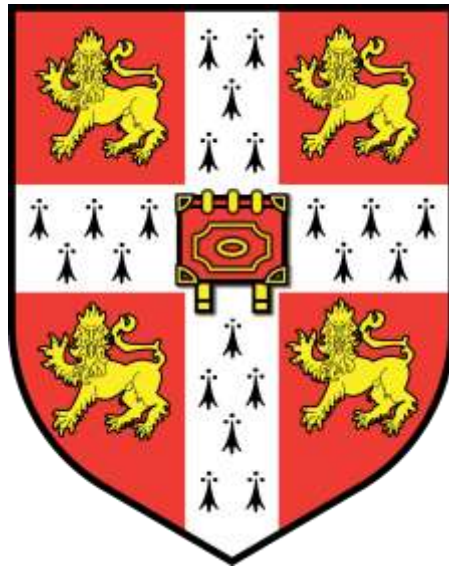


Investigation into the Production of Carbonates and Oxides from Synthetic Brine through Carbon Sequestration



Department of Engineering
University of Cambridge

This dissertation is submitted for the degree of
Doctor of Philosophy by

Rui Hao

Fitzwilliam College

February, 2017

Acknowledgments

This work was undertaken in the Geotechnical and Environmental Research Group, Department of Engineering at the University of Cambridge in academic year 2012-2016.

I would like to express my sincere thanks to my supervisor, Professor Abir Al-Tabbaa, who has provided me this valuable opportunity to advance my research skills and work on such an interesting topic, for her continuous support, advice, guidance, encouragement and motivation, and especially for her kind help with part funding. I also appreciate the recommendations from my adviser Dr. Stuart Scott during the review meetings and his generous advice throughout my PhD. I am also very grateful to my college tutors Dr. David Coomes and Dr. Susan Larsen who have provided me with long-term support and assistance during the course of my studies. Other special thanks go to English tutors in Language Unit of the department, Mrs Nicola Cavaleri, Dr. Denise Chappell, and Dr. Helen East, who has improved my writing English.

I am also thankful to all the technicians in geotechnical, superconductivity, and SEM groups, especially Chris Knight in the experimental conduction, Anthony Dennis in the XRD operation, and Sam Griggs in the SEM manipulation. Other great thanks are to postdocs Dr. Fei Jin, Dr. Chrysoula Litina, and Dr. Antonis Kanellopoulos, and PhD student Regeane Bagonyi in the group, for their guidance. Finally grateful expression goes to Time Ablett, who has always provided me with technical support throughout my study.

In addition, thanks to my colleagues in the GRO, especially Deyi, Zhengtao, Tiffany, Mingzhi, Petros, Oliver, Yunhui, Yiyun, Wenting, for their much valued friendship and support.

I would like to thank the Faculty for the Future, Chinese Student Awards for partial funding of my study; and Fitzwilliam College, the Engineering Department University of Cambridge, and Cambridge Philosophical Society for conference subsidies towards my PhD accomplishment.

Finally, my special and grateful thanks are to my parents for the majority of my funding, their continuous help, great encouragement and significant motivation; without them, I couldnot have achieved anything.

Declaration

I hereby declare that, this dissertation is the result of my own work and has no collaboration work except where specifically indicated in the text. This dissertation has not been submitted in whole or in part for any other degree, diploma or other qualifications to this university or other institutions.

This dissertation has not exceeded upper limit 65,000 words, inclusive of appendices, footnotes, tables and equations, and contains less than 150 figures.

Rui Hao

February 2017

Dedicated to my family...

Abstract

The cement industry contributes around 5-7% of man-made CO₂ emissions globally because of the Portland Cement (PC) production. Therefore, innovative reactive magnesia cement, with significant sustainable and technical advantages, has been proposed by blending reactive MgO and hydraulic binders in various proportions. MgO is currently produced from the calcination of magnesite (MgCO₃), emitting more CO₂ than the production of PC, or from seawater/brine which is also extremely energy intensive. Hence this research aims to investigate an innovative method to produce MgO from reject brine, a waste Mg source, through carbon sequestration, by its reaction with CO₂, to provide a comparable low carbon manufacturing process due to the recycling of CO₂. The produced deposits are then calcined to oxides with potential usage in construction industry. The entire system is a closed loop to achieve both environmental optimisation and good productivity. This research focuses on the chemical manufacturing process, integrated with material science knowledge and advancements, instead of concentrating purely on chemistry evaluations.

Six series of studies were conducted, utilising MgCl₂, CaCl₂, MgCl₂-CaCl₂, MgCl₂-CaCl₂-NaCl, and MgCl₂-CaCl₂-NaCl-KCl to react with CO₂ under alkaline conditions. The precipitates include hydrated magnesium carbonates, calcium carbonates and magnesian calcite. Generated carbonates were then calcined in a furnace to obtain MgO, CaO or dolime (CaO•MgO). All six series of carbonation processes were carried out under a controlled pH level, to study the constant pH's effect on the process and resulting precipitates. Other controllable factors include pH, temperature, initial concentration, stirring speed, and CO₂ flux rate.

In an individual-ion system, sodium distorts the hydrated magnesium carbonates (HMCs) formation with the production of hydromagnesite (HM), dypingite (D) and nesquehonite (N) mixture in the short time when the pH is above 10. However, ammonia shows nesquehonite only because of its good buffering capacity and evaporation properties, providing gradual phase transformation. Nesquehonite is needle-like in shape, produced at a relative low temperature, low carbonates and low pH level. Dissimilarly, hydromagnesite and dypingite are rosette-like, flower-like or accumulated sheet-like morphologies, produced in the presence of sodium when pH \geq 10 or more complex systems. In terms of calcium carbonates,

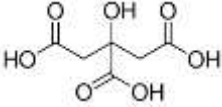
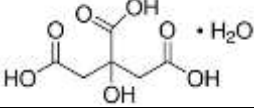
calcite (C) is rhombic in shape, considered as the most stable formation, produced at an ambient temperature. While vaterite (V) is spherical in shape, produced at a lower supersaturation, and aragonite (A) is arrow-like in shape, produced at a high temperature (60 to 80°C). Both vaterite and aragonite are metastable phases, and transfer into calcite finally in the ambient surroundings.

In a dual-ion system, the importance of parameters were investigated and ranked as pH > temperature > CO₂ infusion rate > stirring speed during the carbonation process. Magnesian calcite has four stages of formation: initial stage, intermediate stage, transitional stage and completed stage, dependent on magnesium incorporation within the precipitates. Regarding the mineralisation process, carbonates tend to aggregate into granules of the more abundant element of the initial reactants, such as when reactants are MgCl₂ > CaCl₂ in concentration. The formation mechanism from inner to outer layers of produced particles is magnesium calcium carbonates, calcium carbonates, and magnesium carbonates respectively. A higher calcined temperature requires a longer time to accomplish the oxides reactivity tests because of their reduced porosity and particle sizes. The decarbonation process happens at around 300-600°C for magnesium carbonates, and > 700°C for calcium carbonates. All three heating profiles 650°C, 800°C, and 1000°C are not adequate to fully breakdown the carbonates.

In a multiple-ion system, both sodium and potassium addition accelerate the magnesium participation, and sodium has a better performance than potassium in magnesium capture. Sodium addition increases the impurity level and extends the oxides' completion time in a reactivity test, while the potassium has the propensity to reduce this time.

In conclusion, the optimum parameters for the production of the carbonated precipitates are: 0.25MgCl₂ + 0.05CaCl₂ + 2.35NaCl + 0.05KCl, 700rpm stirring speed, 25°C room temperature, pH=10.5, and 500cm³/min CO₂ infusion rate. Reaction time is within a day. These parameters are chosen based on the sequestration level, particle performance morphology and the operational convenience. The optimum calcination parameters are at 800°C heating temperature with a 4h retention time.

Glossary

Anhydrous citric acid	
Aragonite (A), calcite (C), vaterite (V)	CaCO_3
Artinite	$\text{Mg}_2(\text{CO}_3)(\text{OH})_2 \cdot 3\text{H}_2\text{O}$
Barringtonite	$\text{MgCO}_3 \cdot 2\text{H}_2\text{O}$
Brucite	$\text{Mg}(\text{OH})_2$
CCS	Carbon capture and storage
CCSU	Carbon capture, storage and utilisation
Dolomite (DM)	$\text{CaMg}(\text{CO}_3)_2$
Dolime	$\text{CaO} \cdot \text{MgO}$
Dypingite (D)	$\text{Mg}_5(\text{CO}_3)_4(\text{OH})_2 \cdot 5\text{H}_2\text{O}$
Giorgiosite	$\text{Mg}_5(\text{CO}_3)_4(\text{OH})_2 \cdot 5\text{-}6\text{H}_2\text{O}$
HMCs	Hydrated magnesium carbonates
Halite	NaCl
Hexahydrate calcium carbonate	$\text{CaCO}_3 \cdot 6\text{H}_2\text{O}$
Huntite (HT)	$\text{Mg}_3\text{Ca}(\text{CO}_3)_4$
Hydromagnesite (HM)	$\text{Mg}_5(\text{CO}_3)_4(\text{OH})_2 \cdot 4\text{H}_2\text{O}$
Hydrous citric acid	
ICP-OES	Inductively coupled plasma optical electron spectroscopy
Lansfordite	$\text{MgCO}_3 \cdot 5\text{H}_2\text{O}$
Lime (L)	CaO
Lime stone/calcite	CaCO_3
Magnesia (M)	MgO
Magnesite	MgCO_3
Magnesium calcium carbonate/ Magnesian calcite (MC)	$(\text{Mg}_{0.064}\text{Ca}_{0.936})\text{CO}_3$, $(\text{Mg}_{0.1}\text{Ca}_{0.9})\text{CO}_3$, $(\text{Mg}_{0.129}\text{Ca}_{0.871})\text{CO}_3$, $(\text{Mg}_{0.03}\text{Ca}_{0.97})\text{CO}_3$, $(\text{Mg}_{0.06}\text{Ca}_{0.94})\text{CO}_3$
Monohydrated calcium carbonate/Monohydrocalcite (MHC)	$\text{CaCO}_3 \cdot \text{H}_2\text{O}$
Nesquehonite (N)	$\text{MgCO}_3 \cdot 3\text{H}_2\text{O}$
Olivine	$(\text{Mg, Fe})_2\text{SiO}_4$
PC	Portland cement
Pokrovskite	$\text{Mg}_2(\text{CO}_3)(\text{OH})_2 \cdot 0.5\text{H}_2\text{O}$
Portlandite (PD)	$\text{Ca}(\text{OH})_2$
SEM	Standard electron microscopy
Serpentine	$(\text{Mg, Fe})_3(\text{OH})_4(\text{Si}_3\text{O}_5)$
SI	Saturation index
Slaked lime	$\text{Ca}(\text{OH})_2$
TGA	Thermo-gravimetric
Wollastonite	CaSiO_3
XRD	X-ray diffraction

Contents

Acknowledgments.....	i
Declaration	ii
Abstract	iv
Glossary.....	vi
Chapter 1: Introduction	1
1.1 Background	1
1.2 Aims and Objectives of this Research.....	3
1.3 The Structure of Thesis	4
Chapter 2: Literature Review	6
2.1 Climate Change and Carbon Mitigation	6
2.2 Traditional Cement Sustainability and Its Alternative	7
2.2.1 Current Portland Cement Manufacturing and Alternative MgO-Cement ..	7
2.2.2 The Global Resources of MgO and the Current Production Process of MgO.....	10
2.3 Seawater and Reject Brine	13
2.4 Relevant CO ₂ systems.....	15
2.4.1 The Thermodynamic Properties of CO ₂	15
2.4.2 CO ₂ Dissolution in Seawater and Reject Brine	17
2.4.3 Ternary CO ₂ -NH ₃ -H ₂ O System.....	20
2.5 Magnesium Carbonates and MgO Production	22
2.5.1 Magnesium Carbonates Production with Various Chemical Reagents	22
2.5.2 The Classification and Properties of Magnesium Carbonates	26
2.5.3 The Stability of Magnesium Carbonates.....	29
2.5.4 MgO Grades and Utilisation	31
2.6 Parameters Affecting Magnesium Carbonation.....	32

2.7 Calcium Carbonates and CaO Production	36
2.7.1 Current Precipitated Calcium Carbonates (PCC) and Lime Process, and Its Alternative Carbonation Production from Calcium Ores.....	37
2.7.2 Calcium Carbonates Production with Various Chemical Reagents	38
2.7.3 The Mechanism of Calcium Carbonates Formation	39
2.7.4 The Classifications and Properties of Calcium Carbonates.....	41
2.7.5 The Stability of Calcium Carbonates and Phase Transformation	44
2.7.6 CaCO₃ and CaO Utilisation	47
2.8 Parameters Affecting Calcium Carbonation	48
2.9 Magnesium Calcium Carbonates.....	56
2.10 Parameters Affecting Magnesium Calcium Carbonation.....	58
2.11 The Influences of Impurities on Magnesian Calcites.....	63
2.11.1 Sodium Addition	63
2.11.2 Potassium Addition.....	66
2.11.3 Alkaline Metal Ions Addition & Comparisons.....	68
2.11.4 Other Additives	71
2.12 The Thermal Decomposition of Magnesian Calcites	72
2.13 Thermodynamic Modelling	74
2.14 Missing Gaps for Research Design	77
Chapter 3: Materials and Experimental Methodology.....	80
3.1 Introduction.....	80
3.2 Materials.....	80
3.2.1 Chemical Reactants	80
3.2.2 Magnesium Oxides.....	81
3.3 Apparatus Settings and Operational Procedures.....	83
3.3.1 The Production of Carbonates.....	83

3.3.2 The Production of the Oxides	85
3.4 Experimental Procedures	88
3.4.1 Carbonation Studies	88
3.4.2 pH Stability and Adjustment Studies	89
3.4.3 Reaction Kinetic Studies	90
3.4.4 Calcination Studies	91
3.5 Analytical Measurements	91
3.5.1 Inductively Coupled Plasma-Optical Emission Spectrometry (ICP-OES) 92	
3.5.2 X-Ray Diffraction (XRD)	93
3.5.3 Scanning Electron Microscopy-Energy Dispersive X-ray spectroscopy (SEM-EDX)	94
3.5.4 Thermo-Gravimetric (TGA)	97
Chapter 4: Individual Ion Carbonation and Calcination	99
4.1 Introduction	99
4.2 Preliminary Trial Experiments	99
4.2.1 Experimental Design	100
4.2.2 Carbonation Studies and Basic Analysis	100
4.3 Model Code & Experimental Design Mechanism for SI & SII	105
4.4 Series I-Individual Magnesium Ion System with Ammonia	105
4.4.1 Model for Series I	105
4.4.2 Series I-Experimental Design	106
4.4.3 Series I-Carbonation	111
4.5 Series II-Individual Magnesium Ion System with Sodium Hydroxide	126
4.5.1 Model for Series II	126
4.5.2 Series II.I-Experimental Design	127
4.5.3 Series II.I-Carbonation	132

4.5.4 Series II.I-Thermal Property and Calcination	143
4.5.5 Series II.II-Miscellaneous Studies	153
4.6 Series III-Individual Calcium Ion System with Sodium Hydroxide.....	159
4.6.1 Model for Series III	159
4.6.2 Series III-Experimental Design	159
4.6.3 Series III-Carbonation.....	164
4.6.4 Series III-Thermal Property and Calcination	175
4.7 Conclusions	179
Chapter 5: Dual Ions Carbonation and Calcination	182
5.1 Introduction.....	182
5.2 Series IV-Dual Ions Complex System.....	183
5.2.1 Model for Series IV.....	183
5.2.2 Series IV-Experimental Design.....	184
5.2.3 Series IV-Carbonation	197
5.2.4 Series IV-Thermal Property and Calcination	234
5.3 Conclusions	261
Chapter 6: Multiple Ions Carbonation and Calcination	263
6.1 Introduction.....	263
6.2 Series V-Triple Ions Complex System	263
6.2.1 Model for Series V	263
6.2.2 Series V-Experimental Design	263
6.2.3 Series V-Carbonation	266
6.2.4 Series V-Thermal Property and Calcination.....	277
6.3 Series VI-Quadruple Ions Complex System.....	289
6.3.1 Model for Series VI.....	289
6.3.2 Series VI-Experimental Design.....	289

6.3.3 Series VI-Carbonation	290
6.3.4 Series VI-Thermal Property and Calcination	299
6.4 Conclusions	305
Chapter 7: Conclusions & Recommendations for Future Research	307
7.1 Conclusions	307
7.2 Literature Review	307
7.3 Materials and Experimental Methodology	310
7.4 Series I- Individual Magnesium Ion System with Ammonia	311
7.5 Series II-Individual Magnesium Ion System with Sodium Hydroxide	311
7.6 Series III-Individual Calcium Ion System with Sodium Hydroxide	314
7.7 Series IV-Dual Ions Complex System (Mg²⁺, Ca²⁺)	315
7.8 Series V-Triple Ions Complex System (Mg²⁺, Ca²⁺, Na⁺)	317
7.9 Series VI-Quadruple Ions Complex System (Mg²⁺, Ca²⁺, Na⁺, K⁺)	318
7.10 Recommendations for Future Research	320
References:	322

Chapter 1: Introduction

1.1 Background

The rapid increase of carbon dioxide and methane emitted from the energy industries in the atmosphere is considered as the main cause of global warming. More than 30 billion tonnes of carbon dioxide is produced and released into the atmosphere annually (DECC, 2013), and the main sources of CO₂ are from combustion of fossil fuel (coal, oil and natural gas) to provide energy, industrial processes (e.g. cement production) and land use change. As a consequence, this affects the overall water cycle and ocean circulation patterns, leading to further widespread snow and ice melt and sea level rise, which will particularly threaten some low-altitude cities (Hardy, 2003).

Concrete, as the most commonly used construction material on earth, is a primary contributor to CO₂ emissions. This is because the cement component within the concrete is usually Portland Cement (PC), which accounts for around 5% of global anthropogenic CO₂ emissions (WBCSD, 2012). PC is currently produced at a global rate of over 4 billion tonnes/year (USGS, 2016), and 1 tonne of PC will produce around 0.9-1.1 tonne of CO₂ into surroundings from its production process (NRMCA, 2012). The projected emission from the cement industry is estimated to about 5 billion tonnes by 2050 based on the current progression.

Significant improvements in the properties of PC have been made as well as its sustainable initiative alternatives. These initiatives include the utilisation of renewable energies, the partial substitution of cements with low-carbon materials, such as industrial by-products or wastes, and the development of novel cements with less energy requirements and CO₂ emissions. Among all these developments, the recent emergence of reactive magnesia (MgO) cement is considered a good replacement with its superior mechanical properties and sustainability advantages. It has lower manufacturing temperatures, a higher ability to sequester CO₂, better durability, a better capacity of waste binding, as well as a high extent of recyclability from its produced magnesium carbonates after exposure to the atmosphere.

MgO is graded by the various calcination temperatures. Reactive MgO is produced at a low range of 700-1000°C, which results in larger surface areas of particles and a higher reactivity. On the other hand, dead burned MgO is manufactured at a temperature range of 1400°C-2000°C resulting in MgOs with much lower surface areas and reactivity and is considered the main source of detrimental delayed expansion in concrete. Different grades of MgO have different applications, where the reactive MgO is used in horticultural and water treatment applications and the dead burned MgO for refractory applications. Global production of dead burned MgO is dominant at approximate 80%. Research over the past 15 years has highlighted the potential for applications in reactive MgO in cement systems.

The main production route of MgO is from the calcination of magnesite. This leads to significant CO₂ emissions since 2.1 tonnes of magnesite needed to produce 1 tonne of MgO and leads to 1.4 tonnes of CO₂ emissions. Another production route is from seawater and brine, which results in less CO₂ emissions. But this process is extremely energy intensive and costly. To conclude, traditional MgO production from both magnesite and seawater has the high CO₂ emissions, which has hindered the interest of MgO usage in the constructions.

Hence a sustainable approach for the production of MgO can use the industrial by-products and waste, especially those with high magnesium contents. A major potential waste source is reject brine. According to Ferrini et al. (2009), around 70 billion barrels of waste water are generated globally every year, comprising a drainage system, a desalination plant, subsurface brines and salt lakes. The majority of brackish water is directly disposed into concentrated ponds, surface waters and other water bodies, which will impair aquatic life, seawater quality, soil deterioration and groundwater contamination (Al-handhaly et al.2003; Culligan, et al. 2010;). The use of reject brine to produce MgO through a carbon sequestration process can provide a sustainable solution to convert the wastes into valuable products.

In this thesis, a fundamental study is carried out using synthetic brine investigating the performance of each compound, e.g. magnesium chloride and calcium chloride, and then exploring the performance of a mixture of both. Finally, impurities sodium and potassium will be added to mimic the natural brine (seawater) constitutions. This study covers almost all practical ions except unusual and poisonous elements.

1.2 Aims and Objectives of this Research

This research aims to investigate an innovative method to produce MgO from reject brine/seawater, a waste magnesium source, through carbon sequestration, by reacting with CO₂ to provide a process which has a comparable low carbon footprint. The produced carbonates in the reaction are then calcined to their oxides.

The objectives are to:

- a) Perform an extensive and critical relevant literature review to present an overview of the relevant aspects and the latest research developments on magnesium carbonates, calcium carbonates and their mixed carbonates, and calcined products magnesia, lime and dolime. This will also involve a focus on the chemical production process and the factors that affect the precipitates of carbonates in solution, as well as differences in high temperature calcination.
- b) Test and investigate the reaction parameters and hence precipitation products by identifying the influences of the variable parameters, including different chemical base reagents, pH, temperatures, reactants concentration, CO₂ flux rate, and stirring speed.
- c) Investigate the production of magnesium carbonate alone, calcium carbonate alone and then their mixture and then investigate the effects of sodium and potassium on the production process as well as the calcination process and the properties of the resulting oxides.
- d) Operate analytical measurements to explore the properties of the precipitates and their subsequent calcined oxides and the differences between them, including XRD for the determination of crystalline compounds, SEM for microstructure observation, ICP-OES for aqueous ion analysis, TGA for thermal analysis, and a chemical reactivity test for oxides neutralisation.
- e) Explore the carbonation process using different mixtures and mixture ratios, by introducing ions gradually, forming into multiple ions, triple ions, and quadruple ions.
- f) Investigate the mechanism behind the carbonation reaction, such as nucleation, crystallisation and transformation stages; as well as to understand the different elements or impurities effects on oxides and their consequential properties.

1.3 The Structure of Thesis

The summarised work over the past four years of this research project is elaborated into 7 chapters as follows:

Chapter 1: Introduction—presenting an introduction to the problems and describing the overview of research, the rationale for the proposed work and the aims and objectives of the thesis.

Chapter 2: Literature Review—demonstrating a comprehensive related literature work, starting with construction materials and relevant environmental issues, and then focusing on magnesium carbonates, calcium carbonates, and magnesium calcium carbonates areas. Different chemical reagents as well as the carbonation affecting factors are carefully elaborated in this chapter to provide forefront knowledge. These carbonates are also accompanied by further oxides production, grades and utilisations for the completed cycle of magnesia, calcia or dolime manufacturing. Moreover, modelling is described in the final discussion to present its utilisation.

Chapter 3: Materials and Experimental Methodology—summarising materials used in the experiments, sample preparations, apparatus settings, operational procedures, various experimental studies and analytical measurements, in order to provide a solid analysis of experiments.

Chapter 4: Individual Ion Carbonation and Calcination— showing and discussing preliminary trial experiments and the derived main results. Sodium hydroxide is used to substitute the ammonia later on as the alkaline adjustment to maintain a constant pH level. Two comparisons are made during the magnesium carbonates investigation. Calcination is directly followed afterwards for various heating temperatures. Calcium carbonates are also elaborated in this segment as the sequential exploration of the individual ion.

Chapter 5: Dual Ions Carbonation and Calcination— exploring the carbonation processes of the mixed magnesium and calcium ions and their calcination profiles. Ten samples are analysed, in order to discover the reaction mechanism and the effects of various parameters.

Chapter 6: Multiple Ions Carbonation and Calcination—describing the phenomena of series V triple ions and series VI quadruple ions based on the previous results. Sodium and potassium are added to simulate the synthetic brine except the uncommon and hazardous elements. This chapter analyses the potential optimum condition in carbon sequestration and calcination process by using seawater/brine as raw materials.

Chapter 7: Conclusions and Recommendations for Future Research— giving a summary of the general literature review, experimental operations, and all the main findings in the results chapters, as well as proposing future work on relevant studies.

Chapter 2: Literature Review

2.1 Climate Change and Carbon Mitigation

Carbon dioxide and methane are both considered as the key factors of climate change; more than 30 billion tonnes of carbon dioxide are produced and released annually (DECC, 2013), main causes of which are fossil fuels (coal, oil and natural gas) combustion, industrial manufacturing (e.g. cement production) and urbanisation process. However the progress towards a low carbon-dependent society is still slow, due to poor improvement in energy efficiency and the low level of renewable integration into energy generation. Hence carbon capture storage and utilisation (CCSU) technique offers a good substitution for CO₂ reduction, providing a potential high storage capacity with a reasonable cost, as well as producing valuable products. The concept of CCSU is to capture the produced CO₂ during the chemical energy in fossil fuels transferring to electrical energy, and sequester the carbon elsewhere rather than the atmosphere (Nordbottne & Celia, 2012; International Energy Agency, 2010). It includes the capture, transportation and subsequent storage of CO₂ in suitable geological and ocean sites, or storage as carbonates/bicarbonates via mineral carbonation process (Peter Styring, 2011). Globally, this technology is well under exploration and development in the UK, mainland Europe, the U.S. and Australia at the moment (Peter Styring et al., 2011).

This thesis focuses on carbon sequestration and its application on construction, due to high carbon emissions and tightened carbon reduction obligations. The construction industry is expected to enhance and better protect the natural environment, deliver buildings and structures that provide greater satisfaction, and minimise its impact on the consumption of energy (Bishop et al., 2005). Carbon mineralisation, with permanent calcium and magnesium carbonates storage (Bert et al., 2005), is the process of either chemical or physical capture through product transformation by breaking and reforming structural bonds under certain conditions (Teir, 2008). It provides good solutions in long-term storage, large sequestration quantities, and waste reuse strengths (Lackner et al., 1995). Especially for the UK, it is critical to study the mineralisation due to limited geological sites, thus

related information in carbon storage and utilisation technology is also briefly considered here.

Ca- and Mg-bearing minerals are widely used as feedstocks due to their natural abundance and availability; moreover, manufacturing alkaline wastes are also applied for CO₂ fixation, such as stainless steel slag, fly ash, and cement kiln dust. These raw materials are more reactive, but sequestration capacity of CO₂ is only 200-300Mt annually because of the availability of resources and the maturity of the technologies, compared to the potential 10,000-1,000,000Gt in geological reserves (Styring, et al., 2015).

Mineralisation can also apply in solidifying hazardous contaminants from wastes through pH neutralising, precipitating carbonates and diminishing the porosity of carbonate crystal formation (Fernández et al., 2004; Gunning et al., 2010). This reaction is a fast and permanent process, compared to slow progress in underground CO₂ injection and limited accessibility. Furthermore, it will not release CO₂ till pH<2, and pH of acid rain is unlikely to happen below 2.5 in nature (Brownlow, 1996), therefore the normal environment will not affect the magnesium carbonates' dissolution. However the cost is still not as competitive as geological storage (Zevenhoven et al., 2009). Naturally, the formation process of carbonation is very slow, hence a key challenge of large-scale industrial development of CO₂ is to accelerate the carbonation, using heat, pressure, mechanical and chemical pretreatment of the minerals (Styring et al., 2011).

2.2 Traditional Cement Sustainability and Its Alternative

2.2.1 Current Portland Cement Manufacturing and Alternative MgO-Cement

Concrete, the second most consumed product on earth after water (WBCSD, 2007), is mainly composed of Portland cement, involving an energy-intensive process during production. The process of production is extracting limestone (calcium carbonate) rock, chalk, shale or clay, and crushing into a fine powder, when adding supplemented minerals, obtained from waste or by-products from other industries, such as paper ash, to ensure the proper chemical composition at the same time. This pretreated material is then heated to ~1500°C, forming cement clinker containing hydraulic calcium silicates. Once it cools, 3-5% of gypsum is added to the clinker to control the setting time of the end product (Lafarge,

2013). Because of the high temperature used during calcination, cement manufacturing is incredibly energy intensive.

In the process of PC production, CO₂ emissions are significant during fossil fuels combustion, and the calcination phase of manufacturing. According to Taylor (1997), 1 tonne of PC releases around 1 tonne of CO₂ into atmosphere, taking into account calcium carbonate decomposition, carbon fuel burning, and electrical energy supply. Projected global carbon emissions from cement industry in 2050, are expected to reach ~5 billion tonnes ([Figure 2. 1](#)), assuming no change in current practices. Among these emissions, 50% is from chemical processing, 40% is from fuel burning, 5% is from transportation and 5% is from electricity used during production (WBCSD, 2002). The world's five biggest cement producers are Lafarge, Holcim, Cemex, Heidelberg Cement, and Italcementi.

With severe CO₂ emission in traditional cement manufacture; it is important to invent novel methodologies. Major solutions on emission reduction in this industry are emphasised by three initiatives: (1) partial cement replacement with low carbon materials, industrial by-products and wastes such as pulverised fly ash (PFA) and ground granulated blast slag (GGBS) (Schneider et al, 2011); (2) enhancements of the overall energy efficiency with the use of alternative raw materials, such as renewable energy sources, and low-energy production methods; and (3) development of new cement formulations with lower energy consumption and carbon footprint (Gartner, 2004; PCA, 2009), such as the recently emerged reactive MgO cement.

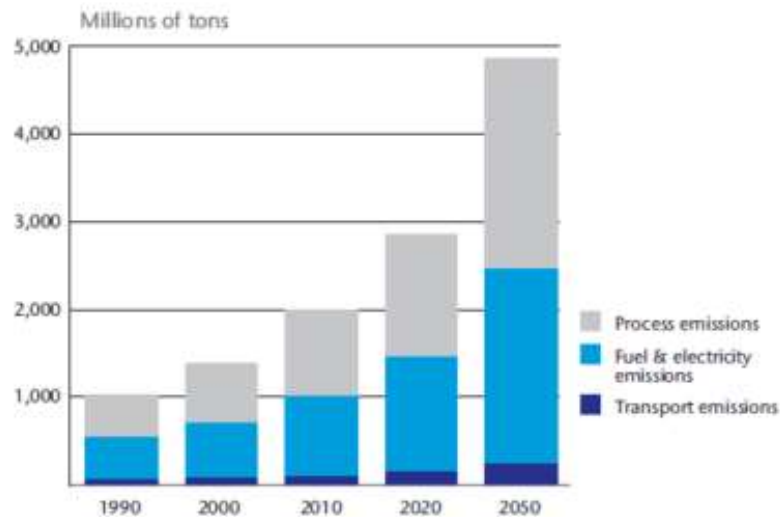


Figure 2. 1: Projected CO₂ emissions from global cement industry (WBCSD, 2007)

Reactive MgO-cement has appeared to be a potential substitute for PC with superior technical and sustainable advantages, which was developed and patented by an Australian Scientist, John Harrison (Harrison, 2001). Reactive MgO is light-burned, which is calcined at a low temperature 700-1000°C, providing the highest reactivity and greatest specific surface area of MgO (Harrison, 2004a-c). Three main formulations are classified with different reactive MgO and PC ratios: Tec-cement with PC>> MgO, Environ-cement with PC= MgO and Eco-cement with MgO >> PC (Harrison, 2001). The advantages of MgO cement are both environmental and technical. The calcination temperature of reactive MgO is ~700-800°C, which is much lower than ~1500°C temperature in PC production. MgO has a high propensity for binding with waste (Harrison, 2001), and thus can be mixed with much larger quantities of industrial by-products such as fly ash, slag and red mud (a by-product of aluminum production). MgO is also much more recyclable as it can hydrate to magnesium hydroxide or carbonate to magnesium carbonates, from which MgO can be reproduced through calcination, hence significantly reducing the waste production. Although the production of 1 tonne of MgO, from magnesite, leads to the production of 1.4 tonnes of CO₂, which is higher than the 0.9 tonne CO₂ emission from the 1 tonne of PC production, MgO can be carbonated completely while PC can only be carbonated by 30% (Taylor, 1997), therefore overall MgO can have much lower CO₂ emissions.

From the technical improvements, MgO-cement achieves high strength and durability via carbonation and hydration processes. However some limitations exist in regulations, PC has

been well-known, documented and relied on for hundreds of years, which has contributed to high market confidence. Obligations on structural engineers and regularity authorities' restriction on new product and process, make MgO-cement relatively hard to be accepted by construction industry and the public (Unluer, 2012) in a short term.

MgO-cements have the potential to be used in mortars, renders, grouts, and drill hole cement; porous pavement, bricks, blocks and pavers; and lightweight disposable high thermal capacity insulated packaging. Moreover, they are applied as stabilising agents, in soil stabilisation/solidification and waste utilisation and capture techniques, and other aspects such as fire retarding. In the long term, as they become more widely accepted and their engineering properties get quantified, MgO-cements and future derivatives have the possibility to target a wider range of PC applications (Unluer, 2012). However, at the moment, the MgO content in cement is only restricted to 5% usage (Taylor, 1997) in existing Codes of Practice. It is important to identify the availability of raw materials of MgO production. Magnesite--the most utilised raw materials is widely found in other countries except UK, and there are significant deposits in China and Australia, which may cause long distance transportation cost as well as the subsequent environmental impact.

2.2.2 The Global Resources of MgO and the Current Production Process of MgO

Magnesium carbonate (MgCO_3) is mainly composed of 90-95% purity level in magnesite deposits. Total estimate of known global reserve is around 12-13 billion tonnes, in addition to several million tons of brucite ($\text{Mg}(\text{OH})_2$) (U.S. Geological Survey, 2013). The dominant producers of magnesite are North Korea, China, Slovakia, Turkey, Russia, Austria, and India, taking up 75% of world output (Shand, 2006). Other reserves of magnesium-ore, including dolomite ($\text{CaMg}(\text{CO}_3)_2$), forsterite (Mg_2SiO_4), magnesium-bearing evaporate minerals, as well as magnesia-bearing brines, are considered to possess billions of tonnes globally. Another typical method is to use the synthetic brine production. There are approximate 20 manufacturers to supply magnesia through seawater or brine resources, accounting for 14% of the world magnesia production (Table 2. 1).

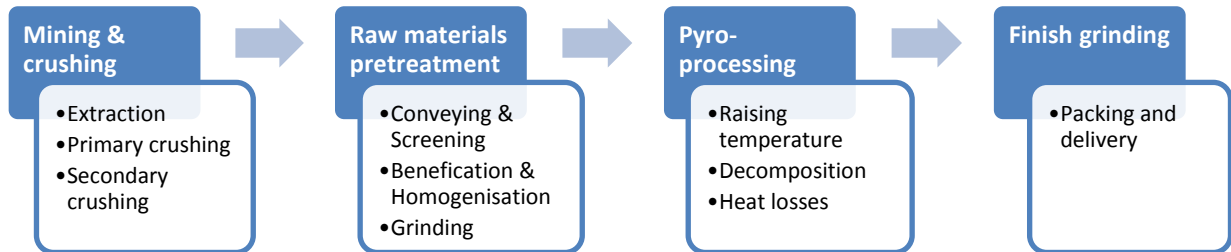
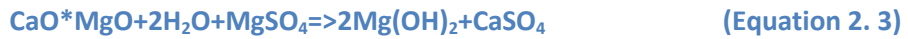
There are four stages of producing MgO from magnesite: mining and crushing, pre-treatment, calcination/pyro-processing and grinding; whereas the production of MgO from seawater/brine comprises three main stages: extraction, pre-treatment, and

calcination/pyro-processing (Figure 2.2a-b). The majority of magnesite mining is conducted using open-pit mining methods with extraction and crushing, and further treatment into intermediate materials, followed by calcination of products under high temperatures.

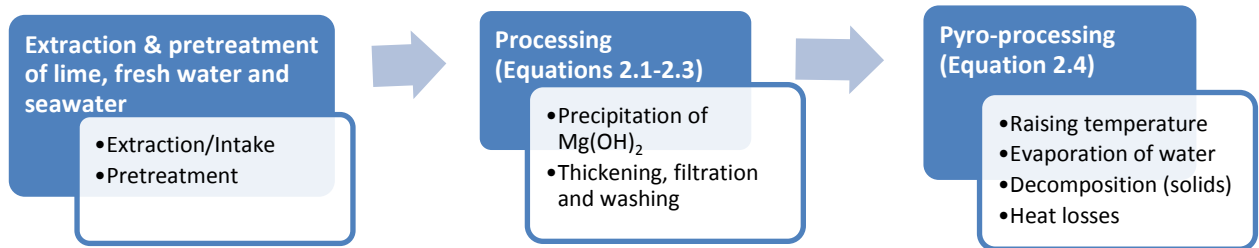
For the synthetic brine production, brine wells and lakes need extraction of the magnesium salt solutions, while seawater is used directly. Magnesium-rich solution is pretreated before entering the reactor, which involves a screening and filtration method to remove the suspended particles such as silts, sand, and marine creatures, followed by the decarbonation process. After that, it is pumped into an agitated reactor vessel where it is contacted with a strong alkali, usually either lime or dolime (Equations 2.1-2.3).

Table 2. 1: Synthetic MgO manufacturers (Shand, 2006)

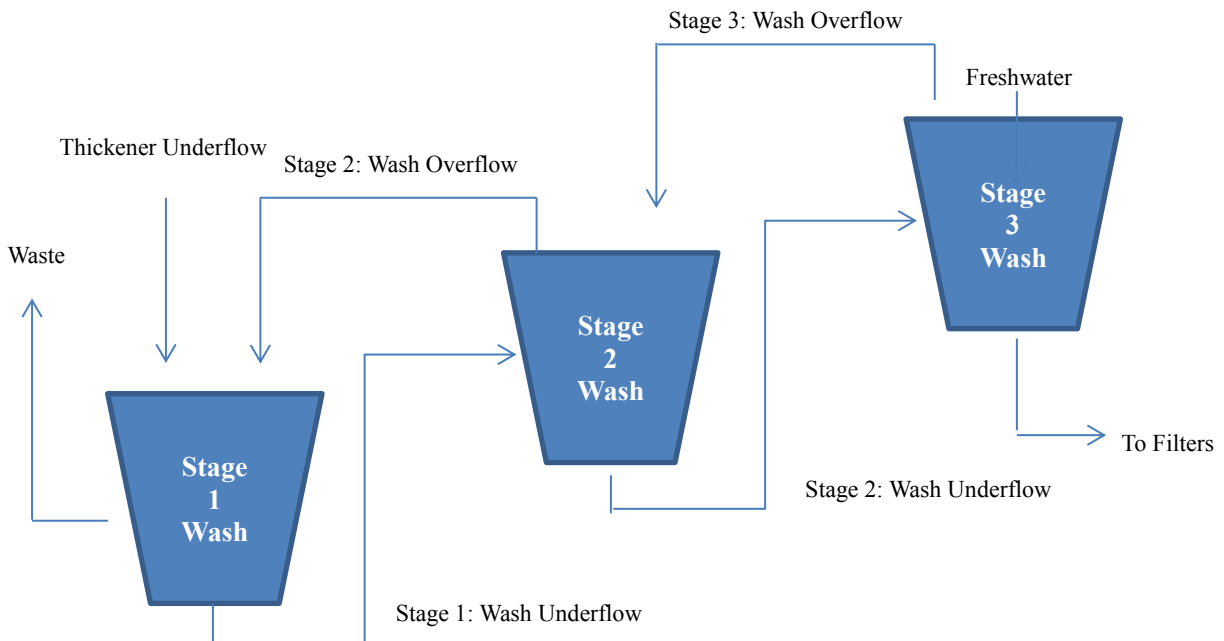
Location	Company	Yearly Production Capacity
China	Manchurian Seawater Works	10,000t dead-burnt MgO
	Jiaozhou Guhe Magnesium Salt Factory	3,000t caustic-calcined MgO
France	Scora	<10,000Mt caustic-calcined MgO (dolomitic purification)
Ireland	Premier Periclase (MgO)	90,000t dead-burnt MgO
Israel	Dead Sea Periclase (MgO)	10,000t caustic-calcined MgO, 60,000t dead-burnt MgO
Jordan	Jordan Magnesia Company Ltd.	50,000t dead-burnt and 10,000t caustic-calcined MgO and Mg(OH) ₂
South Korea	Sam Hwa Chemical Co.	50,000t dead-burnt MgO
Japan	UBE Material Industries Co., Ltd.	250,000t dead-burnt MgO
	Shin Nihon Salt Co., Ltd.	40,000t 35-40% Mg(OH) ₂ slurry
	Naikai Salt Ind. Co., Ltd.	20,000t Mg(OH) ₂ slurry, 2,000t Mg(OH) ₂ powder
	Ako Kasei Co., Ltd.	Mg(OH) ₂ /MgO
	Tateho Chemical Ind. Co., Ltd.	Fused MgO/Mg(OH) ₂
	Konoshima Chemical Co.	12-15,000t Mg(OH) ₂
	TMG Corp.	10,000t Mg(OH) ₂
	Nihon Kaisui Kako	8,000t Mg(OH) ₂ slurry ,24,000t MgO/Mg(OH) ₂ powder
United States	Premier Chemicals, LLC	50,000t Mg(OH) ₂ /caustic-calcined MgO
	Martin Marietta	80,000t caustic-calcined MgO
	Rohm & Haas	10,000t caustic-calcined MgO
	SPI-Pharma	Pharmaceutical-grade magnesium hydroxide
Brazil	Buschle & Lepper	High-purity seawater-grade magnesium oxide and hydroxide
Mexico	Penoles, S.A. de C.V.	Brine precipitation approx. 40,000t caustic, fused, hydroxide, and dead burn



(a): The industrial production route of MgO from magnesite



(b): The industrial production route of MgO from seawater/brine



(c): Three-stage countercurrents wash flow

Figure 2. 2: MgO production from magnesite (a) and seawater (b) and the solids washing procedures (c)

The overflow from the reactor takes the precipitated $\text{Mg}(\text{OH})_2$ into a large settling tank, prior to countercurrent washing. Normally two to three countercurrent washing stages are employed to get rid of dissolved salts such as NaCl from the settled solids ([Figure 2.2c](#)). It is considered as an economical method of the process of pumping slurry uphill, and then the large amounts of freshwater flow downhill by gravity. This method ensures the most efficient usage of freshwater for each successive stage. This operation gives a guidance of washing times within the experimental design. After final wash, the underflow from wash tank is transferred to the filtration system. Produced precipitates are then calcined under a desired temperature to obtain the required specific surface area of the finished products. Finally, various mills are used to grind magnesia to the preferred sizes.

2.3 Seawater and Reject Brine

The composition of seawater is mainly chloride, sodium and magnesium ions ([Table 2. 2](#)), with ~20,000 ppm; 10,000ppm and 1300ppm respectively. Eleven major ions account for 99.5% of the total solutes in seawater, they are chloride, sulphate, bicarbonate, bromide, fluoride, sodium, magnesium, calcium, potassium strontium and boron; and significantly determine the chemistry of seawater.

Seawater is slightly alkaline with a pH range between 7.8 and 8.3 and is buffered by the carbonate system (equilibrium reactions see [Section.2.4.3](#)). Under the natural equilibrium system within the atmosphere, around 87% of ionic carbonate presents as bicarbonate ion (HCO_3^-), and the remaining is carbonate (CO_3^{2-}) ([Shand, 2006](#)). Based on [Table 2. 2a](#), around 125 gallons of seawater will produce 1kg of MgO ([Shand, 2006](#)).

Brine is a more salt-concentrated solution than seawater and is naturally presented in arid and semiarid environments, such as Dead Sea in Jordan and Israel, and Great Salt Lake in Utah. Reject brine, also called produced water (PW), is effluent from manufacturing processes, such as oil and gas production, mineral extraction, cooling towers in power stations, desalination plants and other chemical industries ([Wang, 2012](#)). Salt concentration may vary from 1000-250,000ppm, or up to ~3000,000ppm ([Fakhru'l-Razi et al., 2009](#)).

Around 70 billion barrels of PW are generated worldwide every year ([Ferrini et al. 2009](#); [Veil et al, 2004](#); [Kanagy et al. 2008](#)), the majority of which is directly disposed into concentrated ponds, surface waters and other water bodies. [Table 2.2b](#) displays the percentages of brine

disposal method in the USA. As a long term, this behaviour will impair aquatic life, seawater quality, and lead to soil deterioration and groundwater contamination (Al-handhaly et al.2003; Culligan, et al. 2010; Lattemann & Höpner, 2008; Mohamed et al. 2005; Danoun, 2007; Peters & Pintó, 2008; Vito et al., 2010). The composition of saline water varies by different locations, and some of the representative resources worldwide are compiled in **Table 2. 2c**.

Table 2. 2: Seawater (a) composition, brine disposal in USA (b) & reject brines (c) compositions

(a): Seawater composition (Shand, 2006)

Element	Abundance (ppm)	Principal Species
Cl	19,353	Cl ⁻
Na	10,760	Na ⁺
Mg	1,294	Mg ²⁺ , MgSO ₄
S	812	SO ₄ ²⁻
Ca	413	Ca ²⁺ , CaSO ₄
K	387	K ⁺
Br	67.3	Br ⁻
C	28	HCO ₃ ⁻ , H ₂ CO ₃ , CO ₃ ²⁻ Organic compounds
Sr	8.0	Sr ²⁺ , SrSO ₄
B	4.6	B(OH) ₃ , B(OH) ₂ O ⁻
Si	3	Si(OH) ₄ , Si(OH) ₃ O ⁻
F	1.3	F ⁻ , MgF ⁺

(b): The methods of brine disposal in the USA (Mohamed et al., 2005)

Method of disposal	(%)
Surface water	48
Discharged to wastewater treatment plants	23
Land application	13
Deep well injection	10
Evaporation ponds	6

(c): Some reject brines or salt lake chemical compositions --NR: Not reported

	Drainage system, Iran, 2011 (Aghakhani et al, 2011)	Desalination plant Doha, 1997 (El-Naas, 2011)	Subsurface brines, US, 2006 (Shand, 2006)	Chaka salt lake, China, 2004 (Xingqi et al., 2008)
pH	8.5	8.2	4-5	7
Na ⁺ (ppm)	984,400	NR	50,000	56,120
Ca ²⁺ (ppm)	160,000	1,300-1,400	230,000	125
Mg ²⁺ (ppm)	120,000	7,600-7,700	122,000	45,160
K ⁺ (ppm)	9,750	NR	NR	6,500
Cl ⁻ (ppm)	1,331,000	29,000	768,000	191,230
HCO ₃ ⁻ (ppm)	366,000	3,900	NR	1,200
SO ₄ ²⁻ (ppm)	825,600	3,900	NR	44,400

2.4 Relevant CO₂ systems

2.4.1 The Thermodynamic Properties of CO₂

It is important to investigate the behavior of solid, liquid and vapor phases for CO₂, H₂O and CO₂-H₂O at certain conditions, or coexisting points at equilibrium. All the chemical properties (e.g. ΔG , molar volume etc.) and physical properties (e.g. density, structure etc.) are different at a specific phase. Their thermodynamic properties can be depicted by using a P-T diagram (Figure 2. 3). Both CO₂ and H₂O critical points and triple points are shown in Table 2. 3.

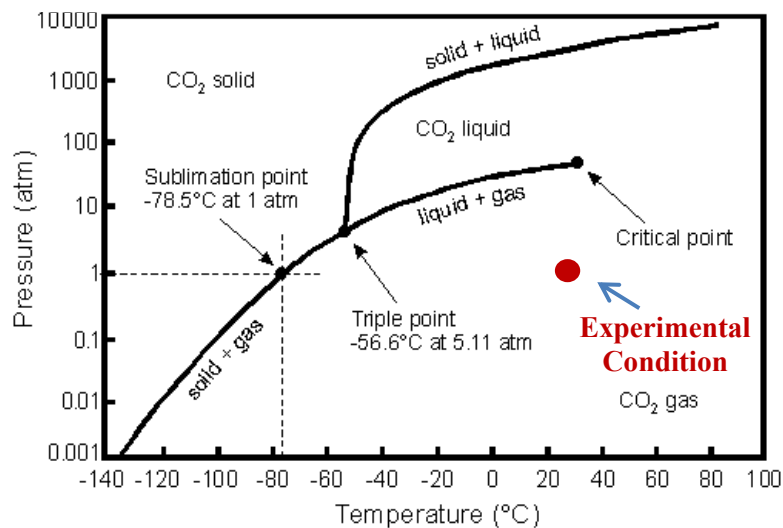
Table 2. 3: The critical properties of CO₂ and H₂O (summarised from Figure 2. 3)

Component	CO ₂ (Span & Wagner, 1996)	H ₂ O (Wagner et al., 2000)
T _c (°C)	30.9782	373.946
P _c (pressure at critical point)(bar)	73.773	220.64
ρ_c (kg/m ³)	467.6	322
		H ₂ O (Lide, 2004)
T _t (°C)	-56.558	0.01
P _t (pressure at triple point) (bar)	5.1795	6.1173*10 ⁻³

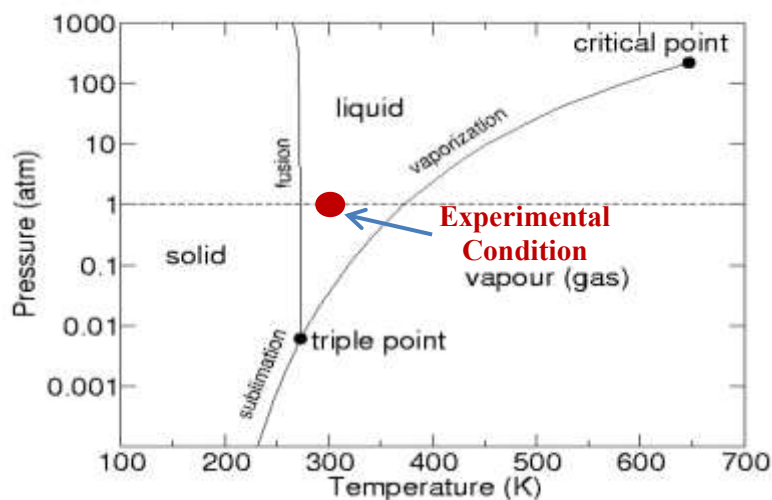
At triple point, three phases coexist, while beyond the critical point, carbon dioxide and water change into supercritical fluids, a phase that is neither liquid nor gas (Hangx, 2005).

Each of curves represents a phase transformation: solid to liquid (melting line), liquid to vapour (saturation line), and solid to vapour (sublimation line). **Figure 2. 3a** shows that CO₂ stays in gas form at atmospheric pressure at any temperatures, but will transfer into liquid under the pressure 30 atmospheres at 20°C (Shakhashiri, 2006).

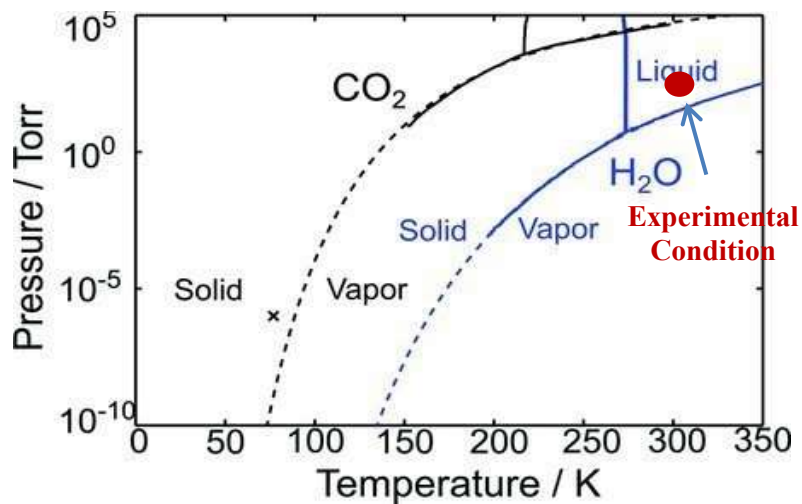
Following the phase diagrams of pure CO₂ and pure water, a mixed CO₂-H₂O aqueous phase P-T graph is shown in **Figure 2.3c**. Based on this figure, H₂O rich liquid phase and CO₂ vapour phase are presented in this experimental condition at the atmospheric pressure ~760 Torr (1 atm = 0.101325Mpa, 1 torr = 13.3*10⁻⁵Mpa) and at a room temperature ~300K (0 Kelvin = -273.15°C) (**Figure 2. 3b, Figure 2.3c**).



(a): Pressure-Temperature phase diagram for pure CO₂ (modified from Shakhashiri, 2006)



(b): Pressure-Temperature phase diagram for H₂O (modified from Goddard, 2011)

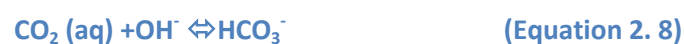


(c): Pressure-Temperature phase diagram for CO₂-H₂O (modified from Jager et al., 2013; Span et al., 2013)

Figure 2. 3: Pressure-Temperature phase diagrams for CO₂ (a), H₂O (b) and CO₂-H₂O binary system (c)

2.4.2 CO₂ Dissolution in Seawater and Reject Brine

CO₂ dissolution in seawater or reject brine needs to be examined, in relation to its reaction with the brine's cation content, forming mineral carbonate precipitates. Reactions are reported by several scholars displayed as below (Druckenmiller et al, 2006; Druckenmiller & Maroto-Valer, 2005; Soong et al 2004; Maries & Hills, 2013):



Eqn 2.5, CO₂ gas going into solution, is greatly dependent on temperature, pressure, and brine salinity (**Figure 2.4**) (Hangx, 2005). According to these graphs, the following effects can be concluded:

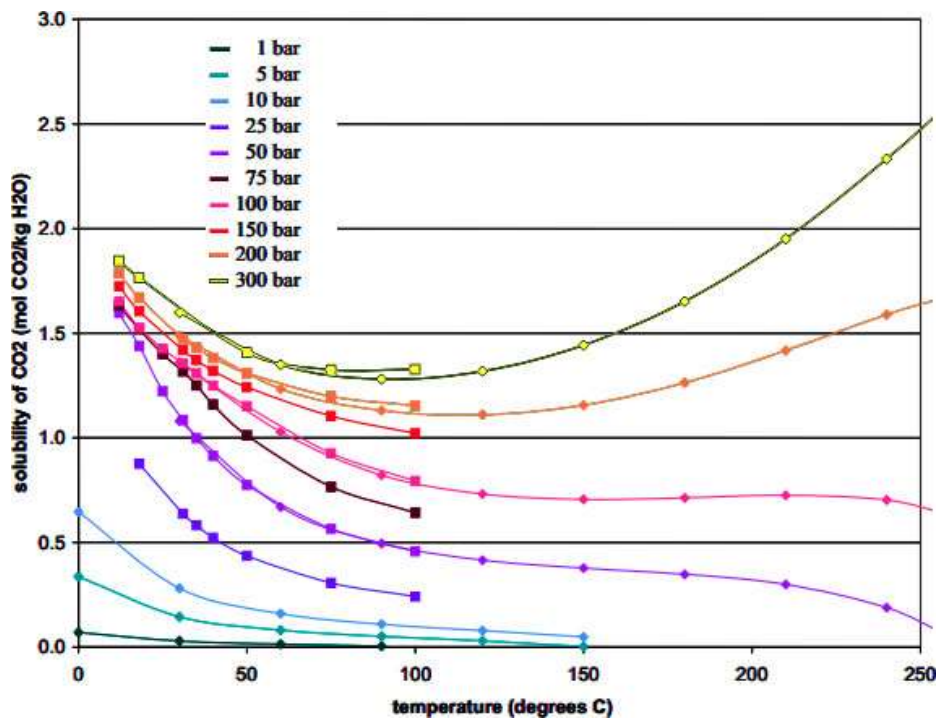
Temperature: The solubility of CO₂ decreases with an increased temperature, under a constant pressure and salinity. Particularly between 25°C and 60°C, CO₂ solubility is dominant. However, when the temperature is beyond 100°C, solubility rises again with temperatures (Al-Anezi, Somerfield, Mee, & Hilal, 2008).

Pressure: With a higher pressure, at a constant temperature and salinity, the solubility of CO₂ in solution grows. It is apparent to see that a lower pressure between 0-200bar has a more obvious effect on CO₂ solubility than a higher pressure.

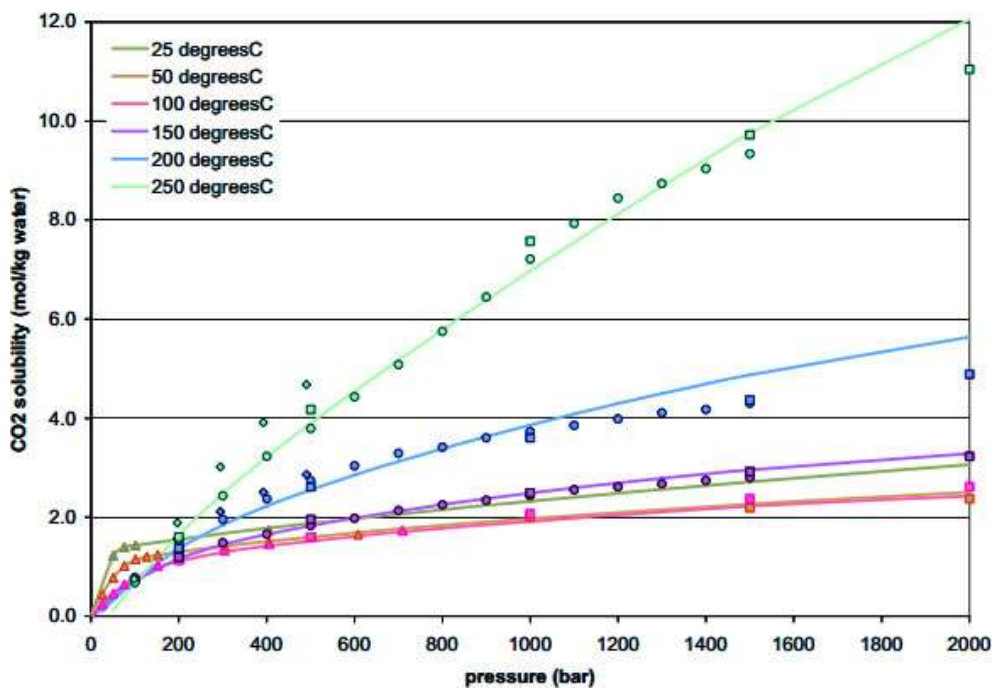
Salinity: The addition of salts to the solution results in lower CO₂ solubility, which is usually named as “salting out effect” (Al-Anezi et al, 2008; Webb et al, 1941; Yoshida, 1979). The magnitude of this effect is controlled by the composition of salts: monovalent salts’ solutions (e.g. NaCl or KCl) have fewer constrains on CO₂ dissolution compared to divalent salt solutions (e.g. CaCl₂ or MgCl₂) (**Figure 2.4c**). This is due to the higher alkaline concentration of divalent salt solutions leading to a more fully saturated level, hence reducing the CO₂ solubility.

Eqn 2.6-2.8 present the carbonic acid formation and its dissociation, reducing the pH in the system. Bicarbonates are then dissociated into carbonates (**Eqn 2.9-2.10**), forming calcite, magnesite and dolomite instantaneously in natural brine through nucleation and subsequent crystal growth (**Eqn 2.11-2.13**) (Druckenmiller & Maroto-Valer, 2005; Lackner, 2002). But in a single chemical reagent system, only calcite or magnesite will be precipitated.

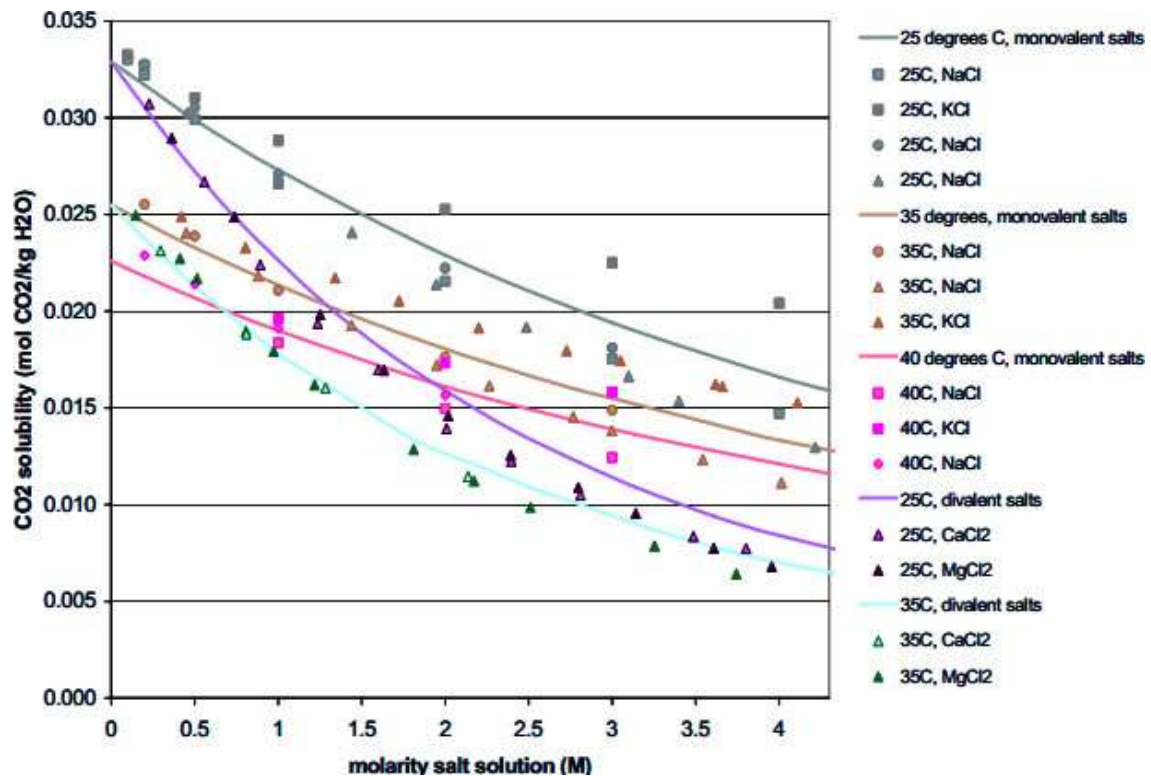
Usually, in the alkaline condition, CO₂ hydrates with OH⁻ ions firstly and then dissociates into bicarbonate and carbonate as shown in **Eqn 2.8-2.9**. It is noted that the formation of bicarbonate is generally the rate limiting step in precipitation, thus an additional alkaline is necessary to assist the precipitations (Bond et al., 2001; Maries & Hills, 2013, Dreybrodt, et al., 1997).



(a): CO₂ solubility as a function of temperature. ◆ Duan & Sun (2003) ■ Wiebe & Gaddy (1939)



(b): CO₂ solubility as a function of pressure. ▲ Wiebe & Gaddy (1939) ■ Todheide and Franck (1963) ● Takenouchi & Kennedy (1964) ◆ Malinin (1959)



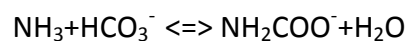
(c): CO₂ solubility as a function of molarity salt solution at 1 atm pressure. ▲ Markham & Kobe (1941), ■ Harned & Davis (1942), ◆ Yoshida (1979)

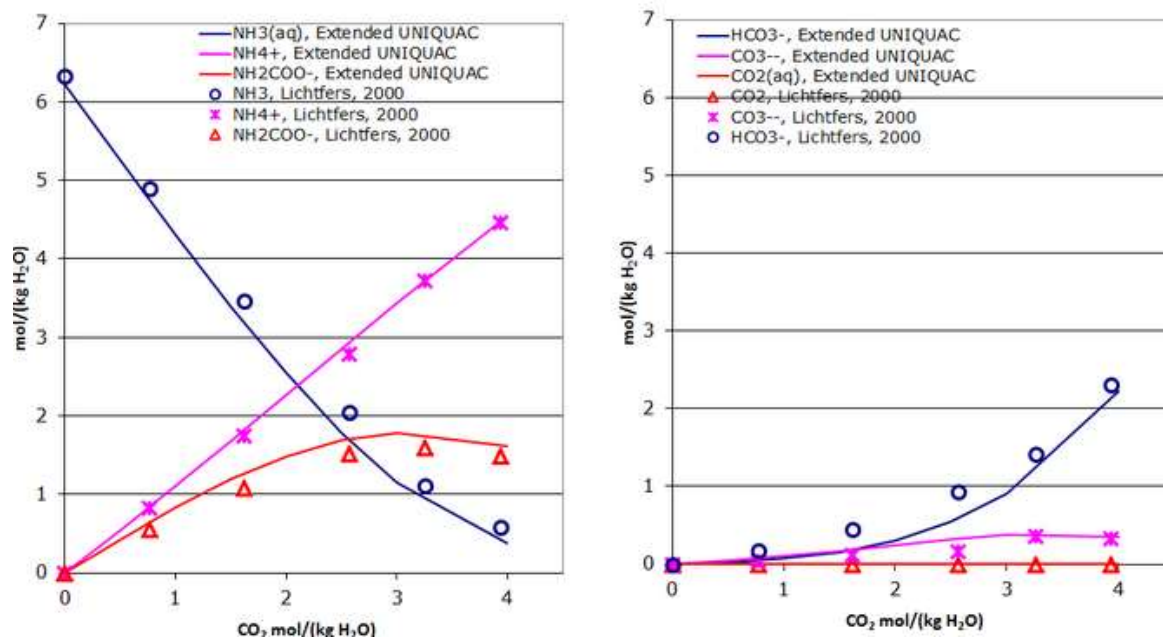
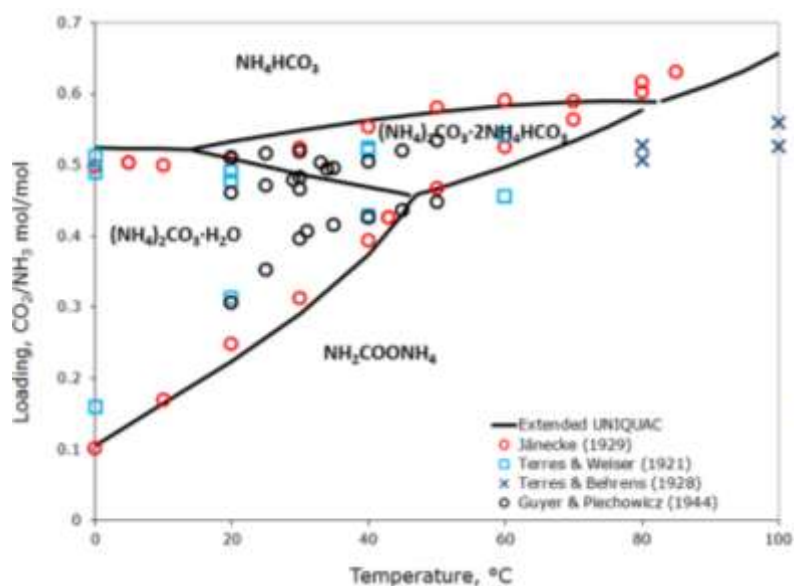
Figure 2. 4: CO₂ solubility dependence: (a) temperature; (b) pressure; (c) salinity

2.4.3 Ternary CO₂-NH₃-H₂O System

This research utilises alkaline solution to maintain a constant pH level, ammonia is used during the experiments, following from Djihan's (2013) and Ferrini's (2009) work, which is also a widely operated chilled ammonia process in industry to remove CO₂ from flue gas in a post combustion carbon capture process. In a chilled ammonia progression, slurry consisting of a liquid in equilibrium with solid ammonia bicarbonates (NH₄HCO₃) is generated in an absorber.

The CO₂-NH₃-H₂O system is investigated as a ternary integration, where the following ions are produced in different amounts: H⁺, OH⁻, NH₄⁺, NH₂COO⁻, HCO₃⁻, and CO₃²⁻. The carbamate (NH₂COO⁻) is the intermediate product for the reaction derived by:



(a): CO₂-NH₃-CO₂ ternary system: ammonia salts(b): CO₂-NH₃-CO₂ ternary system: carbonates

(c): Solid-liquid equilibrium in a chilled ammonia process

Figure 2. 5: Ternary CO₂-NH₃-H₂O system (a-b) & products formation (c) (Aqueous Salt Solutions, 2017)

This ternary system was modeled with the “Extended UNIQUAC model” (Aqueous Salt Solutions, 2017) and the experimental measurements. The amounts of NH₃, NH₄⁺ and NH₂COO⁻ are displayed in the left figure, and the amounts of CO₂, CO₃²⁻, and HCO₃⁻ in the same solution are shown to the right (Figure 2.5a-b). Moreover, the solid-liquid equilibrium

phase diagram exhibits the composition and the temperature range of different solid precipitates. The diagram only depicts the ratio between CO_2 and NH_3 . At 40°C , four solids are precipitated according to the experimental figure in sufficient ammonia solution with CO_2 participation. In this three-composition-four-phases solution (**Figure 2. 5c**), if the composition of the gas phase or solid phase alters, the pressure will change. This part of research phase diagram will be helpful to the determination of the produced ammonia salts in Chapter 4.

2.5 Magnesium Carbonates and MgO Production

Since the manufacture of cement is heavily dependent on the accessibility of raw materials and the suitability of the production facilities, it is important to consider these options when assessing social, environmental and economic impacts. The mineral magnesite, which is a preferred raw material, is not widely available in the UK. Therefore for the UK and most of the European and coastal countries, seawater or reject brine is thought as a good substitute. However, traditional MgO production from brine suffers from the difficulties of the minor impurity uptake, and solid-liquid separation process of $\text{Mg}(\text{OH})_2$ suspension, because of its small particle size and gelatinous state (Cheng & Li, 2009). In comparison, magnesium compounds through other productions, such as nesquehonite or hydromagnesite, have higher purity, and better filtration properties.

2.5.1 Magnesium Carbonates Production with Various Chemical Reagents

In flue gases CO_2 removal techniques, strong alkaline (NaOH or KOH) and buffering (Na_2CO_3 and NaHCO_3) aqueous solutions are considered as the most effective chemical solvents (Georgiou et al, 2007; Astarita,1967). Applying this concept to hydrated magnesium carbonates production, chemical reagents of strong base and buffer solutions have been studied by many researchers.

In contrast, some reactions used in this section are part of the process, which may be modified to some extent. Similar to the mineralisation carbon sequestration work of Maroto-Valer (2005), Park (2004), and Teir (2007), magnesium ores' dissolution, pH swing, and carbonations were integrated as a whole process, but only the relevant procedure is mentioned here. In addition, to cope with this research aim by precipitating carbonates from MgCl_2 of seawater or reject brine, all the dissolved magnesium ions in the process

from other authors are considered as the MgCl_2 ; although they may be demonstrated as another magnesium salt originally, for example MgSO_4 . Particularly, a variant Solvay process is attracting more and more interest gradually, by sequestering CO_2 straightway compared to the indirect carbonate salts, which will also be explained here in this section.

MgCl₂ with KOH: In a underground carbon storage process, both brine and oil-fields brine are naturally acidic (pH is around 2 to 5), and when CO_2 is injected in, the situation becomes even worse (Liu & Maroto-Valer, 2010; Soong et al., 2006). Therefore KOH is used for brine pH stability, to raise the solution from an acidic to a base condition, reaching the precipitation baseline, around 9 or above (Druckenmiller & Maroto-Valer, 2005, 2006; Liu & Maroto-Valer, 2010). The reaction is expected as below:



MgCl₂ with NaOH: In Teir's research (Teir et al., 2007), HCl and HNO_3 acid are applied to dissolve serpentine, while NaOH is utilised for pH-adjustment and carbonation steps, by bubbling CO_2 through the extracted magnesium solution, to obtain the precipitates at a room temperature. Reactions are reported as below:



Hydromagnesite is noted to be formed, attributing to the high temperature used for a sample drying, around 120°C - 135°C (Teir et al, 2007), so as to decompose the estimated primitive product nesquehonite. Therefore this equation cannot fully represent the reaction at room temperature (20°C).

MgCl₂ with NaHCO₃ and Other Buffers: Druckenmiller et al. (2006) mentioned that buffer solutions have better buffering capacity to adjust the brine pH than strong base. So NaCl/NaHCO₃ buffer is investigated by Liu & Maroto-Valer (2010). Another four organic or inorganic buffer solutions (pH>9) are further studied later on (Liu & Maroto-Valer, 2012). They are selected by two criteria: the fundamental one is pH>9, in order to keep the pH in a certain range and a maintained level; and the second one is no bicarbonate or carbonate existing, hence to avoid its interference of precipitates, for instance the uncertainty of carbonate in the formation of calcite/magnesite either from CO_2 or from NaCl/NaHCO₃ (Liu & Maroto-Valer, 2010, 2012).

MgCl₂ with Na₂CO₃: Na₂CO₃ is operated to recover MgCl₂ in solution, forming nesquehonite directly (Li & Demopoulos, 2009; Cheng & Li, 2009; Guo et al., 2010; Jarosinsk & Madejska, 2010; Kloprogge et al., 2003; Wang & Xue, 2006). The reaction happens as below:



Cheng and Li (2009) investigated nesquehonite production at 10-40°C in the supersaturated MgCl₂ and Na₂CO₃ solutions, which is a convenient and energy saving process. They studied the nucleation kinetics and the growth mechanisms of nesquehonite within this system, with and without NaCl in a supersaturation range. This work is meaningful, because of the NaCl's dominance in brine (Cheng & Li, 2010). While Guo et al. (2010) studied MgCl₂ with Na₂CO₃ under the influence of polyacrylamide (PAM) additives. Hänchen et al. (2008) also did reaction under CO₂ atmosphere to understand high pressure and high temperature influence on the reaction. This relevant phenomenon will be further expanded in the following sections.

MgCl₂ with Ammonia Buffers: In the carbon mineralisation process, ammonia salts not only behave as a buffer (ammonia base) in the carbonation step, but can also be recycled back to the dissolution step, which is a significant advantage compared to other methods by using strong acid and base (Kodama et al. 2008; Park & Fan, 2004; Wang & Maroto-Valer, 2011a-b). NH₄HCO₃ and (NH₄)₂CO₃ (50/50 mixture) were added in the carbonation reaction (Sanna et al, 2012; Wang & Maroto-Valer, 2011b):



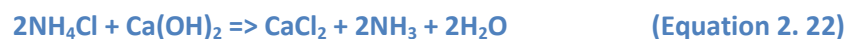
Hydromagnesite was formed in the experiments, due to the high temperatures involved during the operations, starting from 50°C to 100°C. They reported that the highest Mg²⁺ conversion rate to precipitate is 93.5% at 80°C with 1:4:3 Mg:NH₄ salts:NH₃ molar ratio, meanwhile the process sequestrates total 62.6% CO₂ (Sanna et al, 2012). Wang et al (2008) proposed that:



by investigating reaction temperature, initial concentration, stirring speed, alkaline titration speed, and reaction equilibrium time.

Solvay Process and Its Variant: The Solvay process was named after Ernst Solvay who was the first person to develop and use the process in 1881 effectively. It was developed to produce sodium carbonate firstly from a saturated sodium chloride solution, a main component in concentrated brine. The NaCl reacts with ammonia and CO₂, forming sodium bicarbonates and ammonium chloride (Eqn 2.21) at first, the results of which then react with calcium hydroxide to recover and reclaim the ammonia (Eqn 2.22). But from the brine management point of view, this process is to convert water-soluble sodium chloride into less soluble sodium bicarbonate, which will be further removed through a filtration process (El-Naas, 2011).

Even though ammonia is not used in the overall reaction, it still plays an important role in the intermediate reactions, providing a basic condition to form precipitate. Sodium bicarbonate is then converted to the sodium carbonate at around 200°C, generating water and CO₂ as by-products (Eqn 2.23). A good designed and operated Solvay factory can recycle nearly all its ammonia, and consumes only small amounts of additional ammonia to make up for losses. According to Eqn 2.24, major feedstock for the Solvay process is sodium chloride (NaCl) and limestone (CaCO₃), with the only major by-product calcium chloride (CaCl₂), sold as road salt or desiccant (El-Naas, 2011).



The overall reaction is:



The modified Solvay process (Eqn 2.25-2.27), involving CO₂ in the presence of ammonia, has been introduced into produced water management, to transform the reject brine into a profitable and reusable product (El-Naas et al., 2010 & 2011.; Ferrini et al., 2009; Mignardi et al, 2011). Meanwhile, the treated brackish water can be utilised for irrigation. Another benefit is to sequester CO₂, which indicates that it can be used for flue gas carbon capture (El-Naas, 2011). Park & Fan (2004) also conducted the same method during the pH swing process and in the carbonation steps of the mineralisation process.



Mignardi et al., (2011) investigated various MgCl_2 concentrations, and concluded that the coprecipitation of chloride-bearing carbonates (e.g. chlorartinite- $\text{Mg}_2(\text{CO}_3)\text{Cl}(\text{OH})_3 \cdot 3\text{H}_2\text{O}$) with nesquehonite can be easily avoided, when using the magnesium solutions of lower than 32 g/l; a CO_2 : Mg ratio (1:1) close to that of nesquehonite will prevent the precipitation of amorphous carbonates.

Possible Solutions and Resources by Using Ammonia Buffers: Ammonia buffer method can produce high-quality MgO , but leaving NH_4Cl regenerating or recovering problems. Two approaches at the moment applied in the industry for regeneration are called a Solvay soda process, in which ammonia is recovered either by lime or by Hou's combination soda.

In the Solvay soda reaction, lime hinders the production due to the limestone calcinations emitting CO_2 and energy intensive process. Also CaCl_2 containing waste is discarded to the environment (Huang et al, 2001). In Hou's process, NH_4Cl is recovered as a saleable product by crystallisation with the aid of common-ion effect of NaCl addition to NH_4Cl rich solutions (Wang & Li, 2011). Referring to Hou's soda method, an alternative routine is to use MgCl_2 instead of NaCl , providing a stronger common-ion effect because MgCl_2 yields two Cl^- ions compared to one Cl^- in NaCl (Wang & Li, 2011).

All solutions can be done by mimicking natural denitrification process through denitrifying bacteria, such as *Bacillus*, *Paracoccus*, and *Pseudomonas* (The water planet company, 2013.; Seitzinger et al., 2006; Zehr & Kudela, 2011). Furthermore, possible ammonia sources are from nitrification reaction by microorganisms, the compositions of urea and waste water, and composting gas (The water planet company, 2013.; Jeong & Hwang, 2005; Zehr & Kudela, 2011).

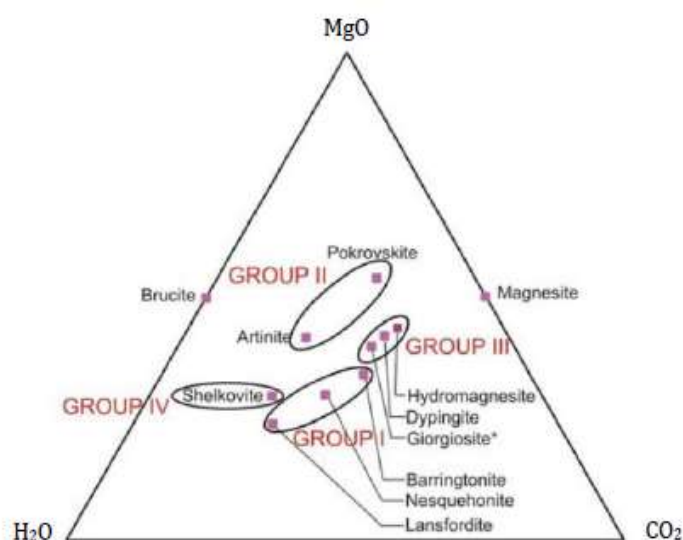
2.5.2 The Classification and Properties of Magnesium Carbonates

Carbonate precipitates obtained with $\text{MgO-CO}_2\text{-H}_2\text{O}$ compositions are shown in **Table 2. 4** based on the number of Mg ions, and **Figure 2.6a** of their compositions. The solubility of magnesite decreases with the rising temperature, and increases with the growing CO_2 partial pressure, the presence of chlorides, sulphates and nitrates (Shand, 2006). A

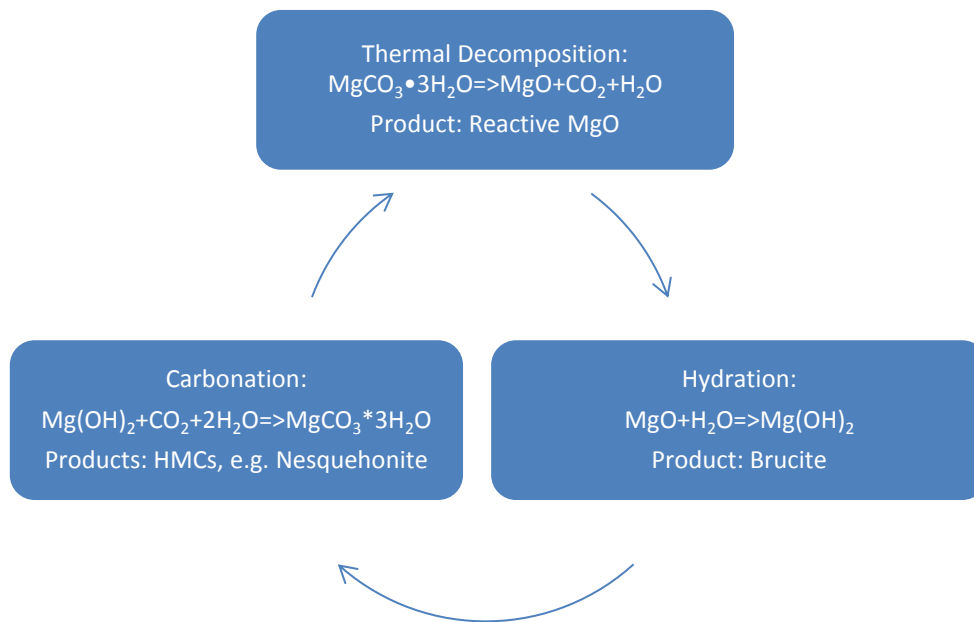
magnesium reaction cycle is presented in [Figure 2.6b](#) and typical SEM micrographs of some HMCs are in [Figure 2.7](#). This SEM illustrates HMCs microstructure, indicating good interlocking characteristics on the higher incorporation of waste materials in mixtures. The elongated needle-like nesquehonite decreases the porosity and improves stiffness, elevating the solid volume by a factor of 2.34 compared to the equivalent brucite.

Table 2. 4: Magnesium carbonate compounds forming in a MgO-CO₂-H₂O composition system (summarised from Canterford et al., 1984)

Groups	Number of Mg ions	Compound	Chemical Formula
Group I	1	Brucite	Mg(OH) ₂
		Magnesite	MgCO ₃
		Barringtonite	MgCO ₃ •2H ₂ O
		Nesquehonite	MgCO ₃ •3H ₂ O
		Lansfordite	MgCO ₃ •5H ₂ O
Group II	2	Pokrovskite	Mg ₂ (CO ₃)(OH) ₂ •0.5H ₂ O
		Artinite	Mg ₂ (CO ₃)(OH) ₂ •3H ₂ O
Group III	5	Hydromagnesite	Mg ₅ (CO ₃) ₄ (OH) ₂ •4H ₂ O
		Dypingite	Mg ₅ (CO ₃) ₄ (OH) ₂ •5H ₂ O
		Giorgiosite	Mg ₅ (CO ₃) ₄ (OH) ₂ •5-6H ₂ O
Group IV	7	Shelkovite	Mg ₇ (CO ₃) ₅ (OH) ₄ •24H ₂ O

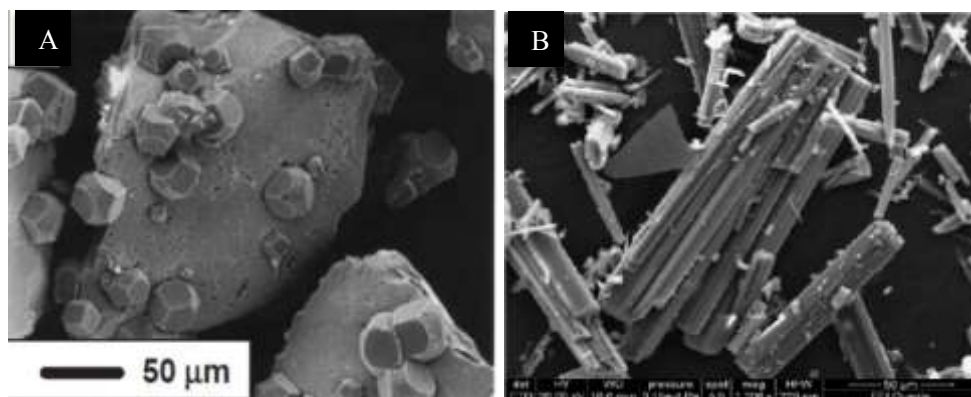


(a): The classification of hydrated magnesium carbonates in a MgO-CO₂-H₂O composition system (webmineral, 2009) *For better visibility giorgiosite is described as a component of 6H₂O molecules.



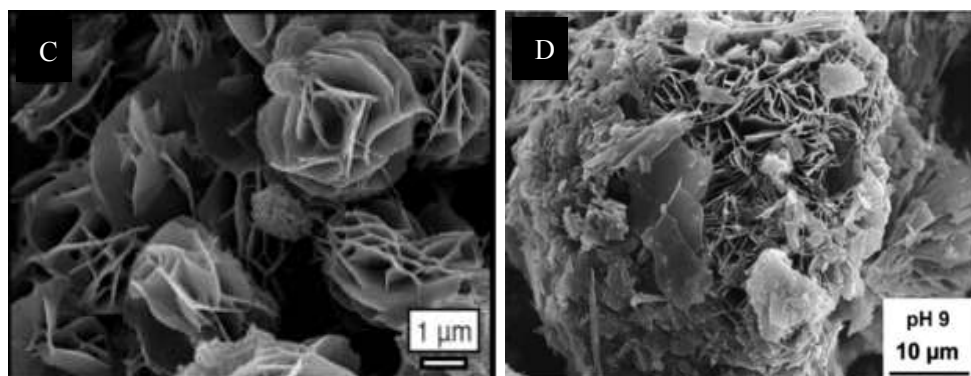
(b): A simplified magnesium related thermodynamic cycle (summarised from Shand, 2006)

Figure 2.6: HMCs classifications (a) and the related thermodynamic cycle (b)



(A) Magnesite (Giammar et al., 2005)

(B) Nesquehonite (Ferrini et al., 2009)



(C) Dypingite (Power et al., 2007)

(D) Hydromagnesite (Teir et al., 2007)



(E) Artinite (Caponera et al., 2013)

Figure 2. 7: The typical SEM images of some magnesium carbonates

2.5.3 The Stability of Magnesium Carbonates

In the MgO-CO₂-H₂O composition system, magnesite and brucite are the only two stable products (Königsberger et al., 1999). Other HMCs precipitates mainly depend on the temperatures and CO₂ concentration. Table 2. 5 summarises the influences of various temperatures and CO₂ pressures on the formation of HMCs. An increased temperature results in less hydrated precipitates, while changing CO₂ concentration leads to various phases (Xiong & Lord, 2008). This section is relevant because some carbonates may convert to other compositions in ambient conditions.

Table 2. 5: Temperatures and CO₂ conditions on the formation of HMCs (Unluer, 2012)

Temperature/ CO ₂		Temperature	
		Ambient	Elevated
CO ₂	Ambient	Hyromagnesite, dypingite, artinite	Hydromagnesite, (preceding magnesite)
	Elevated	Nesquehonite, landfordite	Hydromagnesite (65°C), magnesite (120°C)

Decomposition 1 Lansfordite=>Nesquehonite

Lansfordite has a lower stability than nesquehonite (Ming & Franklin, 1985) and transforms into it when a temperature is higher than 10°C (Dell & Weller, 1959; Langmuir, 1965)

Decomposition 2 Nesquehonite=>Dypingite=>Hydromagnesite

Nesquehonite begins to decompose at approximately 50°C, but the process is still not clear. Dell & Weller (1959) demonstrated that nesquehonite will change into hydromagnesite,

while Davies & Bubela (1973) discussed a protohydromagnesite, a phase similar to dypingite, turns up as an intermediate component between them; this theory has also been proved by Botha & Strydom (2001) and Power et al. (2007). A range of intermediate phases between these transformations is revealed as the following equation (Canterford et al., 1984):



In this equation, x represents 4,5,6,8 and 11; while the number 5 and 6 are the composition of dypingite and giorgiosite respectively.

Although Harrison (2004) records that nesquehonite is unlikely to lose CO₂ and H₂O from its structure naturally under ambient conditions to form into others, numerous researchers still report that it can be decomposed (Davies, Bubela, & Ferguson, 1977; Xiong & Lord, 2008).

Decomposition 3 Hydromagnesite=>Magnesite

Hydromagnesite decomposes into magnesite at elevated temperatures, such as 126°C (Sayles & Fyfe, 1973). In Hänchen et al. (2008) experiment, magnesite is obtained under a high temperature (120°C) and a high pressure system. This transformation is found to be in both ambient and accelerated CO₂ conditions, while the latter one is more influential to the process.

Decomposition 4 Artinite=>Pokrovskite

The stability field of artinite is still not clear because there is no supportive experimental data; but Canterford et al. (1984) claimed that the decomposition of HMCs depends on the loss of water, therefore pokrovskite is expected to form with less water in its component.

Besides CO₂ concentration and temperature, other parameters, such as water activity or pH, also affect the formation of different HMCs. Generally, the transformation flowchart is summarised in [Figure 2.8](#). Nesquehonite is usually formed at a room temperature, which can be used to produce other magnesium-based chemicals, flooring, fireproofing, cosmetics (toothpastes, face powders, etc.), pharmaceuticals (antacids, laxatives, cardiac regulators), food additives, paints, pigments and rubbers (Jarosinsk & Madejska, 2010).

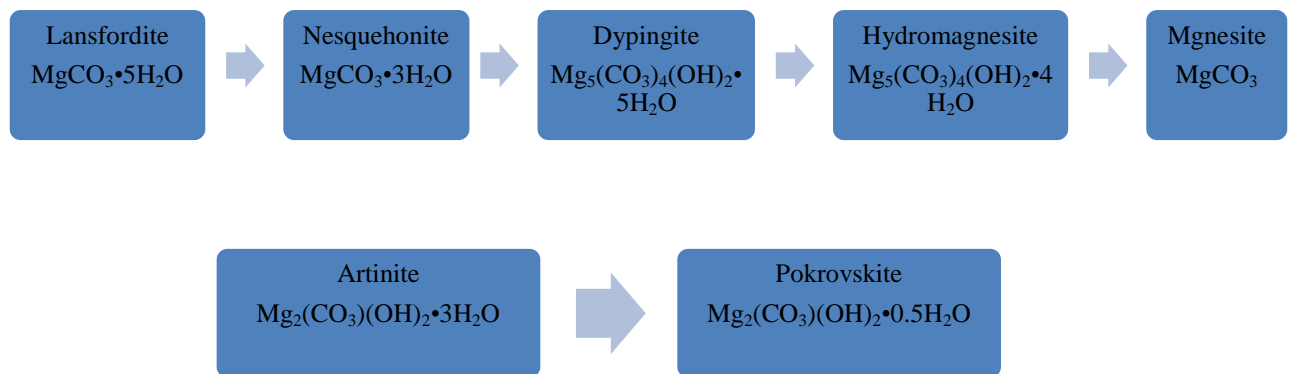


Figure 2. 8: The transformation pathway of magnesium carbonates

2.5.4 MgO Grades and Utilisation

Magnesium carbonates are then calcined into MgO with four grades, categorised by different calcination temperatures. These temperatures affect the particle size and specific surface area, thus resulting in various reactivities:

- Light-burned (reactive or caustic-calcined) MgO is calcined at the lower end of the temperature stream, typically 700-1000°C. It possesses the highest reactivity and the great specific surface area of the entire MgO category (Harrison, 2004a-d). Besides cement, it is also widely used in agricultural, flue gas absorption and waste water-treatment plants (Lacson et al., 2000). Experimental used MgO N50 places within this calcination range.
- Hard-burned MgO is calcined at 1000-1400°C temperature, and has a lower reactivity and surface area than reactive MgO, it has been used in China as an expansive additive in concrete and to compensate for drying shrinkage in a dam construction. The MgO 92-200 which was used lies within this heating area.
- Dead-burned MgO (periclase) is produced at the temperature higher than 1400°C, causing a very small surface area which makes it unreactive. Around 65% of the total consumption of magnesium compounds is dead-burned, used for refractory in furnace lining to deal with molten steel in iron and steel industry (Lacson et al., 2000; USGS, 2001).
- Fused magnesia, produced at temperatures above the fusion point, higher than 2800°C, is the least reactive. It has the advantages in strength, abrasive resistance, and chemical stability compared with dead-burned magnesia. It is mainly applied in water-

heating elements, welding machines and other general heating systems, and electrical insulating markets (Lacson et al., 2000).

2.6 Parameters Affecting Magnesium Carbonation

Synthesis of materials with a specific size and morphology is usually driven by the industry requirements in diverse areas (Jarosinsk & Madejska, 2010). The design and fabrication of inorganic materials with a well-controlled morphology have potential in the application of new materials and devices, such as catalysts, medicine, electronics, ceramics, pigments, and cosmetics, etc. (Zhang et al., 2006).

There are several affecting parameters in the carbonation process. Soong et al. (2004) and Druckenmiller & Maroto-Valer (2005) claimed that pH has a dramatic effect on both conversion rates and certain precipitated species, pH>9 is a key role in precipitates, whereas temperature and CO₂ pressure have less impact on the formation of carbonate minerals. This has also been proved by combined experimental and modelling data. Wang et al.(2008) concluded temperature, initial concentration and (ammonia/NaOH) titration speed have important effects of nesquehonite's crystal morphology and particle size distribution through SEM observation, while stirring speed and reaction time have some influences on its properties. XRD displayed that crystals compositions are largely affected by the reaction temperature(Druckenmiller et al., 2006; Druckenmiller & Maroto-Valer, 2005).

pH: pH can significantly influence sediments' formation, morphology and the particle size distribution (Park et al., 2008; Yan & Xue, 2005). **Figure 2.9** displays carbonate species distribution. At a pH=4, H₂CO₃ molecular is a main component, at a pH=6, HCO₃⁻ dominates, and at a high pH=9 or above, CO₃²⁻ plays a key role. Thus in a low to mid pH range, the rate limiting step is the CO₂ hydration process to acquire carbonic acid, whereas in the high pH range, the rate limiting step is the carbonic acid dissociation to bicarbonate (Bond et al., 2001; Soong et al., 2004). At lower temperatures (20-55°C) and lower pH values, HMCs are prone to be needle-like morphology (**Figure 2.10A**); with further increase of temperatures (60-95°C) and pH values, the sheet-like crystallites become the preferred morphology (**Figure 2.10B**); when the temperature and pH keep rising, these crystallites tend to assemble into layer-like structures with diverse morphologies, such as spherical-like particles with rosette-like structure (**Figure 2.10C-D**) and cakelike particles built from sheet-like structure (**Figure**

2.10E-F (Zhang et al., 2006). It is thought that a higher pH will enhance the reaction and further aggregate particles.

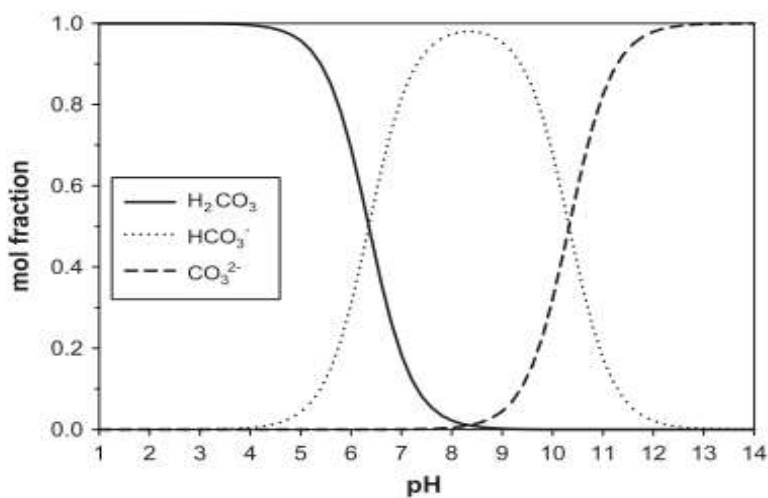
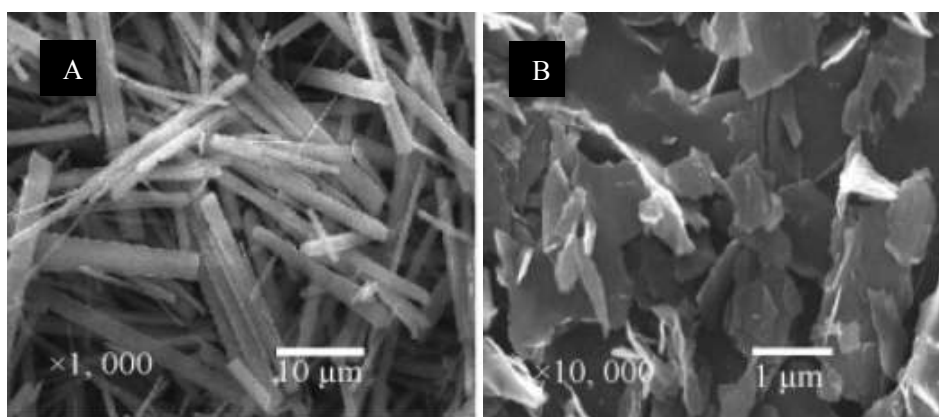
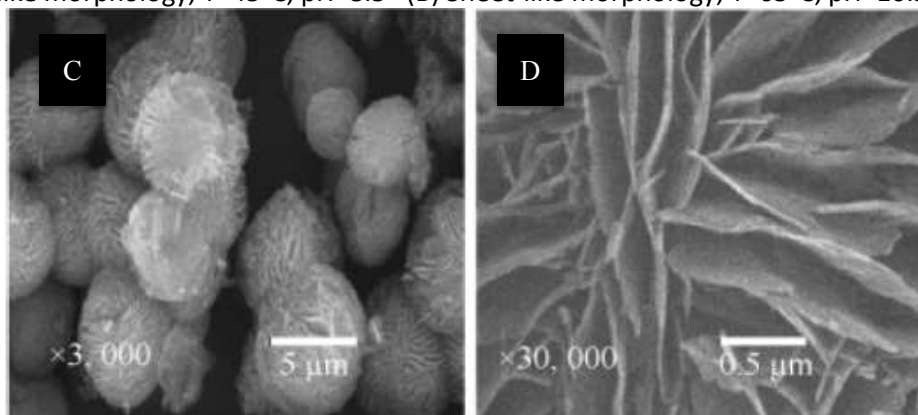


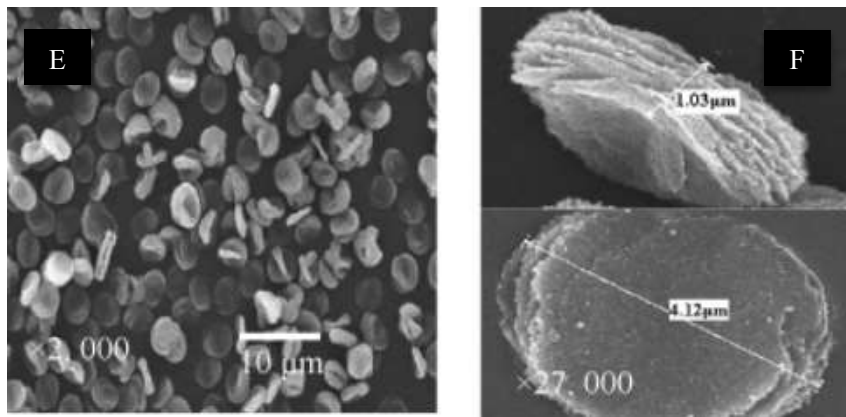
Figure 2. 9: The equilibrium distribution of H₂CO₃, HCO₃⁻, and CO₃²⁻ species in a solution (Lackner, 2002; Steel et al, 2013)



(A) Needle-like morphology, T=45°C, pH=8.5 (B) Sheet-like morphology, T=65°C, pH=10.5



(C) (D) Spherical-like morphology with rosette-like structure, T=45°C, pH= 12; (D) is the magnification image of an individual particle in (C)



(E) Cake-like morphology with sheet-like structure, $T=65^{\circ}\text{C}$, $\text{pH}=12.5$; (F) is the magnification image of an individual particle in (E)

Figure 2. 10: The typical SEM morphologies of HMCs under different pH values and temperatures (Z. Zhang et al., 2006)

Temperature: Temperature is considered as a second leading parameter in the reaction, which can affect size and morphology of precipitates, as a higher temperature tends to boost carbonates' nucleation rate, hence resulting in the growth of nuclei into smaller particles (Cheng & Li, 2010; Zhao et al., 2010). It also accelerates the formation of carbonates due to the increased pH. This is because the carbonic acid (H_2CO_3) formation decreases from the CO_2 hydration process with the rising temperature (Read, 1975). Moreover, the CO_3^{2-} activity is reported to be increased with temperature, and to reach its maximum at $90\text{-}100^{\circ}\text{C}$, which can enhance Mg^{2+} precipitation significantly (Zhang et al, 2012). Therefore, generally higher temperatures will lead to a faster reaction.

In the temperatures $10\text{-}40^{\circ}\text{C}$, nesquehonite forms needle-like or gel-like crystals (Figure 2.11) (Cheng & Li, 2009); however, Jarosinsk & Madejska(2010) said that these types of crystal are only identified at 40°C , a lower temperature and a shorter reaction time (10°C , several minutes) produce poor crystalline or amorphous precipitates. It also influences the compositions of products significantly (Guo et al., 2010). Under atmospheric pressure, at a room temperature, nesquehonite is expected to be obtained, while hydromagnesite is generated at an elevated temperature above $40\text{-}50^{\circ}\text{C}$ according to Section 2.5.3 (Cheng & Li, 2009; Lanas & Alvarez, 2004; Liebermann, 1967; Wang et al., 2008).

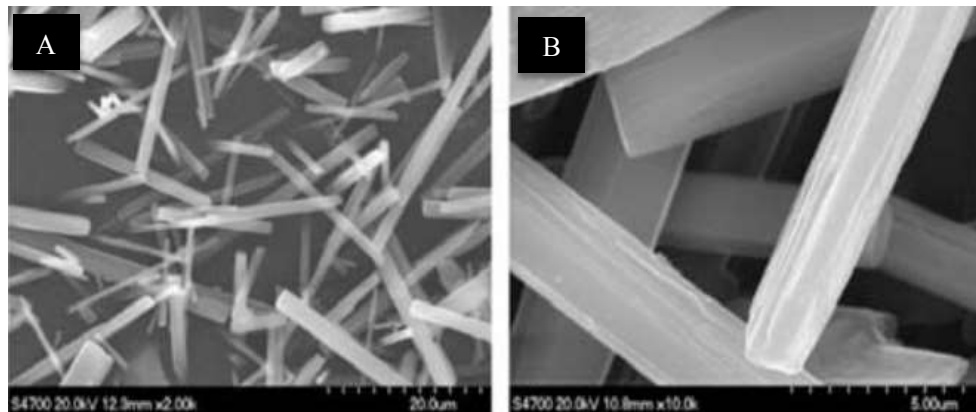


Figure 2. 11: A typical SEM morphology for HMCs at temperature 10°C. (B) is the magnification image of (A) (Cheng & Li, 2009)

Magnesium Concentration: An increase in the concentration of reactants will result in a corresponding increased reaction rate due to higher number of collisions between particles. Usually more precipitates are acquired at relatively higher initial concentrations. However, in a $\text{MgCl}_2\text{-Na}_2\text{CO}_3\text{-NaCl}$ reaction system, nesquehonite induction time decreases when either temperature or supersaturation increases, that is faster reaction; and is prolonged by adding NaCl in solutions at a constant supersaturation, meaning a slower reaction. Induction time is defined as the time passed from the first phase appearance to the creation of supersaturation (Cheng & Li, 2010). Therefore reactants' concentration should be maintained at a certain level to match the final magnesium carbonates supersaturation status.

The concentrations of reactants also affect the final morphology (Wang and Xue, 2006). Particles' length, width and surface smoothness vary with temperatures and supersaturation conditions (Cheng & Li, 2009). A lower supersaturation can be beneficial to produce high quality crystals (Hassan, 2014).

Stirring Speed: It is important to products' morphology, and governs particle size and its distribution (Guo et al., 2010; Wang et al., 2008). Higher stirring speed can accelerate the formation of viable nuclei; but can also accelerate the dissolution of the viable nucleus or crystals to reduce the rate of crystal growth at the same time, thus a suitable stirring is necessary to obtain the uniform crystals (Wang et al., 2008). Hassan (2014) added that a higher stirring speed may also affect the precipitate composition, through slightly increased temperatures, such as more dypingite transformed from nesquehonite.

Reaction Time: Time helps to reach equilibrium, but varies under different concentrations; longer time tends to produce more uniform crystallisation (Ferrini et al., 2009; Y. Wang et al., 2008). The crystal dimension increases with a longer reaction time, or a lower initial concentration of reactants at the same temperature (Cheng & Li, 2009). It is caused by enhanced particle aggregation from the accelerated reaction.

In addition, a higher initial concentration may lead to longer reaction time. In Mignardi et al.'s (2011) work, a kinetic study showed that the reaction nearly completes within 10 min in 7g/l Mg^{2+} , while the reaction happens continuously for 15 days in 16g/l Mg^{2+} and 30 days in 32g/l Mg^{2+} respectively. All three solutions form nesquehonite finally, but 16g/l and 32g/l Mg^{2+} also acquire amorphous carbonates and chlorartinite in the first 2 days. Moreover, Hassan (2014) discussed that the reaction time has no effect on the composition of precipitates by using 24g/l Mg^{2+} within a maximum 2h reaction.

CO₂ Partial Pressure: Pressure affects precipitate formation and growth rate (Hänchen et al., 2008), but is less significant than pH and temperature (Druckenmiller & Maroto-Valer, 2005). At a room temperature and normal pressure, 25°C and $P_{CO_2}=1$ bar, only nesquehonite forms; at a high temperature and pressure, ($P_{CO_2}=3$ bar, 120°C) hydromagnesite is formed and transformed into magnesite within 5-15h; and at an even higher pressure ($P_{CO_2}=100$ bar, 120°C) direct formation of magnesite is observed (Hänchen et al., 2008).

Catalysts and Additives: Catalysts can accelerate chemical reactions without changing final products. The dissociation and hydration of CO₂ is considered as the rate limiting step in precipitates formation (see Section 2.3). As a result, it has been extensively studied by many researchers, to enhance its dissolution rate, by using biocatalysts and chemical catalysts. Bacteria, enzymes, and algae can all be used as bio-catalysts in magnesium carbonates reaction, by introducing the whole process as biomineralisation. Halophilic aerobic bacteria may facilitate the mineral precipitation, such as dolomite, huntite and hydromagnesite, at their undersaturated or kinetically inhibited conditions (Sánchez-Román et al., 2011).

2.7 Calcium Carbonates and CaO Production

Calcium carbonates ($CaCO_3$) are one of the most common and widely dispersed minerals, occurring as limestone, chalk, and also biominerals. Commercial $CaCO_3$ grades, with the

form of powders, granules and slurries, are produced either through the extraction and processing of natural ores or through the chemical precipitation. In 2012, the demand for CaCO_3 and CaO was around at 7655 tons and 6050 tons respectively. This figure will increase to approximate 13,561 tons and 21,840 tons by the year 2018 and year 2023 respectively (Embassy of The Federal Democratic Republic of Ethiopia in London, 2012). This chapter will focus on calcium carbonates and lime (CaO) production as well as their relevant properties.

2.7.1 Current Precipitated Calcium Carbonates (PCC) and Lime Process, and Its Alternative Carbonation Production from Calcium Ores

The current production process of precipitated CaCO_3 has the following steps: calcination, slaking, and carbonation, drying and packing (Figure 2.12), with lime obtained in the first stage. In a commercial precipitated calcium carbonate (PCC) process, limestone is converted into calcium oxide (CaO , lime) and CO_2 over 900°C . CaO is then hydrated into calcium hydroxide (Ca(OH)_2 , slaked lime), subsequently by the carbonation of hydroxide, see Equations 2.29-2.31 (Teir et al., 2007). Although the total amounts of CO_2 emission is close to zero from the equations, a large amount of emissions are still caused from the high temperature lime production (Teir et al., 2005).

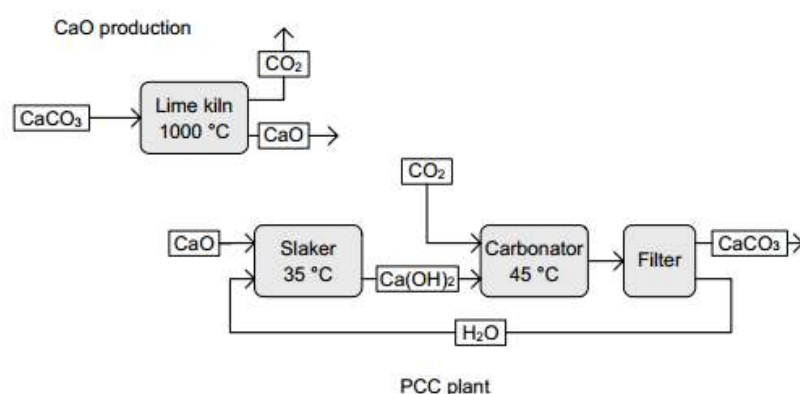


Figure 2.12: Lime and PCC production (Teir et al., 2009)

An alternative process for calcium carbonate production is from calcium silicates, which is abundant in wollastonite, CaSiO_3 minerals, as well as calcium oxide rich rock, basalt.

Wollastonite mainly exists in crystalline limestone with pure chemical composition CaSiO_3 ,

which is formed under high temperatures and pressures from the interaction of calcite (CaCO_3) and silica (SiO_2). This mineral is used in the plastic, ceramic and metallurgical industry as a filler and additive for various applications, as well as asbestos replacement (USGS, 2002). The other minerals, such as rock and basalt, are also considered when wollastonite deposits are not adequate or available.

2.7.2 Calcium Carbonates Production with Various Chemical Reagents

A few chemical reactions are illustrated in this section, in order to provide the references for the experiments.

$\text{CaCl}_2 + \text{CO}_3^{2-}$: Ogino, Suzuki, & Sawada (1987) conducted experiments at various temperatures (14-80°C) by adding CaCl_2 to Na_2CO_3 solution, to investigate the transformation of CaCO_3 from unstable to stable form. Wray and Daniels (1957) also studied the precipitation condition of pure calcite, pure aragonite, or specific mixtures of the two. They used calcium nitrate/calcium chloride ($\text{Ca}(\text{NO}_3)_2/\text{CaCl}_2$) and sodium carbonate (Na_2CO_3), operating temperatures from 30°C to 70°C. Chen & Xiang (2009) investigated CaCl_2 and NH_4HCO_3 reaction under 30-80°C with a double injection method into the distilled water. Reaction is as bellow:



$\text{Ca}(\text{OH})_2 + \text{Na}_2\text{CO}_3$: In a chemical recovery process of NaOH in the Kraft pulping method, CaCO_3 is crystallised as a by-product of the NaOH production by the reactions shown by [Eqns 2.33-34](#). The second one is usually called the causticising reaction (Kitamura et al., 2002). Konno et al. (2002, 2003) used Na_2CO_3 addition into the $\text{Ca}(\text{OH})_2$ to crystallise CaCO_3 under various temperatures.



$\text{CaCl}_2 + \text{CO}_2/\text{N}_2 + \text{Alkali}$: Han et al. (2005) utilised CaCl_2 and ammonia, mixing with CO_2/N_2 gas under 25°C, 400rpm stirring speed conditions, to study the effects of flux rate and CO_2 content on the phase and morphology of the precipitated CaCO_3 , with the following equations:





2.7.3 The Mechanism of Calcium Carbonates Formation

The crystallisation of calcium carbonate polymorphs usually include three steps: nucleation, growth and transformation (Kitamura, 2002). Equations demonstrate in this section will illustrate the theoretical formation.

Calcium Carbonate Nucleation: Kralj & Brecevic (1990) concluded that the calcium carbonate nucleation is not homogeneous but heterogeneous. Gibbs-Thomson formula is considered as a classical nucleation theory:

$$J = A \exp[-B(\ln S)^{-2}], \quad (\text{Equation 2.37})$$

$$S = \sqrt{\frac{[\text{Ca}^{2+}][\text{CO}_3^{2-}]r^2}{K_{\text{so}}}}, \quad (\text{Equation 2.38})$$

Where J and S are the nucleation rate and supersaturation ratio, r is the activity coefficient of divalent ions, K_{so} is the solubility product of calcium carbonate, A is a constant, B is related to the interfacial energy of polymorphs, which can be expressed as below (Kitamura, 2002):

$$B = 16\pi\gamma^3 v^2 / 3(kT)^3, \quad (\text{Equation 2.39})$$

Where k and T are Boltzmann constant and absolute temperature respectively; γ is the interfacial free energy, v is solid density.

Calcium Carbonate Crystallisation: After the nucleation stage, crystals start to grow and aggregate, which is termed as crystallisation process, at the high supersaturation condition according to Kralj and Brecevic (1990):

$$dr/dt = k(S - 1)^2, \quad (\text{Equation 2.40})$$

Where dr/dt denotes the growth rate of crystal, and k and S-1 are the rate of constant and the supersaturation ratio, respectively.

It is obvious that, with a higher supersaturation, the growth rate of crystal is higher, so the precipitation reaction proceeds faster and finishes in a shorter time. However, this causes

more nuclei formation on the other hand, resulting in more metastable particles formation instead of stable ones (Kitamura, 2001; Nielsen & Sohnel, 1971).

Calcium Carbonate Transformation: Followed by crystals agglomeration, metastable phase will transfer into a stable one, which is recognised as Ostwald Law. According to this regulation, the least stable phase with the highest solubility precipitates at first and subsequently transforms into the more stable one. A typical example about vaterite is demonstrated here: nano-sized vaterite nuclei agglomerate together and form the stable spherical particles to meet the rule of lowest energy (**Figure 2.13**), which can be demonstrated as below (Kitamura, 2001; Nielsen & Sohnel, 1971):

$$\ln C(r)/C^e = 2M\gamma/(RT\rho r) \quad (\text{Equation 2.41})$$

Where $C(r)$ is the solubility of particle with radius r , C^e is the usual solubility, T is an absolute temperature, M is the molecular weight, γ is the interfacial free energy, and ρ is the crystal density. So when radius r of particles is small, the solubility of the particles is high, meaning that fine vaterite particles can be dissolved easily and then recrystallise into calcite.

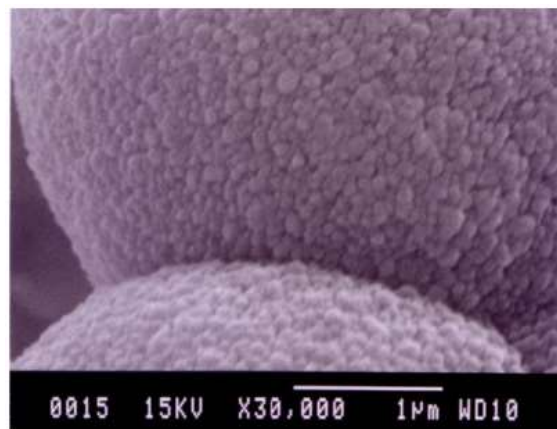


Figure 2.13: The SEM image of the magnified vaterite particles

There are two ways for this transformation: the solid-state transition and the solution-mediated transition. In calcium carbonate transformation process, the solution-mediated transition occurs simultaneously (Davey et al., 1986; Kralj et al., 1997) according to the following equations (Spanos & Koutsoukos, 1998):

$$\Delta G_v = -R_g T \ln S_v, \quad (\text{Equation 2.42})$$

Where ΔG_v is the change in Gibbs free energy going from the supersaturated solution to equilibrium, R_g is the gas constant, T is the absolute temperature and S_v is the supersaturation ratio:

$$S_v = \{IAP/IAP_{eq,v}\}^{1/2}, \quad \text{(Equation 2.43)}$$

Where IAP and $IAP_{eq,v}$ are the ionic activity products in a supersaturated solution and in equilibrium with the polymorph of vaterite, respectively. If we assume the driving force for the stabilisation of vaterite at two supersaturation values S_{v1} and S_{v2} , where $S_{v1} > S_{v2}$, then

$$(\Delta G_v)_1 = -R_g T \ln S_{v1}, \quad \text{(Equation 2.44)}$$

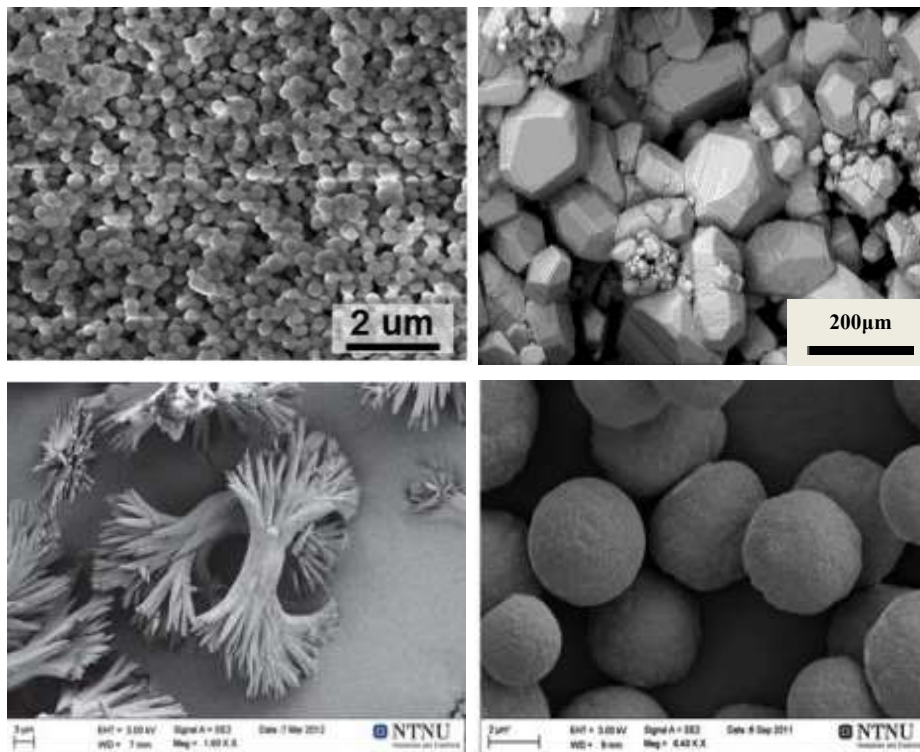
$$(\Delta G_v)_2 = -R_g T \ln S_{v2}, \quad \text{(Equation 2.45)}$$

$$\Delta(\Delta G_v) = (\Delta G_v)_2 - (\Delta G_v)_1 = -R_g T \ln(S_{v2}/S_{v1}). \quad \text{(Equation 2.46)}$$

So the relative stability of vaterite at a higher supersaturation will be more favorable since the $S_{v2}/S_{v1} < 1$, $\Delta(\Delta G_v) > 0$ (Han et al., 2005). This equation has proved that metastable phase is preferable under high solution concentrations, and is used to illustrate the phase transformation under various supersaturations.

2.7.4 The Classifications and Properties of Calcium Carbonates

There are mainly three anhydrous polymorph crystallisations of calcium carbonates (CaCO_3): calcite (trigonal-rhombohedral/rhombohedra), aragonite (orthorhombic system with acicular crystals/needles), and vaterite (polycrystalline spheres/hexagonal) (Figure 2.14). It is important to understand all their morphologies and properties because they are the main differentiated indicators.



ACC (300nm diameter particles; $\text{CaCl}_2 + \text{Na}_2\text{CO}_3$, pH=11.2) (Tobler et al., 2014) (top left);

Calcite (Calcite crystals, 2015) (top right);

Aragonite (scale bar = 3 μm) (Andreassen et al., 2012) (bottom left);

Vaterite (scale bar = 2 μm) (Andreassen et al., 2012) (bottom right)

Figure 2.14: Calcium carbonates polymorphs

The microstructure of three carbonates is seen in [Figure 2.15](#) (Blanco-Gutierrez, Demourgues, Jubera and Gaudon, 2014). In vaterite, the cation is enclosed by six equidistant oxygen atoms. Two oxygen atoms are at a longer distance, leading to an overall 6+2 coordination geometry ([Figure 2.15a](#)). In calcite, the cation is surrounded by six oxygen atoms in a regular octahedron ([Figure 2.15b](#)). In aragonite, the first coordination sphere is formed by nine oxygen atoms ([Figure 2.15c](#)). In short, vaterite occurs in a hexagonal crystal system, calcite is a trigonal system, and the aragonite forms in an orthorhombic system.

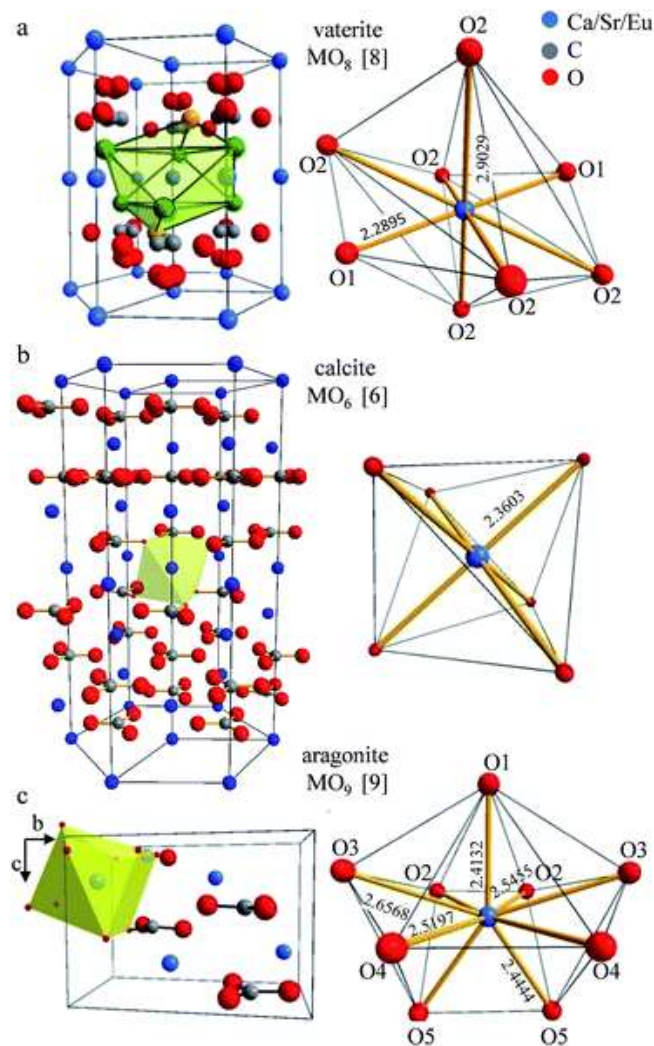


Figure 2.15: Structural cells corresponding to vaterite (a), calcite (b), and aragonite(c) (Blanco-Gutierrez, Demourgues, Jubera and Gaudon, 2014)

Calcite: It is thermodynamically the most stable form under an ambient condition and atmospheric pressure, and is often found in biominerals (Colfen, 2003; Kato et al., 2002; Nan et al., 2008; Wray & Daniels, 1957).

Aragonite: It is often found in biominerals, and formed at high temperature, high pressure or high supersaturation solutions. Threshold temperature for the aragonite structure is around 50°C (Kato et al., 2002; Mathur & Way, 2001). Sulfate and magnesium ions, called calcite kinetic inhibitors, have the tendency to promote the aragonite formation instead of calcite (Farm et al., 1997).

Vaterite: It is the most unstable carbonates among these three, considered as an intermediate phase between calcite and aragonite; and different from those two above, it rarely sees in organism (Ogino et al., 1987).

Unlike anhydrous carbonates, the hydrated forms have not been investigated in depth, probably due to their low stability (Elfil & Roquesb, 2001). Both crystalline mono- ($\text{CaCO}_3 \cdot \text{H}_2\text{O}$) and hexahydrates ($\text{CaCO}_3 \cdot 6\text{H}_2\text{O}$) are considered as amorphous calcium carbonate (ACC), which is the most unstable form, and usually described as spherical shapes of diameter lower than one micron (**Figure 2.14**) (Aizenberg et al., 2002; Colfen, 2003). It is recognised that the presence of this precursor may play an important role in the nucleation behavior of the polymorphs and cause the morphological change from a micro-structure point of view (Kitamura, 2001).

Monohydrated Calcium Carbonate (MHC): It is found mostly in saline alkaline lakes, and reported in carbonate deposits in the shore zone of Lake Lssyk Kul in Kyrgyzstan. It crystallises in a hexagonal form, which is considered as an accessory to aragonite (Clarkson et al., 1992; Nishiyama et al., 2013). The synthesis of this mineral requires the presence of Mg^{2+} and some other ions (seawater constituents) as well as organic material (Kralj & Brečević, 1995). Lippman (1973) mentioned that the magnesium ions allow the monohydrocalcite to precipitate with the minimum concentration of 0.01M (Mg^{2+}), from temperatures 0 to 40°C. It is moderately stable and can be dried at 100°C, with little decomposition. Under room temperature, it decomposes slowly and eventually forms into anhydrous CaCO_3 , even after one year at a room temperature, a small amounts of monohydrate can also be detected occasionally by XRD (Brooks et al., 1950).

Hexahydrate Calcium Carbonate: It crystallises both in nature and in lab (in a monoclinic system) at a temperature near 0°C, but rapidly decomposes to anhydrous forms at warmer ones (Brečević & Nielsen, 1993).

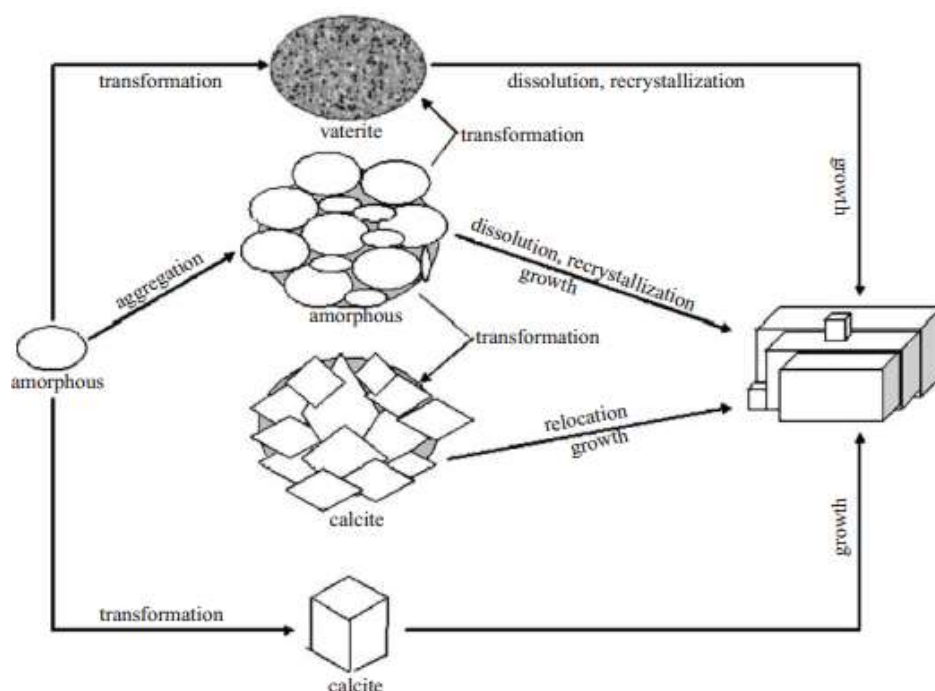
2.7.5 The Stability of Calcium Carbonates and Phase Transformation

Various calcium carbonate phases (polymorphs, hydrates, or amorphous phases) have different thermodynamic stabilities. There are usually two possible methods from unstable into stable ones: 1) solid-state transition and 2) solution-mediated transition. In the first case, internal rearrangement of the crystal lattice occurs to form the new stable structure.

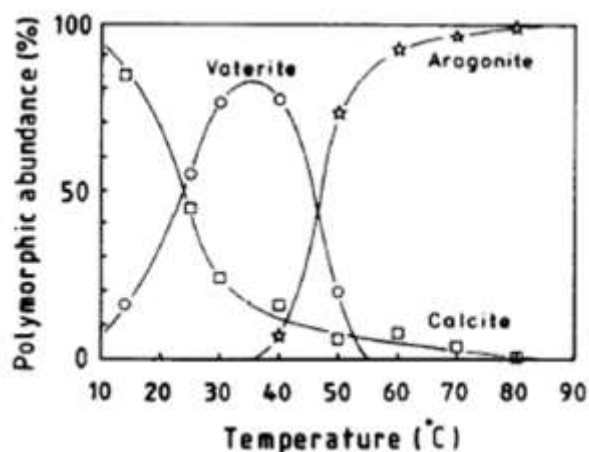
While in the second, the transformation takes place through the dissolution of the unstable phase, and then re-nucleation and growing into the stable one simultaneously (Davey et al., 1986).

Solution-Mediated Transformation: In the solution-solid transformation, there are three crystallisation process steps: the formation of amorphous precursor, the nucleation and growth of the calcite and vaterite with dissolving of precursor, and the transformation from vaterite and calcite (Kitamura, 2001, 2002). A conclusion of the precipitation process is demonstrated in [Figure 2.16a](#) (Wei et al., 2003). Initial product amorphous calcium carbonate (ACC) is the most unstable phase, and then quickly changes within a few minutes into two crystalline phases (vaterite and calcite). Vaterite has high surface area, and high solubility, which easily transfers to rhombic calcite. It happens through the dissolution of vaterite and recrystallization of calcite under ambient condition (Sawada, 1997).

It is also heavily dependent on temperature in this solution-mediated transformation. Phase alteration in the mixture of crystalline can be seen in [Figure 2.16b](#): ACC into vaterite and calcite at a low temperature (14 to 30°C), into aragonite and calcite at a high temperature (60 to 80°C), and into all three polymorphs at an intermediate temperature (40-50°C) within a few minutes (Colfen, 2003; Elfil & Roquesb, 2001; Ogino et al., 1987).



(a): A schematic depiction for the formation of CaCO_3 (Wei et al., 2003)



(b): The plots of abundance of crystalline CaCO_3 at the early metastable stage as a function of temperatures (Sawada, 1997)

Figure 2.16: The solution-mediated phase transformations of CaCO_3 : (a) Schematic description; (b) Plot description overt temperatures

Solid-State Transformation: The rate of change of solid-state transformation in the dry state is extremely slow at a room temperature, compared to a solution-mediated transformation. However, researchers have investigated the aragonite and calcite transformation at high temperatures and high pressure conditions, together with a combined phase diagram produced by Boettcher & Wyllie (1968) (Figure 2.17).

Boettcher & Wyllie (1968) investigated the calcite-aragonite transition boundary: the changed slope happens at 480°C , and the highest point measured on the aragonite-calcite is 800°C at 19.8Kb. The author used Crawford & Fyfe (1964) experiments' data at first, and then provided the extension of this transition boundary up to higher temperatures. The calcite I-calcite II transition was located by Boeke (1912) at point B. The difference of these two is from the absence of (113) peak that presented in calcite I in XRD; however, the structure of calcite II remains unknown. Davis (1964) suggested that calcite II has a similar structure as KNO_3 III, in which the CO_3 groups are oriented unidirectionally. In conclusion, the phase diagram shows that calcite is a stable form under ambient conditions, while it changes into dry aragonite spontaneously at a high pressure and a high temperature. But at an even higher temperature, it is possible for aragonite transition back to calcite (Wray & Daniels, 1957).

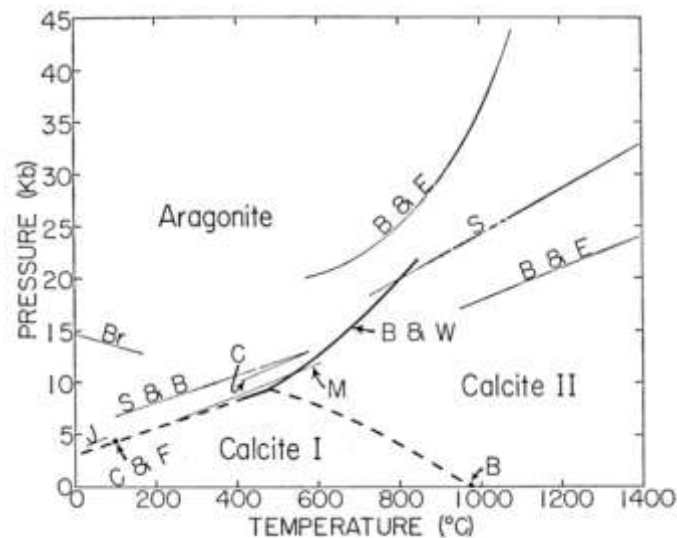


Figure 2.17: The comparison phase diagram of the solid-state transformation between aragonite and calcite

Abbreviations are B =Boeke (1912), Br=Bridgman (1939), J=Jamieson (1953), M=MacDonald, (1956), C=Clark (1957), S=Sclar et al. (1962), S&B=Simmons & Bell (1963), B&E=Bell & England (1964), C&F=Crawford & Fyfe (1964), B&W=Boettcher & Wyllie (1968)

2.7.6 CaCO₃ and CaO Utilisation

Calcium carbonates play an important position in inorganic chemistry, geochemistry and bio-mineralisation (Sawada, 1997). Industrially, calcium carbonates are much more widely used than magnesium carbonates (Zevenhoven et al., 2009). In the US, 1 Gt of limestone was used in the year 2003 for construction, chemical, metallurgical and agricultural uses (USGS, 2003).

The reason of its importance comes from its harmless properties and inexpensiveness, and can be used as neutralising agent, filler, cement, medical supply, food, papers, plastic, printing ink, and its well-studied mineral system (Colfen, 2003). In the paper industry, CaCO₃ has been increasingly used as filler and pigment, to improve the properties such as opacity, printing characteristic, brightness and colour, as well as to reduce the cost (Konno et al., 2003). Additionally, calcite offers weather resistance properties, low abrasiveness, low electrolyte content, and pH stabilising effects; and also has the ability to improve anti-corrosion and rheological properties of coatings (Embassy of The Federal Democratic Republic of Ethiopia in London, 2012).

Lime (CaO) is an inorganic chemical compound, which is generally thought as quick lime or non-slaked lime, obtained from over 900°C calcination of limestone deposit. Quick lime is widely used in construction industry with the preparation of mortar and plasters, and for white washing of houses and building (USGS, 2013). Iron and steel plants, as well as foundries, use lime as a fluxing agent in steel refining or a binder in construction materials. Furthermore, it is also applied in some drugs, pharmaceuticals, paper mills, pesticides formulation plants, chemical processing industries, waste water treatment, air emission remediation, as well as an additive in agriculture to remove the excess soil acidity (Dowling et al., 2015).

2.8 Parameters Affecting Calcium Carbonation

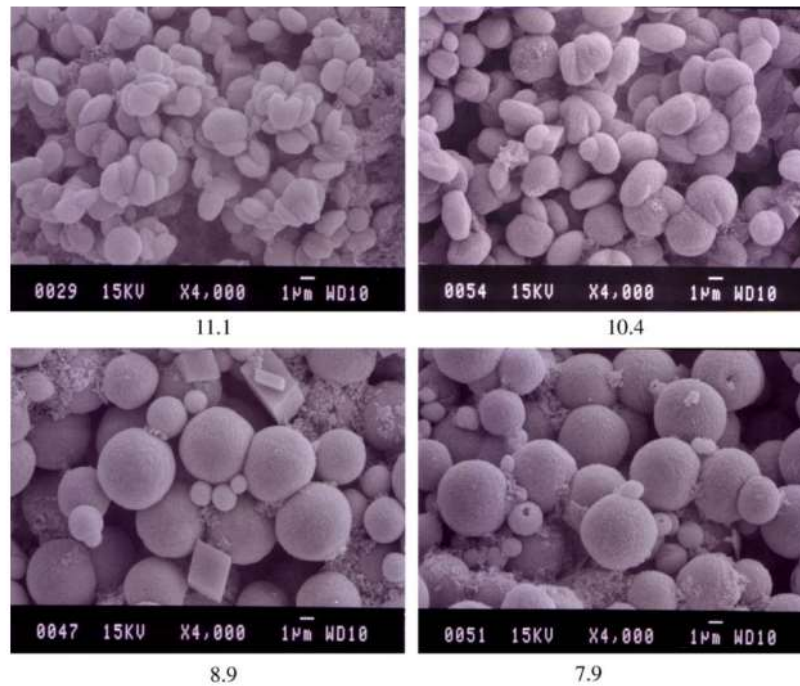
Particle size, distribution, shapes, and the surface properties of calcium carbonates can be controlled through various parameters, such as pH, temperature, reactant concentration, stirring speed, reaction time, CO₂ flux rate, and additives (Teir et al., 2005; BCCF, 2015). Han et al. (2006) also mentioned that initial CaCl₂ concentration, CO₂ flow rate, and temperature play an important role on phase and morphology changes while the bubbling time and stirring rate do not show apparent effect. Because calcium carbonate series are mainly identified through morphology; hence almost all the demonstrations are involved with SEM observation.

pH: pH affects the particle morphology and reaction time. In general, a lower pH tends to induce metastable phase vaterite, while a higher pH is more likely to produce aragonite in a comparably short time. Moreover, an elevated pH leads to a shorter reaction time according to crystallisation equations.

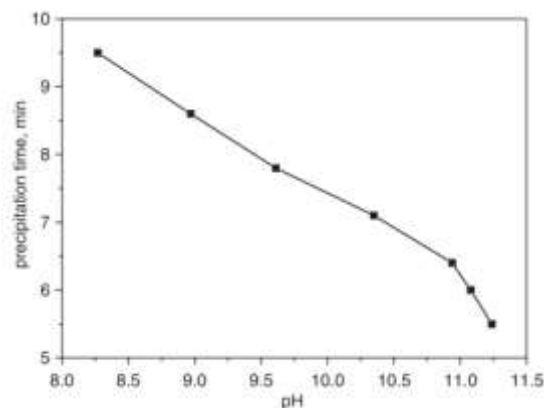
Based on various research, highly alkaline solutions are beneficial for the nucleation of aragonite and the formation starts from pH ≥ 13.5 (Kitamura et al., 2002; Hu & Deng, 2004). Konno et al. (2002) investigated the 1 mol/l NaOH effect at various temperatures in a batch reaction with Na₂CO₃ and Ca(OH)₂. The addition of NaOH increases the aragonite formation at all temperatures. It is thought that this addition stimulates crystal nucleation and aragonite growth (Konno et al., 2003; Han et al., 2006). Han et al. (2005) studied the various CO₂ contents, leading to various pH ranges, from 33.3 to 66.6 vol% at a flow rate of 0.9 l/min on the reactants. They mentioned that there was no obvious morphology change detected

by SEM, but the fraction of vaterite increased with CO₂ content. This is due to a higher CO₃²⁻ concentration, which prevents the vaterite- calcite transformation. Han et al. (2006) studied the produced calcium carbonate particles by passing mixed CO₂/N₂ gas into a CaCl₂ solution under a controlled pH of 7.5-11.5. The pH was kept constant during the precipitation by the addition of ammonia, to investigate the influence on CaCO₃ polymorphs.

Rhombic calcite is composed of a higher proportion of the precipitates with a gradually increasing pH. According to Han et al. (2006) (**Figure 2.18a**), at a pH of 11.1, spherical particles were most abundant and mixed with some rhombic particles, while at a pH of 7.9, they were all spherical with different sizes. It is thought that some nuclei in the later stage of the process did not have sufficient time to grow, thus resulting in smaller sizes with a higher pH. In summary, at a high pH level (pH>10), irregular congeries resulting from vaterite are formed, while at a low pH (pH<9), spherical conglomerations with different sizes are formed. Supersaturation increases with a high pH and more nuclei form, which improves the particles' agglomeration and the growth of metastable phase, thus inhibiting the transformation from a metastable state into a stable state (Han et al., 2006). At a lower level of pH, supersaturation decreases with the change of CO₃²⁻ to HCO₃⁻. The other explanation for rhombic calcite particles' formation can be ascribed to the quick completion of the precipitation reaction at a high pH (**Figure 2.18b**), resulting in a relatively long time for the phase transformation (Han et al., 2006). The reaction completion time is usually determined by a measurement of a constant pH.



(a): SEM of samples prepared at different pH (Han et al. 2006)

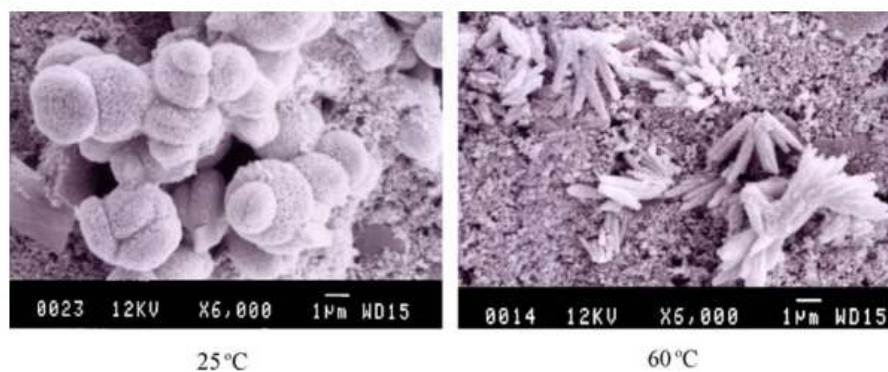


(b): Precipitation time changing with various pH (Han et al., 2006)

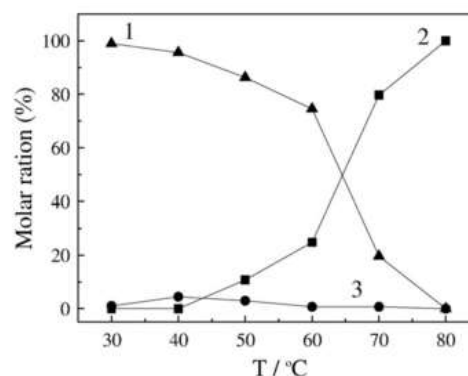
Figure 2.18: pH influences on CaCO₃: (a): Morphology; (b) Completion time

Temperature: Temperature is a determining factor in the crystallisation behavior of polymorphs. Konno et al. (2003) stated that reaction temperature exerts a strong influence on the size, shape, and polymorphs of CaCO₃. Aragonite is predominantly precipitated at a higher temperature (50°C and above), and starts to form at around 40°C. Vaterite is precipitated at a lower temperature (30°C), but both vaterite and aragonite are transformed into calcite (Mathur & Way, 2001; Wray & Daniels, 1957).

Han et al. (2006) show from the applicable SEM graphs, that spherical particles are formed at 25°C whereas needle-like particles are formed at 60°C, illustrating that vaterite is mainly formed at lower temperatures while aragonite is formed at higher temperatures. This is also confirmed by Zhan & Guo (2015) demonstrating that spherical calcium carbonate is favourable at lower reaction temperatures. Chen & Xiang (2009) also studied the phase transformation over temperature by injecting CaCl_2 and NH_4HCO_3 solutions at 30-40°C and 80°C respectively (Figure 2.19a). It can be seen that vaterite altered into aragonite gradually, and calcite kept at a nearly constant ratio of temperatures. Generally, at a higher temperature, the number of calcite crystals behaving as nuclei for further growth is much lower, leading to a slower transformation from aragonite to calcite, but if there are enough crystals, for example an initial mixture of both aragonite and calcite, a higher temperature leads to a faster rate of transformation to stable calcite (Figure 2.19b) (Wray & Daniels, 1957).



(a): SEM images of calcium carbonates at different temperatures (Chen & Xiang, 2009)

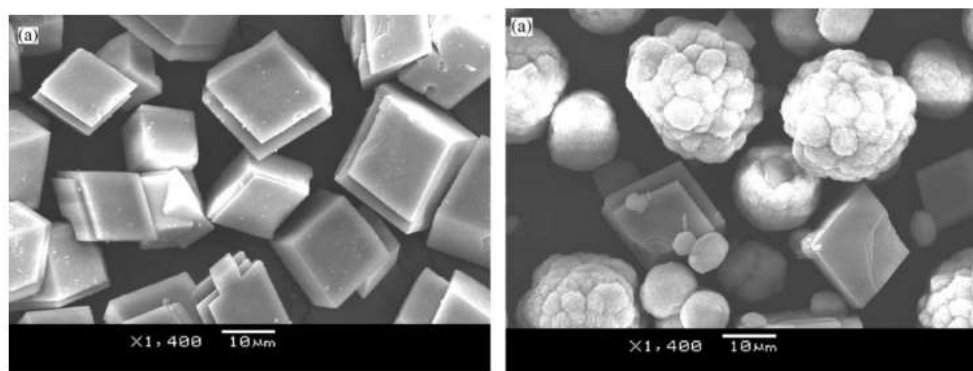


(b): Influence of temperature on the composition of calcite 1. Vaterite 2. Aragonite 3. Calcite (Wray & Daniels, 1957)

Figure 2.19: Temperature influences on CaCO_3 : (a) Morphology; (b) Precipitates compositions

Calcium Concentration: It is well-known that both the nucleation and growth of crystalline depend on the supersaturation of the solution. The morphology of calcite and vaterite crystals was observed to be influenced by the concentrations of reactant solutions.

Figure 2.20 displays the crystals obtained with the 0.05mol/l and 0.2ml/l of calcium hydroxide at rate of 5ml/s Na_2CO_3 addition, where the proportion of vaterite in the precipitates formed at 0.2mol/l is more than 0.05mol/l. Moreover, the crystal size is likely to decrease with the concentrations, which may be caused by the high nucleation rate with a high supersaturation (0.2 mol/l) (Kitamura, 2002). This result follows the “Ostwald’s step rule”, that is at low supersaturation solution, the difference of the supersaturation ratio (S) between the polymorphs is influential on the crystallisation and the most stable form may preferentially precipitate. On the other hand, at a high supersaturation, the difference of the interfacial energy (γ) between the polymorphs becomes to be relatively dominated and the metastable form may tend to precipitate. However, some authors argued that the morphology of CaCO_3 is sensitive to the variations of the initial reactant CaCl_2 concentration (Han et al., 2006). A low initial concentration (0.001M-0.1M) is favourable to the vaterite formation, but when concentration increases to 0.3M, only calcite is observed. The difference between this study and the one above is due to the different solubility of $\text{Ca}(\text{OH})_2$ and CaCl_2 (Han et al., 2006).



(a): CaCO_3 obtained in 0.05mol/l $\text{Ca}(\text{OH})_2$ (b): CaCO_3 obtained in 0.2mol/l $\text{Ca}(\text{OH})_2$

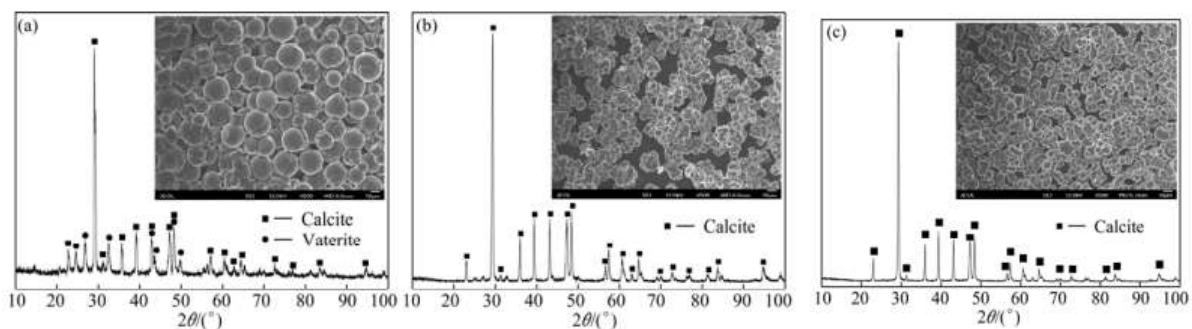
Figure 2.20: Concentration influences on CaCO_3 at $\text{Ca}(\text{OH})_2=0.05$ mol/l (a) & $\text{Ca}(\text{OH})_2=0.2$ mol/l (b) (Kitamura, 2002)

In conclusion, a relatively high concentration is suitable for the stable phase calcite formation; however, with an even higher reactants concentration, a metastable phase is preferred. It is also important to know that metastable phases can frequently occur under

an extreme supersaturation, by economic constraints during industry processing. But these phases are prone to transform into stable ones, which may result in processing and filtration problems, as well as product stability, due to crystal growth in a stored formulation such as creams and tablets (Davey et al., 1986).

Stirring Speed: Stirring speed has an effect on particle morphologies. A higher stirring speed increases the discrete needle-like aragonite, whereas at a low stirring rate, the agglomerated calcite is formed (Kitamura et al., 2002). Similar to Kitamura's work, Han et al. (2006) demonstrated that at a low stirring rate, the fine particles are aggregated and form into dense particles, while the particles prepared at a high stirring rate look loose. This result can be ascribed to the influence of hydrodynamics on particles formation. The initial formed spherical ACC is not stable due to its high surface free energy, and has the tendency to achieve a minimum total surface free energy through aggregation. But at a high stirring speed, it will disturb this aggregation to form a looser particle group.

However, Zhan & Guo (2015) expressed a different opinion on accelerated stirring speed, which can transform unstable vaterite towards more stable calcite, because the enhanced turbulence can increase the collisions and agglomeration among calcium carbonate particles. The stirring intensity can promote the liquids mixture, reduce the deposits in size, and roughen the particles surface (Figure 2.21).

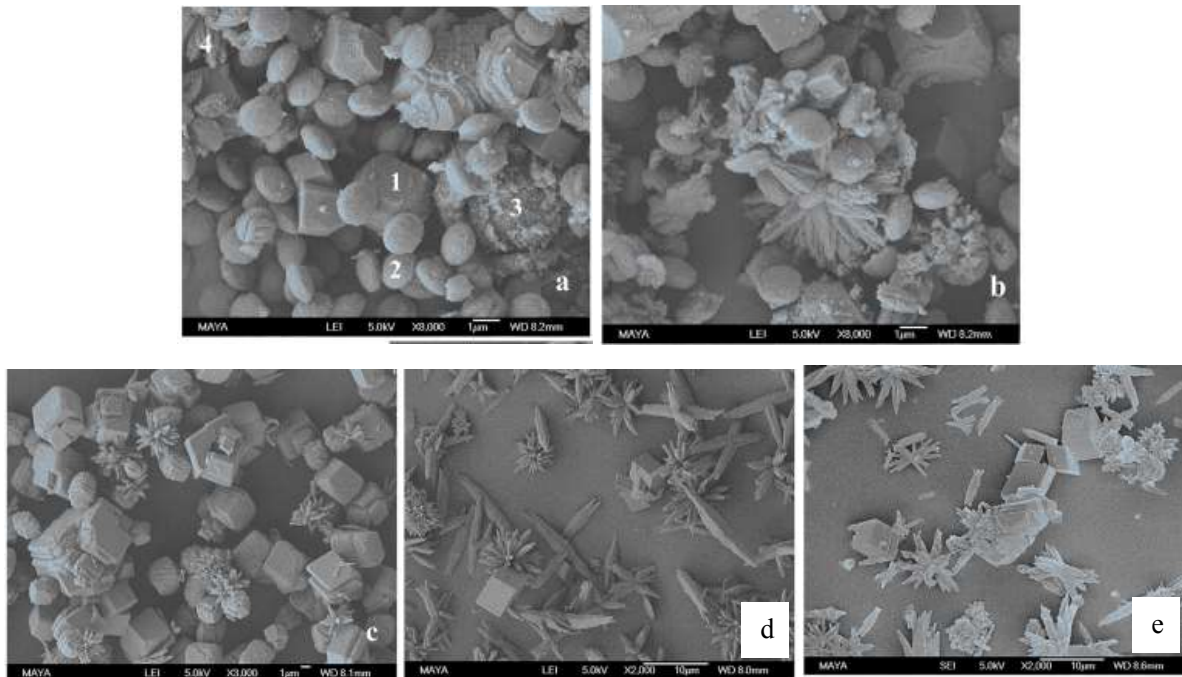


(a)200r/min; (b)400r/min; (c)600r/min (concentration 0.6M/L Na_2CO_3 , flow rate 1mL/min; temperature 20°C, equilibrium time: 0min)

Figure 2.21: Stirring speed influences on CaCO_3 (Zhan & Guo, 2015)

Reaction Time: Reaction time has an effect on phase transformation, meaning metastable polymorphs gradually transform into the stable calcite form. Towards the final stage, the

supersaturation of the solution is relatively low due to the complete consumption of Ca^{2+} and the metastable particles are ready to dissolve and change into calcite. However, this transformation into calcite is usually terminated when the precipitate is vaterite, or prolonged when the precipitate is aragonite after filtration (Han et al., 2006). Wang et al. (2013) also studied CaCO_3 formation under various reaction times and temperatures (Figure 2.22).



a) $T=25^{\circ}\text{C}$, $\text{pH}=10$, 1min; b) $T=25^{\circ}\text{C}$, $\text{pH}=10$, 1h; c) $T=25^{\circ}\text{C}$, $\text{pH}=10$, 15h; d) $T=55^{\circ}\text{C}$, $\text{pH}=10$, 1h; e) $T=55^{\circ}\text{C}$, $\text{pH}=10$, 15h. No. in picture a) 1,2,3 and 4 represent calcite, vaterite, ACC, and aragonite respectively.

Figure 2.22: The reaction time influences on CaCO_3 (Wang et al., 2013)

All phases are formed in the first minute of reaction, ACC less than 0.1 μm diameters are unstable and aggregated into larger particles. Over time, vaterite/aragonite particles are progressively transformed into calcite crystals, and gradually go larger with an initial rough surface; however, as long as the steady state is approached after 15h, the morphologies appear smoother. Under higher temperature conditions, aragonite is preferred with polymorphous, such as leaflike, needlelike, and flowerlike shapes (Wang et al., 2013). With b&d, c&e comparisons, aragonite tends to have longer time to complete transition. Ogino et al. (1987) also demonstrated that: at a low temperature (25-40 $^{\circ}\text{C}$) the transformation of amorphous CaCO_3 to calcite via the vaterite intermediate phase is three to six times faster than via the aragonite intermediate phase at a high temperature (50-80 $^{\circ}\text{C}$) in general. But

the crystallisation rate from aragonite to calcite increases with a higher concentration of Ca^{2+} and temperatures, while Mg^{2+} will retard this crystallisation (Ogino et al., 1987). According to Hu & Deng (2003, 2004), a marked transformation of aragonite to calcite was just found in 24h, Kitamura et al. (2002) reported that aragonite is formed after 10min Na_2CO_3 addition and increases with time. After 25h, the aragonite to calcite transformation is complete.

CO₂ Flux Rate: CO₂ flux rate has an effect on pH, reaction time and the degree of supersaturation, leading to various precipitates and morphologies. [Figure 2.23](#) displays the morphologies of CaCO₃ particles prepared at different flow rates: the CO₂ content in the mixed gas (N₂+CO₂) kept at 33.3 vol%. It can be seen that the rhombic particles (calcite) with different sizes synthesized at a low flow rate. With the increase of flow rate, the particles changed to a spherical form (vaterite). This phenomenon may be attributed to the increasing supersaturation degree of solution in accordance with a higher CO₂ flux rate, resulting in a preferred metastable phase formation. In terms of reaction duration, lower flow rates extended the reaction time due to the insufficient supply of CO₂. However in morphology terms, the only significant influence of CO₂ bubbling time was on particle sizes, i.e., a shorter bubbling time produced more small particles, while a prolonged bubbling time was advantageous for the particles' growth and aggregation (Han et al., 2006).

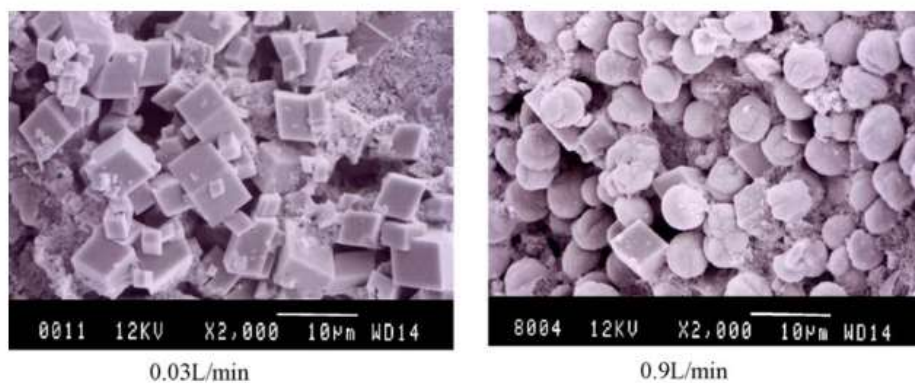


Figure 2.23: The SEM images of CaCO₃ precipitated at different flow rates (Han et al., 2005, 2006)

Additives: Additives usually have effects on both stable and metastable polymorphs by altering the formation. Many approaches with additives have been developed to control the phase and the morphologies of CaCO₃ in order to meet the demands in practical applications.

The previous methods mainly focus on the study of organic additives in the crystallisation of calcium carbonates. While some researchers are also concerned with the impact of inorganic additives (Mg^{2+} , Fe^{2+} , Ni^{2+} and Zn^{2+} etc.) on the formation of calcium carbonates (Kitamura, 2001; Loste et al., 2003; Ota et al., 1995). The effects of Mg^{2+} , Na^+ and K^+ will be studied and summarised in Section 2.11.

2.9 Magnesium Calcium Carbonates

Magnesian calcium carbonates are the members of minerals in the $\text{CaCO}_3\text{-MgCO}_3\text{-H}_2\text{O}$ system. Dolomite and huntite are typical crystals and demonstrated separately below and other formulae are summarised as magnesian calcite in the last section. Deelman (1999) & Liebermann (1967) experimented that the nucleation of huntite and dolomite can be attained at temperatures between 313K and 333K under atmospheric pressure; but details of the formation of huntite and dolomite are not clear. The associated chemical conditions include high Mg^{2+} or CO_3^{2-} concentration, high temperature, high pressure, high ionic strength of solution, and additives introduction (Davies et al., 1977).

Dolomite [$\text{CaMg}(\text{CO}_3)_2$]: Most modern dolomite is found to be formed under anaerobic conditions in supersaturated saline lagoons, or from high ionic strength solutions that are derived from the evaporation of seawater or lakes in arid regions. However, it is often thought that dolomite will develop only with the help of bacteria. Naturally the formation of dolomite, such as modern marine sediments and sediment burial to moderate depths, is largely controlled by reaction kinetics that is slow at even high supersaturations, with the theoretical content of 45.7% MgCO_3 and 54.3% CaCO_3 , equivalent content of MgO 22% (Morse et al., 2007). The most common is dolomitic limestone which contains more than 20% of MgCO_3 , while 5-15% component is termed as magnesian limestone. The ideal ratio of dolomite crystal is 1:1 on CaCO_3 and MgCO_3 . A plausible explanation for this slow kinetics of dolomite is that the requirement of cation ordering has a significant limit on the rate of phase form. Owing to this slow process under normal conditions, experiments on dolomite reaction kinetics have generally been conducted at an elevated temperature (typically between 100 and 300°C).

The mineral dolomite has been synthesised at a high temperature and pressure. A few representatives are selected here to show their experimental productions, providing

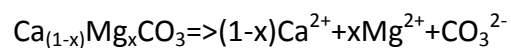
literature guidance to this investigation. Medlin (1956) synthesised dolomite at 150°C under a few atmospheres of CO₂. Baron (1960), similarly, synthesised dolomite in a mixture at 100°C and under a few atmospheres of CO₂. Ordered dolomite appeared in the synthesis experiments of Graf & Goldsmith (1955) at the temperatures of 200°C and above at unspecified pressures. Siegel (1961) prepared a variety of mixtures of calcium and magnesium carbonates mainly in the temperature range of 50-100°C. Some experiments at 25°C give mixtures of very poor crystallinity, illustrating that dolomite is preferred at high temperatures. Lippman (1973) mentioned that a high concentration of CO₃²⁻ is important in the formation of dolomite because of its ability to dehydrate the Mg²⁺ ion. He further suggested that nesquehonite/hydromagnesite might be precursors to dolomite formation. Kinsman (1967) and Davies et al. (1977) demonstrated that if alkalinity production is rapid, then hydrous magnesium carbonates may precipitate as precursors to dolomite. Graf and Goldsmith (1956) made a product which they called “protodolomite” by forming a Ca, Mg carbonate gel from very concentrated solutions and treating it hydrothermally at 70°C under CO₂ pressure. Baron (1960) has prepared high Mg calcites and “protodolomite” at temperatures as low as 25°C under a few atmospheres of CO₂ pressure.

Huntite: Huntite [Mg₃Ca(CO₃)₄] has been found in variety of environments, such as carbonate sediments of tidal flats, seasonal salt lakes, lacustrine deposits, and caves, etc. particularly caves with the low-temperature formation of huntite (Deelman, 2011).

Experimentally, Kinsman (1967) suggested that huntite is a precursor mineral to dolomite, and Lippman (1973) indicated that huntite will grow before dolomite because its more exposed crystalline structure will make easier Mg decarbonation. A high-temperature synthesis of huntite was firstly started by Biedl & Preisinger (1962) when producing huntite in hydrothermal tests with MgO, SiO₂ and Ca²⁺ under conditions 373K and 3.2 bar CO₂ pressure. Oomori et al. (1983) claimed the synthesis of huntite at 33°C when adding Na₂CO₃ solution to concentrated sea water saturated with Ca(HCO₃)₂. Zaitseva et al. (2006) also found huntite at a room temperature and an atmospheric pressure with cyanobacteria as cultures. Davies et al. (1977) precipitated huntite combined with dolomite, magnesium hydroxide carbonate, calcite, and monohydrocalcite with the aid of abundant microbial population after ten months at a room temperature.

Magnesian Calcite: Most of the calcite precipitated by marine organisms includes a certain percentage of magnesium; such calcite is called magnesian calcite (10 to >30mol% of MgCO_3 in solid solution), and divided into low-magnesium calcite and high-magnesium calcite at $\geq 4\%$ MgCO_3 content. Usually the more advanced organism produces less magnesium in the calcite.

Magnesian carbonates display a wide range of morphologies and compositions, which are determined by many factors, such as the temperatures, CO_3^{2-} concentration (pH and CO_2 pressure), $\text{Mg}^{2+}:\text{Ca}^{2+}$ ratios, time and other additives (Meldrum & Hyde, 2001). The crystal morphology and degree of incorporation of Mg within the calcite lattice is based on the Mg:Ca ratios in solution, but the growth conditions remain under discussion (Meldrum & Hyde, 2001; Mucci & Morse, 1983). Formation of magnesian calcite can be expressed as (Bertram et al., 1991; Morse et al., 2007):



There is also evidence that illustrates magnesium's importance in introducing water into the calcite structure; for example, Lippmann (1973) indicated water molecules may be incorporated in magnesian calcite, to avoid the large amount of energy usage in Mg^{2+} dehydration process during the precipitation.

2.10 Parameters Affecting Magnesium Calcium Carbonation

Temperature: The influence of temperature is significant. Early researchers discovered that the positive magnesium content of calcite increases with respect to a higher temperature because of a faster reaction (Glover & Sippel, 1967; Goldsmith et al., 1955; Graf & Goldsmith, 1955; Katz, 1973; Kinsman & Holland, 1969; Morse & Mackenzie, 1990). **Figure 2.24** shows various results on the extent of magnesium uptake. It is clear to see that, with NaCl addition, more magnesium will be trapped, which is also well matched with the findings from Section 6.2.3.3.

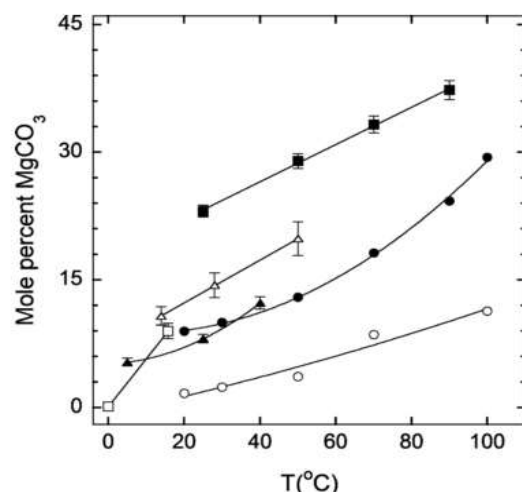


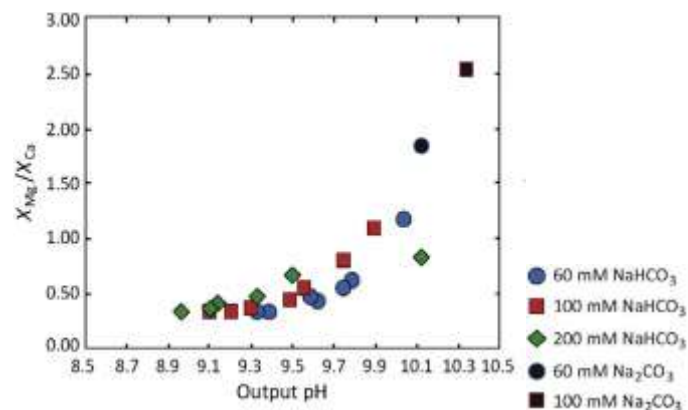
Figure 2.24: The variations of MgCO₃ content of the magnesian calcite with temperatures, precipitated in seawater or synthetic seawater-like solutions (Mucci, 1987).

(Solid squares are CaCl₂+MgCl₂+NaCl; Solid circles are seawater+Na₂CO₃+ Ca(HCO₃)₂; Open circles are seawater+Na₂CO₃; Open triangles are CaCl₂+MgCl₂+Na₂CO₃; Open squares are seawater+Na₂CO₃+aragonite seeds; Solid triangles are seawater + calcite seeds)

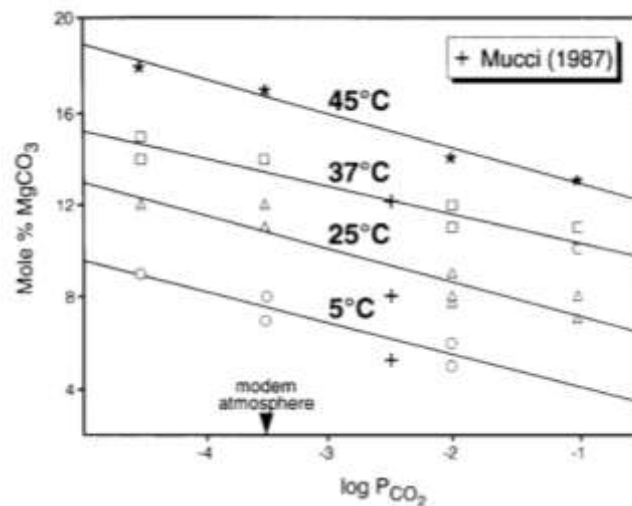
CO₃²⁻ Concentration: Various initial reactant concentrations, pH and CO₂ pressures can lead to different carbonate concentrations. Blue & Dove (2015) investigated amorphous magnesium calcium carbonate (ACMC) formation under controlled chemical conditions to determine the relationship between composition and inorganic solution chemistry. They used mixed flow reactors with two syringes: one with 100ml of MgCl₂ and CaCl₂ solution at a 5:1 ratio, and one with 100ml of NaHCO₃ or Na₂CO₃ solution at variable concentrations (Figure 2.25a). The results show that ACMC with the highest Mg content was predominantly comprised of coalesced particles, and higher pH solutions promoted a greater Mg content. This was due to the higher pH leading to larger amounts of carbonate at a steady state; therefore there were more lattices within precipitates.

CO₂ pressure is another important parameter of magnesian calcite formation. With a decreased partial pressure of CO₂, magnesium concentration in calcite should increase, while an increased P_{CO₂} results in the decrease of MgCO₃ incorporation. This phenomenon shows a parallel dependence on partial pressure at the temperatures of 5°C, 37°C and 45°C. The relationship between MgCO₃ incorporation percentage, temperatures and CO₂ partial pressure is shown in Figure 2.25b (Burton, 1993). It can be seen that in normal seawater, the

temperature varies from 5°C to 45°C, with changes in P_{CO_2} from 10^{-1} to $10^{-4.5}$ atm respectively. The Mg-calcite compositions range from 6 to 18 mole% MgCO_3 .



(a): Various initial reactant concentrations (Blue & Dove, 2015)



(b): The relationship of CO_2 partial pressures, temperatures and percentages of MgCO_3 incorporation into calcite (Burton, 1993) (★ experimental results at 45°C; □ experimental results at 37°C; △ experimental results at 25°C; ○ experimental results at 5°C)

Figure 2.25: The influences of variables on magnesian calcite: (a) Initial reactants; (b) CO_2 partial pressures & temperatures

$\text{Mg}^{2+}/\text{Ca}^{2+}$ Ratio: $\text{Mg}^{2+}/\text{Ca}^{2+}$ ratio has an effect on magnesian calcite morphology (Loste et al., 2003). Raz et al. (2000) performed crystallisation experiments in high magnesium concentrations solution ($\text{Mg}^{2+}/\text{Ca}^{2+} \geq 4$) without any additives. Although $\text{Mg}^{2+}/\text{Ca}^{2+}$ equates to 4:1 in this experiment, magnesium in produced crystals is not uniformly

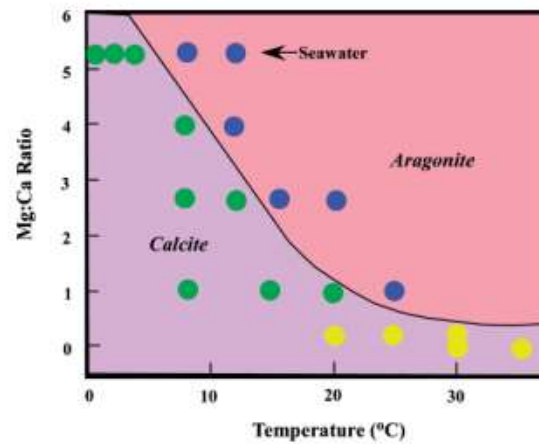
distributed. SEM displays that magnesian calcite precipitates in dumbbell shapes, round shapes, and elongated shapes (**Figure 2.26a**); among which elongated morphology contains the most abundant magnesium concentration. Mixed particles comprising a polycrystalline magnesian calcite core in an envelope of polycrystalline aragonite is showed in **Figure 2.26b**. Observation by this microscopy reveals that the magnesian calcite core forms first, and then aragonite deposits following around the core. In a short time, precipitate generates into a precursor amorphous phase, and then subsequently transforms into calcite, aragonite, and high magnesian calcite, depending upon the conditions of operation (Raz et al., 2000; Reddy & Gaillard, 1981).



(a): The SEM of precipitates grown in the presence of 4:1 Mg/Ca solution from left to right-- Magnesian calcite spherulite with typical dumbbell morphology; Polycrystalline aragonitic spherulite, with the needle shaped morphology of single crystallites with magnesian calcite core(see next figure); Elongated magnesian calcite particles, such particles contain the highest magnesium contents (Raz et al., 2000)



(b): A mixed particle with a core of polycrystalline magnesian calcite and an outer shell of polycrystalline aragonite (Raz et al., 2000)



(c): The influence of seawater $\text{Mg}^{2+}/\text{Ca}^{2+}$ ratios and temperatures on the nucleation of CaCO_3 from seawater. Blue circles are aragonite, yellow are calcite, green are initially calcite with aragonite overgrowths (Morse et al., 2007).

Figure 2.26: Influences of $\text{Mg}^{2+}:\text{Ca}^{2+}$ ratios on magnesian calcite (MC) formation: (a) MC spherulite; (b) Mixed particles; (c) Seawater profile

Mg^{2+} can either be incorporated within the calcite lattice when the $\text{Mg}^{2+}/\text{Ca}^{2+}$ ratio in solution is low, or accelerate the formation of aragonite when the $\text{Mg}^{2+}/\text{Ca}^{2+}$ ratio is ≥ 4 (Bischoff et al., 1987; Brooks et al., 1950; Falini et al., 1996; Loste et al., 2003; Raz et al., 2000). Magnesium can only integrate within the defects of calcite but not adhere to the calcite surface or combine with aragonite. Morse et al. (2007) demonstrated that calcite forms over a wide range of temperatures (0-35°C) in Mg-free seawater, but only forms below 8°C in seawater when the $\text{Mg}^{2+}:\text{Ca}^{2+}$ ratio is 5:1. From the [Figure 2.26c](#), it is evident that the $\text{Mg}^{2+}:\text{Ca}^{2+}$ ratio and temperature control the type of CaCO_3 mineral. It can be seen that both higher magnesium concentration and higher temperature promote aragonite formation.

In conclusion, the addition of Mg^{2+} ions to the crystallising solutions results in two effects: 1) a much wider range of morphology; 2) a transition from single crystal to crystallite aggregates, which means that it can affect crystal morphologies by both their adsorption on specific crystal faces and by altering the calcite nucleation and growth process.

Time: Loste et al. (2003) used NaHCO_3 , $\text{MgCl}_2 \cdot 6\text{H}_2\text{O}$, and CaCl_2 as reactants under various $\text{Mg}^{2+}/\text{Ca}^{2+}$ ratios to investigate time effect on magnesian calcite formation. A typical 10:1 $\text{Mg}^{2+}/\text{Ca}^{2+}$ ratio is presented in [Figure 2.27](#), and it is concluded that a longer time will result in

a more stable phase. Amorphous calcium carbonate (ACC) forms under a high supersaturation and then combines with small amounts of calcite after 24h. In 14 days, nesquehonite (48%), monohydrated calcite (38%), and magnesium calcite (14%) are observed. From another ratios study, they also mentioned that magnesium content is determined by a Mg^{2+}/Ca^{2+} ratio, that is a higher ratio tends to possess a larger concentration of Mg^{2+} in product and produce more stable crystallisation.

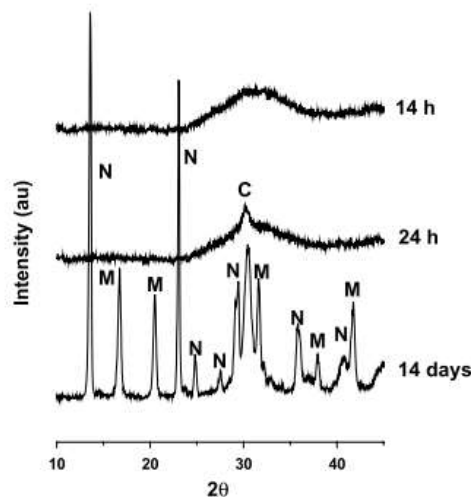


Figure 2.27: XRD results with 10:1 Mg/Ca ratio at times indicated (Loste et al., 2003) (N: Nesquehonite, M: Magnesite, C: Calcite)

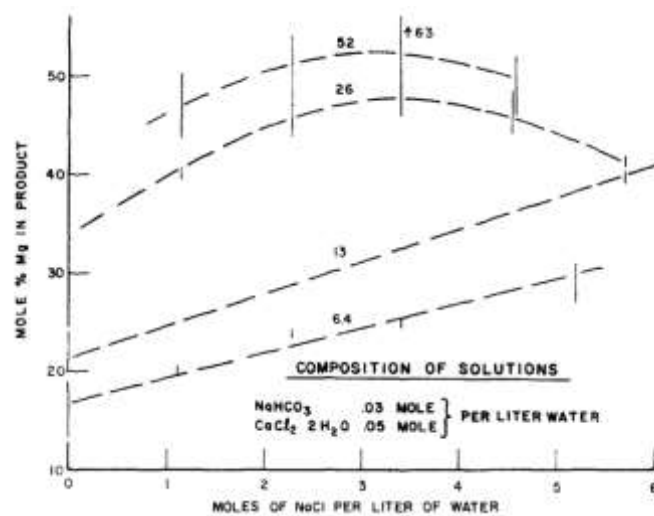
2.11 The Influences of Impurities on Magnesian Calcites

In this study, all elements are considered impurities, apart from magnesium carbonates, calcium carbonates and magnesian calcite. Sodium and potassium are singled out based on the research aim, to better understand these coprecipitates with magnesium or calcium carbonates. Finally various alkaline metal ions and other additives are introduced to make comparisons.

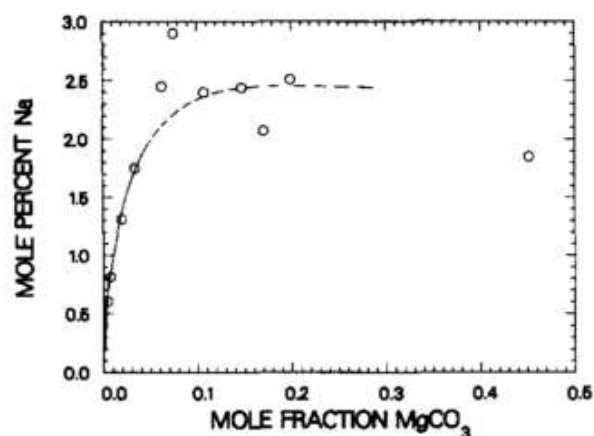
2.11.1 Sodium Addition

Glover & Sippel (1967) used $MgCl_2 \cdot 6H_2O$, $CaCl_2 \cdot 2H_2O$ and $NaHCO_3$ to study precipitates. They found that the initial precipitates slowly disappear after a few hours, especially high magnesian calcite, followed by aragonite formation. Additionally, $NaCl$, together with a higher temperature can improve magnesium concentration in sediments, based on [Figure 2.28a](#). Ishikawa & Ichikuni (1984) also investigated the mixture of coprecipitated sodium with calcite, and demonstrated that Na^+ is located at interstitial sites of the calcite lattice,

which was similar to Busenberg & Plummer (1985)'s study, whose results agreed with the earlier concepts that: 1) normal solid solution coprecipitation does not happen, but just exists in crystal defects; 2) the amount of incorporated Na^+ in the calcite structure is determined by the number of lattices. Busenberg & Plummer (1985) also suggested that the presence of Na^+ and SO_4^{2-} can increase interstitial voids. **Figure 2.28b** displays the results of a $\text{NaCl-MgCl}_2\text{-CaCl}_2\text{-Na}_2\text{CO}_3\text{-NaHCO}_3$ aqueous reaction system, noting the MgCO_3 increases with a higher fraction of Na^+ from 0 to 2.4 percent, but stays constant after that (Busenberg & Plummer, 1989).



(a): NaCl will enhance Mg% in the product under various temperatures (dash lines—temperature) (Glover & Sippel, 1967)



(b): Molar Na^+ concentrations in the synthetic magnesian calcite as a function of MgCO_3 mole fraction (Busenberg & Plummer, 1989)

Figure 2.28: Sodium influence on magnesian calcite (a-b)

Experimental results from White (1977) show that a lower pH leads to fewer defects, due to the slower crystal growth rates of calcites, and therefore lower level of Na^+ intersection; vice versa, increased calcite crystal growth with higher pH values will result in more defects, thus enhancing the Na^+ substitution. Sulfate ions distort the calcite crystal structure and cause sodium coprecipitation. The presence of dissolved sulfate reduces the rate of crystal growth of calcite in artificial sea water dramatically (Busenberg & Plummer, 1985). White (1978) suggested that magnesium has no influence on sodium substitution; however, Okumura & Kitano(1986) argues magnesium ions in the reactant solution increase the Na^+ coprecipitation within calcite, but decreases the Na^+ coprecipitation within aragonite.

Crystal morphology is progressively less perfect with higher reactant concentrations. In the system $\text{NaCl-MgCl}_2\text{-CaCl}_2\text{-Na}_2\text{CO}_3\text{-NaHCO}_3$, when a small amount of MgCO_3 forms in magnesian calcite, crystals appear similar to the calcite phases with well-defined faces. However, when $\text{Mg}^{2+}/\text{Ca}^{2+}$ ratios increase, spherical to needle-shaped magnesium calcite occurs (Figure 2.29), which is caused by the reduced rate of crystal growth and the elongation of internal structure in specific directions, such as towards edges or corners (Berner, 1975; Busenberg & Plummer, 1985; Given & Wilkinson, 1985; Mucci, 1988; Paquette & Reeder, 1995). Both Folk (1974) and Lahann(1978) also concluded that hydrous Mg^{2+} distorts the lattice structure on side faces. This phenomenon is verified in Section 2.10, where morphologies change under various $\text{Mg}^{2+}/\text{Ca}^{2+}$ ratios.



A ———

B ———

C ———

From left to right--a) 2.4 mol% of MgCO_3 ; b) 6 mol% of MgCO_3 ; c) 20 mol% of MgCO_3 . Bars equal 10 μm . (Busenberg & Plummer, 1989)

Figure 2.29: Morphologies under various MgCO_3 mole percentages

2.11.2 Potassium Addition

Potassium is another addition in this experiment, and a few authors have studied its effect. Potassium exerts the same influence as sodium during the analysis of carbonates as an altrivalent (“altrivalent” ions mean the spontaneous incorporation of other ions with different valences from host-crystal ions). Potassium or sodium can be substituted within the carbonate lattices, but not the solid nanocarbonate impurities or fluid inclusions. This section will describe this phenomenon with respect to concentrations, pH, temperatures, and substitution mechanisms.

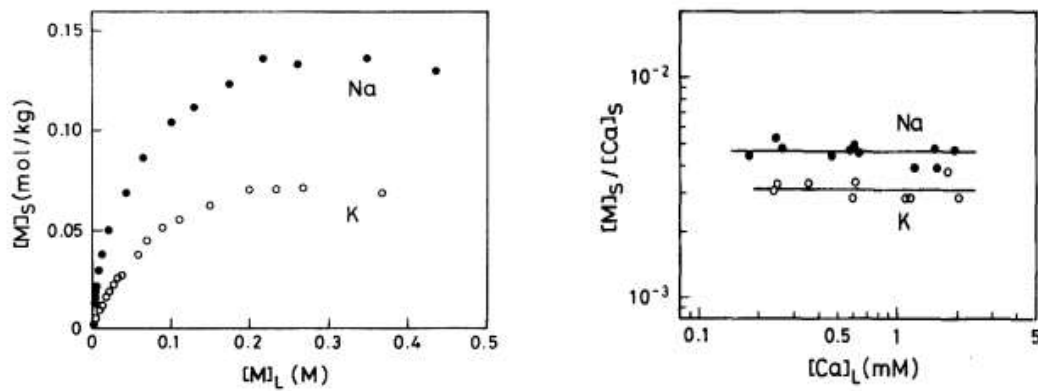
White (1977) summarised that increasing the amounts of sodium decreases the concentration of coprecipitated potassium. Although sodium can inhibit potassium incorporation efficiently, the effect of potassium on sodium coprecipitation is very minor. When pH is reduced, co-precipitated sodium and potassium are decreased in a positive correlation. However, when solvent aqueous calcium’s activity increases under the equilibrated system with aragonite at lower pH levels, the retarded influence on sodium and potassium incorporation will be observed by limiting the quantities of vacant exchange sites.

Both sodium and potassium demonstrated reduced incorporation with calcium at raised temperatures. This can be attributed to energy heterogeneity, which is caused by the defective structures and varieties in type, geometry, and coordination of adjacent atoms. According to Kinsman & Holland (1969), the first step of coprecipitation is usually surface adsorption at the interface of the growing particles. The distribution of cations between the surface and the coexisting aqueous solution are determined by exchange equilibrium on free energies of two states. As the crystal is growing, the coordination numbers of the absorbed cations at the original interface will propagate as the number of neighbour atoms increase. This will alter the energy configuration of the initial distribution and the equilibrium distribution between the solid and aqueous phases. Hence the ions will be instantly attempting to re-equilibrate with the aqueous, because of the enclosed growing crystals. At a certain point in this dynamics, the cations will stick to the particle structure rather than solution media.

The mechanism controlling the incorporation of sodium and potassium in aragonite depends on the heterogeneity of interactive energy either at the surface or within the solid

solution, that is a new atom can be successfully introduced to the crystal lattice of the host atom, based on the similarities of ionic radius and bond type. Sodium and calcium have a closer relationship of those properties, hence having more completed available sites than potassium. The physical separation of sodium and potassium is from their monovalent natural exclusive interaction, to avoid the mutual substitution. Owing to the insufficient replacements of anions, charge imbalances caused by polyvalent cation coprecipitation can be balanced by another mechanism, usually through defect structures within the particles. Particularly, two kinds of defects are classified as vacancy sites and interstitial replacements (White, 1977).

This heterogeneous energy distribution mechanism is capable of incorporating sodium and potassium ions with aragonite and aqueous solution, as well as calcite only at lower aqueous sodium/potassium concentrations, but not at higher ones (White, 1978). However, Busenberg & Plummer (1985) mentioned that the mechanism of sodium and potassium ions coprecipitation into calcite is that: both ions are physically occupied in interstitial sites. These voids are formed during the rearrangement of the growing crystals where Na^+ and K^+ are independent from the aqueous calcium concentration. Ishikawa & Ichikuni (1984) studied calcite adsorption specifically by using the different proportions of sodium and potassium solutions in a constant calcium concentration (0.6mM). Both Na^+ and K^+ display the growth of coprecipitated amounts with the growth of aqueous concentration, and then the saturation point in the calcite phase (Figure 2.30). It is also demonstrated that $[\text{M}]_s/[\text{Ca}]_s$ was independent of $[\text{Ca}]_L$. This result indicates the available positions of sodium or potassium are not calcium lattice locations. If the sites were Ca places, the occupation of M with Ca led to the dependence of $[\text{M}]_s/[\text{Ca}]_s$ on $[\text{Ca}]_L$. Therefore the most sites are interstitial lattice positions where calcium cannot be located.



The incorporated amounts of sodium and potassium against their aqueous concentration (left); Na/Ca and K/Ca ratios in calcite plotted against aqueous calcium concentrations (right). $[M]_s = [Na/K]$ solid coprecipitated with calcite, $[M]_L = [Na/K]$ liquid concentration (left) (Ishikawa & Ichikuni, 1984)

Figure 2.30: The influences of potassium addition on magnesian calcite

2.11.3 Alkaline Metal Ions Addition & Comparisons

The sodium substitution of carbonate rock is considered as a useful indicator of depositional condition and a diagenetic history of sediments (Land & Hoops, 1973; White, 1978). Sodium incorporation into marine calcareous skeletons, carbonate sediments and the carbonate rocks are replaced by the sodium ion to calcium ion in the calcium carbonate crystal lattices (Land & Hoops, 1973), while potassium also has a similar exchange (Amiel et al., 1973), but a real place of potassium ions in aragonite particles is still unknown. Other alkaline metals lithium and rubidium are seldom explored, and their presence in marine calcareous skeletons is within the range of several tenths to several ppm.

As demonstrated in the previous segment, the amounts of alkali metal adsorption with aragonite and calcite are different in mechanism, such alterations can be partially assumed from the different ionic radii of alkali metal ions. **Figure 2.31a** presents the relationship between the quantities of alkali metal ions incorporated with aragonite or calcite and ionic radii. The graph implies a parabolic curve with the peak at sodium 1.01 ionic radii in aragonite, and gradual shrinks with increasing ionic radius from lithium to rubidium in calcite.

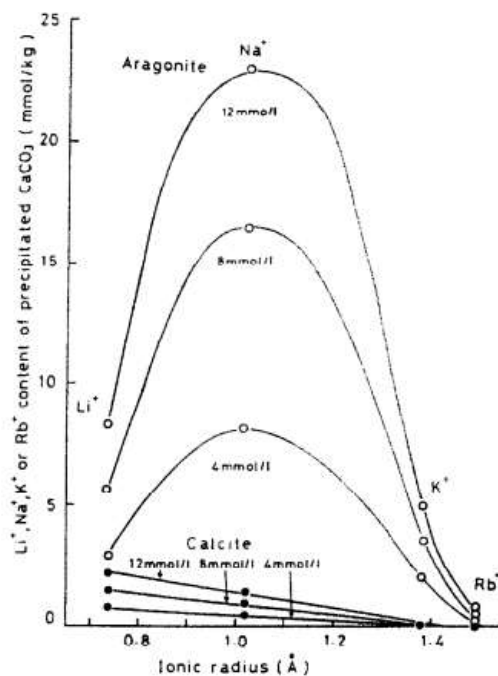
Divalent metals (e.g. magnesium) coprecipitate into calcium carbonate through the replacement of metal ions of calcium in calcium carbonate, that is, the ion-exchange process generates a solid solution between divalent metal carbonate and calcium carbonate. In this

process, the ionic radius of the divalent metals largely influences the incorporation of metal into calcium carbonate. The distribution coefficients of divalent metals between calcium carbonate and the solution are enhanced with elevated ionic radius to reach a maximum, and then are lowered with further increasing ionic radius. It is caused by the similarity of divalent metals and the exchange site in ionic size, while the smaller or larger ions are more difficult to incorporate (Okumura & Kitano, 1986). This profile implies that sodium replaces calcium successfully in the structure of aragonite due to the equality of sodium's and calcium's ionic radius, while other alkali metals are considerably different from that of calcium ions, resulting in less favorable substitution.

Several researchers (Busenberg & Plummer, 1985; Ishikawa & Ichikuni, 1984) commented that calcite replacement is caused by interstitial sites of calcium, because the amounts of substitution are dependent on the alkali metal ion concentration but not on calcium ion concentration in the parent aqueous phase. It is then accepted that smaller particles are easily occupied into interstitial positions to produce an interstitial solid solution. Hence lithium ions are more favoured to incorporate with calcite, relative to larger ions. Generally, the amounts of alkali metals incorporated with aragonite are much larger than calcite due to its possibly denser structure in aragonite.

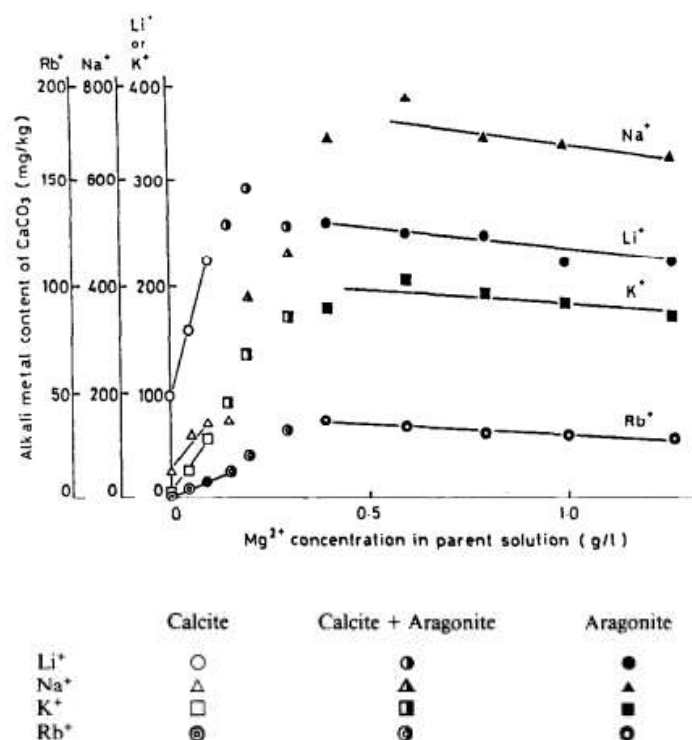
Okumura & Kitano (1986) also studied the interference of magnesium on the incorporation of the alkali metals with calcium carbonate. It has been widely proven that aragonite is more obvious in the presence of magnesium. [Figure 2.31b](#) demonstrates the quantity of alkali metal increases with a higher level of magnesium ions in a parent solution during the calcite phase, while alkali metal decreases gradually in later aragonite conditions. The reason for the reduction of the alkali metal in aragonite is explained by the shrinkage in the activities of alkali metal ions in the aqueous phase, due to the enhanced concentration of magnesium chloride, accompanied by increasing ionic strength. It is documented that magnesium is inserted randomly in the calcite structure to generate precipitates between calcitic CaCO_3 and MgCO_3 (low Mg-calcite). A considerable distortion occurs during the substitution of smaller magnesium ions with larger calcium ions, and alkali metal ions coprecipitate into the deposit during this interference. Sodium has the same tendency of the decreased coprecipitation within the aragonite when the sodium chloride concentration is increased. This is due to the fact that aragonite, combined with sodium and other

incorporated alkali metals, has a strong capacity to coprecipitate because the ion exchange process is increased. In conclusion, alkali metals are easier to precipitate with aragonite than calcite. The quantity of coprecipitation in aragonite is $\text{Na}^+ > \text{Li}^+ > \text{K}^+ > \text{Rb}^+$, and the incorporation with calcite is $\text{Li}^+ > \text{Na}^+ > \text{K}^+ > \text{Rb}^+$ (Figure 2.31b). The figure shows the different formation processes between calcite and aragonite. Magnesium can enhance the alkali metals' coprecipitation with calcite but can decrease it with aragonite. Finally sodium-bearing aragonite reduces other alkali metals (Li^+ , K^+ and Rb^+) because of sodium's competitiveness in ion-exchange as its ionic radius is similar to that of calcium.



(a): A relationship between alkali metals of calcium carbonate (aragonite and calcite) and ionic radii.

Aragonite ○ Calcite ● (Land & Hoops, 1973)



(b): Effects on the magnesium chloride concentration in a parent solution on the quantities of alkali metal ions coprecipitated with calcium carbonate. $\text{Ca}(\text{HCO}_3)_2$ (Ca^{2+} :360mg/l)+LiCl, NaCl, KCl or RbCl (Li^+ , Na^+ , K^+ or Rb^+ ; 0.4g/l) + MgCl_2 (Mg^{2+} , 0 to 1.27g/l) \Rightarrow Calcite and/or Aragonite (Okumura & Kitano, 1986)

Figure 2.31: Alkaline metal ions influences on magnesian calcite: (a) Ionic radii; (b) Reactants concentrations

2.11.4 Other Additives

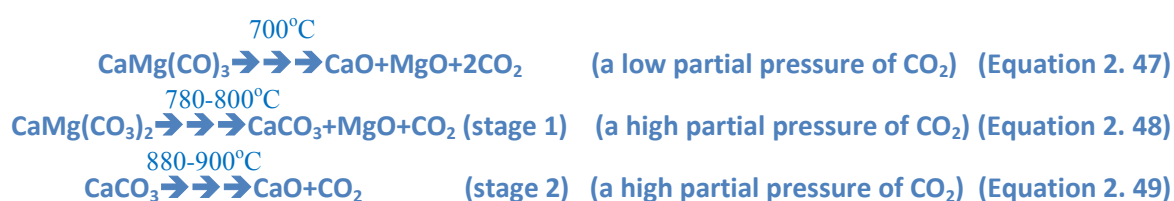
Sulfate is also recognised as an important coprecipitating anion in calcite formation. It leads to a metastable phase formation, with small amounts of sulfate (<3 mole %) coprecipitated, it prefers to form the vaterite structure, and is unfavourable in calcite and the least favourable in aragonite formation (Fernandez-Diaz et al., 2010). According to Kitano et al. (1975), sodium is more favoured to aragonite rather than calcite, and this incorporation is enhanced by the uptake of sulfate ions in aragonite, and sodium presents partly as sodium sulfate in aragonite. However, chloride ions do not influence the sodium incorporation, i.e., sodium ions do not exist as sodium chlorides. But individually, the chloride inclusion of aragonite is much bigger than that of calcite.

Other ions like Sr^{2+} and phosphate also inhibit calcite formation (House, 1987; Reddy & Gaillard, 1981; Reddy, 1977); in terms of organic matter, Berner et al. (1978) illustrated that the introduction of carboxylic, humic and fulvic acids will inhibit the nucleation of aragonite

in supersaturated seawater. But the presence of organic materials, for instance citrate and malate, dramatically enhances the quantities of Na^+ , Mg^{2+} , and F^- incorporation with calcite (White, 1978). Differently, the effect of organic matters in the parent solution on the combination of alkali metal ions with aragonite has not been fully investigated. Usually, the biomineralisation process is different from that inorganic mineralisation.

2.12 The Thermal Decomposition of Magnesian Calcites

Calcination of magnesian calcium carbonates or dolomitic limestone will lead to dolime ($\text{CaO}\cdot\text{MgO}$) formation. Most studies of dolomite show a single decomposition step (Equation 2.47), whereas in some cases, two steps decomposition are documented (Equations 2.48-2.49) (Bandi & Krapf, 1976; McCauley & Johnson, 1991; McIntosh et al., 1990).



This is caused by the different CO_2 partial pressures. One step occurs at a low partial pressure of CO_2 , and two steps happen at a high partial pressure. In a two-step process, initial reaction (first-step) is followed by a fast reprecipitation of CaO to CaCO_3 . While in the latter process (second-step), a lower temperature leads to the decomposition of the dolomitic structure, releasing CO_2 from the ions associated with magnesium when the concentration of alkali metal salts and other diverse ions are low (780°C), followed by the formation of calcite and magnesia (880°C). After that, a higher temperature applies to decompose calcite with the evolution of CO_2 (McIntosh et al., 1990). The partial pressure of CO_2 relies on the rate of diffusion on CO_2 in samples, which in turn is dependent on sample size, particle size, sample-compartment size, use of sample lids, use of static or dynamic surroundings and other controllable factors. Peak temperature is also affected by the introduced atmosphere, for instance the evolution of CO_2 single step takes place at 640 and 720°C in vacuum and nitrogen, at 610 to 800°C in air, and at 680°C in low CO_2 pressures. CO_2 pressure may display the effect on thermal decomposition: the partial pressure of CO_2 cause a higher temperature of second peak, and a lower temperature on first peak with minimum of 10-20% CO_2 mixture (Bandi & Krapf, 1976; McIntosh et al., 1990).

Based on various temperatures' calcination, dolime will be separated into half-burnt dolomite ($\text{CaCO}_3 \cdot \text{MgO}$), where only magnesium carbonates are decomposed; and dolime ($\text{CaO} \cdot \text{MgO}$), where fully thermal decomposition occurs with temperatures around or higher than 900°C (Lhoist, 2016; Dowling et al., 2015). However, CaO is highly reactive with water into half-hydrated dolime ($\text{Ca}(\text{OH})_2 \cdot \text{MgO}$) under normal conditions.

There is sufficient evidence demonstrating that typical salts affect the low-temperature endotherm when the decomposition of dolomite occurs in the presence of CO_2 . Salt catalyses the rearrangement of Ca^{2+} , Mg^{2+} and CO_3^{2-} , and distorts the lattices to lower activation energy. The influence of salts not only reduces the temperature of first decomposition, but also changes the rate of decomposition. For example, a 750°C peak temperature with $10^\circ\text{C}/\text{min}$ heating rate of dolomite can be reduced to 640°C peak temperature with $2^\circ\text{C}/\text{min}$ heating rate when precipitate is salt-bearing dolomite (Bandi & Krapf, 1976). It is also possible to break down the carbonates if a typical salt's concentration is high enough.

The addition of NaCl can lead to uncommon curves during dolomite decomposition. When the concentration of salt is increased, more abnormalities are displayed. NaCl reduces the decomposition temperature in the first stage, since the salt can rearrange the calcium and magnesium ions (McIntosh et al., 1990). It is recognised that salt reduces the thermal decomposition peak of magnesite. The differences in the thermal response of ordinary and salt-bearing dolomites are caused by the endotherm shifting of MgO formation. Hence the existence of salt may lead to a larger extent of the peak temperature movement during the thermal decomposition of magnesian calcite compared to CO_2 partial pressure. Typically, when the salt concentration is high enough, the original 780°C endotherm is altered to a temperature as low as 580°C .

In conclusion, with the salt-bearing dolomites, there is a preferred formation of MgO at which calcite isn't decomposed. This phenomenon is supported by Garn's theory, where the activation energy decreases because the salt disorders the lattice structure (Bandi & Krapf, 1976). More importantly, the decomposition of magnesium carbonates shows lower temperature with the increased presence of salt. There are two mechanisms behind it: 1) salt-bearing magnesian calcite involves the solid-state rearrangement of calcium and

magnesium ions to form calcite and MgO; 2) salt presence causes step-wise process by forming small amounts of magnesite and calcite before the MgO obtained (Bandi & Krapf, 1976).

2.13 Thermodynamic Modelling

Modelling is important to provide an indication of the thermodynamic estimated precipitates; two widely used software in chemistry reaction PHREEQC and Visual Minteq are reviewed in this section in accordance with their databases.

PHREEQC & Visual Minteq Description: PHREEQC, widely used to conduct the varieties of the aqueous geochemical calculations, is a computer program written in C & C++ languages (Parkhurst & Appelo, 2013). It is operated to simulate the reactions in a complex aqueous system and produce the equilibrated thermodynamic results. The most limited constraint for this software is that the chemical reaction progresses under a room temperature and atmospheric pressure only, due to its lacking of a high temperature-high pressure database.

Visual Minteq, widely used modelling software for chemistry reaction, is a chemical equilibrium model to calculate the resulting compositions in solution contacting with gases, solid compounds and particle surfaces. It is well-applied for the inorganic ions and complexes in solutions, to evaluate the effect of dissolution or precipitations in water chemistry. This model operates easily, but has several deficiencies, such as transport calculations, organic compounds, non-equilibrium processes, and reactions under a high temperature-high pressure, which all cannot be utilised. Summary of the two models is seen below:

Table 2. 6: The comparisons of two models: Visual Minteq and PHREEQC

	Visual Minteq (ion association models)	PHREEQC (various models)	Comments
Transport model	No (Only to calculate the chemical composition in one single point)	Yes (However in this study, the type of model is not pursued)	Transport model is to simulate one component transferring into another substance, such as the transport rate of heavy metals from a contaminant source to a water body.
Organic compound	No (No database for this kind of calculations)	Yes	
Non-equilibrium processes	No (A natural process, which cannot be modelled through this chemical equilibrium software, such as weathering or biological degradation.)	Yes	
High T, high P	No (Operated within 0-40°C range, in aqueous phase, under atmospheric pressure)	No (room temp only)	Simulations about deep geological formations are not possibly modelled by both. Special databases have to be assembled.
Ionic strength	Very low <1 (Diluted concentration)	Not specific, but higher than Visual Minteq	Ionic strength is a measure of ion concentrations in the solution.
Inorganic ions and complexes in water	Yes	Yes	
Dissolve or precipitate solid phases on water chemistry	Yes	Yes	
Redox reaction	Yes	Yes	

Database Description: PHREEQC manipulates several aqueous models corresponding to various databases: 1) two ion-association aqueous models (WATEQ4F), 2) a Pitzer specific-ion-interaction aqueous model, 3) the SIT (Specific ion Interaction Theory) aqueous model. The code from Visual Minteq builds on solution-based ion-association interactions. The fundamental differences of these manipulations are from their various activity coefficients, which are the functions of ionic strength over the changed aqueous phases ([Table 2.7a](#)). The thermodynamic data used during this experimental study are then summarised in [Table 2.7b](#) and [Table 2.7c](#), corresponding to PHREEQC Sit. dat and Visual Minteq Thermo. dat respectively.

Table 2. 7: The comparisons of databases (a) and the thermodynamic data (b-c) used in the tests

(a): Aqueous models and comparisons

	Pitzer database-PHREEQC	Sit database-PHREEQC	Ion-association approach (Waterq4f-PHREEQC, Visual Minteq)
Limitations	Limited elements; Temperature dependence; Limited for redox reaction	Temperature dependence	Ionic strength <1, very diluted; Best only in NaCl medium; Inconsistent thermodynamic data; Temperature dependence
Advantages	High ionic strength; Thermodynamic consistency for mixtures of electrolytes	Higher ionic strength than ion association; Fewer parameters, easier to operate than Pitzer; suitable for redox reaction	Redox reaction; Data for most elements (Al, Si); Very basic

(b): Sit. dat thermodynamic data used in the simulations

PHASE	Equilibrium	log K
Brucite	$\text{Mg}(\text{OH})_2 = +1.000\text{Mg}^{+2} - 2.000\text{H}^+ + 2.000\text{H}_2\text{O}$	17.1
Artinite	$\text{Mg}_2(\text{CO}_3)(\text{OH})_2 \cdot 3\text{H}_2\text{O} = +2.000\text{Mg}^{+2} + -2.000\text{H}^+ + 1.000\text{CO}_3^{-2} + 5.000\text{H}_2\text{O}$	9.81
$\text{Mg}_5(\text{CO}_3)_4(\text{OH})_2 \cdot 4\text{H}_2\text{O}$	$\text{Mg}_5(\text{CO}_3)_4(\text{OH})_2 \cdot 4\text{H}_2\text{O} = +5.000\text{Mg}^{+2} + -2.000\text{H}^+ + 4.000\text{CO}_3^{-2} + 6.000\text{H}_2\text{O}$	-10.31
Magnesite	$\text{MgCO}_3 = +1.000\text{Mg}^{+2} + 1.000\text{CO}_3^{-2}$	-8.91
Nesquehonite	$\text{Mg}(\text{CO}_3) \cdot 3\text{H}_2\text{O} = +1.000\text{Mg}^{+2} + 1.000\text{CO}_3^{-2} + 3.000\text{H}_2\text{O}$	-5.1
Lansfordite	$\text{MgCO}_3 \cdot 5\text{H}_2\text{O} = +1.000\text{Mg}^{+2} + 1.000\text{CO}_3^{-2} + 5.000\text{H}_2\text{O}$	-5.04
Aragonite	$\text{CaCO}_3 = +1.000\text{Ca}^{2+} + 1.000\text{CO}_3^{-2}$	-8.31
$\text{CaCO}_3 \cdot \text{H}_2\text{O}$ (s)	$\text{CaCO}_3 = +1.000\text{Ca}^{2+} + 1.000\text{CO}_3^{-2} + 1.000 \text{H}_2\text{O}$	-7.6
Calcite	$\text{CaCO}_3 = +1.000\text{Ca}^{2+} + 1.000\text{CO}_3^{-2}$	-8.48
Vaterite	$\text{CaCO}_3 = +1.000\text{Ca}^{2+} + 1.000\text{CO}_3^{-2}$	-7.9
Dolomite	$\text{CaMg}(\text{CO}_3)_2 = +1.000\text{Ca}^{+2} + 1.000\text{Mg}^{+2} + 2.000\text{CO}_3^{-2}$	-17.12
$\text{CaMg}_3(\text{CO}_3)_4$ (s)	$\text{CaMg}_3(\text{CO}_3)_4 = +1.000\text{Ca}^{+2} + 3.000\text{Mg}^{+2} + 4.000\text{CO}_3^{-2}$	-30.81

(c): Thermo. dat thermodynamic data used in the simulations

PHASE	Equilibrium	log K
Brucite	$\text{Mg}(\text{OH})_2 = +1.000\text{Mg}^{+2} - 2.000\text{H}^+ + 2.000\text{H}_2\text{O}$	17.1
Artinite	$\text{Mg}_2(\text{CO}_3)(\text{OH})_2 \cdot 3\text{H}_2\text{O} = +2.000\text{Mg}^{+2} + -2.000\text{H}^+ + 1.000\text{CO}_3^{-2} + 5.000\text{H}_2\text{O}$	9.6
$\text{Mg}_5(\text{CO}_3)_4(\text{OH})_2 \cdot 4\text{H}_2\text{O}$	$\text{Mg}_5(\text{CO}_3)_4(\text{OH})_2 \cdot 4\text{H}_2\text{O} = +5.000\text{Mg}^{+2} + -2.000\text{H}^+ + 4.000\text{CO}_3^{-2} + 6.000\text{H}_2\text{O}$	-8.77
Magnesite	$\text{MgCO}_3 = +1.000\text{Mg}^{+2} + 1.000\text{CO}_3^{-2}$	-7.46
Nesquehonite	$\text{Mg}(\text{CO}_3) \cdot 3\text{H}_2\text{O} = +1.000\text{Mg}^{+2} + 1.000\text{CO}_3^{-2} + 3.000\text{H}_2\text{O}$	-4.67
Lansfordite	$\text{MgCO}_3 \cdot 5\text{H}_2\text{O} = +1.000\text{Mg}^{+2} + 1.000\text{CO}_3^{-2} + 5.000\text{H}_2\text{O}$	-4.54
Aragonite	$\text{CaCO}_3 = +1.000\text{Ca}^{2+} + 1.000\text{CO}_3^{-2}$	-8.34
$\text{CaCO}_3 \cdot \text{H}_2\text{O}$ (s)	$\text{CaCO}_3 = +1.000\text{Ca}^{2+} + 1.000\text{CO}_3^{-2} + 1.000 \text{H}_2\text{O}$	-7.14
Calcite	$\text{CaCO}_3 = +1.000\text{Ca}^{2+} + 1.000\text{CO}_3^{-2}$	-8.48
Vaterite	$\text{CaCO}_3 = +1.000\text{Ca}^{2+} + 1.000\text{CO}_3^{-2}$	-7.91

After modelling, Saturation Index (SI) is a determination of the precipitates existence in the equilibrium.

$$\text{SI} = \log_{10} (\text{IAP}/\text{K}) \quad (\text{Equation 2. 50})$$

Where IAP is ion activity product; and K is equilibrium constant (K=activity product/activity coefficient).

When $\text{SI} < 0$, minerals dissolve and the dissolution rate > precipitation rate. When $\text{SI} = 0$, the solution reaches equilibrium, i.e., dissolution rate = precipitation rate, and when $\text{SI} > 0$, minerals precipitate, i.e., dissolution rate < precipitation rate.

Both models are used to estimate the potential precipitates by identifying the Saturation Index. It can be concluded that PHREEQC has a wider application but is limited to room temperature simulations, so Visual Minteq is substituted instead at 40°C in a diluted solution. The Sit database (Table 2.7a) is selected together with PHREEQC for its relatively complete database of elements and for its limited constraints during operation.

2.14 Missing Gaps for Research Design

As reviewed, Portland cement is an energy intensive process; alternative MgO cement is utilised to reduce the carbon emission. Current manufacturing procedures of MgO are from either magnesite ore or seawater extraction. Considering UK and most of the European countries' geographic locations, seawater and reject brines are thought to be good resources. However, the conventional industrial process through $\text{Mg}(\text{OH})_2$ intermediate

suffers from impurities and the solid-liquid separation of magnesium hydroxide suspension due to its small particle sizes and gelatinous properties. In comparison, magnesium compounds through magnesium carbonates production have a better purity level and filtration convenience. In this study, innovative carbon dioxide is added from the first stage to achieve carbon mineralisation storage and utilisation target at the same time.

Traditional chemical reactions and their influential parameters in magnesium carbonates, calcium carbonates, magnesian calcites production, as well as their corresponding heating stages, have been carefully summarised and evaluated in this chapter. In view of the current research, there is a need at the moment to fully understand the reactions between constituents in seawater and CO₂ participation, as well as their calcination products. Previous studies have mainly assessed pure chemical processes by using simple reagents, which is not as complex as the experiments in this research. Therefore the current research gaps in developing reactive MgO through carbonation are outlined below.

There is lack of understanding of magnesium carbonates' formation in both sodium hydroxide and CO₂ systems at a controlled pH level, particularly in sophisticated pH adjustment studies and reaction kinetic studies. A better understanding of magnesium carbonates will not only facilitate the interpretation of precipitate phase crystallisation and transformation, but also provide a solid foundation for subsequent multiple ions systems. The innovative reactions in calcium carbonates have not yet been fully addressed by other researchers. Although some authors have explored the generation of typical calcites, the addition of CO₂ in this process is novel. Particularly during the test of chemical reactivity after calcination, magnesia citric acid is substituted in this novel research rather than using the traditional slaking rate method, in order to keep the consistency. In Chapter 4, the analysis of this individual calcium element helps to improve the understanding of the brine system.

Magnesian calcites have been explored to some extent mainly in seawater sedimentary minerals. However, there is lack of applications in industrial manufacturing, and anthropogenic chemical reactions. This study proposes the chemical transformation mechanism and a new chemical optimisation process.

Inorganic impurities, such as F^- , Na^+ , K^+ , Sr^+ etc., within magnesian calcite have been previously investigated from literature. However they are less researched in seawater and brine. Hence this novel research will aim to fill the gaps of the existing findings.

All the produced carbonates and their calcination processes need further improvement to fulfil the conditions of various heating temperatures and their resulting reactivity.

Hence this thesis will focus on sustainable MgO production from waste magnesium resources, such as reject brines or seawater, through carbon sequestration, to provide a comparably low carbon manufacturing process. The produced minerals are further calcined and utilised in the construction materials' industry. The entire system is a closed loop to achieve environmental optimisation and efficient productivity.

Chapter 3: Materials and Experimental Methodology

3.1 Introduction

This chapter introduces all the materials used during the experiments and the experimental methodologies. Firstly, the experimental materials are described according to their physical properties and chemical compositions. Secondly, the apparatus settings are demonstrated along with a description of the operational procedures. Next, the experimental processes are illustrated in detail, as they form foundation for the results Chapters 4, 5 and 6. Finally the analytical measurements are presented, including pH and the temperature indicator, ICP-OES, XRD, SEM-EDX, TGA and a reactivity test, while test for chemical and physical aspects, to confirm the data and thoroughly analyse to the obtained products. Overall, this chapter provides detailed explanations for the full project and its methodology.

3.2 Materials

3.2.1 Chemical Reactants

Preliminary ammonia trials were developed from Mignardi et al. (2009) and Hassan (2013), to further investigate the impact of variables, particularly the controlled pH effect. Considering availability, operation safety, and cost, ammonia is substituted by NaOH in the main experiment subsequently. Other major components CaCl₂, NaCl, and KCl in brine/seawater and their mixtures are further investigated, to study both individual and combined phenomena in this novel system. The carbonation process can occur under ambient conditions; whereas the calcination part requires a high temperature operation in furnace. In a well-controlled process, the by-product CO₂ and the mixed NH₄⁺ in the preliminary experiments can be recycled back to assist the first procedure of the reaction, which will avoid the further environmental pollution.

All pure chemicals displayed in multiple systems are employed, based on the requirements of chemical process, including MgCl₂•6H₂O, NH₃•H₂O, CaCl₂, NaOH, NaCl, KCl and CO₂; as well as anhydrous citric acid, bromothymol blue indicator, and fisher produced commercial CaO. The chemical and physical properties of those materials provided by manufactures are presented in [Table 3. 2](#). All materials except CO₂ are supplied by Fisher Scientific, UK, in

laboratory reagent grade. While CO₂ (g), stored in a cylinder, is supplied by BOC, with a purity level 99.5% and molecular weight 44.

3.2.2 Magnesium Oxides

Two different standard MgOs were utilised in this experiment as references: N50, and RBH 92-200, originally manufactured from seawater and magnesite ores respectively, to compare the effect of reactivity from diverse production routes. The chemical compositions and physical properties of MgOs as well as their corresponding reactivities (citric acid method) provided by suppliers are summarised in [Table 3. 1](#).

Table 3. 1: The chemical compositions of commercial MgO

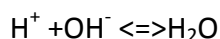
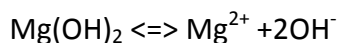
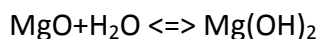
Composition/Property	N50 (Brine)—(Source: Lehmann&Voss)	RBH 92-200 (Magnesite Ore)—(Source: RBH, UK)
MgO	97.5%	91.5%
CaO	1%	1.6%
Fe	0.07%	--
SO ₃	0.85%	--
SiO ₂	--	2%
R ₂ O ₃	--	1%
Cl	0.2%	--
Mn	0.006%	--
Insoluble in HCl	0.1%	--
Loss on drying	1%	--
Loss on ignition	8%	4%
Average particle size	3um	--
Citric acid reactivity (s)	10	150

The citric acid reactivity test conducted at a room temperature was used to assess the reactivity of the magnesium oxides as well as the other alkaline oxides. The chemical reactivity test is operated to measure the time required to neutralise an acidic solution using MgO or CaO or combined dolime, together with a pH indicator to compare the various produced chemicals' reactivity. The method was firstly applied by the magnesia industry to evaluate the quality of MgO, but developed into more diversified segments in this exploration, in order to keep consistency.

Table 3. 2: Materials used during the experiments

CAS	Chemicals	Physical Form	Purity Level	Formula Weight (g/mol)	Density (g/cm ³)	pH	Melting Point (°C)	Water Solubility (g/l at 20°C)	Boiling Point (°C)
7791-18-6	MgCl ₂ •6H ₂ O (s)	Powder, Solid	≥ 99.9%	203.3	1.56	4.5-7	117	543	1412
10043-52-4	CaCl ₂ (s)	White powder	>95%	111	2.15	8-9	772-775	745	1935
1310-73-2	NaOH(s)	Solid	>95%	40	2.13	14	318	1110	1390
7647-14-5	NaCl (s)	Solid	≥ 99.9%	58.44	2.17	5-8	801	359	1461
7447-40-7	KCl (s)	Solid	≥ 99%	74.55	1.98	6	770	25.39% (20°C)	1420
77-92-9	C ₆ H ₈ O ₇ (Citric acid anhydrous)	Solid	≥ 99.5%	192.13	1.67	1.7	153	1477.6	310
1305-78-8	CaO	Powder, Solid	≥ 99.95%	56.08	3.34	12.5	2570	Reacts to form Ca(OH) ₂	2850
1336-21-6	NH ₃ •H ₂ O (aq)	Liquid	25%	35.05	0.91	12	-57.5	Miscible	37.7
34722-90-2	Bromothymol Blue	Liquid	0.04%	624.38	1.25	6 (Yellow)- 7.6 (Blue)	202	Sparingly soluble	N/A

The shorter time for neutralisation corresponds to a higher reactivity of alkaline oxides. Mechanism equations are seen as below; in a similar way, MgO can be replaced by CaO or mixed dolime:



There are several acidified tests in industry; however, taking amounts of the desired samples obtained after 800°C with 4h calcined time, citric acid methodology was selected, because of its low dependence on the sample's weight. In order to rationalise the results, for practical operation, products with ground 250 µm particle sizes were conducted in sequence.

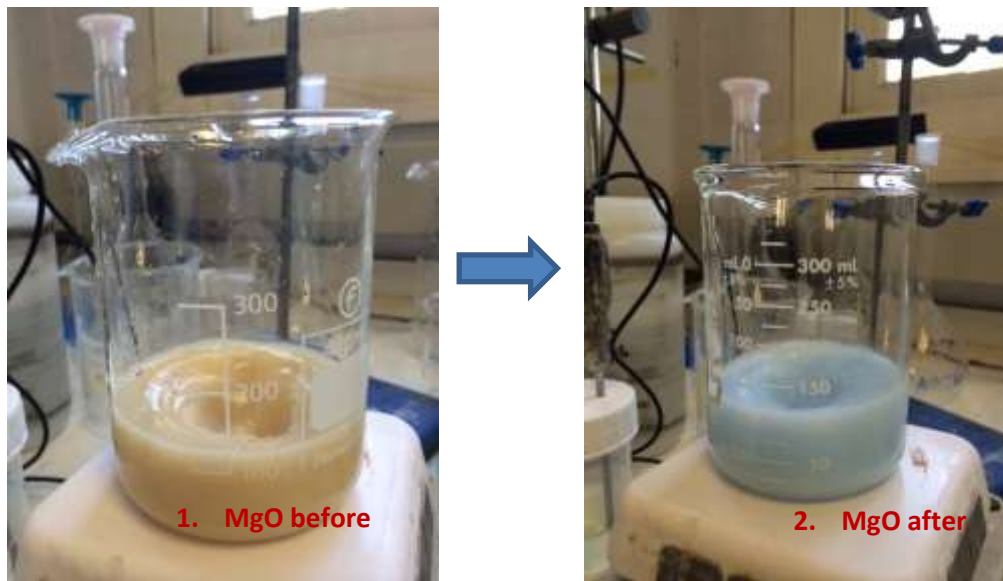
The procedures of reactivity citric acid testing is firstly to weigh 2g sample of MgO or CaO or dolime into a beaker, and then take 100ml citric acid and 0.3ml bromothymol blue indicator. Finally the solution is mixed up, together with a time recorded for colour changes from yellow into light blue (**Figure 3. 1**). The change in colour indicates the completion of neutralisation. MgO's colour is darker than dolime due its impurities.

3.3 Apparatus Settings and Operational Procedures

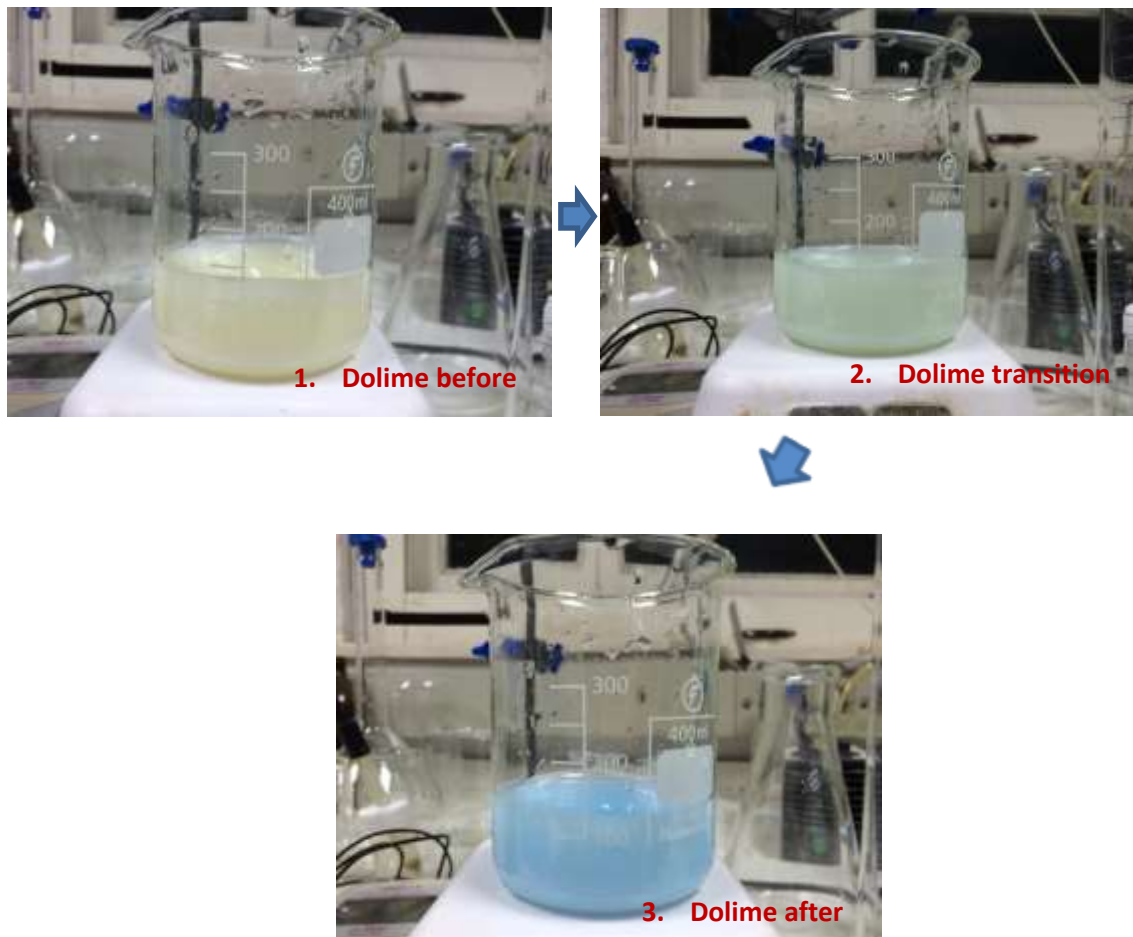
Equipment was set up in several ways based on the operational needs. The main sections are carbonation and calcination, including the pre-treatment of products before the physical and chemical analytical measurements.

3.3.1 The Production of Carbonates

This carbonation work is conducted to investigate the effects of various parameters, such as temperatures, initial reactant's concentration, stirring speed, pH, and CO₂ flux rate. In order to achieve the objectives mentioned above, ammonia/NaOH was added into the solution through a rotational pump, to control the pH level; magnesium chloride solution was placed on a hot plate, to provide a stirring speed with a magnetic stirrer together and temperatures; and pure CO₂ was infused into the solution through a sparger, to deliver smaller CO₂ bubbles and control its flux rate. The whole operation was carried out in a fume hood. The outline of the apparatus and photograph are presented in **Figure 3. 2**.



(a): MgO reactivity test



(b): MgO-CaO binary system reactivity test

Figure 3. 1: Citric acid reactivity test: (a) MgO test; (b) Dolime test

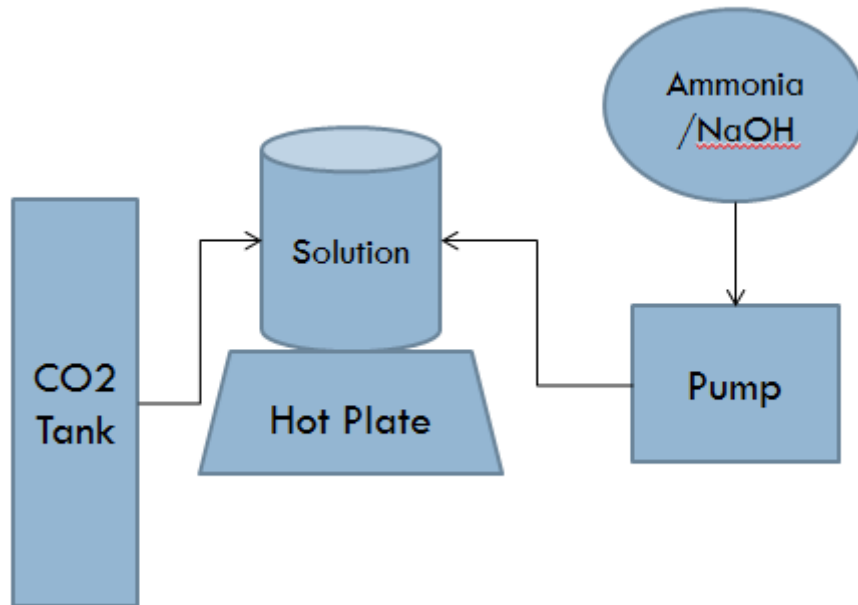
The reactants were firstly added to a beaker, which was placed on a hot plate with a magnetic stirrer. If the reaction requires heating, the hot plate works to the desired temperature in solution. Subsequently, the CO₂ and the alkaline solution were infused, accompanied by an agitation based on the experimental design. pH was controlled manually when required. During the reaction process, it is important to record the pH and temperatures at regular intervals. Finally, the precipitates were collected, filtered and washed with deionised water. For safety, in preliminary ammonia involved experiments, the whole setup is operated in a fume hood, while NaOH can be conducted on a bench.

Precipitates obtained during carbonation process need to be filtrated for further analytical tests. To facilitate the liquid solid separation, it was centrifuged at 3,000-4,000 rpm for 3 min; a conventional filtration process was then operated by using a paper filter to isolate two phases of the products. A vacuum pump was connected to liquid collecting flask for air extraction, to enhance the filtration efficiency. Afterwards, solids were washed with deionised water to remove the remaining impure ions, and dried in an oven at 35°C till constant mass was achieved ([Figure 3.3a](#)). This temperature ensured the drying efficiency and avoided mixed nesquehonite decomposition.

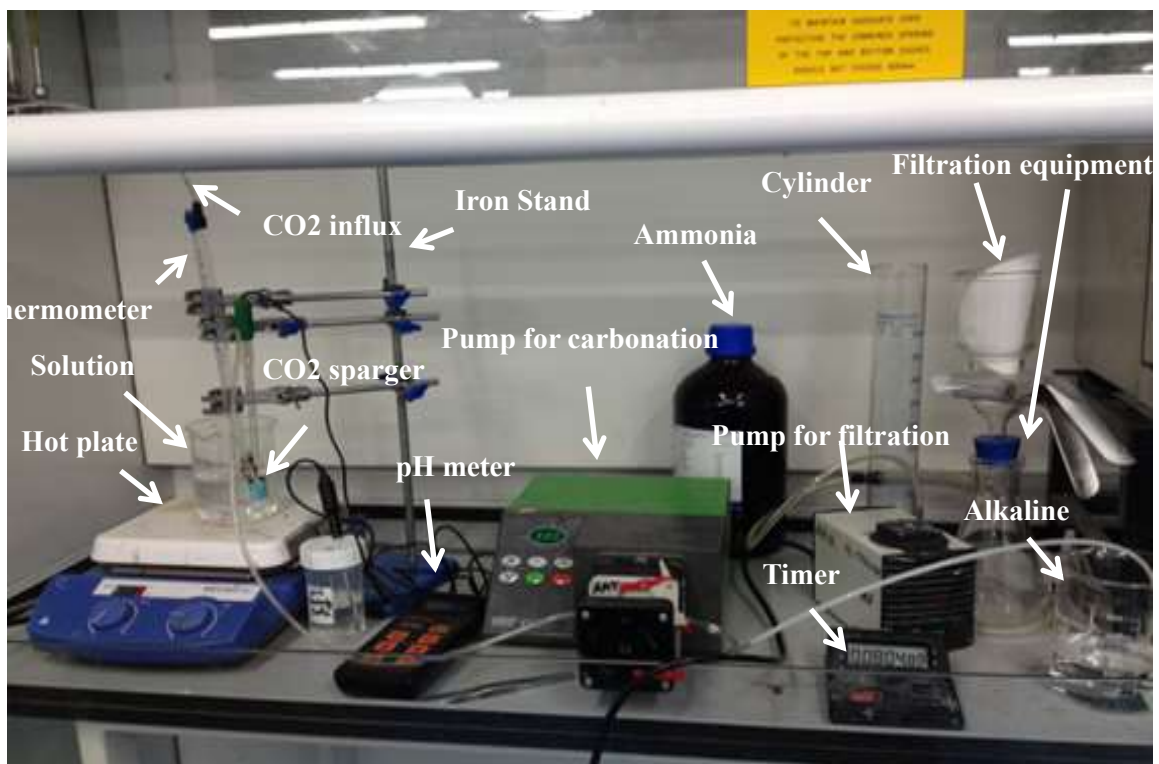
3.3.2 The Production of the Oxides

The other target for this study is to produce MgO; the light-burned threshold temperature of magnesia is 700°C. In order to achieve this high heat, a Carbolite furnace, shown in [Figure 3.3b](#) is used, heating at a constant rate of 10°C/min to 800°C with a 4-hour retention time. Samples were then taken out after the oven naturally cooled down.

The next step for calcined oxides is to test their reactivities with citric acid. Neutralisation rate has significant effect on particle size; in order to ensure the uniformity of the results, all calcined samples are ground down to dimension <250 µm. This size proposed here is convenient for the operation as well as to guarantee the sufficient amounts for a reactivity investigation. The grinding process is completed by a mortar and pestle, followed by a sieve with a mesh size smaller than 250 µm ([Figure 3.3c](#)).

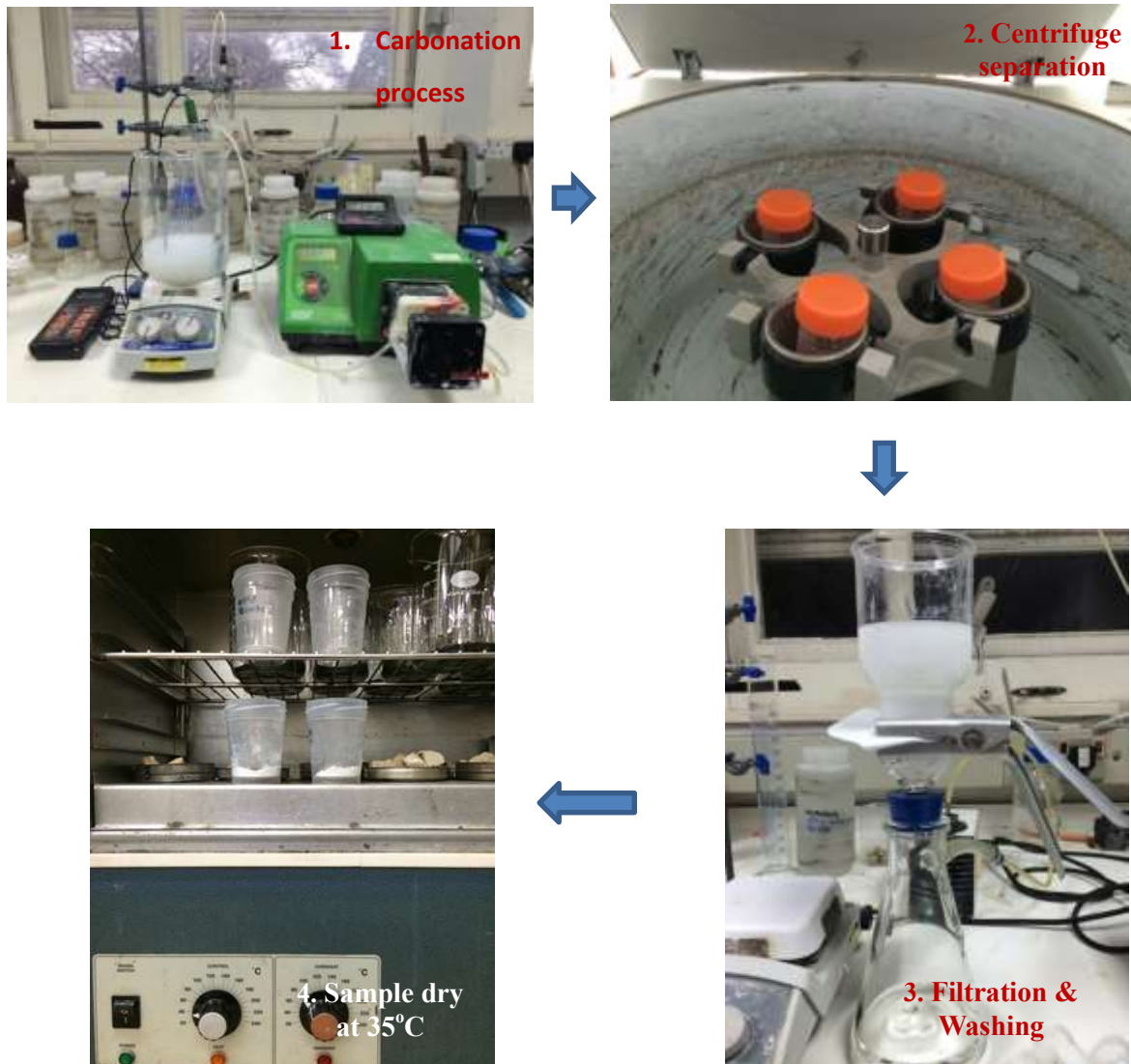


(a): An outline of the experimental apparatus



(b): A picture of the experimental apparatus

Figure 3. 2: Experimental apparatus: (a) An outline of apparatus; (b) A picture of apparatus



(a): The preparation of carbonates for further analytical measurements



(b): Furnace used in calcinaing HMCs



(c): The preparation of oxides for a reactivity test

Figure 3. 3: The preparations of carbonates (a) and oxides (b-c)

3.4 Experimental Procedures

In this section, detailed experimental procedures will be introduced, in preliminary trial tests, only carbonation studies were conducted, while in the main experiments, all studies were carried out. Some complementary information, elaborative data analysis method and relevant collecting points will be clarified later in Chapters 4, 5 and 6.

3.4.1 Carbonation Studies

This process is a key stage to produce desired sediments; therefore procedures were designed and operated carefully. CO_2 dissolution is considered to be a rate limitation step in the reaction, thus in order to enhance the whole efficiency, it was sparged into solution firstly until the pH is constant, ensuring the full saturation. This process will last around a few minutes. After that, alkaline solution (ammonia or NaOH), utilised to raise the pH for

precipitation, was pumped in through a rotational pump with CO₂ all together until a certain reaction time. The solution was gently stirred on a hot plate throughout the reaction, to improve the chemical dissolution and provide a homogenous system. The operations were carried out at an ambient temperature and an open system. pH and temperatures were recorded during the reaction.

Precipitates' nuclei formation and crystal growth increase with a longer time, so in the main experiments, another 1h was operated on the bench at a controlled pH level for the individual element ion, and 1.5h was studied for multiple elements. This time was thought as reasonable to get an amount of precipitates. In order to differentiate this reaction from the filtrate reaction mentioned below, it is called "bench reaction" (usually 1-1.5 hours), whereas the other is called "free reaction" (usually 1-3 days). The whole carbonation process is a prolonged reaction, continuing over days based on the different reactants' concentration; but in this report, carbonation studies refer in particular to the observations during the "bench study" and its consequential weight of precipitates. Typical "bench" and "free" carbonation studies are shown in [Figure 3. 4](#). The obtained precipitates are then be analysed by various analytical measurements.



Figure 3. 4: A typical bench reaction when reactants addition in the first 10min (left);

Bench reaction without reactants addition in the rest of 50min or 80min (middle);

Free reaction after filtration for 1-3 days or a longer time (right);

3.4.2 pH Stability and Adjustment Studies

pH stability is an essential element in this experiment, as a result, liquid obtained (filtrate) after filtration process was monitored at an ambient temperature and pressure over a

period of 1-3 days as a “free reaction”. These filtrates were stored in a closed system, which only indicated the primary effect of initial buffer solution used $\text{NH}_3\cdot\text{H}_2\text{O}$ and partially formed buffer solution $(\text{NH}_4)_2\text{CO}_3$ during the reaction, without atmospheric CO_2 influences. This closed system altered into an alkaline NaOH condition in the main experiment and mixed multiple ions system subsequently; however the operating target was the same as before.

This stability test was used to monitor the constancy of pH during the reaction. The test was performed with two groups under a room temperature: one group comprised of regular samples collections and pH recordings at a particular interval, while the other group was for pH adjustment studies when the pH dropped out of a standard range (standard $\text{pH}\pm 0.1$). According to the primary ammonia study of reaction, several main experiments with NaOH were also conducted later on in the stability studies.

The pH stability test was operated under an ambient temperature and pressure over 1-3 days, aiming to provide a controlled experiment, hence to further understand pH effect over time. The filtrates were stored in a closed system as mentioned above without atmospheric influence, and then to readjust back to a certain standard pH level by using $\text{NH}_3\cdot\text{H}_2\text{O}$ when the solution was out of the designed standard range (standard $\text{pH}\pm 0.1$). As the NaOH and ammonia had the same effects on final products and solution phenomenon, particularly from the preliminary study, showing no significant differences in sequestration efficiency, so there was no further adjustment studies in the NaOH main's and multiple ions' experiments.

3.4.3 Reaction Kinetic Studies

Reaction kinetics, also known as chemical kinetics, is the study of rates of chemical processes, involving different experimental influences on the speed of a chemical reaction, and its resulting yield information, as well as the mathematical models construction that can depict the characteristics of a reaction. The main factors include: the physical state of the reactants, the concentration of reactants, the temperature involved, and catalysts used in the reaction. These parameters affecting the carbonation process have been described in the literature review and some of the experimental design. It is a general whole concept to describe a reaction, but in this experiment, the reaction kinetics studies mainly concentrate on the continuing carbonation process over time in “free reaction” and its resulting magnesium sequestration efficiency. Samples were collected from filtrates at the same time

as pH stability tests, at intervals over 1-3 days, and acidified using HNO_3 (70%) to prevent further reaction. Therefore the result accurately described the metals' concentration at a specific time. The solution was then diluted and ready to be used in ICP to quantify the metals' (Mg^{2+} , Ca^{2+} , Na^+ , K^+) concentration left in the aqueous phase. In the preliminary experiment, ammonia proved to obtain sufficient precipitates within one day; hence in the main experiments, all samples were collected within 24 hours.

3.4.4 Calcination Studies

The calcination temperature is a main factor affecting the surface area and the reactivity of MgO. Calcination at 800°C with 4h duration was first referenced by Cheng and Li (2009) and Wang et al. (2008), and subsequently used by Dijihan (2013). The experiments were mainly operated at 800°C , followed by additional light-burn at 650°C and hard-burn at 1000°C , to study the influences of differentiated heating profiles. Typical samples of before and after calcination are shown in [Figure 3. 5](#). It can be observed that carbonates are colloidal at first but shrink into aggregated blocks after heating due to the weight loss of dehydration and decarbonation.



Figure 3. 5: Carbonates with colloidal property before calcination (left), oxides with aggregated chunks after calcination (right).

3.5 Analytical Measurements

Analytical measurement is a professional evaluative approach to identify the materials and their compositions. For this project, a pH indicator and thermometer are utilised during the carbonation aqueous phase reaction, where HANNA HI8424 is used and calibrated by standard buffer solutions on pH 4 and 7 before every usage, guaranteeing a sustainable pH

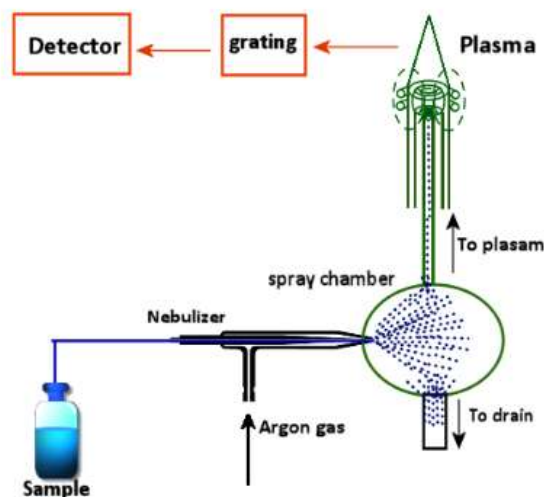
balance. Other machines, such as ICP-OES, XRD, SEM-EDX, and TGA/DTA, are operated for the obtained precipitates and solutions.

3.5.1 Inductively Coupled Plasma-Optical Emission Spectrometry (ICP-OES)

ICP has been widely accepted for inorganic analysis, compared to traditional atomic absorption spectrophotometers (AAS), the excitation temperatures of ICP by argon gas can reach up to 5000 to 7000K, compared to air-acetylene flame in AAS with 2000 to 3000K only. Higher excitation temperature has better capacity in multiple elements diagnosis, and inert gas (argon) reduces the oxidisation and nitration efficiently.

The working mechanism of an ICP-OES is from the external plasma's excitation on the analysed atoms, when these excited samples return to low energy state, light rays (spectrum rays) are emitted and corresponding photon wavelengths are then recorded. The element type is identified according to the wavelength, while the composition of each element is determined based on the rays' intensity. In order to produce plasma, argon gas is connected to a torch coil, and high frequency electric current is utilised to the coil at the end of torch tube, which generates the electromagnetic field to ionise argon gas for plasma preparation. This type of plasma has high electron density and temperature (1000K), which is implemented in the samples' excitation. Solution samples are injected into the plasma in an atomised state through the narrowed center of torch tube ([Figure 3. 6a](#)).

In this test, ICP was employed to determine the metals' concentration (Mg^{2+} , Ca^{2+} , Na^+ , and K^+) left in the solution. Calibration samples were from Fisher and Sigma Aldrich with 1000ppm initial concentration, which was subsequently diluted to 0.1ppm, 1ppm, 10ppm, and 100ppm. Measured samples were taken at certain intervals and acidified using HNO_3 (70%), then diluted maximum 1000 times to be tested in the range of 0.1ppm to 100ppm. Before the operation, samples were collected by a syringe, and then injected through a 0.2 μm pore size PVDF membrane filter, to avoid the suspended solids blockage for equipment.



(a): The diagram of working principle on ICP-OES (Chemias FT, 2017)



(b): ICP-OES equipment



(c): Typical acidified samples for ICP testing

Figure 3. 6: ICP working mechanism (a) and operation (b-c)

3.5.2 X-Ray Diffraction (XRD)

X-Ray Diffraction (XRD) was employed to study crystal structures and atomic spacing, in order to further define the precipitates' composition, which relies on the constructive interference of monochromatic X-rays and crystalline samples. These X-rays are created by a cathode ray tube, filtered to generate monochromatic radiation, collimated to concentrate and then head towards the sample. The interaction of instant rays and the sample diffracted pattern or spots satisfies Bragg's Law ($n\lambda=2d \sin \theta$). This law counts the wavelength of electromagnetic radiation to the diffraction angle and the lattice spacing in the crystals. The reflected X-rays are then detected, processed and counted. At the high purity level of samples, X-ray diffraction can determine the mean chemical bond lengths and angles within

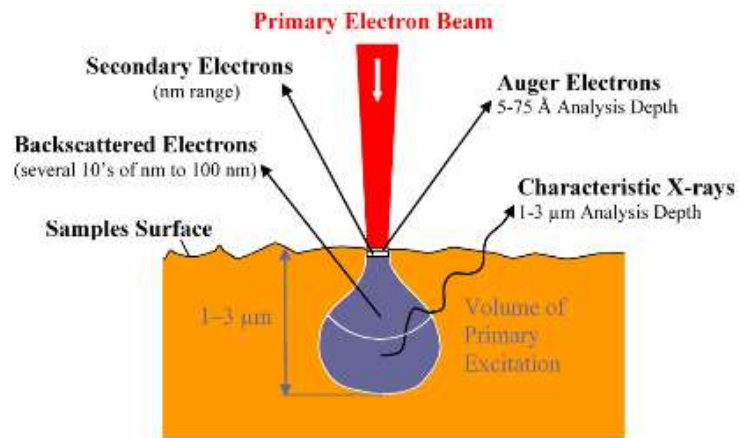
the thousands of recorded samples' databases. During the experiment, the samples were obtained by vacuum-drying, grinding and sieving of representative material to less than 600 μm . The analysis was performed using a powder diffractometer Bruker D8 Advance, Bruker AXS Inc., Madison, WI, with a Cu $K\alpha$ source operating at 40 kV and 40 mA (Figure 3. 7), emitting radiation at a wavelength of 1.5405 Angstroms. XRD samples were prepared by grinding and sieving through 75 μm pore sizes. XRD patterns were operated from 5° to 60°, where most of the related compounds exist; and operation 2 θ value was at the rate of 0.05° per step with a 1s per step counting time.



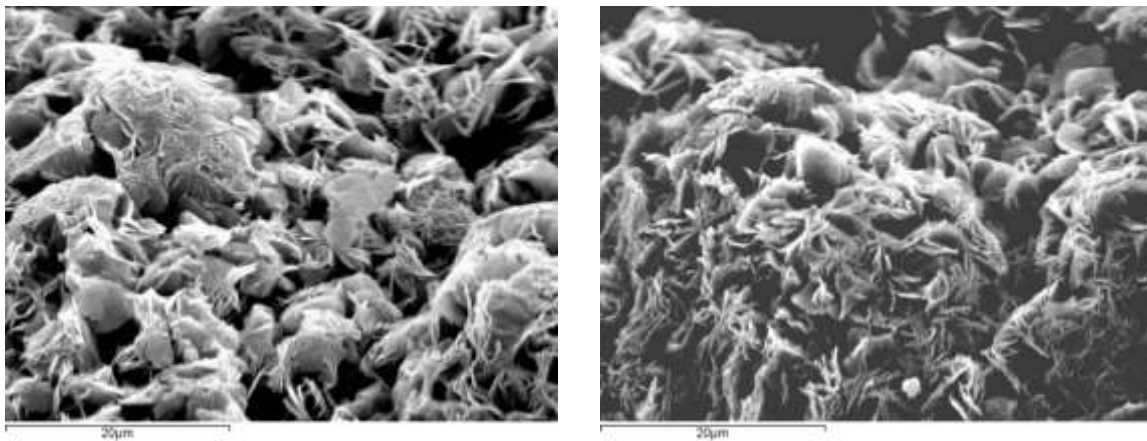
Figure 3. 7: XRD equipment

3.5.3 Scanning Electron Microscopy-Energy Dispersive X-ray spectroscopy (SEM-EDX)

SEM-EDX is the most recognised and popular-used of the fracture surface analytical techniques. High resolution images for superficial topography, with prominent depth of area, are generated by a highly-concentrated, scanning (primary) electron beam. This Initial beam then results in a number of different waves when contacting with particles surfaces, including secondary electrons, back-scattered electrons, X-rays, photons, and auger electrons etc. Secondary electrons and back-scattered electrons are for imaging while the characteristic X-rays presents the chemical information of the emitting atoms. Further explanations about those three are described below.

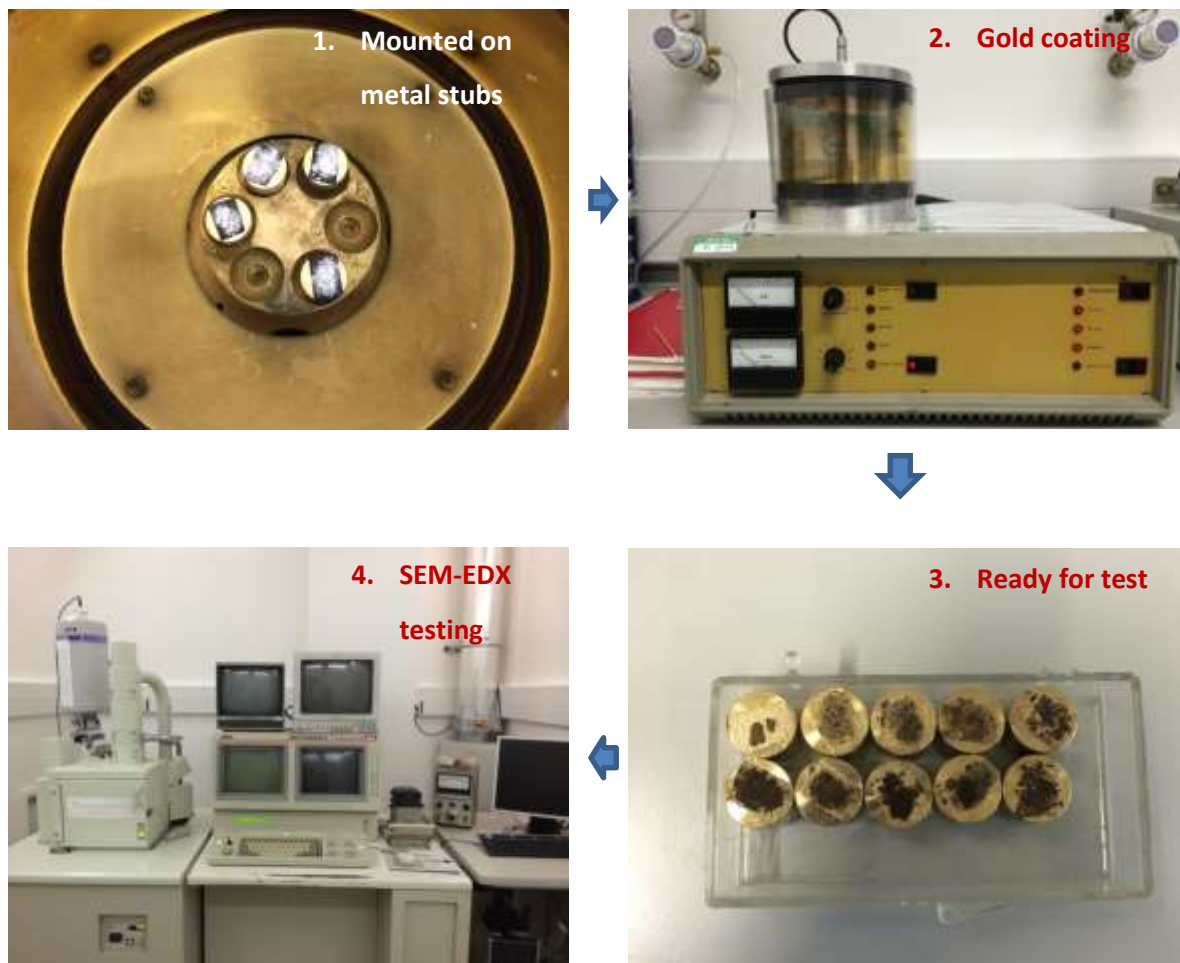


(a): SEM electrons working mechanism (SURF, 2017)



(b): Same samples (Mg4) using secondary- image (left), backscattered (right)

The primary electrons have access to a surface with an energy voltage of 0.5-30kV and produce low energy secondary electrons, while the intensity of these secondary electrons is determined by the surface topography of the sample. An image of the sample surface is then fabricated by quantifying secondary electron intensity as a function of the position of the scanning primary electron beam. A high spatial resolution is promising due to the small area that primary electron beam focuses on (<10nm). High sensitivity to topographic structures on the outermost surface (<5nm) can be reached even when using a primary electron beam with an energy <1kV. A typical pictures produced by secondary scanning is seen in [Figure 3. 8a](#).



(c): SEM-EDX operation procedures

Figure 3. 8: SEM-EDX working mechanism (a), secondary and back-scattered images (b) & operation procedures (c)

Besides low energy secondary electrons, backscattered electrons and X-rays are generated by primary electron bombardment. The intensity of backscattered electrons can be linked to the atomic number of elements within the sampling volume, meaning the deeper permeation of the samples compared to secondary beams. Hence, some qualitative elemental information can be achieved by this scan; however, backscattered pictures are normally darker with higher energy intensive to produce the electron beams, compared to secondary, thus it is not recommended unless necessary (Figure 3. 8b).

In addition, the analysis of characteristic X-rays (EDX) released from a sample provides more quantitative elemental information. Combined SEM-EDX analysis delivers a generally rapid, inexpensive, and fundamentally non-destructive approach to surface analysis. It is often

used to monitor surface analytical problems before proceeding to techniques that are more surface-sensitive and dedicated.

In this experiment, the microstructure of precipitated samples was examined by optical microscope JOEL-5800 (**Figure 3. 8c**), targeting to analyse samples through magnifying 1000x, 3000x, and 5000x with accelerated 15kV. Moreover, EDX was also widely used for selected samples. The taken images are then compared with the normalised micro-graph to identify the components, together with EDX and XRD multiple verifications. Before placing the holder into SEM, samples are mounted on metal stubs and coated with a thin layer of gold by low vacuum sputter coating.

3.5.4 Thermo-Gravimetric (TGA)

TGA analysis is a widely-used analytical measurement in quantifying the hydration and carbonation degree of certain materials. It measures the alterations in the mass of a sample over a range of temperatures, to justify the component of a material or its thermal stability, up to 1000°C. Generally a sample loses weight when heated up due to decomposition, reduction or evaporation; while a sample can gain weight according to oxidisation or absorption. During the operation, TGA records weight variations via a microgram balance, when temperature is monitored via a thermocouple. Data is then graphed as weight percentage (%) vs temperature (°C).

The instrument used was a Perkin Elmer STA 6000 TGA controlled by Pyris software shown in **Figure 3. 9**. Samples were placed in a crucible and then heated in air at a rate of 10°C/min from room temperature to 800°C. Additional 1000°C calcination tests were run subsequently, to investigate the thermal process of various heating temperatures up to 1000°C. The change in mass of carbonated precipitates accompanied with increased heat, due to the loss of CO₂ and H₂O, was recorded to provide samples' qualitative and quantitative information for further analysis. It is essential to turn on water for machine cooling during the operation, and samples used for this investigation are the same as XRD ground particles.



Figure 3. 9: Perkin Elmer STA 6000 TGA (left); Samples used for both XRD and TGA (right)

Chapter 4: Individual Ion Carbonation and Calcination

4.1 Introduction

This chapter investigates the production of magnesium and calcium carbonates from magnesium and calcium chlorides respectively, before the dual-ion-system in Chapter 5. The production of magnesium carbonates is based on the successful work of Ferrini et al. (2009) and Hassan (2013). Hydrated magnesium carbonates (HMCs) are precipitated from the reaction of MgCl_2 and NH_4OH when sparging with CO_2 , according to the equation:



The preliminary tests and the series I tests used this method to prove the feasibility of the proposed novel study. However, considering the high costs and the undesirable production of ammonia, sodium hydroxide was substituted subsequently in the main experiment series II tests, to achieve long-term sustainability and cost-effectiveness. Finally calcium was examined to elucidate the reaction mechanism, on the basis of comprehensive literature reviews on calcium carbonates.

In all reactions, different factors were considered comprising of: stirring speed, pH, reaction temperature, initial reactants concentrations, and CO_2 flux rate. Further calcination was then undertaken at 800°C for 4h time in SII and SIII experiments. Particularly 650°C and 800°C were further employed to evaluate the various endothermal effects in Series II. All carbonates and oxides were analysed using XRD to determine the components, SEM to observe the morphology, ICP to quantify the remaining metal ions in the aqueous solutions, and thermal degradation (TGA) to examine the reaction products. Finally, the reactivity of the produced calcined products was tested in order to be compared with the commercial oxides.

4.2 Preliminary Trial Experiments

This primary test aimed to verify the apparatus setting and the production process, including the testing methods and mechanical analysis. Hence limited samples and stages were undertaken.

4.2.1 Experimental Design

Two different MgCl_2 concentrations were refined in order to identify the concentration effect. CO_2 flux rate varied from $50\text{cm}^3/\text{min}$ to $450\text{cm}^3/\text{min}$, and the $\text{NH}_3\cdot\text{H}_2\text{O}$ titration was achieved by a rotational pump, while the stirring speed for the solution was with a magnetic stirrer on the hot plate. **Table 4. 1** presents the detailed programme. Run time represents the reactants' addition time, and all other parameters are constant.

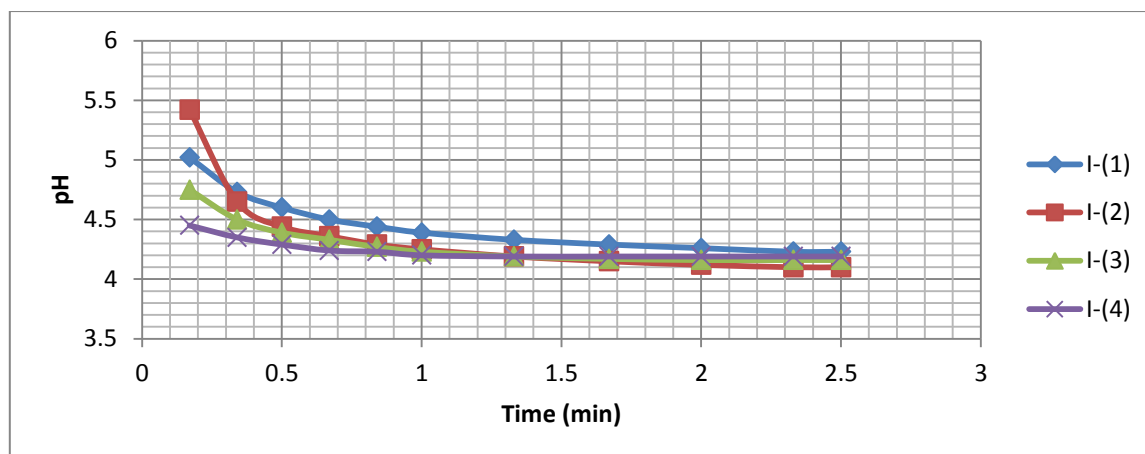
Table 4. 1: Preliminary experimental design

Sample	Solution Volume (ml)	Initial Mg^{2+} Concentration (mol/l)	CO_2 flux rate (cm^3/min)	Run Time (min)	NH_3 Titration Speed (rpm)	Stirring Speed (rpm)
PI-(1)	80	0.25	50	6	35	150
PI-(2)			150		35	
PI-(3)			250		35	
PI-(4)			350		35	
PII-(1)	80	0.5	50	6	35	150
PII-(2)			150			
PII-(3)			250			
PII-(4)			350			
PII-(5)			450			

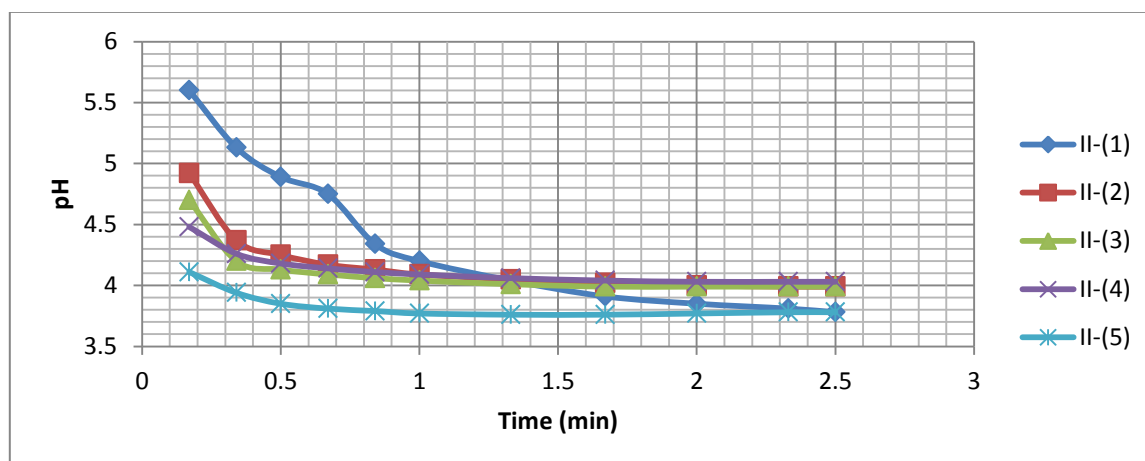
4.2.2 Carbonation Studies and Basic Analysis

4.2.2.1 The Effects of CO_2 Sparging on pH

The initial measured MgCl_2 solution pH range varied from 5 to 6.4, in agreement with the datasheet provided by Fisher Scientific. This was possibly caused by the different Mg^{2+} hydrolysis in an aqueous phase. To improve the overall reaction rate, CO_2 was flushed into the solutions prior to other additions until the pH became constant, providing stabilised fully saturated conditions. The pH was recorded every 10s within 1min, and every 20s after that. **Figure 4. 1** shows that the pH is almost steady after 2min, implying 2.5 min sparging time is sufficient for most of the solutions. In the end, $\text{pH}\approx 4$ is reached at CO_2 saturation. Temperature keeps constant during the procedure.



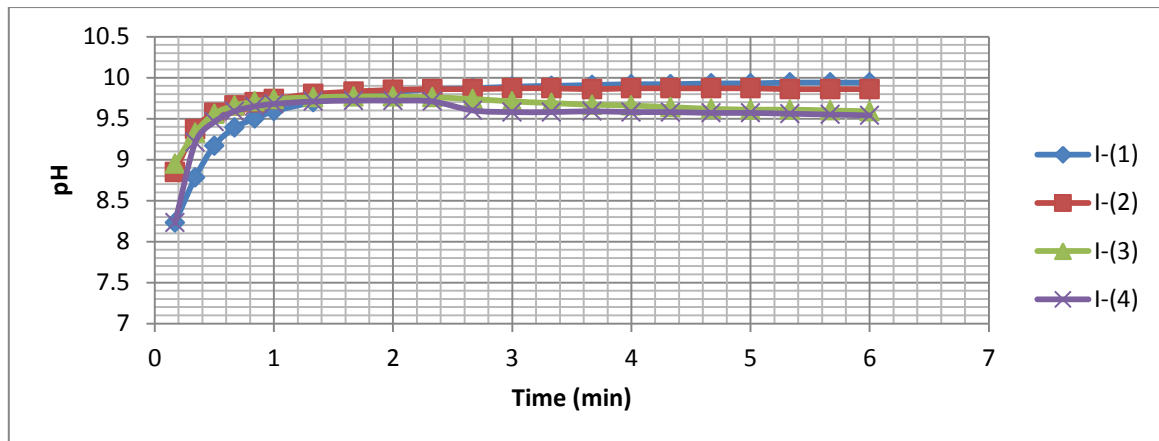
(a): Samples I for preliminary tests shown in Table 4.1



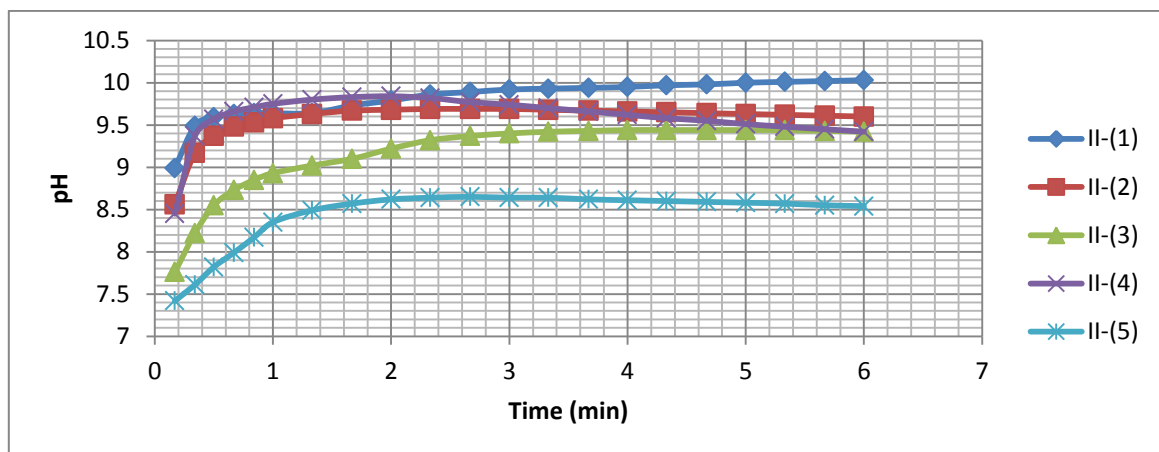
(b): Duplicated samples II for preliminary tests shown in Table 4.1

Figure 4. 1: The effects of CO₂ sparging on pH for the preliminary experiments shown in Table 4.1

Information on the dynamic pH values after $\text{NH}_3 \cdot \text{H}_2\text{O}$ addition, are shown in [Figure 4. 2](#). It is found that the pH rises up immediately within 1min after alkaline reagent diffused into the solution, and remains at a roughly constant level for the rest of time. A higher CO_2 flux rate usually has a lower pH profile in reaction, due to the acidic properties of dissolved CO_2 . The only exception II-(4) is attributed to the use of newly poured ammonia with less molecular decomposition. All solutions reach $\text{pH} > 9$ in the end, except for II-(5). The result is slightly different from Hassan (2013), who performed a similar process with maximum pH range from 8.5 to 9. This is caused by a much higher CO_2 flux rate utilised by the author.



(a): Samples I for preliminary tests shown in Table 4.1



(b): Duplicated samples II for preliminary tests shown in Table 4.1

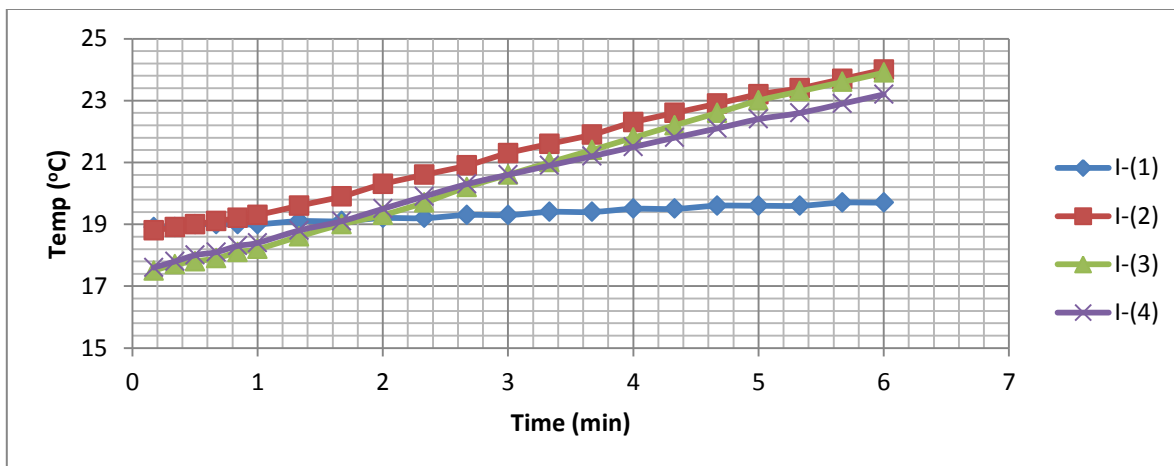
Figure 4. 2: pH stability vs time when ammonia addition for the preliminary experiments

4.2.2.2 Reaction Temperature

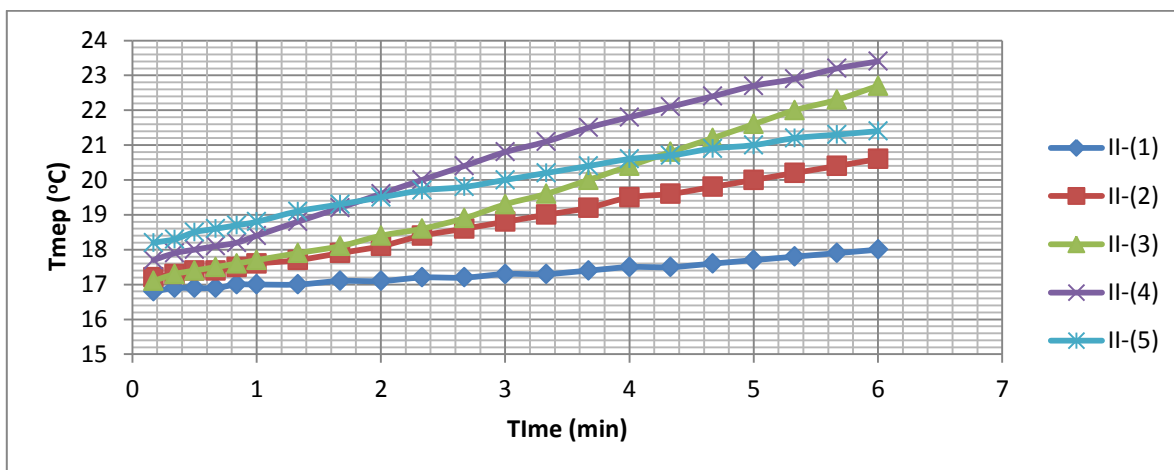
The experiment was operated at a room temperature, ranged from 16.7-18.8°C.

Temperature is a macroscopic manifestation of molecular motion. Faster molecular motion can generate more energy, presenting as higher temperature, whereas a slower one produces less energy and thus lower temperature. One indicator of exothermal reaction is increased temperature variations. [Figure 4. 3](#) illustrates the dynamic temperature profile during the reaction time, which has substantiated the reaction's exothermal properties, by an increased temperature. From a microscopic point of view, this can be attributed to the accelerated movements of molecules in solution when reactants infused, increasing the collision probabilities. It is obvious that a higher CO₂ flux rate tends to generate more heat,

but excess rate reverses this observation, as in the case of I-(4) and II-(5), where heat loss is seen with surplus CO₂.



(a): Samples I for preliminary tests shown in Table 4.1



(b): Duplicated samples II for preliminary tests shown in Table 4.1

Figure 4. 3: Temperatures vs time with ammonia addition for the preliminary experiments

4.2.2.3 The Quantification of Precipitates

The weight of precipitates is another indication of the reaction degree. Higher concentrated reactants can produce more precipitates under identical conditions within the same time scale (Figure 4. 4). Similar to the temperature variations, CO₂ flux rate has a role in optimising precipitates: in I-(x) series, the best performance appears at 150 cm³/min, followed by 250cm³/min; while in II-(x) series, best is at 250cm³/min and 350cm³/min. Flux rate over 450cm³/min is excluded from further investigations.

In this experiment, the starting concentration of Mg^{2+} equalling 0.25mol/l (=6g/l) was expected to yield 34.5g/l precipitates, supposing that all magnesium formed into nesquehonite, which the literature review depicted as the main product in the precipitates. This programme utilised 80ml $MgCl_2$ solution; hence the assumed total weight of sediments was estimated at 2.76g. Similarly, this figure was doubled to 5.52g with $Mg^{2+}=0.5mol/l$ initial concentration. As a consequence, the highest produced amount in each series I-(2) 1.73g, as well as II-(3) 2.51g and II-(4) 2.47g, accounted for 62.68%, 45.47% and 44.75% respectively of the total theoretical weight of the precipitates. This difference was attributed to the non-crystallisation of the sequestered element, operational error, or other mixed impurities and formations. Thus this method, through assuming the total weight of carbonates to evaluate the metal's sequestration level, is still ambiguous and can only provide a general indication of the metal's capture to some extent. Consequently, ICP is manipulated in the main experiments to provide more accurate measurements.

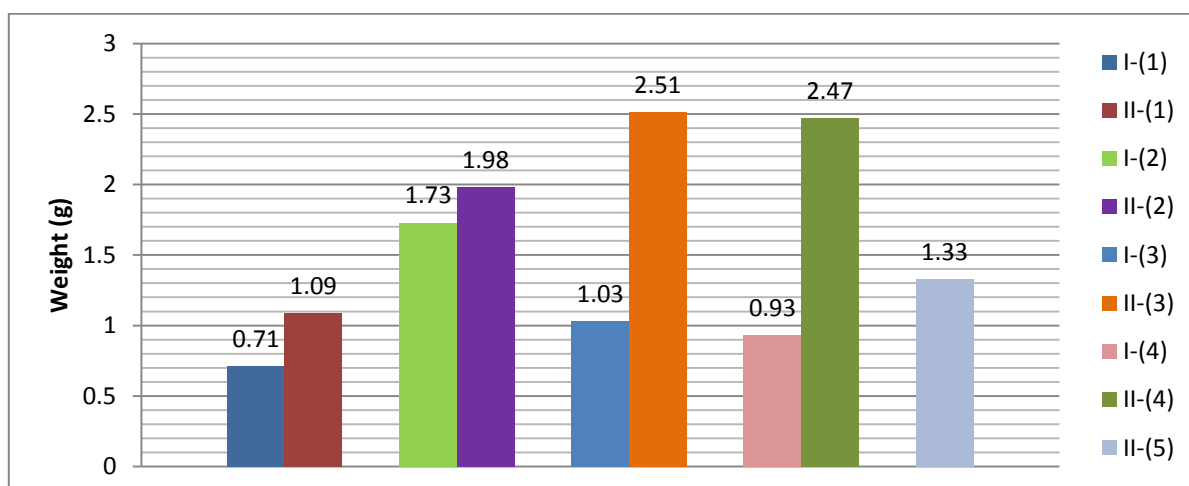


Figure 4. 4: The weight of precipitates for the preliminary experiments shown in Table 4.1

In conclusion, this process is an exothermic reaction, and pH is a determining factor of precipitates, when the majority of sediments are obtained at $pH > 9$, in accordance with the literature review. A higher concentration of reactants tends to generate more precipitates in total, but its efficiency of formation declines to some extent. This preliminary test has proved the apparatus and confirmed the validity of operational procedures.

4.3 Model Code & Experimental Design Mechanism for SI & SII

The modelling is elaborated in this section for magnesium carbonates formation in SI & SII. It uses the PHREEQC model of Sit.dat and the Visual Minteq model of Thermo.dat. They both were applied to solution-based chemical reaction, and performed as mutual verification.

In this chapter, three systems are considered: (i) ammonia engagement with MgCl_2 (SI); (ii) sodium hydroxide participation instead of ammonia with MgCl_2 (SII); (iii) sodium hydroxide solution with CaCl_2 (SIII). In SI system, input constituents consisted of 0.25mol/l MgCl_2 and 250cm³/min carbon dioxide, with the exception of ammonia due to its large molar concentration ($\text{NH}_4^+=26\text{M}$ in 25% Fisher Scientific ammonia solution) resulting in high ionic strength. This alkaline condition was illustrated by hydroxide ions addition in PHREEQC and fixed pH value in Visual Minteq. In SII, the input codes are 0.25mol/l MgCl_2 , and 1mol/l Na^+ , together with 500cm³/min carbon dioxide. Finally, in SIII, inputs are 0.5mol/l CaCl_2 , and 1mol/l Na^+ with the diffusion of 500cm³/min carbon dioxide. All three were run at an atmospheric pressure CO_2 and a room temperature under high alkalinity condition. Results focused on the saturation index parameter. When saturation index > 0.0 the selected phase can thermodynamically be found in the solid state; but the practical formation should be determined by the surroundings and experimental conditions.

Based on the findings of previous trial tests, experiments were carried out under constant pH control conditions for at least one day. During the reactants' additional time, the pH was maintained at a constant value throughout the reaction, which is a novel and different approach to that of others. Additionally, it has good indication to industrial practice, when the production of a certain precipitate under a desired pH level is required. Each series has a specific parameter design, which is elaborated in the following sections.

4.4 Series I-Individual Magnesium Ion System with Ammonia

4.4.1 Model for Series I

According to PHREEQC simulation the pH of the final solution is 9.902, which is an acceptable approximation considering the experiments variation from 9 to 10.5. In terms of the solid phase, the presence of brucite is thermodynamically favourable (SI = 0.22), which is consistent with the experimental results demonstrated below, agreeing with the literature.

The presence of nesquehonite is also expected; however, the calculated Saturation Index is -0.25, indicating its non-existence in the precipitates. That suggested its long-term conversion into other phases containing magnesium and carbonate such as artinite ($\text{Mg}_2(\text{CO}_3)(\text{OH})_2 \cdot 3\text{H}_2\text{O}$), magnesite and $\text{Mg}_5(\text{CO}_3)_4(\text{OH})_2 \cdot 4\text{H}_2\text{O}$, of which the calculated Saturation Indexes are 2.16, 3.57 and 6.25, respectively. It is also important to highlight that thermodynamic simulations can achieve the final equilibrium over a long period of time, while laboratory experiments are performed only in a limited timeframe.

At the same pH level, two more deposits are approximated in Visual Minteq, nesquehonite and lansfordite ($\text{MgCO}_3 \cdot 5\text{H}_2\text{O}$) besides other precipitates presented in PHREEQC. Both SI and SII studies share the same outcomes of modelling, because they both use the magnesium chloride solution.

4.4.2 Series I-Experimental Design

4.4.2.1 Experimental Parameters

Both sets of experiments (SI.I and SI.II) have the same operation programme, all the parameters are fixed except pH variables, displayed in **Table 4. 2**. While the data is selected from the literature and trial testing, explained in **Table 4. 3**. The reaction lasts for 1 hour.

Table 4. 2: Parameters in main experiments in series I

Solution Vol	Initial Mg^{2+} concentration	CO_2 flux rate	Stirring speed	Temp	Pressure
100ml	6g/l=0.25mol/l	250cm ³ /min	150rpm	Room temp, around 20°C	Atmospheric
The pH variables were 8, 8.5, 8.75, 9, 9.25, 9.5, 10, 10.3* (max); ± 0.1 .					

* The pH=10.3 is considered as a max, because max pump rate, 55rpm, is reached.

Table 4. 3: Parameters selection criteria

Parameter	Data	Reasons
Solution Volume	100ml	From preliminary result, this amount is sufficient to produce precipitates for analysis.
Initial Mg^{2+} concentration	6g/l=0.25mol/l	From preliminary result, this amount is sufficient to produce precipitates for the analysis. Also it is 1/10 of produced water in Rome (Mignardi, De Vito, Ferrini, & Martin, 2011) and 1/5 of subsurface

		brine water in the US (Shand, 2006).
CO ₂ flux rate	250cm ³ /min	From preliminary results, this flux rate demonstrates a relatively good performance.
Stirring Speed	150 rpm	It is to provide a gentle speed, avoiding solution splash and turbulence flow, which may dissolve carbonates nuclei reducing the rate of crystalline growth.
Temperature	Room	It is more economic and practical under a room temperature. However, other temperature ranges also need to be investigated further, to distinguish their effects. Temperature is considered as the second most important influential factor from the literature review.
Pressure	Atmospheric	It is more economic and practical at atmospheric pressure in industrial process. Also from the literature review, the majority of researchers studied carbonation process at an ambient pressure.

To reduce the systematic errors, the first set of experiments (SI.I) was duplicated, with 3-day and 2-day monitoring. Subsequently, error analysis was conducted based on both two days' data through calculating average values and its standard deviation. The majority of studies presented in Chapter 3 were reflected in this experiment; including carbonation process, pH stability, reaction kinetics, and precipitates analysis.

Based on the previous results (SI.I), one day experiments (SI.II) were then performed as a supplementary one with several selected typical pH values. Two investigations were duplicated, comprising of the pH stability study and reaction kinetics study. A pH adjustment study was added on the basis of earlier exploration, with one adjusted sample of three days observation. Carbonation process also exists in this reaction; however no recording occurred during the "bench study" in this set of tests, because of its primary one day pH monitoring target.

4.4.2.2 The Analysis of Precipitates

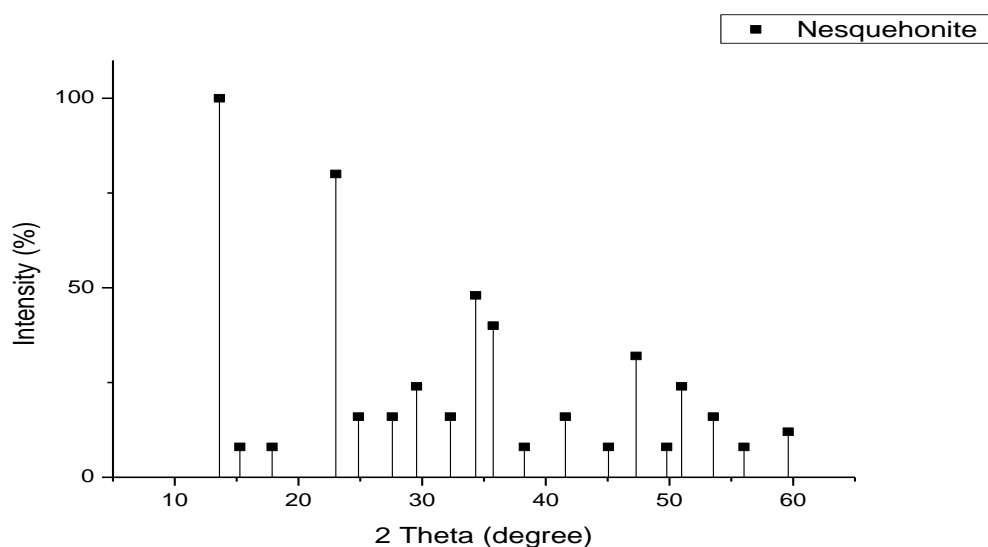
ICP: ICP is used to identify the metal ions left within the solution. Samples were collected from a half day to a maximum of one day. This was concluded from the preliminary trial test as an adequate time frame. Standard calibrations were 0.1ppm, 1ppm, 10ppm and 100ppm.

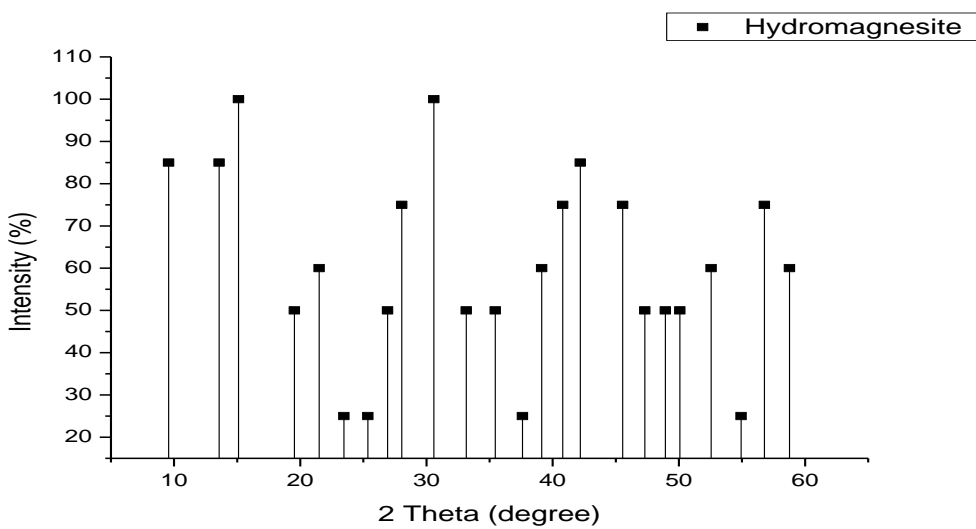
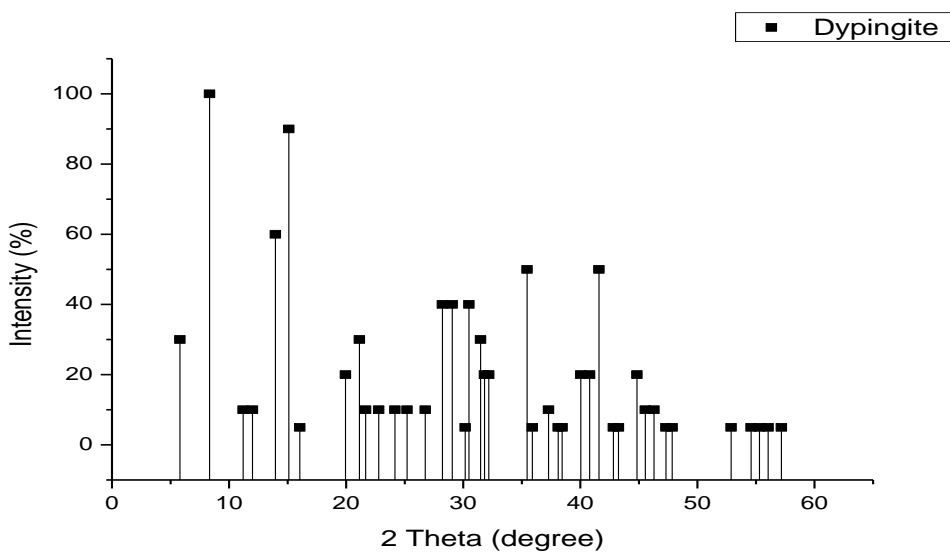
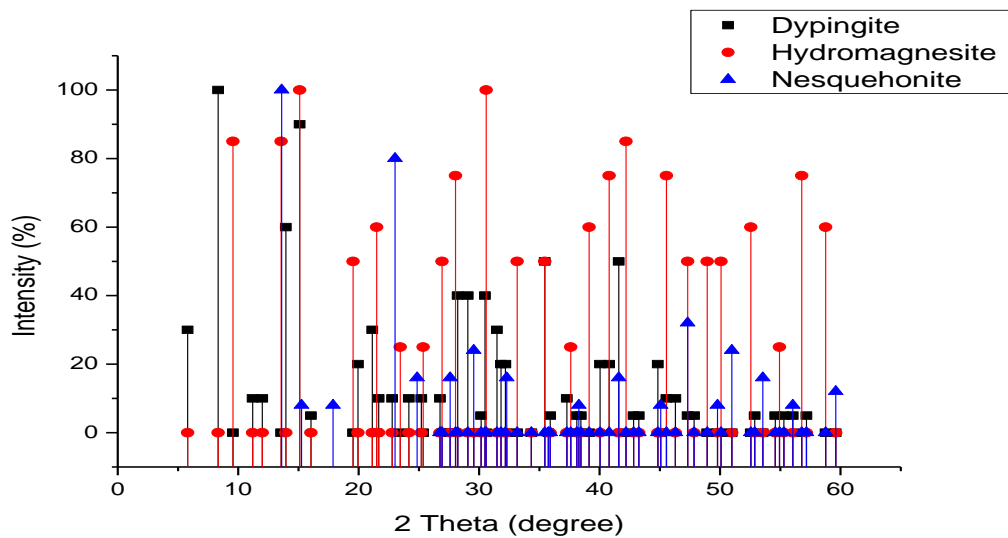
Further complemented data analysis was incorporated to obtain magnesium sequestration efficiency, and detailed kinetics was then carried out to account for the time effect.

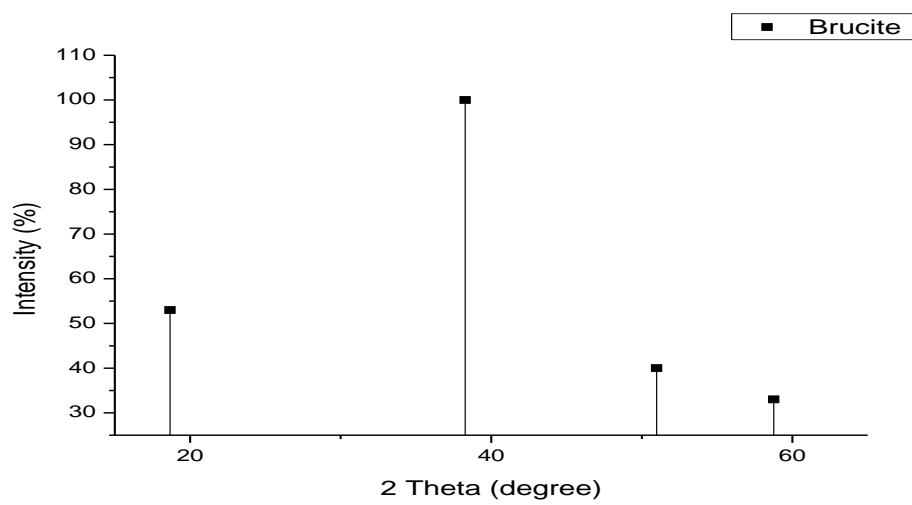
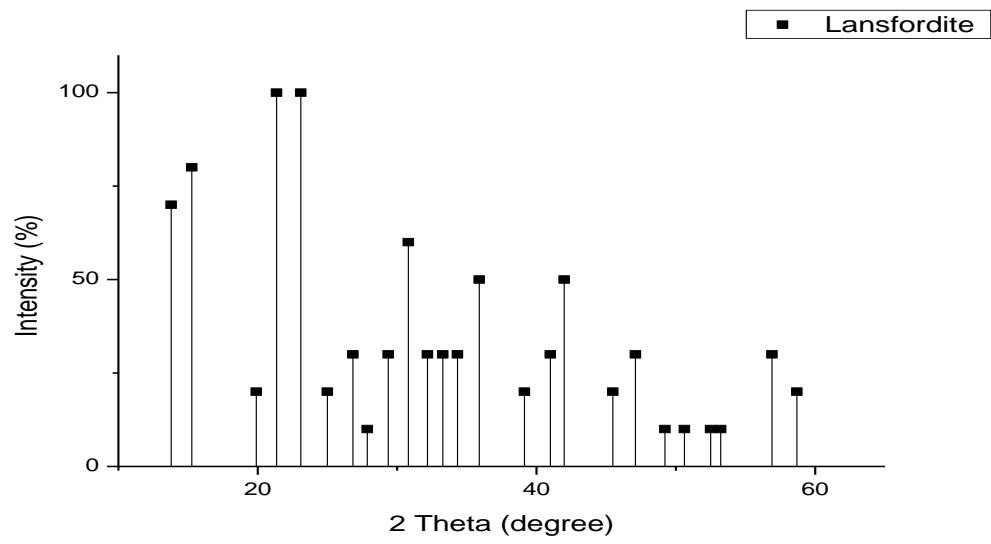
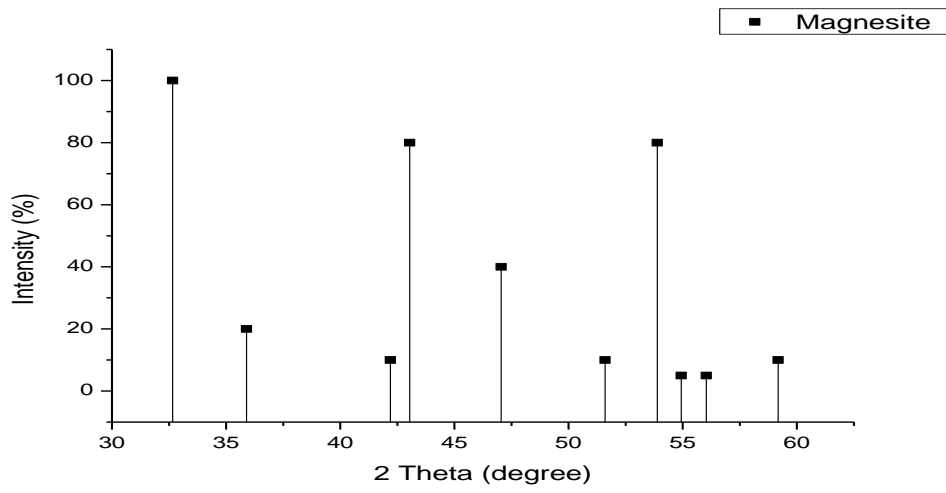
XRD: The chemical compositions of HMCs related to this work are elaborated in [Table 4. 4](#). In addition, the standard XRD diffractograms of the precipitates as well as $\text{Mg}(\text{OH})_2$ and MgO are given in [Figure 4.5](#). Many similarities can be seen through the graphs below, especially among nesquehonite, dypingite and hydro-magnesite, making it a challenge to differentiate from one to another in some cases.

Table 4. 4: The chemical compositions of potentially produced HMCs in SI

Hydrated Magnesium Carbonates	Molecular weight (g/mol)	CO_2 (%)	H_2O (%)	MgO [Mg^{2+}] (%)	Total Weight Loss (%)
$\text{MgCO}_3 \cdot 3\text{H}_2\text{O}$ (Nesquehonite)	138	31.9	39.1	29 [17.4]	71
$4\text{MgCO}_3 \cdot \text{Mg}(\text{OH})_2 \cdot 4\text{H}_2\text{O}$ (Hydromagnesite)	466	37.6	19.2	43.2 [25.6]	56.8
$4\text{MgCO}_3 \cdot \text{Mg}(\text{OH})_2 \cdot 5\text{H}_2\text{O}$ (Dypingite)	484	36.2	22.2	41.6 [24.7]	58.4
MgCO_3 (Magnesite)	84	52.4	0.0	47.6 [28.6]	52.4
$\text{MgCO}_3 \cdot 5\text{H}_2\text{O}$ (Lansfordite)	174	25.3	51.7	23.0 [13.8]	77







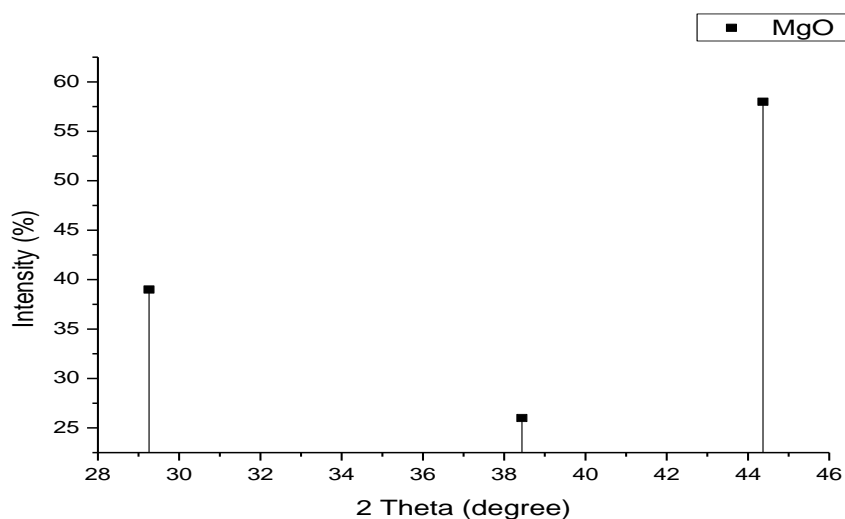


Figure 4. 5: XRD diffractograms for relevant HMCs, magnesium hydroxide & MgO in SI (captions see top right corner)

4.4.3 Series I-Carbonation

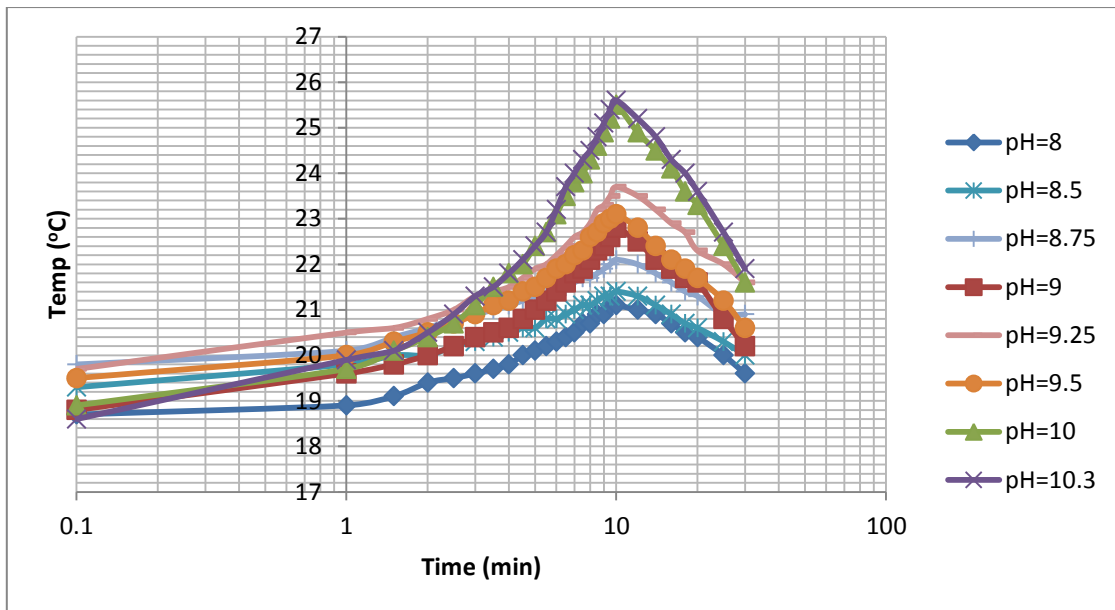
Two sets of tests were undertaken, to get familiar with the whole procedure in SI.I, and investigate the pH effects on precipitates and the sequestered efficiency in SI.II.

4.4.3.1 Series Set I.I

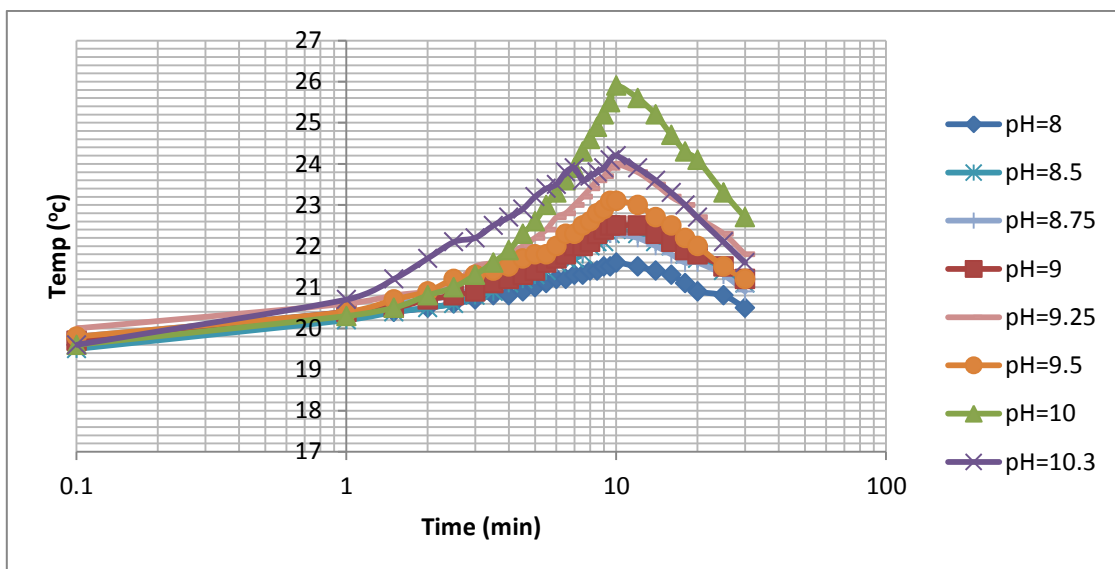
4.4.3.1.1 Carbonation Studies

Carbonation studies aim to explore variations during the first 30min of bench reactions, and the resulting weight of precipitates. It is a crucial step to obtaining the desired precipitates under a controlled pH level, with a reasonable time scale and a relatively convenient operation procedure. Because of the fixed pH property in the reaction, only temperature variations were recorded.

These two temperature profiles show a similar tendency: temperature increased by 3-6°C sharply during the first 10min when reactants infused in; then declined back gradually in the later 20min bench reaction. As demonstrated before, temperature is the macroscopic manifestation of molecular motion; hence this phenomenon can infer the increased molecule movements during reactants additions, triggering higher collision chances among molecules, thus generating more energy in the first 10min. In addition, the energy required to form the precipitates is less than the energy released from the initial reactants, leading to the extra energy release. Overall, temperature increased slightly, once again validating its exothermal characteristic.



(a): Temperature vs time in the first tests of SI.I shown in Table 4.2



(b): Temperature vs time in the duplicated tests of SI.I shown in Table 4.2

Figure 4. 6: Temperature profiles in two tests of SI.I shown in Table 4.2

Figure 4. 6 shows that a higher pH tends to activate a larger temperature. This is explained by more hydroxide ions providing higher collisions' probabilities among particles, so as to produce more energy. The only exception in the graph is pH=10.3. This is to some extent attributed to the decomposition of ammonia when it was kept over a prolonged period of time, or the underestimation of ammonia usage by a supply shortage during the operation.

The weight of precipitates can also reflect the bench reaction in a different aspect. After 30min, sediment was filtered and dried at 35°C. This temperature can provide sufficient heat to dry samples, as well as avoid nesquehonite decomposition. **Figure 4. 7** was derived by averaging two duplicate experiments, and an error bar was drawn from a standard deviation function.

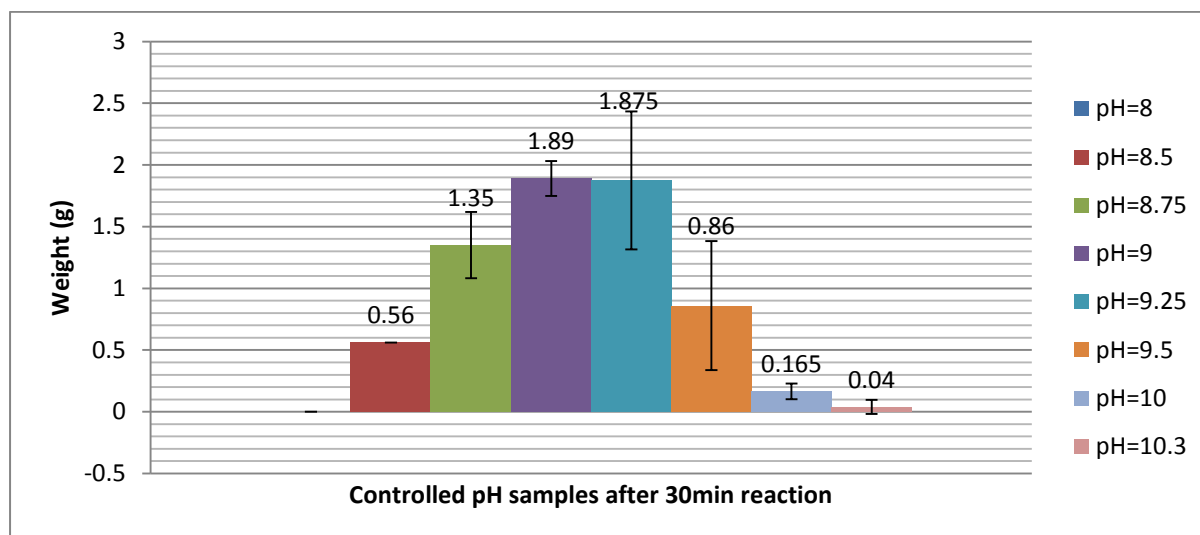


Figure 4. 7: Weight distribution over controlled pH after 30min reaction with STEDV for SI.I

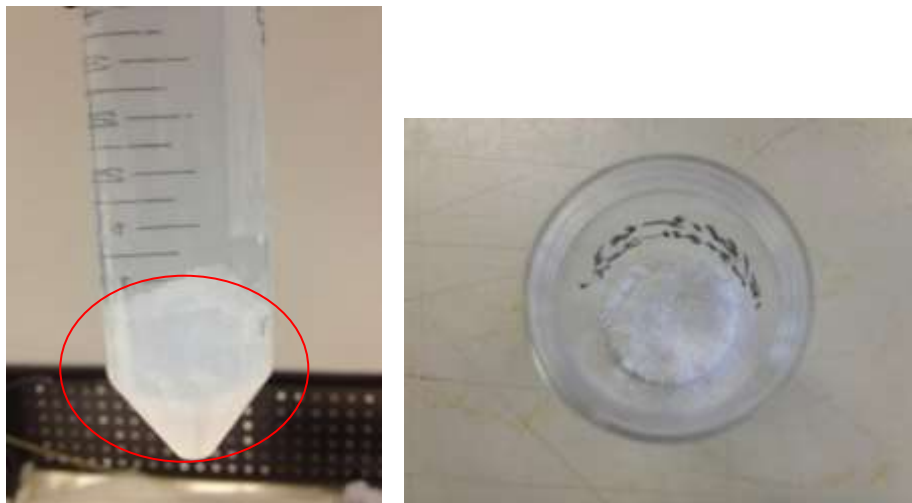
It can be seen that no precipitate is formed at pH=8 after 30min, while the highest amount appears at pH=9 and pH=9.25, with both acquire 1.9g sediments, as well as showing the best magnesium sequestration ability at relevant values. pH=8.75 and pH=9.5 also obtain HMCs to some extent, with 1.3g and 0.8g respectively. By contrast, pH=10 and above has the smallest amounts of precipitates in this series. Consequently, for a short retention time, pH range from 8.5 to 9.5 is recommended, although best performances emerge at 9 and 9.25. No further free reaction sediments weight is measured, considering that the system has changed after filtration, which cannot provide reliable data. This alteration can also not be identified by ICP.

Two representative precipitates photos obtained from pH=8.75 and pH=10 after 30min bench reaction were taken, to record the products' morphology from the macroscopic point of view (**Figure 4. 8**). It is noticeable that a lower pH produces finer aggregated particles compared with a higher one, producing more sheet-like dispersed crystals. This phenomenon is also corresponding to SEM results from other authors in the literature. Lower pH values affect the nucleation rate of HMCs formation due to the bicarbonates'

dominance leading to aggregated nuclei into larger particles. However, with the ascended pH value, the nucleation and crystallisation rate gradually increase forming small independent particles. Further SEM operation needs to be undertaken to verify this effect on the microstructure.



(a): Precipitates obtained from pH =8.75 after 30min bench reaction of SI.I



(b): Precipitates obtained from pH=10 after 30min bench reaction of SI.I

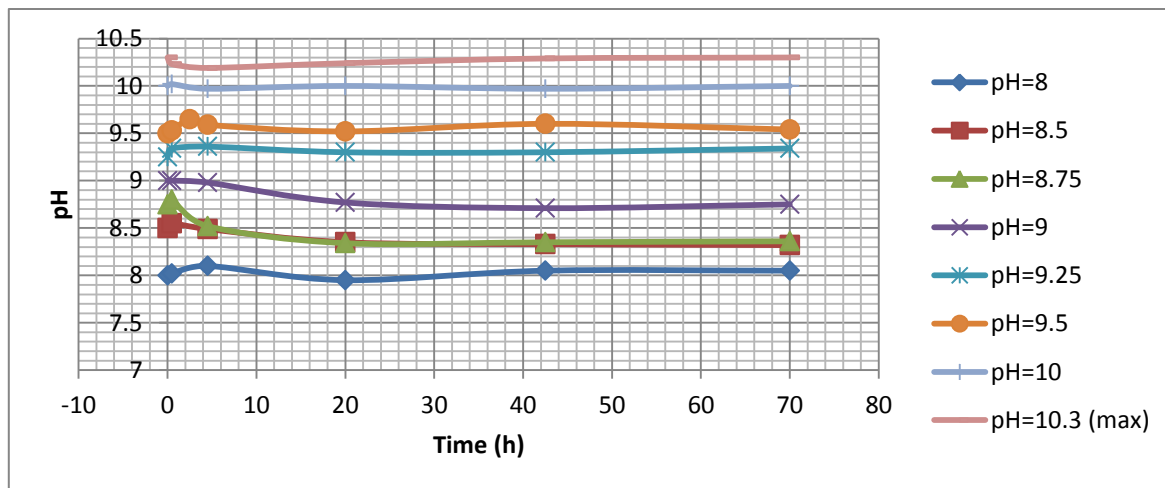
Figure 4. 8: The images of precipitates from pH=8.75 (a) &10 (b) for SI.I shown in Table 4.2

4.4.3.1.2 pH Stability Studies

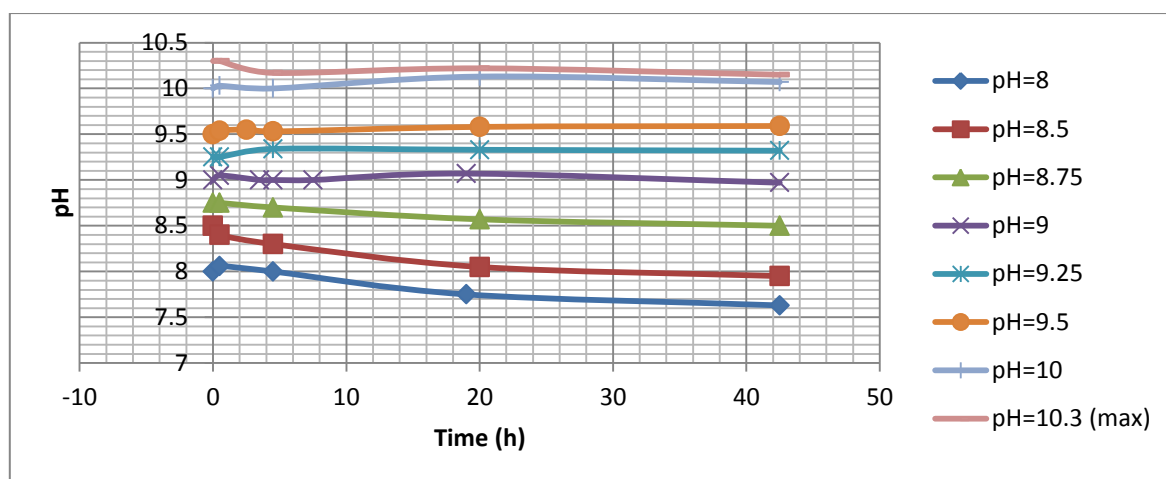
The pH stability study aims to scrutinise pH alteration over a relatively long time. This was firstly introduced by Druckenmiller and Maroto-Valer (2005). They used this method to examine the raised pH from the initial values after KOH addition over 12 days. It was then developed by Liu and Maroto-Valer (2010, 2012) to research the various buffer solutions'

influences on synthetic brine over time, then to select the optimal condition for the subsequent carbonation studies. Unlike them, this experiment conducted carbonation studies firstly by utilising a buffer solution, and explored its long term performance.

In this case, filtrates in free reaction were studied at an ambient temperature and pressure, to identify the pH conditions in an added alkaline buffering solution $\text{NH}_3 \cdot \text{H}_2\text{O}$ and a moderately formed buffering solution $(\text{NH}_4)_2\text{CO}_3$. A closed system was employed to avoid the atmospheric CO_2 influence. Two tests were carried out, one was monitored through three days, selecting 0.5h (30min, after bench reaction), 4.5h, 20h, 42.5h and 70h as testing times, while the other was a two days one, following the same procedures with first four testing points. Starting pH (time=0) was set up as a standard. **Figure 4.9** shows that $\text{pH} > 9$ keeps a constant pH range (standard value ± 0.1) over three days, due to its high buffering capacity from exceeded $\text{NH}_3 \cdot \text{H}_2\text{O}$ or formed $(\text{NH}_4)_2\text{CO}_3$ molecules when pumping CO_2 in it. However, $\text{pH} \leq 9$ has a 0.2-0.5 decrease slowly, starting from 2h, over a long time reaction. This shows that the molecules, which provide a steady pH, are just about to be used up in the precipitates formation, leading to the scarcity of hydroxide ions in solutions.



(a): pH stability tests over 3 days for SI.I



(b): pH stability tests over 2 days for SI.I

Figure 4. 9: pH stability profiles in two experiments for SI.I shown in Table 4.2

4.4.3.1.3 Precipitate Identification

Precipitates from the majority of 30min bench reactions were analysed through XRD to identify their components. Prior to this operation, two duplicated products were fully mixed, to reduce systemic errors. The mixed particles were ground finer than 75 μm . Other affecting conditions were considered, like pressure and temperature, to verify the probabilities of a certain precipitate. Standard XRD diffractograms from the database matched with the experimental product's pattern is a main method of identifying components. The better the match between the diffractograms and the product's pattern means the more likely the existence of the precipitate in the product. In addition, microstructural analyses with SEM are also used to prove the different morphologies and further determine the sediments. [Figure 4. 10](#) indicates that nesquehonite only exists in bench reactions, irrespective of pH values within 30min, with a high purity level by virtue of its solitary presence. This phenomenon matches Hassan's and Ferrini's result, and is achieved by matching the scores and 'semiquants' of the precipitates, which are calculated by the sophisticated XRD analysis software X'Per HighScore Plus.

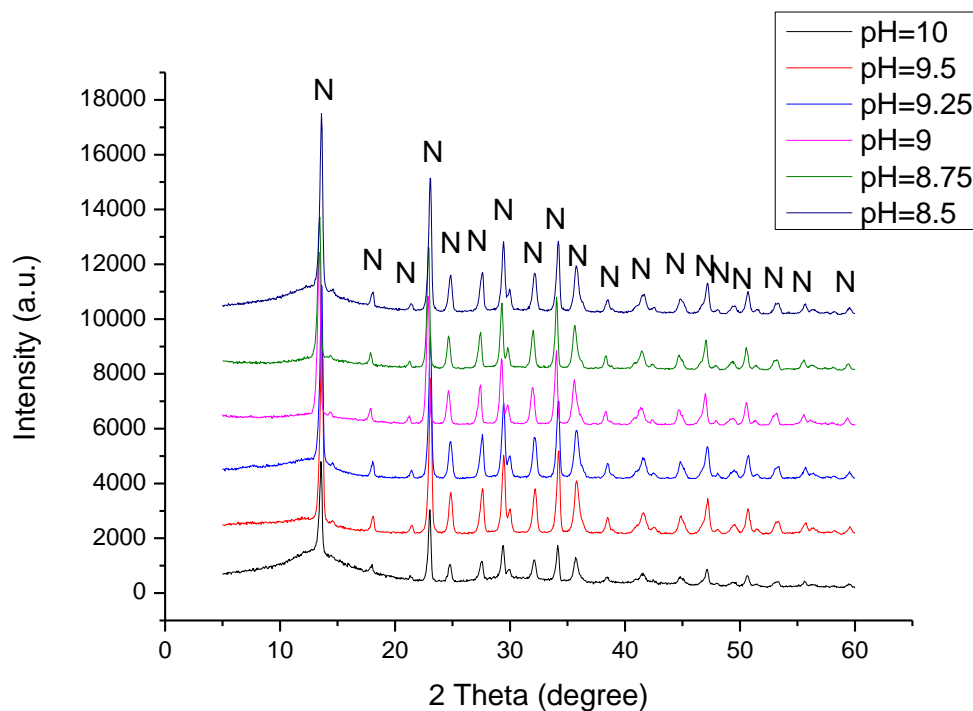


Figure 4. 10: Precipitates within 30min at various pH levels for SI.I (N=Nesquehonite)

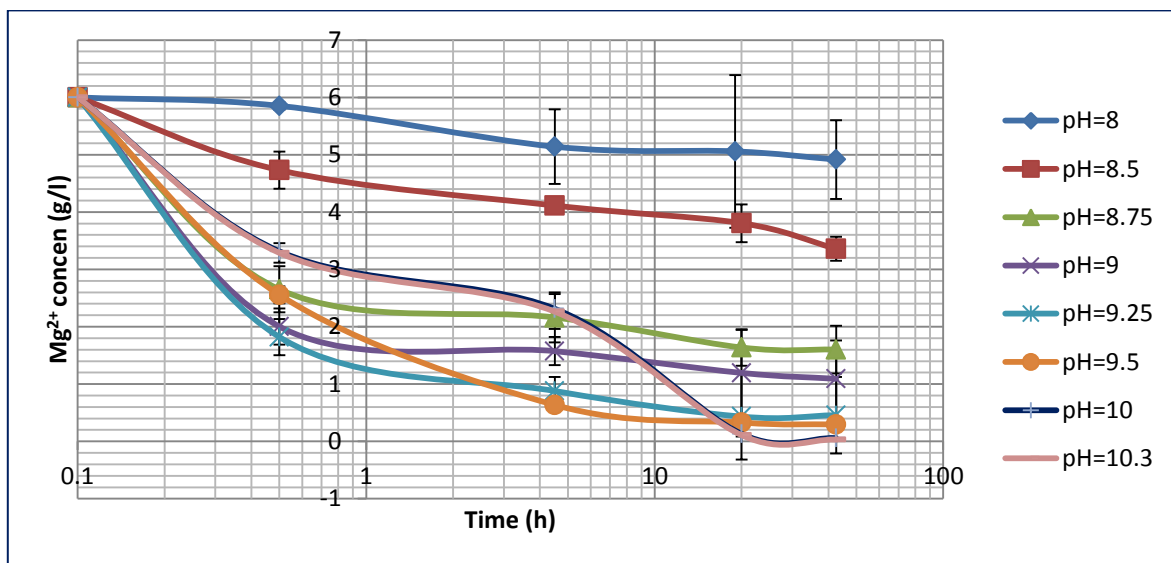
4.4.3.1.4 Reaction Kinetics Studies

Reaction kinetics studies are performed to verify the rate of a chemical process. In a systematic one, experiments are conducted to validate the various affecting factors, and to establish a theoretical reaction model. Given that this experiment mainly focuses on general tendency investigation, only several samples' collecting points are decided in the series. They are the same as pH stability studies. Two tests were conducted as follows: three days reaction was with 0.5h (30min, after bench reaction), 4.5h, 20h, 42.5h and 70h as testing times, while two days had only the first four testing instances. Error analysis was then conducted by both two days' results. Based on that, unreacted magnesium ions percentage and sequestered magnesium percentage over time were drawn, providing a more intuitive graph of the reaction. Starting magnesium concentration was 6g/l.

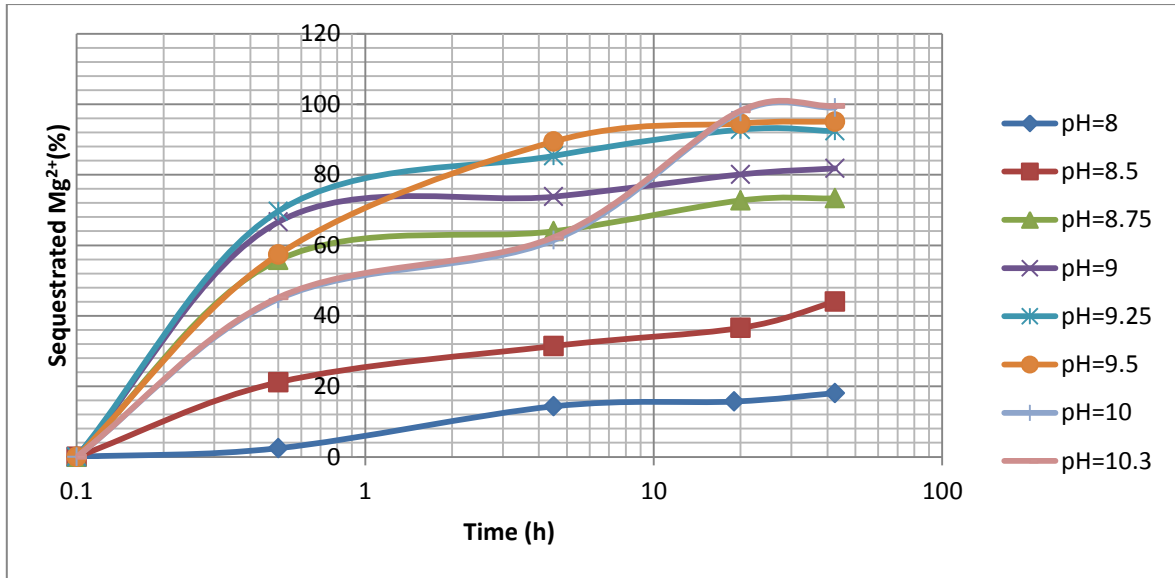
Figure 4. 11 shows that the majority of reactions finishes within the first day, reaching nearly a stable level later on. Samples are placed in line from pH=8 to pH=10.3. Clearly, there is nearly no reaction at pH=8; while higher pH increases the precipitations, because surplus hydroxide ions induce the carbonates formation. Especially when $\text{pH} \geq 10$ (pH=10 & pH=10.3), approximately after 20h, remained magnesium ions in solution are less than 0.1g.

Only less than 1% magnesium ions do not react, with sequestration efficiency being higher than 99%. However, they have a slower initial rate than $9 < \text{pH} < 10$ ($\text{pH}=9.25$ & $\text{pH}=9.5$), which achieve less than 1 g Mg^{2+} after 4.5h, with corresponding sequestration efficiency $>85\%$. These two values finally reach $< 0.4 \text{ g/l Mg}^{2+}$ concentration left in solution and $> 92\%$ sequestration performance after 20h.

In the first 30min, all $8.5 < \text{pH} < 10$ ($\text{pH}=8.75, 9, 9.25, 9.5$) capture Mg^{2+} more than 50%, namely less than 3 g/l Mg^{2+} , which is higher than $\text{pH} \geq 10$ ($\text{pH}=10$ & $\text{pH}=10.3$) 3.5 g/l . Error analysis confirms the data's reliability and the method's efficiency. The good magnesium removal ability accords with the high yield of the precipitates, and the first 30min ICP result matches well with its weight of sediments in [Figure 4.7](#). Long time deposits over 1 and 3 days of $\text{pH}=9, 9.5, \text{ \& } 10$ are identified as nesquehonite through XRD analysis ([Figure 4.12](#)), which are identical results to 30min. It infers that precipitates are generated irrespective of pH condition and time frame in ammonia reactants, similar to Mignardi et al.'s (2009) work.

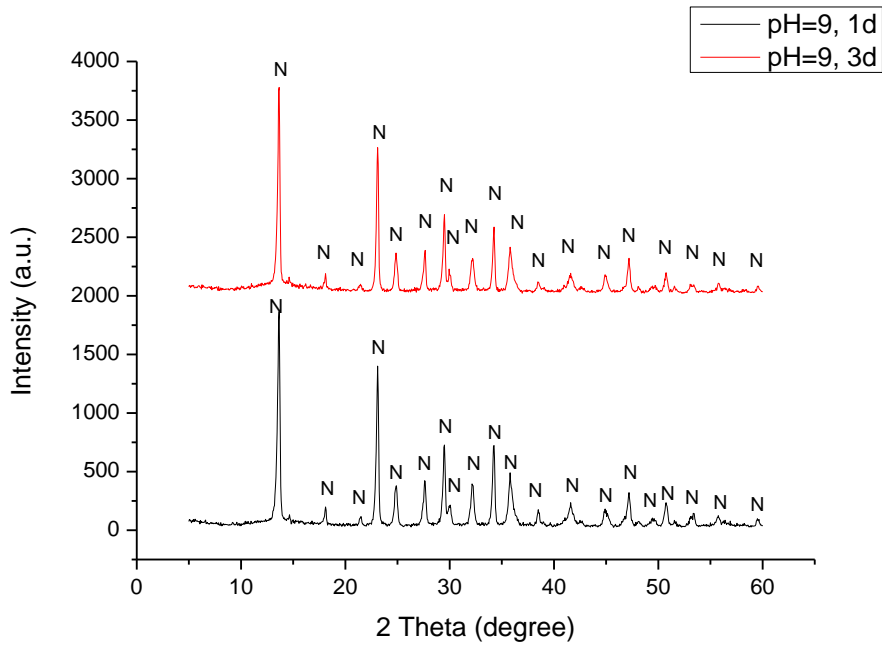


(a): Unreacted Mg^{2+} concentrations vs time with a standard deviation over 2 days on duplicated experiments

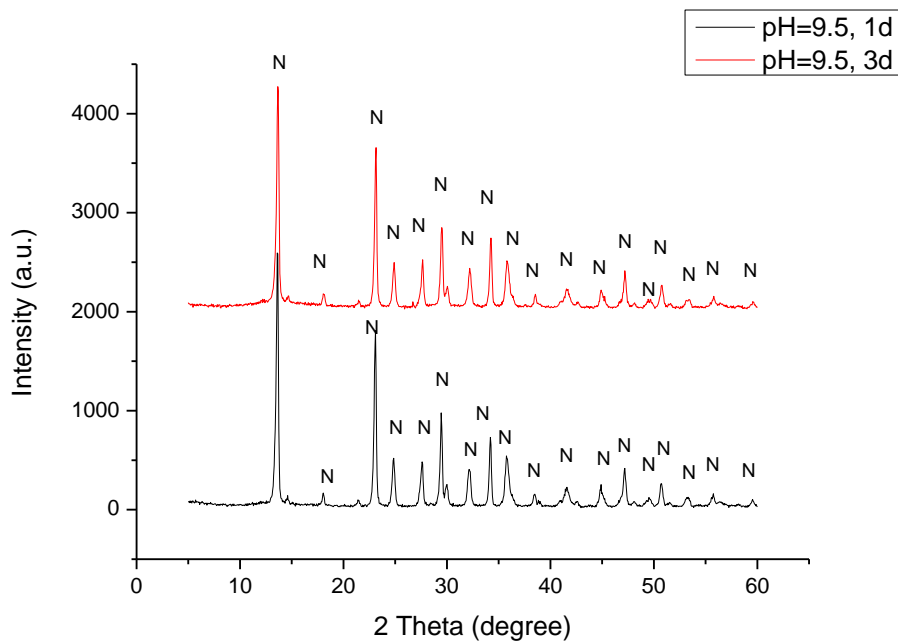


(b): Sequestered Mg²⁺ percentages over 2 days

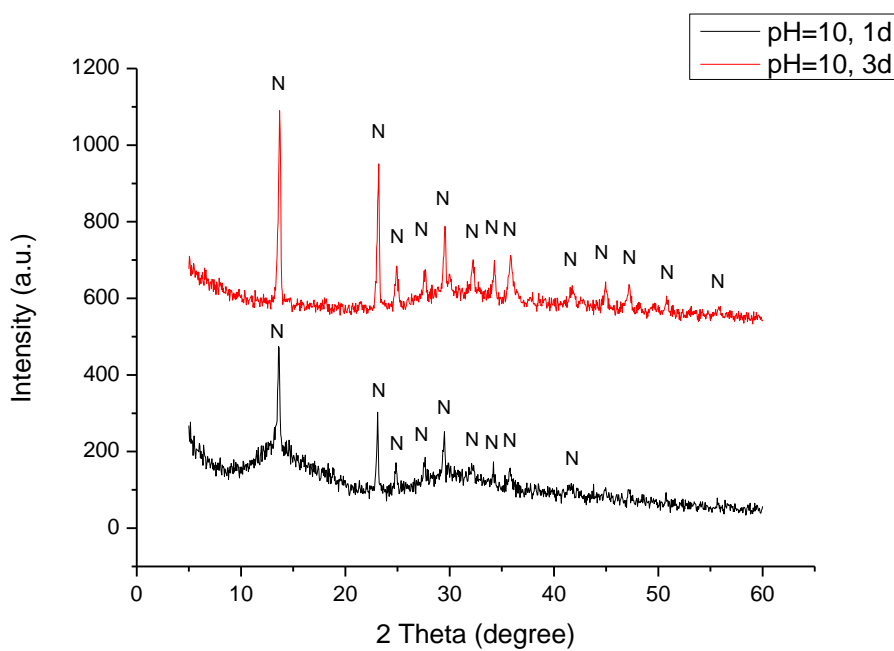
Figure 4. 11: A magnesium kinetics study over two days of duplicated SI.I



(a): pH=9 precipitates over days for SI.I



(b): pH=9.5 precipitates over days for SI.I



(c): pH=10 precipitates over days for SI.I

Figure 4. 12: Precipitates over days with pH=9 (a), pH=9.5 (b), and pH=10 (c) for SI.I shown in Table 4.2

4.4.3.2 Series Set I.II

4.4.3.2.1 pH Stability Studies

The purpose of this study is to validate the pH behaviour within one day. Four typical values, pH=8.5, 9, 9.5 and 10, were selected based on the previous result. They are representative of the pH ranges with the capability of producing precipitates. Samples were taken at 0.5h (after 30min bench reaction), 4.5h, 8.5h, 12.5h, 16.5h and 20.5h. Starting point was set up as a standard pH value.

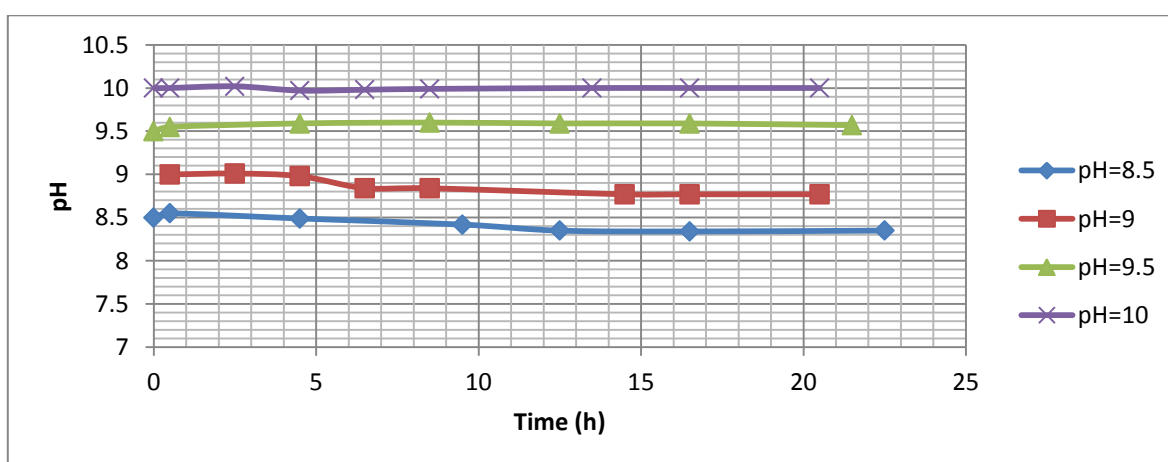


Figure 4. 13: The pH profiles of typical samples within one day in SI.II shown in Table 4.2

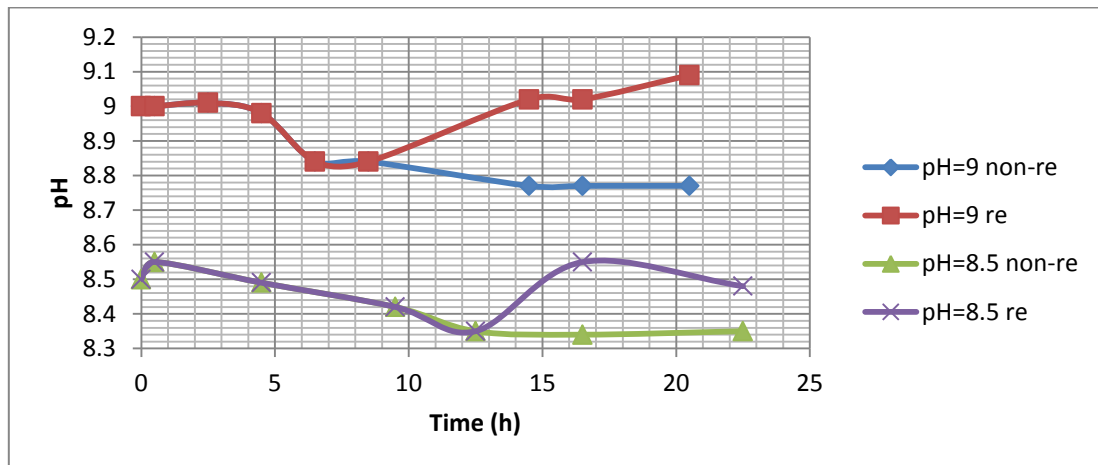
Figure 4. 13 describes that pH=9.5 and pH=10 both have a steady state, whereas pH=9 and pH=8.5 both have an equivalent fall of 0.2. This propensity of deviation from the standard pH starts from approximately 6h. The figure agrees to the broad three days graph, by proving that pH > 9 are favoured.

4.4.3.2.2 pH Adjustment Studies

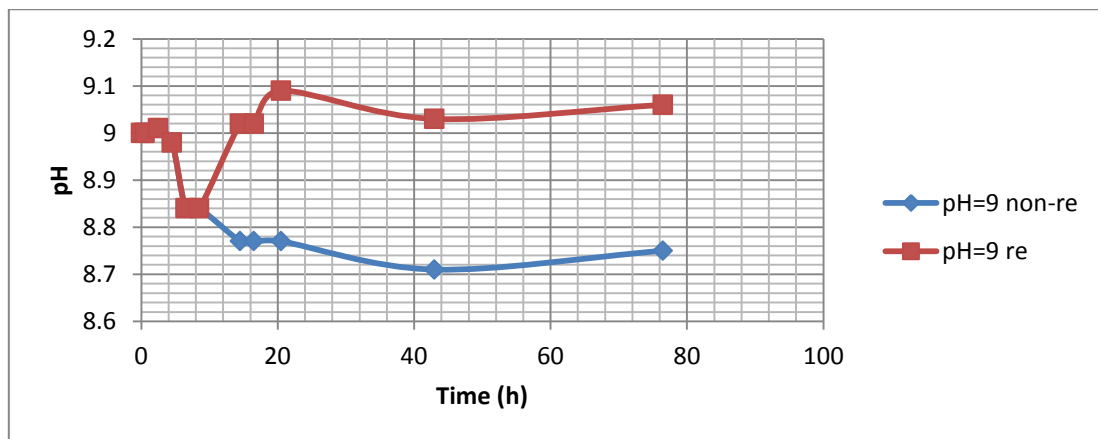
In terms of pH fluctuation, adjustment studies were used to explore the importance of a constant pH over time and the effect of the further added ammonia buffer solutions. In light of Figure 4. 14, pH=8.5 and pH=9 samples were adjusted when they fell over 0.1. In particular, the pH=9 monitoring time lasted for up to three days, with 43h and 76h additional sampling points.

There is an apparent difference between adjustment and non-adjustment samples. pH rises back to an accept error level (standard $\text{pH} \pm 0.1$) after adjusting, while the non-adjusted one continues the previous downward trend. Both non-adjusted samples remain at a roughly

steady situation after 15h, but the adjusted ones have a slight variation to some extent within the error range due to their molecules' decomposition or reaction. This inclination is more noticeable in slight longer time. However, all adjusted and non-adjusted samples maintain approximately at their previous pH levels after three quarters day or one day, with the explanations of a completed reaction by then, supported by ICP results in the following section.



(a): pH adjustment over a day in SI.II



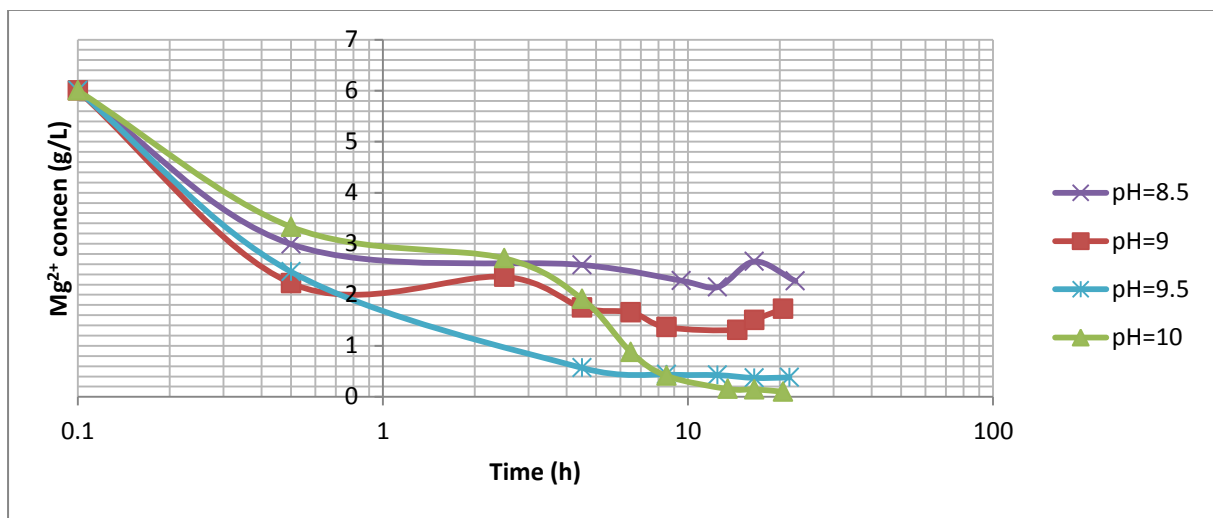
(b): pH adjustment over three days in SI.II

Figure 4. 14: The pH adjustment profiles of typical samples over one day (a) and three days (b) in SI.II

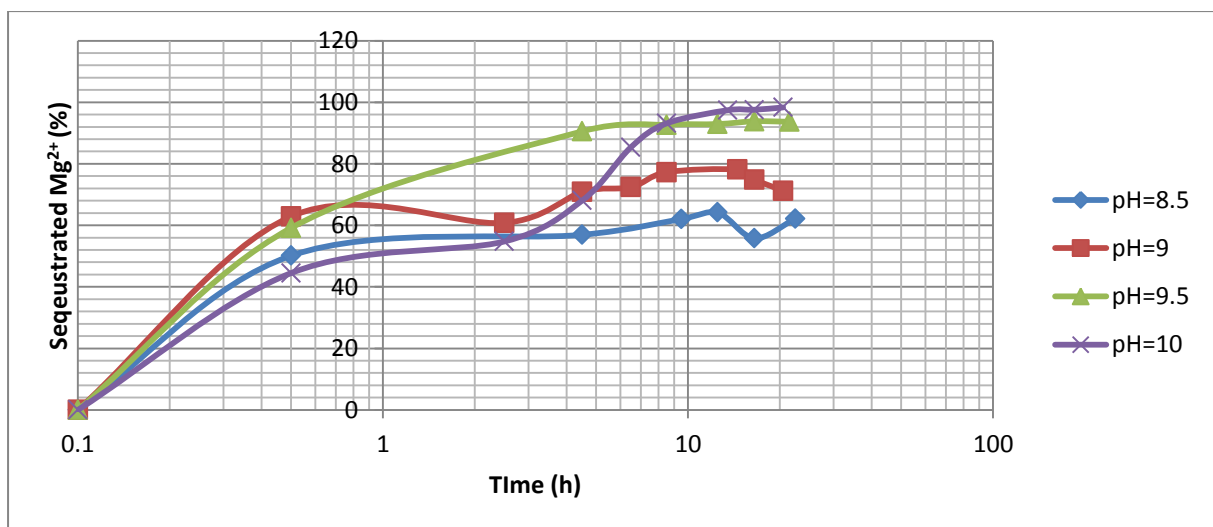
4.4.3.2.3 Reaction Kinetics Studies

Accompanied with pH stability and pH adjustment studies, this programme was carried out to supplement the reactions' extent. Similar to the previous graph, a higher pH has better performances in accelerating carbonation process. pH=10 reaches 0.15 g/l unreacted Mg^{2+}

concentration in a solution at time of 13.5h. This corresponds to 2.57% remaining Mg^{2+} and 97.43% captured Mg^{2+} (Figure 4. 15). This value decreases to 0.1g/l left in the solution, with 1.67% remaining and 98.3% captured after 20.5h. In comparison, pH=9.5 reaches this relatively stable position earlier, at 8.5h, with 0.44g/l (7.32%) Mg^{2+} left in the solution, and 5.56 g/l (92.68%) sequestered. This sequestration efficiency is improved by 1% to 93.67% finally at 21.5h. Hence for $pH < 10$ the completion time is shortened to one third of a day, while for $pH \geq 10$ completion is prolonged to half day. $pH \geq 10$ has a larger sequestration capacity over a longer period because of the higher pH effect, but it has reversed results over a short time due to the ammonia hydrolysis.



(a): Unreacted Mg^{2+} vs time within one day in SI.II



(b): Sequestered Mg^{2+} (%) vs time within one day in SI.II

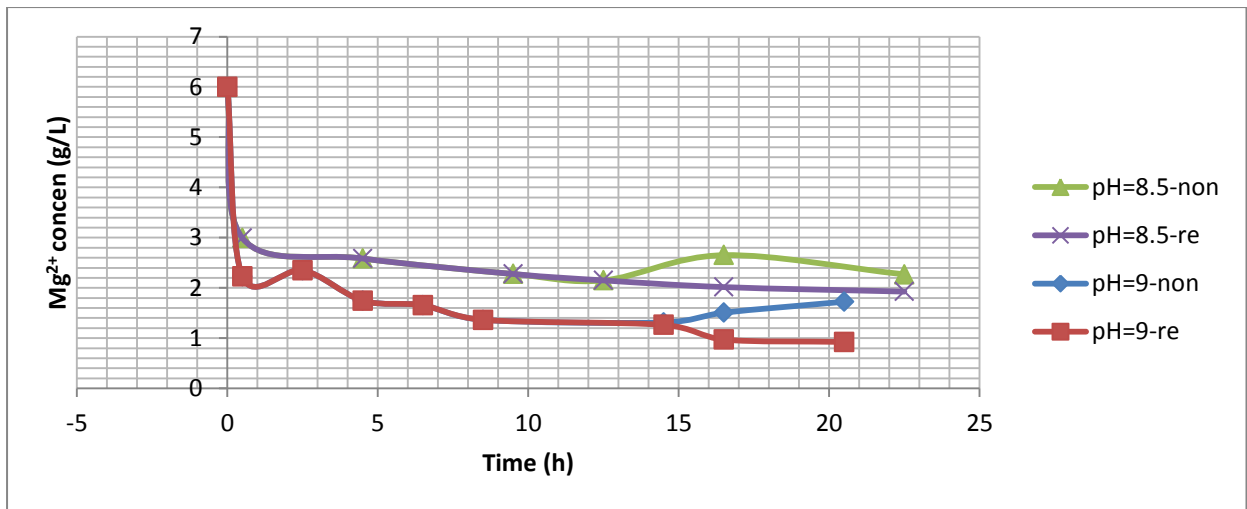
Figure 4. 15: Kinetic studies on typical samples within one day in SI.II shown in Table 4.2

During the whole process, some of Mg^{2+} concentration increases slightly (**Figure 4.16**, pH=8.5 at time 16.5h; pH=9 time at 3.5h and 16.5h; e.g. pH=9, non-re means this sample has no pH adjustment; while pH=9, re means this sample is adjusted), which is explained by Ostwald ripening rule, namely, when solid precipitates are left in their own saturated or supersaturated solution, a propensity exists for smaller particles to dissolve and later deposit into larger particles (Wang, Li, & Demopoulos, 2008). As a result, it is inferred that the time of sampling happens to be at smaller particles' dissolution period.

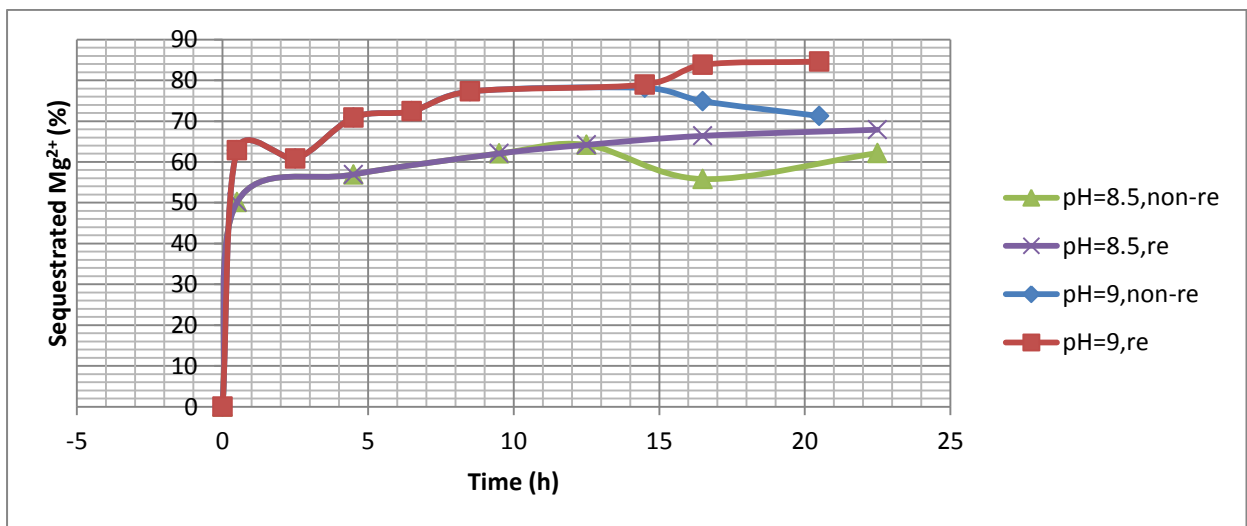
Figure 4.16a and **Figure 4.16b** show that Mg^{2+} has a better conversion after pH adjustment. When pH= 9, 1.36g/l (22.74%) unreacted Mg^{2+} exists at 8.5h. Once the pH adjustment is applied, this number gradually turns into 1.72g/l (28.75%) and 0.92g/l (15.42%) with non-readjustment and readjust respectively at a time of 20.5h. Correspondingly, there is around 13% difference in sequestration profile, with respect to 71.25% on no pH readjusted sample and 84.58% on pH adjusted sample. However, this distinction is much smaller at pH=8.5, with only 0.3g/l (5%) remaining Mg^{2+} and traps Mg^{2+} disparity at final 22.5h.

When time is extended to three days, pH=9 discrepancy is reduced to 0.3g/l (5%) unreacted Mg^{2+} at 76.5h, in accordance to 1.3g/l (21.82%) in a non-readjusted sample and 0.97g/l (16.25%) in a readjusted one. There is not an apparent reduction between the time at 8.5 and 76.5h, which substantiates that the reaction is mostly terminated in the first one third of a day. From the macroscopic perspective, pH reduction correlates to a more active reaction; on the other hand, pH elevation usually illustrates an inactive process.

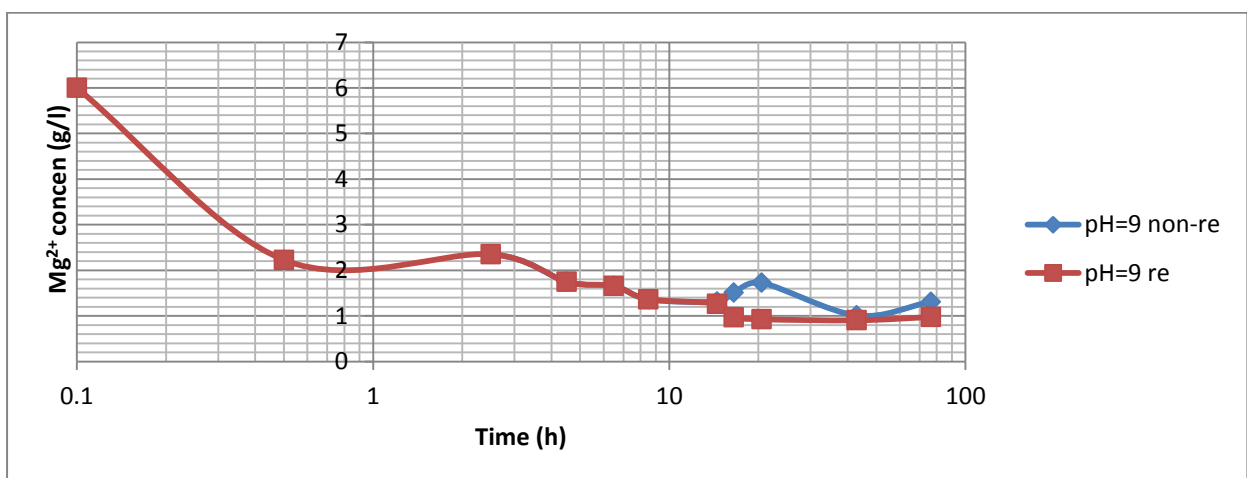
Overall, these studies have confirmed that invariably pH is a significant factor and a higher pH accelerates the precipitation. There is a direct interrelationship between pH variations and the reaction extent, decreased pH reveals a more dynamic progress than the increased one.



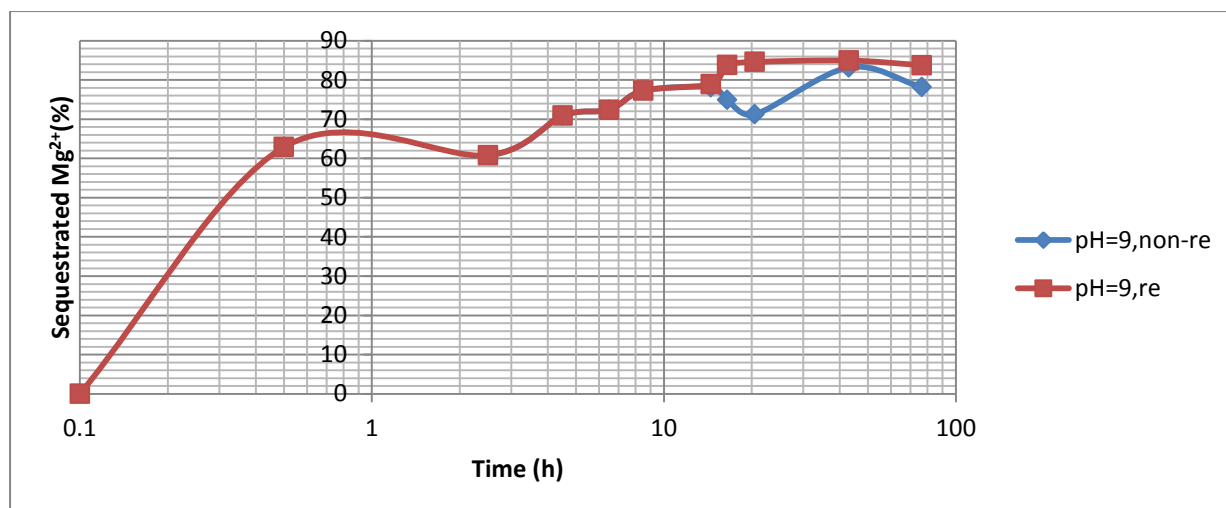
(a): Unreacted Mg^{2+} concentration vs time (pH adjust) in SI.II



(b): Sequestered Mg^{2+} (%) vs time (pH adjust) in SI.II



(c): Unreacted Mg^{2+} concentration vs time (pH adjust) over 3 days in SI.II



(d): Sequestered Mg^{2+} (%) vs time (pH adjust) over 3 days in SI.II

Figure 4. 16: The pH adjustment profiles of typical samples over days in SI.II

4.5 Series II-Individual Magnesium Ion System with Sodium Hydroxide

4.5.1 Model for Series II

In system II, NaOH was used to substitute ammonia in Series I; but operating codes were the same as Series I because the alkaline condition was represented by hydroxide ions only, irrelevant to ammonium and sodium elements. The various proportions of mixtures are summarised below with Saturation Index over pH.

According to [Figure 4. 17](#), within the interested pH range between 9.5 and 10.5, possible precipitates are artinite ($Mg_2(CO_3)(OH)_2 \cdot 3H_2O$), brucite ($Mg(OH)_2$), magnesite ($MgCO_3$), hydromagnesite ($Mg_5(CO_3)_4(OH)_2 \cdot 4H_2O$), and potential nesquehonite ($MgCO_3 \cdot 3H_2O$). Yet the Saturation Index (SI) for nesquehonite is slightly lower than 0, indicating non-existing product, it still presented in the experimental result. The reason for this is due to insufficient time reacting at the lab time frame, while the simulation represents thermodynamic equilibrium outcome, which means prolonged nesquehonite should transfer into other more stable phases.

Visual Minteq shows similar precipitates to PHREEQC within the scope of 9.5 -10.5, but two more precipitates lansfordite ($MgCO_3 \cdot 5H_2O$) and nesquehonite are formed in Visual Minteq model because of the different database usage. Both models point towards a similar thermodynamic conclusion.

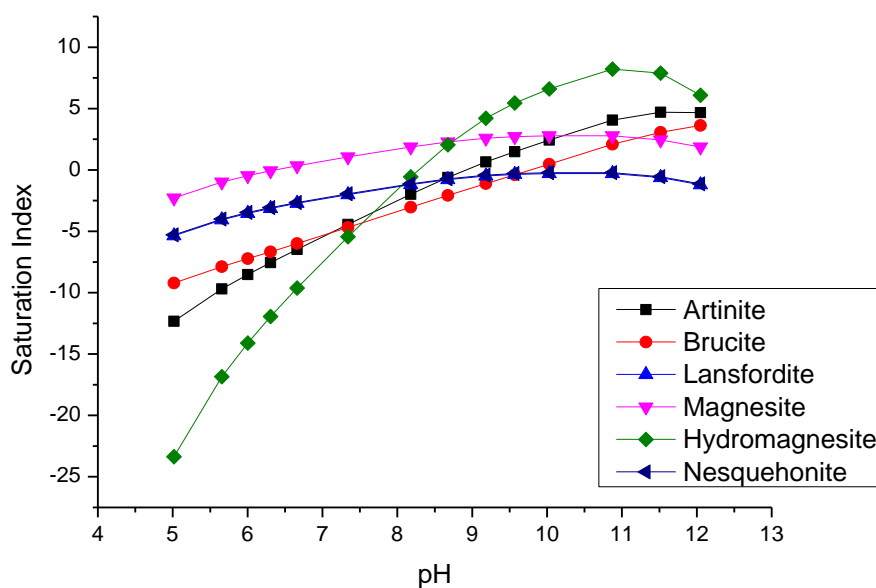


Figure 4. 17: The Saturation Index of HMCs over pH, summarised from PHREEQC for SII

4.5.2 Series II.I-Experimental Design

4.5.2.1 Experimental Parameters

In the main experiment, NaOH was used to replace ammonia considering the economic benefit and operational convenience, with the equation:



Net weights of samples were separated and washed at least three times in centrifuge tubes. As larger amounts of precipitates were required to be assessed, initial solution volume and bench retention time were extended to 200ml and 1h respectively.

Table 4. 5: Main magnesium experimental design parameters for SII

Sample (Mg)	Mg ²⁺ concn (M)	Stirring Speed	Temp (°C)	pH	CO ₂ flux rate (cm ³ /min)
1	0.25	700	25	10.5	500
2	0.5	700	25	10	500
3	0.5	700	25	10.5	500
4	0.25	0	25	10.5	500
5	0.5	700	40	10.5	500
6	0.5	700	25	10.5	150

Expected products are nesquehonite at a room temperature and hydromagnesite at a higher temperature. Precipitates were dried at 35°C avoiding nesquehonite thermal decomposition and then weighed immediately until reaching a constant mass. Table 4.5 is

for test parameters. It is clear to notice that samples 1 & 4 were designed for stirring speed, samples 2 & 3 for pH, samples 1 & 3 for reactant concentration, samples 3 & 5 for temperature, and samples 3 & 6 for CO₂ flux rate comparisons.

4.5.2.2 The Analysis of Precipitates

ICP: According to the previous Series I detailed explorations of a one day kinetics study, sampling time is shortened to the 1h and 1d timeline starting from this series. Standard calibrations are 0.1ppm, 1ppm, 10ppm and 100ppm of magnesium element.

During the analysis, the sequestered amounts of metal are responsible for the calculations of theoretical nesquehonite (N), dypingite (D) and hydromagnesite (HM) masses, to make the comparisons with net weights. Samples 1 and 4 are 0.25M magnesium reactants with 6g/l, while others are 0.5M with 12g/l; and the testing solution is 200ml. Based on the sequestered magnesium element after 1h, assuming all captured metals altered into N, HM and D, the corresponding molecular weights are 138, 466, and 484 individually. The computational equation is then presented as:

$$\frac{\text{Magnesium sequestration efficiency (1h)} * \text{Molar concentration}}{\text{The theoretical amounts of precipitates}} = \frac{M_{Mg}}{M_{N,D,HM}} \quad (\text{Equation 4. 1})$$

Where

Magnesium sequestration efficiency (1h) can be seen from [Table 4.7](#) (page 140) below.

The theoretical amounts of precipitates are unknown

$$M_{Mg} = 24 \text{ g/mol}$$

$$M_N = 138 \text{ g/mol}$$

For example, sample 1

$$\frac{0.9506 * 6 \text{ g/l}}{x} = \frac{24}{138}$$

So

$$x = 32.80 \text{ g/l}$$

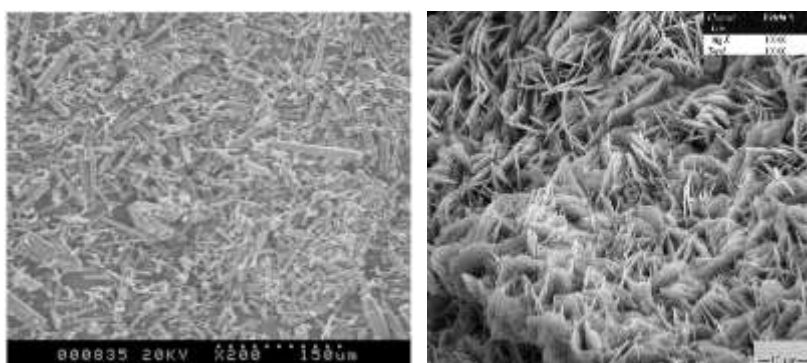
Detailed results are illustrated in Section 4.5.3.4 below to distinguish the ideal HMCs and practical weights.

XRD: Proposed precipitates are estimated from either modelling computations or literature references. Since both sodium and ammonium salts are water soluble compounds, their

combined chloride compounds were washed off during the cleaning process. XRD standard patterns are identical to Series I and not further described here. However in practice, the products should have the differences due to the changed alkaline solution, which may distort the particles' restructuring or rearrangement.

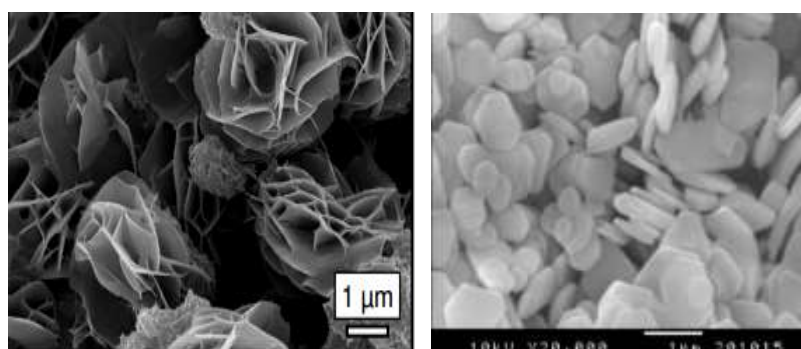
SEM: SEM was used to image the microstructure of precipitates, in accordance with other analytical measurements to determine the physical compositions of sediments.

Nesquehonite is needle-like; hydromagnesite and the intermediate transformation dypingite have a rosette-like morphology, while brucite is a sheet-like particle. Several experimental images were presented in Chapter 2, and the refined reference pictures of each component are further displayed here.



Nesquehonite (Glasser et al., 2016)

Hydromagnesite (Formia et al., 2014)



Dypingite (Power et al., 2007)

Brucite (Kisuma Chemicals, 2015)

Figure 4. 18 : The SEM microstructure of HMCs for SII

TGA: From the literature reviews of HMCs, nesquehonite, dypingite, and hydromagnesite thermal decomposition graphs are demonstrated in [Table 4. 6](#) with a three-step calcination. First two stages are water loss, while the last step is carbon dioxide release. Nesquehonite

has the largest thermal loss with 70.9% in total, and the dypingite as well as hydromagnesite are nearly similar accounting for 58.5% and 56.9% respectively. Nesquehonite has deeper hydrated properties, whereas HM and D have better carbonation degree. Additionally, MgO in brucite takes the amounts of 69%, with the 31% of weight loss.

Reactivity Test: The reactivity test in this section is utilised to quantify the time required for solution neutralisation; the method is elucidated in Section 3.2.2 through using citric acid as an indicator by weighing 2g testing powders. Referenced sample N50 is a light burned product with a particle size less than 2-3 μm and a reactivity test of 10s, while sample 92-200 hard burned calcined magnesia with 150s reactivity and particle size lower than 75 μm . Pictured commercial N50 and 92-200 are presented below (Figure 4. 19), showing particle sizes and porosity condition. N50 has smaller agglomerated granules and looser voids because of its high purity level produced from seawater and lower heating temperatures compared to 92-200.

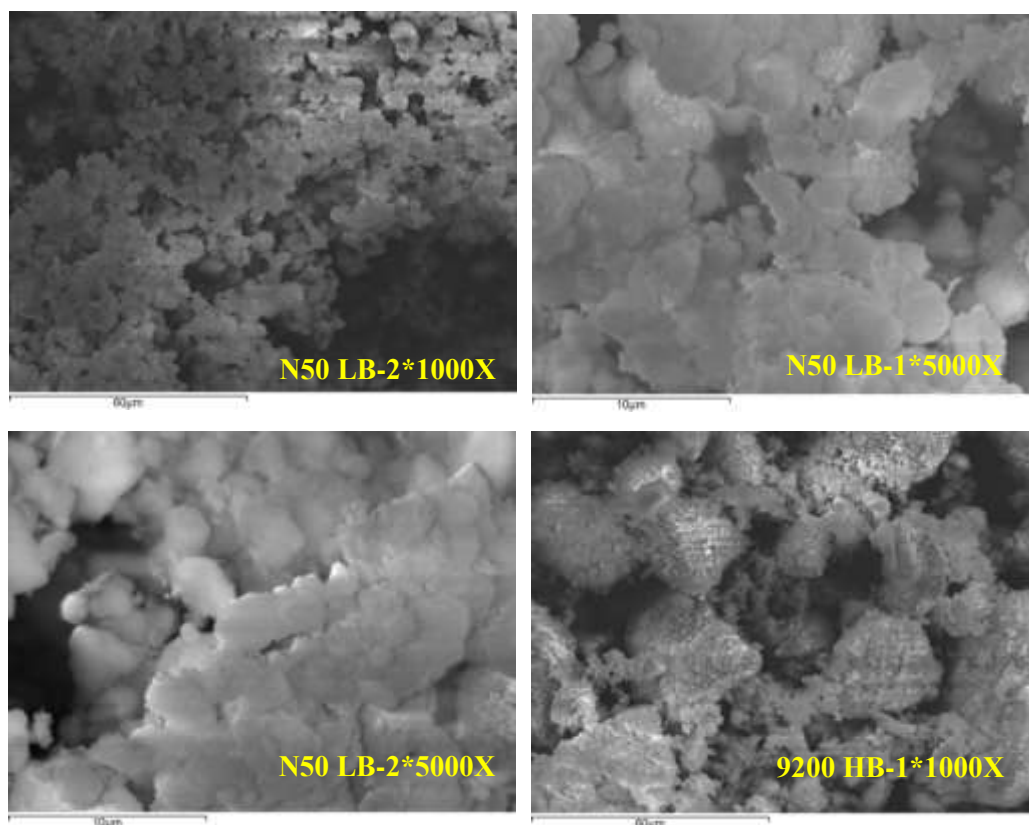


Figure 4. 19: The referenced MgO of N50 and 92-200 for reactivity tests

Table 4. 6: The thermal decomposition of nesquehonite, dypingite and hydromagnesite (Alvaraz & Lanas, 2004)

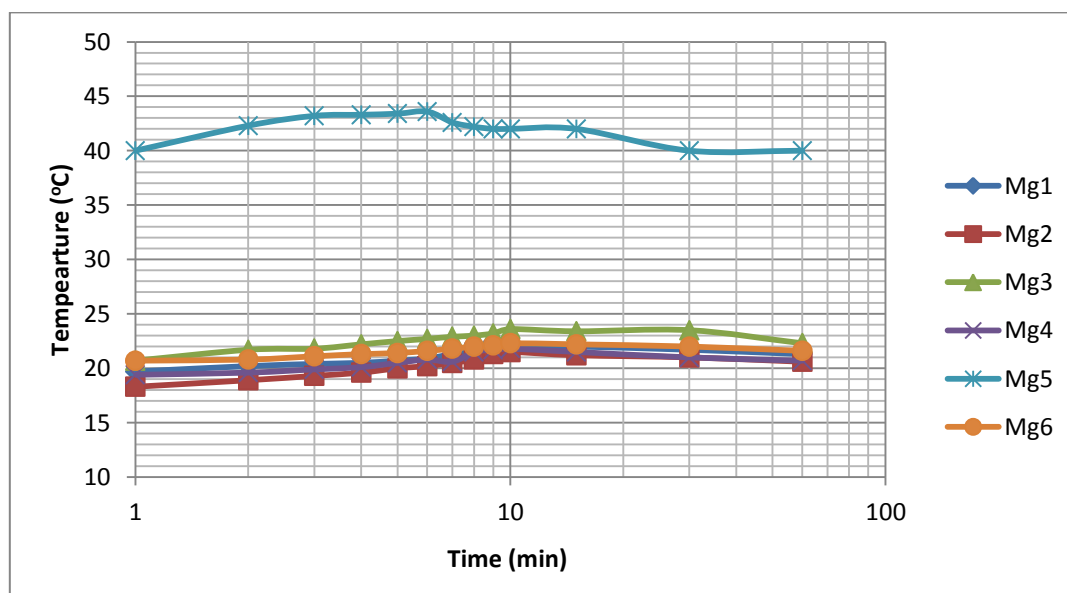
Mineral	Dehydration Step 1: Temp<250°C			Dehydroxylation Step 2: 250<Temp<350°C			Decarbonation Step 3: Temp>350°C			Total Weight loss (%)
	Reaction	Weight loss (%)	Peak temperature (°C)	Reaction	Weight loss (%)	Peak temperature (°C)	Reaction	Weight loss (%)	Peak temperature (°C)	
Nesquehonite	$\text{MgCO}_3 \cdot 3\text{H}_2\text{O} = \text{MgCO}_3 \cdot \text{H}_2\text{O} + 2\text{H}_2\text{O}$	26	200	$\text{MgCO}_3 \cdot \text{H}_2\text{O} = \text{MgCO}_3 + \text{H}_2\text{O}$	13	300	$\text{MgCO}_3 = \text{MgO} + \text{CO}_2$	31.9	550	70.9
Dypingite	$4\text{MgCO}_3 \cdot \text{Mg}(\text{OH})_2 \cdot 5\text{H}_2\text{O} = 4\text{MgCO}_3 \cdot \text{Mg}(\text{OH})_2 + 5\text{H}_2\text{O}$	18.5	54	$4\text{MgCO}_3 \cdot \text{Mg}(\text{OH})_2 = 4\text{MgCO}_3 + \text{MgO} + \text{H}_2\text{O}$	3.7	259	$4\text{MgCO}_3 = 4\text{MgO} + 4\text{CO}_2$	36.3	520	58.5
Hydromagnesite	$4\text{MgCO}_3 \cdot \text{Mg}(\text{OH})_2 \cdot 4\text{H}_2\text{O} = 4\text{MgCO}_3 \cdot \text{Mg}(\text{OH})_2 + 4\text{H}_2\text{O}$	15.4	54	$4\text{MgCO}_3 \cdot \text{Mg}(\text{OH})_2 = 4\text{MgCO}_3 + \text{MgO} + \text{H}_2\text{O}$	3.8	259	$4\text{MgCO}_3 = 4\text{MgO} + 4\text{CO}_2$	37.7	433	56.9

4.5.3 Series II.I-Carbonation

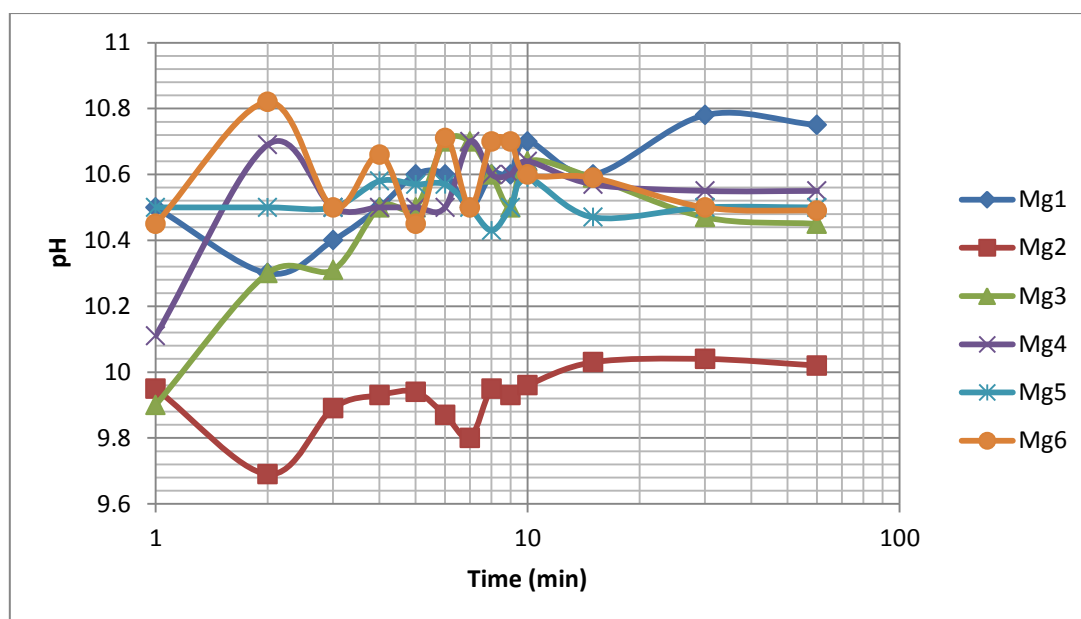
4.5.3.1 Carbonation and pH Stability Studies

Temperature was recorded through 1h bench reaction to monitor the formation of sediments. **Figure 4.20a** indicates that exothermal reaction happens during the reactants addition time, caused by the increased particles' collisions and the exothermal reaction property; but this tendency falls back gradually after 10min. Sample 5 ran at 40°C, which is harder to be controlled because of non-uniform heating.

pH stability testing is used to observe the pH level during the reaction, in order to maintain a constant pH throughout study. Although there is a short fluctuation within first 10min, the solution is still controlled at a reasonable range avoiding high fluctuation. This routine tends to stabilise in the following one hour timeframe, demonstrating a fast completion within a short time. This was also described by authors Han et al. (2006) to determine the completion of process by the unchangeable pH. The results can be combined with subsequent ICP samplings, to show high sequestration outcomes in a limited period.



(a): Carbonation study—temperature vs time in SII.I



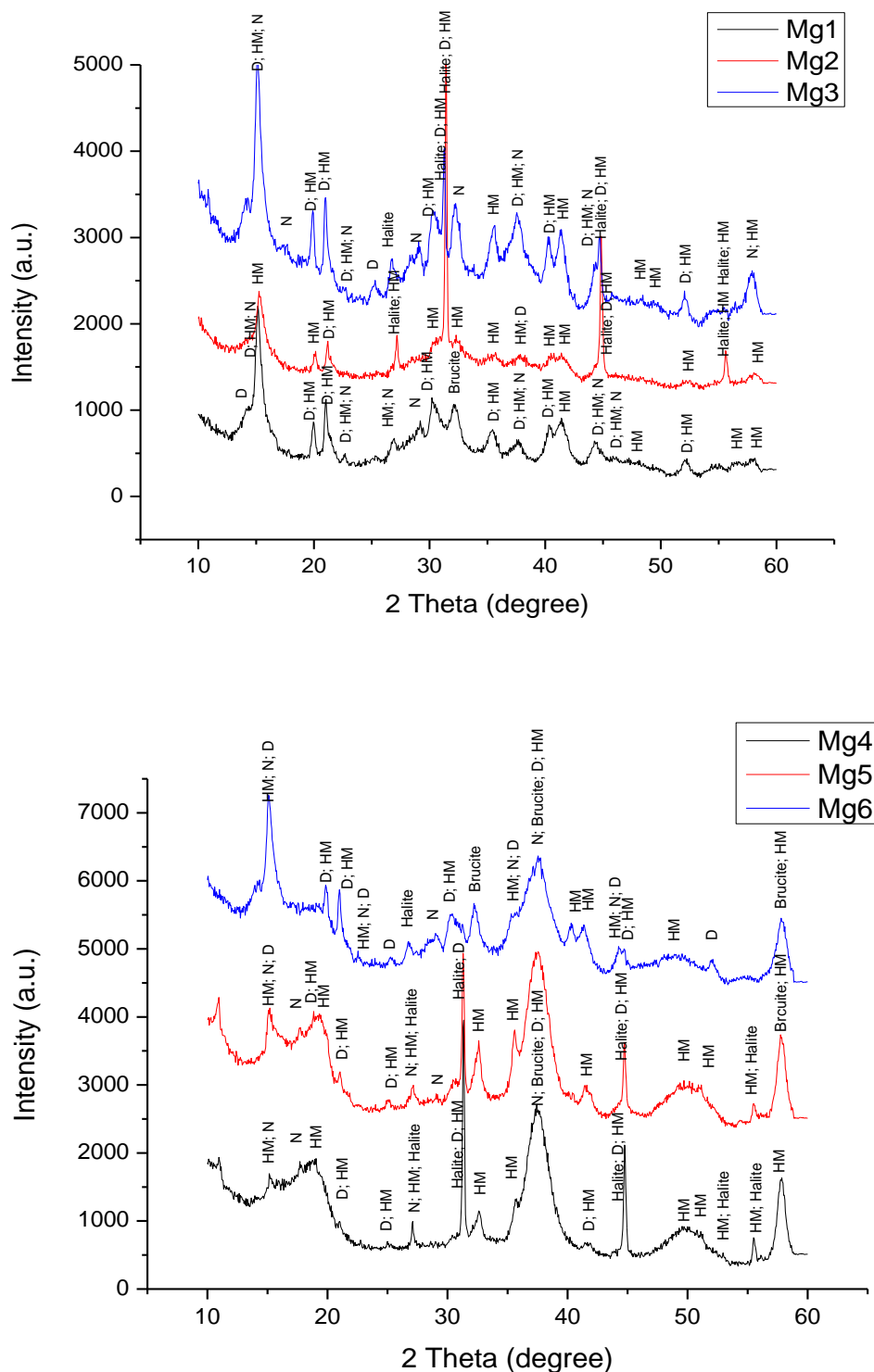
(b): pH stability study—pH vs time in SII.I

Figure 4. 20: Carbonation (a) and pH stability (b) studies for SII.I shown in Table 4.5

4.5.3.2 Precipitates Identification

XRD was utilised to analyse precipitates, based on the samples' crystallisation performance. No landsfordite and magnesite formation was seen according to Chapter 2.5.3, as this test was only conducted at a temperature of 40°C, which is not in the favoured conditions of landsfordite's and magnesite's formation. All deposits are composed of hydromagnesite (HM) or dypingite (D), with several distinct halite (NaCl) peaks caused by sodium chloride incorporation within the HMCs lattices (Figure 4.21a). Sample 3 presents more crystallised hydromagnesite by a higher supersaturation degree than 1, with the appearance of sharper peaks and larger matching scores of Figure 4.21b. This is explained by the faster reaction completion time in 3, which introduces a longer phase transformation period into a more stable one. Compared to that, samples 2 and 3 demonstrate the results of pH effect, inferring a more concentrated solution (sample 3) drives additional metastable HMCs phases (intermediate precipitates N & D) or less uniform structures within the same amount of time. This is in agreement to the literature findings. It is recognised that no stirring speed (sample 4), a higher temperature (sample 5), and a smaller CO₂ sparging rate (sample 6) lead to less CO₂ engagement and defer its dissolution in aqueous phase, based on the observation from samples 4-6 with prominent brucite formation. Broader peaks are with the

nano-particles attendance, proving the reaction is still undergoing in 4-6, while transformed sharper ones imply better crystallisation in 1-3.



(a): The precipitates of HMCs 1-6 for SII.I shown in Table 4.5 (HM=Hydromagnesite, N=Nesquehonite, D=Dypingite, Halite=NaCl)

Sample			Mg1	Mg2	Mg3
Ref. Code	Mineral Name	Chemical Formula	Contained within precipitates? (Score)	Contained within precipitates? (Score)	Contained within precipitates? (Score)
00-023-1218	Dypingite	4MgCO ₃ •Mg(OH) ₂ •5H ₂ O	Yes (36)	Yes (43)	Yes (34)
01-070-0361	Hydromagnesite	4MgCO ₃ •Mg(OH) ₂ •4H ₂ O	Yes (34)	Yes (33)	Yes (39)
00-001-0130	Nesquehonite	MgCO ₃ •3H ₂ O	Yes (26)	No	Yes (16)
00-007-0239	Brucite	Mg(OH) ₂	Yes (11)	No	No
01-072-1668	Halite	NaCl	No	Yes (51)	Yes (47)
Sample			Mg4	Mg5	Mg6
Ref. Code	Mineral Name	Chemical Formula	Contained within precipitates? (Score)	Contained within precipitates? (Score)	Contained within precipitates? (Score)
00-023-1218	Dypingite	4MgCO ₃ •Mg(OH) ₂ •5H ₂ O	Yes (25)	Yes (35)	Yes (62)
01-070-0361	Hydromagnesite	4MgCO ₃ •Mg(OH) ₂ •4H ₂ O	Yes (31)	Yes (39)	Yes (49)
00-001-0130	Nesquehonite	MgCO ₃ •3H ₂ O	Yes (9)	Yes (19)	Yes (26)
00-007-0239	Brucite	Mg(OH) ₂	Yes (38)	Yes (54)	Yes (23)
01-072-1668	Halite	NaCl	Yes (51)	Yes (63)	Yes (40)

(b): The matching scores of Mg1-6 precipitates, calculated by software X'Per HighScore Plus in SII.I
Figure 4. 21: The precipitates of Mg1-6 (a) and their matching scores (b) for SII.I shown in Table 4.5

4.5.3.3 Precipitates Microstructure

SEM was operated to image the microstructure of precipitates; magnesium carbonates from 1 to 6 can be seen in **Figure 4. 22** (e.g. Mg6-1*3000x means sample 6 in **Table 4.5**, location 1, 3000x magnification). Stirring speed, initial concentration corresponding to supersaturation degree, pH, CO₂ flux rate, and temperatures were investigated from a microstructure perspective. Images were taken at 1000x, 3000x, and 5000x magnification, while samples 1, 3 and 4 accompanied by EDX analysis, demonstrated good results of sodium chloride removal, providing the reliability of operations as well as the indications of larger magnesium concentration capture in flower or rosette-like crystals. In general, the SEM micrographs are in good agreement to the XRD implying the same compounds in each sample.

From the reviews, pH is considered as one of the most determining factors in precipitates. Particles are more regulated and have better rosette-like morphologies in 2, due to the

lower supersaturation degree than 3, while more nuclei are formed in 3. In addition, sample 3 presents sharper and better crystallised granules.

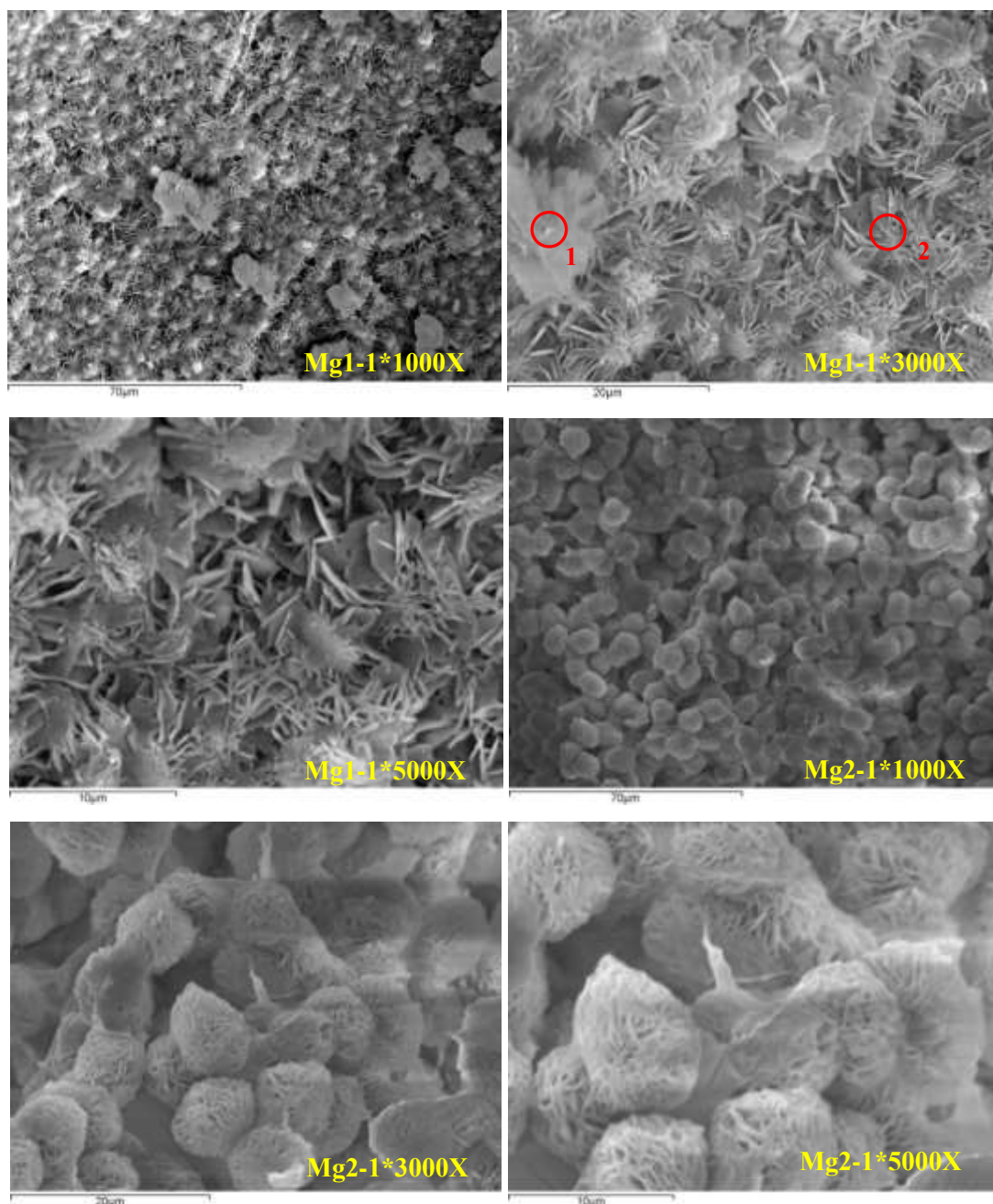
For the temperature differences, nest-like hydromagnesite samples are well observed in 5 with operational level 40°C. These particles mainly consist of nanosheet-like structures, self-assembled into spherical accumulations combined into a tunnel appearance (Figure 4.22, sample 5). While in sample 3, there are more aggregated sheet-like grains formed by needled nesquehonite, and some rosette-like hydromagnesite. This is caused by the elevated heating condition, resulting in enhanced carbonates' nucleation rate. Moreover, the increased rate further improves the growth of nuclei assembling into smaller particles based on Chapter 2.6. A higher temperature also accelerates the carbonations because it raises the pH level and further increased the carbonates' activity. Similarly, researcher Zhang et al. (2006) reported the phase transformation from rosette-like into cake-like assemblies of sheet-like structures with higher temperature and pH level.

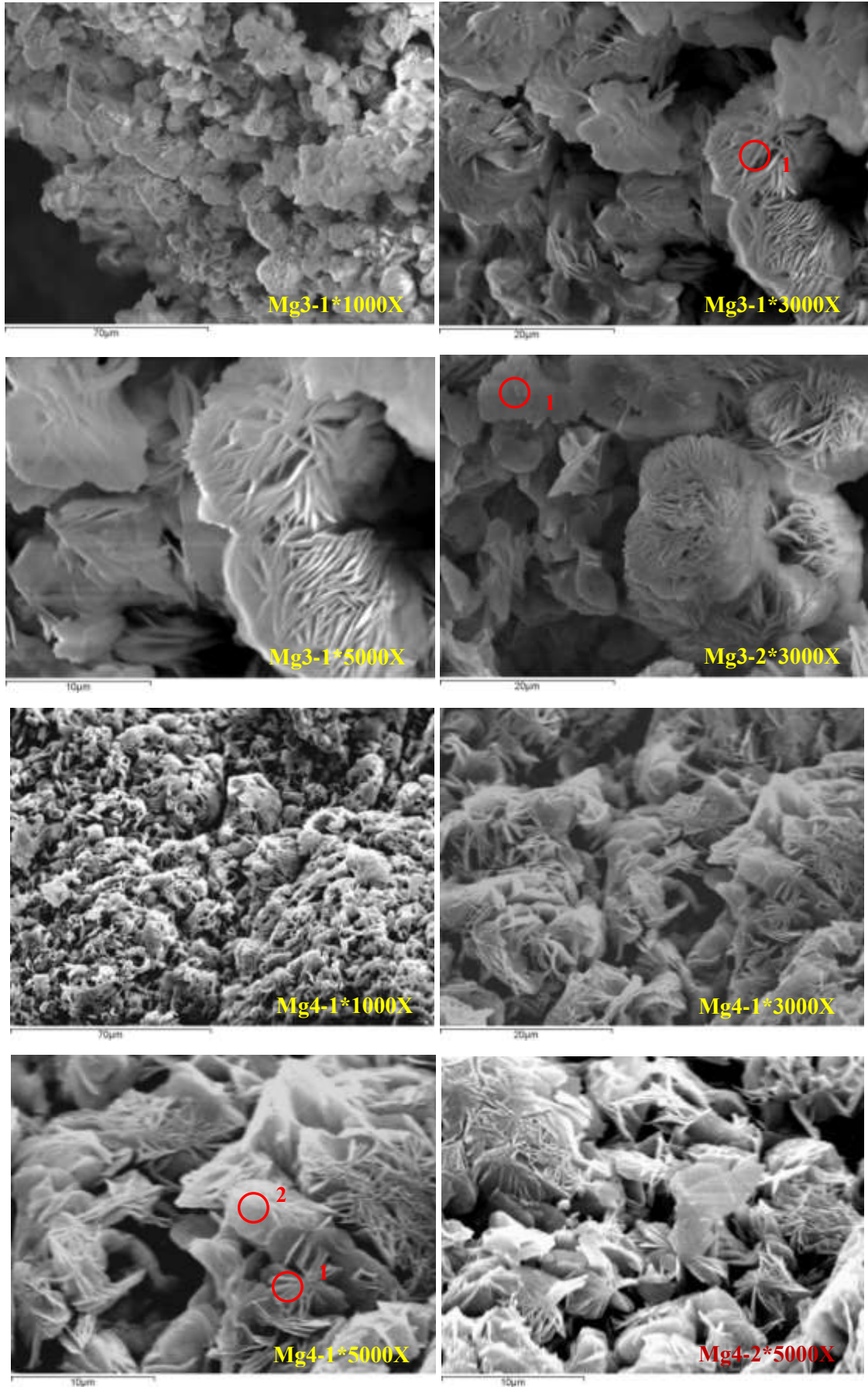
From the initial concentration perspective, supersaturation is a driving force for both original nucleation step and the following crystallisation growth. It is clear that sample 1 with lower supersaturation has more uniform and smoother particle morphologies than 3 due to less micro-collision, indicating its benefit in producing high quality crystals. This is in agreement with Hassan's work.

Stirring speed governs the particle size and particle distribution. On one hand, it can accelerate the formation of nuclei through increasing the rate of nucleation; on the other hand, it can also enhance the dissolution of the crystals by reducing the rate of their growth, thus breaking agglomerated blocks down. Sample 4 contains both sheet-like and flower-like crystals compared to 1. Evaluating both of them, it can be seen that 1 has more uniform morphology and crystallised structure due to the good mixture and particle agglomeration during the reaction. Thus it is important to ensure that a suitable stirring speed is employed to obtain the homogeneous crystals since they will affect the quality of precipitate. A relatively higher stirring speed leads to a more homogenous solution with better consistent particles generation, which was also in accordance with Wang et al. (2008).

Comparing samples 3 and 6, CO₂ flux rate is considered to have an effect on morphology formation. Higher carbonate ions production highlights the influence of CO₂ flux rate, which

reduces the reaction time. This faster reaction accomplishment provides a longer phase transformation from nesquehonite into hydromagnesite. Hence sample 3 accounts for more intensive hydromagnesite agglomerated clusters, confirming Hassan's work, while sample 6 has the assembled needle-like nesquehonite forming into tabular-shape particulates and obvious flat brucite particles, based on literature and XRD diffractograms above. Besides brucite gelatinous property, it is more desirable to deal with larger crystals with uniform size distribution during washing, filtering and storage, as larger particles are easier to be filtered out of a solution and have smaller surface area to volume ratio resulting in a higher purity from their less contact with the mother solution which contains impurities.





Sample	Spectrum	C	O	Na	Mg	Cl
Mg1-1*3000X	Spectrum 1	23.64	60.23	0.71	15.32	Not tested
	Spectrum 2	18.44	64.23	Not tested	17.33	Not tested
Mg3-1*3000X	Spectrum 1	1.98	69.95	1.67	25.56	0.84
Mg3-2*3000X	Spectrum 1	Not tested	58.23	6.94	13.29	21.54
Mg4-1*5000X	Spectrum 1	20.01	57.18	3.46	18.98	0.37
	Spectrum 2	21	56.83	3.32	18.46	0.4

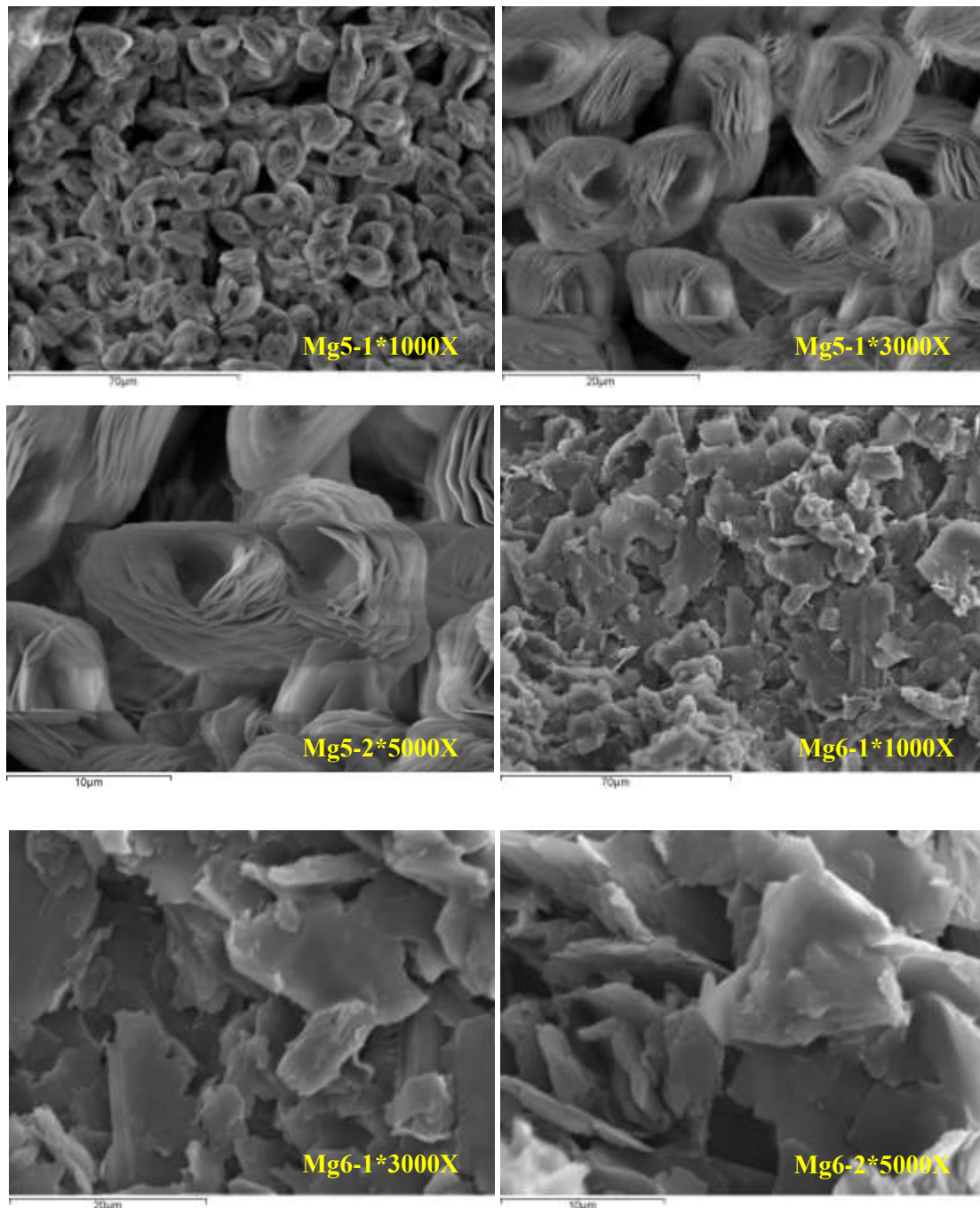


Figure 4. 22: The precipitates of microstructures of Mg1-6 and their correlated EDX results for SII.I shown in Table 4.5

4.5.3.4 Reaction Kinetics Studies

A bench study was operated at 1h at a controlled pH range; samples were then collected and tested. The remaining filtrates were subsequently kept within a sealed centrifuge tube, used for pH stability and kinetics test.

1h results demonstrated in [Table 4. 7](#) displaying that all magnesium sequestration efficiency is higher than 90%; particularly in sample 5, magnesium capture is over 99% at an elevated temperature. In one day measurement, there is not a significant difference in magnesium sequestration over time; hence 1h shows a promising functional period in magnesium removal.

Table 4. 7: The kinetic studies of Mg1-6 for SII.I shown in Table 4.5

Sample (Mg)	Mg ²⁺ concn (M)	Stirring Speed	Temp (oC)	pH	CO ₂ flux rate (cm ³ /min)	Net weight (g)	ICP result (g/l-1 h)	Sequestration%
1	0.25	700	25	10.5	500	4.07	0.3	95.06
2	0.5	700	25	10	500	8.18	0.86	92.79
3	0.5	700	25	10.5	500	7.9	0.28	97.63
4	0.25	0	25	10.5	500	3.26	0.36	94.01
5	0.5	700	40	10.5	500	7.85	0.03	99.75
6	0.5	700	25	10.5	150	8.31	0.16	98.71

Furthermore, according to the [Equation 4.1](#) in 4.5.2.2, the theoretical computed figures (maximum weight of a specific precipitate) and obtained weights after 1h are summarised in [Figure 4.23](#) (where AW=Actual Weight, TN=Theoretical calculated N, THM=Theoretical calculated HM, TD=Theoretical calculated D). Calculated hypothetical figure shows no AW matching with theoretical ones, proving that 1h is not sufficient to induce full crystallisation. The sequestered metals are either incorporated within the formed lattices or produced as nuclei only.

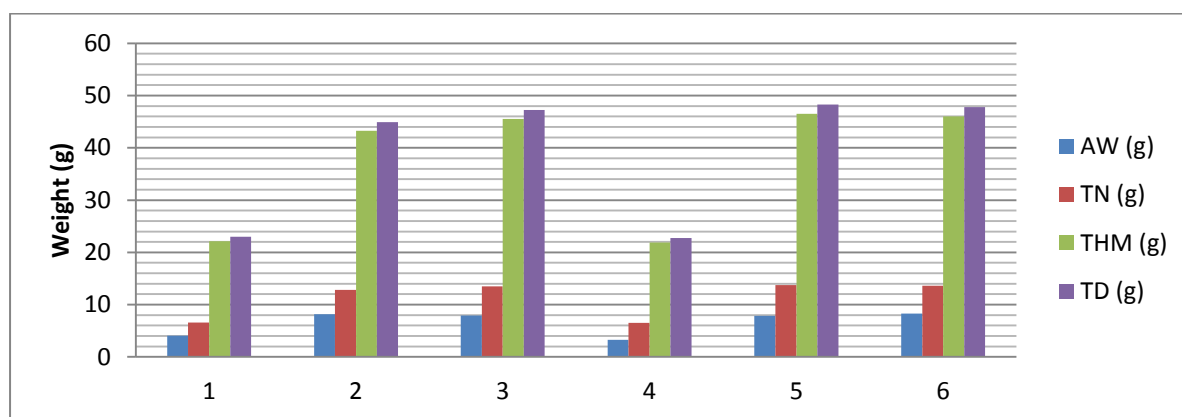
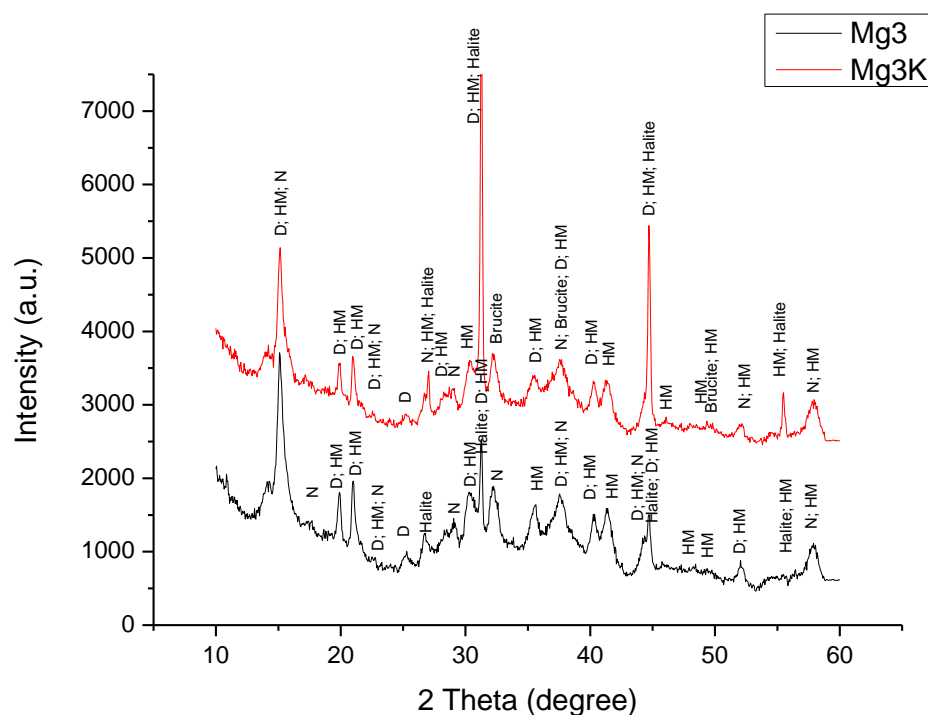


Figure 4. 23: The theoretical and actual weight comparisons of Mg1-6 for SII.I shown in Table 4.5

Among all samples, test 3 was selected for a continuing one day investigation, exhibiting overall the most appropriate performance in terms of kinetics, produced weight, XRD analysis and microstructure. **Figure 4. 24** presents Mg3 one day pattern and analysis, noticing more obvious shaper peaks formed after 1d, and more HMCs produced/crystallised from the matching scores.

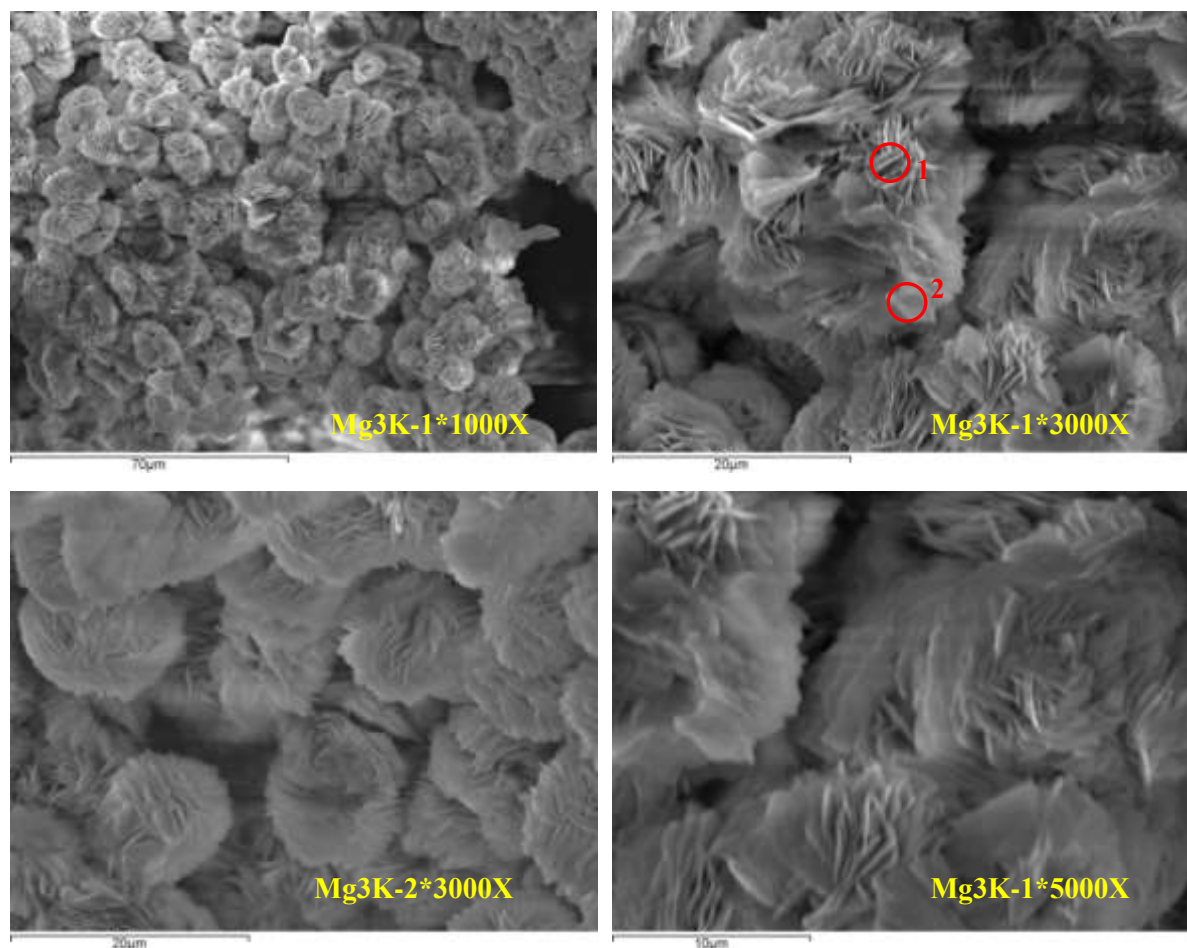


Sample			Mg3 (1h precipitates)	Mg3K (1d precipitates)
Ref. Code	Mineral Name	Chemical Formula	Contained within precipitates? (Score)	Contained within precipitates? (Score)
00-023-1218	Dypingite	$4\text{MgCO}_3 \cdot \text{Mg}(\text{OH})_2 \cdot 5\text{H}_2\text{O}$	Yes (34)	Yes (66)
01-070-0361	Hydromagnesite	$4\text{MgCO}_3 \cdot \text{Mg}(\text{OH})_2 \cdot 4\text{H}_2\text{O}$	Yes (39)	Yes (55)
00-001-0130	Nesquehonite	$\text{MgCO}_3 \cdot 3\text{H}_2\text{O}$	Yes (16)	Yes (42)
00-007-0239	Brucite	$\text{Mg}(\text{OH})_2$	No	Yes (53)
01-072-1668	Halite	NaCl	Yes (47)	Yes (69)

Figure 4. 24: Mg3 kinetic precipitates over a day (top) and the corresponded calculated scores (bottom) for SI.II

Microscopy was also conducted to image the one day kinetics, pictured at 1000x, 3000x, and 5000x magnification. Higher amounts of rosette-like hydromagnesite than sheet-like assembled HMCs appear after one day duration compared to the 1h reaction, illustrating the increased quantities of nesquehonite transforming into a more stable carbonate

hydromagnesite as **Figure 4. 25** shows (Mg3K refers to a one day sample of Mg3). Additionally, more uniform and homogenous crystals are also generated with a longer retention time. This phenomenon proves precipitates' conversion progressively from N to HM, demonstrating that a longer retention time speeds up this transformation process, equivalent to the effect of increased temperatures.



Sample	Spectrum	O	Na	Mg	Cl
Mg3K-1*3000	Spectrum 1	66.6	2.86	30.01	0.53
	Spectrum 2	66.31	2.94	29.23	1.52

Figure 4. 25: Mg3 kinetics one day microstructure for SII.I shown in Table 4.5

It is summarised that, during a short period of time, pH=10 is beneficial to particles observed from the prominent peaks performance and the regulated morphologies; but over a long-time period, pH=10.5 has a better result as it supplies sufficient reactants and provides the adequate crystallisation/transformation time.

4.5.4 Series II.I-Thermal Property and Calcination

4.5.4.1 The Analysis of Thermal Property

The thermal decomposition of all samples was undertaken to help the identification of the precipitates, to better understand their thermal properties and to quantify the degree of hydration and carbonation that occurred during the experiment. Results shown below are the mixtures of brucite, nesquehonite, dypingite and hydromagnesite as well as sodium impurity. Figures were assessed according to the referenced thermal estimation in Section 4.5.2.2, under atmospheric CO₂ pressure and air infusion gas. **Table 4. 8** summarises the weight loss and the corresponding peak temperatures of the samples, where the operations are heated up to 800°C in TGA.

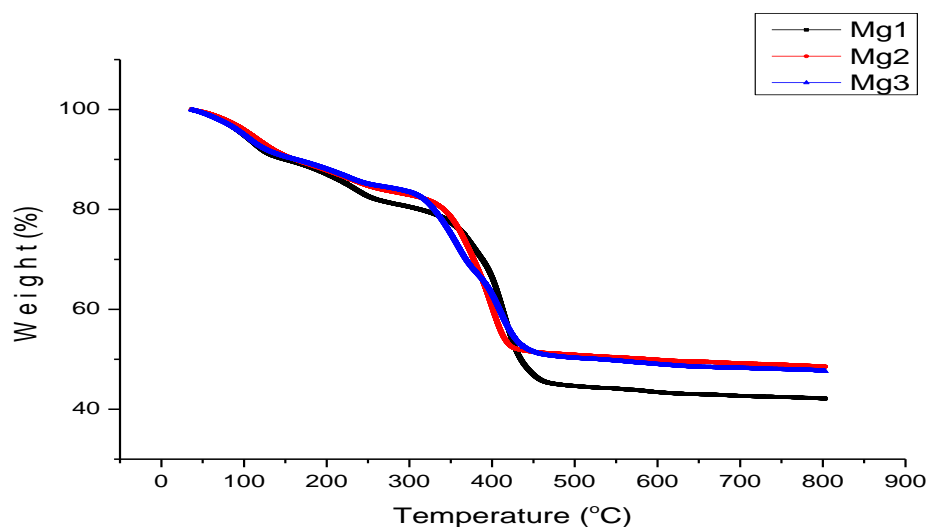
During step 1, the smaller amounts of water release (10-13%) compared to the standard (15-26%) is attributed to two possibilities: over dried in the oven beforehand and NaCl contamination. In terms of the over-burned situation, it was also noticed in samples' net weight Section 4.5.3.4. During step 2, it is expected that H₂O keeps releasing from the system, continuing dehydration process from the step 1. The decrease in sample mass varies from 1.8% to 6.5%, the majority of which is within the expected range except 5 with a lower weight loss of typical HMCs given in **Table 4. 6**. In step 3, the weight loss percentage is similar to the dypingite and hydromagnesite theoretical thermal decomposition profiles and the predicted CO₂ release amounts of 36.3% & 37.7% respectively except for sample 5.

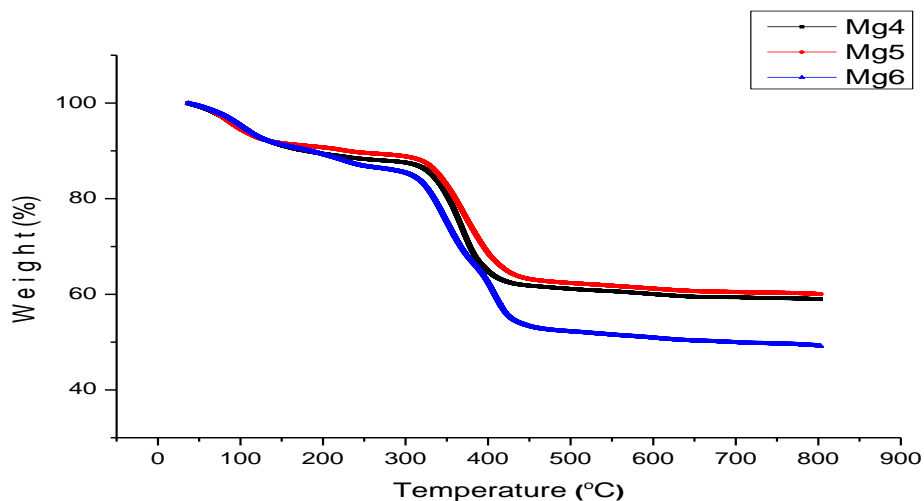
Table 4. 8: The thermal decomposition stages of Mg1-6 and Mg3 one day sample for SII.I shown in Table 4.5

Sample	Step 1: Temp <200°C		Step 2: Temp 200°C-300°C		Hydration degree (%)	Step 3: Temp >300°C		Total weight loss (%)
	Peak temp (°C)	Weight loss (%)	Peak temp (°C)	Weight loss (%)		Peak temp (°C)	Weight loss (%)	
1	114.59	12.86	234.69	6.54	19.40	416.78	38.22	57.62
2	110.71	12.16	233.03	4.89	17.05	395.03	34.26	51.30
3	108.59	11.82	229.92	4.59	16.41	358.06/409.36	36.71	52.13
4	107.65	11.73	228.10	4.01	15.75	367.92/411.06	33.47	49.21
5	95.63	10.54	226.42	1.84	12.38	362.41	28.42	40.80
6	109.86	10.65	230.93	3.83	14.48	335.64/406.16	36.06	50.54
3-1d	107.65	11.73	230.29	4.01	15.75	367.92/409.20	33.47	49.21

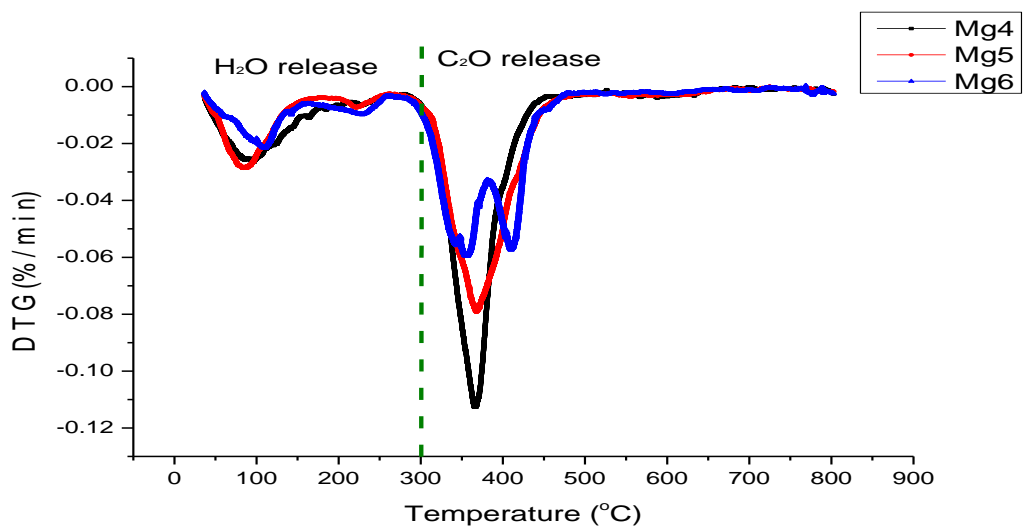
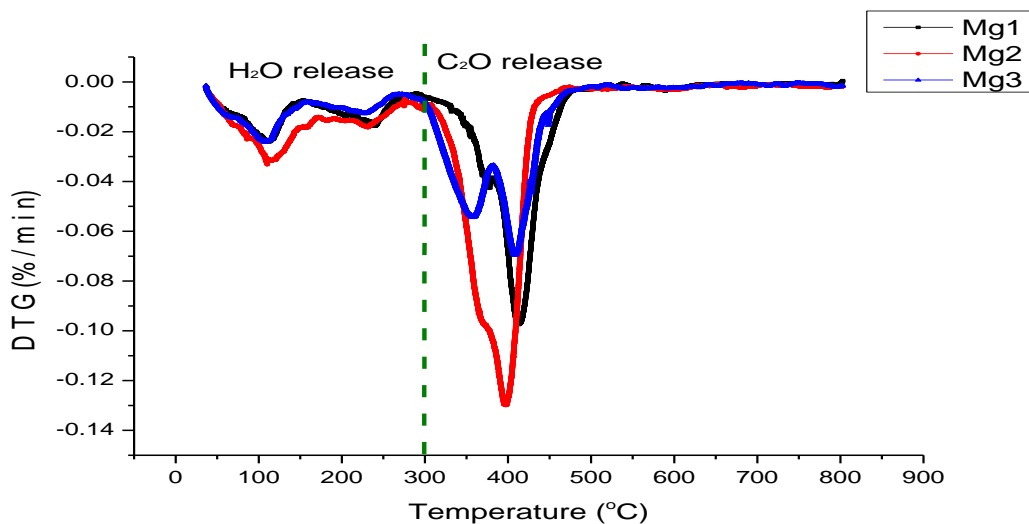
Sample 5 has the lowest H₂O and CO₂ weight loss, estimated from a higher temperature used in carbonation stage, resulting in less H₂O incorporation and less CO₂ dissolution in water by forming carbonate ions because of solubility. Thus its hydration and carbonation degrees are generally lower compared to others. Moreover, considerable amounts of sodium participated in this sample, which was also confirmed by Section 4.5.3.3 XRD identification. Samples 4-6 show more obvious brucite peak, leading to a slightly lower weight loss than samples 1-3. Similar to 5, sample 4 has no stirring speed, so less CO₂ is dissolved through either diffusion or its solubility capacity, while sample 6 has directly smaller CO₂ dissolution. It is therefore concluded that samples 4-6 all have the potential to form extensive brucite together with hydromagnesite and dypingite. In terms of Mg3 one day observation, there is no significant change in weight loss. But the reduced amount over a day can be explained by better crystallisation formation leading to more absorbed incorporated halite, or natural decomposition over the retention time.

This peak temperature observed within the experiment is similar to Hassan's work, but several profiles present two peaks in the range of 300-450°C (Figure 4.26, DTG = Differential Thermogravimetry). This can be possibly attributed to two-step decomposition. Immediate re-carbonation with original powders directly resulted in a second procedure, reported by authors Bandi & Krapf (1976) and McIntosh et al. (1990). This re-carbonation can be caused by several parameters like, particle sizes, sample lid, atmosphere diffusion and ventilation situation, etc.

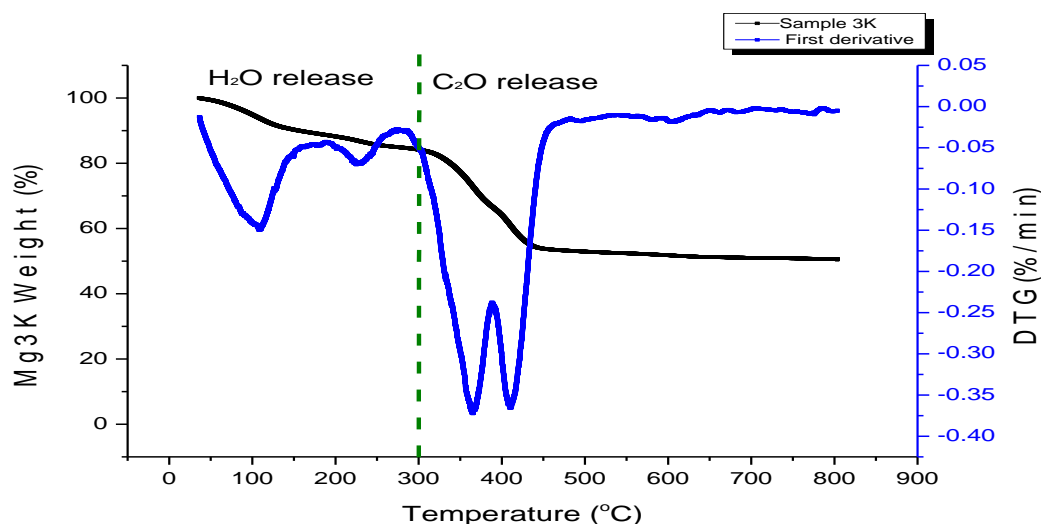




(a): The weight% profiles of Mg1-6 calcination for SII.I shown in Table 4.5



(b): The derivative profiles of Mg1-6 calcination for SII.I shown in Table 4.5

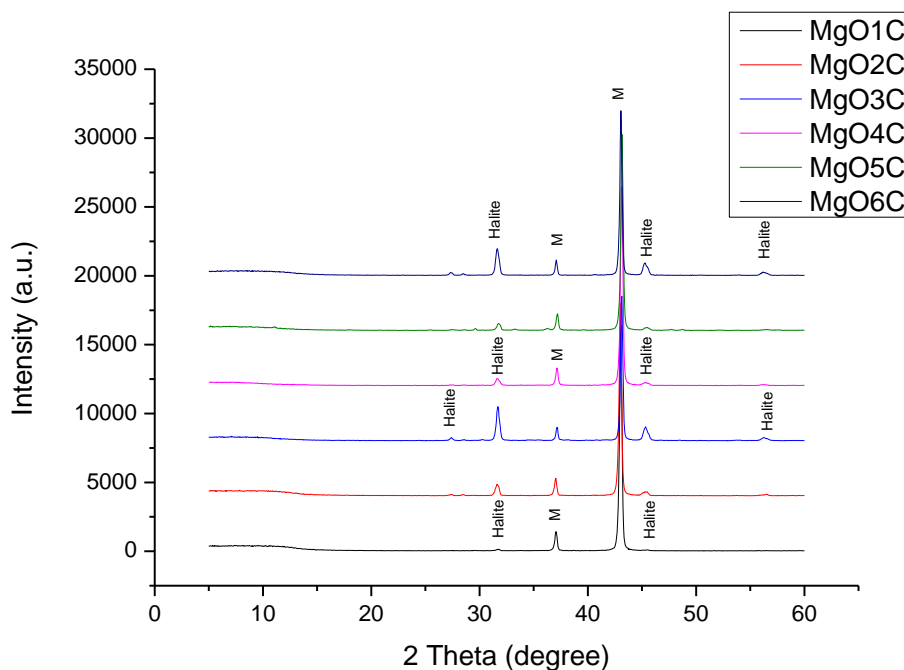


(c): The Mg3 one day (Mg3K) thermal profile weight % and its first derivative for SII.I

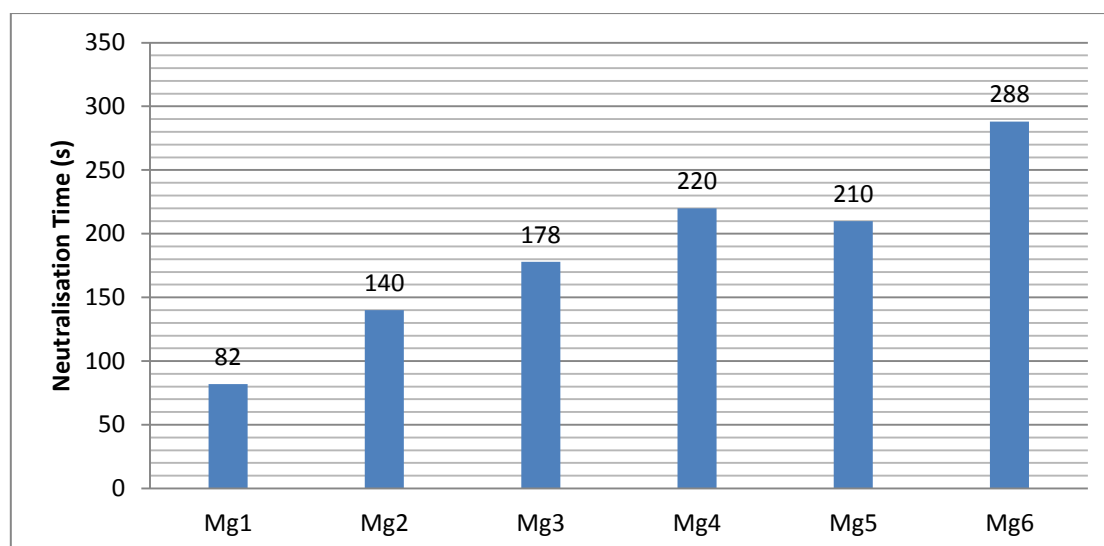
Figure 4. 26: The TGA thermal (a) and the analysed first derivative (b) profiles of Mg1-6, and Mg3 one day sample (c) for SII shown in Table 4.5 (captions see top right corner)

4.5.4.2 The Analysis of Calcination at a Certain Temperature

MgO is produced at a temperature of 800°C initially; this section illustrates the calcined products as well as their reactivities. XRD results in Figure 4. 27a demonstrate that all the decomposed precipitates are MgO completely, with some NaCl impurity incorporation.



(a): The calcined products of Mg1-6 for SII.I shown in Table 4.5 (Halite=NaCl, M=MgO)



(b): The MgO reactivity tests of Mg1-6 for SII.I shown in Table 4.5

Figure 4. 27: The calcination products of Mg1-6 (a) and MgO reactivity tests of Mg1-6 for SII.I (b)

All other sample sizes tested were less than 250 μm . It is clear that particle size affected the reactivity result. For example, without the grinding of sample 3, reactivity was more than 8min, compared to only 3min of the same sample after grinding.

Lower reactant concentration (sample 1) presents better reactivity when comparing 1 and 3 (**Figure 4. 27b**), which is caused by more uniform particles' morphology during the carbonation and calcination processes. Samples 2 and 3 show pH effect: when pH is higher, a longer reactivity appears, caused by the surplus hydroxide ions. Subsequently, in temperature differences (samples 3 and 5), a higher temperature (Mg5) usually leads to a larger pH value and more abundant hydroxide ions existence within the solution of lower reactivity, while finally sample 6 has the longest neutralisation time because of less CO_2 infusion. On one hand, it is due to more sheet-like aggregated particles that lead to the reduced porosity. On the other hand, it can be indicative of halite incorporation, as shown by XRD. There are large differences in comparison to the references in Section 4.5.2.2, which are caused by much larger particle sizes in the experiments. This grinding size was decided by the products' property and the working suitability.

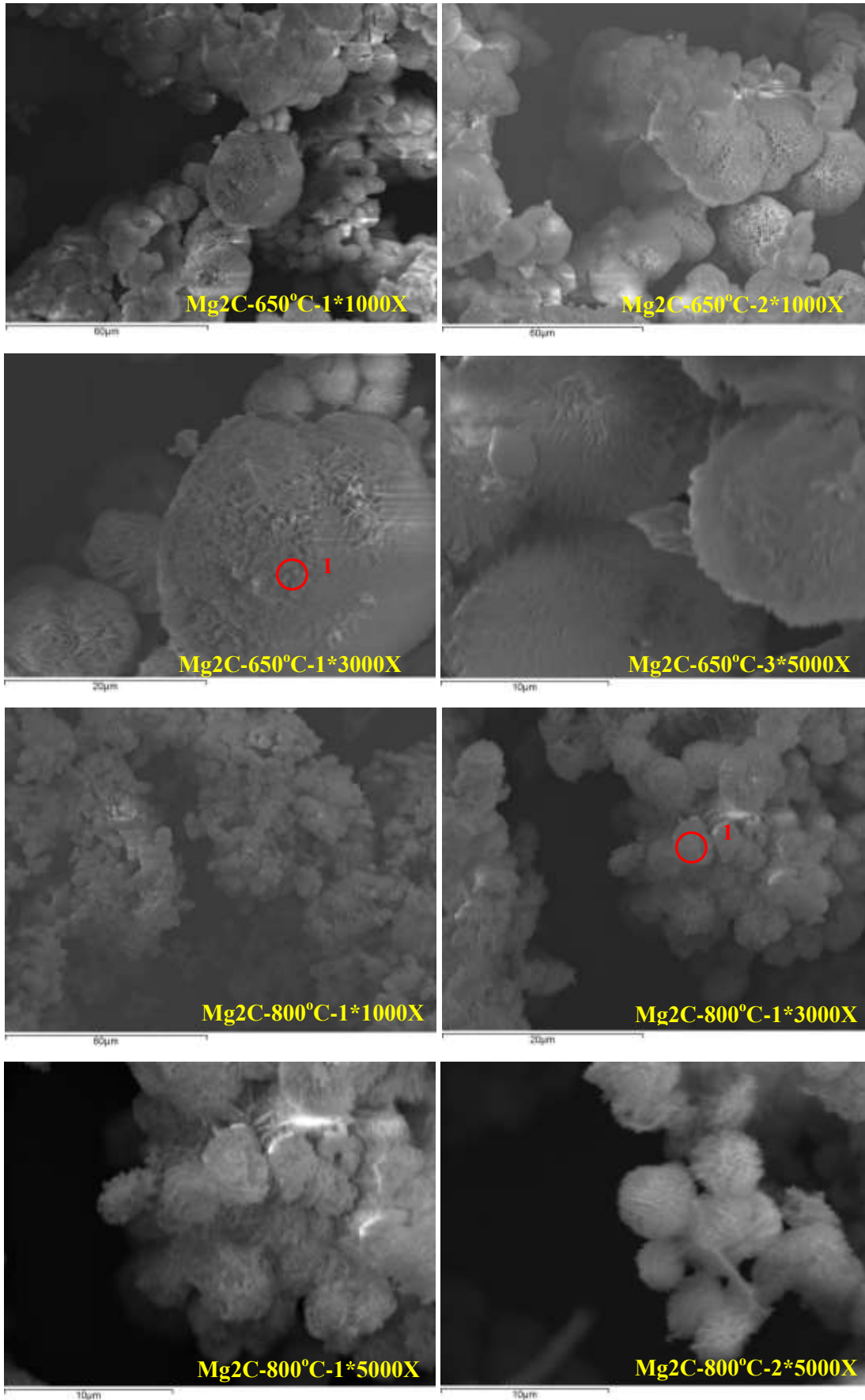
It is concluded that supersaturation degree and carbonates' morphologies affect resulting MgO reactivity. Usually a higher supersaturation will enhance the MgO reaction time with non-uniform or sheet-like particles performance or direct higher quantities of hydroxide

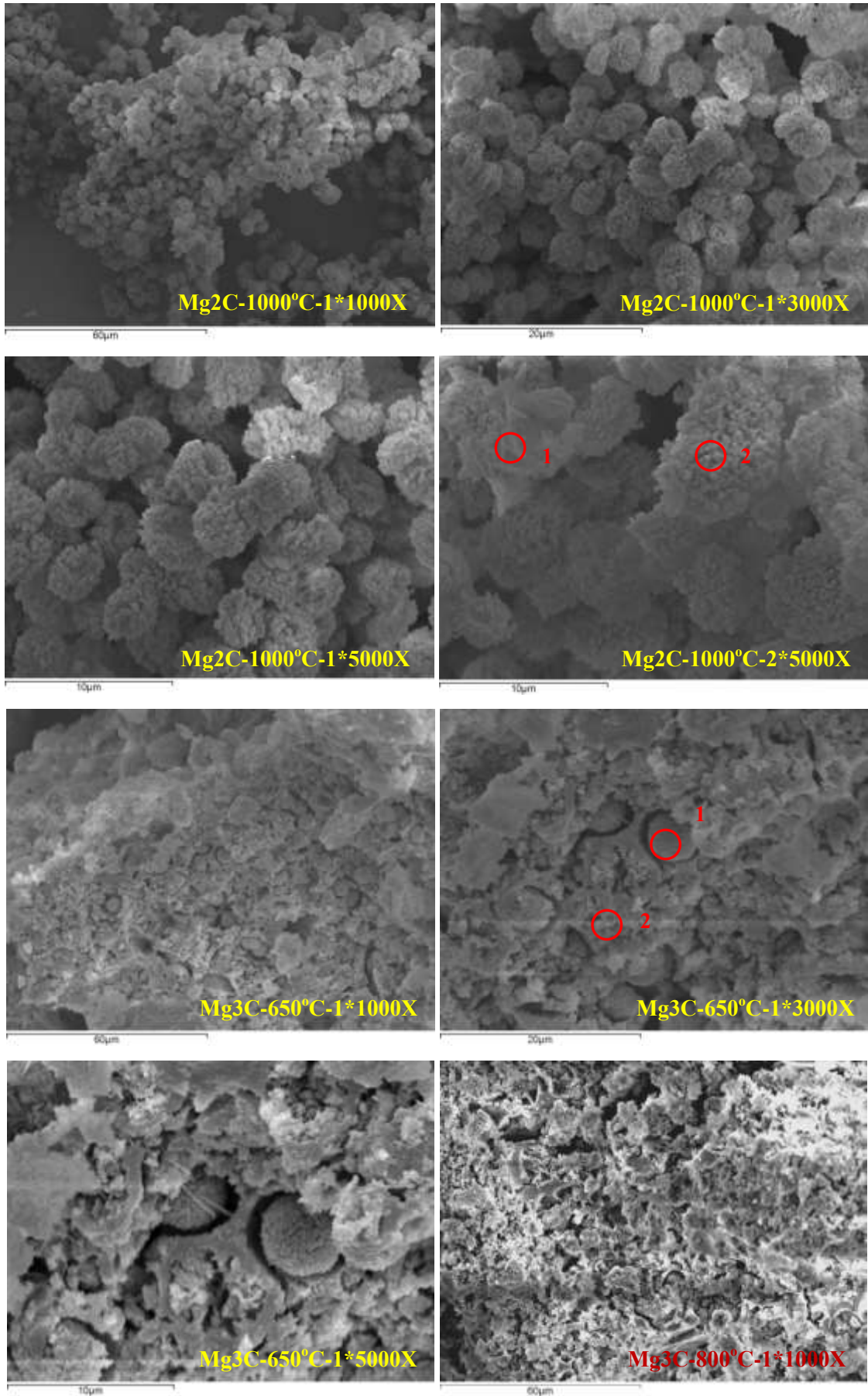
compounds. This was also demonstrated in Hassan's project. Additionally, impurity can further delay the neutralisation progression, such as halite intersection within the lattices of products in this study.

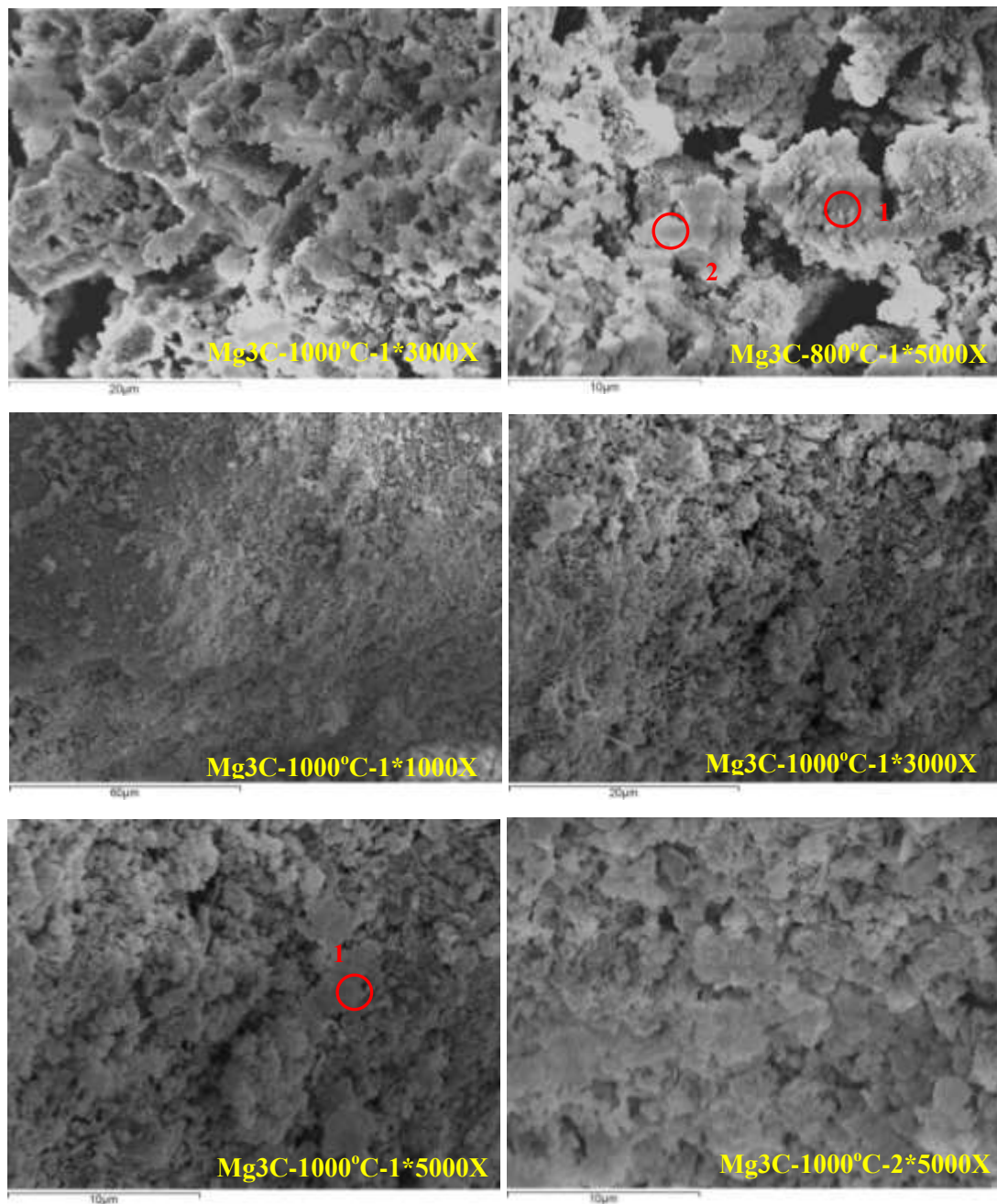
4.5.4.3 The Analysis of Calcination at Various Temperatures

Three calcination temperatures 650°C, 800°C and 1000°C were undertaken by a furnace to better understand the decomposed properties of the selected samples Mg2-3. In [Figure 4.28](#), 650°C treated samples have larger rounded particles and this pore size gradually decreases with the increasing temperature. It is noticeable that 1000°C is not sufficient to fully decompose the carbonates by the retained carbon appearance from samples Mg2-3-1000°C. The explanation of no carbon detected at the lower temperatures of 650°C and 800°C is the random selection and the limitations of surface detection, which cannot represent the entire situation. Carbonation occurs naturally during the grinding stage or during long-time storage before testing when the powder is more likely to come in contact with the atmosphere. Mg2 has a better shape than 3, while the latter has more agglomerated blocks, as a result of higher pH and supersaturation degree level. This elevated pH induces a more complex turbulence than 2, and increases the nuclei generation. Therefore these smaller sizes tend to agglomerate. Conversely, system 2 is relative simple, and the particles have sufficient space and time in which to crystallise. Overall the EDX results imply good sodium elimination and magnesium sequestration.

Two TGA profiles up to 1000°C were measured afterwards. Both of them present only one prominent peak at around 400°C, coping well with conventional magnesium products ([Figure 4.29a-b](#)). However, EDX detection contradicts the theoretical assumption of no carbonates appearance beyond 600°C, and the completed decarbonation process cannot be identified as the upper limit of TGA at 1000°C. There is a larger weight loss in 2 than 3. From the previous investigation (Section 4.5.4.1), sample 2 has a higher degree of hydration but lower carbonation until 800°C. This extended heating profile implies that the enclosed carbonates can be released at higher temperatures.

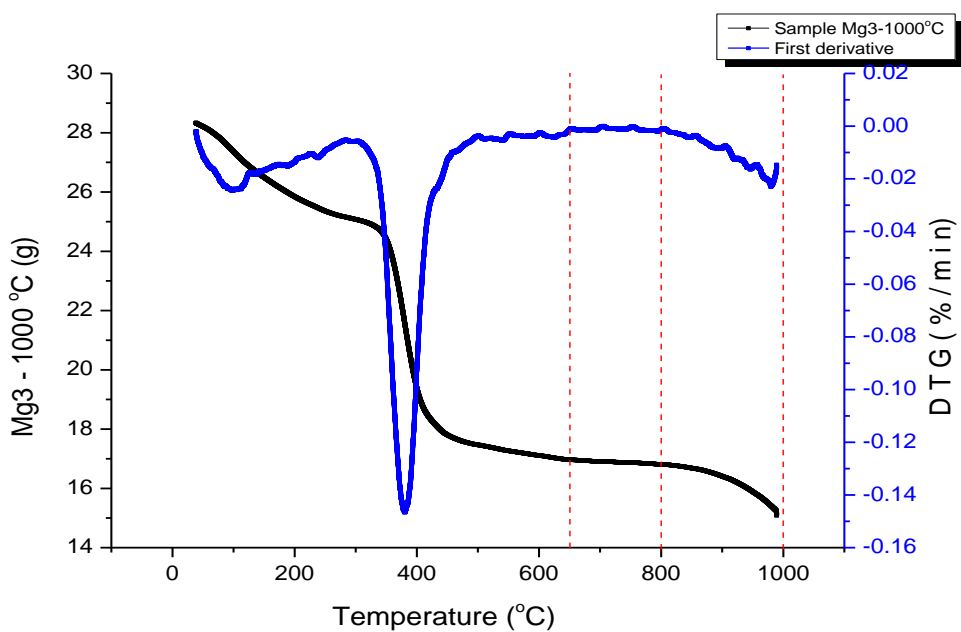
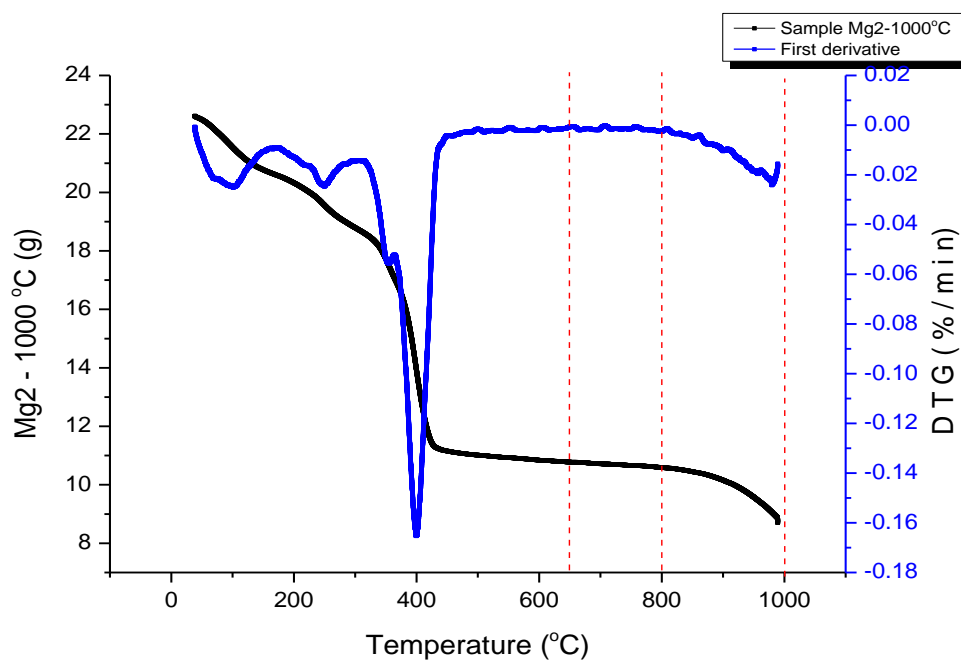






Sample	Spectrum	C	O	Na	Mg	Cl
Mg2C-650°C-1*3000X	Spectrum 1	Not tested	42.8	0.99	55.13	1.07
Mg2C-800°C-1*3000X	Spectrum 1	Not tested	50.39	Not tested	49.61	Not tested
Mg2C-1000°C-2*5000X	Spectrum 1	14.82	43.01	0.08	42.09	Not tested
	Spectrum 2	16.71	23.28	3.26	56.76	Not tested
Mg3C-650°C-1*3000X	Spectrum 1	29.61	29.87	7.03	33.5	Not tested
	Spectrum 2	12.82	39.44	2.37	45.36	Not tested
Mg3C-800°C-1*5000X	Spectrum 1	Not tested	32.36	10.51	31.52	25.6
	Spectrum 2	Not tested	53.43	1.92	43.66	0.99
Mg3C-1000°C-1*5000X	Spectrum 1	26.16	36.02	1.22	36.61	Not tested

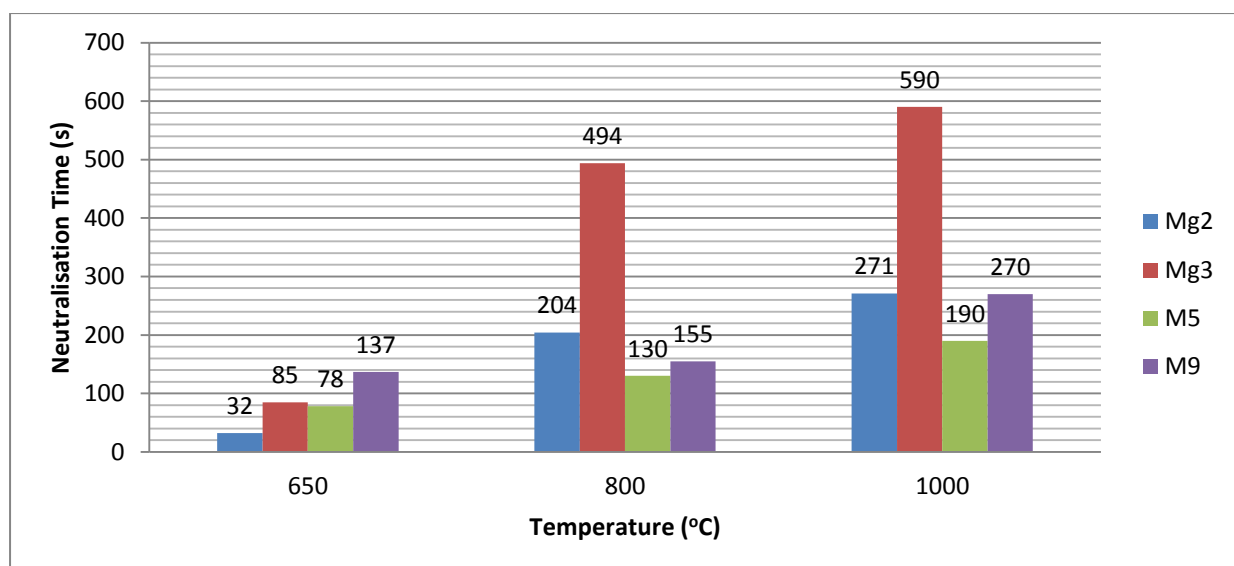
Figure 4. 28: The microstructure of calcination products Mg2&3 & their corresponded EDX results for SII.I shown in Table 4.5



(a): The TGA thermal profiles of Mg2-1000°C (top) and Mg3-1000°C (bottom) for SII.I

Sample	T < 650°C		650°C < T < 800°C		800°C < T < 1000°C		Total weight loss (%)	
	Peak (°C)	T	Weight loss (%)	Peak (°C)	T	Weight loss (%)		
Mg2-1000°C	400.5		52.33	N/A	1.74	986.67	17.8	71.87
Mg3-1000°C	382.96		40.13	N/A	0.94	986.97	10.24	51.31

(b): The TGA thermal stages of Mg2/3-1000°C for SII.I



(c): The reactivity tests of Mg2 and Mg3 at various calcination temperatures and their comparisons for SII.I

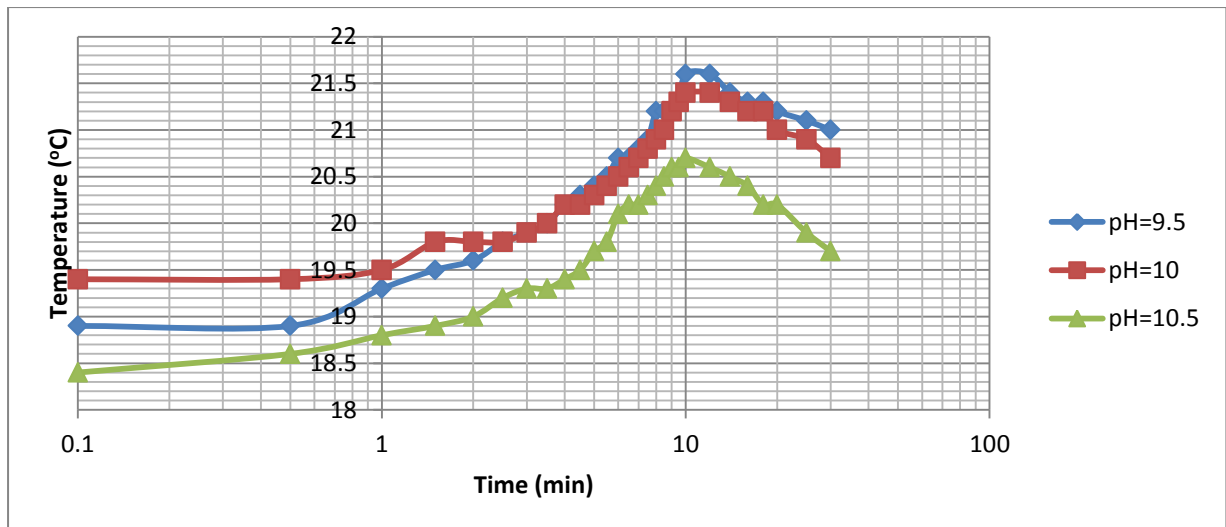
Figure 4. 29: The TGA profiles of Mg2/3 1000°C calcination (a) & their calcination stages (b), and the reactivity tests of Mg2-3 at various calcination temperatures (c)

Finally, reactivity testing outcomes agree fully with the prediction that a higher calcination requires a longer neutralisation period because of the reduced voids and the granular sizes. Mg2 & M9 were then paired together as Group 1 and Mg3 & M5 as Group 2 (Figure 4. 29c), because the parameter design was identical for each pair with the exception of calcium addition in M5 & M9. Group 2 shows greater reactivity compared to Group 1 at all temperatures. This is caused by the higher pH level resulting in larger quantities of hydroxide ions and further complicating the formed system involving possibly more impurities. MgOs has a longer neutralisation time than the mixed oxides, while the latter is reduced by the addition of CaO.

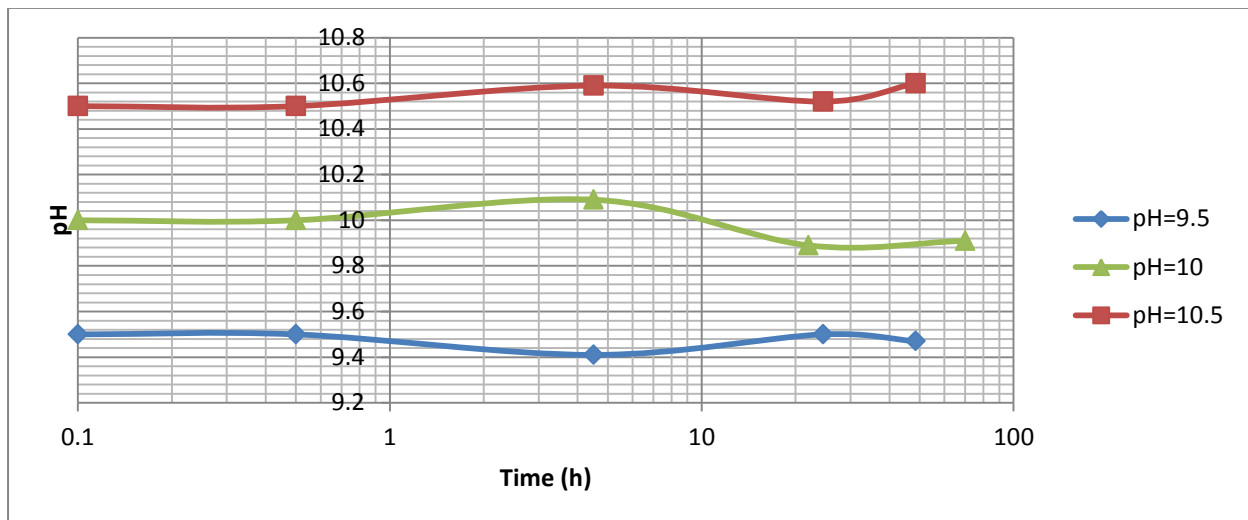
4.5.5 Series II.II-Miscellaneous Studies

4.5.5.1 Series II.II-The Comparison Studies of Ammonia and Sodium Hydroxide

Three pH numbers 9.5, 10 and 10.5 were chosen reacting with NaOH using the identical controlled parameters as Series I. It is mainly evaluated from the carbonation studies, pH stability studies, precipitate identification and kinetics reaction.



(a): Temperature vs time (NaOH) +CO₂ for SII.II using the parameters in Table 4.2



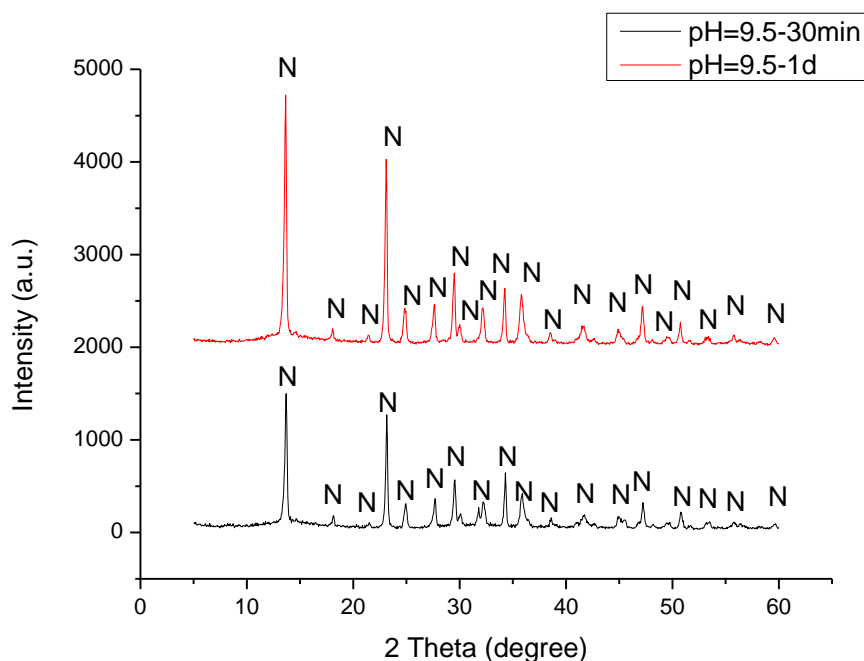
(b): pH stability vs time (NaOH) +CO₂ for SII.II using the parameters in Table 4.2

Figure 4. 30: Carbonation (a) and pH stability (b) studies using NaOH as an alkali for SII.II with the same parameters used in Table 4.2

Figure 4.30a shows a similar tendency with ammonia but with less obvious gradients and thermal elevation due to the reduced grain sizes within the solution. Ammonia is a gas-liquid mixture, where atoms are generally more active than the sodium solid-liquid mixture. The pH stability studies show a slight fluctuation compared to ammonia, implying a good buffering capacity in ammonium salts. Sodium stability is within the acceptable deviation errors (standard value ± 0.1) of a standard pH.

It is worth noting that XRD pattern has demonstrated interesting precipitates (**Figure 4.31a**): when the pH is lower than 9.5, nesquehonite is formed similar to Series I, but at a higher alkaline level, hydromagnesite and dypingite are formed instead (within a 30min timeframe) (**Figure 4.31b**). This performance then alters from HM+D to nesquehonite at pH=10 after a day (**Figure 4.31c**), contradicting the literature findings of the more stable D and HM than N. It is therefore considered that samples are changed by natural decarbonation or decomposition from the atmosphere over time. However, this is not the case at a higher pH level (pH=10.5) that surplus hydroxide ions inhibit the automatic phenomenon (Mg3K).

The precipitates show that nesquehonite become present in ammonia utilisation, whereas hydromagnesite and dypingite become present in NaOH usage, when comparing SI and SII.II. This phenomenon is illustrated by the atom disturbance due to sodium, while ammonia is easy to evaporate which reduces this effect. The buffering capacity of ammonia also partially contributes to the feasibility of the phase transformation; in contrast, sodium works more rapidly due to its strong alkalinity. The higher pH in the ammonia solution produces bigger crystals more easily filtrated and ground, but in the NaOH solution, the higher pH tends to generate finer brucite particles instead from the surplus hydroxide ions leading to the particles' gelatinous characteristics.



(a): pH=9.5 over 30min and one day for SII.II using the parameters in Table 4.2 (N=Nesquehonite)

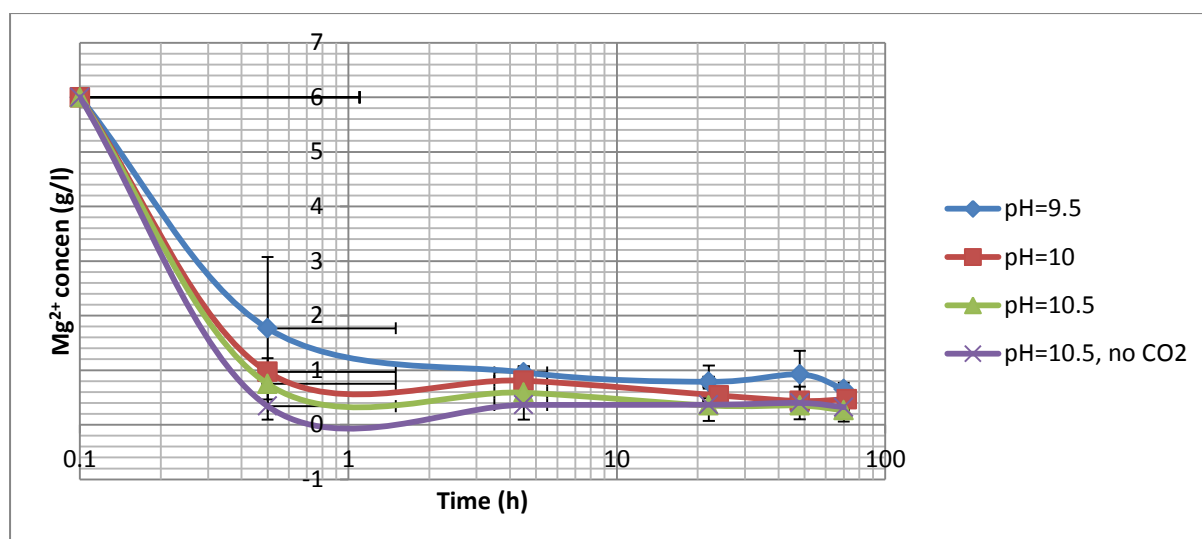


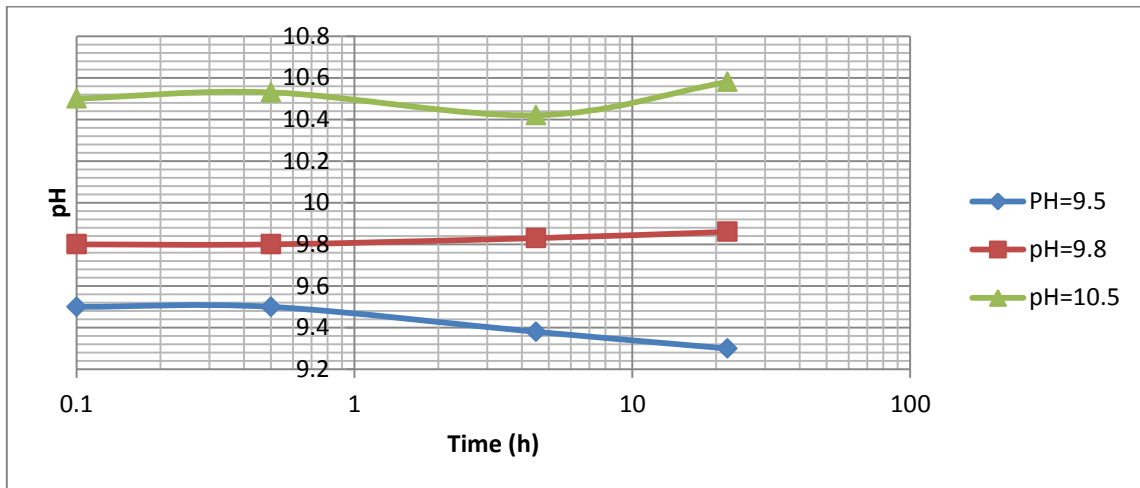
Figure 4. 32: Unreacted Mg^{2+} concentration with NaOH vs time with STEDV over 3 days for SII.II using the same parameters in Table 4.2

Both ammonium and sodium hydroxide have good magnesium sequestration, and prove that a higher pH can capture more metals. Moreover the majority of the reaction is completed within a half-day. Dissimilarly, all precipitates of $pH > 9.5$ achieves more than 80% sequestration after 1h with less 1g remaining in NaOH, and the larger pH can initiate the higher capture percentage; but this pH level in ammonia changes into $pH < 10$, where the larger pH has less sequestered efficiency initially. This is considered from the weak base property of ammonia, indicating that the weak alkali stays at molecular form at first and then gradually decomposes to an ionised appearance. Conversely, the sodium hydroxide exists as a strong base with the directly dissociated sodium and hydroxide ions within the solution from the first step. In summary, sodium hydroxide has advantages over ammonia because it theoretically needs a shorter time to reach the balance and also has cost competitiveness as well as operational convenience.

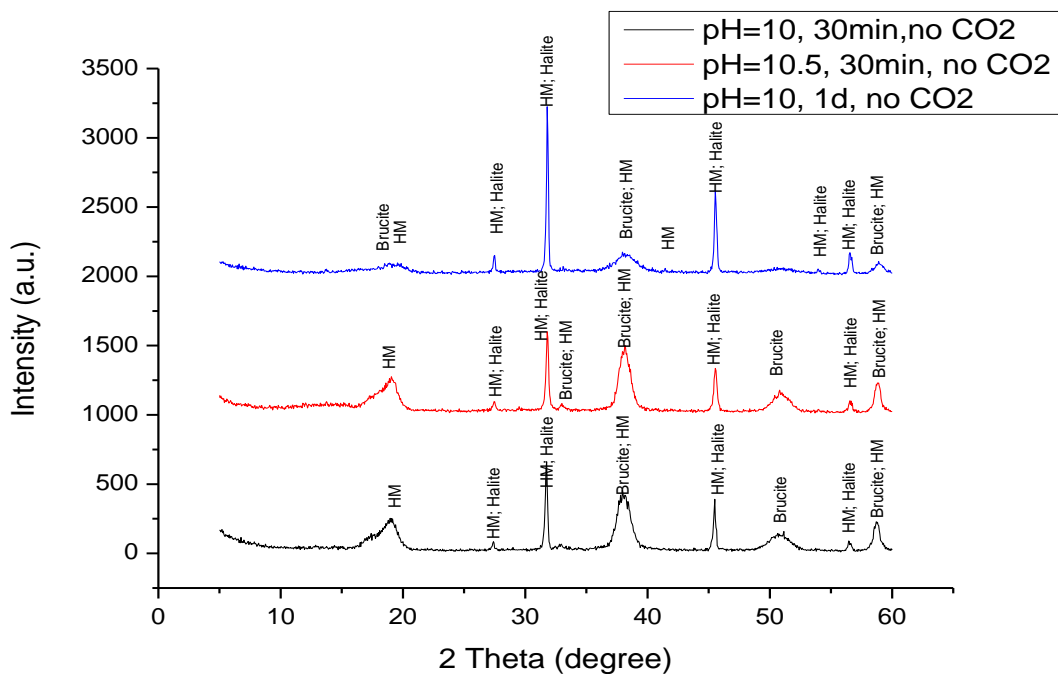
4.5.5.2 Series II.II-The Addition and Elimination Studies of CO_2

This experiment of no CO_2 diffusion into $MgCl_2$ solution was operated together with the Section 4.5.5.1 NaOH comparison studies above. Ideally, no carbon involvement leads to brucite formation instead. A pH stability test indicates that it is harder to control the pH level when CO_2 is eliminated due to the lack of weak base hydrolysis (Figure 4. 33a). The carbonates that existed in precipitates (Figure 4. 33b) are considered to be the result of natural carbon dioxide contact from the atmosphere. In the no- CO_2 system, products are

more gelatinous, leading to severe problems in filtration, and it is also observed that in both NaOH+CO₂ and NaOH-CO₂ situations, pH=10.5 is hard to achieve, while the convenient pH range is around 9.8<10<10.3. Hence CO₂ helps to control the pH in a solution effectively.



(a): pH stability vs time (no CO₂) for SII.II using the same parameters in Table 4.2



(b): Precipitates produced in various pH (no CO₂) for SII.II using the same parameters in Table 4.2 (HM=Hydromagnesite, Halite=NaCl)

Figure 4. 33: pH stability study (a) and precipitates produced in various pH without CO₂ (b) for SII.II

4.6 Series III-Individual Calcium Ion System with Sodium Hydroxide

4.6.1 Model for Series III

On the basis of PHREEQC modelling, thermodynamic favoured prospective precipitates with a Saturation Index over pH are summarised in **Figure 4. 34**. In this figure, $\text{CaCO}_3 \cdot \text{H}_2\text{O}$ has the highest pH=7.2, when the Saturation Index=0, while calcite has the least pH=6.4 when the SI=0. This is explained by monohydrated calcite hydrophilic property, providing a higher tolerance to maintain the reversible balance between hydrogen and hydroxide ions. The same tendency also presents in magnesium series, deducing that materials with stronger hydrophilic groups require larger pH to settle down. Between 9.5 and 10.5, all types of calcium carbonates can be formed, namely aragonite, $\text{CaCO}_3 \cdot \text{H}_2\text{O}$, calcite and vaterite. These four carbonates have no significant fundamental differences but appear with different structures and crystallised orders.

Visual Minteq was run at both room temperature and 40°C at fixed pH of 10 and 10.5. Calculated ionic strength is less than 1, indicating the reliability of results. It presents the same precipitates as PHREEQC, of aragonite, $\text{CaCO}_3 \cdot \text{H}_2\text{O}$, calcite and vaterite formation. Thus both models point towards the same conclusion.

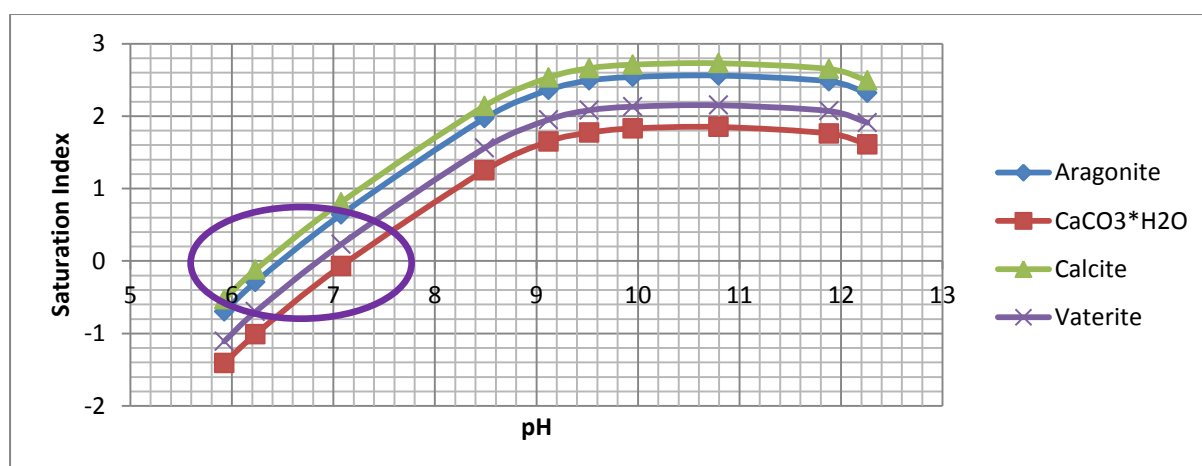
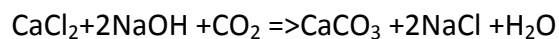


Figure 4. 34: The Saturation Index of calcium carbonates over pH, summarised from PHREEQC for SIII

4.6.2 Series III-Experimental Design

4.6.2.1 Experimental Parameters

In this individual calcium study, NaOH was used as an alkali with the equation:



Other design variables can be seen in [Table 4. 9](#), where samples 1 & 4 were designed for stirring speed, samples 2 & 3 for pH, samples 1 & 3 for reactant concentration, samples 3 & 5 for temperature, and samples 3 & 6 for CO₂ flux rate comparison respectively. The pH was controlled with a pump at different rates throughout the reaction. The initial operating CaCl₂ solution was 200ml, and the expected formations were vaterite and calcite. Net weights of samples were washed at least three times in centrifuge tubes, and then dried at 35°C consistent with SII, and finally weighed immediately after reaching a constant mass. The NaOH used is 1mol/l.

Table 4. 9: Calcium experimental design parameters for SIII

Sample (Ca ²⁺)	Ca ²⁺ concentration (M)	Stirring speed (rpm)	Temperature (°C)	pH	CO ₂ flux rate (ml/min)
1	0.1	700	25	10.5	500
2	0.5	700	25	10	500
3	0.5	700	25	10.5	500
4	0.1	0	25	10.5	500
5	0.5	700	40	10.5	500
6	0.5	700	25	10.5	150

4.6.2.2 Analytical Measurements

ICP: ICP is used to identify the concentration of metal ions left within solution; collecting times for samples were at 1h and 1d. Standard calcium calibrations used were 0.1ppm, 1ppm, 10ppm and 100ppm. The obtained ICP is also utilised to calculate the theoretical precipitates and make the comparisons with practical measured weight. For instance, samples 1 and 4 are 0.1M (=4g/l) calcium reactants and others are 0.5M (=20g/l). A test solution is 200ml. Assuming all captured metals transform into calcium carbonates in the end, as three types of carbonates vaterite, calcite, and aragonite have identical chemical form (CaCO₃), molecular weight of each calcium carbonate is the same. After measuring the one hour sequestered calcium, we can use the following equation:

$$\frac{\text{Calcium sequestration efficiency (1h)} * \text{Molar concentration}}{\text{The theoretical amounts of precipitates}} = \frac{M_{Ca}}{M_{CaCO_3}} \quad \text{(Equation 4. 2)}$$

Where

Calcium sequestration efficiency (1h) can be seen from **Table 4. 12** (Section 4.6.3.4, page 173) below.

The theoretical amounts of precipitates are unknown

$$M_{\text{Ca}} = 40 \text{ g/mol}$$

$$M_{\text{CaCO}_3} = 100 \text{ g/mol}$$

For example, sample 1

$$\frac{0.9889 * 4 \text{ g/l}}{x} = \frac{40}{100}$$

So

$$x = 9.89 \text{ g/l}$$

Given solution volume is 200ml

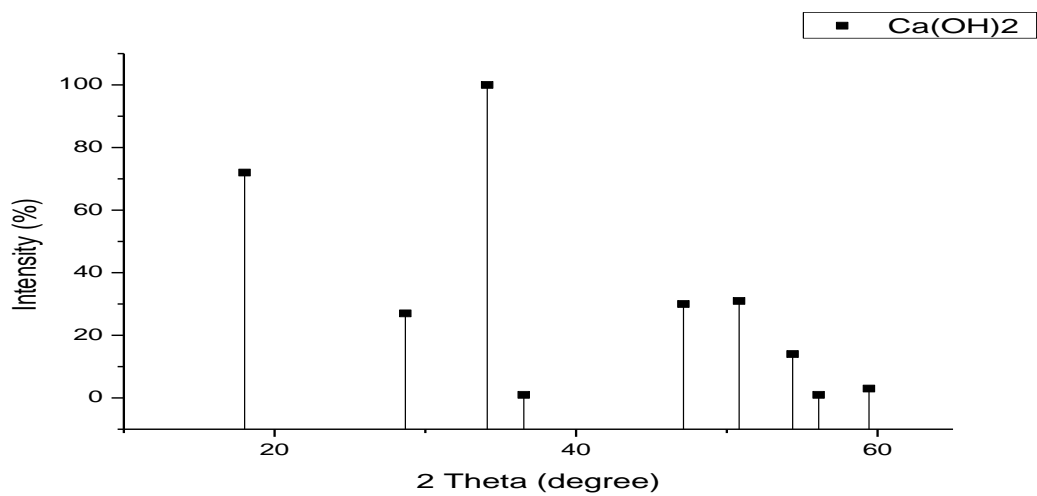
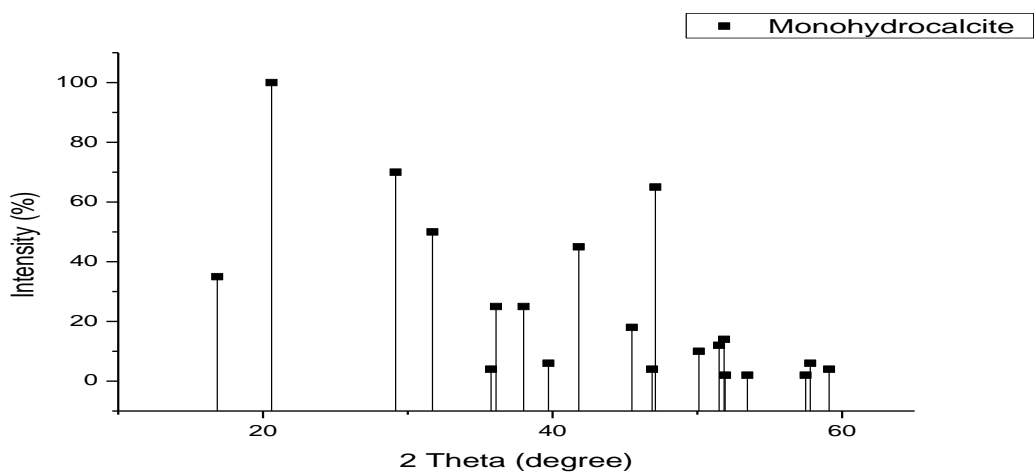
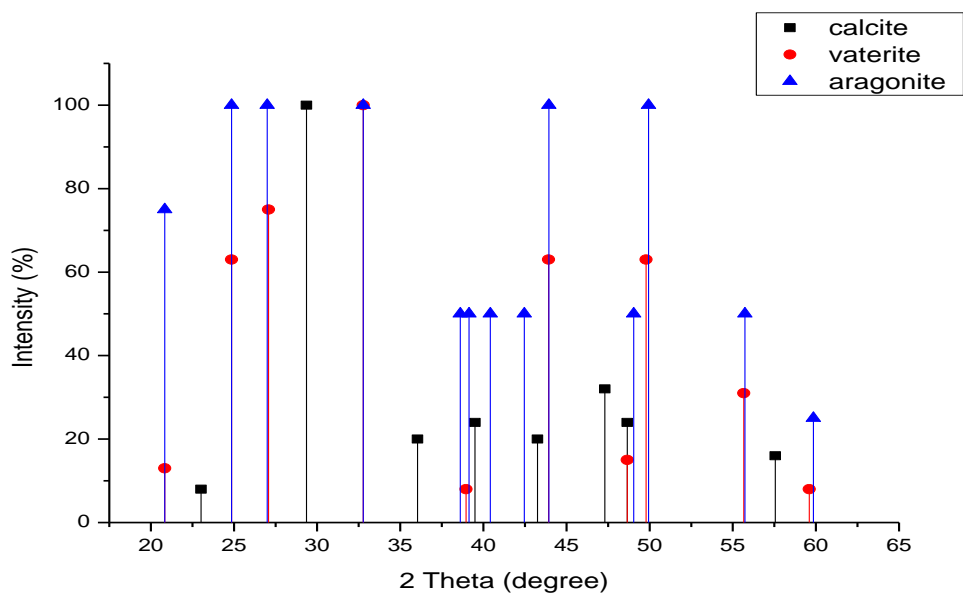
$$\text{Total weight} = 9.89 \text{ g/l} * 0.2 \text{ l} = 1.98 \text{ g}$$

In sample 2, initial molar concentration changes from 4 g/l into 20 g/l by using the same equation; so the theoretical weight of sample 2 can be calculated as 9.65g, based on the method above.

XRD: The chemical compositions of the calcium carbonates related to this work are described in **Table 4. 10**. In addition, the standard XRD diffractograms of the precipitates as well as portlandite and lime are given in **Figure 4. 35**. Many similarities among aragonite, vaterite and calcite can be seen below, which is caused by the identical chemical formula but different molecular structures and make it a challenge in some cases to differentiate them from another.

Table 4. 10: The chemical compositions of potential formed calcium carbonates in the precipitates for SIII

Calcium carbonates	Chemical Formula	CO ₂ (%)	H ₂ O (%)	CaO [Ca ²⁺] (%)	Total Loss (%)
Aragonite (A)	CaCO ₃	44	N/A	56 [40]	44
Vaterite (V)	CaCO ₃	44	N/A	56 [40]	44
Calcite (C)	CaCO ₃	44	N/A	56 [40]	44
Monohydrated calcite (MHC)	CaCO ₃ •H ₂ O	37.3	15.3	47.5 [33.9]	52.6



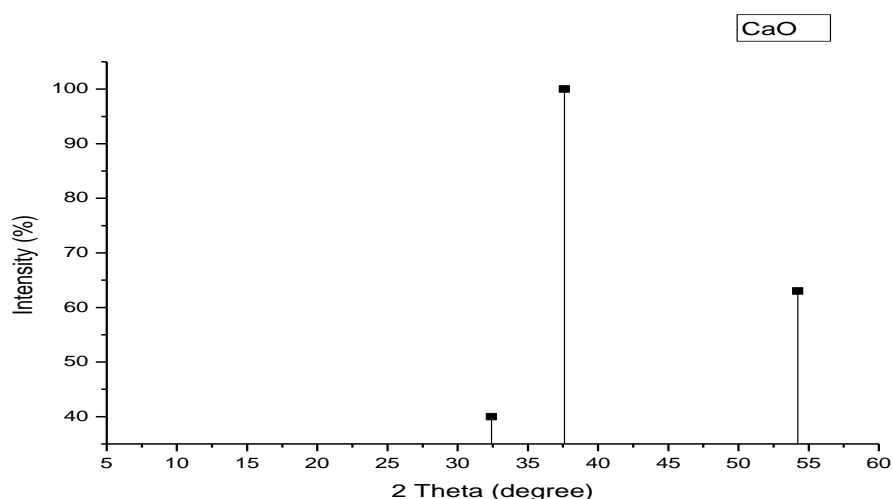
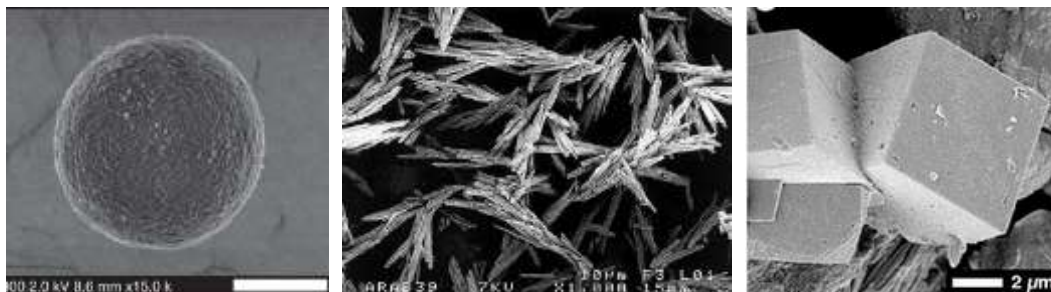


Figure 4. 35: The standard XRD patterns of calcium carbonates, Ca(OH)_2 and CaO (captions see top right corner)

SEM: Microstructure is used as the main differentiator in calcium carbonates group and the referenced pictures of each is presented in **Figure 4. 36**. Microscopy aims to analyse precipitates through their unique appearances (rounded, needle-like, & cubic) and in cooperation with other analytical measurements, to identify the final precipitates.



Vaterite (mean diameter of $4.40 \pm 0.05 \mu\text{m}$) (Arita, 2013)--left; Aragonite (bar = $10 \mu\text{m}$)(Lucas-Girot et al., 2005)--middle; Calcite (Brian & Peng, 2014)--right

Figure 4. 36: The microstructure of calcium carbonates

TGA: Aragonite, calcite and vaterite thermal decomposition graphs are shown in **Table 4. 11**. The thermal stage only has one step because of the non-hydrated property of calcium carbonate. Because aragonite, calcite and vaterite have the identical chemical formulae, theoretically, the thermal decomposition procedures of them are the same. Calcite is the most stable phase in this series, and temperature peaks between 700°C - 800°C . The weight loss is $44/100=44\%$ by CO_2 emission according to the molecular balance. The thermal decomposition equation in one step is:



Table 4. 11: The thermal decomposition properties of aragonite, calcite and vaterite (Kristóf-Makó & Juhász, 1999)

Mineral	Decarbonation Step: Temperature >700°C		
	Reaction	Weight loss (%)	Peak temperature (°C)
Aragonite	$\text{CaCO}_3 \Rightarrow \text{CaO} + \text{CO}_2$	44	750
Calcite	$\text{CaCO}_3 \Rightarrow \text{CaO} + \text{CO}_2$	44	750
Vaterite	$\text{CaCO}_3 \Rightarrow \text{CaO} + \text{CO}_2$	44	750

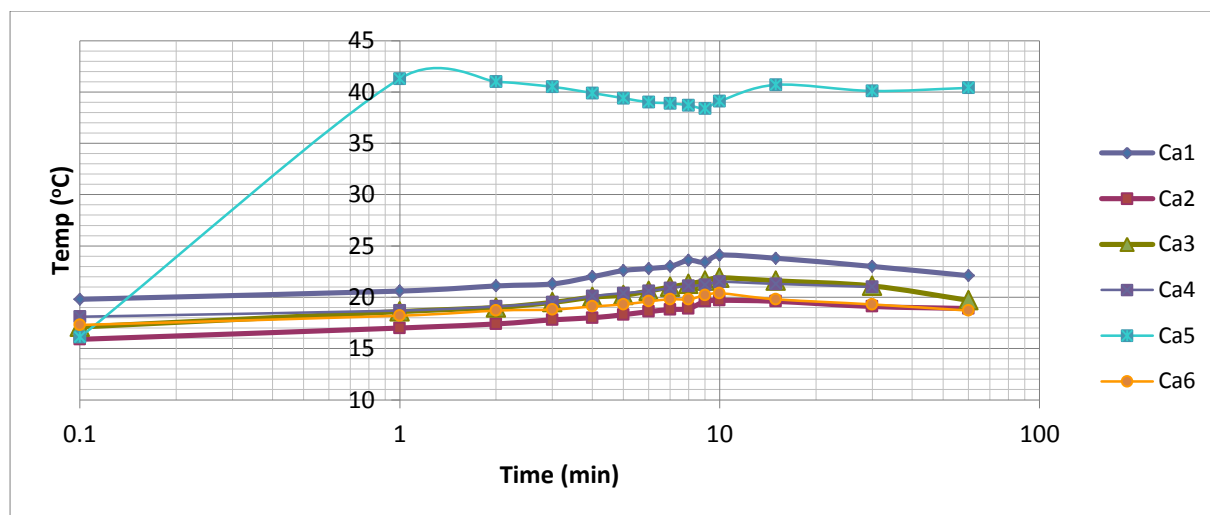
Reactivity Test: This experiment aims to compare the reactivity within each individual ion, in order to provide a good knowledge for the subsequent complex systems presented in the next two chapters. In order to keep consistency within all sets of work, the same reactivity test used for MgO was applied based on the citric acid method shown in Chapter 3.2.2, instead of the CaO conventional evaluation “Quicklime Slaking Test”.

4.6.3 Series III-Carbonation

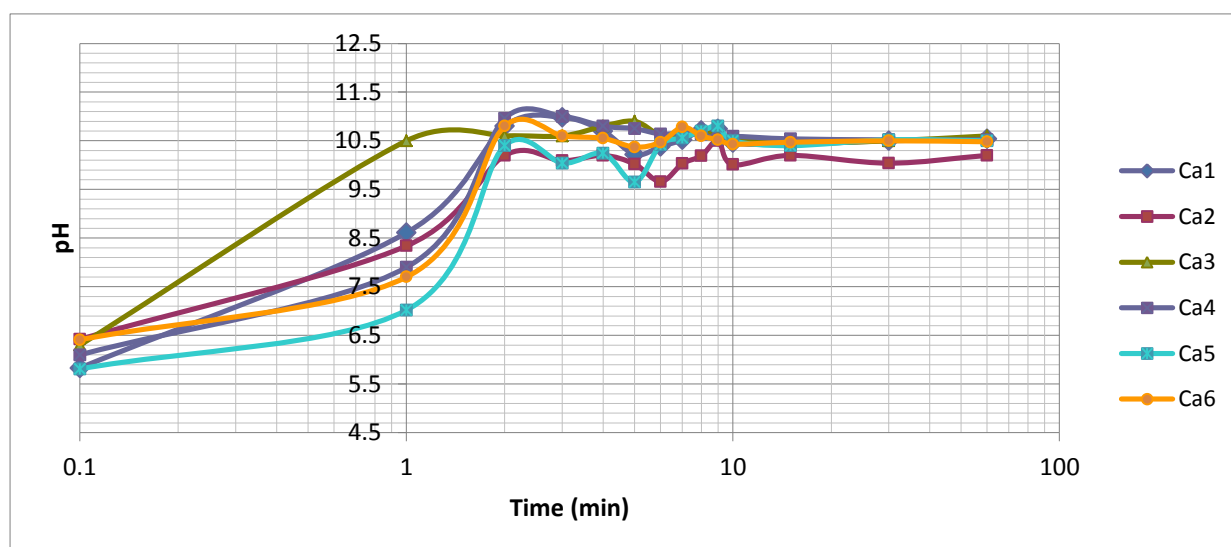
4.6.3.1 Carbonation and pH Stability Studies

Carbonation studies aims to explore the temperature variations in order to monitor the progress within the one hour bench experiment. Sample five was conducted at 40°C, while the others were at a room temperature. It is easy to observe the increased heat during the reactants addition (10min), but this tendency gradually decreases during the bench reaction, due to the fewer molecules' collision energy produced. In total, all end temperatures are higher than the initial ones, demonstrating the reaction's exothermic property.

Tested CaCl_2 pH is around 5.8-6.4, lying within the reasonable limits of chemicals by Fisher Scientific. Operated pH is restricted to equivalent 10 or 10.5. **Figure 4. 37** illustrates no apparent pH drop after 10min, validating the well-controlled operation and the reliability of this test within one hour, as well as reflecting the fast completion of carbonation process.



(a): The temperature profile in calcium carbonation studies



(b): The pH stability profile in calcium carbonation studies

Figure 4. 37: Carbonation (a) and pH stability (b) studies of calcium solution for SIII shown in Table 4.10

4.6.3.2 Precipitates Identification

Calcite, vaterite and aragonite are present in all samples after one hour's bench reaction (Figure 4. 38). All samples have obvious calcite mixture. Peaks are well distributed with the additional vaterite in samples 1 & 4 and extra vaterite/aragonite in sample 5. Lower calcium reactants' concentration (samples 1&4) retards the phase transformation into a more stable one through surplus carbonates, supported by Han et al. (2006), while a higher temperature is favourable for the metastable precipitates(vaterite and aragonite) formation in sample 5.

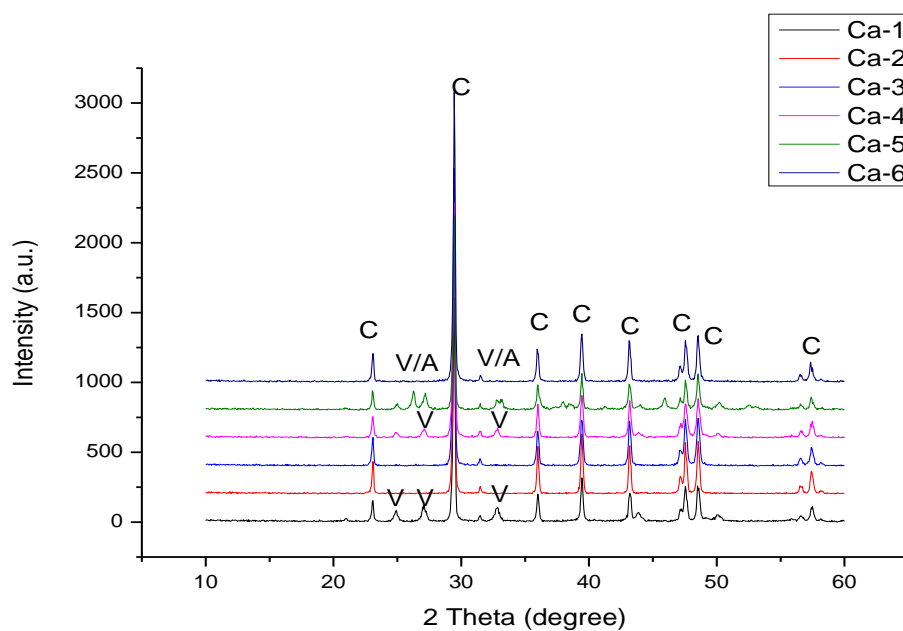


Figure 4. 38: Calcium carbonates of Ca1-6 for SIII shown in Table 4.10

4.6.3.3 Precipitates Microstructure

This section describes observed microstructure from SEM imaging conducting at 1000x, 3000x, 5000x and 10000x magnifications (**Figure 4. 40**; e.g. Ca6-1*5000X means sample 6 in **Table 4.10**, location 1, 5000x magnification). All samples were dried after one hour bench reaction. As SEM is the main tool used to determine the morphological differences between each sample, the main comparison work with other researchers on influential variables is presented in this section. Although added reactants are different, the main products remain identical because calcium carbonate has good non-hydrous characteristics. Hence EDX is not described here, by giving more focus on morphologies instead.

Generally, SEM has a good agreement to XRD diffractograms indicating the same compounds. Overall, samples 1 and 4 have vaterite and calcite-like appearance, while sample 5 has vaterite/aragonite and calcite, and the others are calcite. At 10000x magnification, calcite is clearly observed to be formed by sheet-like layered structures; and vaterite is an entire spherical shape, but the morphology was disturbed or damaged by mechanical collisions (Ca5-3*5000x). Especially in sample 5, picture Ca5-1*10000x shows the phase alteration procedure from calcite into aragonite, affected by a high temperature.

pH has an important influence on particle morphology and samples 2 and 3 were selected to evaluate this phenomenon. Both samples exhibit good cubic calcite production, differently from that documented in Section 2.8. In literature, authors Han et al. (2006) operated at pH=7.9-11.1, which is a larger pH range than this test. However sample 3 shows denser and aggregated particles, while sample 2 displays more uniform and individual ones. It is thought that a higher supersaturation degree leads to more nucleation generation and less nuclei dissolution, thus preserving the crystal seeds and enhancing its growth. Although ICP does not agree (see Section 4.6.3.4), the difference is estimated from the lack of crystallisation of sequestered nuclei, demonstrating the reliability of the analysis above. But the pH difference in this experiment is not as significant as that found in Han et al.'s (2006) work (Chapter 2.8), as this test is optimised based on the preliminary findings from the first stage; hence the repeated section is not conducted.

Unlike magnesium carbonates, where pH is the most important, temperature is crucial to precipitates in calcium carbonates. Samples 3 and 5 were analysed to show this importance. Only calcite is formed in sample 3; whilst in sample 5, sediments alter to vaterite, aragonite and calcite. This can be explained by a higher temperature influence resulting in phase transformation into metastable precipitates. Apparently, sample 3 has better shape models than 5. Meanwhile it also obeys the "Ostwald's step rule" under the same pH condition, where lower temperature will bring in smaller supersaturation. Ostwald further demonstrates that at a low supersaturated aqueous phase, the difference of supersaturation ratio (S) between the polymorphs plays the influential role on the crystallisation and according to equation in Section 2.7.3, the stable form may preferentially deposit in this case. On the other hand, at high supersaturation, the difference of the interfacial energy (γ) between the polymorphs starts to be relatively dominant and the metastable phase tends to precipitate, based on [Equations 2.37-2.39](#). This explanation has also been widely accepted by other researchers.

Initial concentration, which has the direct relationship with supersaturation degree due to the ion denseness, was assessed in samples 1 and 3. Sample 1 has both vaterite and calcite from the observation, while sample 3 consists of calcite only. The higher concentration of reactants or a higher supersaturation degree can lead to more rhombic particle formation. Because of a larger Ca^{2+} /carbonate ions ratio increases the equal adsorption of the surface

of calcite, resulting in the enhanced growth of calcite. This result agrees well with Han et al.'s (2006) work (Figure 4. 39).

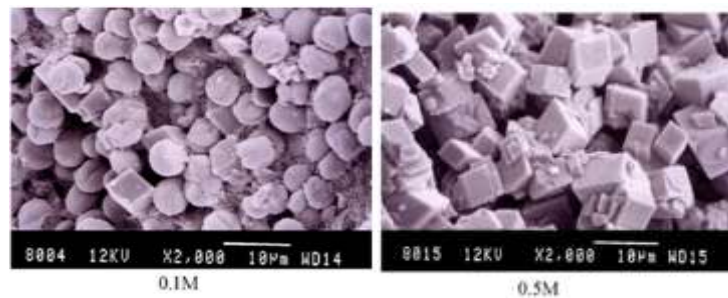
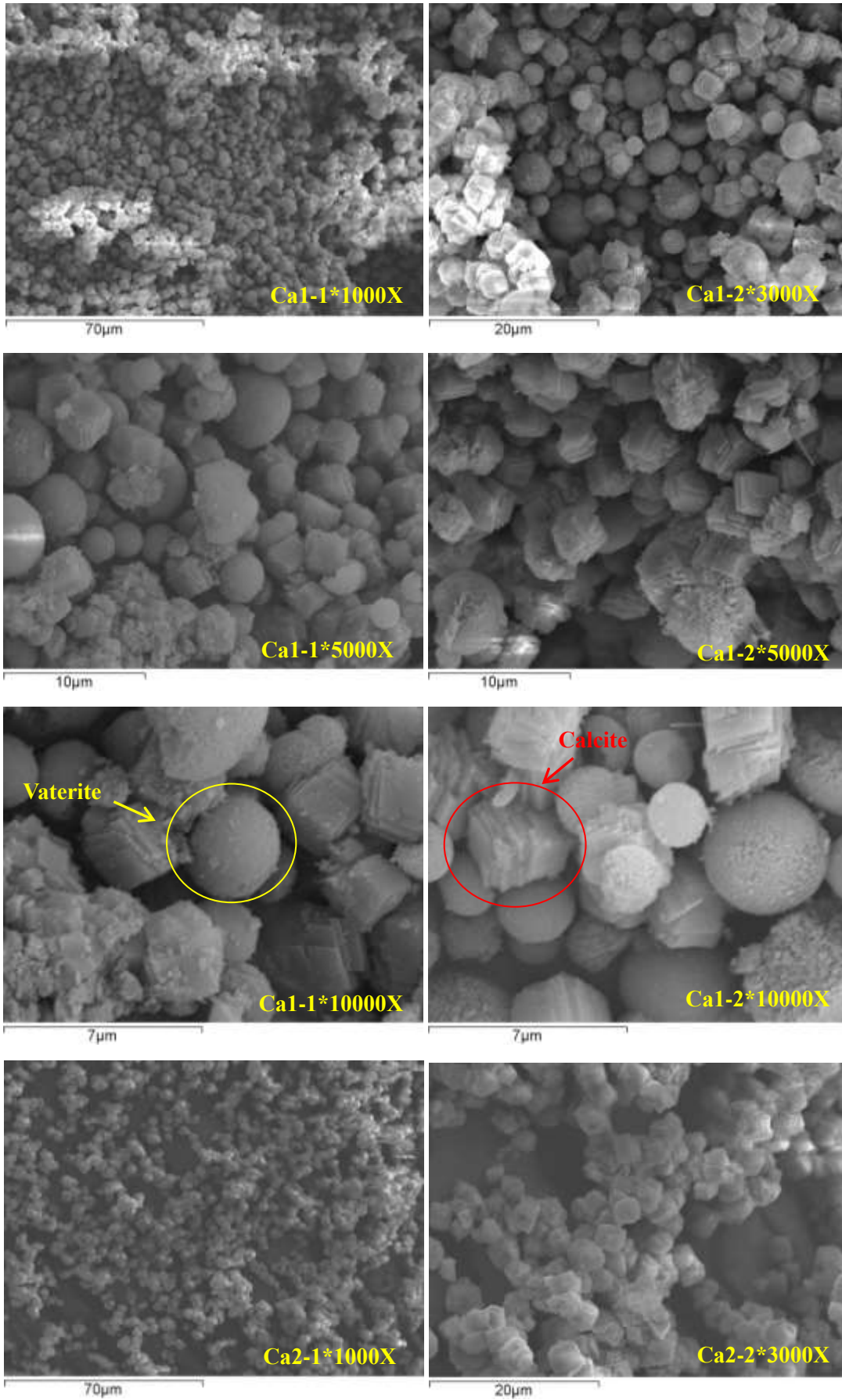
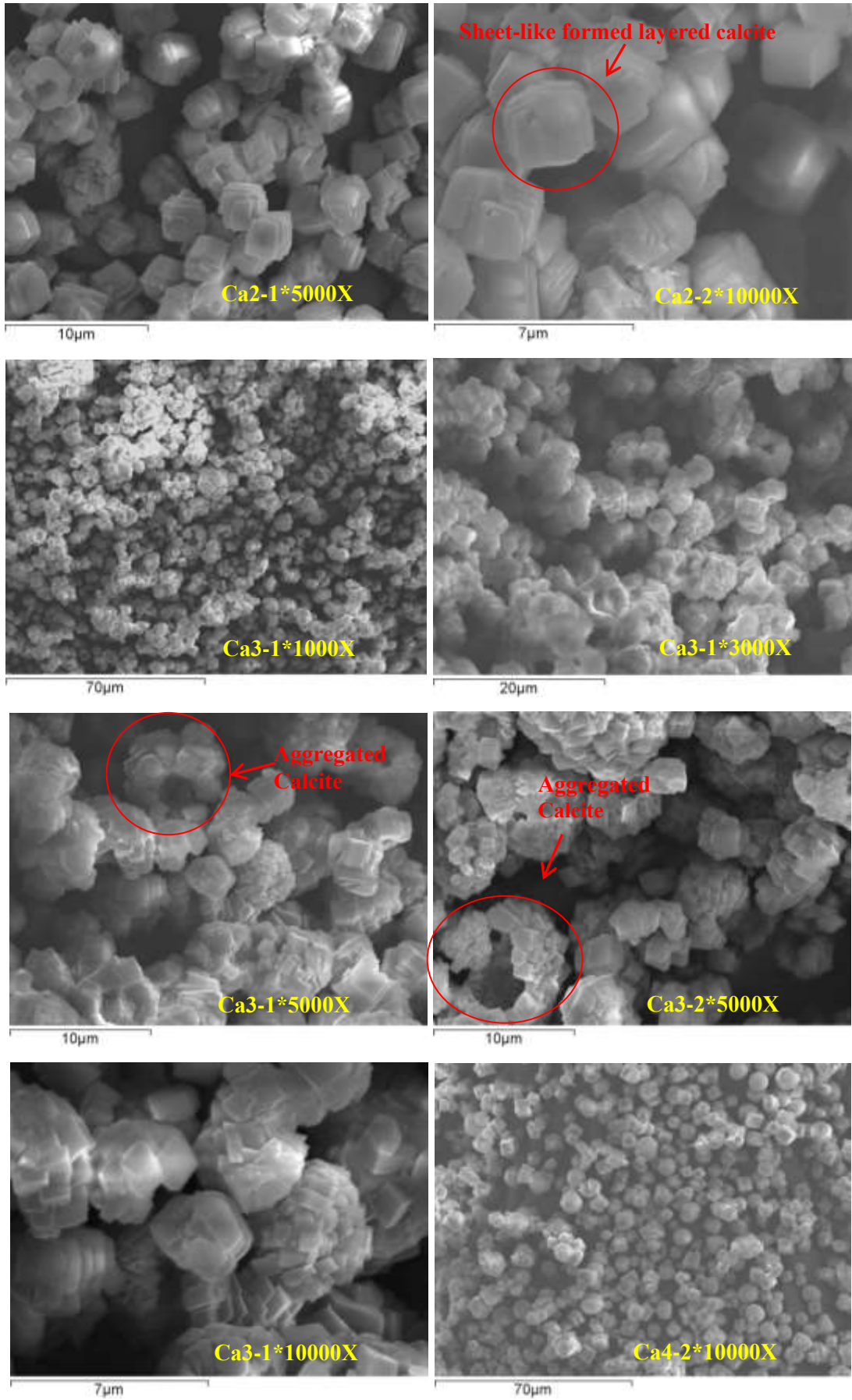


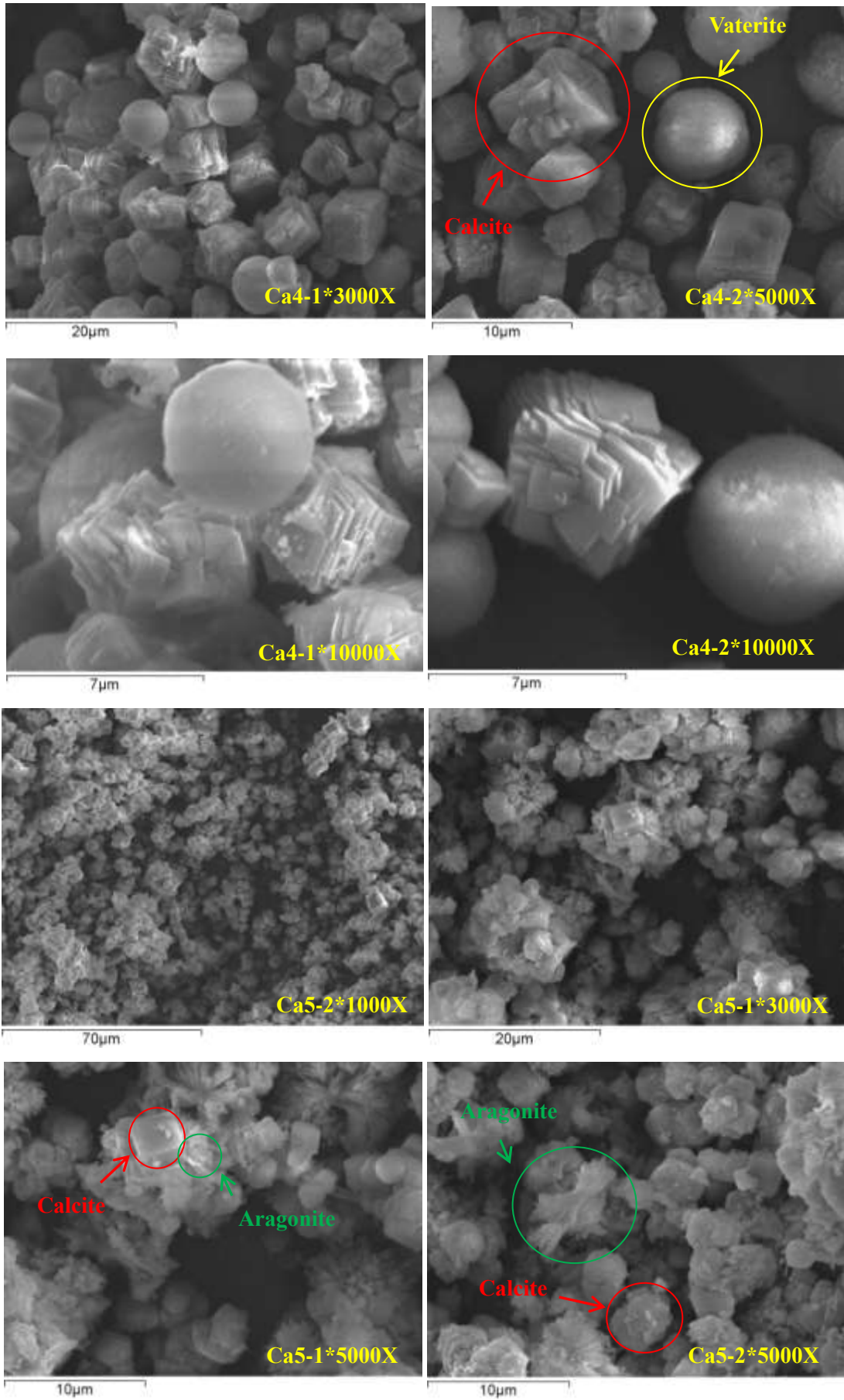
Figure 4. 39: Han's SEM for calcium carbonates prepared at different initial CaCl_2 concentrations (Han et al., 2006)

Stirring speed has an effect on particles' morphologies to some extent, as can be identified from samples 1 and 4. Under microscopy, 4 is more uniform and well-shaped than 1. A high stirring speed can affect the morphology mechanically, although in some ranges stirring speed can improve the reaction efficiency; but excessively speedy agitation may also have a negative effect on sequestration, as happened in this case (see Section 4.6.3.4). However there is not a significant difference between two results (samples 1 and 4) in SEM. This experiment shows the dissimilar appearance compared to Kitamura et al. (2002) and Han et al. (2006). Both stated that a higher stirring speed provides looser particles, while a lower stirring speed tends to aggregate the denser ones. This contrast is not a dramatic issue in SEM imaging, as the picturing areas were randomly selected based on the most individual representatives due to the importance of calcium carbonates morphology and the optimum quality of resolution, which did not represent the entire sample.

CO_2 has a direct effect on pH, reaction time and supersaturation degree, as samples 3 and 6 imply. Sample 3 displays bigger aggregated particles with more edges and corners, caused by larger deposits, while sample 6 presents well-uniform individual grains. It is estimated that a higher flux rate leads to more carbonate ions formation, resulting in a larger supersaturation degree, accompanied by more nucleation and denser products generation. But in this set of CO_2 flux rate, the dissimilarities between the two samples are not as large as Han et al.'s (2005) work (Section 2.8).







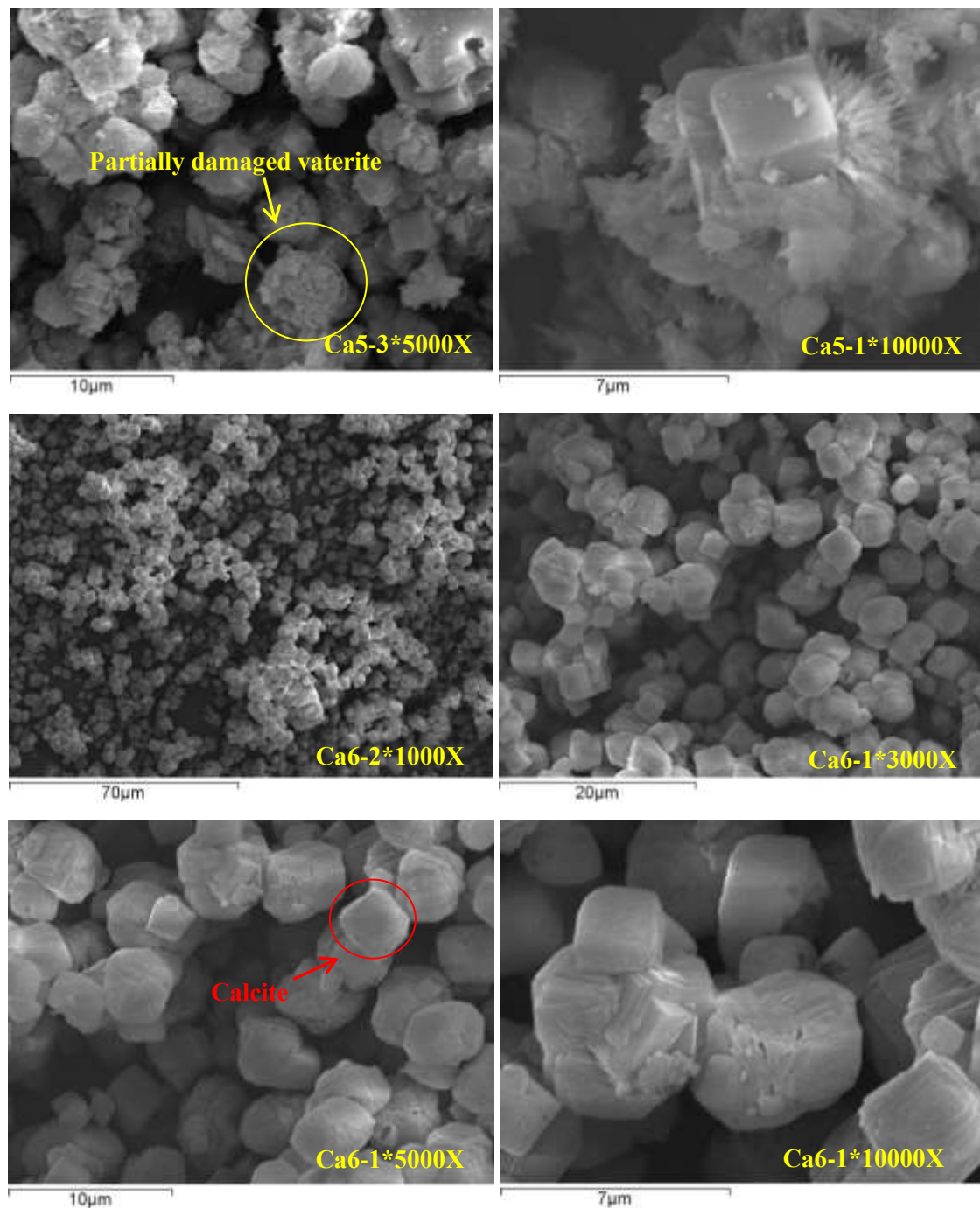


Figure 4. 40: The SEM microstructure of CaCO_3 in Ca1-6 for SIII shown in Table 4.10

4.6.3.4 Reaction Kinetics Studies

Table 4. 12 presents the calcium sequestrated efficiency. It is clear that the small improvement over one day's calcium capture cannot compensate for the overall associated economic, environmental and social inefficiency, compared to a one hour completion time. Based on the Equation 4.2 in 4.6.2.2, the theoretical computed figures and obtained weights

after 1h are summarised in **Figure 4. 41** (where AW=Actual weight, TCC=Theoretical calculated calcium carbonates).

Table 4. 12: 1h samples' net weights and the sequestered calcium for SIII

Sam ple	Ca ²⁺ concentra tion (M)	Stirring speed (rpm)	Tempe rature (°C)	pH	CO ₂ flux rate (ml/min)	Net weight (g)	Remaine d calcium (%)-1h	Calcium sequestration efficiency (%)-1h
1	0.1	700	25	10.5	500	1.52	1.11	98.89
2	0.5	700	25	10	500	7.53	3.53	96.47
3	0.5	700	25	10.5	500	9.07	9.48	90.52
4	0.1	0	25	10.5	500	1.79	0.37	99.63
5	0.5	700	40	10.5	500	7.62	0.12	99.88
6	0.5	700	25	10.5	150	5.28	22.85	77.15

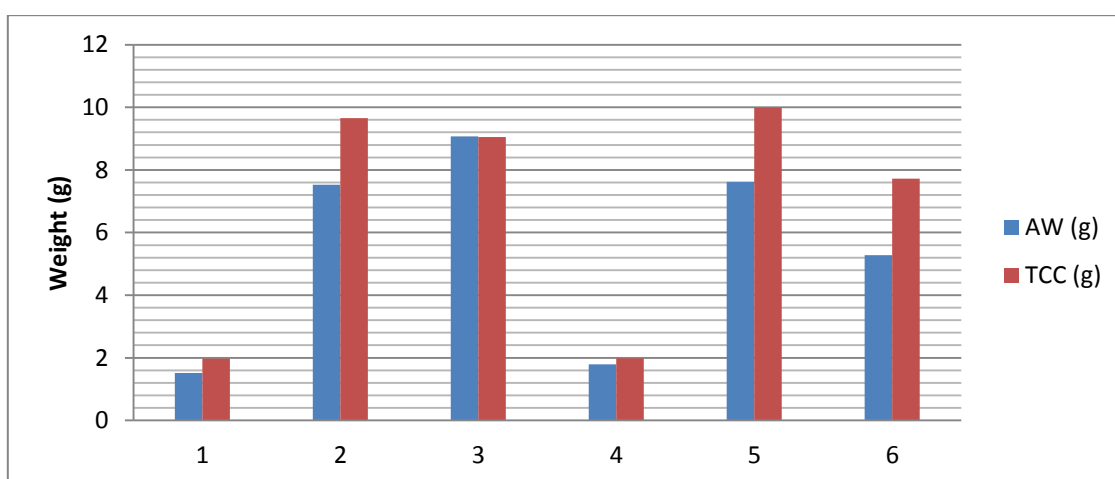


Figure 4. 41: The comparisons of actual weight and theoretical weight for SIII shown in Table 4.10

From this analysis, almost all samples have a good sequestration degree (over 90%) except 6, which has the lowest CO₂ flux rate resulting in reduced carbonates addition. Generally, initial 0.1M reactant has better sequestration results, as less particulate within the solution enhances the mutual interactive opportunities. However, comparing actual and theoretical percentage differences, there are no significant variances between 0.1M and 0.5M primary reactants. The gap between the reality and idealisation is caused by either operational errors or insufficient filtration processes leading to no removal of aggregated adherence nuclei to the precipitates' surface before its crystallisation. In conclusion, from the perspectives of operation and crystal formation, sample 3 has the best behaviour; the slight additional weight above the theoretical estimation is attributed to some impurities, such as

NaCl. However, it needs to be mentioned that this contamination level is extremely low, and even cannot be identified by XRD.

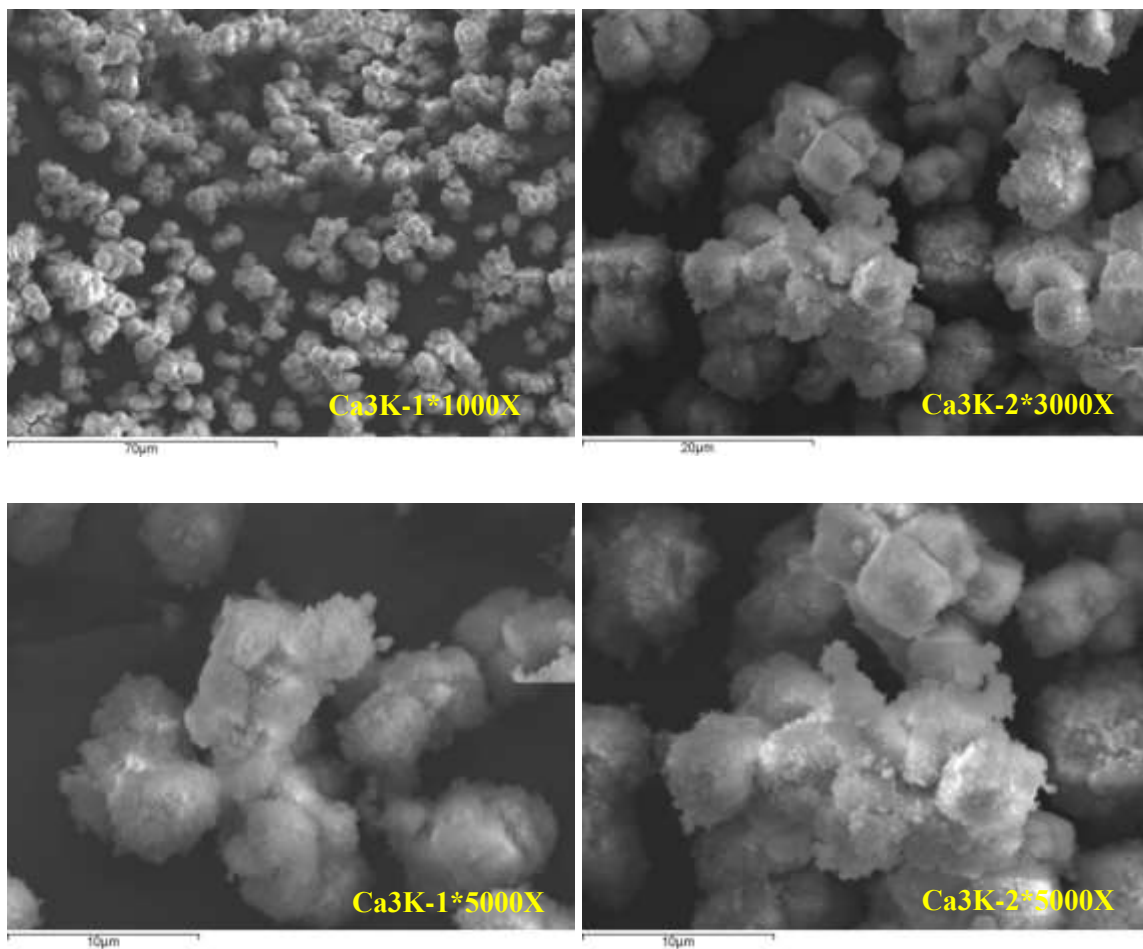


Figure 4. 42: Ca3 one day (Ca3K) microstructure for SIII shown in Table 4.10

SEM was further incorporated to validate the reaction kinetics. Sample 3 was selected from ICP results. **Figure 4. 42** displays that one day morphology is less uniform compared to one hour products. As theorised by Ostwald's rule, nuclei dissolve and reform into larger particles over time; hence the more ragged surfaces appear after a day indicating the effect of this dissolve-reform transaction model. In short, sample 3 is the optimal sample from its regulated morphology, the uniform calcite formation, and the remarkable calcium removal efficiency, through the analysis of SEM, XRD, and ICP respectively.

4.6.4 Series III-Thermal Property and Calcination

4.6.4.1 The Analysis of Thermal Property

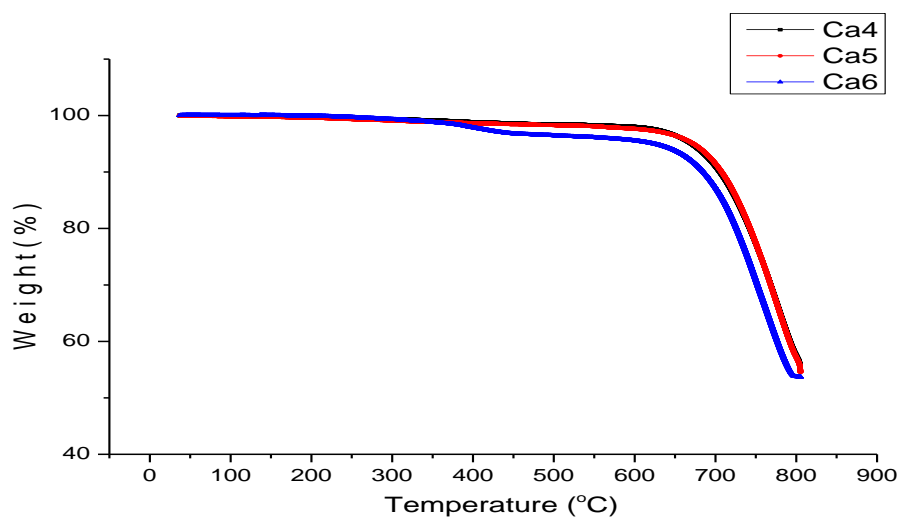
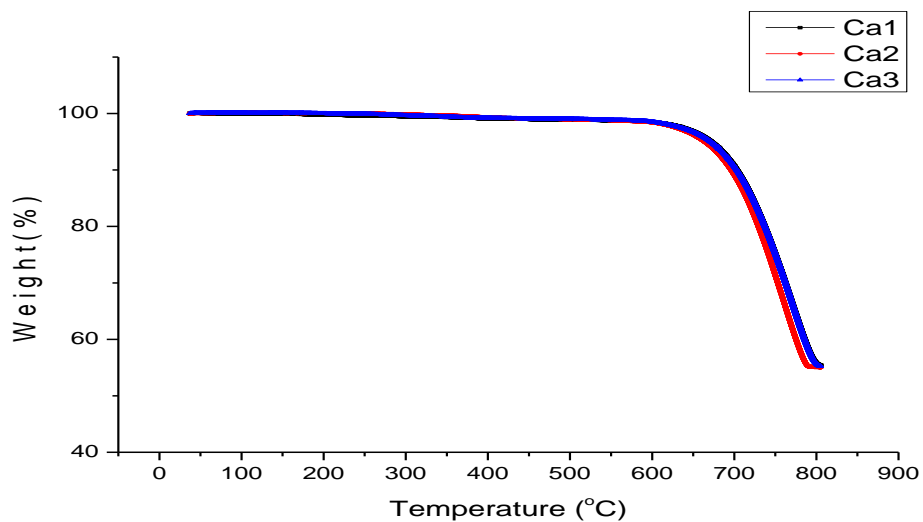
The thermal decomposition of samples through TGA was studied to identify the sediments' thermal properties, as well as to quantify the degree of CO₂ sequestration. **Figure 4. 43** (DTG = Differential Thermogravimetry) shows the weight losses and relevant peak temperatures for this calcium carbonation study, where the deposits were heated up to 800°C. The heating temperature followed Djihan's investigation (2013), and met the requirement of the reactive magnesia heating profile.

During this single step of thermal decomposition, all samples' weight losses have a good match with the theoretical calculation on 44% reduction in mass, implying good non-hydrophilic properties, except higher numbers in samples 5 and 6. These are attributed to incomplete drying. Moreover, the one day test depicts higher weight loss due to a longer induction time of more surface water attachment.

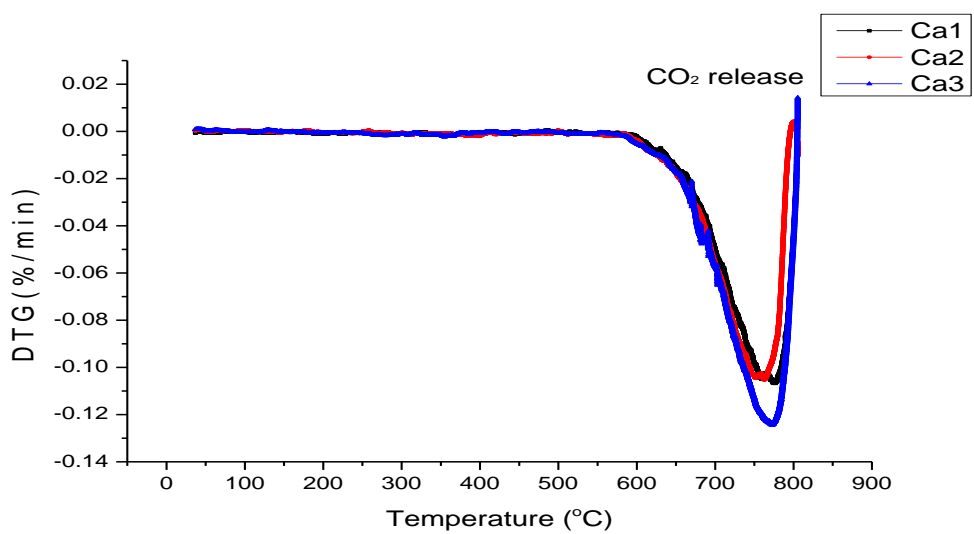
All samples' peak temperatures are slightly higher than literature values at 750°C. However, considering that carbon loss is a gradual procedure starting from 700°C while other unexpected and uncontrollable factors may occur, this set of tests lies within the error tolerance. Each individual TGA profile is seen below with the carbon release of all samples at $\geq 700^\circ\text{C}$, determined by the first derivative calculation.

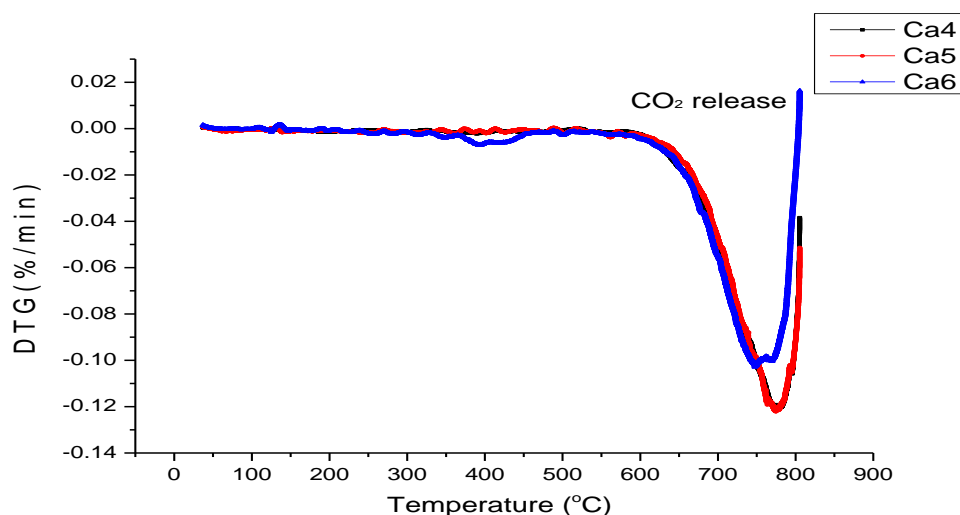
Sample	Peak Temp (°C)	Weight loss (%)
1	766.64	44.592
2	765.53	44.951
3	771.97	44.782
4	786.17	44.562
5	777.07	45.403
6	760.04	46.299
3-1d	775.58	45.356

(a): The thermal stage of Ca1-3 calcination for SIII shown in Table 4.10

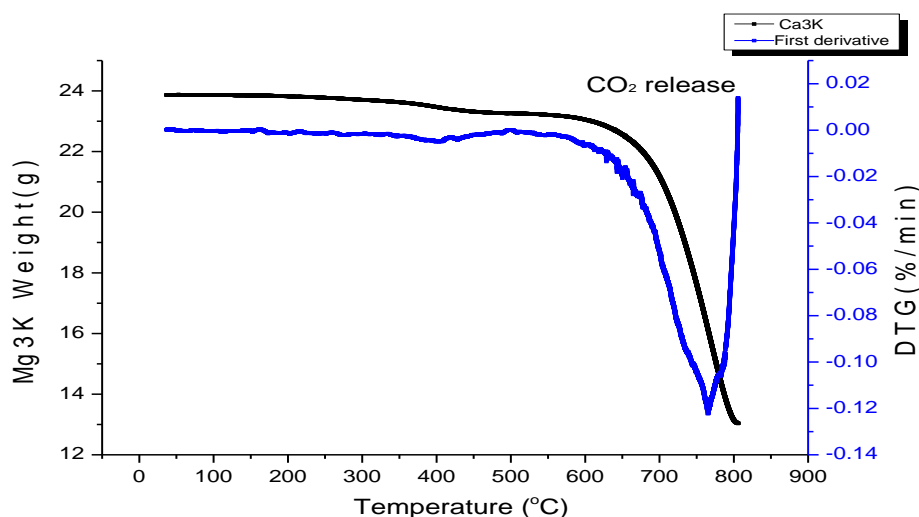


(b): The weight% profiles of Ca1-6 calcination for SIII shown in Table 4.10





(c): The derivative profiles of Ca 1-6 calcination for SIII shown in Table 4.10



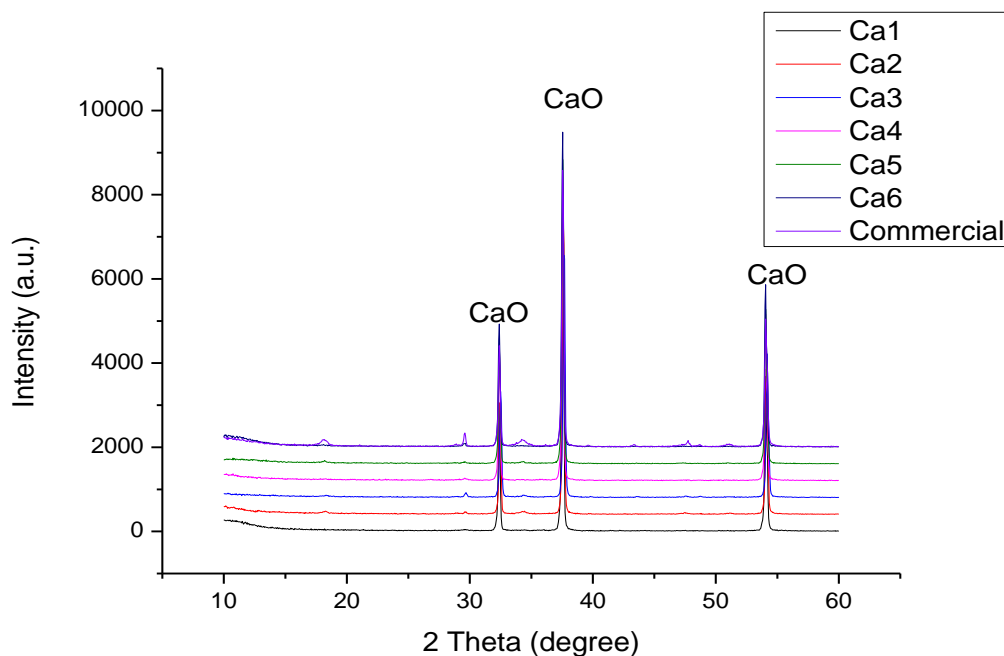
(d): The Ca3 one day thermal profile weight (g) and first derivative for sample Ca3K in SIII

Figure 4. 43: The TGA thermal stage (a), thermal profiles (b) and analysed first derivative profiles (c) of Ca1-6, and Ca3 one day sample (d) for SIII shown in Table 4.10 (captions see top right corner)

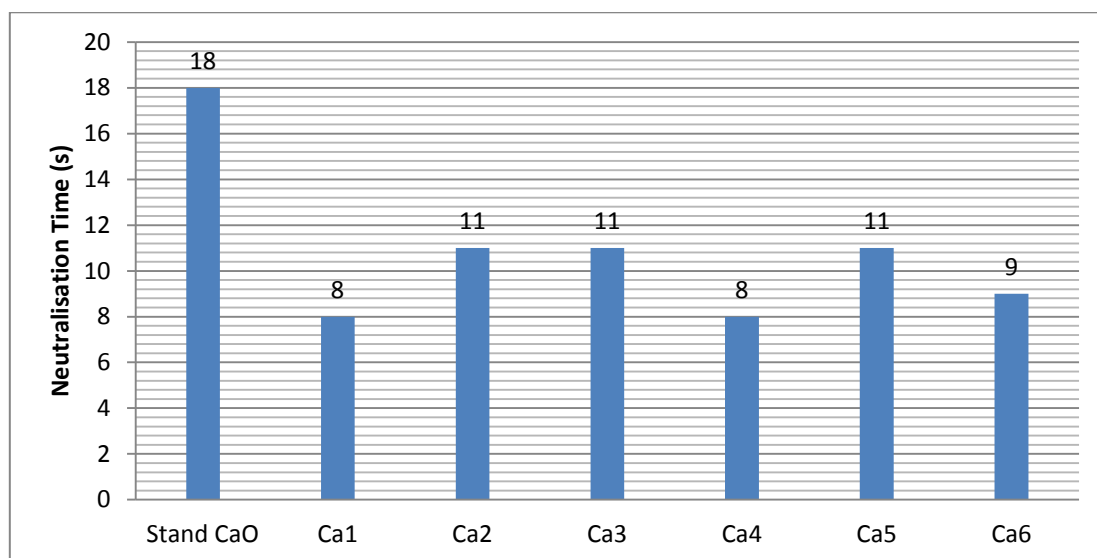
4.6.4.2 The Analysis of Calcination at a Certain Temperature

Calcined products CaO were analysed through reactivity testing and XRD. Although there is an existing standard quicklime slaking test, the MgO citric acid method used is demonstrated in Chapter 3.2.2 in order to stay the consistency with the other results' chapters. From [Figure 4. 44a](#), it can be concluded that this set of tests is successful and reliable, since the reactivity results show better performance than a commercial product which may be stagnated by a long time storage and experience an increase in the level of

impurities. In addition, the well-matched XRD graphs with a commercial profile (Figure 4. 44b) demonstrate that all samples are fully decomposed up to 800°C and the precursor carbonates are generated at a high purity level.



(a): Experimental calcined CaO of SIII with commercial CaO comparisons



(b): CaO reactivity tests for SIII shown in Table 4.10

Figure 4. 44: Experimental calcined Ca1-6 (a) and their reactivity tests (b) for SIII

4.7 Conclusions

This chapter started from a preliminary trial in order to prove the apparatus setting's reliability and the initialised operational processes. After validating all the experimental equipment and the analysed studies, main tests were conducted in three series.

Ammonia was used to produce precipitates in SI. Both PHREEQC and Visual Minteq were run to record the estimated precipitates, in which nesquehonite, artinite, magnesite, hydromagnesite and lasfordite were thermodynamically favoured when equilibrium was reached. Precipitates started to appear from pH=8.5 and reached a maximum at 9 and 9.25. A lower pH produced finer aggregations from macro-reflection. In the ammonia reaction, pH stability was well maintained because of the ammonia's strong buffering capacity. The precipitates formed were nesquehonite, which was irrelevant to pH value and the retention time over 3 days. Moreover, in order to justify the importance of pH level during the operation, pH adjustment studies were further operated in SI.II, to examine whether magnesium had better sequestration after adjustment.

In SII study, ammonia was replaced by NaOH to ensure cost effectiveness and safe operation. All products were found to have a mixture of HM, D and N. In addition, halite was also well incorporated into the deposits' lattices, implying good hydrophilic properties of HMCs and strong NaCl attachment through the dissociation into an aqueous phase. XRD diffractograms indicated that a higher pH level increased the metastable phase appearance while no stirring speed, a high temperature as well as a smaller CO₂ infusion all induced brucite formation. The microstructure of the samples demonstrated observed nest-like HM nano-sheet accumulation at an elevated temperature. Sample 3 depicted complex agglomeration combined with sheet-like particles assembled by needle-like nesquehonite and rosette-like HM caused by a raised temperature. Moreover, lower initial reactants induced more uniform particles and an appropriate stirring speed accelerated the homogenous solution. Regarding the kinetics results, there were not significant differences in 1h and 1d, but a short time (1h) was insufficient for complete crystallisation. Finally, sample 3 with the parameters 0.5M MgCl₂, a 700 stirring speed, a 25°C room temperature, a pH=10.5 and a 500 cm³/min CO₂ flux rate, was selected as the most appropriate specimen due to its sequestration efficiencies, particle performance and morphology, as well as its operational convenience.

Thermal decomposition was evaluated through TGA. The sample prepared with raised temperatures experienced the smallest weight loss, while samples with brucite mixture had less mass than the rest because of the reduced degree of carbonation. The reactivity test was manipulated to suggest that a higher supersaturation solution prolonged the MgO reaction time, as seen by the sheet-like particle performance and the existence of higher amounts of hydroxide ions existing. Moreover, NaCl impurity also inhibited the neutralisation. Two other temperatures were used: 650°C led to the biggest voids in spherical morphology, but the porosity was steadily reduced with the increasing temperatures. It was also found that 1000°C did not decompose all carbonates, which was contrary to the references, due to its natural carbonation or long-time storage before the test. TGA profiles up to 1000°C also partially proved this evaluation. Reactivity tests with various temperatures agreed with the primary predictions: elevated calcinations required extended neutralisation time due to the decreased voids and granular sizes. In the end, pure MgO was slower in powder neutralisation than the mixture dolime in the reactivity test, which was caused by the CaO composition in the dolime that shortened the final result.

In SII.II, NaOH had lower gradients in the temperature profile than ammonia, as the gas-liquid phase was more active than the solid-liquid solution. Its stability was imperfect compared to ammonia, because the latter has a good buffering capacity. The precipitates were heavily dependent on the pH level. When the pH equalled 9.5, nesquehonite was generated irrespective of the time lapsed, but when the pH was higher than 10, HM and D formed within the carbonates. Conversely, at pH=10 after a 24-hour reaction, nesquehonite was observed from the natural decomposition or the decarbonation of HM&D after this extended time. In general, ammonia showed a good tendency to produce nesquehonite because of its evaporation characteristics, and NaOH was favourable for the existence of HM and D. These precipitates were caused by the atom disturbance of sodium participation. So the alkalis buffering solution smoothed the phase transformation, while sodium was a strong alkali to initiate a direct chemical reaction. More importantly, the higher pH exhibited good sequestration efficiency during the primary stage of NaOH addition, whereas ammonium salts presented reversed these effects with the identical pH. In the no-CO₂ reaction, brucite formed instead of HMCs, but small quantities of carbonates were observed

within the samples generated by the natural carbonation processes when the precipitates made contact with the atmosphere.

In the calcium carbonates series, both PHREEQC and Visual Minteq estimated thermodynamic favoured precipitates, comprising of aragonite, $\text{CaCO}_3 \cdot \text{H}_2\text{O}$, calcite and vaterite. However, from the literature, it is known that monohydrocalcite can only be produced in the presence of magnesium or some organic materials. In this series, calcite is the most stable product within the calcium carbonates series, and their transformations are heavily dependent on temperature: sample 5 with elevated temperature had a vaterite/aragonite mixture, and lower initial reactants samples 1 and 4 exhibited vaterite formation because of the inhibition of phase transformations from surplus carbonates.

At a 10000x magnification of microscope, calcite was observed with a sheet-like layered structure, and vaterite was an integrated sphere, but was damaged moderately. A higher supersaturation degree led to more nucleation generation and less nuclei dissolution, in order to protect the crystal seeds and thus accelerate growth. Moreover, a higher concentration of reactants or a larger supersaturation degree resulted in more cubic granules, because of larger Ca^{2+} /carbonate ions ratio increasing the equal adsorption of the surface of calcite, inducing the growth of calcite. In this case, the sample without agitation had more uniform and well-shaped particles. Furthermore, a higher CO_2 flux rate led to more nuclei appearance and denser products generation, while the lower one presented more uniform independent particles.

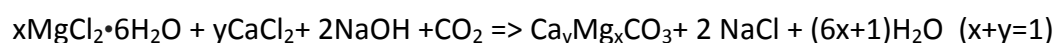
Kinetics showed an impressive sequestration performance at over 90% mostly. The gap between the theoretical and practical weights was attributed to either operational error or the insufficient time of nuclei crystallisation. The thermal profile indicated good numerical scaled 44% weight loss in all samples, validating its high purity level with a good match of theoretical prediction; and the peak temperature was also placed within an appropriate range of references. Calcined products CaO was highly reactive with only 10s neutralisation time using citric acid method, in a good agreement with the commercial one.

Chapter 5: Dual Ions Carbonation and Calcination

5.1 Introduction

It is important to investigate a complex multiple-ion system, in order to accomplish the target of using synthetic brine as a raw material. Principally, this chapter, the essence of the entire study, expands on the previous individual magnesium and calcium ion explorations. All of the planned works are designed scientifically, based on the natural seawater constitutions. Studied components in these two Chapters 5 and 6 include almost all of the practical ions, except for uncommon and dangerous elements. According to Section 2.3, the main components of seawater are sodium, magnesium, calcium and potassium. While other minority constitutions, such as strontium, boron and silicon are not considered in this study due to their minute amounts as well as the hazardous property in the combined compounds during the lab operation. Chlorine is used as an anion to balance aqueous electric charge. Inorganic compounds derived from carbon elements are substituted by CO₂ during the mimic process. Fluorine is rarely present in solution, because of the poisonous feature of most fluoride salts, which have potential to endanger the operation. Three experimental designs of Chapters 5 and 6 are upgraded gradually from the multiple magnesium and calcium ions into the triple combination of magnesium, calcium and sodium ions, until the last addition of potassium.

Considering the industrialised synthetic seawater/brine process, this study provides a relatively elaborate innovative experimental methodology and analysis to indicate the potential optimum conditions in the carbon sequestration procedure starting with seawater/brine. All of the variables in this chapter are studied using the same procedures as previously, with the equation:



but targeted samples are narrowed down in Chapter 6 based on the created knowledge. Various calcined conditions are also applied in Series IV (SIV) and Series V (SV), to identify the most suitable heating temperature, as well as the deposits' thermal properties.

The model PHREEQC was utilised to simulate the possible precipitates throughout Saturation Index ≥ 0 to identify the thermodynamically favored products. Various obtained sediments were subsequently run by evaluation tools, such as XRD for component identification, SEM for microstructure observation, ICP for remained metal measurement, and TGA for thermal decomposition property. Three heating temperatures (650°C, 800°C, 1000°C) were utilised to explore the different thermal phenomenon. The calcined deposits were then tested using the citric acid method to work out their reactivity performance by an initialised testing standard, as the mixed CaO-MgO binary system has no industrialised acid neutralisation approach, because of the less usage of a CaO-MgO binary system than an individual CaO system and MgO system.

5.2 Series IV-Dual Ions Complex System

This series plays an important role in a complex system investigation, as both magnesium and calcium are the desired compounds in cement construction, after eliminating the sodium, potassium and other impurities. Following the individual element study, a combined approach worked towards the preliminary verification on the two most required metals (Mg, Ca), to further discuss the manufacturing properties from potential seawater/brine. In short, this process is abbreviated as a $\text{MgCl}_2\text{-CaCl}_2$ system.

5.2.1 Model for Series IV

Due to the restriction of non-application on a high ionic strength in the solution of Visual Minteq in Series IV (SIV) from the Section 2.13, the majority of calculations then depended on PHREEQC. The input code encompasses the speciation-solution head sentences: SOLUTION, GAS_PHASE and MIX together to explain the contact of CO_2 (500 cm^3/min) with various ratios of $\text{MgCl}_2\text{-CaCl}_2$ at room temperature over 10min. The input components included 0.5mol/l MgCl_2 , 0.1mol/l CaCl_2 , and 1 mol/l Na^+ , operating at atmospheric pressured CO_2 and room temperature. Results concentrate on the Saturation Index (SI), where Saturation Index ≥ 0.0 , the selected product, is thermodynamically possible to be formed in the solid precipitates. However this is only a guideline for the precipitates generation, as each component will have special conditions to be produced in nature and experiments.

In addition to the combination of previous chapters magnesium carbonates and calcium carbonates deposits, two typical mixtures of magnesian calcite are dolomite and huntite ($\text{CaMg}_3(\text{CO}_3)_4$). The most common Mg:Ca equivalent to 5:1 ratio extracted from seawater under a different pH level is drawn below, accompanied by all prospective products from the composition. To scrutinise the pH equaling 10 and 10.5, it can be observed that potential precipitates are aragonite, artinite, brucite, $\text{CaCO}_3 \cdot \text{H}_2\text{O}$, calcite, huntite, dolomite, magnesite, hydromagnesite and vaterite (Figure 5. 1).

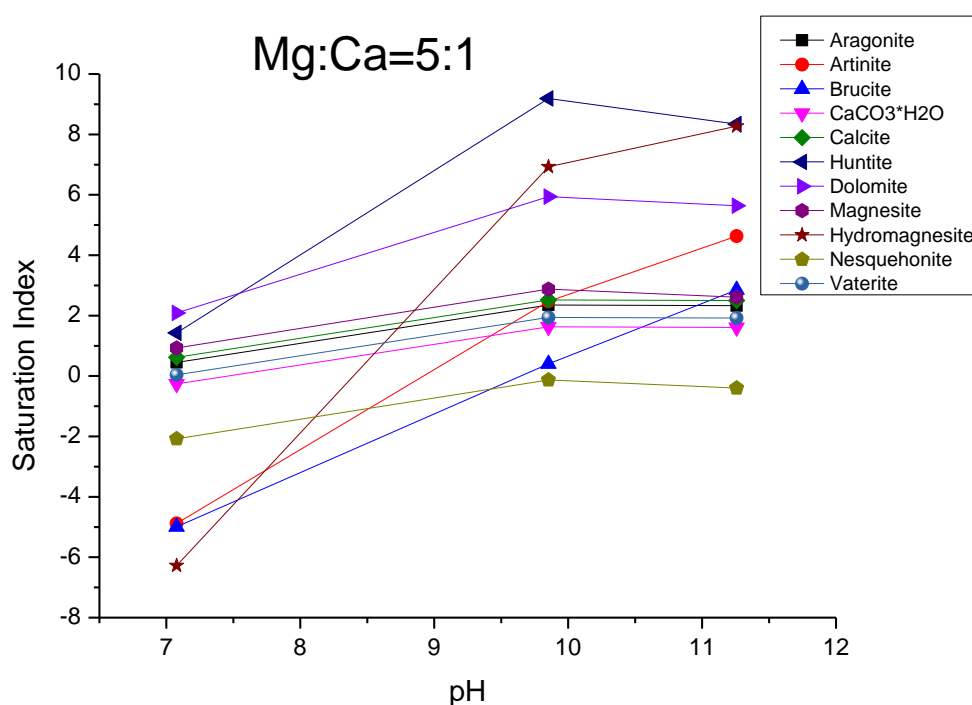


Figure 5. 1: The Saturation Index of potential precipitates over pH, summarised from PHREEQC for SIV

5.2.2 Series IV-Experimental Design

This section aims to provide the knowledge of testing parameters and the applicable reference standards for all analytical measurements, in order to satisfy the fundamental approach towards the precipitates' analysis.

5.2.2.1 Experimental Parameters

There are two tables in this part, one is for carbonation study, and the other one is for calcination analysis. Parameters include stirring speed, pH, temperature, and CO_2 flux rate; samples 5 to 10 were designed specifically to use the ratio of calcium: magnesium (1:5)

proportions in seawater, but controlled parameters varied from one to another. Both concentrations 0.1M on Ca^{2+} and 0.5M on Mg^{2+} were 10 times larger than the original seawater concentration level. Samples 1 to 4 are the converse of samples 5 to 10 by selecting relatively good performance sets, in order to study the distinguished calcium over magnesium ratios. A 200ml solution was weighed and 1.5 hours reaction as standard bench test was used in terms of multiple ions involvement. Although both ions ideally reacted with carbonates independently, based on the mutual ions interaction, working efficiency is lower than separate aqueous phase due to the common ions' effect. So 50% additional time was added on the basis of previous individual calcium and magnesium standard bench reactions. Besides carbonation assessment, several thermal calcinations were conducted further from the chosen samples, selected from Chapters 4 and 5, in order to measure the differences of temperatures (Table 5. 1).

Table 5. 1: Carbonation (a) and calcination (b) designed samples

(a): Carbonation designed samples

Sample (Mixture)	Ca^{2+} concentration (M)	Mg^{2+} concentration (M)	Stirring Speed (rpm)	pH	Temp ($^{\circ}\text{C}$)	CO_2 flux rate (cm^3/min)	Net Weight (g)
M1	0.5	0.1	700	10.5	25	500	7.46
M2	0.5	0.25	700	10.5	25	500	9.34
M3	0.5	0.1	700	10.5	40	500	10.61
M4	0.5	0.25	700	10.5	40	500	12.54
M5	0.1	0.5	700	10.5	25	500	11.4
M6	0.1	0.5	700	10.5	40	500	8.64
M7	0.1	0.5	0	10.5	25	500	10.14
M8	0.1	0.5	700	10.5	25	150	10.61
M9	0.1	0.5	700	10	25	500	10.66
M10	0.1	0.5	700	10	40	500	10.37

(b): Calcination designed samples

Sample (Mixture)	Mg^{2+} concentration (M)	Ca^{2+} concentration (M)	Stirring Speed (rpm)	CO_2 flux rate (cm^3/min)	pH	Temp ($^{\circ}\text{C}$)
SI-M5	0.5	0.1	700	500	10.5	25
SI- M9	0.5	0.1	700	500	10	25

5.2.2.2 The Analysis of Precipitates

ICP: In this set of experiment, ICP was employed to measure the unreacted metals in solutions, interval samples were 1.5h and 1 day, based on the previous knowledge of the majority metal's capture within 1.5h. The standard calibrations of both calcium and magnesium were 0.1ppm, 1ppm, 10ppm and 100ppm; and both of them existed independently during the reference preparation, meaning that they had no influences on each other when diluting and mixing.

In addition, ICP was also deployed to calculate the ideal carbonates with the evaluations of weighed samples. Assuming all the calcium would transform into calcium carbonates, and all the magnesium transforms into nesquehonite, dypingite or hydromagnesite, which are the three most possible generated precipitates within this experimental condition and time scale, approved by other researchers, the produced theoretical weight shall be calculated as:

$$\frac{\text{Calcium or Magnesium sequestration efficiency (1.5h)} * \text{Molar concentration}}{\frac{\text{The theoretical amounts of precipitates}}{M_{Ca} \text{ or } M_{Mg}}} = \text{Equation 5. 1}$$

$$\frac{M_{CaCO_3} \text{ or } M_{nesquehonite} \text{ or } M_{dypingite} \text{ or } M_{hydromagnesite}}$$

Where

Calcium or magnesium sequestration efficiency (1.5h) can be observed from [Table 5. 5](#) (Section 5.2.3.4, page 221) below.

The theoretical amounts of precipitates are the required sediments for calculation in this section with the listing molecular weight (unit: g/mol):

$$M_{Ca} = 40; M_{CaCO_3} = 100; M_{Mg} = 24; M_{nesquehonite} = 138;$$

$$M_{hydromagnesite} = 466; M_{dypingite} = 484$$

For example, sample 1:

$$\text{Assuming all is calcium carbonates} \Rightarrow \frac{0.8839 * 20 \text{ g/l}}{x} = \frac{40}{100} \Rightarrow x = 44.20 \text{ g/l}$$

$$\text{Assuming all is nesquehonite} \Rightarrow \frac{0.9671 * 2.4 \text{ g/l}}{x} = \frac{24}{138} \Rightarrow x = 13.35 \text{ g/l}$$

$$\text{Assuming all is hydromagnesite} \Rightarrow \frac{0.9671 * 2.4 \text{ g/l}}{x} = \frac{24}{466} \Rightarrow x = 45.07 \text{ g/l}$$

$$\text{Assuming all is dypingite} \Rightarrow \frac{0.9671 \cdot 2.4 \text{ g/l}}{x} = \frac{24}{484} \Rightarrow x = 46.81 \text{ g/l}$$

Given solution volume is 200ml,

Total weight: All calcium carbonates = 44.20 g/l * 0.2 l = 8.84 g

All nesquehonite = 13.35 g/l * 0.2 l = 2.67 g

All hydromagnesite = 45.07 g/l * 0.2 l = 9.01 g

All dypingite = 46.81 g/l * 0.2 l = 9.36 g

Figures will demonstrate the differences between the hypothetical and the actual weights of samples in Section 5.2.3.4.

XRD: It is used to match and score the products' peaks with a typical reference material.

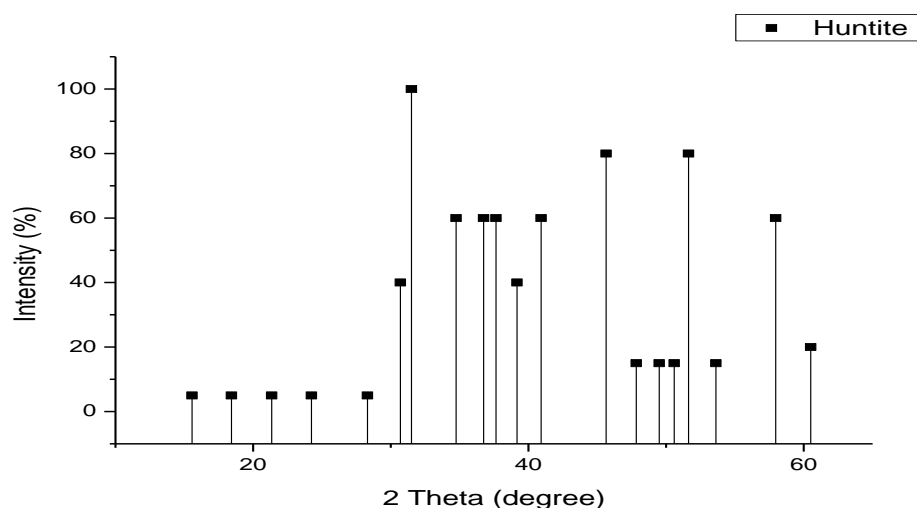
According to model estimation, at pH=10, aragonite (SI=2.35), artinite (SI=2.47), brucite (SI=0.4), monohydrocalcite written as $\text{CaCO}_3 \cdot \text{H}_2\text{O}$ (SI=1.63), calcite (SI=2.52), huntite (SI=9.19), dolomite (SI=5.94), magnesite (SI=2.88), hydromagnesite (SI=6.93), and vaterite (SI=1.94) are the possible formed products. Taking NaCl into consideration, halite (NaCl) is likely mixed or incorporated within the sample lattice, and other random combined magnesian calcite, different from the well-recognised dolomite and huntite, with various ratios of $\text{MgCO}_3 \cdot \text{CaCO}_3$.

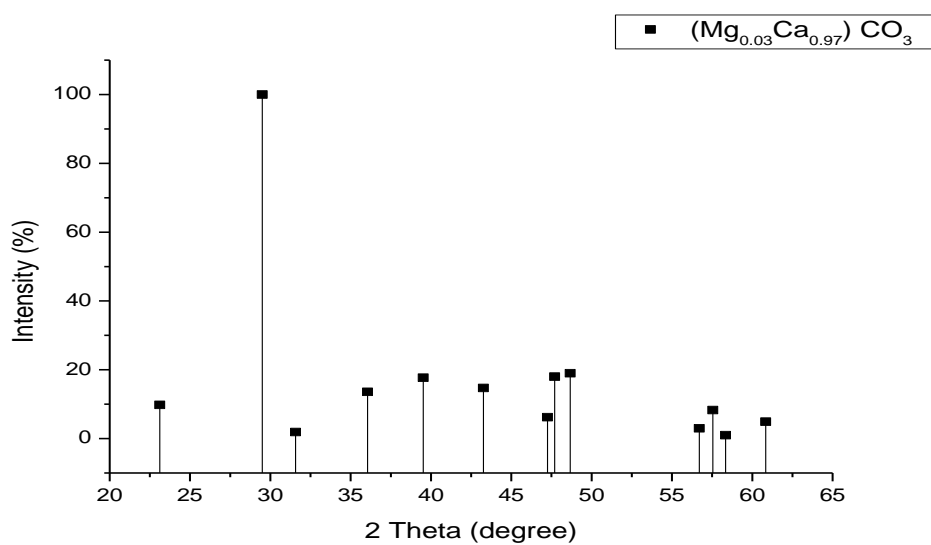
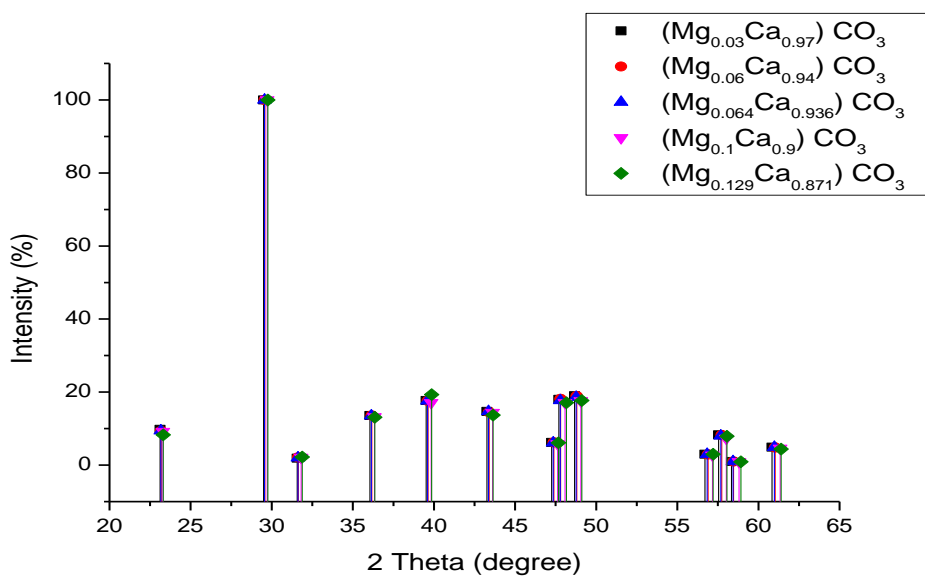
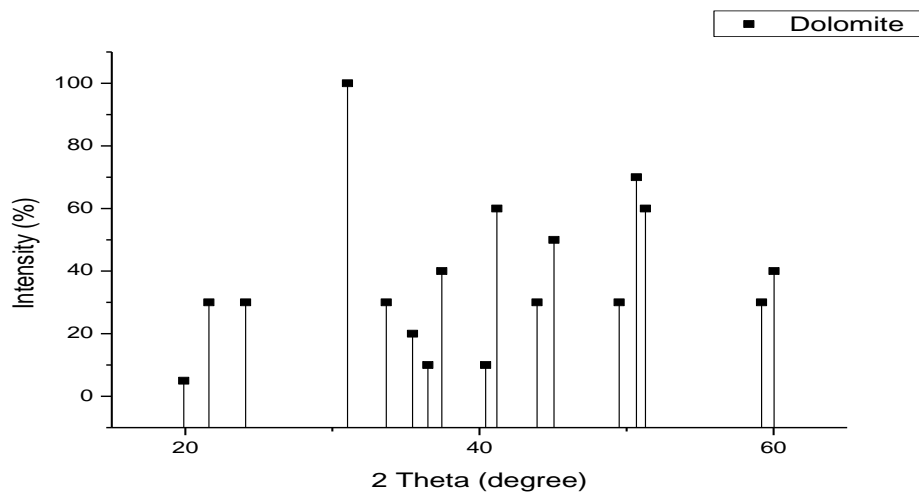
Considering all individual magnesium carbonates and calcium carbonates have been demonstrated in the previous two chapters, only huntite, dolomite, halite and particularly magnesian calcite are displayed here. There are seven relevant phases of magnesian calcite, although overlapped peaks don't have significant differences presented from the corresponded version, they are particularly useful in the semiquants (semiquant is less accurate than quantitative analysis, but provides a quantitative information to some extent) data analysis in XRD, as well as its further derived mechanics study. The practical range of XRD crystal examination is from 5 to 60 degrees based on the operational XRD requirements; and the potential calcined products are CaO and MgO or the combination of the two. Strictly speaking, although both huntite and dolomite are part of the magnesian calcite mineral compound, they are more widely distributed and studied. With regard to the common

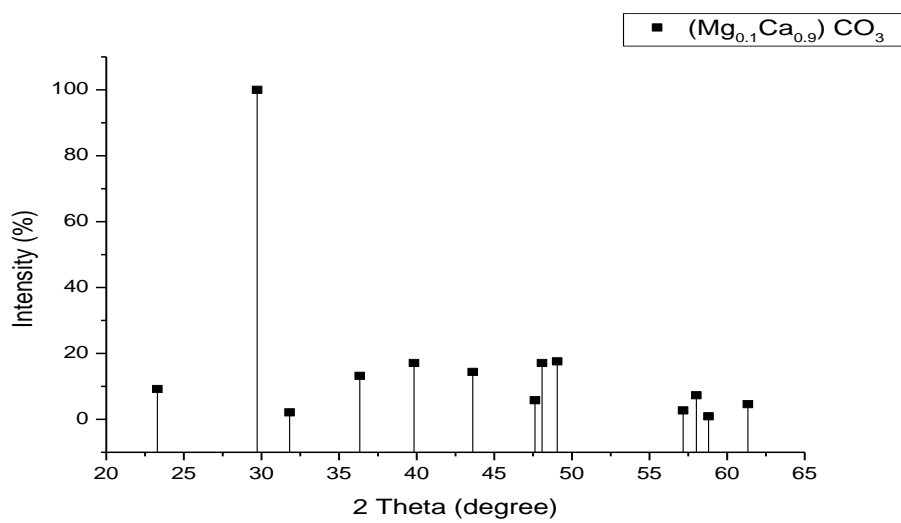
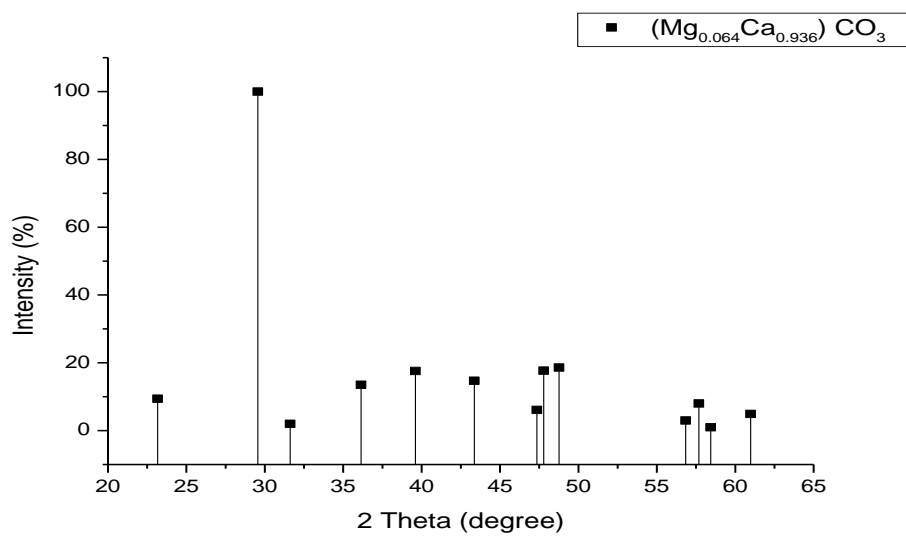
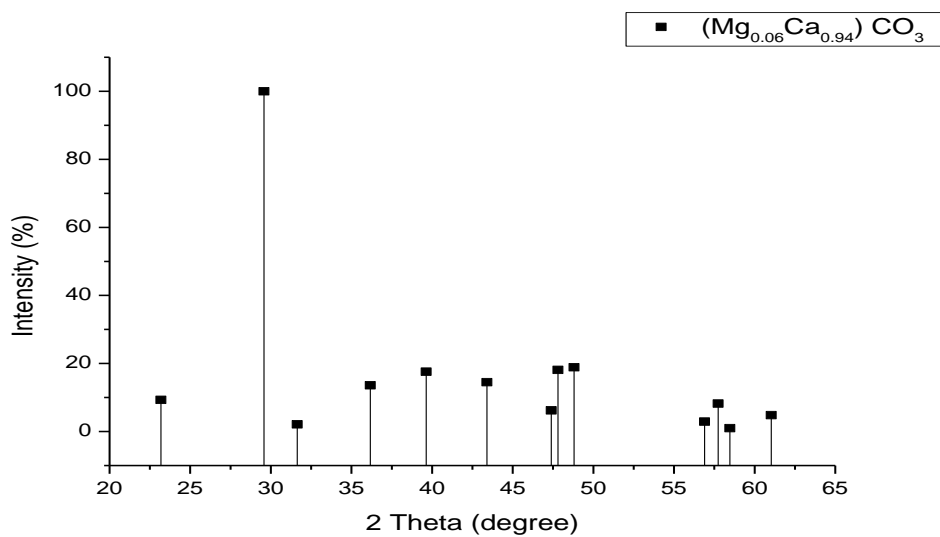
acceptance of huntite and dolomite and the rest of strong overlapped XRD patterns, all the other magnesian calcites (MC) are presented as a big group in their abbreviations and peaks except huntite and dolomite (Figure 5.2).

Table 5. 2: The chemical compositions of HMCs in the precipitates for SIV shown in Table 5.1

Magnesium Calcium Carbonates	Abbreviation symbol	Molecular weight	CO ₂ (%)	MgO [Mg ²⁺] (%)	CaO [Ca ²⁺] (%)	Total loss (%)
Mg₃Ca(CO₃)₄ (Huntite)	HT	352	50	34.1 [20.5]	15.9 [11.4]	50
MgCa(CO₃)₂ (Dolomite)	DM	184	47.8	21.7 [13]	30.4 [21.7]	47.8
(Mg_{0.064}Ca_{0.936})CO₃ (Magnesian calcite)	MC	99	44.4	2.6 [1.6]	52.9 [37.8]	44.4
(Mg_{0.1}Ca_{0.9})CO₃ (Magnesian calcite)	MC	98.4	44.7	4.1 [2.4]	44.7 [36.6]	44.7
(Mg_{0.129}Ca_{0.871})CO₃ (Magnesian calcite)	MC	97.9	44.9	5.3 [3.2]	49.8 [35.6]	44.9
(Mg_{0.03}Ca_{0.97})CO₃ (Magnesian calcite)	MC	99.5	44.2	1.2 [0.7]	54.6 [39]	44.2
(Mg_{0.06}Ca_{0.94})CO₃ (Magnesian calcite)	MC	99	44.4	2.4 [1.5]	52.6 [38]	44.4
NaCl (Halite,syn)	Halite	58.5	N/A	N/A	N/A	N/A







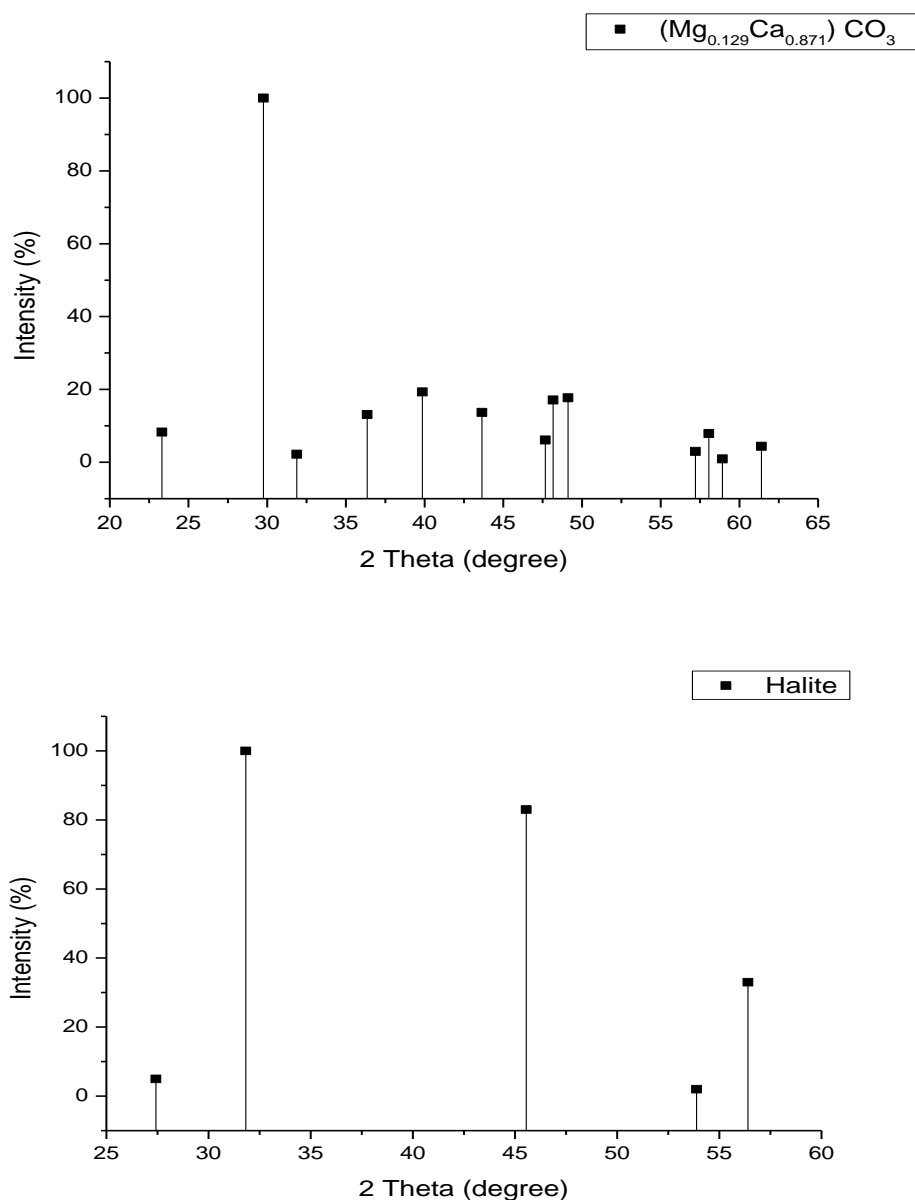
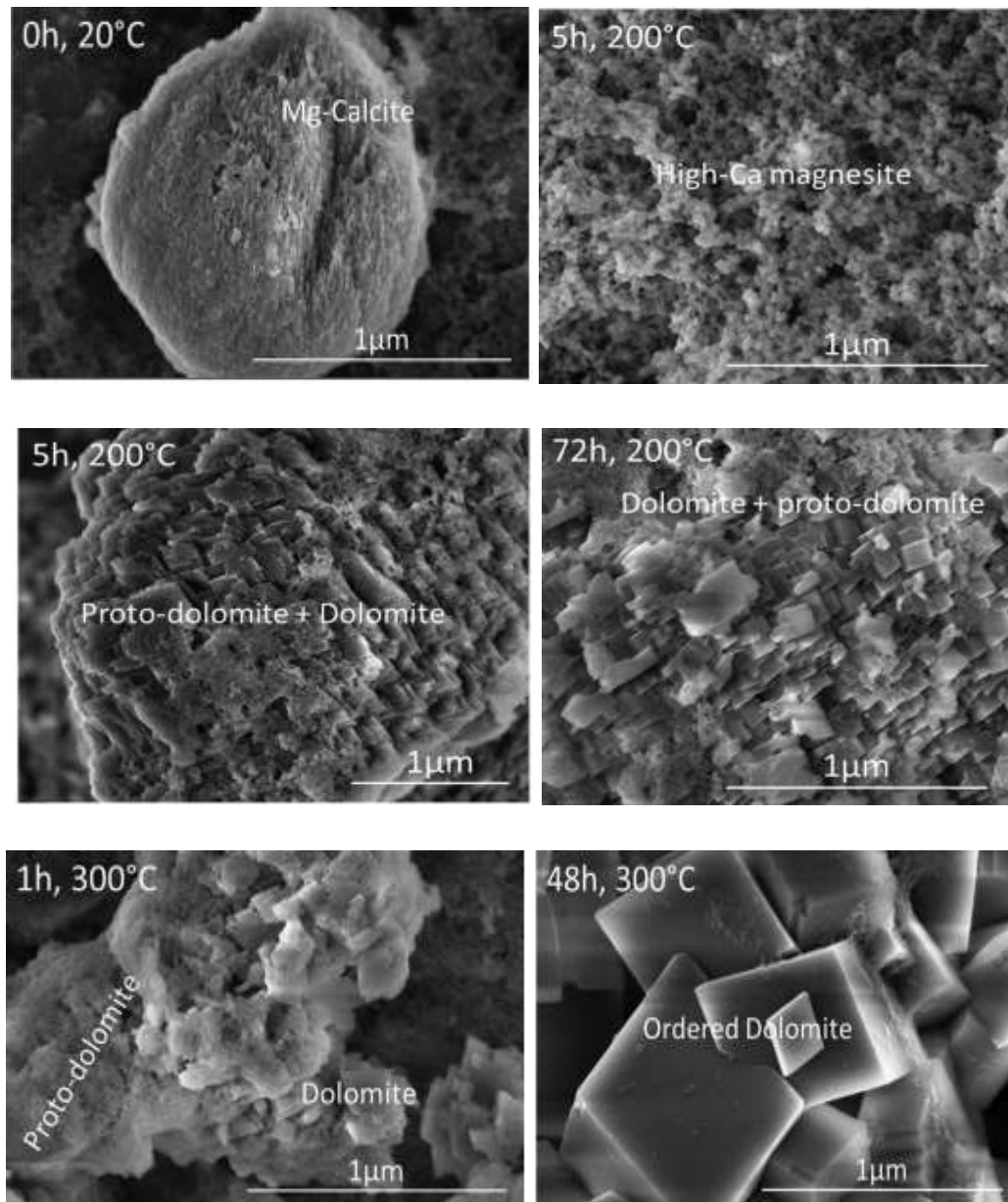


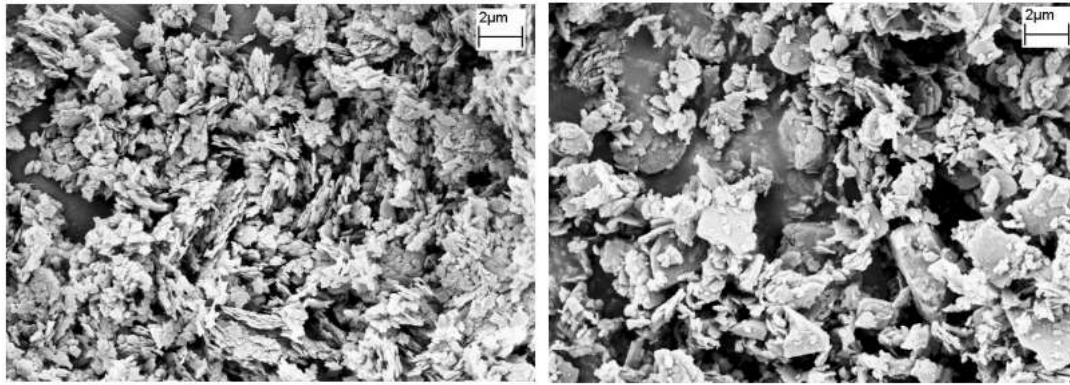
Figure 5. 2: XRD diffractograms for huntite, dolomite, magnesian calcite and halite (captions see top right corner)

SEM: SEM aims to provide microstructure observation. All the referenced pictures of potential sediments mentioned in Section 5.2.1 are shown in [Figure 5. 3](#). The figure does not have magnesian calcite, which has been demonstrated in Chapter 4. Hydromagnesite naturally occurs as a mixture with huntite. Its commercial application as a fire retardant was first investigated in the late 1980s. [Figure 5. 3b](#) presents the phenomenon of larger hydromagnesite particles interspersed with smaller platy huntite particles. Author Montes-Hernandez, Findling and Renard (2016) used 0.25mol NaOH, 0.25mol $\text{MgCl}_2 \cdot 6\text{H}_2\text{O}$ and

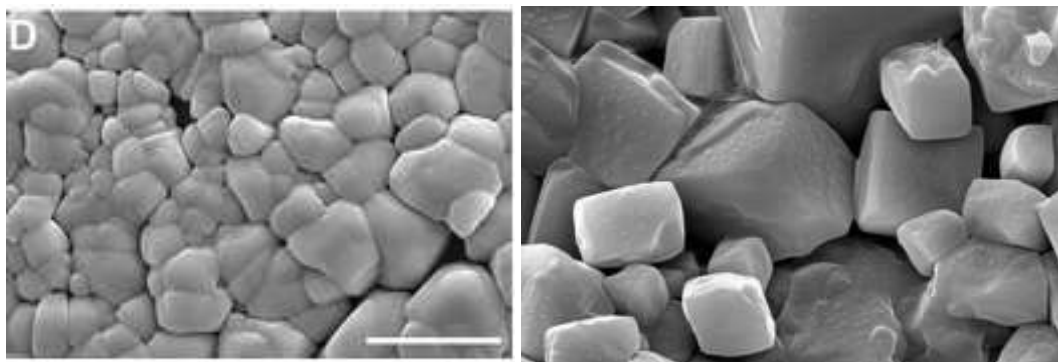
0.25mol $\text{Ca}(\text{OH})_2$, as well as CO_2 injection to generate dolomite and magnesian calcite with heating temperatures from 20°C to 300°C at various retention times. **Figure 5. 3a** illustrates a guidance in morphology on the presence of either magnesian calcite or dolomite. The image of NaCl demonstrates the bright-shining scaly agglomerates, which are significant different from other carbonates, providing its first impressions of halite contamination within sediments from SEM examination (**Figure 5. 3c**).



(a): Magnesian calcite (top two); Protodolomite (middle two +bottom left); Ordered dolomite (bottom right) (Montes-Hernandez et al., 2016)



(b): Huntite particles (left); A mixture of hydromagnesite and huntite particles (right) (Hollingbery & Hull, 2010)



(c): NaCl (Halit)--Individual NaCl grains ranged between 200nm and 5um (left)(Zawko & Schmidt, 2010); NaCl (Salt)—natural Margarita salt (The National, 2014).

Figure 5. 3: The referenced pictures of possible precipitates: (a) Magnesian calcite; (b) Huntite, and hydromagnesite and huntite mixture; (c) NaCl

TGA: Dolomite thermal decomposition has been extensively studied by researchers, whereas huntite and magnesian calcite are lack of references. It is because the commercial characteristic of huntite has not been widely explored, and magnesian calcite is a main production of this experiment only. Ideally the mixed components of huntite and magnesian calcite can be recognised as an MgCO_3 and CaCO_3 combination in various ratios, so their thermal property provides an insight into the decomposition procedures of both individual magnesium carbonates and individual calcium carbonates, and the precipitates are broken down into two steps if the partial pressure of CO_2 is high enough: 1) MgCO_3 decomposition at lower temperatures around $300\text{--}400^\circ\text{C}$; 2) CaCO_3 decomposition at higher temperatures around $700\text{--}800^\circ\text{C}$, and the two decomposition stages integrate into one process due to low

partial pressure of CO₂ (Table 5. 3). In contrast, there are differences in peak temperatures to some extent with the additional elements, based on researchers McIntosh et al. (1990).

Table 5. 3: The thermal decomposition stages of dolomite, huntite and magnesian calcite: (a) Two-stage; (b) One-stage (summarised from McIntosh et al. 1990)

(a): A two-stage thermal decomposition of precipitates (a high CO₂ partial pressure)

Mineral	Thermal Decomposition Steps
MgCa(CO₃)₂ (Dolomite)	MgCa(CO ₃) ₂ => CaCO ₃ + MgO + CO ₂ CaCO ₃ => CaO + CO ₂
Mg₃Ca(CO₃)₄ (Huntite)	Mg ₃ Ca(CO ₃) ₄ => CaCO ₃ + 3MgO + 3CO ₂ CaCO ₃ => CaO + CO ₂
(Mg_{0.064}Ca_{0.936})CO₃ (Magnesian calcite)	(Mg _{0.064} Ca _{0.936})CO ₃ => 0.936CaCO ₃ + 0.064 MgO + 0.064CO ₂ 0.936CaCO ₃ => 0.936CaO + 0.936CO ₂
(Mg_{0.1}Ca_{0.9})CO₃ (Magnesian calcite)	(Mg _{0.1} Ca _{0.9})CO ₃ => 0.9 CaCO ₃ + 0.1 MgO + 0.1 CO ₂ 0.9 CaCO ₃ => 0.9 CaO + 0.9 CO ₂
(Mg_{0.129}Ca_{0.871})CO₃ (Magnesian calcite)	(Mg _{0.129} Ca _{0.871})CO ₃ => 0.871CaCO ₃ + 0.129MgO + 0.129CO ₂ 0.871CaCO ₃ => 0.871CaO + 0.871CO ₂
(Mg_{0.03}Ca_{0.97})CO₃ (Magnesian calcite)	(Mg _{0.03} Ca _{0.97})CO ₃ => 0.97CaCO ₃ + 0.03 MgO + 0.03CO ₂ 0.97CaCO ₃ => 0.97CaO + 0.97CO ₂
(Mg_{0.06}Ca_{0.94})CO₃ (Magnesian calcite)	(Mg _{0.06} Ca _{0.94})CO ₃ => 0.94CaCO ₃ + 0.06 MgO + 0.06CO ₂ 0.94CaCO ₃ => 0.94CaO + 0.94CO ₂

(b): A one stage thermal decomposition of precipitates (a low CO₂ partial pressure)

Mineral	Thermal Decomposition Reaction
Dolomite	MgCa(CO ₃) ₂ => CaO + MgO + 2CO ₂
Huntite	Mg ₃ Ca(CO ₃) ₄ => 3MgO + CaO + 4CO ₂
(Mg_{0.064}Ca_{0.936})CO₃	(Mg _{0.064} Ca _{0.936})CO ₃ => 0.064MgO + 0.936CaO + CO ₂
(Mg_{0.1}Ca_{0.9})CO₃	(Mg _{0.1} Ca _{0.9})CO ₃ => 0.1MgO + 0.9CaO + CO ₂
(Mg_{0.129}Ca_{0.871})CO₃	(Mg _{0.129} Ca _{0.871})CO ₃ => 0.129MgO + 0.871CaO + CO ₂
(Mg_{0.03}Ca_{0.97})CO₃	(Mg _{0.03} Ca _{0.97})CO ₃ => 0.03MgO + 0.97CaO + CO ₂
(Mg_{0.06}Ca_{0.94})CO₃	(Mg _{0.06} Ca _{0.94})CO ₃ => 0.06MgO + 0.94CaO + CO ₂

Tables above provide the information on typical mixed magnesium calcium carbonates.

However, according to the results from modelling, the more types of magnesium carbonates or calcium carbonates are expected to form or mix into products, such as N, HM, D, V, C, and A. Because they were all demonstrated in Chapter 4, no further TGA will be summarised here for those precipitates.

In this work the ordinary air was used as the working gas in TGA, hence the heating profiles with regard to the peak temperatures were also operated in air diffusion. It is worth noting

that DT, HT and MC have no attached water molecule, first two dehydration stages are negligible; hence the table starts from the decarbonation stage 3. In particular, magnesian calcite does not have a standard reference peak, as it can vary from the $\text{MgCO}_3 \cdot \text{CaCO}_3$ ratios. Estimated peak temperature is thus equivalent to calcite at 750°C , as its major component is calcium (Table 5. 4).

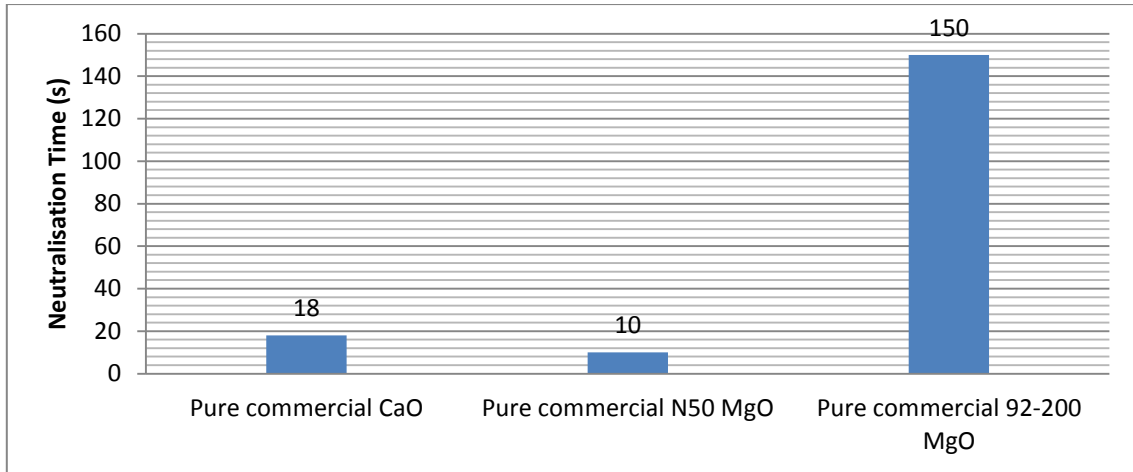
Reactivity Test: In terms of citric acid measurement, there is no difference between this reactivity test and those demonstrated in Chapter 4. The aim of it is to keep the consistency, as well as to make the general comparisons based on the previous results. However, there is not a typical test for this mixture, thus a reference experiment used in the following, is particularly designed for this section. All particles have been ground less than $250\ \mu\text{m}$ to unify the reaction.

Several hypotheses were initiated, such as CaO slaking methodology to estimate the lime reactivity; however, it is considered not reliable due to the unachievable high temperature at the slaking standard, and the other concern specifically for this study is from the high level of MgO mixture, which may lead to only partial dissolution from CaO. Therefore a more explicit design, on different proportions of MgO: CaO corresponding to the equivalent Mg^{2+} : Ca^{2+} ratios, was conducted to generate a base line for the experimental reactivity test. Citric acid testing methodology was utilised in the various mixed proportions on commercial N50 or 92-200 MgO combined with commercial CaO with the total amount of 2g.

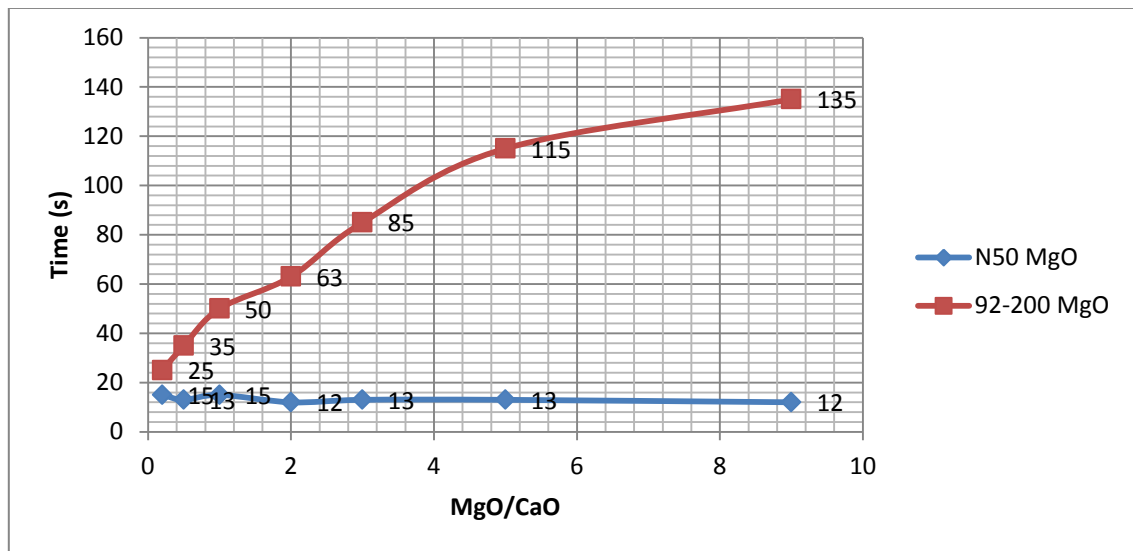
From Figure 5. 4, it can be seen that the reactivity tendency of the N50 commercial MgO mixture stays almost at the same level across the different mixture ratios; however, the 92-200 mixture exhibits much higher reactivity results accompanied by the larger mixture of MgO, displaying an almost linear tendency. This is due to the good reactivity of N50, produced from seawater with an extremely high purity level. Thus there is not a significant increase of reactivity when further N50 MgO is added. Moreover, a commercial CaO test is only 18 seconds, 8 seconds more than N50, which cannot lead to a significant increase in the neutralisation time of the N50 mixed dolime.

Table 5. 4: The thermal decomposition profiles of dolomite (Engler et al., 1988), huntite (Hollingbery &Hull,2010) and magnesian calcite (summarised from calcite)

Mineral	Magnesium Decarbonation Step 3: 300°C <Temp < 600°C			Calcium Decarbonation Step 4: 600°C<Temp < 800°C			Total Weight Loss (%)
	Reaction	Weight loss (%)	Peak temp (°C)	Reaction	Weight loss (%)	Peak temp (°C)	
Dolomite				$\text{MgCa}(\text{CO}_3)_2 \Rightarrow \text{CaO} + \text{MgO} + 2\text{CO}_2$	47.8	750	47.8
Huntite	$\text{Mg}_3\text{Ca}(\text{CO}_3)_4 \Rightarrow \text{CaCO}_3 + 3\text{MgO} + 3\text{CO}_2$	37.5	570	$\text{CaCO}_3 \Rightarrow \text{CaO} + \text{CO}_2$	12.5	714	50
$(\text{Mg}_{0.064}\text{Ca}_{0.936})\text{CO}_3$ (MC)				$(\text{Mg}_{0.064}\text{Ca}_{0.936})\text{CO}_3 \Rightarrow 0.064\text{MgO} + 0.936\text{CaO} + \text{CO}_2$	44.4	750	44.4
$(\text{Mg}_{0.1}\text{Ca}_{0.9})\text{CO}_3$ (MC)				$(\text{Mg}_{0.1}\text{Ca}_{0.9})\text{CO}_3 \Rightarrow 0.1\text{MgO} + 0.9\text{CaO} + \text{CO}_2$	44.7	750	44.7
$(\text{Mg}_{0.129}\text{Ca}_{0.871})\text{CO}_3$ (MC)				$(\text{Mg}_{0.129}\text{Ca}_{0.871})\text{CO}_3 \Rightarrow 0.129\text{MgO} + 0.871\text{CaO} + \text{CO}_2$	44.9	750	44.9
$(\text{Mg}_{0.03}\text{Ca}_{0.97})\text{CO}_3$ (MC)				$(\text{Mg}_{0.03}\text{Ca}_{0.97})\text{CO}_3 \Rightarrow 0.03\text{MgO} + 0.97\text{CaO} + \text{CO}_2$	44.2	750	44.2
$(\text{Mg}_{0.06}\text{Ca}_{0.94})\text{CO}_3$ (MC)				$(\text{Mg}_{0.06}\text{Ca}_{0.94})\text{CO}_3 \Rightarrow 0.06\text{MgO} + 0.94\text{CaO} + \text{CO}_2$	44.4	750	44.4



(a): The reactivity tests of commercial MgO and CaO, used as a standard (citric acid method)



(b): The initial reactivity tests of a MgO•CaO mixture, used as a standard (citric acid method)

Figure 5. 4: The reactivity tests of the calcination products, used as standards: (a) MgO and CaO individual reactivity tests; (b) Dolime mixture reactivity tests

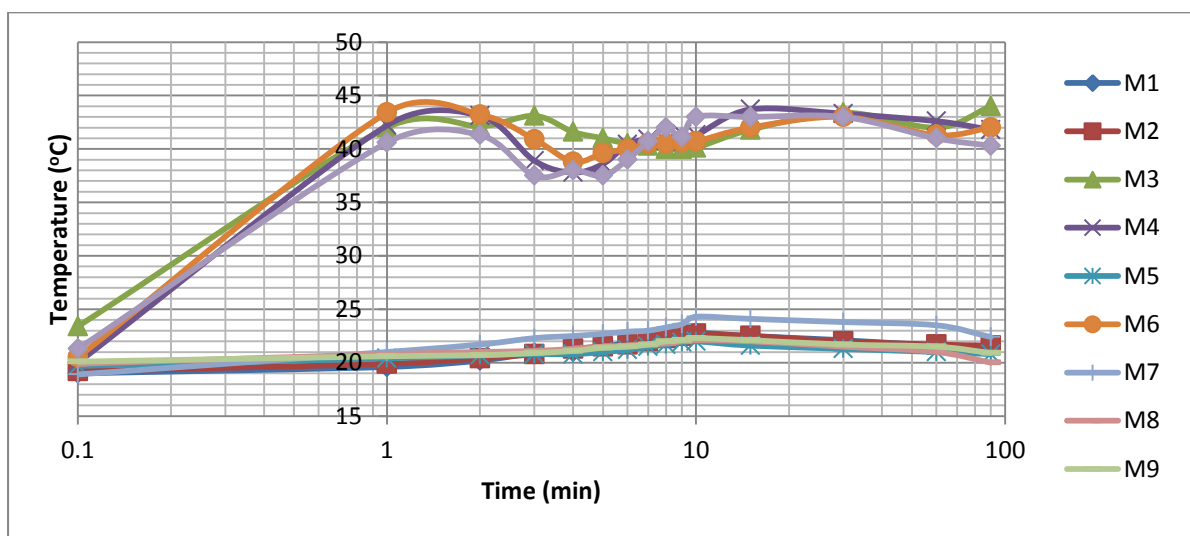
5.2.3 Series IV-Carbonation

5.2.3.1 Carbonation and pH Stability Studies

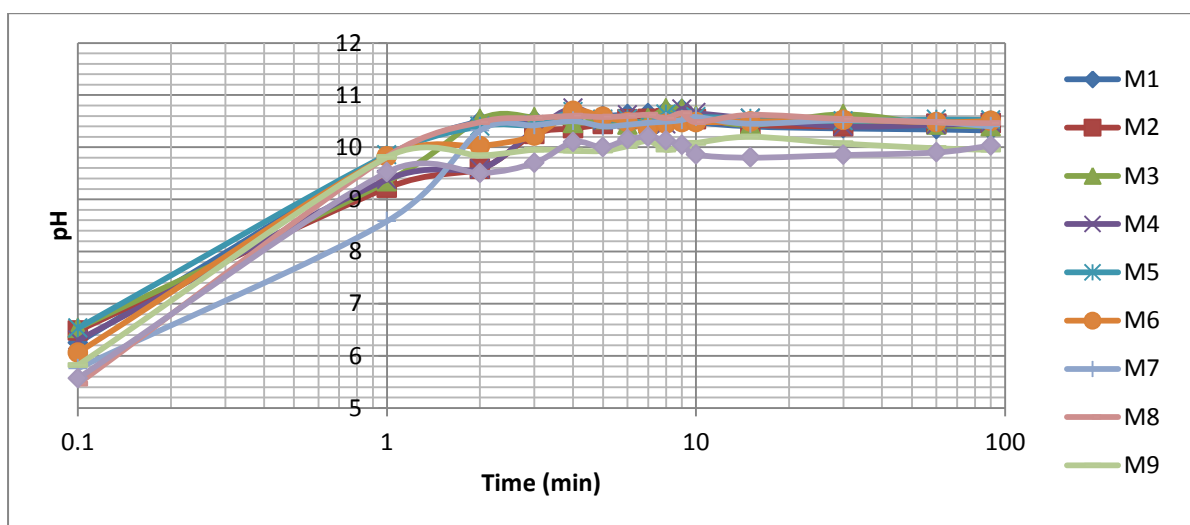
The measurement was recorded during the operation level of 1.5h standard period in multiple ions bench reaction (Figure 5. 5). All samples were taken at a room temperature except M3, M4, M6 and M10, which were run at 40°C. The higher temperature experiment is more difficult to maintain at a constant level because of the significant heat accumulation at the bottom of beaker in a short time; natural reaction thermal release also contributes to it in a small proportion. Hence higher temperature profiles on those four samples conducted

at higher heat are expected to fluctuate, while the other samples at room temperatures display more regular exothermal reaction.

A pH stability test was accompanied with temperature measurements, which was measured throughout the entire operation of 1.5h (bench reaction) and 1d (free reaction), in order to monitor and maintain a constant pH. Starting pH ranges from 5.5 to 6.5 within the normal area of $MgCl_2$ and $CaCl_2$ reactants, this figure is then elevated to around 10 or 10.5 within 2min by introducing an alkaline solution, and further keeps in a relative reasonable fluctuation phase over a day to ensure the reliability of this experiment.



(a): Carbonation study--temperature vs time for SIV shown in Table 5.1



(b): pH stability study--pH vs time for SIV shown in Table 5.1

Figure 5. 5: Carbonation (a) and pH stability (b) studies for SIV shown in Table 5.1

5.2.3.2 *Precipitates Identification Studies*

In the sediments' analysis, two precipitates' analytical tables correspond to one graph used to describe the XRD analysis and its related peaks. All of the possible precipitates including all types of magnesian calcites are shown in the first table of its corresponding figure, while the determination based on general matching scores as well as semiquants is displayed in the second.

The score in **Figure 5.10b** indicates the degree to which the scaled peaks match the reference peaks. A larger score represents a stronger matching potential meaning a precipitate is more likely to be formed in the tested sample. However the other indicator semiquants are also important in the samples' identification. A higher figure in this column tends to depict more quants within the composition. Neither the score nor semiquants can work independently; if together they demonstrate a reasonable range or relatively equal high figure, this component is contained in the graph and table.

There are mainly four compound groups in this section: (i) the magnesium calcium carbonate group-- the most important in this mixed carbonation study; (ii) the calcium carbonate group—accompanied as a byproduct of the precipitated magnesian calcite; (iii) the magnesium compound group—accompanied as a byproduct of the desired magnesian calcite; (iv) others—mainly impurities' coprecipitation. In this SIV carbonation study, relevant phases in each categorised group are presented in **Figure 5. 6** based on the importance of the precipitates. This ranking is the result of the software's presentation of the matching possibility of the produced peaks from the precipitation and the referenced peaks from the mineral databases. A higher percentage of magnesium participation in the final products leads to a more stable phase.

Figure 5.10a mainly displays the magnesian calcite and the calcite formation in M1-4 due to the larger initial calcium concentrations ($\text{Ca}^{2+}:\text{Mg}^{2+}=5:1$ or $2:1$). In **Figure 5.10b**, almost all types of the precipitates are produced in M1-4 to some extent except dolomite and brucite, reflecting the difficulties of dolomite formation in lab conditions and the unfavourable factors influencing brucite production in this process. In terms of Magnesian Calcite (MC), there is only one composition [e.g. $(\text{Mg}_{0.03}\text{Ca}_{0.97})\text{CO}_3$] in sample 1, and two more in sample 2, indicating that higher magnesium involvement accelerates magnesium participation within

the product. However, the number of minerals increases to five in samples 3 and 4 because of the elevated temperature enhancing the reaction rate significantly. Brucite only exists in samples 2 and 4, implying the increased value of magnesium within the products by a larger reactants' concentration. This phenomenon is irrelevant to the temperature.

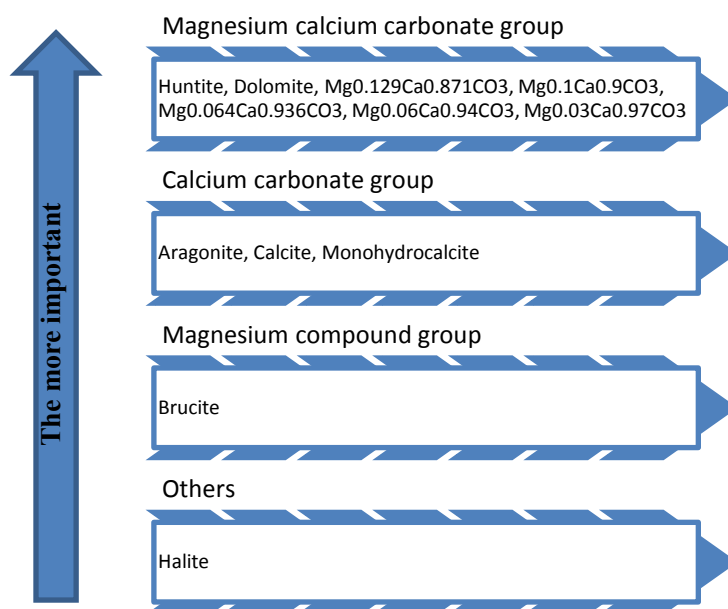


Figure 5. 6: The groups of potential precipitates in SI carbonation study

It is also worth noting that based on this first analysis and prominent quantitative data, magnesium calcium carbonate can be classified into three categories, aiming to differentiate the amounts of magnesium coprecipitation, that is (i) $Mg^{2+} < 0.1$ ($Mg_{0.064}Ca_{0.936}CO_3$, $Mg_{0.03}Ca_{0.97}CO_3$ & $Mg_{0.06}Ca_{0.94}CO_3$), (ii) $0.1 \leq Mg^{2+} < 1$ ($Mg_{0.1}Ca_{0.9}CO_3$ & $Mg_{0.129}Ca_{0.871}CO_3$), and (iii) $Mg^{2+} \geq 1$ (huntite & dolomite); the first two classifications are commonly named as magnesian calcite. Usually, each classification has the appearance of the same group of products all together. For example, when magnesium is not sufficient in the solution, produced precipitates mainly contain the deposits of $Mg^{2+} < 0.1$; but when more magnesium is introduced into the reaction system or the entire process is accelerated by other factors, precipitates with $0.1 \leq Mg^{2+} < 1$ and $Mg^{2+} \geq 1$ are present in the crystalline products. Therefore the magnesium penetration is a good indicator of the carbonation degree. However, as the dolomite is remarkably difficult to synthesise in lab conditions according to research, it is not considered mostly in the precipitates. The exceptions of samples M8-10 are caused by their magnesium dispersions of $Mg^{2+} \geq 1$ with several overlapped peaks of huntite. Theoretically, there is no reason to reject the dolomite crystalloids in XRD evaluation.

Considering the complexity of the mixed carbonates, all possible precipitate formations are summarised in **Figure 5.10c**, where they are scored and analysed. Samples M5-10 possess 10 times the magnesium concentration of natural seawater, with the ratio of $\text{Ca}^{2+}:\text{Mg}^{2+}=1:5$. XRD diffractograms are used to display the varieties of magnesian calcites, including larger proportions of huntite and dolomite in samples 8-10. During the intermediate transformation stage of magnesian calcite, the magnesium element triggers monohydrocalcite and aragonite, as well as an impurity NaCl (with the mineral name halite) in all samples. Additionally brucite is also noticed in samples 6-8 due to an insufficient carbonate supply. In short, all samples are dominated by magnesium interstitial carbonates, which is consistent with the results of Radha et al. (2011) who explained that the crystallisation energetics of amorphous MgCO_3 (AMC) is energetically more metastable than the $\text{MgCO}_3\text{--CaCO}_3$ (AMC–ACC) system, but it is more persistent, probably because of the higher dehydration energy and slower dehydration kinetics of the Mg^{2+} ion.

A more detailed analysis of the magnesium proportion in crystals is conducted during the four stages of the phase transformation process (**Figure 5.7**): (i) an initial stage of $\text{Mg}^{2+}<0.1$ in MC group; (ii) an intermediate stage of $\text{Mg}^{2+}<0.1$ & $0.1\leq\text{Mg}^{2+}$; (iii) a transitional stage of $\text{Mg}^{2+}<0.1$, $0.1\leq\text{Mg}^{2+}<1$ & $\text{Mg}^{2+}\geq 1$; (iv) a completed stage of $\text{Mg}^{2+}\geq 1$. In accordance with the relevant samples, sample 5 is in the initial stage with $\text{Mg}^{2+}<0.1$, while samples 6 and 7 possess both crystals of $\text{Mg}^{2+}<0.1$ and $0.1\leq\text{Mg}^{2+}<1$ in the intermediate stage, caused by the accelerated carbonation from an elevated temperature, and less carbonates participation in a no agitated solution. Dissimilarly, samples 8 and 10 are filled with a variety of MC when they place in the middle of the transitional stage by either less infusion of CO_2 or increased heat. Finally, sample 9 is the most completed specimen possessing $\text{Mg}^{2+}\geq 1$ only in the MC group.

In the calcium carbonate group, monohydrocalcite (MHC) and aragonite (A) are the other two main features in all precipitates. Based on Section 2.7.4, MHC is found mainly in the presence of Mg^{2+} (e.g. saline lakes), while aragonite is also largely derived by Mg^{2+} participation (e.g. natural seawater). The main difference between the two is the magnesium concentration. A more concentrated magnesium solution is more likely to produce MHC. In terms of the magnesium compound group, brucite appears in samples 6-8 caused by inadequate carbonates, hence reflecting the abundancy of magnesium ions. The

contamination of halite occurs in all samples, which is explained by the good hydrophilic characteristics of magnesium incorporated into the soluble NaCl. In the end, samples 5 and 9 are further selected to monitor the kinetics over the course of a day, in order to validate this assumption of reaction degree.

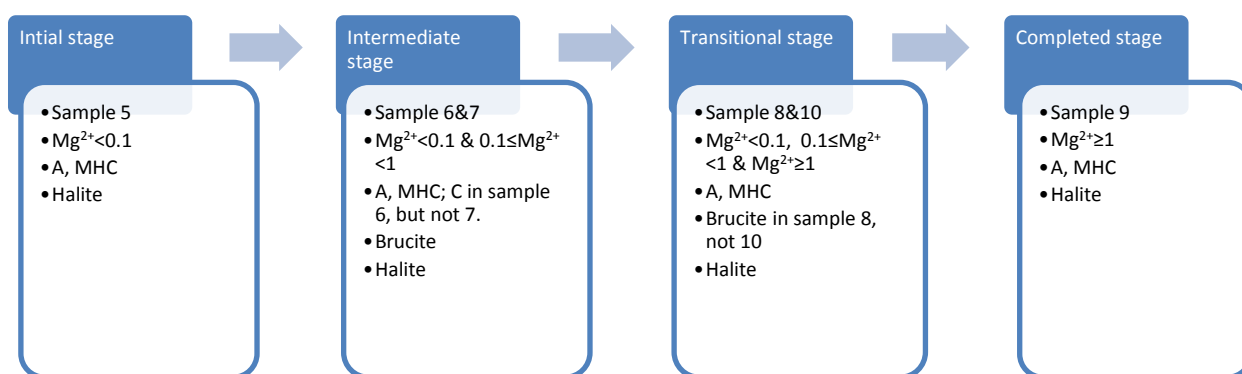


Figure 5. 7: The phase transformation process of the precipitates

Figure 5.10a indicates that brucite is part of the intermediate transaction product, which transforms towards magnesian calcite with sufficient time. Evidence of this is demonstrated by the quantitative analysis of the transitional stage, where brucite exists only in M8 rather than M10. In M10, the amount of MC including huntite and dolomite is 76%, 2% more than M8; this larger number implies a better degree of reaction and phase transformation in M10. The same illustration also applies to samples M7 and 8. M7 only possesses 45% of MC including huntite and dolomite, which is much less than 74% in M8, demonstrating its higher reaction extent. Calcite presented in sample 6 is caused by the insufficient magnesium involvement due to the increased temperature, consistent with the previous demonstration. In this particular case of magnesium participation, aragonite and MHC are grouped as the stable phase, while calcite is considered to be the metastable phase.

The integrated mechanism and the phase transformation process corresponding to each individual sample are presented in Figure 5. 8. Sample 5 is set as a referenced substance; hence all other parameters are then compared to it. These factors comprise elevated temperature, lower stirring speed, lower CO₂ flux rate, and lower pH. They enhance the reaction through an increased stability in phase alteration, which is explained by the insufficiency of one of the reactants' addition, or the reversed effect of various parameters, leading to an earlier process completion and the deposits' immediate conversion (refer to

Chapter 2.10). An increased temperature usually contributes to positive acceleration, but samples 9 and 10 contradict this observation. This graph utilises a ladder shape to evaluate the importance of each parameter, where the larger difference of height stands for a more important factor.

pH is an essential restriction in the carbonation study, where a lower pH can produce more stable precipitates. Conversely, a higher pH tends to continuously sequester the larger amounts of elements, resulting in less crystallisation and reduced transformation time. The second essential factor is temperature, which can have either positive or negative influences: at pH=10.5 (samples 5 and 6), the increased temperature has a positive effect on reaction degree, while at pH=10 (samples 9 and 10), a higher temperature causes the disturbance of magnesium recrystallisation. The next important factor is the CO₂ flux rate, directly linked to the addition of initial reactants. The stirring speed, on the other hand, which contributes to a uniform agitation that provides higher chances of particulate collision, demonstrates the least influence.

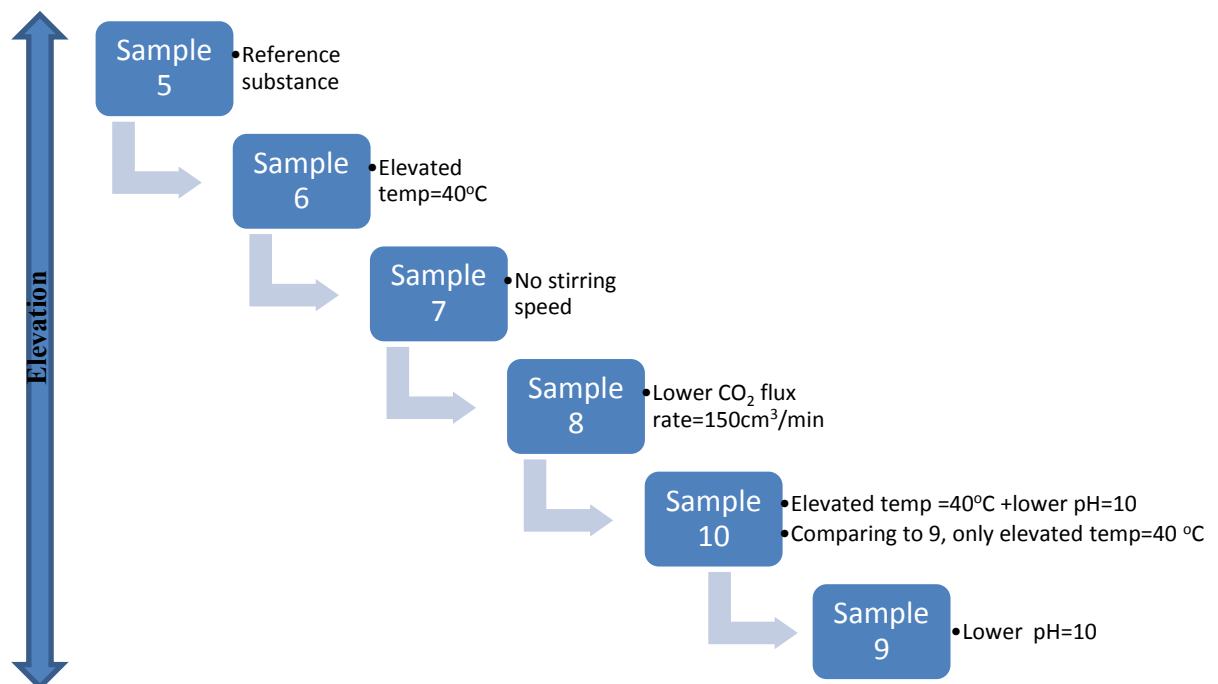


Figure 5. 8: The flow chart of phase transformation corresponding to each individual sample

All samples are divided into two groups, 1-4 and 5-10, according to the integral ratios of Ca²⁺:Mg²⁺ and Mg²⁺:Ca²⁺. The former has MC, C and brucite, while the latter possesses MC+DM+HT, A+MHC, brucite and halite (**Figure 5. 9**). The reason for the huntite and

dolomite presence in group 2 is attributed to the addition of more Mg^{2+} , in line with the theoretical assumption. Similarly, the identical phenomenon in the calcium carbonate group also shows in [Figure 2.26](#) of Section 2.10, where the calcite is obtained at $Mg^{2+}:Ca^{2+}<0.5$ with temperatures lower than $40^{\circ}C$, while the aragonite and MHC present at $Mg^{2+}:Ca^{2+}>1$ at both room and the elevated temperatures.

Halite is present in all samples of group 2 rather than group 1, which agrees with the NaCl incorporation within the carbonated crystal lattices, together with its dissociated ions in water molecules. Therefore, it is indirectly proven that magnesium-based compounds have stronger hydrophilic property, while calcium has a better carbonphilic (rooted from hydrophilic) characteristic than magnesium with a stronger propensity to integrate with CO_3^{2-} . This phenomenon is also validated by SEM and EDX analysis in the following section, on the SEM-EDX analysis of sample 5.

Group 1: Samples 1-4	Group 2: Samples 5-10
<ul style="list-style-type: none">•Magnesium calcium carbonate group: MC•Calcium carbonate group : C•Magnesium compound group: Brucite	<ul style="list-style-type: none">•Magnesium calcium carbonate group: MC+DM +HT•Calcium carbonate group : A+MHC•Magnesium compound group: Brucite•Others: Halite

Figure 5. 9: The comparisons of the precipitates from two groups

Sample			M1		M2		M3		M4	
Ref. Code	Mineral Name	Chemical Formula	Score	SemiQuant (%)	Score	SemiQuant (%)	Score	SemiQuant (%)	Score	SeimiQuant (%)
01-071-1663	Calcite, magnesian	(Mg _{0.1} Ca _{0.9})CO ₃	29	2	43	1	60	15	54	19
01-073-1403	Huntite	Mg ₃ Ca(CO ₃) ₄	16	1	27	2	24	1	37	1
01-083-1766	Dolomite	MgCa(CO ₃) ₂	5	--	5	--	15	--	11	1
01-086-2335	Calcite, magnesian	(Mg _{0.064} Ca _{0.936})CO ₃	42	22	51	22	71	23	70	20
01-086-2336	Calcite, magnesian	(Mg _{0.129} Ca _{0.871})CO ₃	30	1	50	1	55	8	55	9
01-089-1304	Calcite, magnesium, syn	(Mg _{0.03} Ca _{0.97})CO ₃	77	23	69	24	73	21	74	19
01-089-1305	Calcite, magnesium, syn	(Mg _{0.06} Ca _{0.94})CO ₃	36	22	46	22	72	21	72	20
01-072-1652	Calcite	CaCO ₃	92	29	71	25	70	12	73	11
01-074-2220	Brucite	Mg(OH) ₂	44	--	51	3	22	--	48	1
Sample			M1		M2		M3		M4	
Ref. Code	Mineral Name	Chemical Formula	Contained within precipitates ? (Score)	Semi-Quant (%)	Contained within precipitates? (Score)	Semi-Quant (%)	Contained within precipitates ? (Score)	Semi-Quant (%)	Contained within precipitates ? (Score)	Seimi-Quant (%)
01-071-1663	Calcite, magnesian	(Mg _{0.1} Ca _{0.9})CO ₃	No		No		Yes (60)	15	Yes (54)	19
01-073-1403	Huntite	Mg ₃ Ca(CO ₃) ₄	No		No		No		No	
01-083-1766	Dolomite	MgCa(CO ₃) ₂	No		No		No		No	
01-086-2335	Calcite, magnesian	(Mg _{0.064} Ca _{0.936})CO ₃	No		Yes (51)	23	Yes (71)	23	Yes (70)	20
01-086-2336	Calcite, magnesian	(Mg _{0.129} Ca _{0.871})CO ₃	No		No		Yes (55)	8	Yes (55)	9
01-089-1304	Calcite, magnesium, syn	(Mg _{0.03} Ca _{0.97})CO ₃	Yes (77)	45	Yes (69)	25	Yes (73)	21	Yes (74)	19
01-089-1305	Calcite, magnesium, syn	(Mg _{0.06} Ca _{0.94})CO ₃	No		Yes (46)	23	Yes (72)	22	Yes (72)	20
01-072-1652	Calcite	CaCO ₃	Yes (92)	55	Yes (71)	26	Yes (70)	12	Yes (73)	11
01-074-2220	Brucite	Mg(OH) ₂	No		Yes (51)	3	No		Yes (48)	1

(b): The matching scores and semiquants of M1-4 precipitates, calculated by software X'Per HighScore Plus

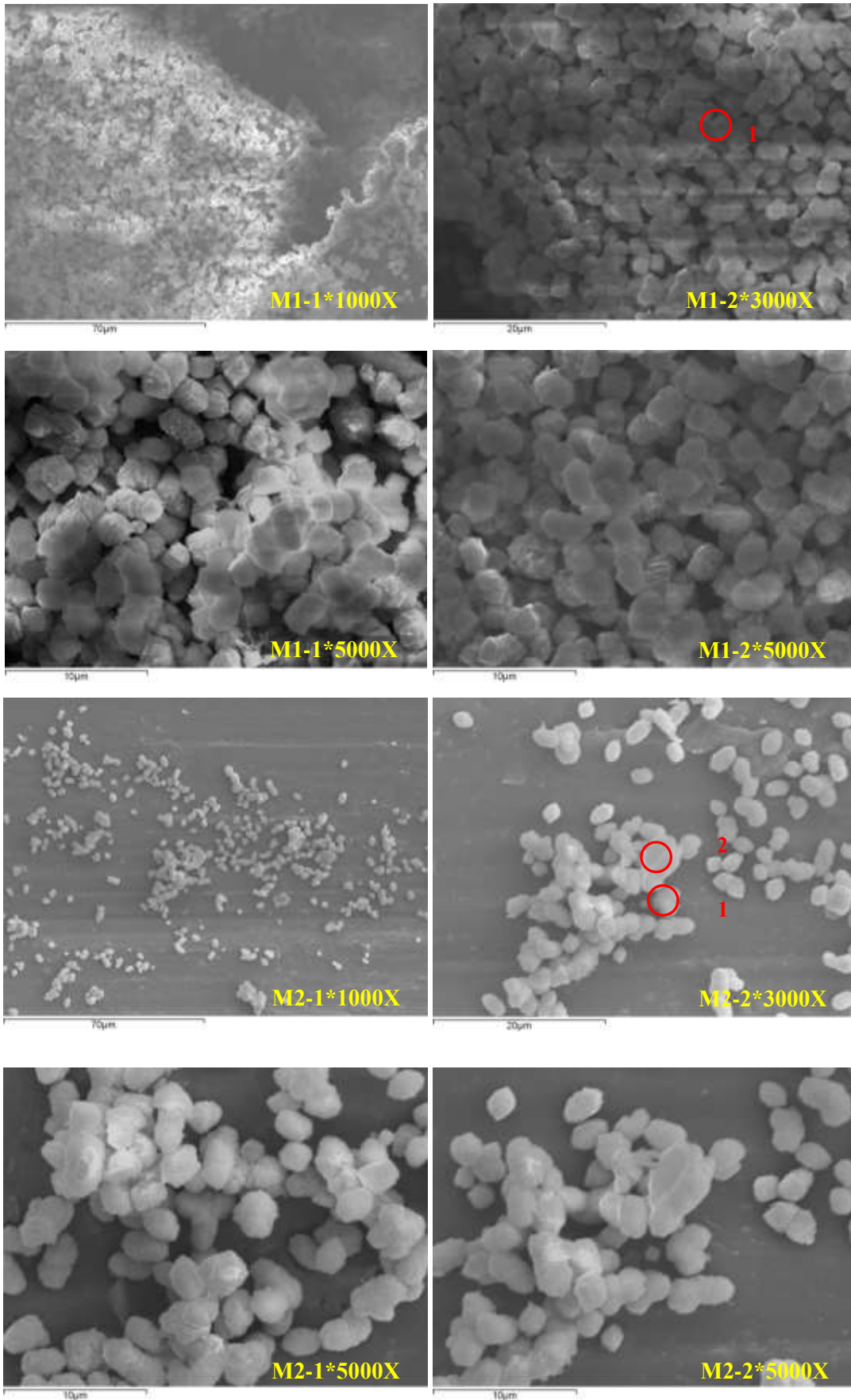
Sample			M5		M6		M7	
Ref. Code	Mineral Name	Chemical Formula	Score	SemiQuant (%)	Score	SemiQuant (%)	Score	SemiQuant (%)
01-071-1663	Calcite, magnesian	(Mg _{0.1} Ca _{0.9})CO ₃	29	5	55	21	64	7
01-073-1403	Huntite	Mg ₃ Ca(CO ₃) ₄	25	6	41	4	39	6
01-083-1766	Dolomite	MgCa(CO ₃) ₂	0	2	24	1	35	3
01-086-2335	Calcite, magnesian	(Mg _{0.064} Ca _{0.936})CO ₃	45	8	45	7	64	10
01-086-2336	Calcite, magnesian	(Mg _{0.129} Ca _{0.871})CO ₃	30	5	54	21	66	7
01-089-1304	Calcite, magnesium, syn	(Mg _{0.03} Ca _{0.97})CO ₃	46	8	54	6	60	6
01-089-1305	Calcite, magnesium, syn	(Mg _{0.06} Ca _{0.94})CO ₃	43	8	48	7	65	10
01-076-0606	Aragonite	CaCO ₃	51	12	28	13	59	13
01-086-0174	Calcite	CaCO ₃	39	10	42	3	57	3
00-044-1482	Brucite	Mg(OH) ₂	39	3	50	8	62	8
01-072-1668	Halite	NaCl	51	20	49	3	66	18
01-083-1923	Monohydrocalcite	CaCO ₃ *H ₂ O	41	16	20	5	35	9
Sample			M8		M9		M10	
Ref. Code	Mineral Name	Chemical Formula	Score	SemiQuant (%)	Score	SemiQuant (%)	Score	SemiQuant (%)
01-071-1663	Calcite, magnesian	(Mg _{0.1} Ca _{0.9})CO ₃	28	3	14	2	54	3
01-073-1403	Huntite	Mg ₃ Ca(CO ₃) ₄	41	9	33	10	47	12
01-083-1766	Dolomite	MgCa(CO ₃) ₂	39	5	33	3	56	7
01-086-2335	Calcite, magnesian	(Mg _{0.064} Ca _{0.936})CO ₃	38	4	9	2	52	4
01-086-2336	Calcite, magnesian	(Mg _{0.129} Ca _{0.871})CO ₃	39	3	15	3	44	2
01-089-1304	Calcite, magnesium, syn	(Mg _{0.03} Ca _{0.97})CO ₃	35	4	15	2	51	4
01-089-1305	Calcite, magnesium, syn	(Mg _{0.06} Ca _{0.94})CO ₃	32	3	13	2	61	4
01-076-0606	Aragonite	CaCO ₃	74	40	71	27	74	33
01-086-0174	Calcite	CaCO ₃	30	4	24	4	45	4
00-044-1482	Brucite	Mg(OH) ₂	45	12	24	6	31	5
01-072-1668	Halite	NaCl	43	2	52	27	53	8
01-083-1923	Monohydrocalcite	CaCO ₃ *H ₂ O	36	11	31	11	45	14
Sample			M5		M6		M7	
Ref. Code	Mineral Name	Chemical Formula	Contained within precipitates? (Score)	SemiQuant (%)	Contained within precipitates? (Score)	SemiQuant (%)	Contained within precipitates? (Score)	SemiQuant (%)

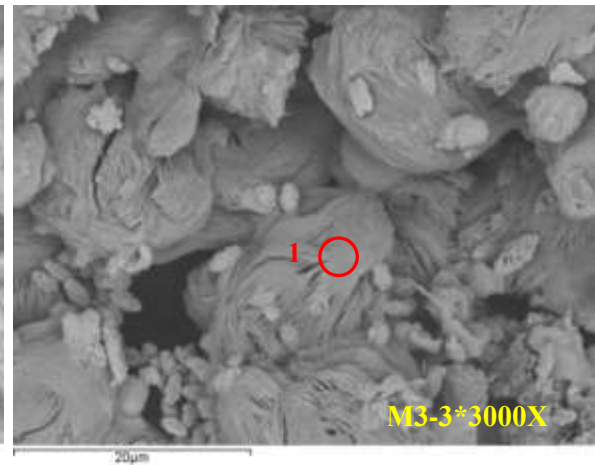
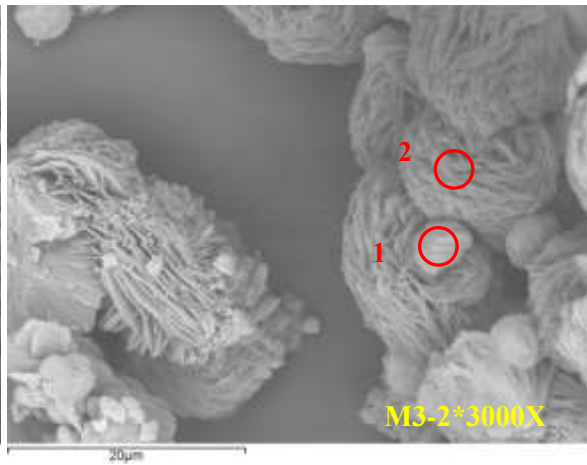
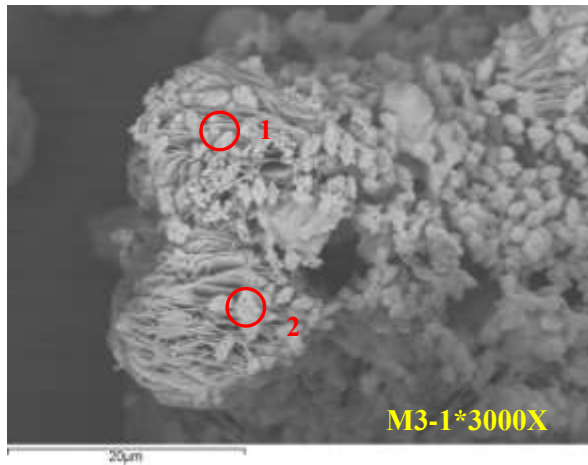
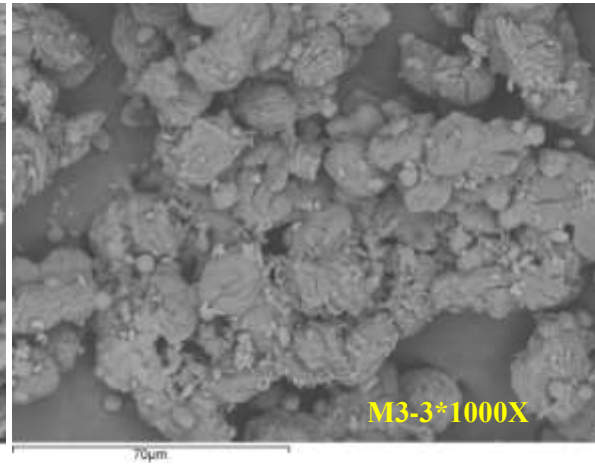
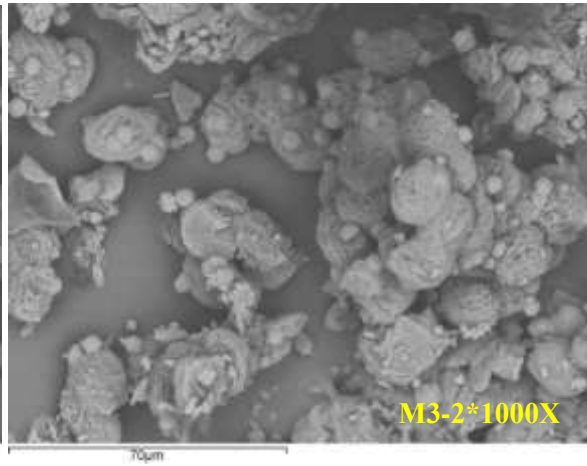
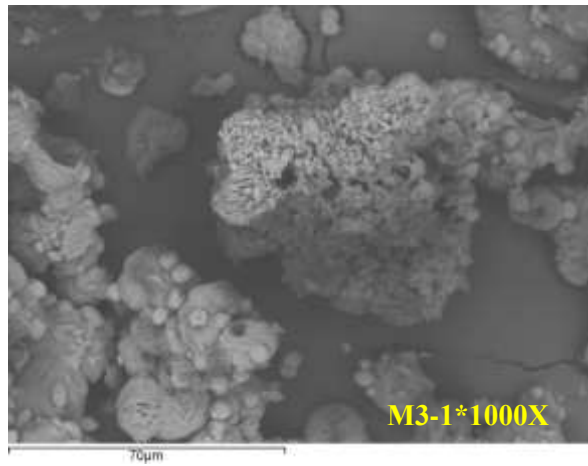
01-071-1663	Calcite, magnesian	$(Mg_{0.1}Ca_{0.9})CO_3$	No		Yes (55)	22	Yes (64)	8
01-073-1403	Huntite	$Mg_3Ca(CO_3)_4$	No		No		No	
01-083-1766	Dolomite	$MgCa(CO_3)_2$	No		No		No	
01-086-2335	Calcite, magnesian	$(Mg_{0.064}Ca_{0.936})CO_3$	Yes (45)	12	Yes (45)	8	Yes (64)	11
01-086-2336	Calcite, magnesian	$(Mg_{0.129}Ca_{0.871})CO_3$	No		Yes (54)	22	Yes (66)	8
01-089-1304	Calcite, magnesium, syn	$(Mg_{0.03}Ca_{0.97})CO_3$	Yes (46)	12	Yes (54)	6	Yes (60)	7
01-089-1305	Calcite, magnesium, syn	$(Mg_{0.06}Ca_{0.94})CO_3$	Yes (43)	12	Yes (48)	8	Yes (65)	11
01-076-0606	Aragonite	$CaCO_3$	Yes (51)	17	Yes (28)	14	Yes (59)	15
01-086-0174	Calcite	$CaCO_3$	No		Yes (42)	3	No	
00-044-1482	Brucite	$Mg(OH)_2$	No		Yes (50)	8	Yes (62)	9
01-072-1668	Halite	$NaCl$	Yes (51)	25	Yes (49)	3	Yes (66)	21
01-083-1923	Monohydrocalcite	$CaCO_3 \cdot H_2O$	Yes (41)	23	Yes (20)	6	Yes (35)	10
Sample			M8		M9		M10	
Ref. Code	Mineral Name	Chemical Formula	Contained within precipitates? (Score)	SemiQuant (%)	Contained within precipitates? (Score)	SemiQuant (%)	Contained within precipitates? (Score)	SemiQuant (%)
01-071-1663	Calcite, magnesian	$(Mg_{0.1}Ca_{0.9})CO_3$	Yes (28)	3	No		Yes (54)	4
01-073-1403	Huntite	$Mg_3Ca(CO_3)_4$	Yes (41)	10	Yes (33)	13	Yes (47)	13
01-083-1766	Dolomite	$MgCa(CO_3)_2$	Yes (39)	5	Yes (33)	4	Yes (56)	8
01-086-2335	Calcite, magnesian	$(Mg_{0.064}Ca_{0.936})CO_3$	Yes (38)	4	No		Yes (52)	4
01-086-2336	Calcite, magnesian	$(Mg_{0.129}Ca_{0.871})CO_3$	Yes (39)	3	No		Yes (44)	3
01-089-1304	Calcite, magnesium, syn	$(Mg_{0.03}Ca_{0.97})CO_3$	Yes (35)	4	No		Yes (51)	4
01-089-1305	Calcite, magnesium, syn	$(Mg_{0.06}Ca_{0.94})CO_3$	Yes (32)	3	No		Yes (61)	4
01-076-0606	Aragonite	$CaCO_3$	Yes (74)	42	Yes (71)	35	Yes (74)	36
01-086-0174	Calcite	$CaCO_3$	No		No		No	
00-044-1482	Brucite	$Mg(OH)_2$	Yes (45)	13	No		No	
01-072-1668	Halite	$NaCl$	Yes (43)	2	Yes (52)	34	Yes (53)	9
01-083-1923	Monohydrocalcite	$CaCO_3 \cdot H_2O$	Yes (36)	11	Yes (31)	14	Yes (45)	15

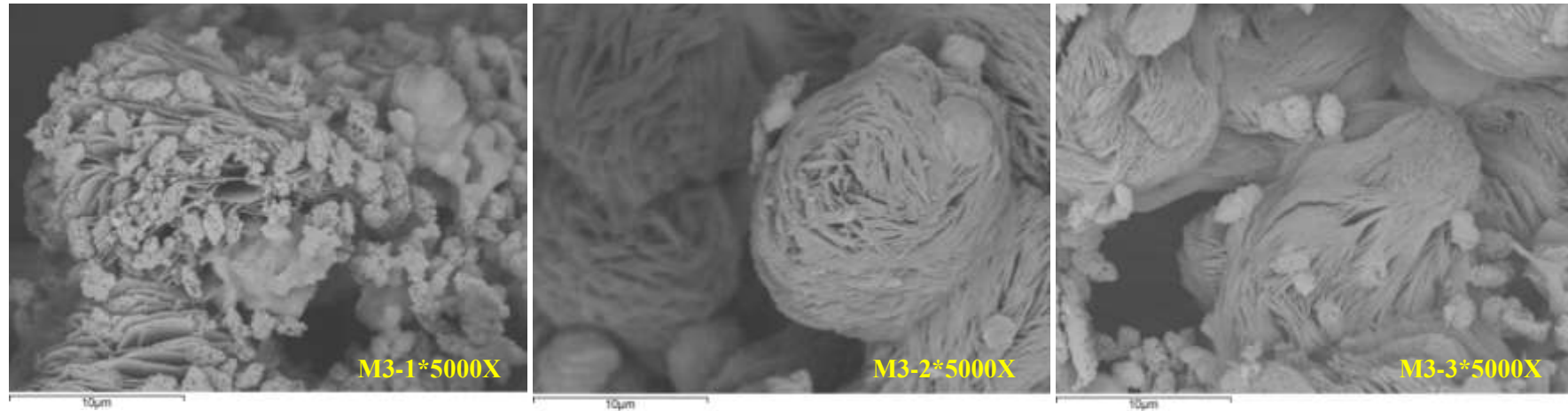
(c): The matching scores and semiquants of M5-10 precipitates, calculated by software X'Per HighScore Plus

Figure 5. 10: The XRD patterns for M1-10 (a), and the matching scores and semiquants of M1-10 precipitates, calculated by software X'Per HighScore Plus (b-c). All samples are for SIV shown in Table 5.1

5.2.3.3 Precipitates Microstructure Studies

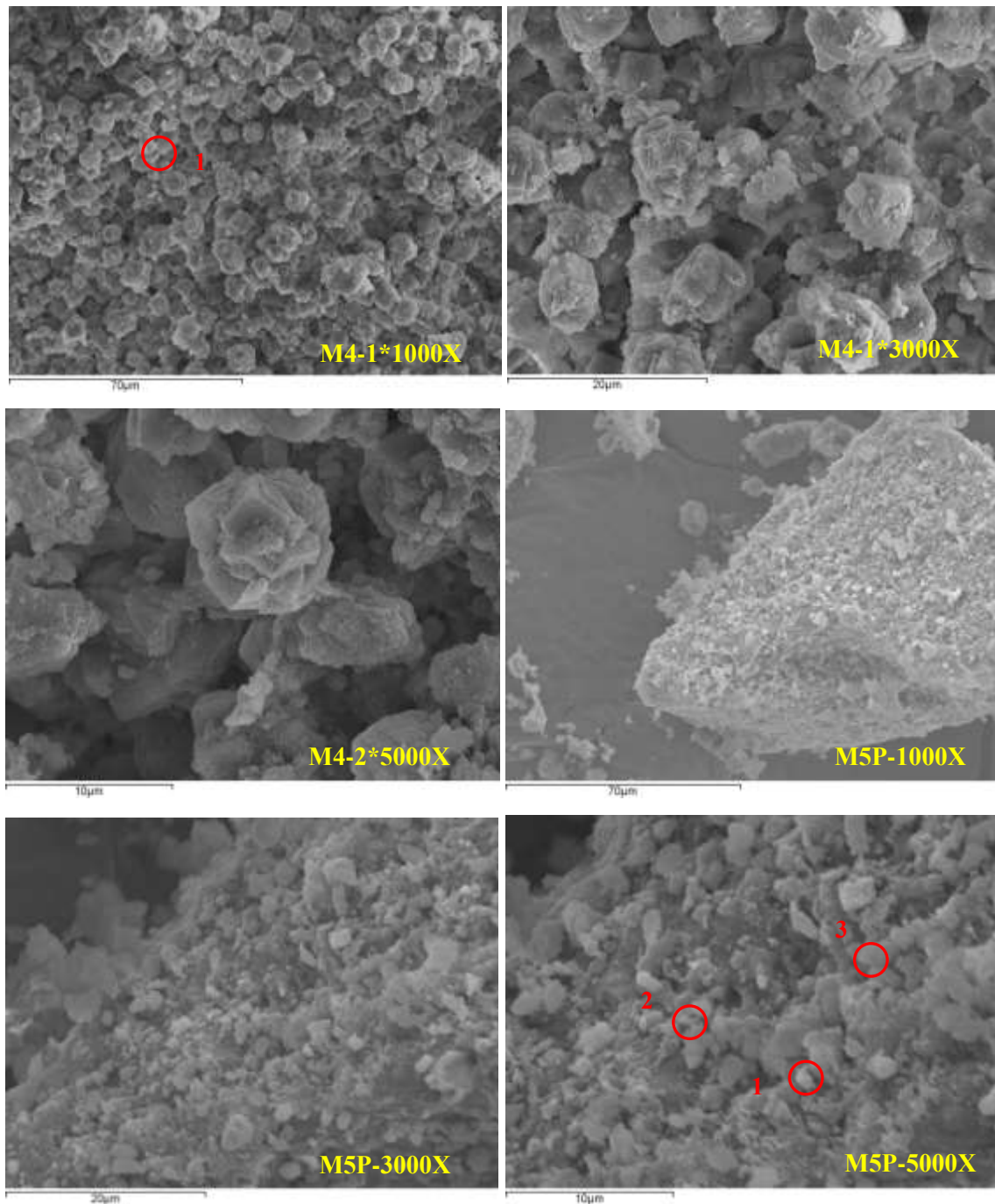






Sample	Spectrum	C	O	Na	Mg	Cl	Ca	Ca ²⁺ :Mg ²⁺
M3-1*3000X	Spectrum 1	19.87	62.57	1.43	9.48	0.26	6.4	0.68
	Spectrum 2	15.33	65.83	1.41	7.46	0.36	9.62	1.29
M3-2*3000X	Spectrum 1	23.23	60.67	1.72	1.46	0.18	12.75	8.73
	Spectrum 2	13.5	69.47	1.85	14.72	0.19	0.26	0.02
M3-3*3000X	Spectrum 1	9.3	69.8	Not tested	20.09	0.31	0.5	0.02

Sample	Spectrum	C	O	Mg	Ca	Ca ²⁺ : Mg ²⁺
M1-2*3000X	Spectrum 1	26.23	49.39	0.92	23.46	25.5
M2-2*3000X	Spectrum 1	9.28	33.58	1.25	55.88	44.70
	Spectrum 2	23.83	49.9	13.03	13.24	1.02



Sample	Spectrum	C	O	Mg	Ca	Ca ²⁺ : Mg ²⁺
M4-1*3000X	Spectrum 1	21.31	52.75	2.28	23.67	10.38

Sample	Spectrum	C	O	Na	Mg	Cl	Ca	Ca ²⁺ : Mg ²⁺
M5P-3000X	Spectrum 1	18.37	52.59	7.28	10.71	6.32	4.73	0.44
	Spectrum 2	20.53	55.28	3.5	11.35	3.76	5.59	0.49
	Spectrum 3	10.27	58.66	5.45	17.7	5.04	2.87	0.16

Figure 5. 11: The microstructure of M1-4 +powdered M5P and their correlated EDX results for SIV (e.g.M5P-3000x means crushed powder M5, 3000x magnification)

Typical particles were imaged by SEM-EDX to indicate and analyse the surface constitutions, where the EDX is expressed by the atomic percentage. However, this number is not used to determine the molecular formulae due to its inability to capture an image of a whole sample and cannot represent the entire sample. The calculated $\text{Ca}^{2+}:\text{Mg}^{2+}$ ratio is presented providing a visual numerical impression of the extent of a solution reaction.

Dominant calcium is observed in sample 1 of the EDX analysis. The morphology of spherulites is rounded and rhombic, mixed with partial elongation on several crystals, while sample 2 shows obvious spherical particles, similar to vaterite, where calcium is the major element (spectrum 1). Unlike circular morphology, tabular grain (M2-2*3000X, spectrum 2) displays dramatic Mg^{2+} sequestration, almost reaching the balance of $\text{Ca}^{2+}:\text{Mg}^{2+}=1:1$. This ratio ($\text{Ca}^{2+}:\text{Mg}^{2+}$) is around 26 in sample 1 (initial $\text{Ca}^{2+}:\text{Mg}^{2+}=5:1$), and increases to 45 in M2-2*3000x spectrum 1 (initial $\text{Ca}^{2+}:\text{Mg}^{2+}=2:1$), due to the addition of larger magnesium reactants resulting in nucleation differences. Based on Section 2.7.3, the classical Gibbs-Thomson nucleation formula is used in this analysis, where the nucleation rate J is the inverse function of the solid density v , from [Equations 2.36-2.38](#). All other parameters are considered as the intrinsic properties; only the solid density is a variable and depends on the designed experiment, which is calculated from the initial mass of reactants over volume. Hence sample 2 possesses a higher preliminary magnesium concentration leading to a larger solid density. A lower nucleation rate leads to less magnesium. Another explanation for the existence of magnesium is that it is due to the particles' coprecipitation throughout a structural embedding, meaning that magnesium grains possibly integrate into calcium carbonate lattices in sample 1, so a surface detector has a better chance of tracing magnesium. The opposite is true in sample 2 with its chemistry nucleation and reformation phenomenon, which reduce its magnesium detection on the surface area.

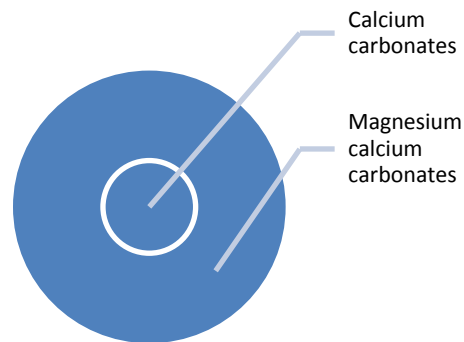
The variety of morphologies in sample 3 are flower-like, rosette-like or flat particulates corresponding to groups 1, 2 and 3 respectively. With the evaluation of all detected areas by EDX, it can be observed that particles are more similar to the magnesium carbonates in morphology and exhibit larger amounts of magnesium mixture in the precipitates, and vice versa. Likewise, the higher matching degree of calcium carbonates presents larger amounts of calcium. The typical shapes of HMCs are flower-like (HM, D), rosette-like (HM, D) and needle-like (N), while the calcium carbonates are spherical-like (V), cubic-like (C) and arrow-

like (A). Finally, the tabular morphology in M3-3*3000x is estimated by the bottom sample extraction from the reaction-vessel.

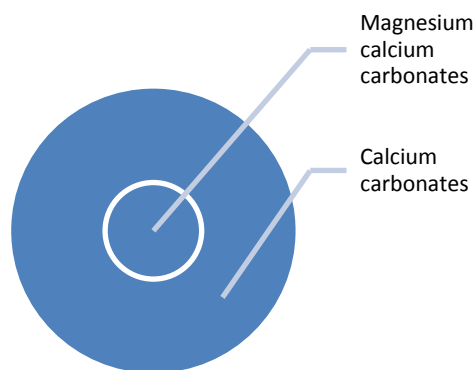
Sodium is still included as an impurity due to its good crystallised characteristic and the amounts of interstitial intersection within these particulates, despite the treble washing procedure conducted before testing. The remaining NaCl distorts the crystal lattices, enabling more magnesium cooperation within the products with the HMCs- like images according to Glover & Sippel (1967). Furthermore, sample 3, which was achieved at an elevated temperature (40°C), reflects more magnesium-like morphology generation and higher magnesium concentration detection, opposed to test 1, which was conducted at a room temperature. It is well known that a higher temperature enhances the reaction rate at pH=10.5. Therefore the evaluation is concluded when calcium reacts with aqueous carbonates faster than magnesium, while the latter gradually precipitates into the deposits afterwards, according to EDX result from samples 1 and 3. A similar phenomenon is also visible in this group of temperature comparisons from samples 2 and 4, further proving this preliminary assumption. Another concern is from initial concentration, demonstrating that the larger amounts of magnesium added led to the appearance of more rounded uniform shapes. Morphology tends to be more similar to the cubic or rounded spherulite of calcium carbonates, from the quantitative analysis of EDX. This result is similar to samples 1 and 2. Additionally, samples 3 and 4 show that a higher initial magnesium concentration reduces the nucleation rate by the increased $\text{Ca}^{2+}:\text{Mg}^{2+}$ value. This summary is also consistent with XRD examination in Section 5.2.3.2, where both samples 3 and 4 at the higher temperature have elevated matching scores and percentage compositions in magnesian calcite (including huntite and dolomite) compared to the samples 1 and 2 of the same products.

The most detailed precipitation mechanism is illustrated in sample 5 above sample 3 in this SIV dual-ion system. Finely ground particles were used to investigate calcium and magnesium carbonates' formation. As the most of 5 to 10 samples present similar spherical or cubic CaCO_3 -like morphology, crushed powder grains specifically for XRD measurement are incorporated to provide the information on potential internal components. Obvious differences can be observed from $\text{Ca}^{2+}:\text{Mg}^{2+}$ ratios, where M5P is smaller than 1, but the usual M5 is infinite. This value from EDX illustrates that magnesium is more concentrated in ordinary M5 than M5P. It further demonstrates that magnesium calcium carbonates form

an internal core at first with the subsequent buildup of calcium carbonates around the core. This phenomenon was also noticed by Raz et al. (2000) (Chapter 2), as well as in the sample 5 particle tests below, where the calcium exhibits significant dominance on the surface area displayed by SEM-EDX. The estimated stage reaction graph is presented below (Figure 5. 12b).



(a): Carbonation stages concluded from SI-(M1-M4)



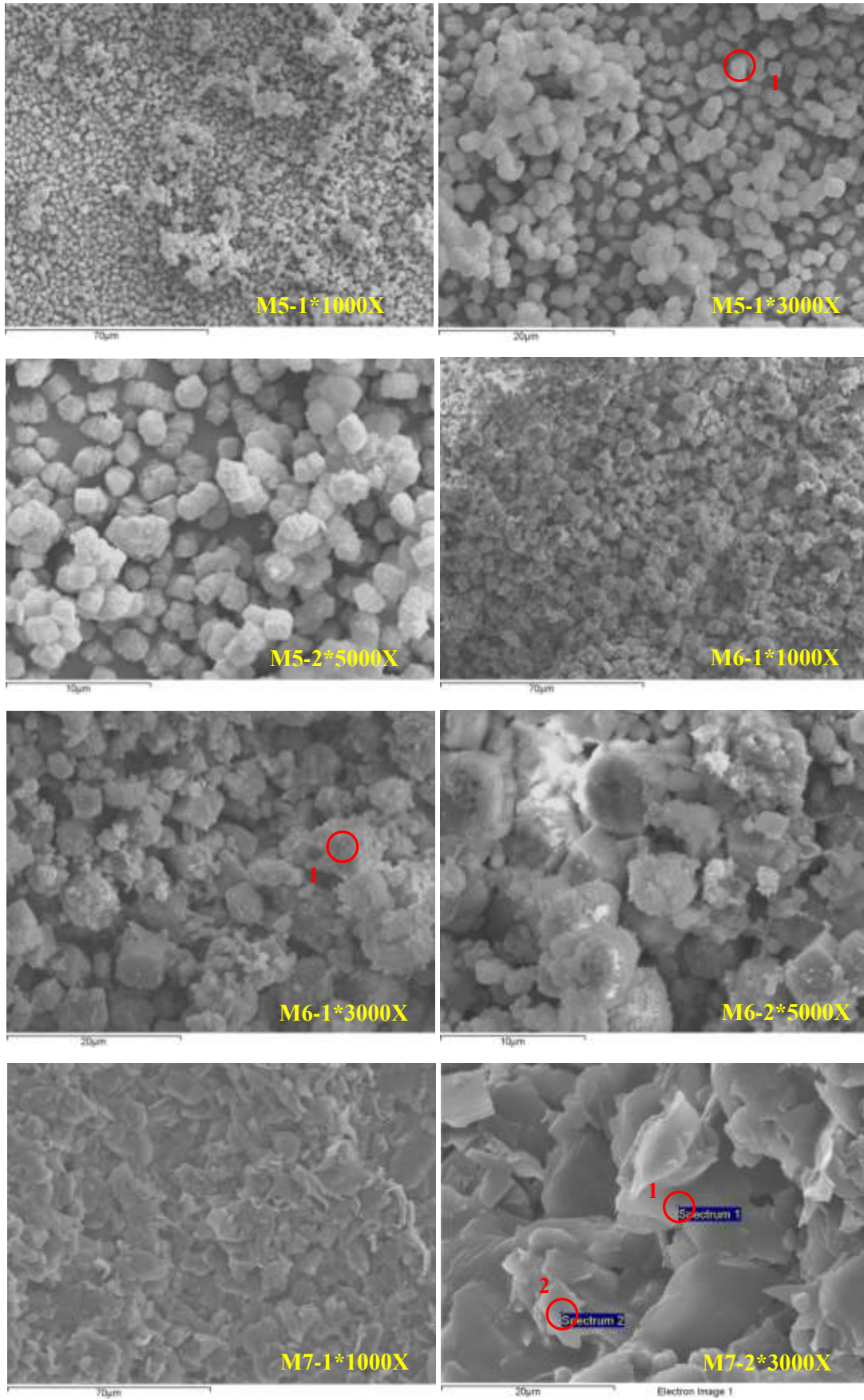
(b): Carbonation stages concluded from SI-M5

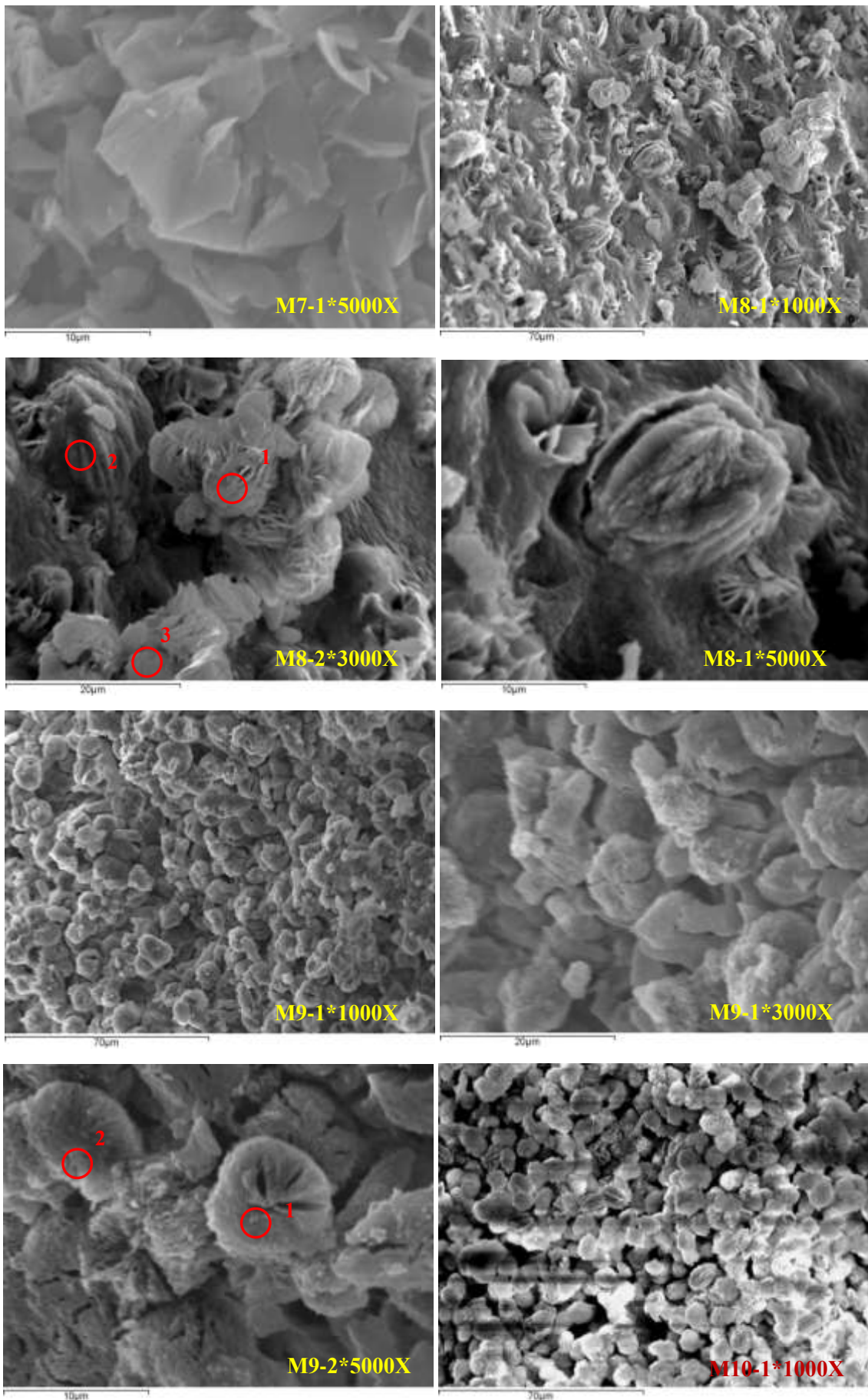
Figure 5. 12: Carbonation stages in samples M1-M4 (a), and M5 (b)

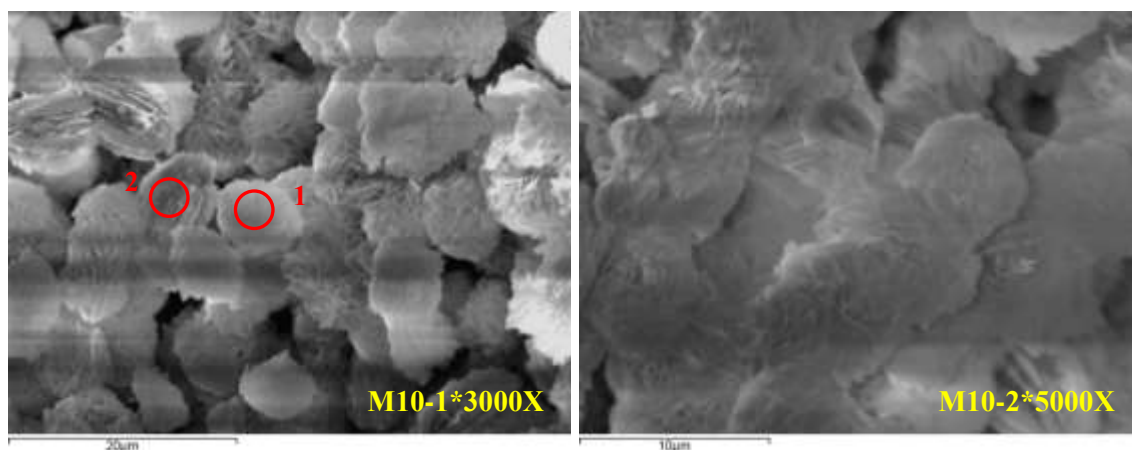
In the ordinary uncrushed sample 5, cubic shapes similar to calcium carbonates are shown from EDX. Particularly in spectrum M5-1*3000x, no magnesium was detected due to its limited amount. The formation stages proved a difference in the hydrophilic and carbonophilic properties of magnesium and calcium, observed in this EDX table, the XRD powered pictures above and the samples 1-4. Tests 5 and 1 are used to compare the initial concentration, which is directly related to the supersaturation degree. Trial 5 has the larger magnesium association from the initial stage, but less magnesium appearance on the surface area of the precipitates according to EDX. This is caused by the higher

supersaturation degree, which has a negative effect on the nucleation rate and further delays the magnesian calcite crystallisation process.

It is known that a higher temperature can accelerate the reaction rate, as more magnesium appears on the reacted surface of sample 6 compared to 5 (**Figure 5. 13**). This is validated by the reduced ratio of $\text{Ca}^{2+}:\text{Mg}^{2+}$ in 5.2.3.2. In addition, this increased condition of temperature also results in less uniform particles than 5, shown in all tests of this study. In sample 7, no magnesium was detected on the surface area by EDX, verifying that the reaction efficiency was significantly decreased without agitation. Comparing to the substance of 5, sample 7 presents more aggregated particles, showing its reversed influence on the crystallisation without stirring. As a result, the precipitates are unlikely to be formed into large independent crystals as sample 5. Moreover, both samples 5 and 7 have magnesian calcite, proving that the crushed particulates used for XRD analysis release more enclosed elements, which is different from the normal generated precipitates. Oval-like as well as flat-rosette-like spherulites appear in sample 8, considering the oval morphology is transformed from the rounded CaCO_3 -like crystals, hence more calcium is measured. This demonstrates that the faster nucleation completion leaves a longer retention time for phase alteration into more magnesium particles, in contrast with 5. A similar explanation also applies to sample 9, with lower pH level reducing the supersaturation degree. It shows triggered tabular, irregular shapes, and rounded spherulites with a good magnesium concentration of less variance on $\text{Ca}^{2+}:\text{Mg}^{2+}$ proportions compared to 5-8. Heating accelerates the magnesium coprecipitation within sample 10, where almost all particles have rounded morphology with a prominent precursor rosette-form. Bright images indicate not sufficient sample coating, resulting in an inability to trace the radioactive reflection from machine.







Sample	Spectrum	C	O	Mg	Ca	Ca ²⁺ :Mg ²⁺
M5-1*3000X	Spectrum 1	23.68	52.57	Not tested	23.74	∞
M6-1*3000X	Spectrum 1	22.04	53.1	4.33	20.53	4.74
M7-2*3000X	Spectrum 1	87.72	11.02	Not tested	1.27	∞
	Spectrum 2	86.78	10.62	Not tested	2.6	∞

Sample	Spectrum	C	O	Na	Mg	Cl	Ca	Ca ²⁺ :Mg ²⁺
M8-2*3000X	Spectrum 1	10.68	62.68	1.34	22.12	2.01	1.17	0.05
	Spectrum 2	6.83	56.88	2.75	3.83	3.92	25.79	6.73
	Spectrum 3	12.91	61.78	0.83	20.19	2.16	2.13	0.11
M9-2*5000X	Spectrum 1	11.63	60.24	1.48	23.38	2.14	1.13	0.05
	Spectrum 2	10.04	57.81	1.66	26.93	3	0.56	0.02
M10-1*3000X	Spectrum 1	10.34	63.01	1.35	23.08	1.56	0.66	0.03
	Spectrum 2	10.57	66.87	0.84	14.82	0.71	6.19	0.42

Figure 5. 13: The microstructure of M5-10 and their correlated EDX results

In summary, all samples point towards one transformation conclusion in this MgCl₂-CaCl₂ system: magnesian calcites form as an inner core at first, followed by calcium carbonate surroundings, and the subsequent participation of the magnesium as an exterior surface. The morphology during this transformation can be summarised as follows: an elongated magnesian calcite appears during the first stage, while in the second stage rounded or rhombic calcite shapes are formed, and then finally flat or rounded rosette-like particles are generated. The shape of crystals can also be considered with respect to growth kinetics that the fastest growing sides disappear to leave behind the slower growing crystal as a facet of the samples. A lower supersaturation degree (a lower pH, a lower CO₂ flux rate) accelerates the process moving towards more magnesium sequestered specimens within 1.5h, while higher temperatures can enhance the reaction by speeding up the process. Additionally, stirring speed causes reversed particle crystallisation. Generally, by washing the particles

three times, a high purity level can be ensured with less NaCl contamination in the EDX results.

5.2.3.4 Reaction Kinetics Studies

According to Chapter 4, 1h was usually sufficient for both individual calcium and magnesium sequestration; however considering the common-ion effect, 1.5 h was used in all multiple ions system. Alongside ICP direct sequestration efficiency, calculated from the remained aqueous metal concentration, the experiments on selected samples one day kinetics morphology and XRD analysis were also analysed to provide a better knowledge of the sediments over time.

Table 5. 5: Ca, Mg sequestration after 1.5h

Sample (Mixture)	Ca ²⁺ concen (M)	Mg ²⁺ concen (M)	Ca Seque% (1.5h)	Mg Seque% (1.5h)	Ca ²⁺ :Mg ²⁺ (seque%:seque%)	Net Weight (g)
1	0.5	0.1	88.39	96.71	0.914	7.46
2	0.5	0.25	89.05	98.71	0.902	9.34
3	0.5	0.1	99.84	99.34	1.005	10.61
4	0.5	0.25	99.96	99.67	1.003	12.54
5	0.1	0.5	98.91	98.71	1.002	11.4
6	0.1	0.5	99.94	99.96	1.000	8.64
7	0.1	0.5	97.84	98.13	0.997	10.14
8	0.1	0.5	99.82	99.54	1.003	10.61
9	0.1	0.5	98.75	95.41	1.035	10.66
10	0.1	0.5	99.92	99.79	1.001	10.37

The table above illustrates the sequestration results on independent calcium and magnesium elements. Samples 1 to 6 aim to deliver the information to identify the different mixture ratios on both Ca²⁺ and Mg²⁺ ions, while samples 5 to 10 are for the various parameters' investigation and optimisation initiated by the original sea water constitution. Clearly, the majority of the metals are trapped after 1.5h with more than 90% transforming into other products. The ratios of Ca²⁺:Mg²⁺ in this set aim to show the tendency of capture efficiency. It appears that both elements' adsorptions are correlated in a line and ranges from 0.90-1.04. It can be seen that that higher magnesium sequestration is always accompanied by a larger percentage of calcium sequestration, showing a positive correlation.

In addition, based on the [Equation 5.1](#) in 5.2.2.2, the ideal calculated data and practical samples after 1.5h are summarised in [Figure 5. 14](#) with their comparisons below (where AW=Actual Weight, TCC=Theoretical calculated Calcium Carbonates, TN=Theoretical calculated N, THM=Theoretical calculated HM, TD=Theoretical calculated D).

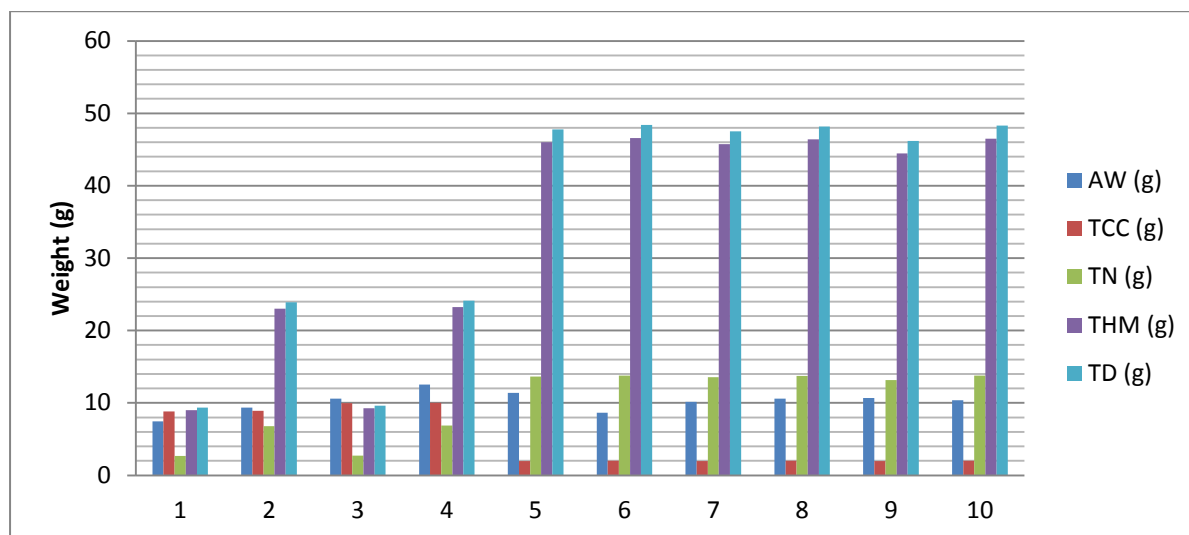
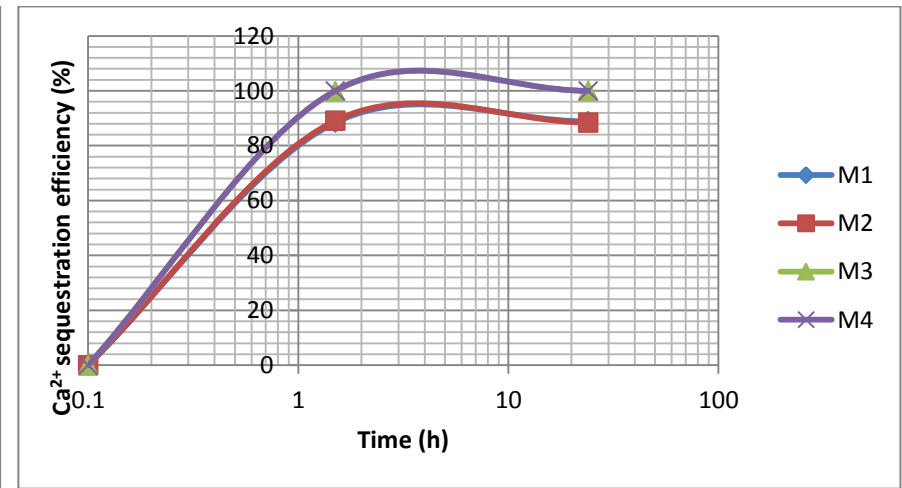
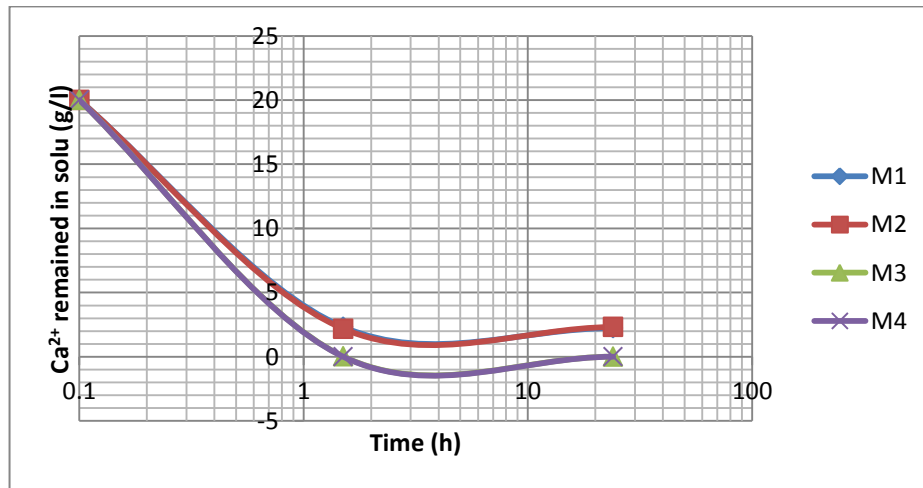
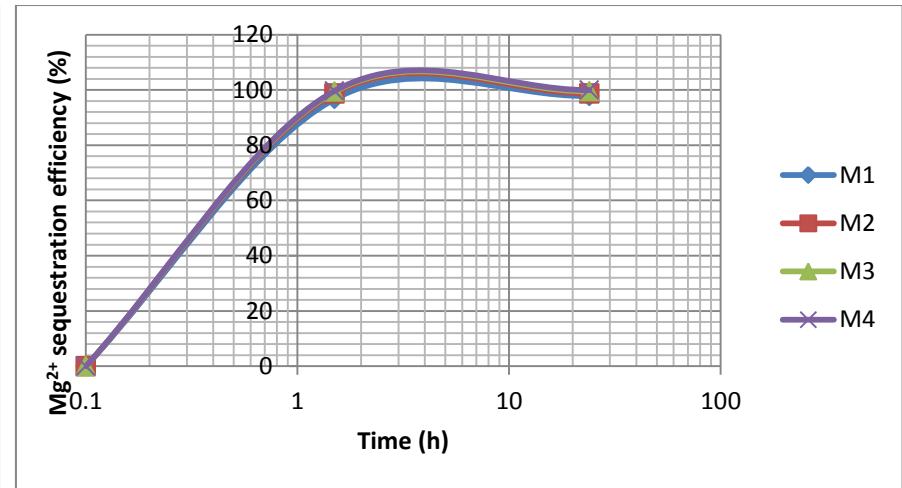
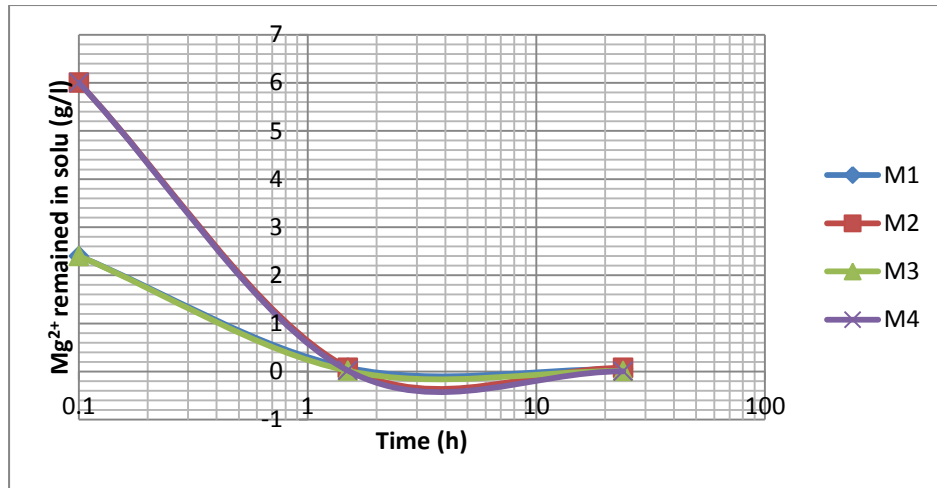


Figure 5. 14: The theoretical and practical weights of potential precipitates

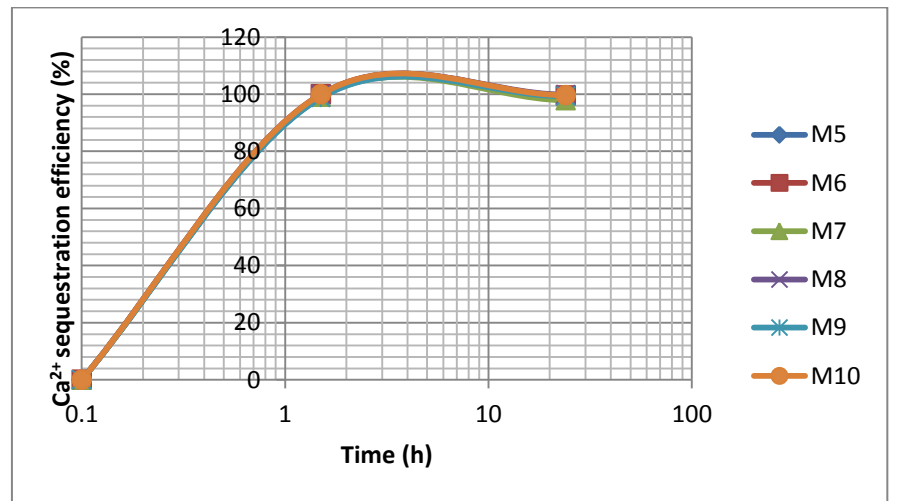
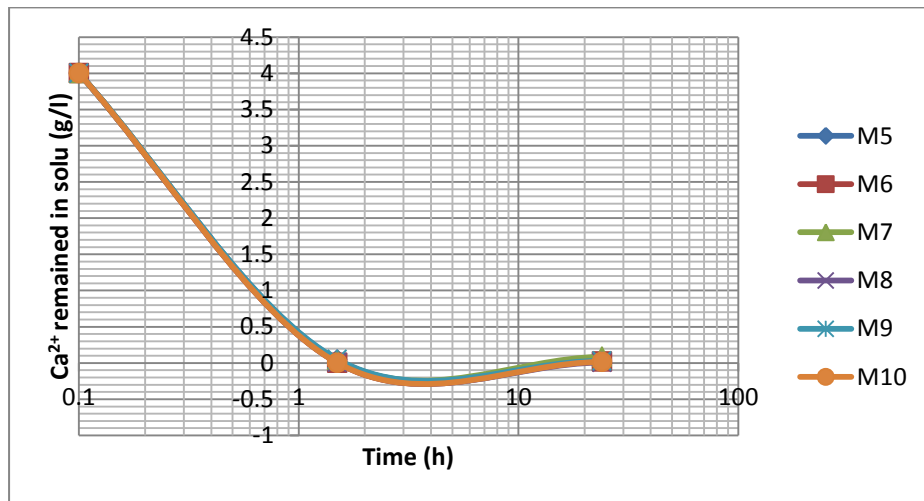
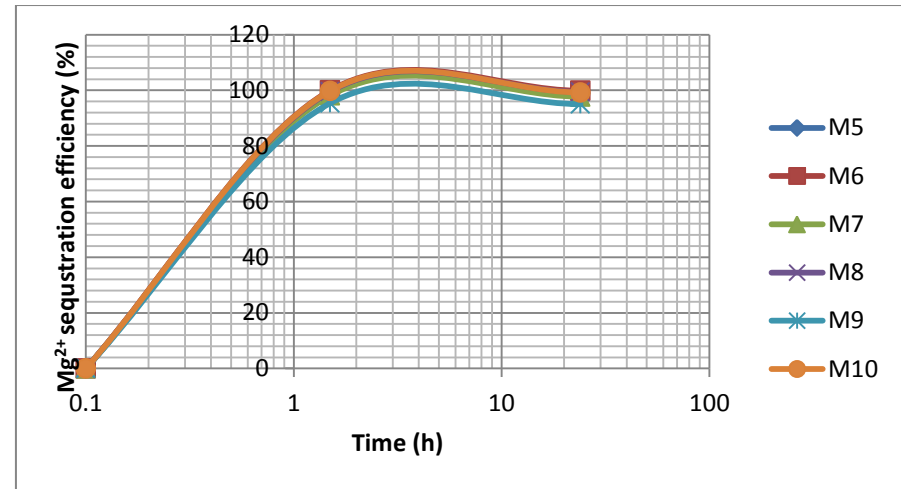
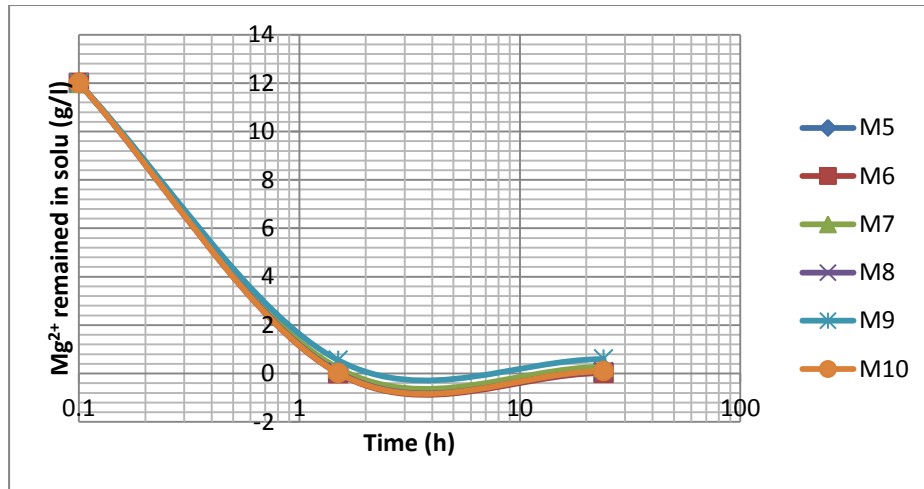
In this experiment, EDX was used to deliver an initial composition of the prospective precipitates. For example, the weight of sample 1 is 7.456g, which is between the range of nesquehonite and other ideal potential deposits, validating the accuracy of this obtained weight. All the produced sediments stay within the acceptable range based on this hypothetical assumption. However, in samples 5 to 10, the results do not correlate with the weights in the HMCs series, although more magnesium is added from the first stage. In contrast, samples 1 to 4 with more calcium participation present fewer different percentages than the theoretical assumption. Operational errors also need to be considered during the transfer stage. Usually higher metal capture produces heavier precipitates, but this is not the same in samples 5 and 6. One reason is the incomplete sample drying; the other is the surface attachment or lattice incorporation prior to actual crystallisation, leading to falsely high sequestration figures.

Samples 6, 8 and 10 have better performed better, but are observed by SEM to be less uniform due to larger amounts of impurities, and the metals' crystallisation of particulates after sequestration. Test 5 was designed as a standard reference, and other samples varied from it. A higher pH has the advantage of capturing larger magnesium ions due to the

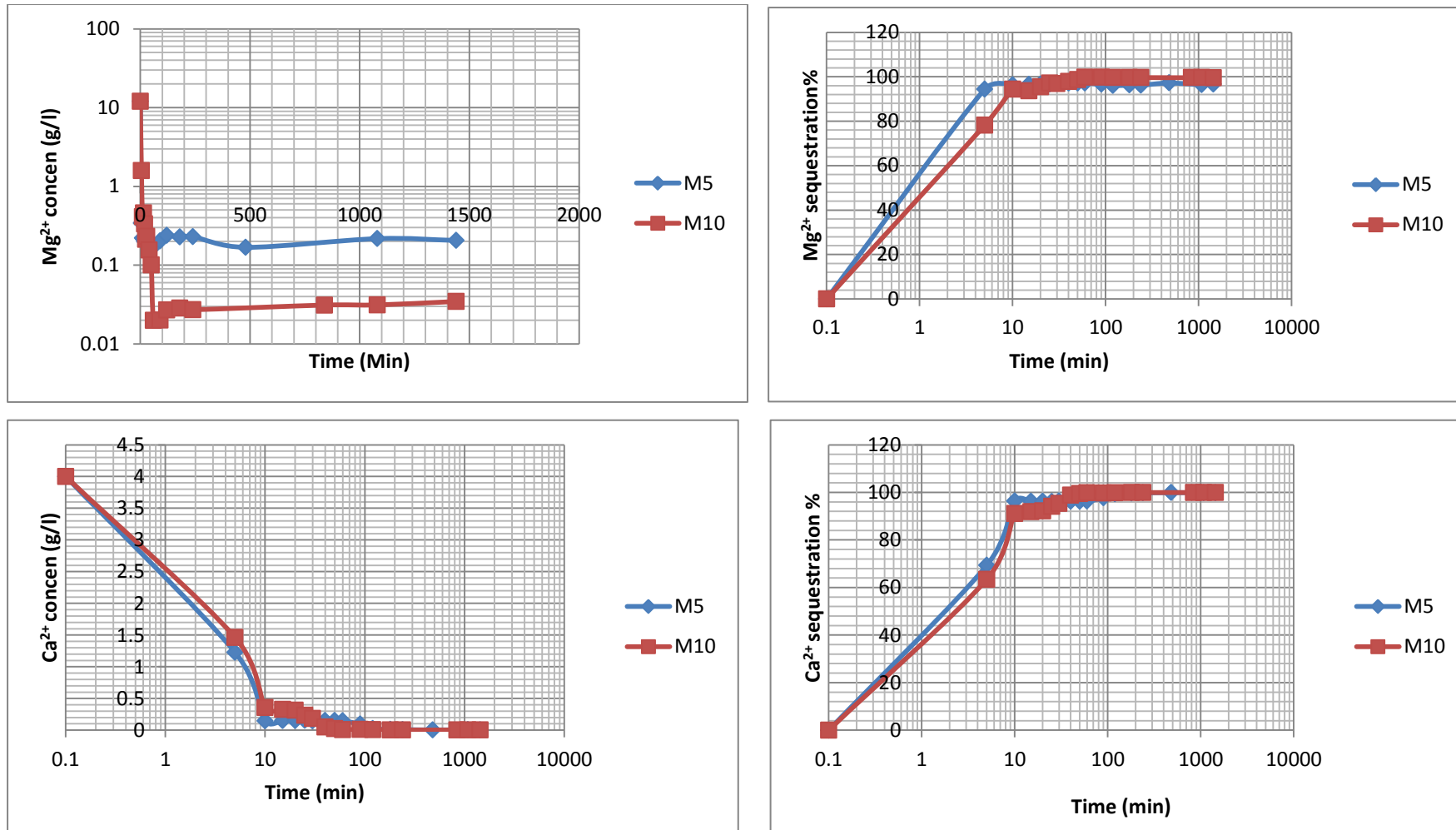
formation of more carbonate ions within the aqueous phase in samples 5 pH=10.5 and 9 pH=10. Sample 5 and sample 9 corresponds to magnesium sequestration of 98.71% and 95.41% and calcium sequestration of 98.91% and 98.75% respectively. In comparison to sample 5, sample 7 (no stirring speed) depicts slightly lower magnesium sequestration. It can be estimated that stirring speed only improves chemical reactions slightly, validating that it is an indeterminate factor among the various relevant parameters. Another control of pH is CO₂ diffusion. Tests 5 and 8 display this pH effect to some extent, since the addition of more CO₂ addition causes an acid environment, leading to less magnesium sequestration (sample 5). Although a lower amount of carbon addition has the benefit on trapping magnesium, 500 cm³/min flux rate is more controllable and operational. Therefore 5 in general is an optimum set from both practical perspective and overall performance. The last comparison is about the temperature (samples 5 and 6). It is well recognised that a higher temperature has a positive effect on the reaction improvement because of more hydroxide ions involvement with elevated heat at the same pH figure. Inevitably, both magnesium and calcium have the larger concentration in sample 6; however considering energy inefficiency during the operation, process 6 is not recommended.



(a): M1-4 remained Mg²⁺ vs time (top left); M1-4 Mg²⁺ sequestered efficiency vs time (top right); M1-4 Ca²⁺ remained vs time (bottom left); M1-4 Ca²⁺ sequestered efficiency vs time (bottom right)

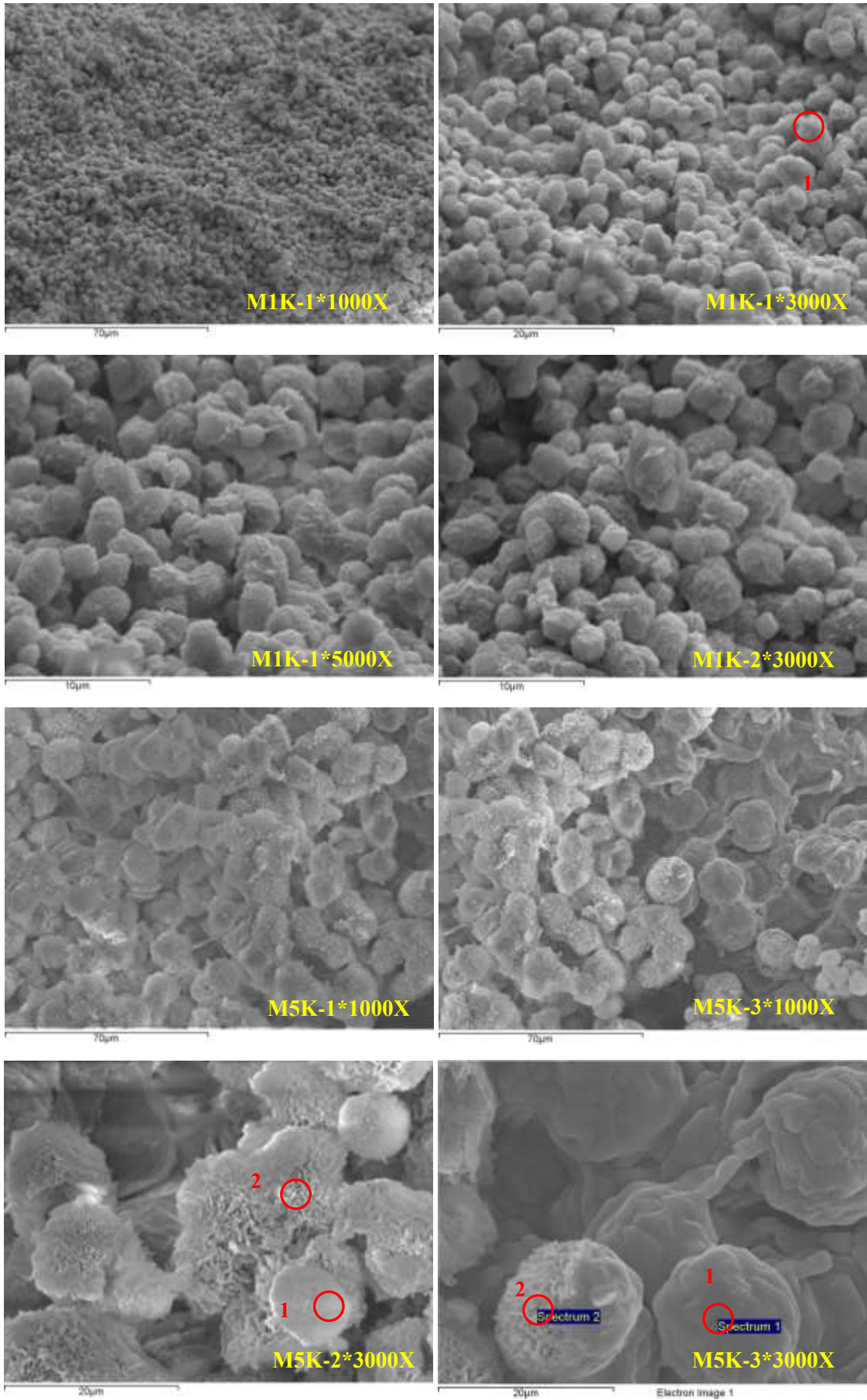


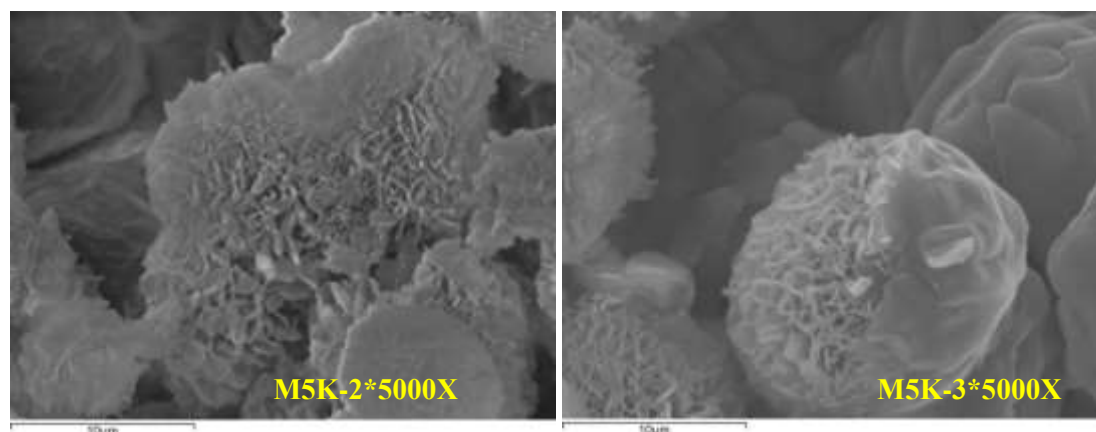
(b): M5-10 Mg²⁺ remained vs time (top left); M5-10 Mg²⁺ sequestrated efficiency vs time (top right); M5-10 Ca²⁺ remained vs time (bottom left); M5-10 Ca²⁺ sequestrated efficiency vs time (bottom right)



(c): M5&10 Mg^{2+} kinetics study over a day (top left); M5&10 Mg^{2+} sequestration% over a day (top right); M5&10 Ca^{2+} kinetics study over a day (bottom left); M5&10 Ca^{2+} sequestration% over a day (bottom right)

Figure 5. 15: M1-10 magnesium and calcium sequestration efficiency, and the selected samples M5&10 one day kinetics studies





Sample	Spectrum	C	O	Mg	Ca	Ca ²⁺ :Mg ²⁺
M1K-1*3000X	Spectrum 1	15.52	57.88	1.16	25.43	21.92

Sample	Spectrum	C	O	Na	Mg	Cl	Ca
M5K-2*3000X	Spectrum 1	11.63	57.98	1.96	26.18	2.24	Not tested
	Spectrum 2	8.96	59.98	1.95	26.69	2.42	Not tested
M5K-3*3000X	Spectrum 1	21.35	10.54	20.81	4.84	42.45	Not tested
	Spectrum 2	13.94	59.62	2.11	21.94	2.39	Not tested

Figure 5. 16: The microstructure of M1&5 one day kinetic studies and their corresponded EDX results

Figure 5.15 depicts a one day reaction, proving that 1.5 hours and one day are reasonable, practical and sufficient collection points in terms of completing the necessary chemical reaction for the experiments in the research. However, different from initial estimation, one day results usually present less capture efficiency corresponding to more ions remained within the solution, explained by Ostwald's Rule. It is possible that nuclei left after 1.5 hours dissolve into the solution and thus have the ability to deposit later into larger particles. Moreover, samples 5 and 10 were randomly selected to do the experiment of the one-day kinetics analysis. In calcium sequestration, two samples have no apparent differences, but magnesium has larger sequestration efficiency in a higher temperature condition. It shows that calcium has a relative good sequestration internally but magnesium requires external assistance to enhance the capture level. Within the 10min reactants' addition time, large amounts of elements are formed into precipitates.

SEM images on one day precipitates were taken and used to make the comparisons of ordinary products through the selected samples 1 and 5 (Figure 5.16), representing Mg^{2+} : Ca^{2+} equivalent to 1:5 and 5:1 respectively. In a short-term (1.5h reaction), no significant distinctions are observed between them, and both are abundant in calcium precipitates rather than magnesium. Sample 1 presents more rounded shapes with small amounts of enclosed Mg^{2+} , while sample 5 is cubic shapes without any Mg^{2+} detection. Over a relatively long period, M1 one day sample displays generally higher calcium concentration, due to its noticeably larger proportions of initial reactants. This difference can be negligible as M1K (Ca^{2+} : $Mg^{2+} \approx 22$) is close to M1 (Ca^{2+} : $Mg^{2+} \approx 26$). M5 one day precipitates have a much higher magnesium accumulation, indicating a phase transformation procedure-- magnesium calcite core forms at first, followed by a calcium carbonate coat, until further magnesium accumulated as an exterior cover. This explains the phenomenon of more magnesium carbonate rosette-like morphology appearance in M5K, proving that reaction degree can be affected by either temperature or duration time, after comparing Ca^{2+} : Mg^{2+} ratios in this and the previous sections. It is concluded that over time, the particles' formation has the tendency to aggregate into a precipitate with the same element participation as the initial surplus reactants, either magnesium or calcium (Figure 5. 18).

It is then easy to assume the particulate reaction mechanism after analysing Sections 5.2.3.3 & 5.2.3.4. In particular, M5-10 inner two layers formation was also proved by Raz et al. (2000) (Chapter 2.10). Magnesium carbonate XRD precipitate analyse show that, in one day sediments, there is not an obvious alteration of M1K as its small amounts of magnesium takes longer to form into final products. More visibly, M5K presents relatively prominent phase transformation after one day, accompanied by the increased magnesian calcite crystallised peaks from XRD demonstration (Figure 5.17). The results of M5K and M1K match well with the SEM-EDX outcome and the primary research questions. It is worth noting that M5K only has aragonite, but not MHC, because of its phase transformation into aragonite over time in a magnesium solution. Aragonite is more stable than calcite when magnesium exists, as proved by Morse et al. (2007) and several other authors in Chapter 2.

Sample			M1K		M5K	
Ref. Code	Mineral Name	Chemical Formula	Score	SemiQuant (%)	Score	SemiQuant (%) (percentages without HMCs addition)
01-071-1663	Calcite, magnesian	(Mg _{0.1} Ca _{0.9})CO ₃	52	10	34	--(3)
01-073-1403	Huntite	Mg ₃ Ca(CO ₃) ₄	22	--	50	--(13)
01-083-1766	Dolomite	MgCa(CO ₃) ₂	21	--	50	--(9)
01-086-2335	Calcite, magnesian	(Mg _{0.064} Ca _{0.936})CO ₃	68	30	43	--(3)
01-086-2336	Calcite, magnesian	(Mg _{0.129} Ca _{0.871})CO ₃	42	10	45	--(3)
01-089-1304	Calcite, magnesium, syn	(Mg _{0.03} Ca _{0.97})CO ₃	61	14	40	--(3)
01-089-1305	Calcite, magnesium, syn	(Mg _{0.06} Ca _{0.94})CO ₃	68	29	49	--(3)
01-072-1652	Calcite	CaCO ₃	66	6		
01-074-2220	Brucite	Mg(OH) ₂	32	--		
01-076-0606	Aragonite	CaCO ₃			71	--(23)
01-086-0174	Calcite	CaCO ₃			36	--(4)
00-044-1482	Brucite	Mg(OH) ₂			36	--(5)
01-072-1668	Halite	NaCl			64	--(24)
01-083-1923	Monohydrocalcite	CaCO ₃ •H ₂ O			44	--(12)
00-003-0093	Hydromagnesite	4MgCO ₃ •Mg(OH) ₂ •4H ₂ O			72	--
00-023-1218	Dypingite	4MgCO ₃ •Mg(OH) ₂ •5H ₂ O			65	--
00-001-0130	Nesquehonite	MgCO ₃ •3H ₂ O			35	

Sample			M1K		M5K	
Ref. Code	Mineral Name	Chemical Formula	Contained within precipitates? (Score)	SemiQuant (%)	Contained within precipitates? (Score)	SemiQuant (%) (percentages without HMCs addition)
01-071-1663	Calcite, magnesian	(Mg _{0.1} Ca _{0.9})CO ₃	Yes (52)	11	Yes (34)	--(4)
01-073-1403	Huntite	Mg ₃ Ca(CO ₃) ₄	No		Yes (50)	--(15)
01-083-1766	Dolomite	MgCa(CO ₃) ₂	No		Yes (50)	--(11)
01-086-2335	Calcite, magnesian	(Mg _{0.064} Ca _{0.936})CO ₃	Yes (68)	30	Yes (43)	--(3)
01-086-2336	Calcite, magnesian	(Mg _{0.129} Ca _{0.871})CO ₃	Yes (42)	10	Yes (45)	--(3)
01-089-1304	Calcite, magnesium, syn	(Mg _{0.03} Ca _{0.97})CO ₃	Yes (61)	15	Yes (40)	--(4)
01-089-1305	Calcite, magnesium, syn	(Mg _{0.06} Ca _{0.94})CO ₃	Yes (68)	29	Yes (49)	--(3)
01-072-1652	Calcite	CaCO ₃	Yes (66)	6		
01-074-2220	Brucite	Mg(OH) ₂	No			
01-076-0606	Aragonite	CaCO ₃			Yes (71)	--(27)
01-086-0174	Calcite	CaCO ₃			No	
00-044-1482	Brucite	Mg(OH) ₂			No	
01-072-1668	Halite	NaCl			Yes (64)	--(28)
01-083-1923	Monohydrocalcite	CaCO ₃ •H ₂ O			No	
00-003-0093	Hydromagnesite	4MgCO ₃ •Mg(OH) ₂ •4H ₂ O			Yes (72)	
00-023-1218	Dypingite	4MgCO ₃ •Mg(OH) ₂ •5H ₂ O			Yes (65)	
00-001-0130	Nesquehonite	MgCO ₃ •3H ₂ O			No	

(b): The matching scores and semiquants of M1K and M5K precipitates, calculated by software X'Per HighScore Plus

Figure 5. 17: M1 one day (M1K) and M5 one day (M5K) kinetics studies (a) and their corresponded matching scores (b) for SIV shown in Table 5.1

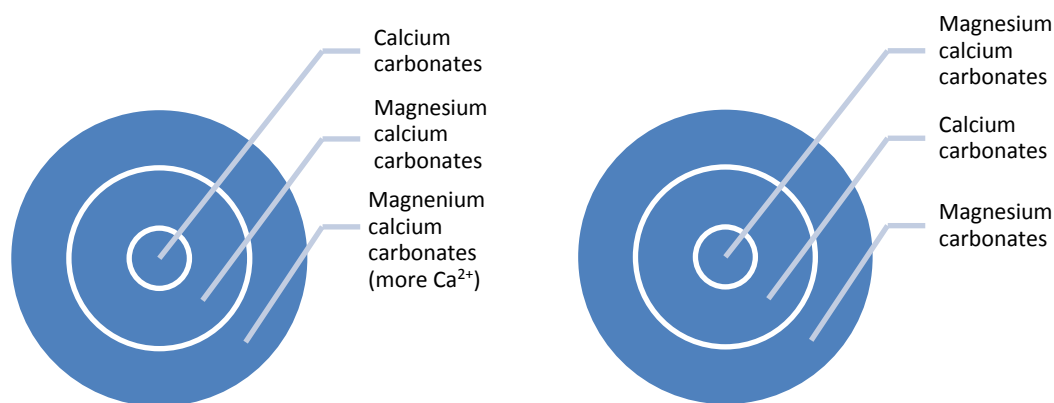
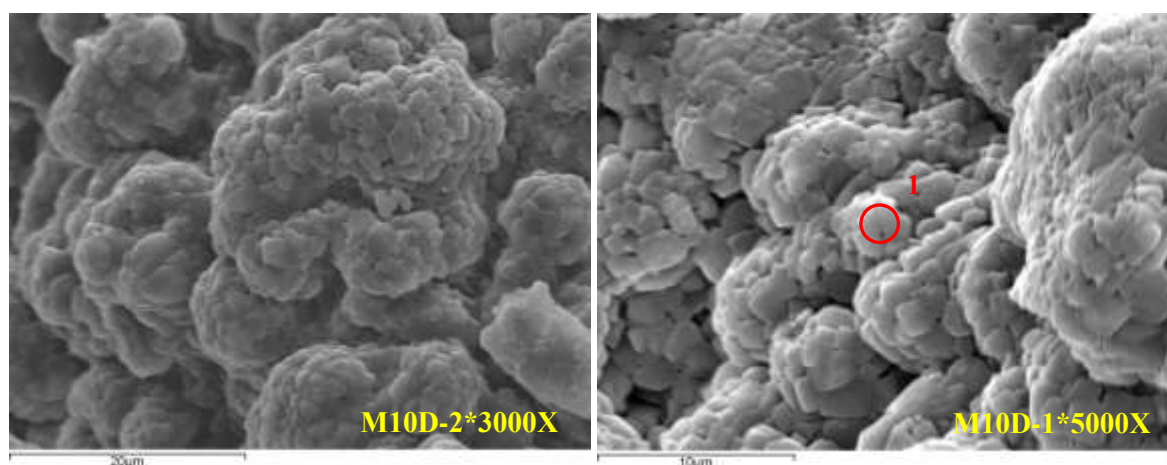


Figure 5. 18: Particles in system M1-4 (left) & M5-10 (right); first two layers (1.5h), outer layer (1d)

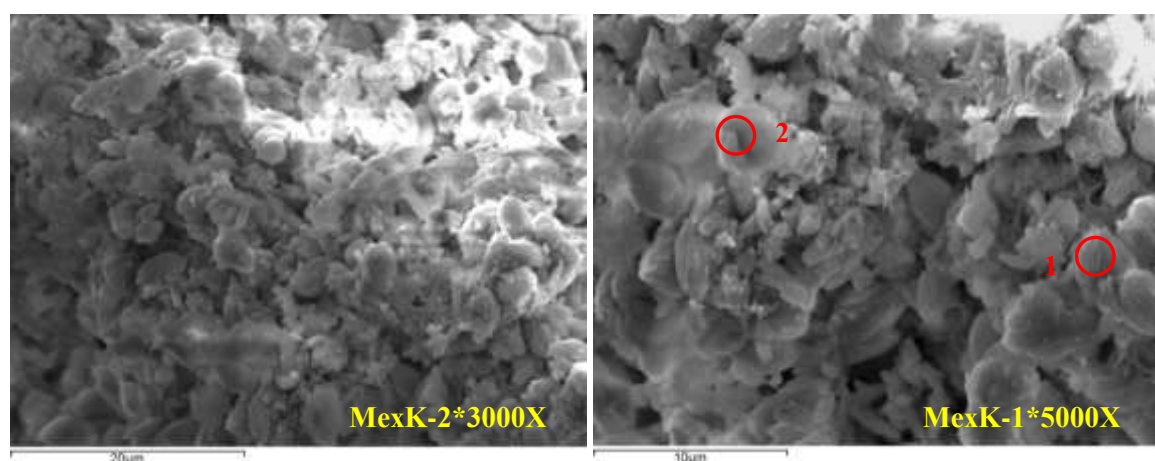
5.2.3.5 Miscellaneous Studies

Concerns were raised in this section with the insufficient washing times, causing further sodium coated precipitates. They are called 'defective products'. Mixture sample 10 with SEM-EDX analysis showed the high amounts of sodium impurities with fish-scale-like morphology. At the same time, there was no calcium element tested and only limited amount of magnesium was detected, which was attributed to the initial larger quantities of magnesium as well as its strong hydrophilic tendency, when NaCl was significantly dissolved in it. Additionally, this image (Figure 5.19, M10D-2*3000x and M10D-1*5000x) is also close to pure NaCl morphology, seen in Section 5.2.2.2. It is therefore a good guidance to identify the impurity presence though the naked eye.

In this study, the ratio of $Mg^{2+}:Ca^{2+}$ is 1:1, in order to study the equal ratio's effect, in addition to the previous studies of M1 ($Mg^{2+}:Ca^{2+}=1:5$) and M5 ($Mg^{2+}:Ca^{2+}=5:1$). These results agree with the preliminary assumption of circular shape possessing more calcium, while this 1 to 1 ratio MexK demonstrates oval-like morphology, which is different from the other two (Figure 5.19). Not only does the MexK picture (oval-like) lie between M1K (rounded and elongated) and M5K (rosette-like) one day graphs, but also the $Ca^{2+}:Mg^{2+}$ proportion ($\approx 3-11$) is within the range (M5K ≈ 0 --M1K ≈ 22).



Sample	Spectrum	C	O	Na	Mg	Cl
M10D-1*5000X	Spectrum 1	27.75	3.65	31.14	1.42	36.03



Sample	Spectrum	C	O	Na	Mg	Cl	Ca	Ca ²⁺ :Mg ²⁺
MexK-1*5000X	Spectrum 1	17.37	64.5	1.04	1.37	0.6	15.11	11.03
	Spectrum 2	15.47	67.1	0.49	3.83	0.55	12.55	3.28

Figure 5. 19: The microstructure of miscellaneous studies and their correlated EDX results

5.2.4 Series IV-Thermal Property and Calcination

Calcination analysis is a necessary step in this study, to complete the closed loop of carbon emission, as well as to produce the usable oxides for the construction industry. 800°C is the most utilised temperature that has been depicted in the first section, and the lighter-burned (650°C) as well as the harder-burned (1000°C) are then roughly equally distributed with the same intervals from the 800°C. However prior to the calcination investigation, a carbonates' thermal property study is undertaken, to understand the initial mechanism during the heating process.

5.2.4.1 The Analysis of Thermal Property

TGA was utilised to test thermal properties of mixed components. The samples are the combination MgCO_3 and CaCO_3 in various ratios, thus 4 steps integrated from earlier studies are broken down. Profile graphs (Figure 5.21) from M1-10 correspond to the theoretical evaluation and the referenced literatures.

In this series, the first two steps when temperatures are lower than 300°C , water molecular loss is measured, while the temperatures above that will be considered by CO_2 release. Weight loss over temperature $300\text{-}600^\circ\text{C}$ is caused by the loss of CO_2 from carbonate groups associated with magnesium ions, while the final weight loss in endotherm between 600°C and 800°C is caused by losing CO_2 from the thermal decomposition of carbonate groups associated with calcium ions. For example, at 800°C hydromagnesite decomposes to leave a magnesium oxide residue, and the huntite decomposes to leave a mixture of calcium oxide and magnesium oxide. Typical carbonate weight loss is seen in Figure 5.21a, but in this system, NaCl mixture should be taken into account as a partial weight, reducing the products' theoretical weight loss.

It can be seen that the first four samples (M1-M4) are well matched, with CaCO_3 TGA graph, having huge peak beyond 700°C ; however, a slightly shallower dip between $300\text{-}400^\circ\text{C}$ shows magnesium mixture, accompanied with calcium carbonate formation. Total weight loss percentage lies in between 43% to 48%, which is slightly less than hypothetical huntite standard, but appears in the calcium carbonates and magnesian calcite series. As magnesian calcite has no molecular water combination within the chemical formulae, the results illustrated in these four samples are the ones with approximately 1-2.5% H_2O loss, indicating magnesium element integration. However, this percentage is insignificant as it is quite different from the purified magnesium carbonates water weight loss starting from 19.2% in hydromagnesite to 39% in nesquehonite.

Samples 5 to 10 present a wider range of entire weight loss, from 39% to 53%. It can be seen that water molecular loss is significantly higher (>10%) than set 1-4. It is found out that the increased amount of magnesium mixture in samples 5-10 can accelerate the hydration degree due to the magnesium's prominent hydrophilic characteristics, from its lower hydration energy level. On the other hand, CO_2 sequestration amount is reduced

dramatically to approximate 30%, compared with M1-4 over 40% losses. This is attributed to the reduced calcium participation. In short, higher amounts of magnesium lead to higher percentages of the products' hydration degree; when more calcium accounts for higher carbonation quantities. This phenomenon is validated by the individual element study in Chapter 4. They both imply that the filtration of HMCs is more difficult than calcium carbonates because of the latter's larger independent particle appearance, while HMCs have partial gelatinous property and the small water-filled particulates. This also proves the impurity of NaCl attachment in HMCs, which is more difficult to be cleaned than calcium carbonates, as halite is used to dissolve into an aqueous phase and incorporate within the crystallised lattices.

The carbonation degree of each sample can significantly reflect the reaction degree, which is identified by CO₂ weight loss. In the referenced magnesian calcite group, the higher magnesium present in the samples corresponds to a higher CO₂ percentage. This percentage is scaled from 44%-50% by their different ratios of Mg²⁺ and Ca²⁺ in the standard MC group. However, the typical magnesium carbonate group (nesquehonite, hydromagnesite & dypingite) has much less weight loss in CO₂ reduction, ranged from around 32% to 38%, which reverses the effect of magnesian calcite CO₂ release to some extent. According to this analysis, a ranking of samples 1-4 & 5-10 on carbonation degrees from small to large is seen in [Figure 5. 20](#).



Figure 5. 20: The carbonation degree of M1-10

Samples 1-4 match with XRD results and the previous analysis perfectly, that is a higher supersaturation degree (samples 2&1; 4&3) will retard the reaction process, but elevated temperature will enhance the reaction rate (samples 4 &2; 3&1). This graph ([Figure 5.20](#)) also proves that a temperature rather than a supersaturation degree is a determining factor. Samples 5-10 are similar to the samples in Section 5.2.3.2 to estimate the reaction degree,

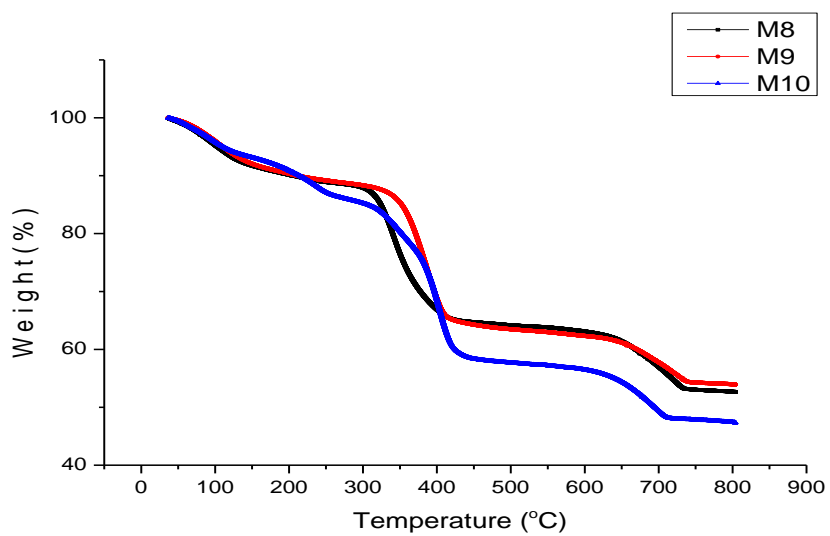
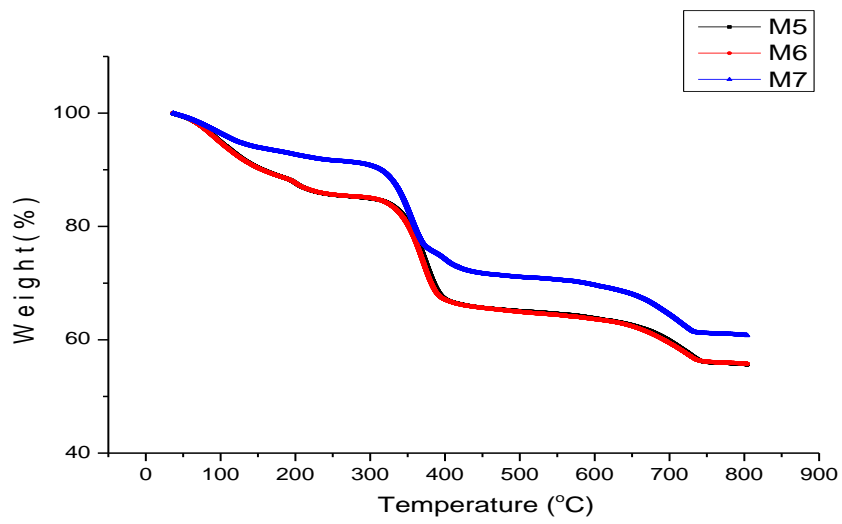
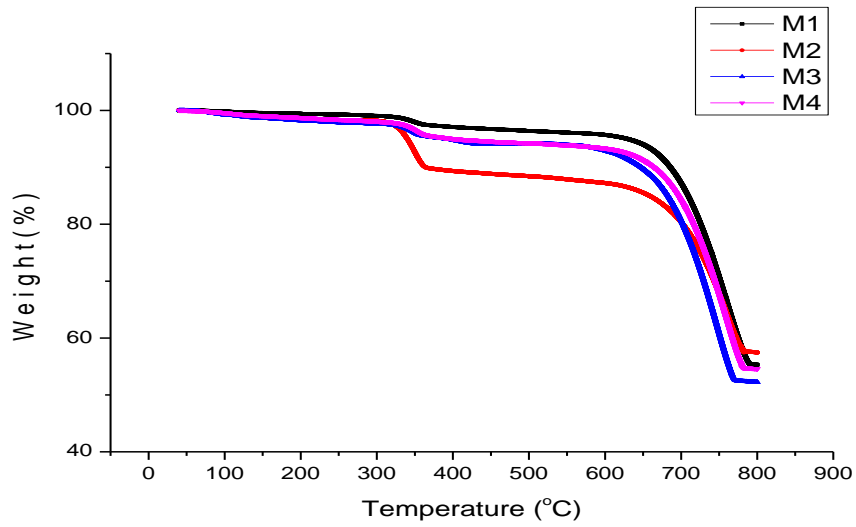
except 9. In the precipitates' identification, specimen 9 ranked last, representing the most completed reaction. While in this study sample 9 appears in the middle, sample 10 illustrates the best finished process, which can be estimated by the considerable amount of halite in 9 (34%) compared to 8 (2%) & 10(9%), reducing the carbon emission percentage.

The thermal property of kinetics was also investigated together with XRD and SEM-EDX. In both samples 1K and 5K water losses ([Figure 5.21d](#), DTG = Differential Thermogravimetry) are reduced while more carbon weight loss is shown. It is worth stating that more carbonates attach to the precipitates or join into the reaction over time, which leads to a higher carbonation degree. However sediment and water molecule amalgamation is faster in the initial stage. From this perspective, it is concluded that magnesian calcite generates the internal core as a central nucleation, because of strong magnesium hydrophilic characteristics. Water was added into this experiment rapidly. However, the outer shell is covered by calcium carbonates instantly, thus the majority of uncrushed samples forms into rounded or rhombic shapes, which is similar to the calcium carbonates' morphology within a short 1.5 hours' reaction. This phenomenon also proves the higher carbonation degree can represent a more accomplished reaction after one day.

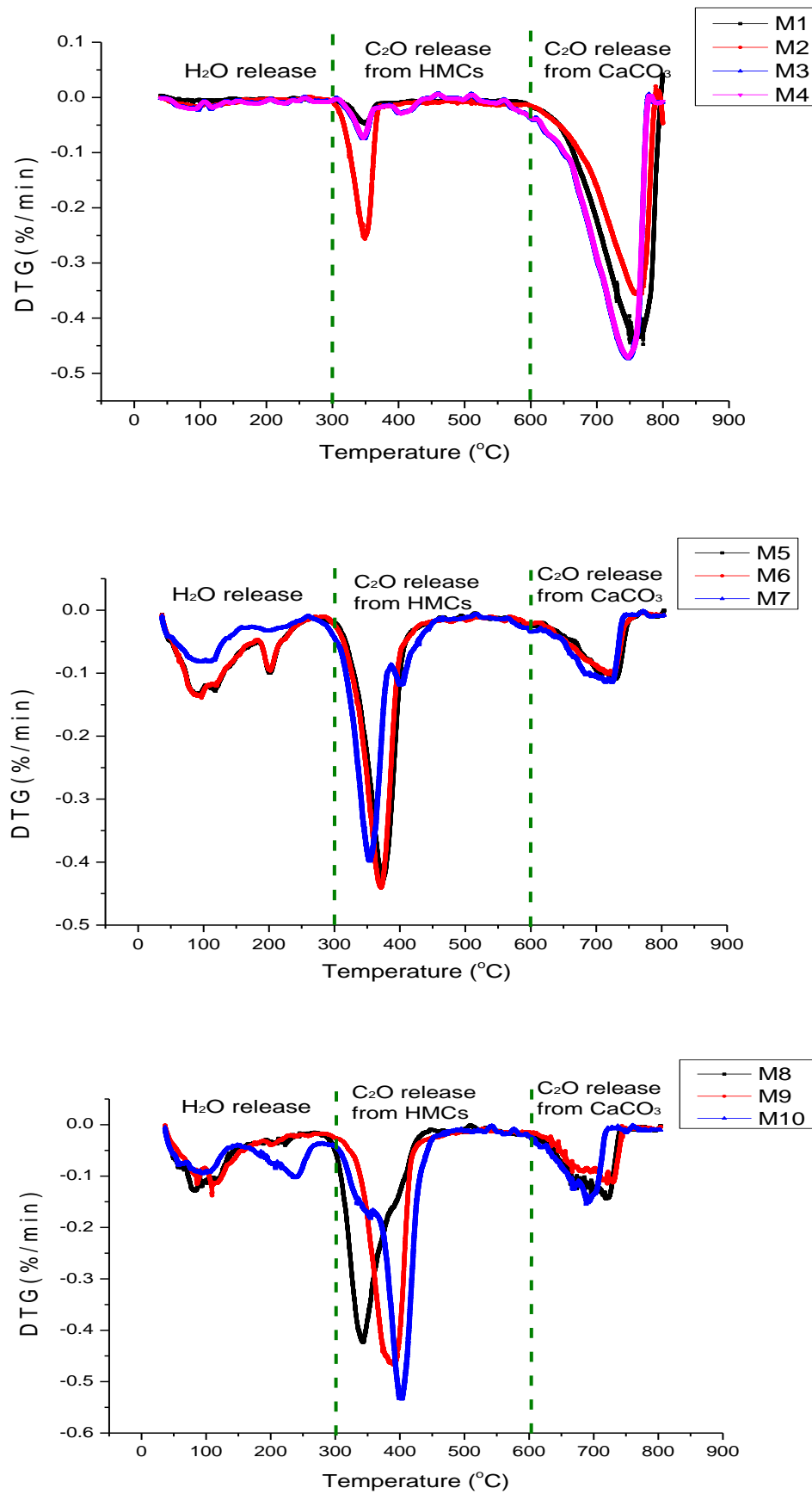
Over time or with the increased temperature, magnesium ions join to substitute the calcium or incorporate within the precipitate lattices, resulting in large phase transformation on spherulites macroscopic images towards the more HMCs' likened shapes. This is in line with EDX outcome with noticeable magnesium detection on the deposit surface. Due to this reacted phase transformation and crystallisation reformation of Mg^{2+} and carbonates incorporation, increased water molecule's attachment indicates magnesium carbonates' hydrophilic property, and therefore reverses the carbonation degree to some extent. Finally although a peak temperature in the last step is slightly different from the theoretical estimation, it is within a tolerance range of 610°C-800°C in air, based on author Bandi & Krapf (1976).

Sample	Step 1: Temp <200°C		Step 2: 200°C <Temp < 300°C		Water weight loss (%) (C3+C5)	Step 3: 300°C <Temp < 600°C		Step 4: 600°C<Temp <800°C		CO ₂ weight loss (%) (C8+C10)	Total weight loss (%) (C6+C11)
	Peak temp (°C)	Weight loss (%)	Peak temp (°C)	Weight loss (%)		Peak temp (°C)	Weight loss (%)	Peak temp (°C)	Weight loss (%)		
1	90.18	0.829	279.08	0.475	1.304	346.17	3.463	776.04	39.879	43.342	44.646
2	104.85	1.552	225.3	0.368	1.92	341.52	10.872	755.03	29.729	40.601	42.521
3	97.93	1.815	233.54	0.605	2.42	343.19	4.767	746.84	40.424	45.191	47.611
4	106.98	1.314	255.13	0.664	1.978	347.5	4.703	765.68	38.654	43.357	45.335
5	94.89	12.271	201.65	2.706	14.977	376.91	21.038	728.26	8.142	29.18	44.157
6	96.38	12.256	202.48	2.632	14.888	374.19	21.326	731.53	7.869	29.195	44.083
7	103.88	7.283	217.88	1.918	9.201	353.08	21.03	717.5	8.853	29.883	39.084
8	103.26	9.784	224.09	2.25	12.034	336.07	24.66	725.87	10.43	35.09	47.124
9	101.93	9.626	205.15	2.015	11.641	382.52	25.945	721.87	8.368	34.313	45.954
10	102.93	9.075	242.05	5.611	14.686	401.72	28.605	700.22	9.141	37.746	52.432
1K-1d	95.41	0.604	269.09	0.238	0.842	343.52	3.73	757.7	40.835	44.565	45.407
5K-1d	98.11	7.985	240.51	6.791	14.776	395.79	28.102	702.14	9.503	37.605	52.381

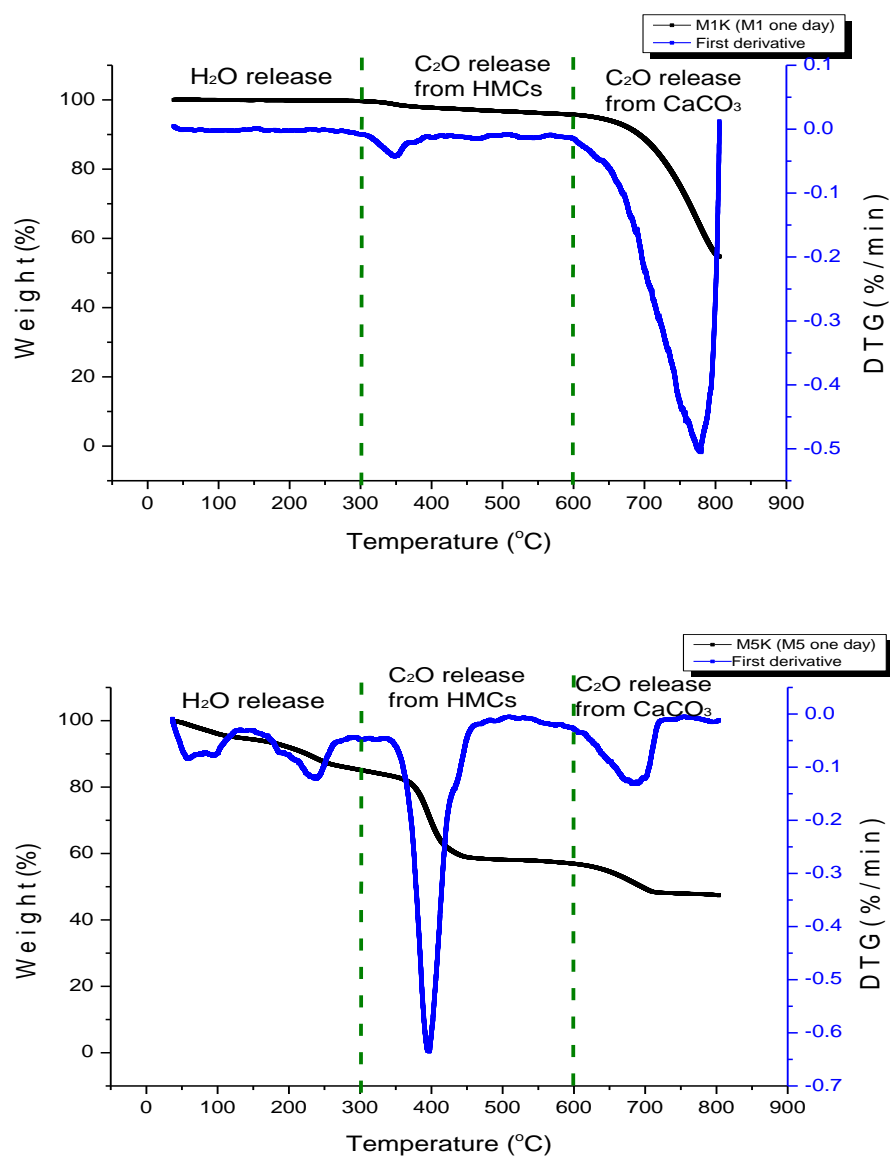
(a): Mixed magnesian calcite TGA (after1.5h)



(b): The weight% profiles of M1-10 calcination for SIV shown in Table 5.1



(c): The derivative profiles of M1-10 calcination for SIV shown in Table 5.1



(d): M1 and M5 one day thermal profiles weight (%) and first derivative for SVI

Figure 5. 21: The TGA thermal stages (a), thermal profiles (b) and analysed first derivative profiles (c) of M1-10, and M1 and M5 one day samples (d) for SIV shown in Table 5.1 (captions see top right corner)

5.2.4.2 Calcination at a Certain Temperature

The XRD analysed compound and its corresponding identical reference code from the database are presented in [Figure 5.22b](#). A higher matched score means the greater possibility to form into a specific precipitate. Several referenced samples cannot be detected in the quantitative analysis. As this non-recognition affected the whole group in the percentage calculation, they were removed from the list. 800°C is a temperature of light burned samples. The portlandite in [Figure 5.22a](#) is caused by the fast hydration in the atmosphere of lime after several days' storage before testing. However this hydration phenomenon from MgO into Mg(OH)₂ is not observed in the HMCs tests. Samples 1 -4 tend to illustrate CaO reactivity while the rest shows more MgO peaks. After analysing these four samples, the only difference is the hydration degree level caused by different storage conditions and the possible retention time. Samples 5 -10 are amalgamated into one category of their larger magnesium reactants. MgO and CaO are the main components, and MgO is the most amounts in all samples, while anhydrous lime reacts into hydrated lime-portlandite immediately (samples 5, 8 &9). This speed can be clearly seen from the lime alkaline-acid neutral reactivity test. The quantities of portlandite cannot be verified, as the retention time for the testing can be varied. The only notable component is the magnesian calcite appearance in M5C and M9C, implying the possible inadequate time or the insufficient calcination temperature.

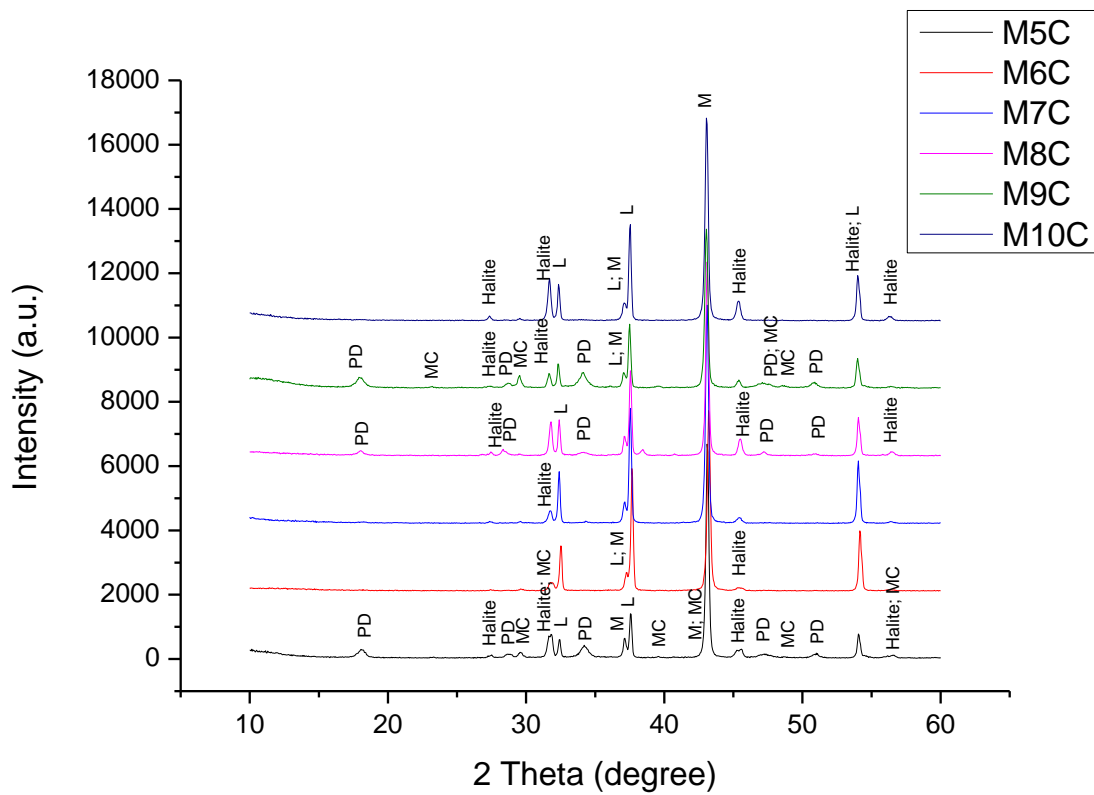
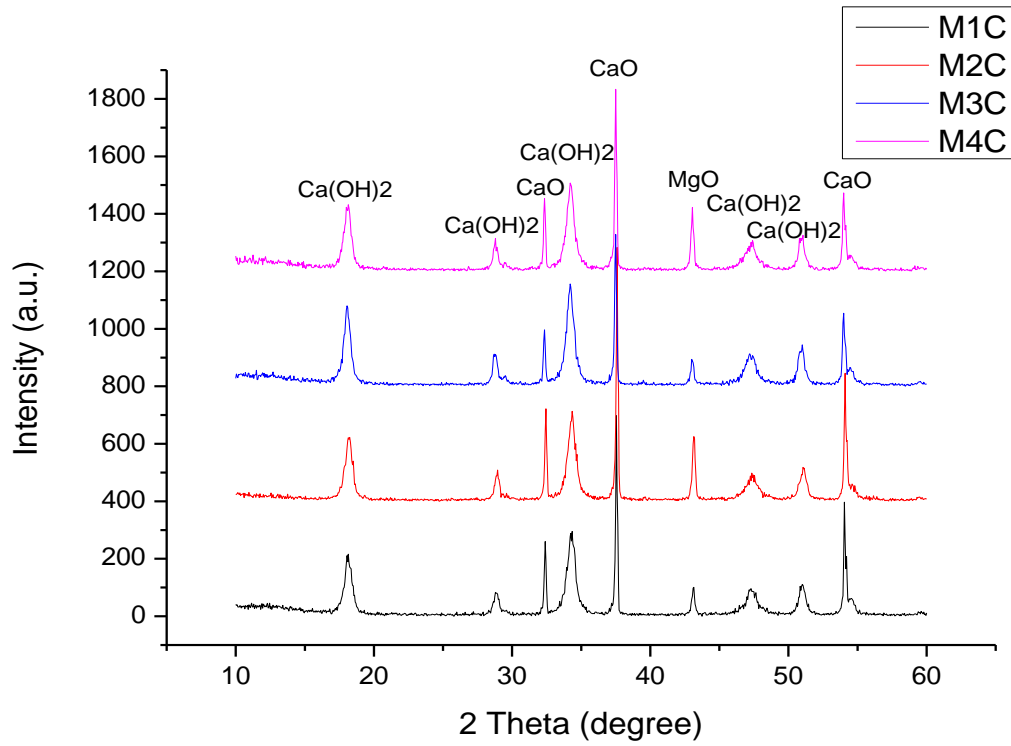
In this section, all samples decomposed at 800°C, consistent with the previous study in Chapter 4. Ideally if the entire amount of calcium and magnesium in aqueous phase was captured, in samples 1-4, the ratio Ca²⁺:Mg²⁺ should be equal to 5 or 2; and the ratio in samples 5-10 should be theoretically 0.2. Some samples need a specific element-setting, that is, a particular component has to be tested irrelevant to its quantity, while the rest is from the automatic search by software.

[Figure 5. 23](#) shows that samples 1 and 2 present fluffy spherical surfaces, and samples 3 and 4 have more individual particles with the elongated version and aggregated round grains. Samples 2 and 4 present more thorough decomposition without carbon appearance and the amounts of carbon in samples 1 and 3 are also insignificant because of its low initial

concentration. The increased magnesium participation reduces the peak temperatures in TGA, highlighted by salts' distortion on the crystalline reformation during the thermal investigation, and the requirement of less heat to break down the samples into magnesium than calcium carbonates.

To analyse samples 5-10, from the microscopic perspective, sample 5 shows the relative shaped circular granules while 6 has more aggregated fine particles. Unlike them, later imaged pictures 7, 8 and 10 all display the large lumps, excluding 9. Example 9 displays incomplete calcination with hidden rosette-like shapes and prominent carbon remained in the EDX result. Additionally, carbon is observed within all samples 7-10 ([Figure 5.22b](#)), which is caused by the natural carbonation of their relative long-time duration periods before the testing. Furthermore, this carbonation process can enhance the particles' conglutination into a bigger block. Theoretically, this (carbonation) chemical reaction will not affect $\text{Ca}^{2+}:\text{Mg}^{2+}$ ratios. In practice, sample 7 is significantly bigger than the others in ratio, partially caused by its multiple locations' selection. It is therefore not representative. In conclusion, samples 5 to 10 have a generally stable condition with similar calcium and magnesium extraction, revealed from the kinetics study and the calcined $\text{Ca}^{2+}:\text{Mg}^{2+}$ ratios. The reason for the carbonation microstructure disclosing big differences on $\text{Ca}^{2+}:\text{Mg}^{2+}$ is caused by the exterior morphology; while higher temperature can break down this molecular bond.

In the reactivity test ([Figure 5.24](#)), samples 1 to 4 are for indication only, where the major element is calcium, leading to a rapid neutralisation with citric acid. These figures are all larger than the standardised reactivity because of the reversed reactivity from its considerable hydration degree of M1C-M4C. Targeted comprehensive analysis of the mixed reactivity tests of M5C-M10C at 800°C is summarised in [Figure 5. 24](#). It varies from 100s to 150s. But in the mixture, the proportion of MgO : CaO is equal to 5 (theoretically). N50 mixture is 13s and ore extracted 92-200 is 115s. Even if choosing other proportions relying on EDX $\text{Ca}^{2+}:\text{Mg}^{2+}$ ratios' table above, the majority of M5C-M10C outcomes are still bigger than the commercial dolime due to the addition of other impurities during the experimental process. A more elaborated demonstration on the reactivity test and its standard can be seen in Section 5.2.2.2.



(a): The calcined products of M1-10C for SIV (PD=Portlandite, Halite=NaCl, MC=Magnesian calcite)

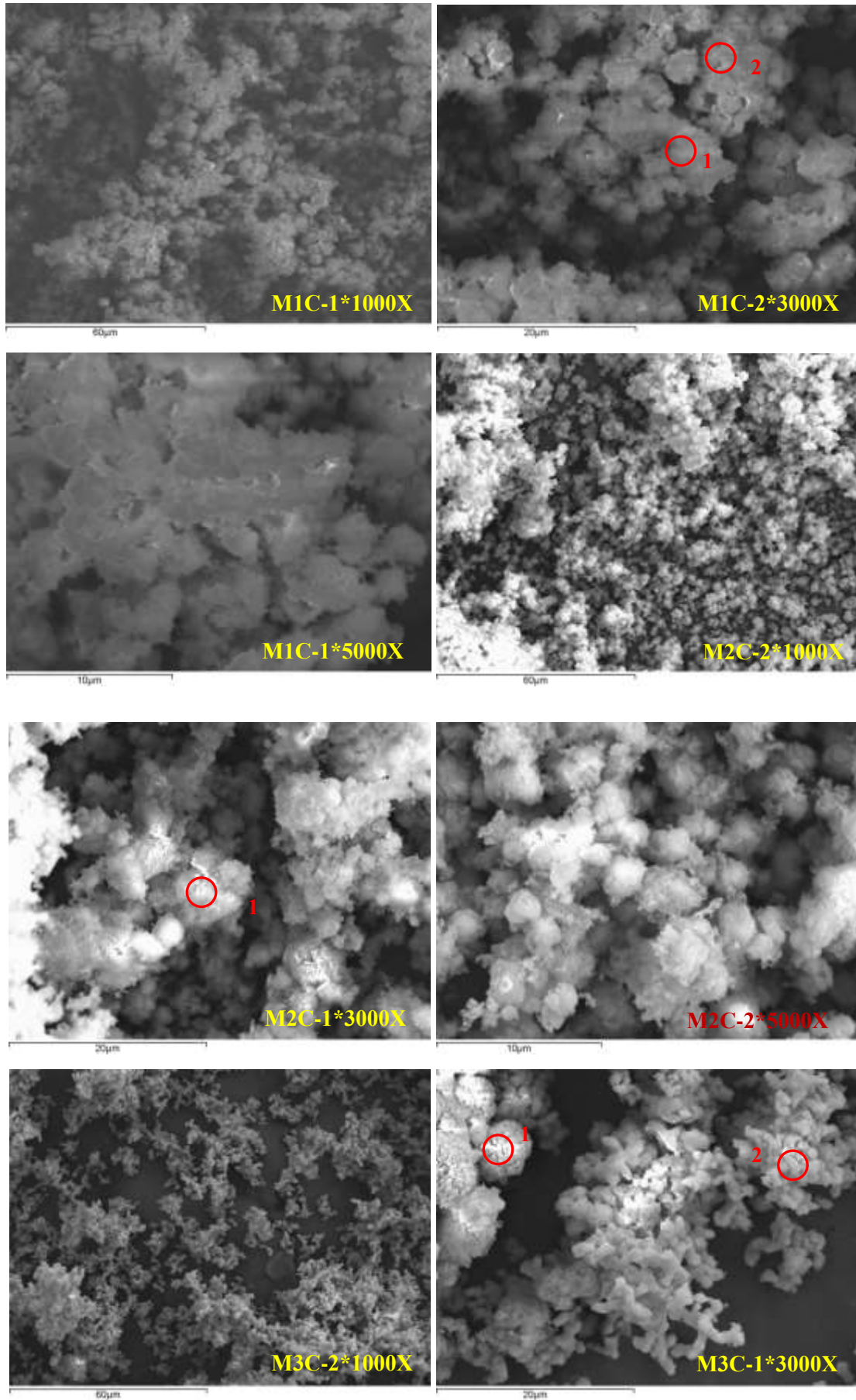
Sample			M1C		M2C		M3C		M4C	
Ref. Code	Mineral Name	Chemical Formula	Score	SemiQuant (%)	Score	SemiQuant (%)	Score	SemiQuant (%)	Score	SeimiQuant (%)
01-076-0570	Portlandite, syn	Ca(OH) ₂	82	--	75	--	78	--	82	--
01-078-0649	Lime	CaO	70	--	63	--	65	--	71	--
00-001-1235	Periclase	MgO	55	--	47	--	46	--	55	--
01-074-2220	Brucite	Mg(OH) ₂	22	--	26	--	18	--	17	--
Sample			M1C		M2C		M3C		M4C	
Ref. Code	Mineral Name	Chemical Formula	Contained within precipitates ? (Score)	SemiQuant (%) (percentage s without Periclase addition)	Contained within precipitates ? (Score)	SemiQuant (%) (percentage s without Periclase addition)	Contained within precipitates ? (Score)	SemiQuant (%) (percentage s without Periclase addition)	Contained within precipitates ? (Score)	SemiQuant (%) (percentage s without Periclase addition)
01-076-0570	Portlandite, syn	Ca(OH) ₂	Yes (82)	-- (70)	Yes (75)	-- (73)	Yes (78)	-- (59)	Yes (82)	-- (57)
01-078-0649	Lime	CaO	Yes (70)	-- (30)	Yes (63)	-- (27)	Yes (65)	-- (41)	Yes (71)	-- (43)
00-001-1235	Periclase	MgO	Yes (55)	--	Yes (47)	--	Yes (46)	--	Yes (55)	--
01-074-2220	Brucite	Mg(OH) ₂	No		No		No		No	

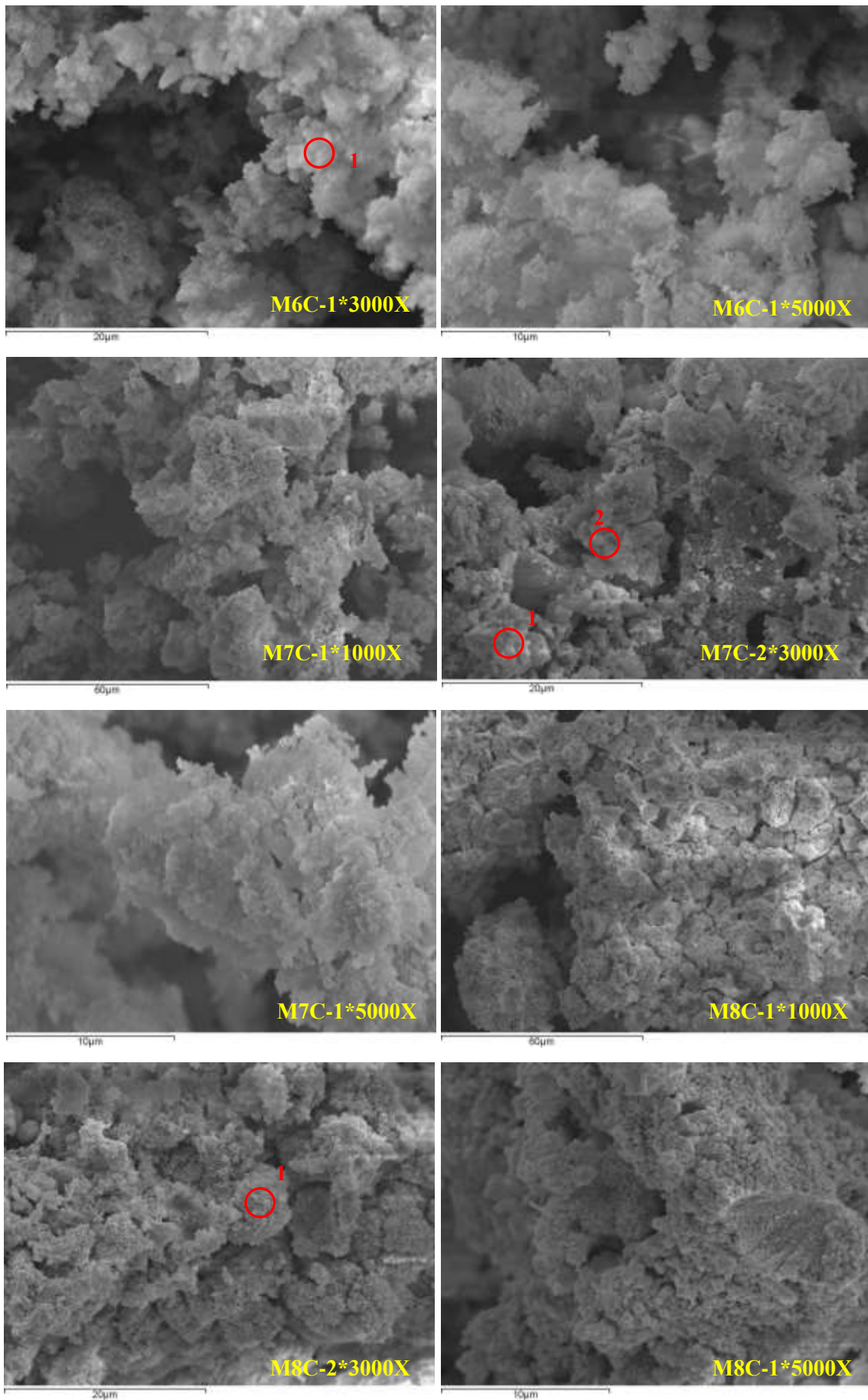
Sample			M5C		M6C		M7C	
Ref. Code	Mineral Name	Chemical Formula	Score	SemiQuant (%)	Score	SemiQuant (%)	Score	SemiQuant (%)
00-004-0829	Magnesia	MgO	44	66	61	41	66	71
01-077-2376	Lime	CaO	49	6	65	9	74	11
00-044-1481	Portlandite, syn	Ca(OH) ₂	58	11	Unmatched Strong	34	Unmatched Strong	10
01-078-0751	Halite, syn	NaCl	51	11	58	6	69	6
01-086-2335	Calcite, magnesian	(Mg _{0.064} Ca _{0.936})CO ₃	42	6	0	10	9	2
Sample			M8C		M9C		M10C	
Ref. Code	Mineral Name	Chemical Formula	Score	SemiQuant (%)	Score	SemiQuant (%)	Score	SemiQuant (%)
00-004-0829	Magnesia	MgO	57	63	47	69	58	71
01-077-2376	Lime	CaO	64	10	53	10	65	10

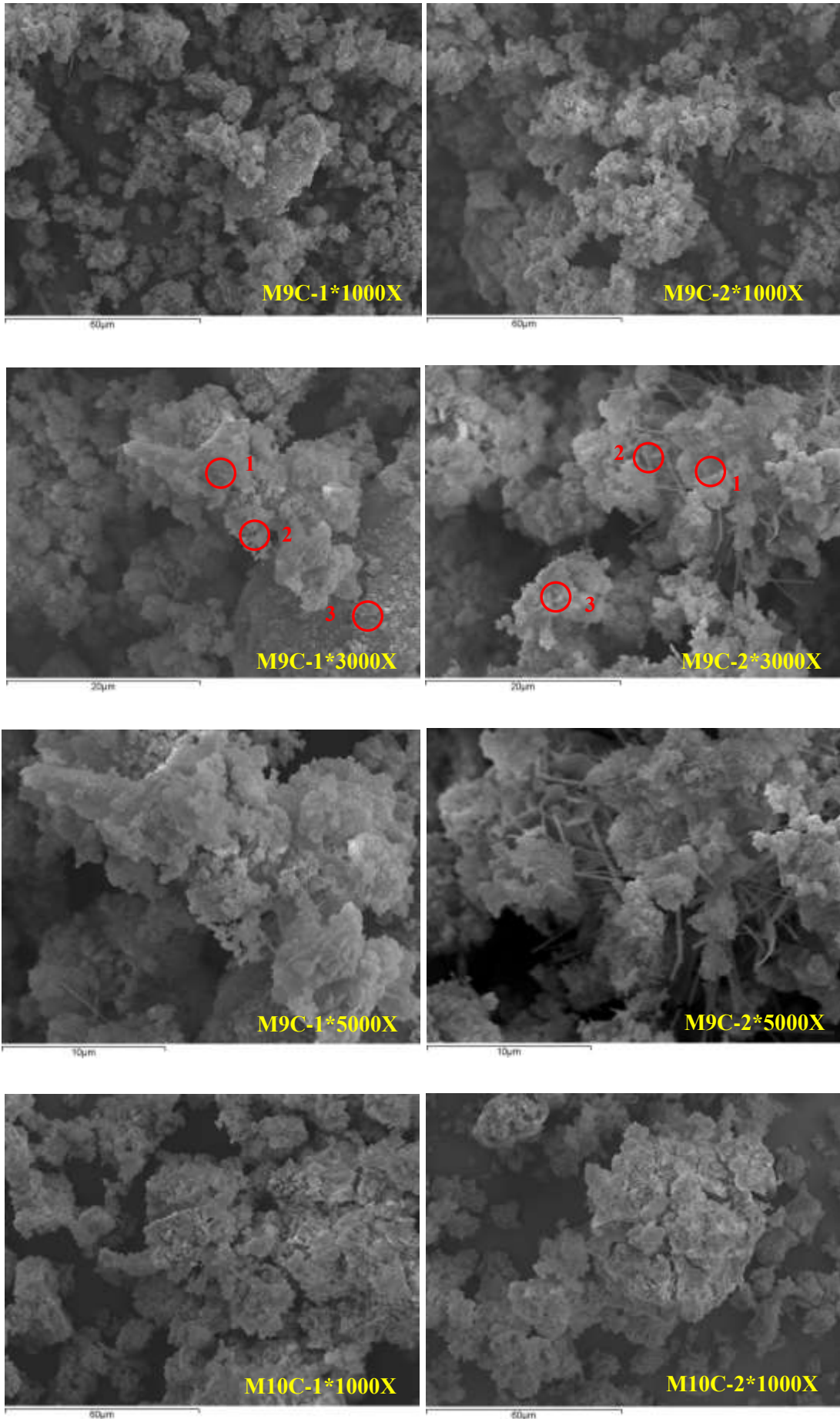
00-044-1481	Portlandite, syn	Ca(OH) ₂	56	5	59	9	Unmatched Strong	3
01-078-0751	Halite, syn	NaCl	66	20	54	5	64	15
01-086-2335	Calcite, magnesian	(Mg _{0.064} Ca _{0.936})CO ₃	3	2	52	7	0	2
Sample			M5C		M6C		M7C	
Ref. Code	Mineral Name	Chemical Formula	Contained within precipitates? (Score)	SemiQuant (%)	Contained within precipitates? (Score)	SemiQuant (%)	Contained within precipitates? (Score)	SemiQuant (%)
00-004-0829	Magnesia	MgO	Yes (44)	66	Yes (61)	74	Yes (66)	81
01-077-2376	Lime	CaO	Yes (49)	6	Yes (65)	16	Yes (74)	12
00-044-1481	Portlandite, syn	Ca(OH) ₂	Yes (58)	11	No		No	
01-078-0751	Halite, syn	NaCl	Yes (51)	11	Yes (58)	10	Yes (69)	7
01-086-2335	Calcite, magnesian	(Mg _{0.064} Ca _{0.936})CO ₃	Yes (42)	6	No		No	
Sample			M8C		M9C		M10C	
Ref. Code	Mineral Name	Chemical Formula	Contained within precipitates? (Score)	SemiQuant (%)	Contained within precipitates? (Score)	SemiQuant (%)	Contained within precipitates? (Score)	SemiQuant (%)
00-004-0829	Magnesia	MgO	Yes (57)	65	Yes (47)	69	Yes (58)	74
01-077-2376	Lime	CaO	Yes (64)	10	Yes (53)	10	Yes (65)	10
00-044-1481	Portlandite, syn	Ca(OH) ₂	Yes (56)	5	Yes (59)	9	No	
01-078-0751	Halite, syn	NaCl	Yes (66)	20	Yes (54)	5	Yes (64)	15
01-086-2335	Calcite, magnesian	(Mg _{0.064} Ca _{0.936})CO ₃	No		Yes (52)	7	No	

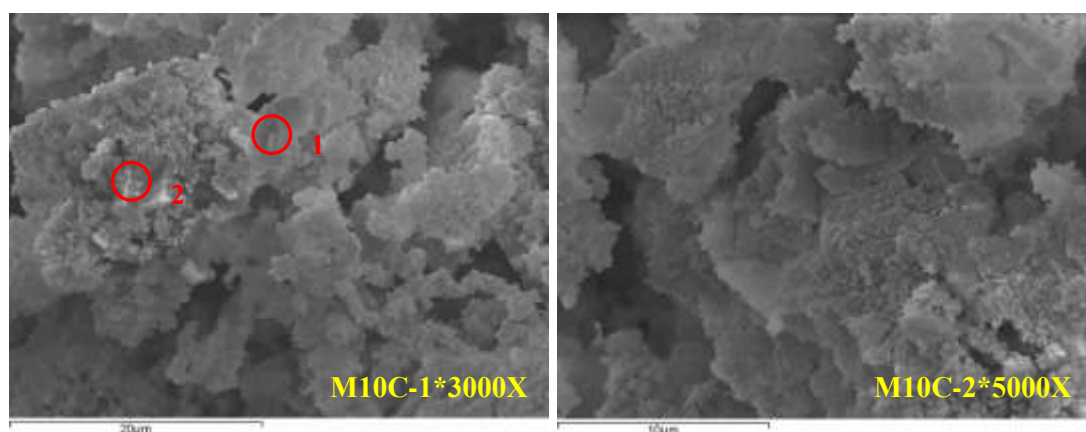
(b): The matching scores and semiquants of calcined M1-10C precipitates, calculated by software X'Per HighScore Plus for SIV

Figure 5. 22: The XRD patterns for M1-10C (a), and the matching scores and semiquants of M1-10 calcination products, calculated by software X'Per HighScore Plus (b). All samples are for SIV shown in Table 5.1









Sample	Spectrum	C	O	Mg	Ca	Ca ²⁺ : Mg ²⁺
M1C-2*3000X	Spectrum 1	9.25	51.82	11.72	27.22	2.32
	Spectrum 2	6.8	51.44	11.66	30.1	2.58
M2C-1*3000X	Spectrum 1	Not tested	27.32	6.72	65.95	9.81
M3C-1*3000X	Spectrum 1	5.49	46.33	2.04	46.14	22.62
	Spectrum 2	0.92	13.25	0.86	84.97	98.80
M4C-2*3000X	Spectrum 1	Not tested	64.13	2.63	33.24	12.64
	Spectrum 2	Not tested	47.39	2.35	50.27	21.39
M5C-1*3000X	Spectrum 1	Not tested	51.27	46.27	2.45	0.05
	Spectrum 2	Not tested	55.42	41.81	2.77	0.07
M6C-1*3000X	Spectrum 1	Not tested	56.77	35.58	7.65	0.22
M8C-2*3000x	Spectrum 1	39.42	27.88	6.43	26.26	4.08
M9C-1*3000X	Spectrum 1	20.46	55.16	10.08	14.3	1.42
	Spectrum 2	25.08	44.47	19.66	10.79	0.55
	Spectrum 3	27.75	38.58	16.57	17.1	1.03
M9C-2*3000X	Spectrum 1	16.53	49.21	27.33	6.93	0.25
	Spectrum 2	15.71	55.46	24.56	4.27	0.17
	Spectrum 3	37.27	41.99	10.09	10.65	1.06
M10C-1*3000x	Spectrum 1	24.01	37.55	37.5	0.93	0.02
	Spectrum 2	18.02	39.16	38.45	4.36	0.11

Sample	Spectrum	C	O	Na	Mg	Ca	Ca ²⁺ : Mg ²⁺
M7C-2*3000X	Spectrum 1	23.64	34.91	2.35	11.95	27.16	2.27
	Spectrum 2	31.86	42.75	1.04	3.42	20.93	6.12

Figure 5. 23: The microstructure of calcined M1-10C and their correlated EDX results for SIV shown in Table 5.1 (e.g. M7C-2*3000X means M7 sample, calcination at 800°C, location 2, 3000x magnification)

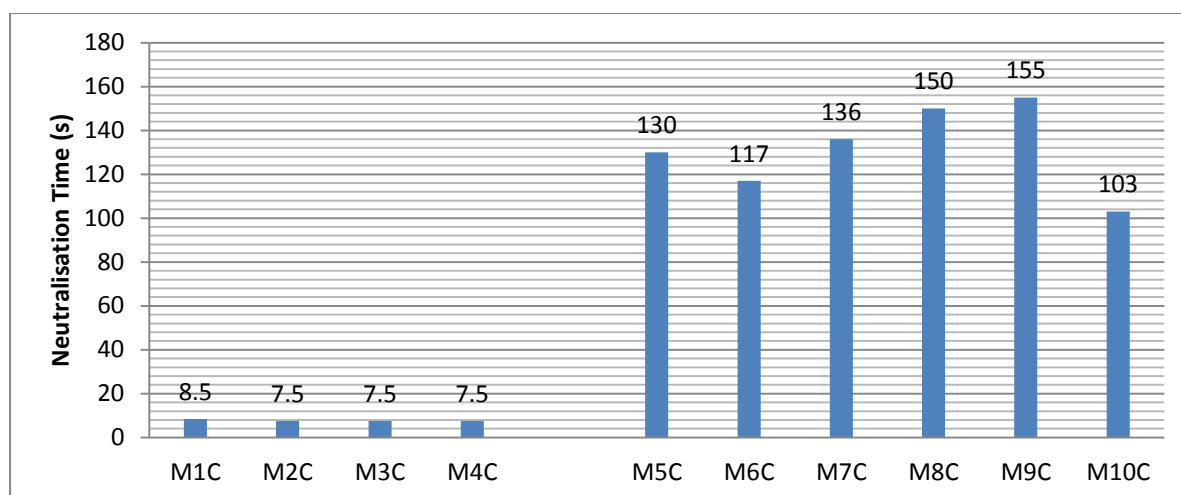
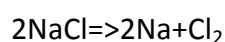


Figure 5. 24: The reactivity tests of calcined M1-10C

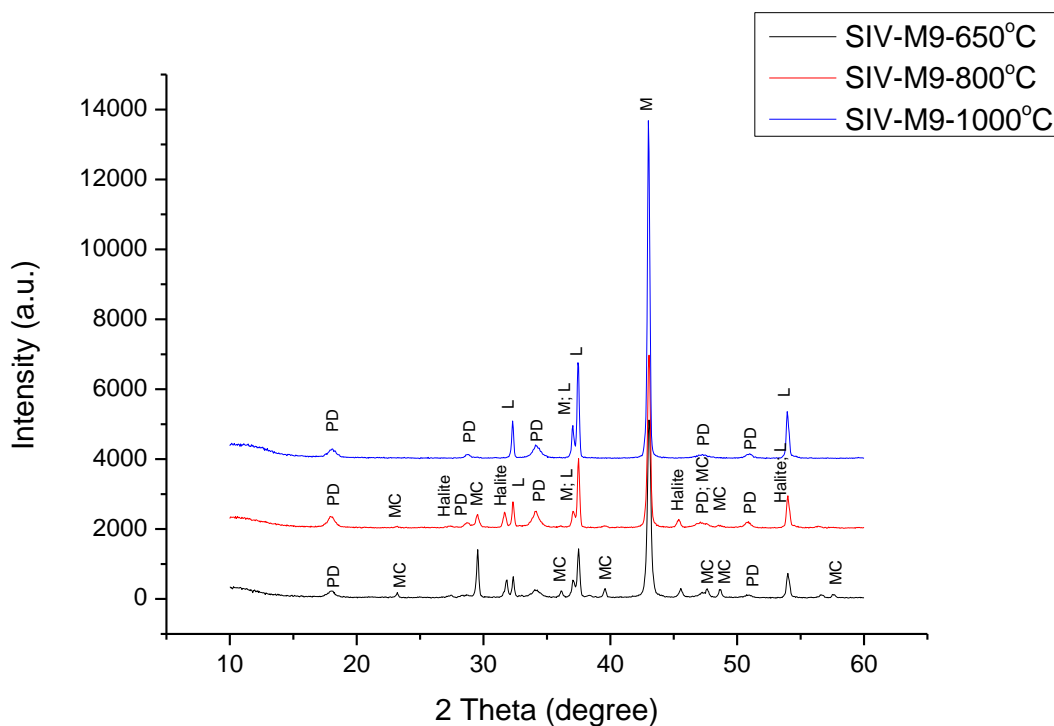
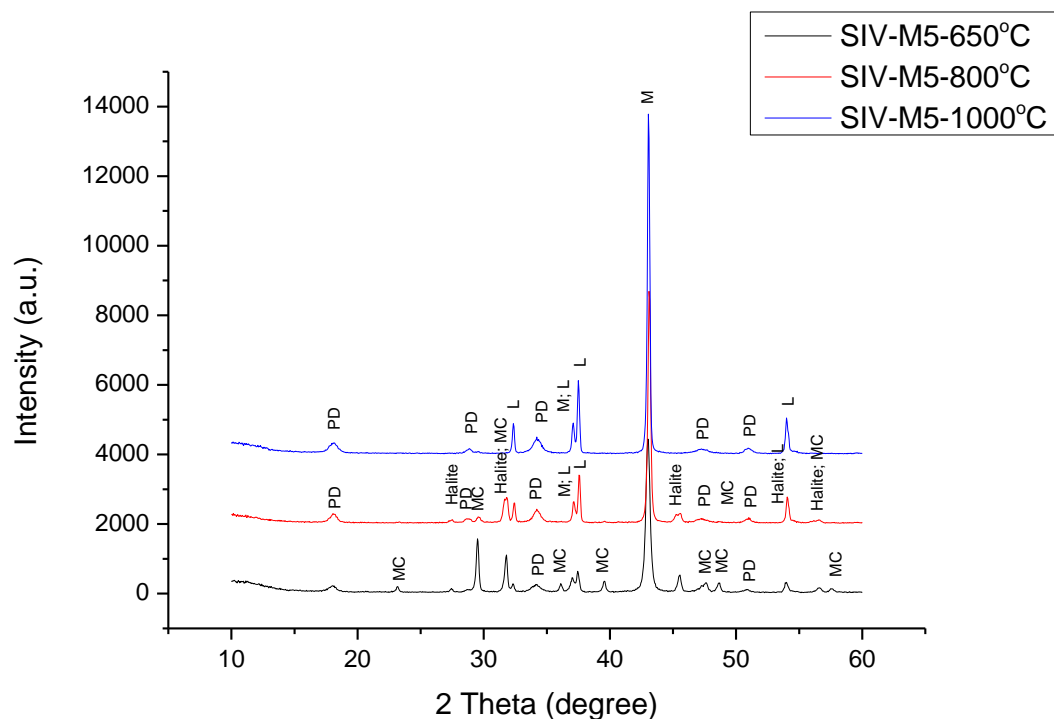
When making evaluations of M5C-M10C, results on reactivity here are numbered as: M9C>M8>M7C>M5C>M6C>M10C, this segment indicates sample 10 is the most reactive effective product. While the ranking in Section 5.2.3.2 on the reaction degree was: M9>M10>M8>M7>M6>M5. As seen, the orders of samples in both tests are very similar except 10. It shows that a higher reaction level can contribute to a poorer reactivity performance to some extent. This is caused by larger magnesium participation leading to a normally more complex system, having the tendency to result in higher impurities addition. While the surrounding temperature is elevated, samples 6 and 10 are likely to induce faster reactivity. A lower stirring speed and CO₂ flux rate (samples 7 and 8) are not positive for a reactivity test, which can also be observed from the MgO samples in Chapter 4. Generally, a higher pH can promote the chemical reactivity, which is equivalent to the effect of the raised temperature leading to an increased pH.

5.2.4.3 The Analysis of Calcination at Various Temperatures

Various temperatures were explored further developing Hassan's work (2013). Relatively reasonable intervals were rewarded, ensuring the uniform distribution of temperatures (650°C, 800°C, and 1000°C). From both graphs and tables (**Figure 5.25**), 650°C MC peaks are obvious, while in 800°C, only small portions are accounted for MC, until the last at 1000°C, where the sample was fully calcined with the no trace of carbonates or halite. The melting point of NaCl is 801°C with the following equation:



This process demonstrates the decomposition of halite into evaporated Cl_2 and independent reactive sodium; hence there is no NaCl detected at 1000°C . The precipitates contain the highest amounts of MgO with a considerable quantity of CaO occupation.



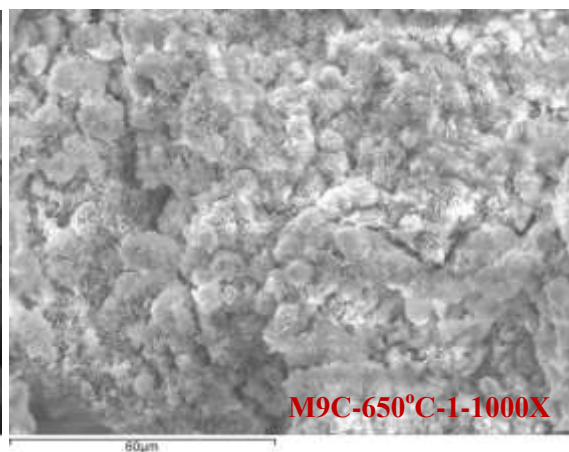
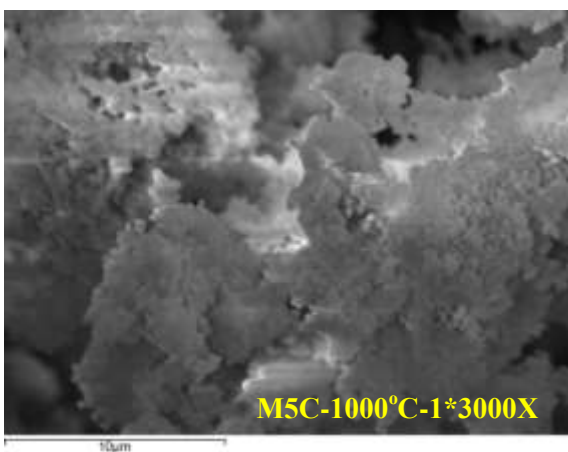
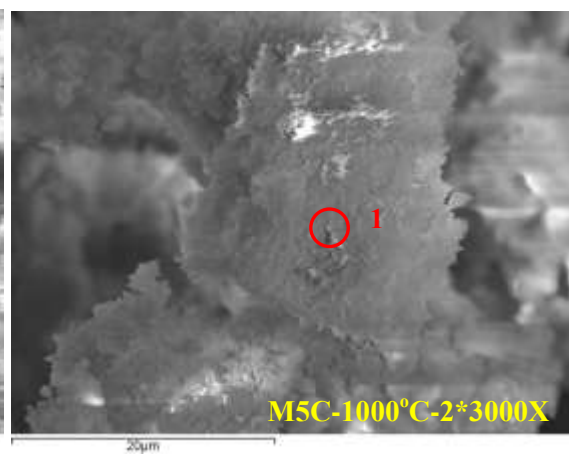
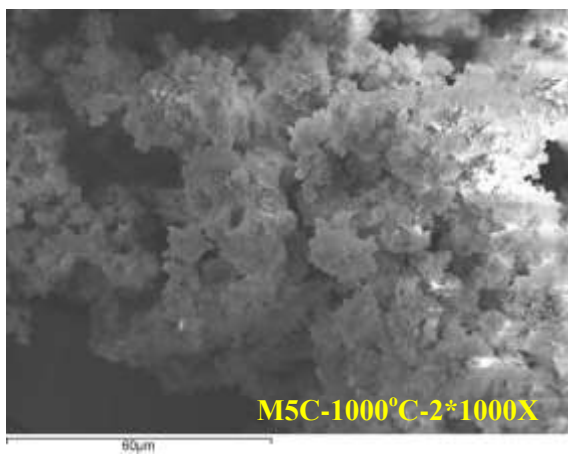
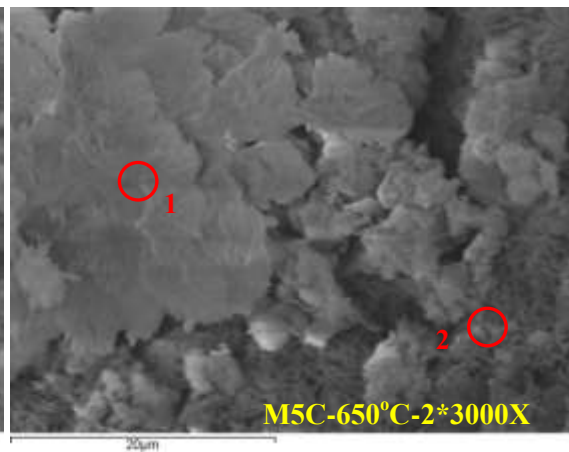
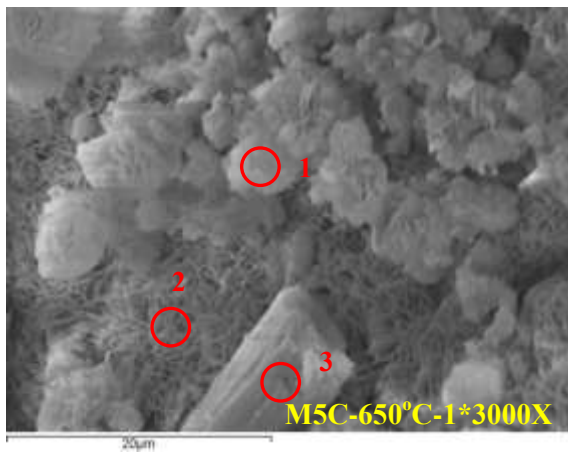
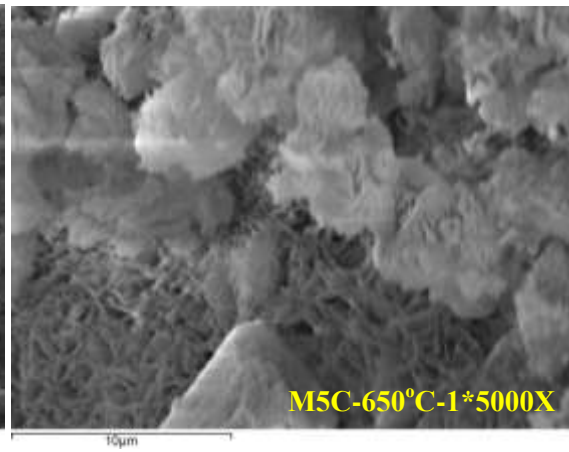
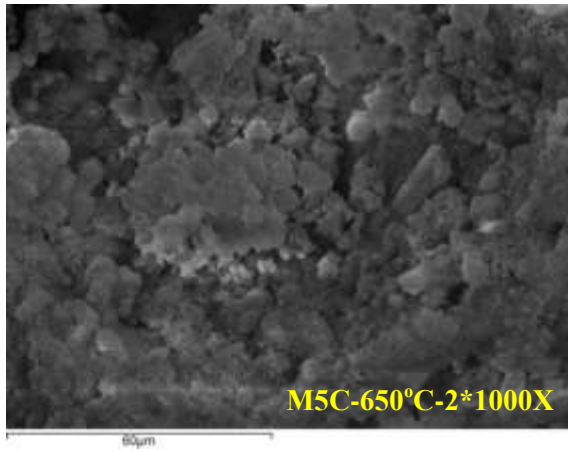
(a): The calcined products of SIV-M5/M9 after various heating temperatures (L=Lime, M=MgO)

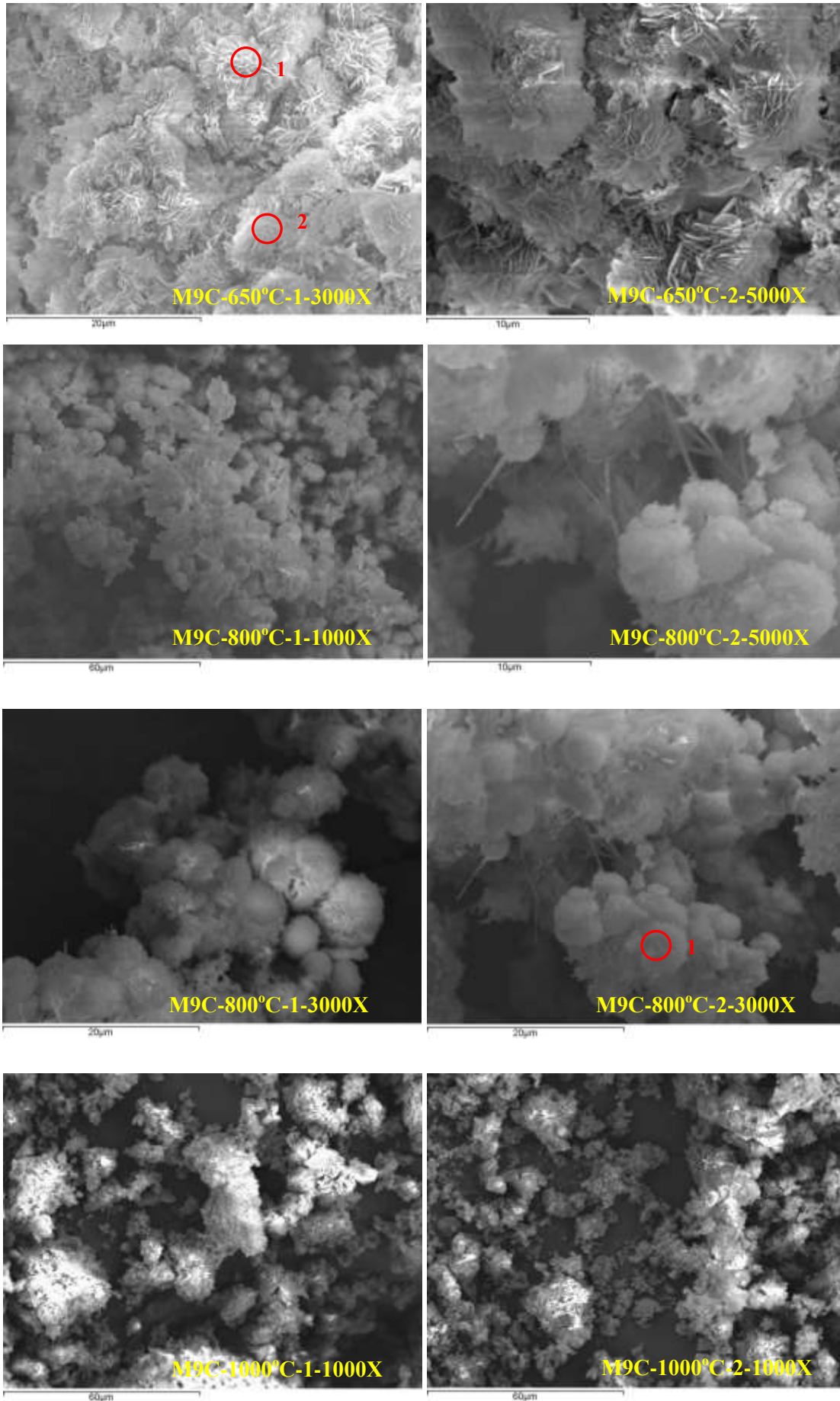
Sample			SIV-M5C-650°C		SIV-M5C-800°C		SIV-M5C-1000°C	
Ref. Code	Mineral Name	Chemical Formula	Score	SemiQuant (%)	Score	SemiQuant (%)	Score	SemiQuant (%)
01-071-1663	Calcite, magnesian	(Mg _{0.1} Ca _{0.9})CO ₃	34	2	34	4	0	--
01-073-1403	Huntite	Mg ₃ Ca(CO ₃) ₄	26	3	26	12	6	2
01-083-1766	Dolomite	MgCa(CO ₃) ₂	9	1	11	2	8	19
01-086-2335	Calcite, magnesian	(Mg _{0.064} Ca _{0.936})CO ₃	54	13	42	4	25	2
01-086-2336	Calcite, magnesian	(Mg _{0.129} Ca _{0.871})CO ₃	34	1	21	2	0	--
01-089-1304	Calcite, magnesium, syn	(Mg _{0.03} Ca _{0.97})CO ₃	59	14	34	7	21	1
01-089-1305	Calcite, magnesium, syn	(Mg _{0.06} Ca _{0.94})CO ₃	48	12	40	4	26	1
00-004-0829	Magnesia	MgO	44	46	44	45	46	62
01-077-2376	Lime	CaO	48	2	49	4	52	6
00-044-1481	Portlandite, syn	Ca(OH) ₂	55	2	58	7	62	5
01-078-0751	Halite, syn	NaCl	51	5	51	8	6	--
Sample			SIV-M5C-650°C		SIV-M5C-800°C		SIV-M5C-1000°C	
Ref. Code	Mineral Name	Chemical Formula	Score	SemiQuant (%)	Score	SemiQuant (%)	Score	SemiQuant (%)
01-071-1663	Calcite, magnesian	(Mg _{0.1} Ca _{0.9})CO ₃	No		No		No	
01-073-1403	Huntite	Mg ₃ Ca(CO ₃) ₄	No		No		No	
01-083-1766	Dolomite	MgCa(CO ₃) ₂	No		No		No	
01-086-2335	Calcite, magnesian	(Mg _{0.064} Ca _{0.936})CO ₃	Yes (54)	14	Yes (42)	5	No	
01-086-2336	Calcite, magnesian	(Mg _{0.129} Ca _{0.871})CO ₃	No		No		No	
01-089-1304	Calcite, magnesium, syn	(Mg _{0.03} Ca _{0.97})CO ₃	Yes (59)	15	Yes (34)	9	No	
01-089-1305	Calcite, magnesium, syn	(Mg _{0.06} Ca _{0.94})CO ₃	Yes (48)	13	Yes (40)	5	No	
00-004-0829	Magnesia	MgO	Yes (44)	49	Yes (44)	57	Yes (46)	85
01-077-2376	Lime	CaO	Yes (48)	2	Yes (49)	5	Yes (52)	8
00-044-1481	Portlandite, syn	Ca(OH) ₂	Yes (55)	2	Yes (58)	9	Yes (62)	7
01-078-0751	Halite, syn	NaCl	Yes (51)	5	Yes (51)	10	No	
Sample			SIV-M9C-650°C		SIV-M9C-800°C		SIV-M9C-1000°C	
Ref. Code	Mineral Name	Chemical Formula	Score	SemiQuant (%)	Score	SemiQuant (%)	Score	SemiQuant (%)
01-071-1663	Calcite, magnesian	(Mg _{0.1} Ca _{0.9})CO ₃	33	2	45	2	0	--
01-073-1403	Huntite	Mg ₃ Ca(CO ₃) ₄	21	2	31	5	6	15

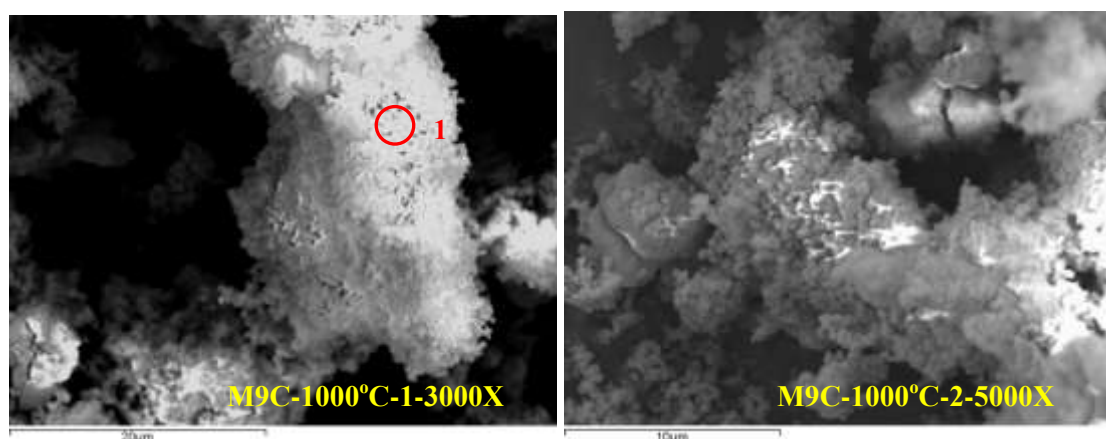
01-083-1766	Dolomite	$\text{MgCa}(\text{CO}_3)_2$	11	1	17	2	5	19
01-086-2335	Calcite, magnesian	$(\text{Mg}_{0.064}\text{Ca}_{0.936})\text{CO}_3$	62	14	52	6	20	--
01-086-2336	Calcite, magnesian	$(\text{Mg}_{0.129}\text{Ca}_{0.871})\text{CO}_3$	31	1	43	2	11	--
01-089-1304	Calcite, magnesium, syn	$(\text{Mg}_{0.03}\text{Ca}_{0.97})\text{CO}_3$	61	15	57	6	22	--
01-089-1305	Calcite, magnesium, syn	$(\text{Mg}_{0.06}\text{Ca}_{0.94})\text{CO}_3$	54	14	52	6	14	--
00-004-0829	Magnesia	MgO	47	42	47	53	47	54
01-077-2376	Lime	CaO	52	4	53	8	53	7
00-044-1481	Portlandite, syn	$\text{Ca}(\text{OH})_2$	61	2	59	7	57	3
01-078-0751	Halite, syn	NaCl	49	2	54	4	0	--
Sample			SIV-M9C-650°C		SIV-M9C-800°C		SIV-M9C-1000°C	
Ref. Code	Mineral Name	Chemical Formula	Score	SemiQuant (%)	Score	SemiQuant (%)	Score	SemiQuant (%)
01-071-1663	Calcite, magnesian	$(\text{Mg}_{0.1}\text{Ca}_{0.9})\text{CO}_3$	No		No		No	
01-073-1403	Huntite	$\text{Mg}_3\text{Ca}(\text{CO}_3)_4$	No		No		No	
01-083-1766	Dolomite	$\text{MgCa}(\text{CO}_3)_2$	No		No		No	
01-086-2335	Calcite, magnesian	$(\text{Mg}_{0.064}\text{Ca}_{0.936})\text{CO}_3$	Yes (62)	15	Yes (52)	7	No	
01-086-2336	Calcite, magnesian	$(\text{Mg}_{0.129}\text{Ca}_{0.871})\text{CO}_3$	No		No		No	
01-089-1304	Calcite, magnesium, syn	$(\text{Mg}_{0.03}\text{Ca}_{0.97})\text{CO}_3$	Yes (61)	16	Yes (57)	7	No	
01-089-1305	Calcite, magnesium, syn	$(\text{Mg}_{0.06}\text{Ca}_{0.94})\text{CO}_3$	Yes (54)	15	Yes (52)	6	No	
00-004-0829	Magnesia	MgO	Yes (47)	45	Yes (47)	60	Yes (47)	85
01-077-2376	Lime	CaO	Yes (52)	4	Yes (53)	9	Yes (53)	11
00-044-1481	Portlandite, syn	$\text{Ca}(\text{OH})_2$	Yes (61)	2	Yes (59)	8	Yes (57)	4
01-078-0751	Halite, syn	NaCl	Yes (49)	2	Yes (54)	4	No	

(b): The matching scores and semiquants of calcined SIV-M5/M9 at different heating temperatures, calculated by software X'Per HighScore Plus

Figure 5. 25: The XRD patterns for M5, M9 at different calcination temperatures (a), and the matching scores and semiquants of M5 and M9 calcination products, calculated by software X'Per HighScore Plus (b). All samples are for SIV shown in Table 5.1







Sample	Spectrum	C	O	Mg	Ca	Ca ²⁺ :Mg ²⁺
M5C-650°C-1*3000X	Spectrum 1	11.28	46.38	40.8	1.54	0.04
	Spectrum 2	5.55	49.97	39.89	4.58	0.11
	Spectrum 3	15.27	42.63	40.96	1.14	0.03
M5C-650°C-2*3000X	Spectrum 1	8.19	41.92	45.64	4.26	0.09
	Spectrum 2	9.82	31.4	53.37	5.41	0.10
M5C-1000°C-2*3000X	Spectrum 1	Not tested	38	58.96	3.04	0.05

Sample	Spectrum	C	O	Mg	Ca	Na	Cl	Ca ²⁺ :Mg ²⁺
M9C-650°C-1-3000X	Spectrum 1	13.61	61.61	18.89	3.77	0.67	1.44	0.20
	Spectrum 2	13.43	66.07	13.42	5.43	0.61	1.04	0.40
M9C-800°C-2-3000X	Spectrum 1	Not tested	45.4	52.42	2.18	Not tested	Not tested	0.04
M9C-1000°C-1-3000X	Spectrum 1	Not tested	47.54	52.32	0.15	Not tested	Not tested	0.00

Figure 5. 26: The microstructure of SIV-M5/M9 after various heating temperatures (e.g. M9C-650°C-1-3000X means, M9 sample, calcination temperature at 650°C, location 1, 3000x magnification)

EDX at 800°C of both samples M5C and M9C can be seen in the previous session; hence only 650°C and 1000°C are recorded here, particularly sample M9C was imaged twice by random selection to verify the reaction's repetition. Both samples are good at impurity sodium elimination. Samples with 650°C have visible carbonate shape, but not in 800°C and 1000°C. Although there is no evidence of carbon in M5C-800°C, the crushed sample in XRD shows its existence, while 1000°C displays thorough calcination in all analytical measurements. The absorbed ratios of Ca²⁺:Mg²⁺ are in both M5C and M9C. Overall, it ranks as M9C>M5C, proving more magnesium is sequestered in a carbonation stage, in accordance to the result of Section 5.2.3.2.

TGA was operated up to 1000°C in order to investigate the essence of reaction procedures.

Figure 5.27b further explains the carbonates presence at 650°C and 800°C calcinations. It is

worth noting that, only the largest peak was counted in this analysis when the temperature is lower than 650°C, in order to simplify the examination.

From other researchers' comments, seen in Section 2.12, on dolomite decomposition, at a high partial pressure of CO₂, the thermal process breaks down into two steps. This pressure has a primary relationship with the rate of air diffusion and other parameters, such as particle size. In this supplemented 1000°C calcination, samples were placed before testing, particles were then further hydrated or carbonated, naturally forming into aggregations. On one hand, these agglomerates can slow down the air diffusion, thus leading to a high partial pressure; and on the other hand, they also increase the weight loss on various stages due to extra hydration and carbonation degrees compared to the samples' weight loss in Section 5.2.4.1. The data obtained on impurity-contained minerals is difficult to be reproduced; therefore it is acceptable to have the different peak temperatures when using exactly the same products as Section 5.2.4.1.

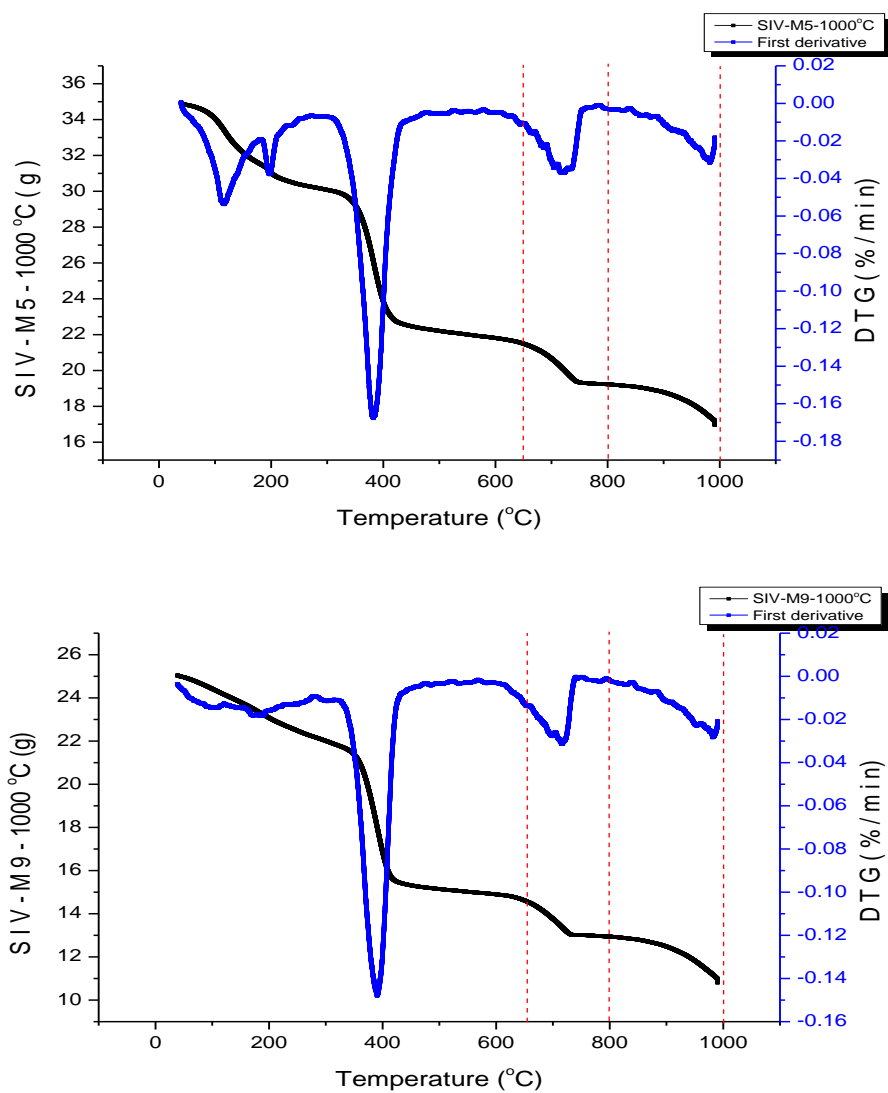
Peak temperatures and accumulated weight loss until 800°C (in both samples M5 & M9) in **Figure 5.27b** increase to some extent, comparing to the previous 800°C calcination. For example, weight loss percentage rises from 44.16% to 48.92% in M5, and 45.96% to 53.09% in M9 respectively. The reason for this growth is because of halite impurity reduction in the different operations, consistent with Bandi & Krapf (1976)'s experiment in Chapter 2.

Another mass reduction happens during the final stage of 800°C and 1000°C, indicating the incomplete decomposition with the designated 800°C calcination temperature.

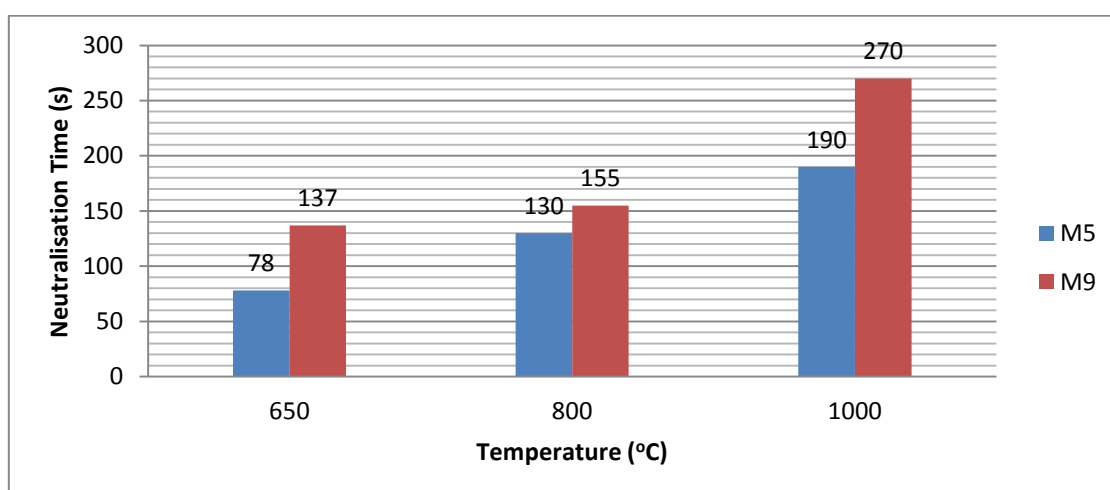
The porosity and particle sizes are reduced gradually from 650°C to 1000°C by observation (**Figure 5. 26**), which is also strongly supported by reactivity tests, based on the increasing figures of completed neutralisation. M9C depicts higher reactivity at all three temperatures compared to M5C (**Figure 5.27c**), which is attributed to more magnesium addition resulting in a higher complex system, leading to more impurities.

Sample	T < 650°C		650°C < T < 800°C		800°C < T < 1000°C	
	Peak T (°C)	Weight loss (%)	Peak T (°C)	Weight loss (%) (accumulation result)	Peak T (°C)	Weight loss (%) (accumulation result)
SI-M5-1000°C	384.78	38.37	730.03	10.55 (48.92)	988.4	11.8 (60.72)
SI-M9-1000°C	393.42	41.63	718.78	11.46 (53.09)	987.88	16.49 (69.58)

(a): The thermal stages of M5 and M9 up to 1000°C



(b): The TGA thermal stages and profiles of SIV-M5/M9 up to 1000°C



(c): The reactivity tests of SIV-M5/M9 at various calcination temperatures

Figure 5. 27: Experimental calcined M5 and M9 up to 1000°C thermal stages (a) and their thermal profiles (b), & relevant reactivity tests (c) for SIV.

5.3 Conclusions

This chapter acts as the most important series in this study, as it is based on the previous results and works towards a deeper understanding of complex seawater components.

Theoretically under this system; the products are divided into known categories, such as a CaCO_3 - Mg_2CO_3 system or a CaO - MgO system as the analysed products are mixed with these two types of compounds in different ratios. However, in practice, it is difficult to distinguish the separated CaCO_3 or Mg_2CO_3 structures; hence the entire compound is evaluated during the experiment, as well as to make further comparisons with the recognised studies.

PHREEQC estimated potential outcomes of aragonite, artinite, brucite, $\text{CaCO}_3 \cdot \text{H}_2\text{O}$, calcite, huntite, dolomite, magnesite, hydromagnesite and vaterite. They are thermodynamically favoured, but precipitates can be different in practical conditions. 10 mixtures were conducted to investigate the experimental parameters' influences on multiple $\text{Mg}^{2+}:\text{Ca}^{2+}$ ratios. Samples 1 to 4 were one group, which had a larger proportion of calcium, while samples 5 to 10 were synthesised based on 10x concentrated seawater. Two selected samples M5 and M9 were subsequently calcined to study the effects of various heating temperatures. All mechanical analyses experiments were undertaken to make a comprehensive and systemic exploration, for instance ICP, XRD, SEM, TGA and reactivity tests. In particular, a special proposed reactivity was utilised in this study due to the absence of documentation.

Carbonation studies continued to present the exothermal reaction and the stable pH during the experiment. It was discovered that, at a high temperature, heat was harder to identify. Therefore room temperature operations were more representative of this exothermal reaction. pH stability remained constant after maximum 2min adjustment, proving the reliability of this test. In XRD precipitates' identification, four stages were summarised during carbonations: initial stage, intermediate stage, transitional stage and completed stage. Brucite had the tendency to transform into magnesian calcite after a long time, and aragonite as well as MHC was more stable in the presence of magnesium. From the analysis, pH was the main determining factor, followed by temperature, CO_2 flux rate and final stirring speed. A lower pH and a higher temperature both had a positive influence on the formation of deposits. MgCO_3 and CaCO_3 were shown in SEM. For example rosette-like shapes had higher amounts of magnesium, while rounded or cubic particles had abundant

calcium. A greater possibility of magnesium's and calcium's capture was caused by the higher pH and the elevated heat, recorded by ICP.

A more sophisticated particles' formation mechanism was found out after combining the three types of the quantitative analysis of XRD, SEM and ICP. This demonstrated that in an exceeded calcium aqueous (samples 1-4) system, calcium carbonates formed at first, accompanied by magnesium incorporation, and then there was more calcium participation as time passed. This was different from a magnesium heavy solution, presenting the magnesium calcium carbonates formed as the inner core, subsequently covered by calcium carbonates, and magnesium carbonates as the exterior surface. Additional impurity (sodium) participation was also pictured with the appearance of the prominent fish-scale-like morphology, while the sample of 1 to 1 ratio in $Mg^{2+}:Ca^{2+}$ displayed ovoid shapes.

Thermal analysis was carried out at $800^{\circ}C$, but increased to $1000^{\circ}C$ in the various calcinations. Peaks that appeared at $300-400^{\circ}C$ were caused by the magnesium carbonates, while peaks that appeared at $700^{\circ}C$ and above were attributed to calcium carbonates. Weight losses were well within the ranges of MC and HMCs, but halite impurity needed to be taken into consideration. $650^{\circ}C$ and $800^{\circ}C$ were not sufficient to break down the entire sample, and the subsequent peak happened at $800-1000^{\circ}C$. Moreover, a further reactivity test was conducted to show the neutralisation property, and that a higher calcination temperature resulted in a longer neutralisation time. In particular, M9C had larger numbers in all three temperatures compared to M5C, which was caused by a more complex system formation in M9, leading to a higher impurity level.

Chapter 6: Multiple Ions Carbonation and Calcination

6.1 Introduction

This chapter continues from the previous one with the subsequent. The main aim of this chapter is to investigate the effects of the additional sodium (Series V) and potassium (Series VI) ions in the selected samples by making comparisons with Chapter 5. The experiments simulate natural seawater in terms of components and mixture ratios. The procedures were similar to those used in Chapters 4 and 5 with respect to modelling, experimental design, carbonation and calcination studies.

6.2 Series V-Triple Ions Complex System

6.2.1 Model for Series V

In this system, Visual Minteq results are unreliable due to the high ionic strength exceeding the software's limitation. According to definition, ionic strength of a solution is a measurement of the ions' concentration in the solution, which is caused by ionic compounds' dissociation. The total electrolyte concentration in solution affects dissociation or the solubility of various salts, which is explained by the common ions' effect.

Therefore, model PHREEQC was conducted instead of Minteq by utilising the process of sodium chloride elimination. The addition of NaCl led to high ionic strength, which was not applicable to Minteq software. Similar to SIV, in triple ions mixture system, the input codes were 0.25mol/l MgCl_2 , 0.05mol/l CaCl_2 , and 1mol/l Na^+ , which mimicked natural seawater ratio; while in quadruple ions combination system, the input figures were 0.25mol/l MgCl_2 , 0.05mol/l CaCl_2 , 0.05mol/l KCl and 1mol/l Na^+ . All simulations were operated under an atmospheric pressured CO_2 at a room temperature.

6.2.2 Series V-Experimental Design

In this series, the most abundant element in seawater sodium was mixed to observe its influence on the process, so the resulting system is MgCl_2 - CaCl_2 -NaCl.

6.2.2.1 Experimental Parameters

M5 and M9 were selected as the representatives. Experimental parameters are in [Table 6.1](#).

Sodium concentration is restricted to 5 times that of natural seawater due to its solubility limitation, with the following equation:

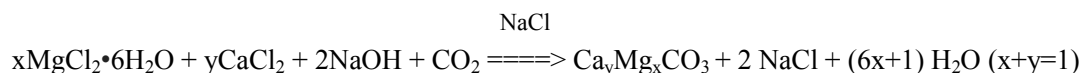


Table 6. 1: Designed parameters in SV

	Na ⁺ (M)	Mg ²⁺ (M)	Ca ²⁺ (M)	Stirring Speed (rpm)	CO ₂ flux (cm ³ /min)	pH	Temp (°C)
SV-M5	2.35	0.25	0.05	700	500	10.5	25
SV-M9	2.35	0.25	0.05	700	500	10	25

All precipitates were washed a minimum of five times. This is different from the previous cases, where deposits were only cleaned 3 times. This segment includes a test to determine NaCl impurities' elimination within the samples.

6.2.2.2 Analytical Measurements

All measurements were employed in this series, in order to make a comprehensive analysis. However, as they were all mostly covered in SIV, this part briefly demonstrates the differences from that.

ICP: Collecting points were 1.5h and 1d in aqueous phase of this study. Standard calibrations of both calcium and magnesium were 0.1ppm, 1ppm, 10ppm, and 100ppm, and their preparations were the same as previous SIV dual ions' complex system. Furthermore, extra sodium was tested independently to simplify the operations, together with individual magnesium and calcium sequestrations.

XRD: In essence, there are no dramatic variances on deposits compared to SIV-dual ions complex system, considering sodium as an impurity which can be washed off immediately after the precipitates' acquisition. In reality, NaCl tends to form into crystalised lattices and present as halite sodium interference should be determined in more detail.

SEM: There are more impurities presented in pictures; previous references are correlated to high purity level, and the deposits' pictures are the same as SIV. Exceeded sodium can be noticed visually from the Section 5.2.3.5.

TGA: Thermal properties are expected to change slightly when NaCl mixes with precipitates. Either in the case of proactive addition or passive impurities, peak temperatures reduce slightly, but decomposition steps keep the same, according to Chapter 2.

Thermal graph is seen below (**Figure 6. 1**) (Bandi & Krapf, 1976), describing that the peak temperature reduced from 750°C to 640°C if sufficient time elapsed. According to this figure, the rest of magnesian calcite (MC) shall be similar to 640°C in the **Table 5.4** of Section 5.2.2.2. However according to Bandi's further investigation, when salt-concentration is sufficient, the original 780°C (750°C is used here as a standard) can reduce to as low as 580°C. The thermal decomposition mechanism of salt-bearing magnesian calcite has two categories, one is physical magnesium and calcium atoms solid-state rearrangement; and the other is a chemical reaction to reform into magnesite and calcite prior to their decomposition.

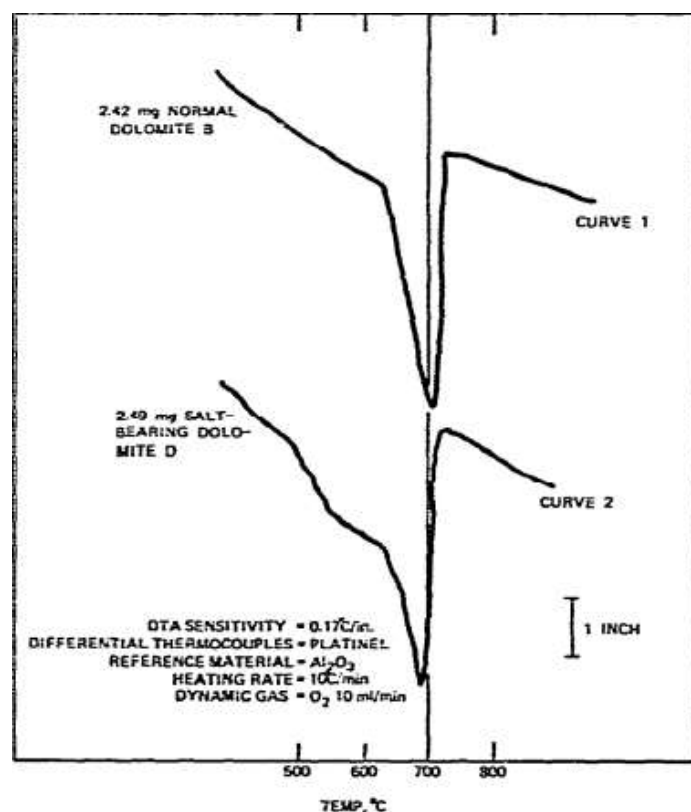


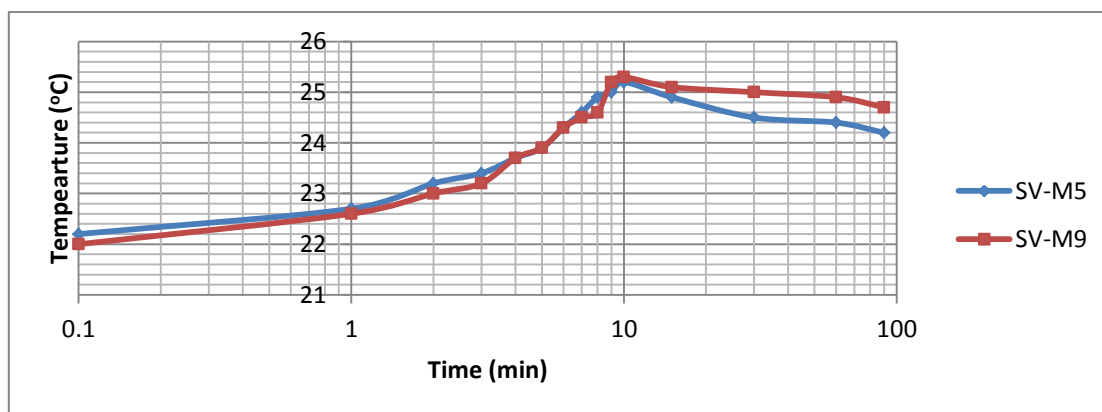
Figure 6. 1: The thermograms of normal and salt-bearing dolomites (Bandi & Krapf, 1976)

Reactivity Test: Assuming all sodium is removed after minimum five times washing of precipitates with water, and only $\text{MgCO}_3 \cdot \text{CaCO}_3$ exists in the sediment after that; so the reference test is used as the same one as SIV's. But the scaled reactivity results in this section may show the influence of sodium presence compared to a no added NaCl solution.

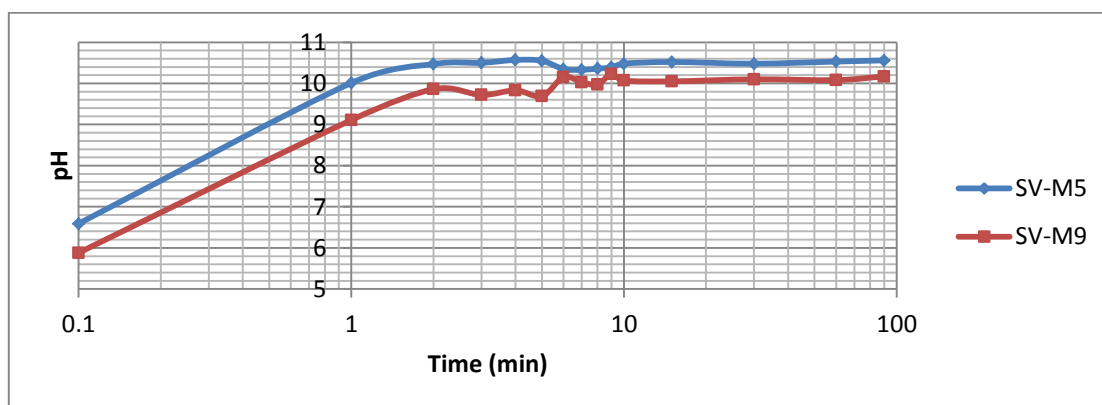
6.2.3 Series V-Carbonation

6.2.3.1 Carbonation and pH Stability Studies

Carbonation studies were accompanied by a temperature measurement. The reaction is an exothermal process, and the temperature continues to rise in the first 10min when reactants are added, and then gradually decreases for the rest of 1.5h (Figure 6. 2a). The cause of the dramatic temperature increase during the initial phase is explained by its natural exothermal reaction and the severe particle collision, which in turn generates more thermo-energy within the solution. pH stability is constant after 1min pH adjustment over 1.5h bench reaction (Figure 6. 2b), ensuring the reliability of experiments' conduction and the results' analysis.



(a): Temperature vs time in SV



(b): pH stability vs time in SV

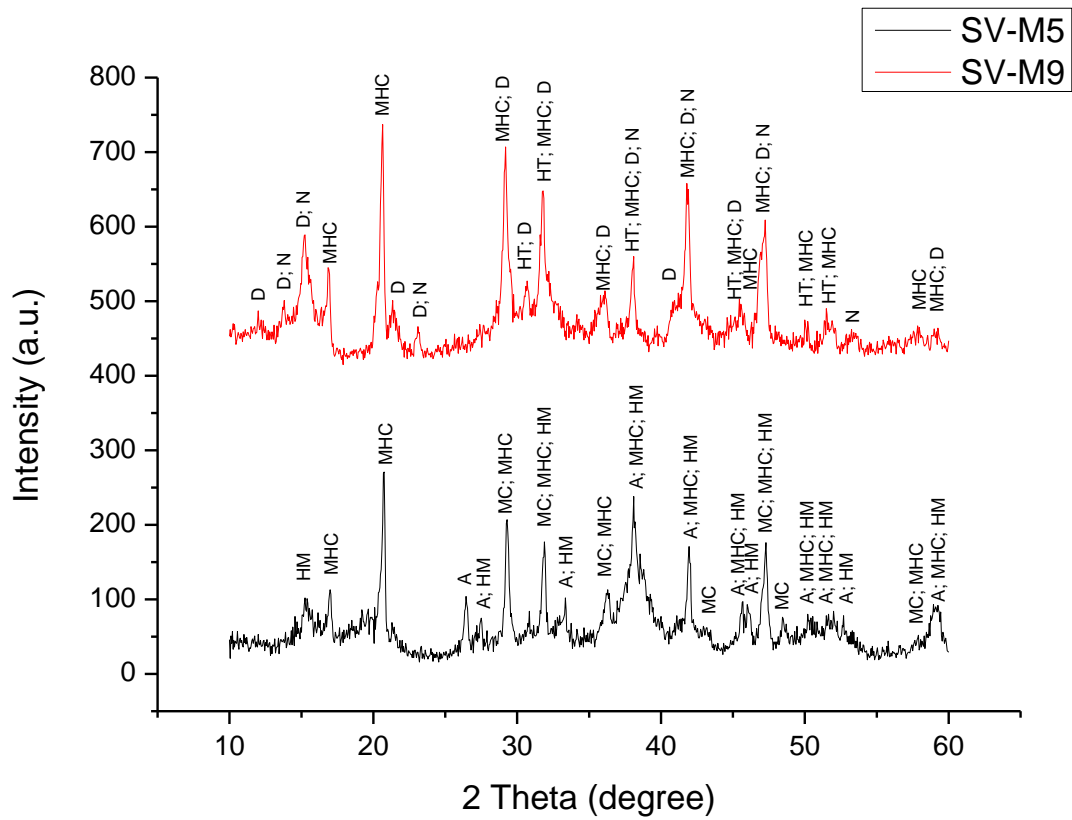
Figure 6. 2: Temperature (a) and pH stability (b) vs time in SVs shown in Table 6.1

6.2.3.2 *Precipitates Identification Studies*

Due to the complexity of magnesium carbonates, 'semiquants' calculated from the X'Per HighScore Plus software are unavailable for most of them, and hence no quantitative data is recorded in [Figure 6.3b](#). The determination of precipitates then mainly relies on the representative peaks in the graph and the matched scores in the table. However, a few semiquants were still possibly calculated by the software after eliminating MHC and HM in the precipitates. Moreover, all types of magnesian calcite components similar to SIV were picked out from the software as reference standards, in order to make the comparisons.

The distinctive HMCs peaks in the graph show that magnesium carbonates are precipitated with the assistance of sodium participation ([Figure 6.3a](#)). This observation validates Glover & Sippel's discovery in 1967, concluding that both NaCl and higher temperature can enhance magnesium addition in products. Similar to SIV, SV-M9 is more carbonated or more sophisticated than M5 due to its additional magnesium peaks and existing huntite. The reason for this is attributed to a lower pH in M9, enhancing the reaction completion, thus leading to a longer phase transformation. In addition, sample M9 passes through the early stage and moves towards the next process with more HMC formation and higher penetration of magnesium in magnesian calcite, but M5 stays at the end of an early stage of the HMC' appearance and the MC starting point.

It is worth mentioning that aragonite (CaCO_3) in M5 transfers into MHC ($\text{CaCO}_3 \cdot \text{H}_2\text{O}$) in M9, which is due to the insufficiency of magnesium concentration, because of its higher penetration degree in M9. The assumption is also supported by Lippman (1973); MHC is stimulated to precipitate at a minimum concentration of 0.01M Mg^{2+} (see Section 2.7.4). Aragonite is generally considered to be formed with higher amounts of magnesium participation with the ratios of $\text{Mg}^{2+}/\text{Ca}^{2+} \geq 4$ (Bischoff, Mackenzie, & Bishops, 1987; Brooks, Clark, & Thurston, 1950; Falini, Gazzanob, & Ripamonti, 1996; Loste, Wilson, Seshadri, & Meldrum, 2003; Raz, Weiner, & Addadi, 2000) (see Section 2.10).



(a): The precipitates of SV in XRD pattern (HT= Huntite, HM=Hydromagnesite, MC=Magnesian calcite, A=aragonite, D=Dypingite, N=Nesquehonite)

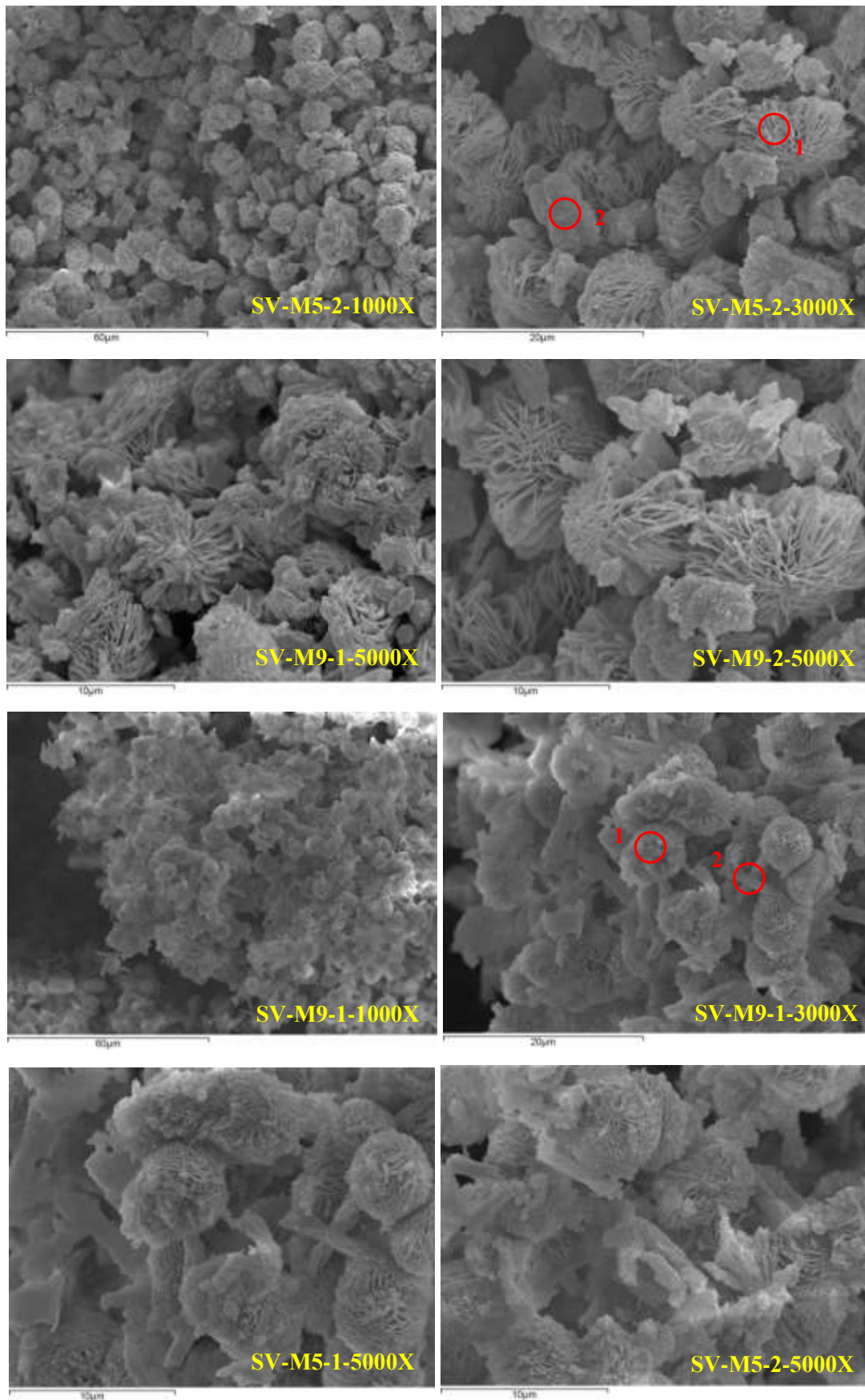
Sample			SV-M5		SV-M9	
Ref. Code	Mineral Name	Chemical Formula	Score	SemiQuant (%)	Score	SemiQuant (%)
01-071-1663	Calcite, magnesian	(Mg _{0.1} Ca _{0.9})CO ₃	25	--	0	--
01-073-1403	Huntite	Mg ₃ Ca(CO ₃) ₄	27	--	43	--
01-083-1766	Dolomite	MgCa(CO ₃) ₂	19	--	23	--
01-086-2335	Calcite, magnesian	(Mg _{0.064} Ca _{0.936})CO ₃	38	--	25	--
01-086-2336	Calcite, magnesian	(Mg _{0.129} Ca _{0.871})CO ₃	15	--	23	--
01-089-1304	Calcite, magnesium, syn	(Mg _{0.03} Ca _{0.97})CO ₃	39	--	28	--
01-089-1305	Calcite, magnesium, syn	(Mg _{0.06} Ca _{0.94})CO ₃	35	--	16	--
01-076-0606	Aragonite	CaCO ₃	51	--	Unmatched Strong	--
01-086-0174	Calcite	CaCO ₃	47	--	21	--
00-044-1482	Brucite	Mg(OH) ₂	41	--	14	--
01-072-1668	Halite	NaCl	36	--	35	--
00-017-0528	Monohydrocalcite (MHC)	CaCO ₃ *H ₂ O	70	--	65	--
00-005-0211	Hydromagnesite (HM)	4MgCO ₃ *Mg(OH) ₂ *4H ₂ O	34	--	33	--
00-023-1218	Dypingite	4MgCO ₃ *Mg(OH) ₂ *5H ₂ O	29	--	44	--
00-001-0130	Nesquehonite	MgCO ₃ *3H ₂ O	Unmatched Strong	--	32	--

Sample			SV-M5		SV-M9	
Ref. Code	Mineral Name	Chemical Formula	Contained in precipitates? (Score)	SemiQuant (%) (after removing HM+MHC)	Contained in precipitates? (Score)	SemiQuant (%)
01-071-1663	Calcite, magnesian	(Mg _{0.1} Ca _{0.9})CO ₃	No		No	--
01-073-1403	Huntite	Mg ₃ Ca(CO ₃) ₄	No		Yes (43)	--
01-083-1766	Dolomite	MgCa(CO ₃) ₂	No		No	--
01-086-2335	Calcite, magnesian	(Mg _{0.064} Ca _{0.936})CO ₃	Yes (38)	18	No	--
01-086-2336	Calcite, magnesian	(Mg _{0.129} Ca _{0.871})CO ₃	No		No	--
01-089-1304	Calcite, magnesium, syn	(Mg _{0.03} Ca _{0.97})CO ₃	Yes (39)	15	No	--
01-089-1305	Calcite, magnesium, syn	(Mg _{0.06} Ca _{0.94})CO ₃	Yes (35)	15	No	--
01-076-0606	Aragonite	CaCO ₃	Yes (51)	52	No	--
01-086-0174	Calcite	CaCO ₃	No		No	--
00-044-1482	Brucite	Mg(OH) ₂	No		No	--
01-072-1668	Halite	NaCl	No		No	--
00-017-0528	Monohydrocalcite (MHC)	CaCO ₃ *H ₂ O	70		Yes (65)	--
00-005-0211	Hydromagnesite (HM)	4MgCO ₃ *Mg(OH) ₂ *4H ₂ O	Yes (34)		No	--
00-023-1218	Dypingite	4MgCO ₃ *Mg(OH) ₂ *5H ₂ O	No		Yes (44)	--
00-001-0130	Nesquehonite	MgCO ₃ *3H ₂ O	No		Yes (32)	--

(b): The matching scores and semiquants of the SV-M5/M9 precipitates, calculated by software X'Per HighScore Plus

Figure 6. 3: The XRD patterns for SV-M5 and SV-M9 (a), and the matching scores and semiquants of MV-M5/M9 precipitates, calculated by software X'Per HighScore Plus (b). All samples are for SV shown in Table 6.1

6.2.3.3 *Precipitates Microstructure Studies*



Sample	Spectrum	C	O	Na	Mg	Ca	Ca ²⁺ :Mg ²⁺
SV-M5-2-3000X	Spectrum 1	43.07	42.06	1.75	11.75	1.36	0.12
	Spectrum 2	33.71	45.02	1.11	4.45	15.71	3.53
SV-M9-1-3000X	Spectrum 1	22.85	56.89	0.86	17.57	1.83	0.10
	Spectrum 2	19.67	65.79	0.19	4.84	9.51	1.96

Figure 6. 4: The SEM images of SV-M5/M9 at various magnifications & corresponded EDX results (e.g. SV-M5-2-3000X means sample SV-M5, location 2, 3000x magnification)

All photos in **Figure 6.4** were carefully selected to show the representative sodium assistance within the initial precipitates. Compared with SIV carbonations, both M5 and M9 present more magnesium carbonates from morphologies, with typical rosette-like style, in accordance with XRD. The ratio of Ca²⁺:Mg²⁺ has undoubtedly pointed out this phenomenon with much smaller numbers than equivalent tests in SIV. Overall, reactants' ratios in M5 and M9 are similar to SIV, but present apparent differences, which can be concluded that sodium addition has the benefit of enhancing magnesium participation, and thus reducing the phenomenon of a lower pH's contribution to magnesium incorporation.

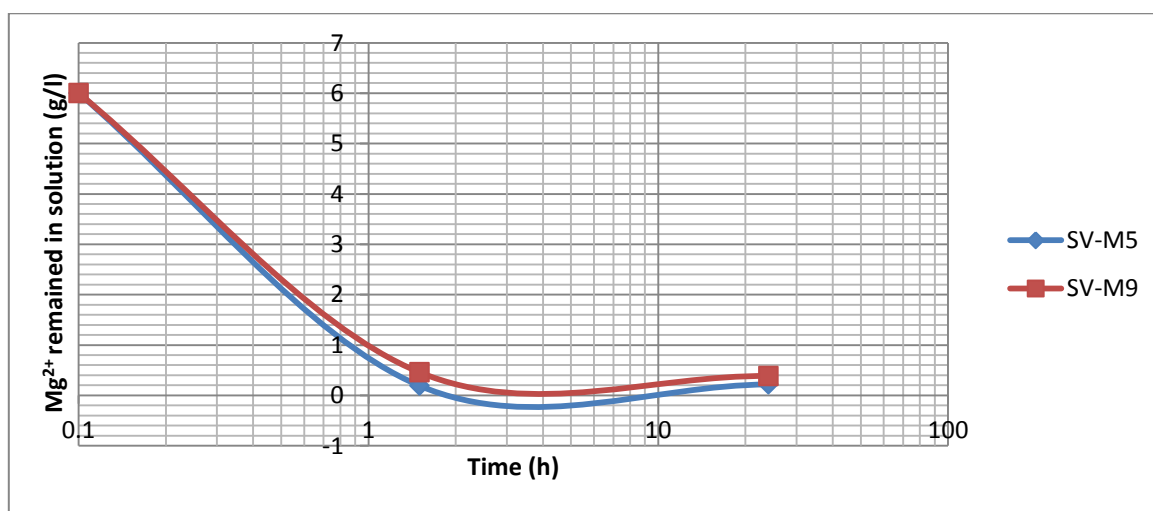
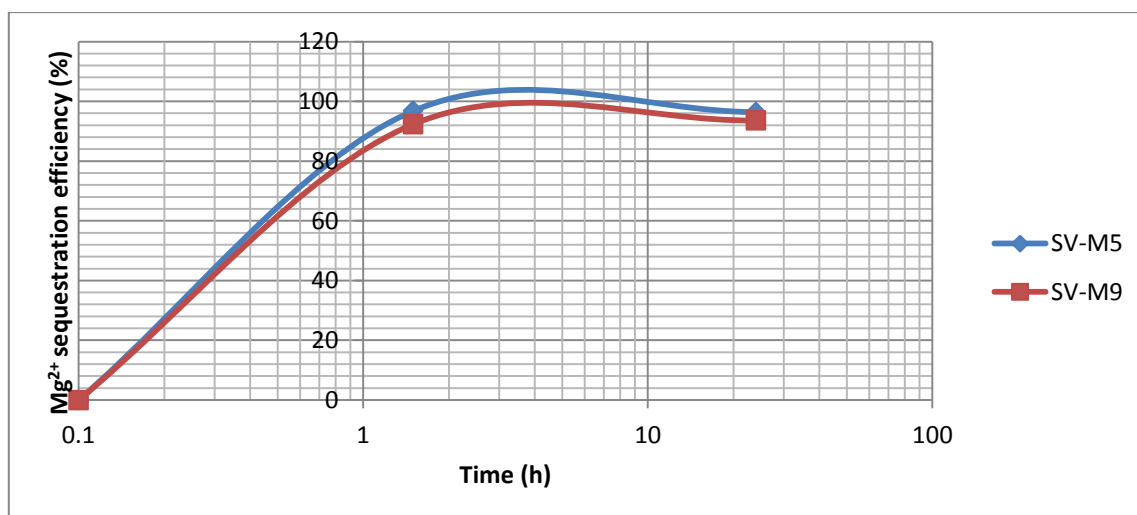
6.2.3.4 Reaction Kinetics Studies

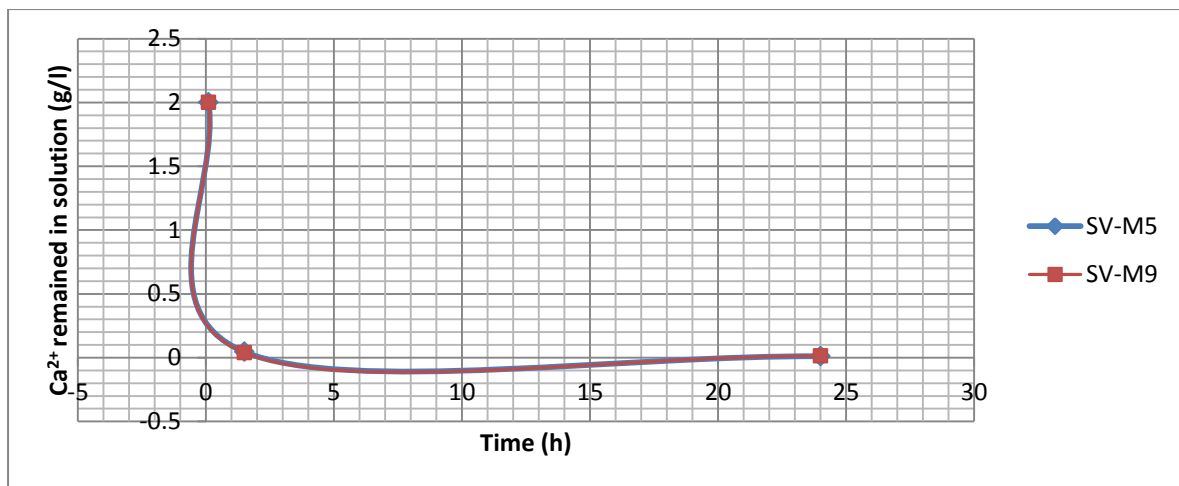
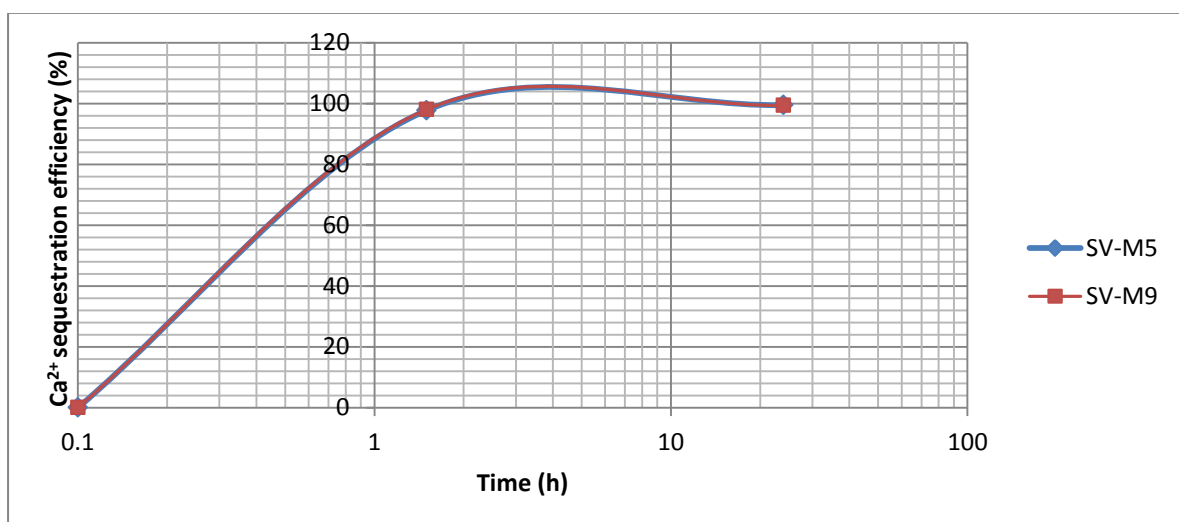
Reaction kinetics studies were carried out with usual 1.5h and 1d collections. Both M5 and M9 display promising calcium capture efficiency, although M5 is less than M9 in this set, the reverse of usual observations (**Figure 6. 5c-d**). It is understandable that the normally presented performance does not apply to all cases in such high sequestration, because any minute uncontrollable factor can affect the results. However, M5 continues the usual trend with a higher magnesium capture level because it has a higher pH degree than M9 (**Figure 6. 5a-b**).

It is assumed that the degree of supersaturation in SV is larger than SIV, with the evaluation of SIV almost reaching the saturation of sodium element. In order to prove this, a more sophisticated calculation is required, as its lower initial Mg²⁺ and Ca²⁺ reactants have reversed the sodium addition effect. It is worth noting that elements' sequestration degrees in SIV are higher than their equivalence in SV, and are highly likely caused by its lower aqueous supersaturation level. These figures again support the 1.5h sufficient time theory for the metal extraction. From a ratio perspective, M5 achieves better performance than M9 due to its surplus of hydroxide ions (**Table 6. 2**).

Table 6. 2: The kinetic studies of SV-M5/M9

Sample	Ca ²⁺ (M)	Mg ²⁺ (M)	Ca ²⁺ (1.5h, g/l)	Sequestrati on%	Mg ²⁺ (1.5h, g/l)	Sequestra tion %	Ca ²⁺ :Mg ²⁺ (seques%: seques%)
SV-M5	0.05	0.25	0.045	97.7	0.192	96.8	1.01
SV-M9	0.05	0.25	0.039	98	0.458	92.4	1.06

(a): Mg²⁺ remained over time for SV(b): Mg²⁺ sequestration efficiency over time for SV

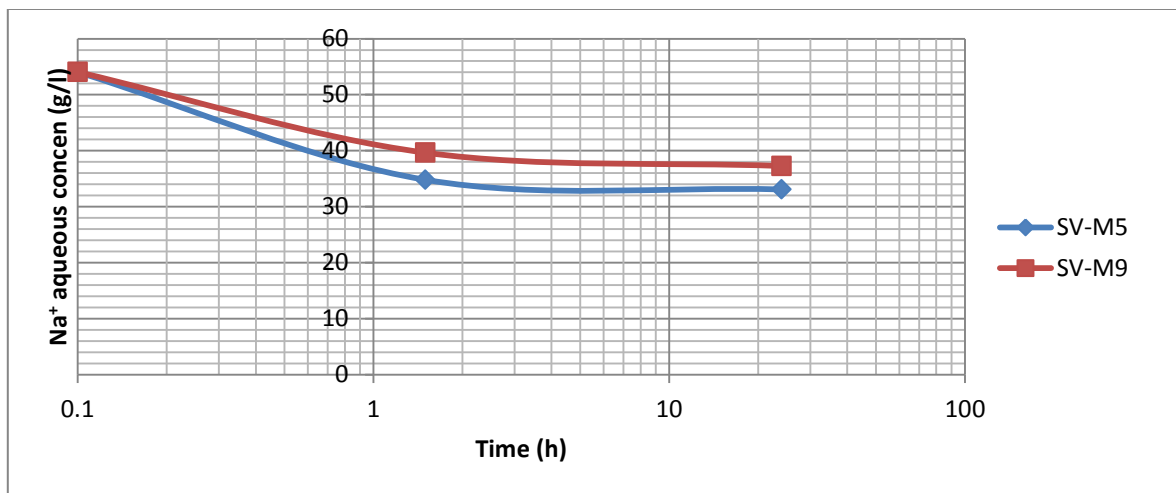
(c): Ca²⁺ remained over time for SV(d): Ca²⁺ sequestration efficiency over time for SV**Figure 6. 5: The kinetic studies of SV-M5/M9 over a day.**

6.2.3.5 Miscellaneous Studies

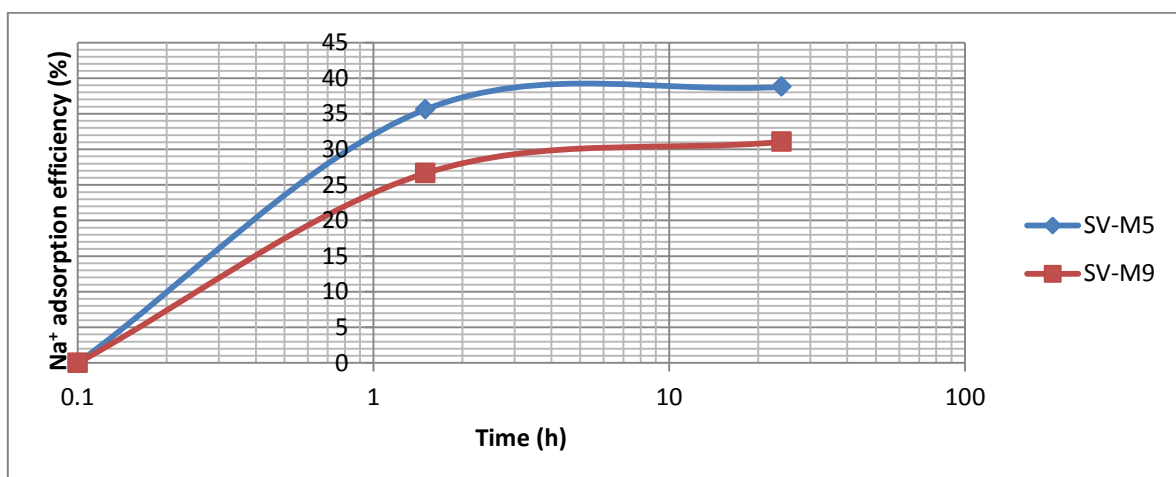
Extra sodium is added in this section of the study. This exploration aims, firstly to investigate the remaining sodium in solution over time, and secondly, the minimum washing times before the precipitates analysis.

In the first case, the sodium remains stable in solution after 1.5h, meaning the majority of sodium attaches or incorporates within sediments within a short time. From its decreasing amounts in M5 & M9 after one day, the adsorption proportions are around up to 40% (33g/l) and 31% (37g/l) respectively, caused by larger amounts of NaOH added initially to achieve

pH=10.5 in M5 (Figure 6. 6a-b). Therefore, a sophisticated cleaning process of this impurity is highly recommended.



(a): SV sodium concentration vs time

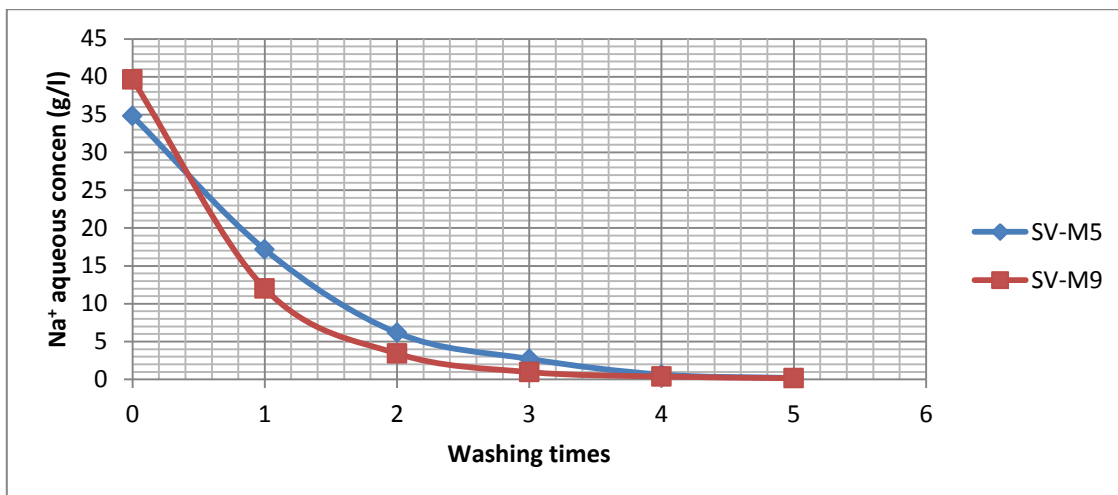


(b): SV sodium adsorption efficiency over time

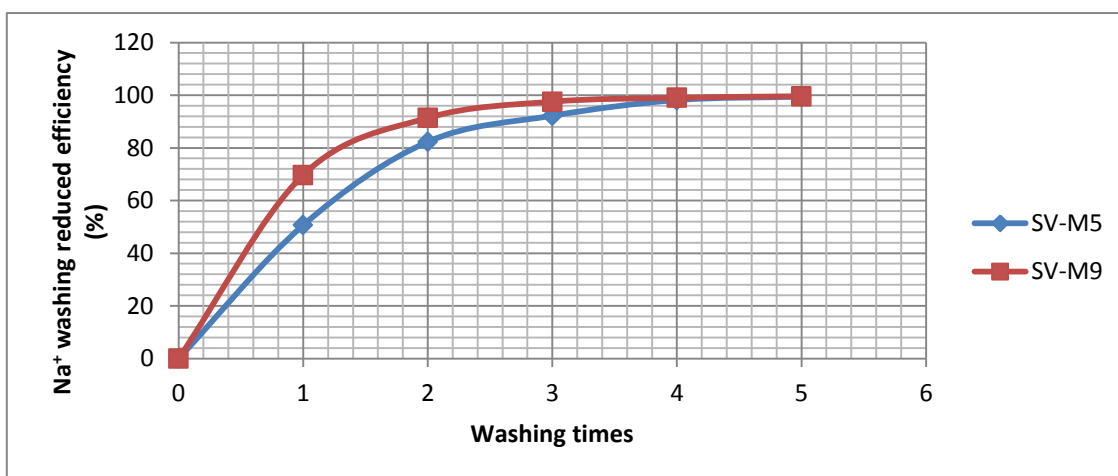
Figure 6. 6: The remained sodium over time for SV

In the second case, five washing procedures were conducted to eliminate sodium. After that, both M5 and M9 have sodium reduction up to 99.45% and 99.61% respectively (Figure 6. 7a-b). However, this figure was only 92% and 97.56% in accordance to Chapters 4 and 5 after three times washing, shown in the adequate cleaning procedures before. Moreover, it is also well accepted that not all the alkali salt can be removed in this manner as some is incorporated within the sediments' crystals (Figure 6. 7c-d).

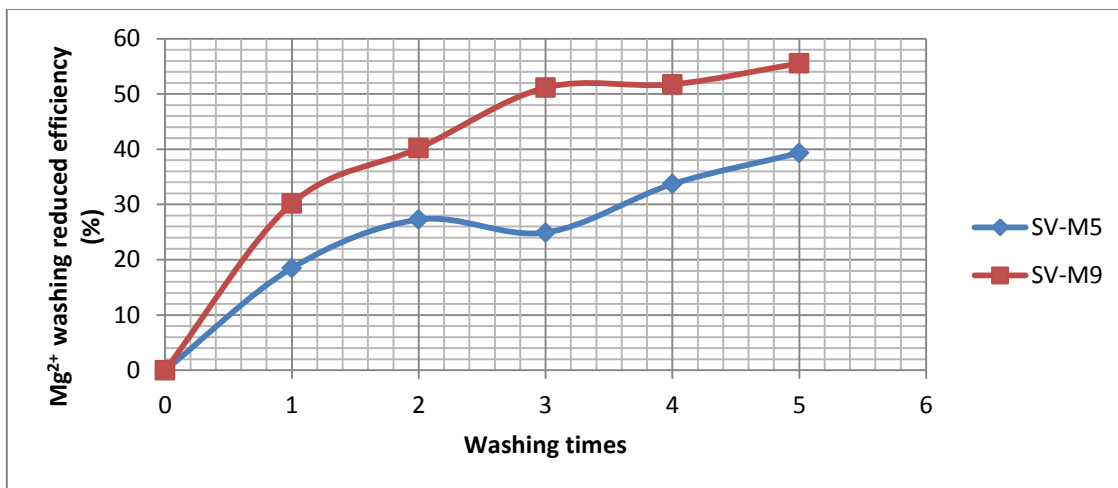
Together with sodium removal, both non-crystallised magnesium and calcium metals are washed off at the same time. It is proved that not all sequestered elements are transferred into a solid product; part of it is mixed or incorporated within the lattices of precipitates, and is similar to sodium which can be eliminated during the purification procedure.



(a): SV sodium concentration vs washing times



(b): SV sodium reduced efficiency after washing vs washing times



(c): SV magnesium reduced efficiency after washing vs washing times



(d): SV calcium reduced efficiency after washing vs washing times

Figure 6. 7: Sodium washing procedures for SV

6.2.4 Series V-Thermal Property and Calcination

6.2.4.1 The Analysis of Thermal Property

Based on the literature review in 2.12, peak temperature decreases in the presence of impurities; however, it is not always the case in practice, such as SV-M9 in the first stage and both SV-M5 & M9 in stage three of this study. Considering M5 and M9 pH differences, it is noticeable that at a lower pH (M9) condition, all stages are higher in peak temperatures except the last one, showing the theory of the more involvement of elements (M5) leading to additional disordered peaks (Figure 6. 8, DTG=Differential Thermogravimetry), mutually verified by McIntosh et al. (1990).

Analysing total weight loss, CO₂ loss significantly increases in SV experiments, which is closer to the theoretical magnesium carbonates percentage loss, although 61.29% (SV-M5) and 78.22% (SV-M9) are above the largest total loss in nesquehonite of 71%. This is attributed to the incomplete drying and a long-term duration time leading to further natural carbonation. Two peaks are shown in M5 step 3, considered by the diffusion rate of air during the process. The rate in turn relies on sample size, particle size, sample size, use of sample lids, use of static or dynamic atmosphere, and other factors according to Chapter 2.12.

6.2.4.2 The Analysis of Calcination at Various Temperatures

It is important to have the view of various temperature conditions, corresponding to different reactivity and microstructure perspectives. All XRD, SEM-EDX and reactivity tests were manipulated to validate the performance of calcined products. Both samples M5 and M9 have carbon remaining in all three calcining products, inferring that sodium addition elevated the completion of calcination temperature for precipitates (**Figure 6.9**). Ca²⁺: Mg²⁺ ratios are similar to SIV with the increased introduction of magnesium element. From a morphology perspective (**Figure 6.10**), the majority shows crushed grains without obvious voids compared to SIV's observation by the naked eye. However, the exception of sample M5C-800°C illustrates elliptical shapes or stripy particles in carbonates.

Similar results can be mutually evaluated from the subsequent TGA operation. In SIV, the last carbonation derivative peak appeared at the final stage, 800°C < T < 1000°C; but in this SV decomposition, it does not show up equivalently. This is caused by low partial pressure CO₂ leading to only one step decomposition, due to the relatively shorter duration of this trial. Two peaks are recorded during the evolution of CO₂ between 500°C and 700°C, indicating MgO is formed by more than one reaction mechanism, such as incomplete carbon release or immediate re-carbonation of MgO after the first peak endotherm. This two-peak phenomenon was found to be more usual in Chapter 4.5.4.

Sample	Step 1: Temp <200°C		Step 2: 200°C <Temp < 300°C		Water weight loss (%) (C3+C5)	Step 3: 300°C <Temp < 600°C		Step 4: 600°C<Temp <800°C		CO ₂ weight loss (%) (C8+C10)	Total weight loss (%) (C6+C11)
	Peak temp (°C)	Weight loss (%)	Peak temp (°C)	Weight loss (%)		Peak temp (°C)	Weight loss (%)	Peak temp (°C)	Weight loss (%)		
SV-M5	84.15	11.83	193.64	4.07	15.9	339.42; 402.33	28.69	712.65	16.70	45.39	61.29
SV-M9	111.61	14.33	199.01	8.18	22.51	425.06	38.75	689.68	16.96	55.71	78.22
SIV-M5	94.89	12.27	201.65	2.71	14.98	376.91	21.04	728.26	8.14	29.18	44.16
SIV-M9	101.93	9.626	205.15	2.015	11.64	382.52	25.95	721.87	8.37	34.32	45.96

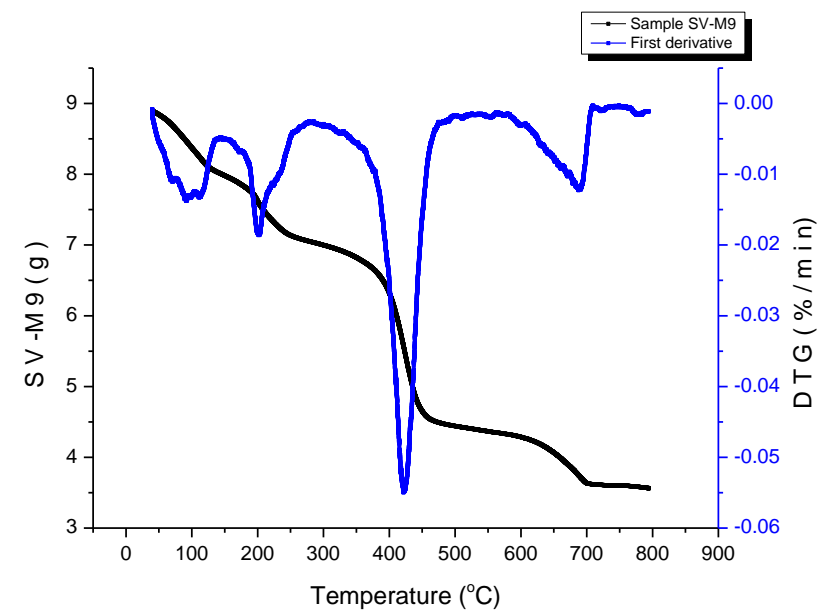
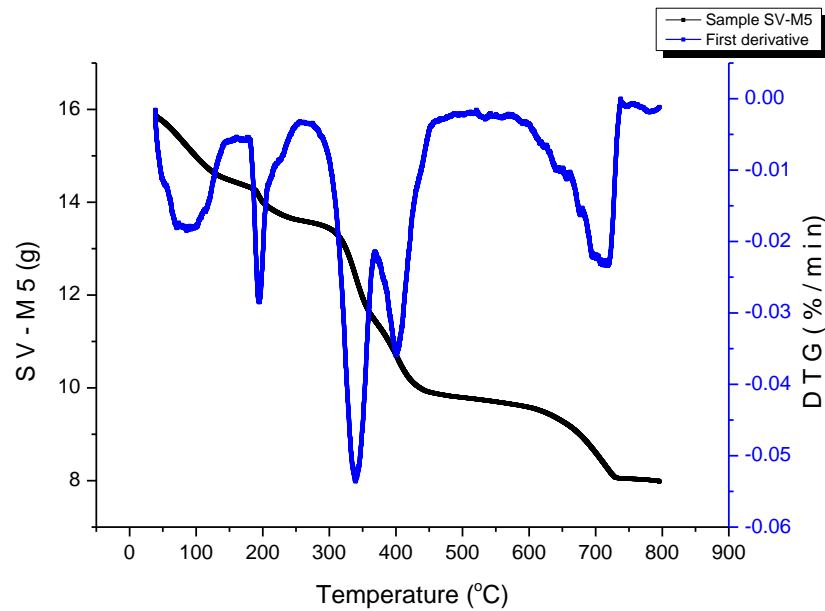
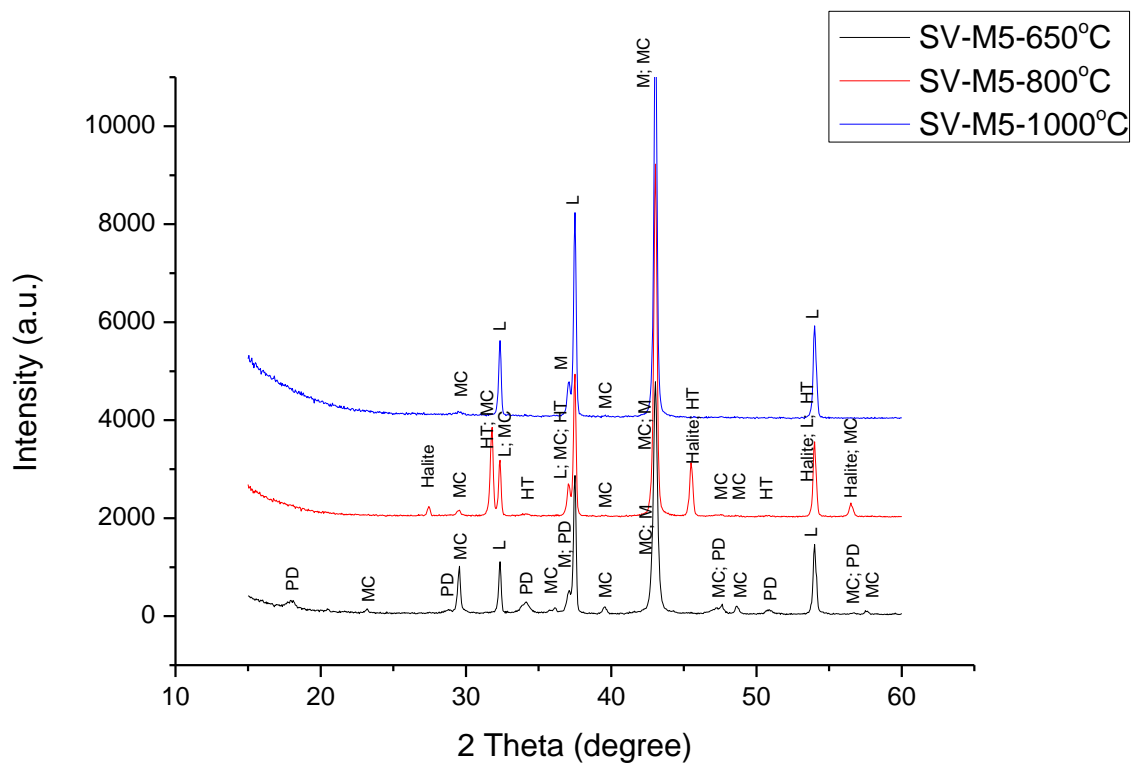
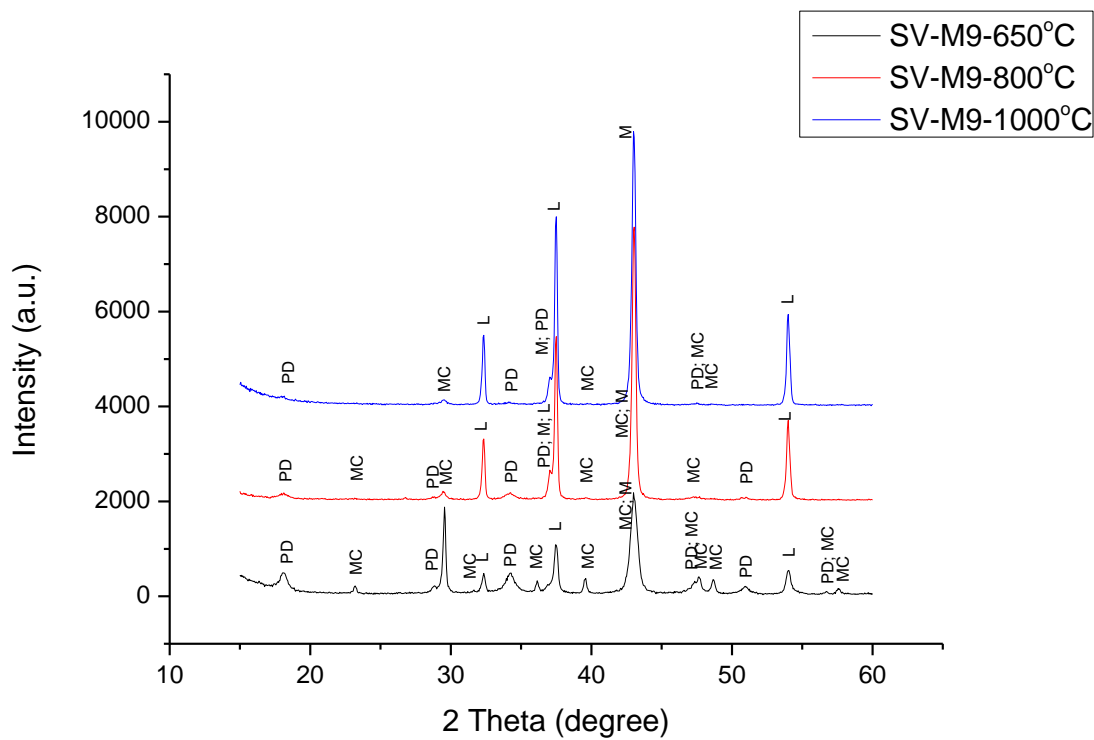


Figure 6. 8: The TGA thermal stages of SV-M5/M9 & SIV-M5/M9 (top); The TGA thermal profiles of SV-M5 (bottom left) & SV-M9 (bottom right)



(a): SV-M5 at various calcined temperatures



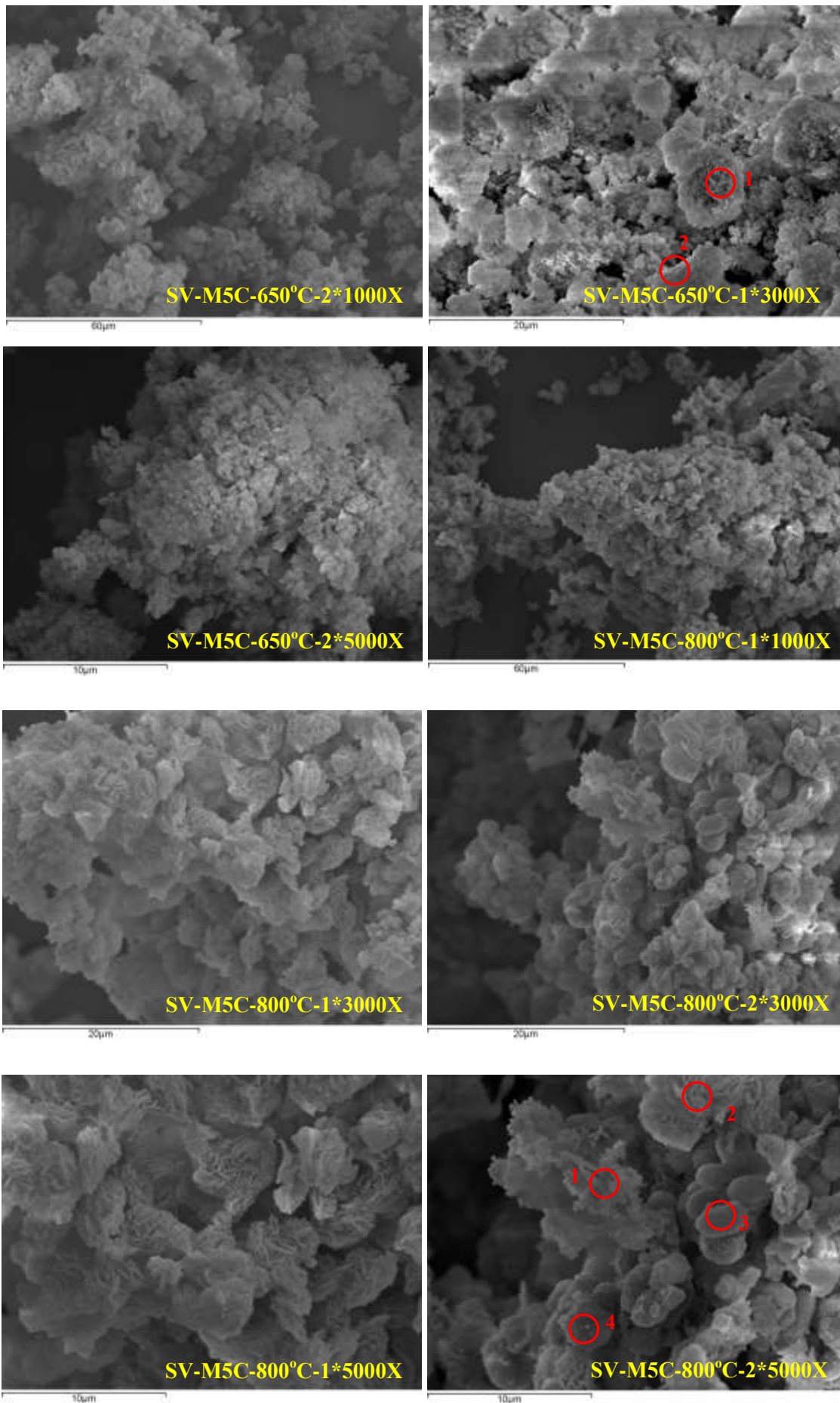
(b): SV-M9 at various calcined temperatures

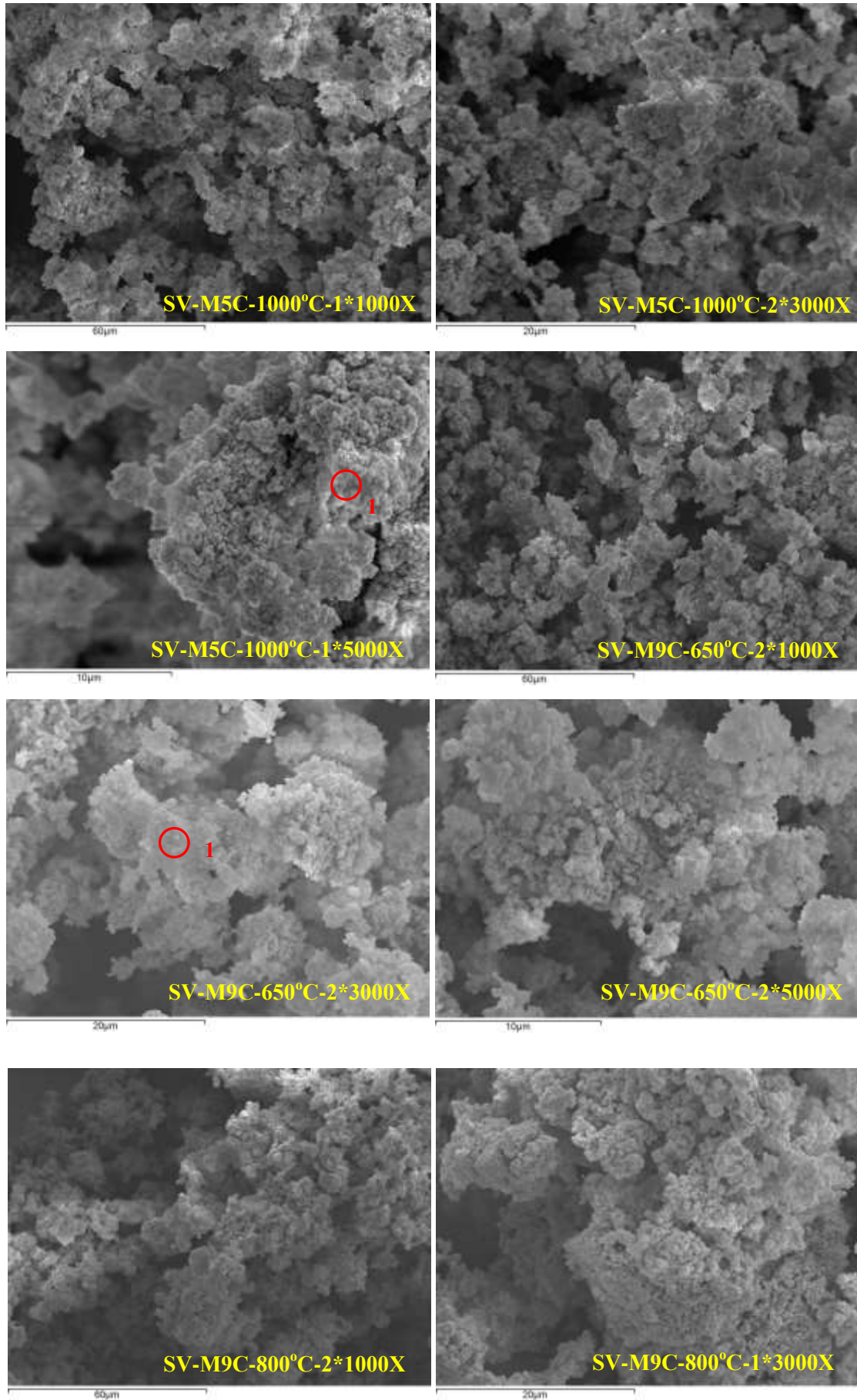
Sample			SV-M5C-650°C		SV-M5C-800°C		SV-M5C-1000°C	
Ref. Code	Mineral Name	Chemical Formula	Score	SemiQuant (%)	Score	SemiQuant (%)	Score	SemiQuant (%)
01-071-1663	Calcite, magnesian	(Mg _{0.1} Ca _{0.9})CO ₃	34	1	14	1	11	--
01-073-1403	Huntite	Mg ₃ Ca(CO ₃) ₄	12	1	24	4	4	5
01-083-1766	Dolomite	MgCa(CO ₃) ₂	6	15	9	2	6	2
01-086-2335	Calcite, magnesian	(Mg _{0.064} Ca _{0.936})CO ₃	53	9	34	1	20	1
01-086-2336	Calcite, magnesian	(Mg _{0.129} Ca _{0.871})CO ₃	32	1	18	1	0	--
01-089-1304	Calcite, magnesium, syn	(Mg _{0.03} Ca _{0.97})CO ₃	58	9	29	1	23	1
01-089-1305	Calcite, magnesium, syn	(Mg _{0.06} Ca _{0.94})CO ₃	49	8	25	1	19	1
00-043-1001	Lime, syn	CaO	49	8	49	8	44	9
03-065-0476	Magnesia, syn	MgO	44	46	43	71	38	80
01-075-0306	Halite	NaCl	5	--	51	10	0	--
01-076-0570	Portlandite, syn	Ca(OH) ₂	51	2	26	--	0	--
Sample			SV-M5C-650°C		SV-M5C-800°C		SV-M5C-1000°C	
Ref. Code	Mineral Name	Chemical Formula	Contained in precipitates? (Score)	SemiQuant (%)	Contained in precipitates? (Score)	SemiQuant (%)	Contained in precipitates? (Score)	SemiQuant (%)
01-071-1663	Calcite, magnesian	(Mg _{0.1} Ca _{0.9})CO ₃	No		No		No	
01-073-1403	Huntite	Mg ₃ Ca(CO ₃) ₄	No		Yes (24)	4	No	
01-083-1766	Dolomite	MgCa(CO ₃) ₂	No		No		No	
01-086-2335	Calcite, magnesian	(Mg _{0.064} Ca _{0.936})CO ₃	Yes (53)	11	Yes (34)	2	No	
01-086-2336	Calcite, magnesian	(Mg _{0.129} Ca _{0.871})CO ₃	No		No		No	
01-089-1304	Calcite, magnesium, syn	(Mg _{0.03} Ca _{0.97})CO ₃	Yes (58)	11	Yes (29)	1	Yes (23)	1
01-089-1305	Calcite, magnesium, syn	(Mg _{0.06} Ca _{0.94})CO ₃	Yes (49)	10	Yes (25)	1	No	
00-043-1001	Lime, syn	CaO	Yes (49)	9	Yes (49)	8	Yes (44)	10
03-065-0476	Magnesia, syn	MgO	Yes (44)	57	Yes (43)	73	Yes (38)	89
01-075-0306	Halite	NaCl	No		Yes (51)	10	No	
01-076-0570	Portlandite, syn	Ca(OH) ₂	Yes (51)	2	No		No	
Sample			SV-M9C-650°C		SV-M9C-800°C		SV-M9C-1000°C	
Ref. Code	Mineral Name	Chemical Formula	Score	SemiQuant (%)	Score	SemiQuant (%)	Score	SemiQuant (%)
01-071-1663	Calcite, magnesian	(Mg _{0.1} Ca _{0.9})CO ₃	39	4	28	1	22	1
01-073-1403	Huntite	Mg ₃ Ca(CO ₃) ₄	22	1	0	1	5	1

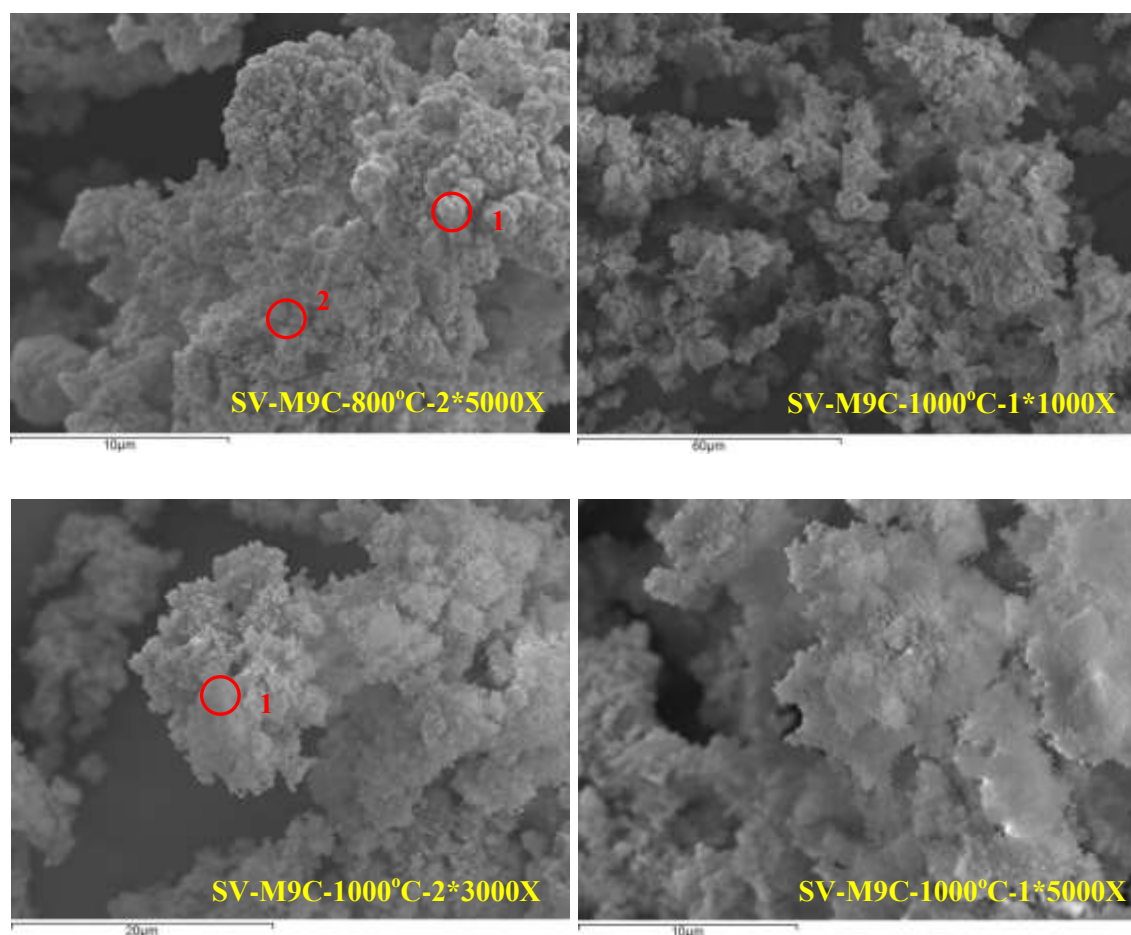
01-083-1766	Dolomite	$\text{MgCa}(\text{CO}_3)_2$	13	2	5	23	9	2
01-086-2335	Calcite, magnesian	$(\text{Mg}_{0.064}\text{Ca}_{0.936})\text{CO}_3$	62	19	35	2	30	2
01-086-2336	Calcite, magnesian	$(\text{Mg}_{0.129}\text{Ca}_{0.871})\text{CO}_3$	30	2	26	1	12	--
01-089-1304	Calcite, magnesium, syn	$(\text{Mg}_{0.03}\text{Ca}_{0.97})\text{CO}_3$	66	19	31	2	29	2
01-089-1305	Calcite, magnesium, syn	$(\text{Mg}_{0.06}\text{Ca}_{0.94})\text{CO}_3$	53	18	32	1	36	1
00-043-1001	Lime, syn	CaO	51	6	52	11	49	15
03-065-0476	Magnesia, syn	MgO	44	24	46	57	44	75
01-075-0306	Halite	NaCl	18	--	4	--	7	--
01-076-0570	Portlandite, syn	$\text{Ca}(\text{OH})_2$	59	4	53	1	27	--
Sample			SV-M9C-650°C		SV-M9C-800°C		SV-M9C-1000°C	
Ref. Code	Mineral Name	Chemical Formula	Contained in precipitates? (Score)	SemiQuant (%)	Contained in precipitates? (Score)	SemiQuant (%)	Contained in precipitates? (Score)	SemiQuant (%)
01-071-1663	Calcite, magnesian	$(\text{Mg}_{0.1}\text{Ca}_{0.9})\text{CO}_3$	No		No		No	
01-073-1403	Huntite	$\text{Mg}_3\text{Ca}(\text{CO}_3)_4$	No		No		No	
01-083-1766	Dolomite	$\text{MgCa}(\text{CO}_3)_2$	No		No		No	
01-086-2335	Calcite, magnesian	$(\text{Mg}_{0.064}\text{Ca}_{0.936})\text{CO}_3$	Yes (62)	21	Yes (35)	2	No	
01-086-2336	Calcite, magnesian	$(\text{Mg}_{0.129}\text{Ca}_{0.871})\text{CO}_3$	No		No		No	
01-089-1304	Calcite, magnesium, syn	$(\text{Mg}_{0.03}\text{Ca}_{0.97})\text{CO}_3$	Yes (66)	21	Yes (31)	3	No	
01-089-1305	Calcite, magnesium, syn	$(\text{Mg}_{0.06}\text{Ca}_{0.94})\text{CO}_3$	Yes (53)	20	Yes (32)	2	Yes (36)	2
00-043-1001	Lime, syn	CaO	Yes (51)	7	Yes (52)	15	Yes (49)	16
03-065-0476	Magnesia, syn	MgO	Yes (44)	27	Yes (46)	77	Yes (44)	82
01-075-0306	Halite	NaCl	No		No		No	
01-076-0570	Portlandite, syn	$\text{Ca}(\text{OH})_2$	Yes (59)	4	Yes (53)	1	Yes (27)	--

(c): The matching scores and semiquants of the SV-M5/M9 calcined precipitates at various temperatures, calculated by software X'Per HighScore Plus

Figure 6. 9: The XRD patterns for SV-M5 at various calcined temperatures (a), and SV-M9 at various calcined temperatures (b), and their matching scores and semiquants, calculated by software X'Per HighScore Plus(c). All samples are for SV shown in Table 6.1







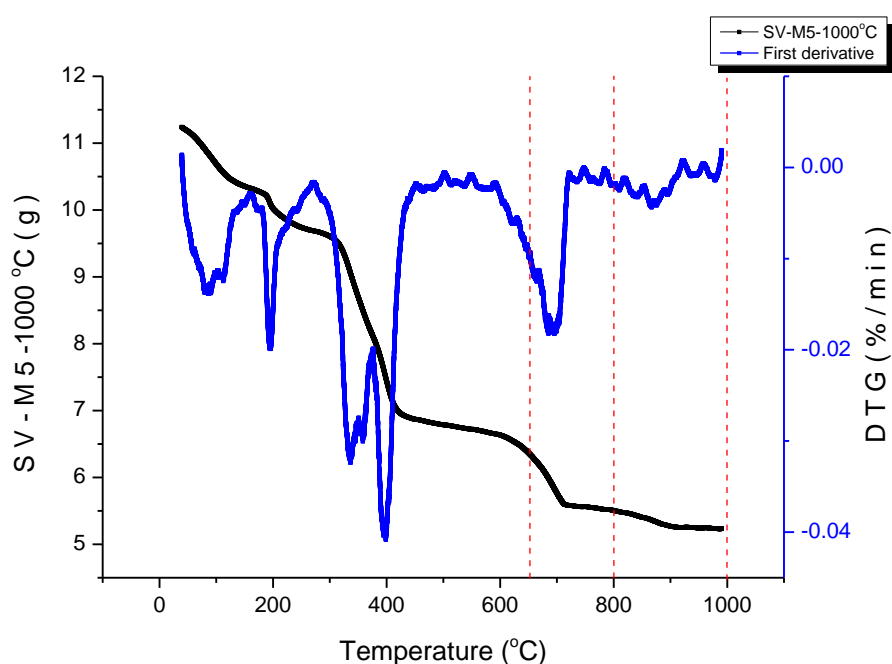
Sample	Spectrum	C	O	Na	Mg	Ca	Ca ²⁺ :Mg ²⁺
SV-M5C-650°C-1*3000X	Spectrum 1	2.38	60.71	0.8	14.57	21.54	1.48
	Spectrum 2	25.41	41.95	1.27	30.95	0.42	0.01
SV-M5C-800°C-2*5000X	Spectrum 1	19.73	44.53	0.85	30.43	4.46	0.15
	Spectrum 2	6.58	47.97	1.71	38.71	5.04	0.13
	Spectrum 3	15.35	57.29	0.69	5.38	21.28	3.96
	Spectrum 4	17.8	51.76	0.91	4.95	24.58	4.97
SV-M5C-1000°C-1*5000X	Spectrum 1	49.07	32.49	1.85	10.63	5.96	0.56
SV-M9C-650°C-2*3000X	Spectrum 1	1.87	51.23	0.69	37.33	8.89	0.24
SV-M9C-800°C-2*5000X	Spectrum 1	14.6	55.9	2.67	21.23	5.6	0.26
	Spectrum 2	53.75	26.15	0.58	18.49	1.03	0.06
SV-M9C-1000°C-2*3000X	Spectrum 1	12.5	68.48	0.21	7.58	11.23	1.48
	Spectrum 2	17.18	42.7	0.48	38.54	1.11	0.03

Figure 6. 10: The SEM images of SV-M5/M9 dolime at various calcined temperatures & corresponded EDX results (e.g. SV-M5C-650°C-1*3000X means sample SV-M5, calcination at 650°C, location 1, 3000x magnification)

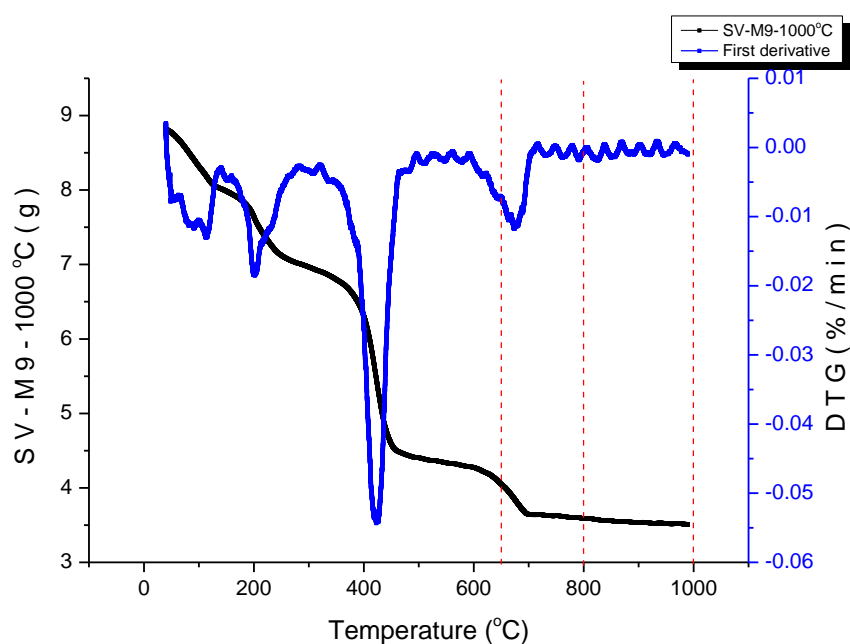
1000°C has a great similarity to thermal property analysis (Section 6.2.4.1), and this is shown by its peak temperatures and weight losses, although it is acceptable that two operations are different even if using the same particles due to the complexity of thermal decomposition. Large variations can be seen in M9 weight loss segment, as in the first test,

SV-M9 reaches 78.22% weight loss towards the end of 800°C, which is much higher than this study of 67.76% weight loss at 1000°C. This difference is estimated by the sample storage condition leading to its natural decomposition, compared to a higher hydration and carbonation degree in the original SV-M9. The continuous small undulation shape, especially in the temperature range 800-1000°C, was caused by the vibration disturbance from other lab machines running at the same time.

The results of the reactivity test are described in [Figure 6.11d](#). During the operation, hydrous citric acid ($C_6H_8O_7 \cdot H_2O$) was substituted for 650°C samples and obvious differences is shown in both M5 and M9 compared to ordinary anhydrous citric acid prescription, and this can be attributed to an additional water molecular introduction in hydrous citric acid leading to its shorter neutralisation time.



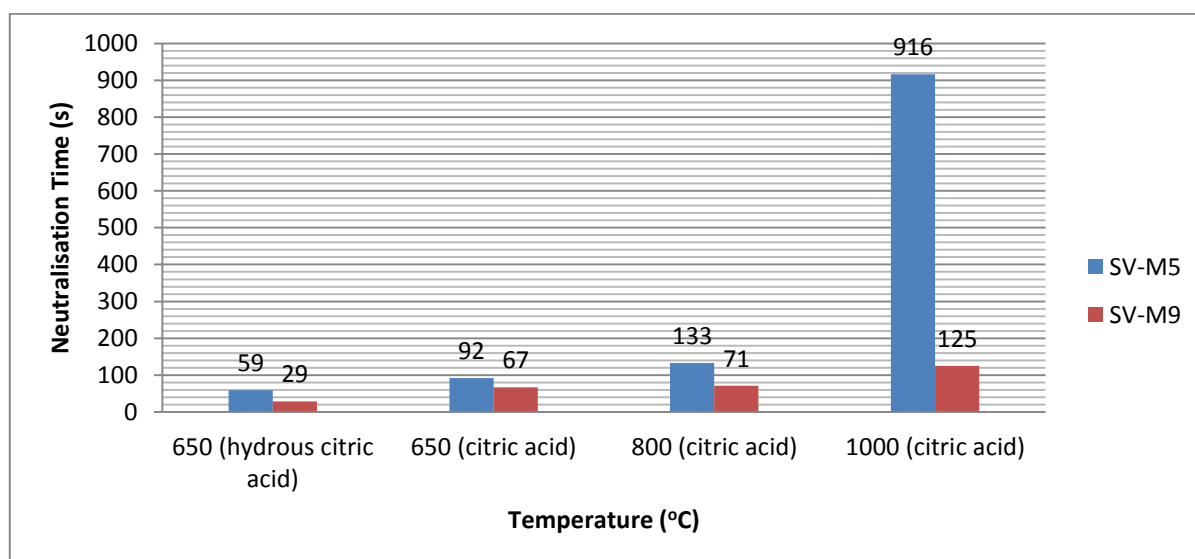
(a): SV-M5-1000°C thermal profile (DTG=Differential Thermogravimetry)



(b): SV-M9-1000°C thermal profile

Sample	T < 650°C		650°C < T < 800°C		800°C < T < 1000°C	
	Peak T (°C)	Weight loss (%)	Peak T (°C)	Weight loss (%) (accumulation result)	Peak T (°C)	Weight loss (%) (accumulation result)
SV-M5-1000°C	400.58	43.34	696.39	13.56 (56.9)	N/A	4.83 (61.73)
SV-M9-1000°C	423.48	54.04	676.07	11.44 (65.48)	N/A	2.26 (67.74)

(c): The TGA thermal stages of SV-M5/M9-1000°C



(d): The dolime reactivity results at various temperatures of SV-M5/M9

Figure 6. 11: The TGA thermal profiles of SV-M5/M9-1000°C (a & b) & TGA thermal stages of SV-M5/M9-1000°C (c), and their reactivity tests at different calcinations (d)

Similar to SIV, the precipitates obtained from the higher temperature results in a longer reactivity time due to the smaller porosity and more aggregated blocks. In addition, SV-M5 has an extended duration to complete the reaction compared to SIV-M5, but this is a reversed case in SV-M9 and SIV-M9, with an estimation of SV-M5 possessing a higher level of impurities than SIV-M5 because of the extra sodium introduction, which cannot be fully washed off in some structured embedded lattices.

The result of the reactivity test in SIV- M9 is larger than SIV-M5, which can be explained by a lower pH level in M9 trapping more magnesium, which in turn leads to a more complicated system with a higher impurity level. Conversely, SV-M9 do not show an advantage in magnesium sequestration, but has fewer hydroxide ions reducing the reaction time directly, as seen from data $SV-M9 < SIV-M9$. Overall the rank can be placed as $SV-M9 < SIV-M5 < SV-M5 < SIV-9$. A comparison graph is illustrated in [Figure 6. 12](#).

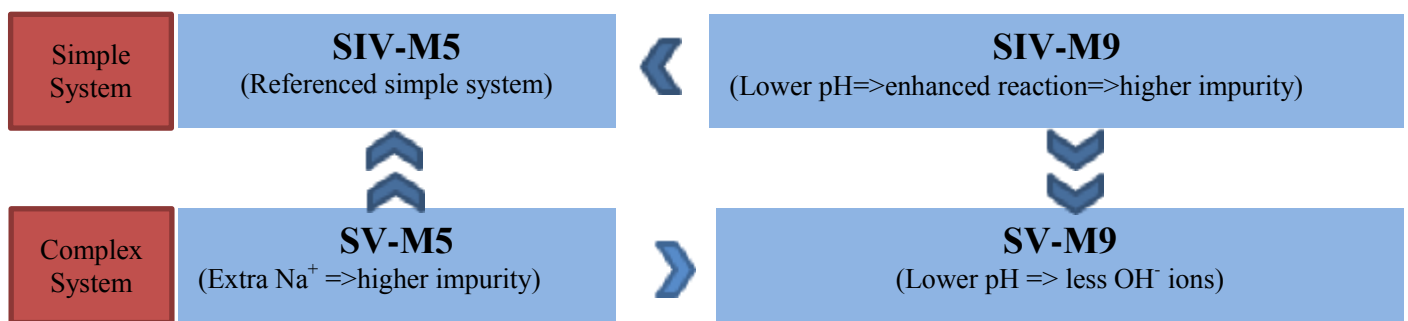


Figure 6. 12: The comparison graph in simple SIV-M5/M9 and complex SV-M5/M9 systems

It is therefore concluded that in an SIV relatively simple system, lower pH has a higher magnesium sequestration, thus increasing the contamination level due to the complex products. While in an existing complex system, such as this case, sodium has reached its maximum capacity to capture magnesium and its corresponding impurity creation; Hence pH has higher influence instead in reactivity test, for instance, more hydroxide ions are expected in a higher pH solution. In summary, it really depends on the complexity of the solution, and suggests giving the priority to firstly create a more comprehensive or supersaturated aqueous system. However, when it reaches a certain level, continuing ions' mutual interaction has no effects as they tend to perform independently instead.

6.3 Series VI-Quadruple Ions Complex System

Finally potassium as a compound of KCl, forming into a quadruple ion complex system, was added to the process, generating MgCl₂-CaCl₂-KCl-NaCl system.

6.3.1 Model for Series VI

The model is essential for this system to estimate the potential outcomes, only PHREEQC was conducted due to its exceeding high ionic strength compared to Visual Minteq. In this series, a new entry KCl was added into the model code, compared to SV; however the calculated potential precipitates were identical to SIV's model. Potassium is an active and highly soluble element. Products K₂CO₃ and KOH have high solubility in water with 112g/100ml (20°C) and 121g/100ml (25°C) respectively. Considering their dissolution, both the modelling codes and the computed results were indistinguishable from those of SIV, so no further figure of the model's result is needed.

6.3.2 Series VI-Experimental Design

This series was the condition of an ambient temperature and an atmospheric pressure operating on the lab bench. By adding a fourth element, the entire system became NaCl-MgCl₂-CaCl₂-KCl.

6.3.2.1 Experimental Parameters

In this last series of tests, potassium was added as the final cation to mimic synthetic brine, and the reactants were concentrated to 5 times more than those from original seawater. Based on the previous results, only one set of factors was selected for this final series. M5's parameters were introduced here specifically, as higher pH produces better performance in element capture, accompanied by an extra sodium participation study (Table 6. 3). The entire process was repeated to prove the reliability of the experiments, and the reaction equation is as below:

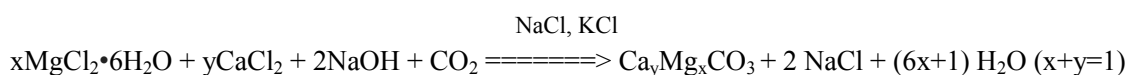


Table 6. 3: Designed parameters in SVI

	Na ⁺ (M)	Mg ²⁺ (M)	Ca ²⁺ (M)	K ⁺ (M)	Stirring Speed (rpm)	CO ₂ flux (cm ³ /min)	pH	Temp (°C)
SVI-1	0	0.25	0.05	0.05	700	500	10.5	25
SVI-2 (Na ⁺)	2.35	0.25	0.05	0.05	700	500	10.5	25

6.3.2.2 Analytical Measurements

ICP: ICP is the main testing method in the condition of ambient environment; specimen collecting points were 1.5h and 1d from the solution. Standard calibrations of calcium, magnesium and potassium were 0.1ppm, 1ppm, 10ppm and 100ppm. Moreover additional sodium was measured separately to complete the operation process.

With respect to the preparation of the standards, all calcium, magnesium and potassium ions interact independently in the solution, having no effect on each other during dilution and mixing. More data was computed from the magnesium, calcium and potassium ions sequestration efficiency and the remained sodium measurement.

XRD: XRD pictures in this section have similar profiles to SIV in 5.2.2.2, evaluated from the formed potassium compounds of large solubility.

SEM: Images may have some disturbance on products' morphologies when potassium is added; however there are not appropriate data in this potassium interference in reference research. Hence no further information is provided under this category.

TGA: Thermal property should have differences compared to non-potassium addition, based on the previous analysis. The increasing amount of salt leads to higher abnormalities of thermal curves. Remained KCl, NaCl, CaCl₂ & MgCl₂ incorporated with samples are expected to have the temperature shifting, according to Bandi and Krapf (1976). However, no specific relevant TGA reference profile can be found online.

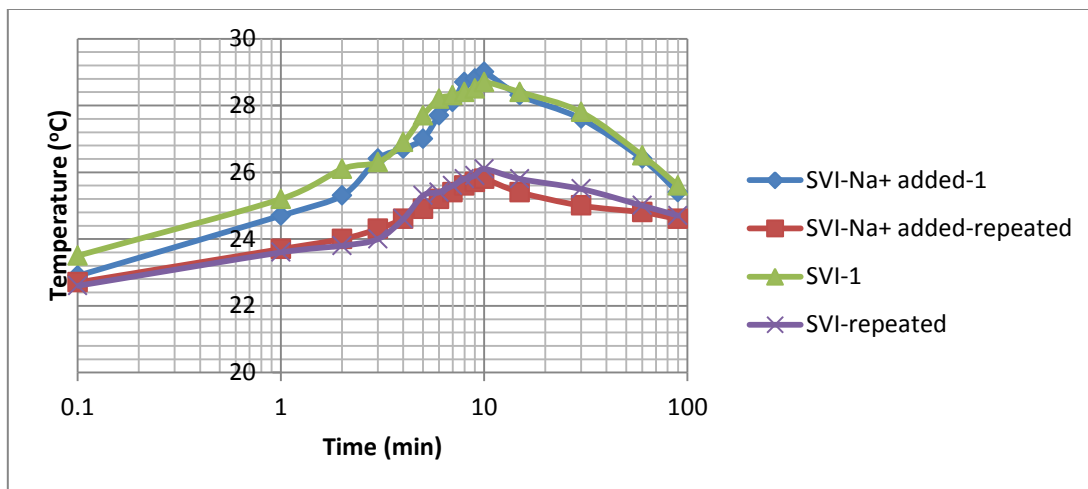
Reactivity Test: Chemical reactivity was tested as before, but physical property has more obvious changes than chemical characteristics, due to their high solubility of K₂CO₃ and KOH.

6.3.3 Series VI-Carbonation

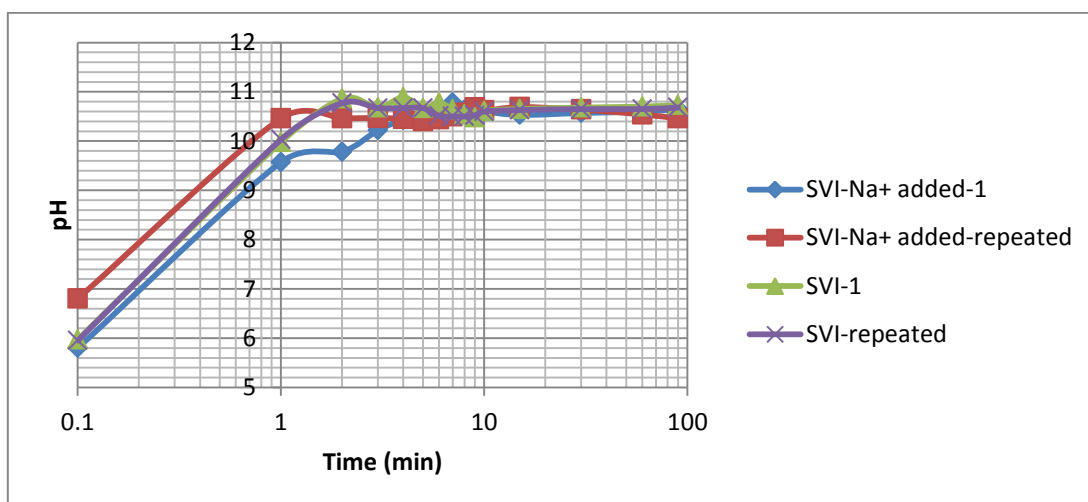
6.3.3.1 Carbonation and pH Stability Studies

Two duplicated tests were conducted, in order to provide reliable data; there was no direct interactive relationship among them. The higher temperature value in the first experiment compared to the second in both sodium-addition and non-addition sets, was caused by the latter's natural process of operation at lower ambient temperatures in the evening. Graph profile shows a similar tendency in all experiments in terms of temperature (**Figure 6. 13a**).

The stability test performs well in maintaining the constant pH level, accompanied with the temperature recording, to demonstrate the validation of this test (Figure 6.13b).



(a): Temperature vs time in SVI



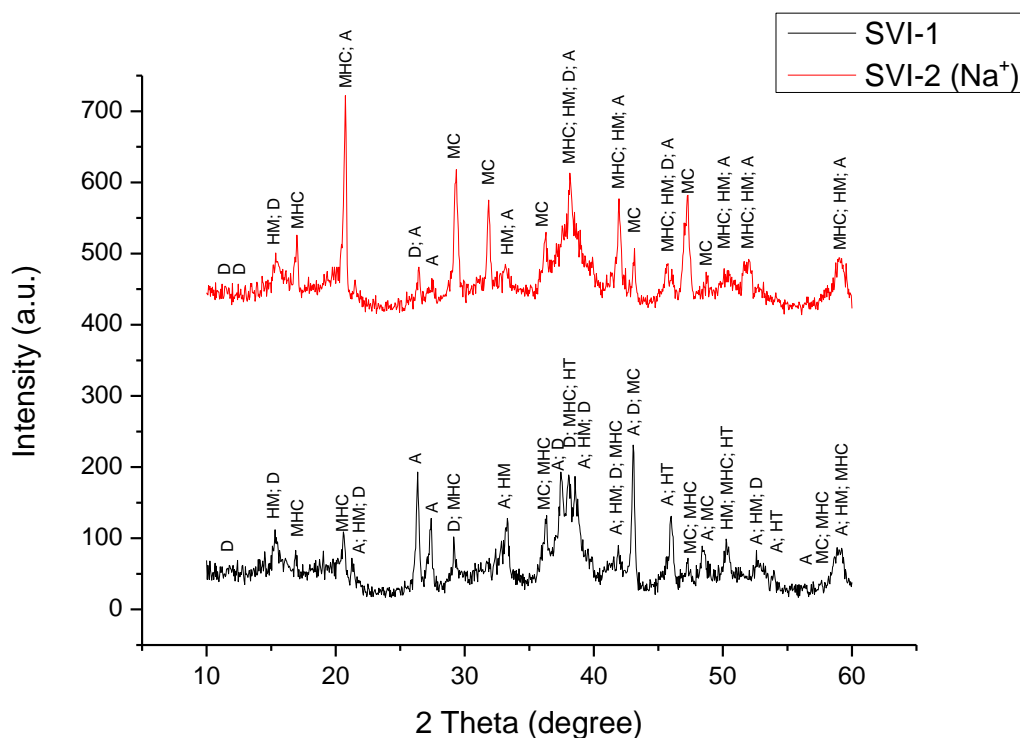
(b): pH stability vs time in SVI

Figure 6.13: Temperature (a) & pH (b) vs time in SVI

6.3.3.2 Precipitates Identification Studies

Because of the complexity of this system, no semiquants are shown in Figure 6.14b. Hence the determination of precipitates can only be justified by the components' specific peaks and scores in combination with each other. Both SVI-1 and SVI-2 (Na^+) are composed of the magnesium carbonates (HM, D), calcium carbonates (MHC, A) and magnesian calcites. Taking into account SIV-M5 (Figure 5.10a) and SV-M5 (Figure 6.9a), potassium has an equal or better effects in enhancing the formation of magnesium carbonates. This is explained by the

sample SIV-M5 without HMCs composition and the sample SV-M5 with only HM presence in HMCs group. However, both HM and D appear in this SVI-1 with the same parameters of SIV/SV-M5 (Figure 6.14a). In the addition to potassium, sodium has no advantages in the acceleration for the formation of magnesium carbonates compared to potassium. However, huntite is also observed in SVI-1, but further actions may be required to validate this, since this is not the main theme of this study.



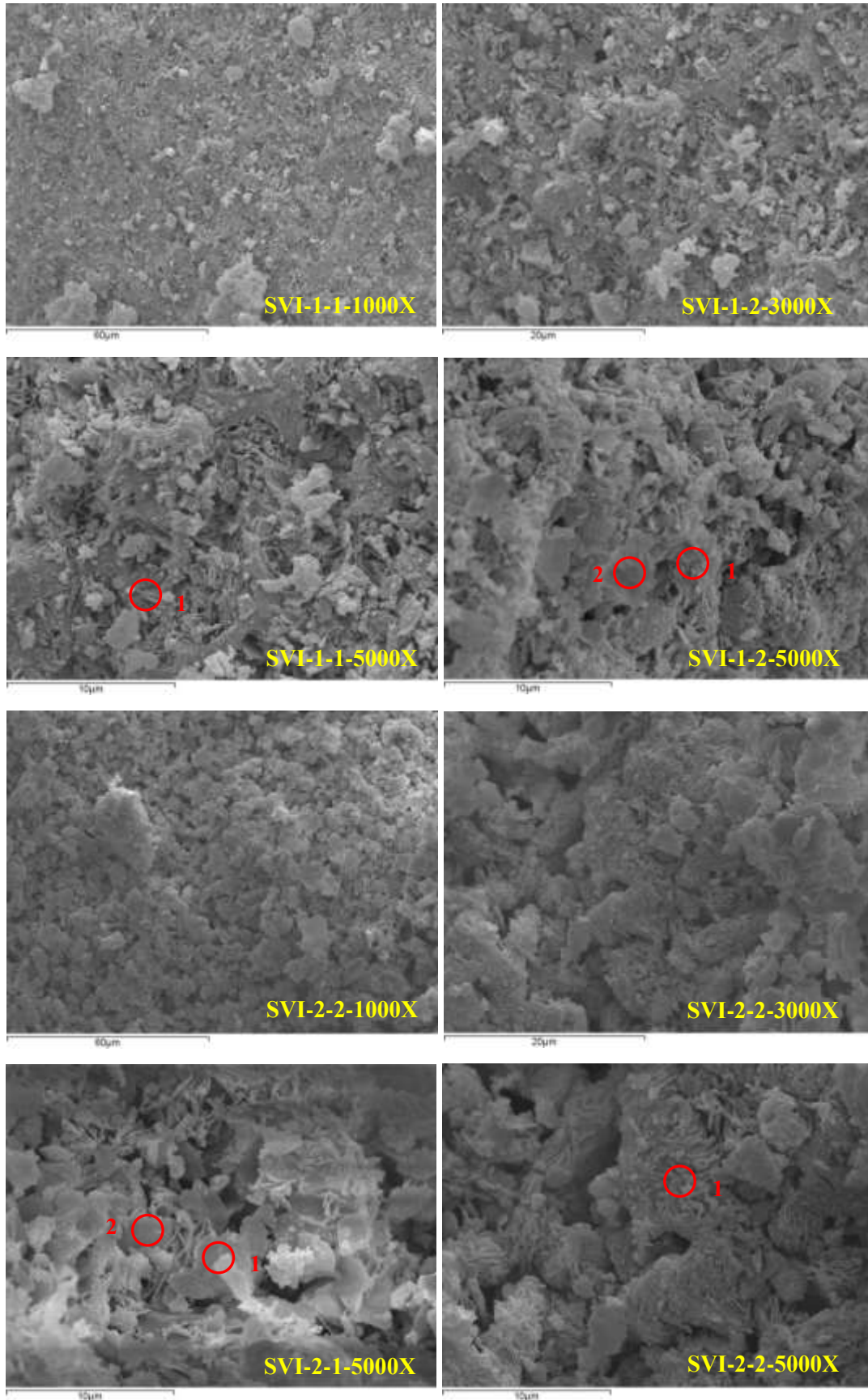
(a): Precipitates of SVI in XRD pattern

Sample			SVI-1		SVI-2 (Na ⁺)	
Ref. Code	Mineral Name	Chemical Formula	Score	SemiQuant (%)	Score	SemiQuant (%)
01-071-1663	Calcite, magnesian	(Mg _{0.1} Ca _{0.9})CO ₃	5	--	20	--
01-073-1403	Huntite	Mg ₃ Ca(CO ₃) ₄	24	--	9	--
01-083-1766	Dolomite	MgCa(CO ₃) ₂	17	--	21	--
01-086-2335	Calcite, magnesian	(Mg _{0.064} Ca _{0.936})CO ₃	19	--	26	--
01-086-2336	Calcite, magnesian	(Mg _{0.129} Ca _{0.871})CO ₃	15	--	23	--
01-089-1304	Calcite, magnesium, syn	(Mg _{0.03} Ca _{0.97})CO ₃	16	--	26	--
01-089-1305	Calcite, magnesium, syn	(Mg _{0.06} Ca _{0.94})CO ₃	19	--	30	--
01-076-0606	Aragonite	CaCO ₃	63	--	46	--
01-086-0174	Calcite	CaCO ₃	26	--	36	--
00-044-1482	Brucite	Mg(OH) ₂	31	--	34	--
01-072-1668	Halite	NaCl	4	--	39	--
00-022-0147	Monohydrocalcite (MHC)	CaCO ₃ •H ₂ O	70	--	66	--
00-005-0210	Hydromagnesite (HM)	4MgCO ₃ •Mg(OH) ₂ •4H ₂ O	31	--	28	--
00-023-1218	Dypingite	4MgCO ₃ •Mg(OH) ₂ •5H ₂ O	24	--	21	--
00-001-0130	Nesquehonite	MgCO ₃ •3H ₂ O	Unmatched Strong	--	17	--
Sample			SVI-1		SVI-2 (Na ⁺)	
Ref. Code	Mineral Name	Chemical Formula	Score	SemiQuant (%)	Score	SemiQuant (%)
01-071-1663	Calcite, magnesian	(Mg _{0.1} Ca _{0.9})CO ₃	No	--	No	--
01-073-1403	Huntite	Mg ₃ Ca(CO ₃) ₄	Yes (24)	--	No	--
01-083-1766	Dolomite	MgCa(CO ₃) ₂	No	--	No	--
01-086-2335	Calcite, magnesian	(Mg _{0.064} Ca _{0.936})CO ₃	Yes (19)	--	Yes (26)	--
01-086-2336	Calcite, magnesian	(Mg _{0.129} Ca _{0.871})CO ₃	No	--	No	--
01-089-1304	Calcite, magnesium, syn	(Mg _{0.03} Ca _{0.97})CO ₃	Yes (16)	--	Yes (26)	--
01-089-1305	Calcite, magnesium, syn	(Mg _{0.06} Ca _{0.94})CO ₃	Yes (19)	--	Yes (30)	--
01-076-0606	Aragonite	CaCO ₃	Yes (63)	--	Yes (46)	--
01-086-0174	Calcite	CaCO ₃	No	--	No	--
00-044-1482	Brucite	Mg(OH) ₂	No	--	No	--
01-072-1668	Halite	NaCl	No	--	No	--
00-022-0147	Monohydrocalcite (MHC)	CaCO ₃ •H ₂ O	Yes (70)	--	Yes (66)	--
00-005-0210	Hydromagnesite (HM)	4MgCO ₃ •Mg(OH) ₂ •4H ₂ O	Yes (31)	--	Yes (28)	--
00-023-1218	Dypingite	4MgCO ₃ •Mg(OH) ₂ •5H ₂ O	Yes (24)	--	Yes (21)	--
00-001-0130	Nesquehonite	MgCO ₃ •3H ₂ O	No	--	No	--

(b): The matching scores and semiquants of the SVI-1/2 (Na⁺) precipitates, calculated by software X'Per HighScore Plus

Figure 6. 14: The XRD patterns for SVI-1 and SVI-2 (a), and their matching scores and semiquants, calculated by software X'Per HighScore Plus(b). All samples are for SVI shown in Table 6.3

6.3.3.3 *Precipitates Microstructure Studies*



Sample	Spectrum	C	O	Na	Mg	K	Ca	Ca ²⁺ :Mg ²⁺
SVI-1-1-5000X	Spectrum 1	40.48	41.55	1.02	15.33	0.48	1.14	0.07
SVI-1-2-5000X	Spectrum 1	82.71	13.67	0.09	2.35	0.57	0.61	0.26
	Spectrum 2	30.02	43.94	0.59	4.86	0.07	20.53	4.22
SVI-2-1-5000X	Spectrum 1	38.31	44.34	0.69	12.95	0.17	3.54	0.27
	Spectrum 2	21.66	51.54	0.29	16.52	0.24	9.75	0.59
SVI-2-2-5000X	Spectrum 1	26.84	52.29	2.52	16.79	0.0	1.75	0.10

Figure 6. 15: The SEM images of SVI-1/2 (Na⁺) at various magnifications & corresponded EDX results (e.g. SVI-2-2-5000X means sample SVI-2, location 2, 5000x magnification)

Figure 6. 15 presents more tabular or fragmented morphology, conglomerating into a big block when potassium was added. The only difference, on SVI-1 no sodium and SVI-2 with sodium participation, is the latter can promote more independent particulates such as magnesium carbonate based rosette-like shapes. Additional sodium has the capability to accelerate the magnesium penetration, when all other factors remain unaltered. This is also observed from the EDX results with generally smaller numbers on Ca²⁺: Mg²⁺ ratios in SVI-2 than SVI-1, inferring the enhanced quantities of magnesium in SVI-1.

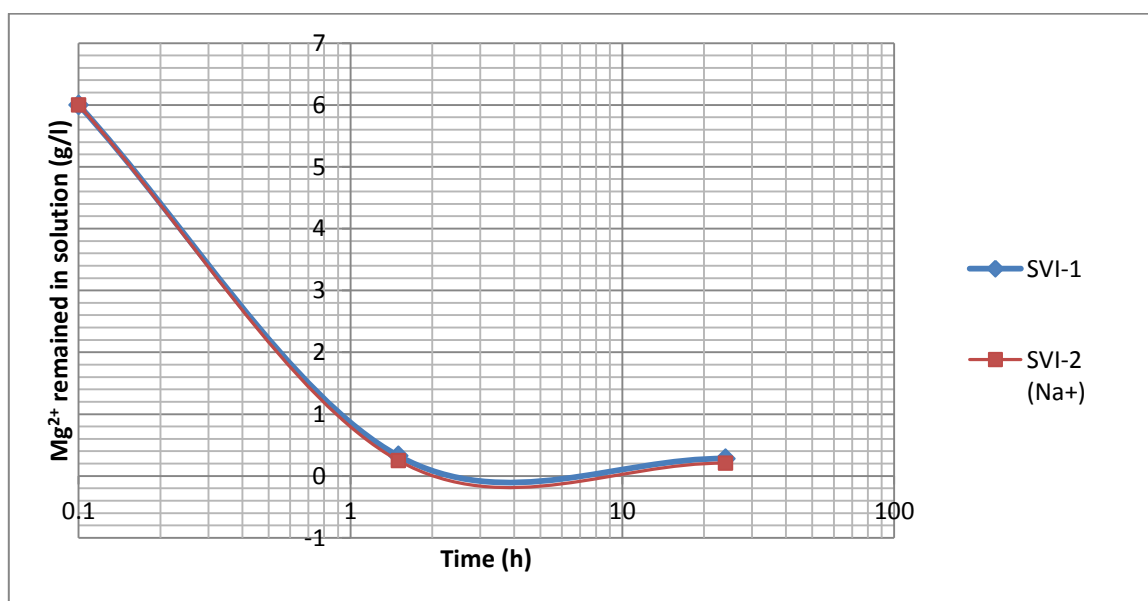
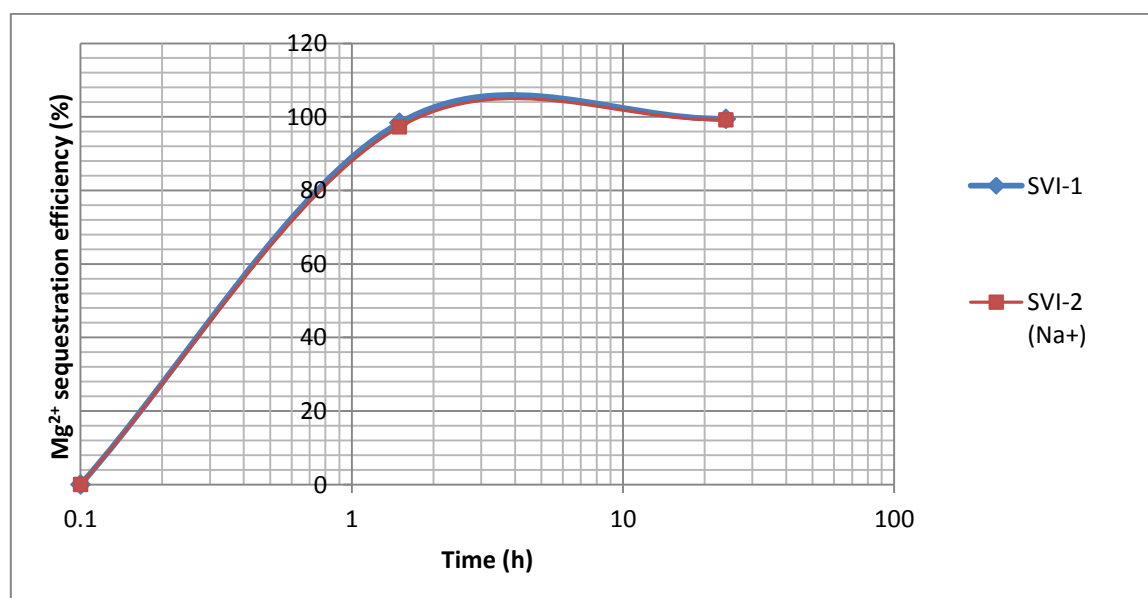
6.3.3.4 Reaction Kinetics Studies

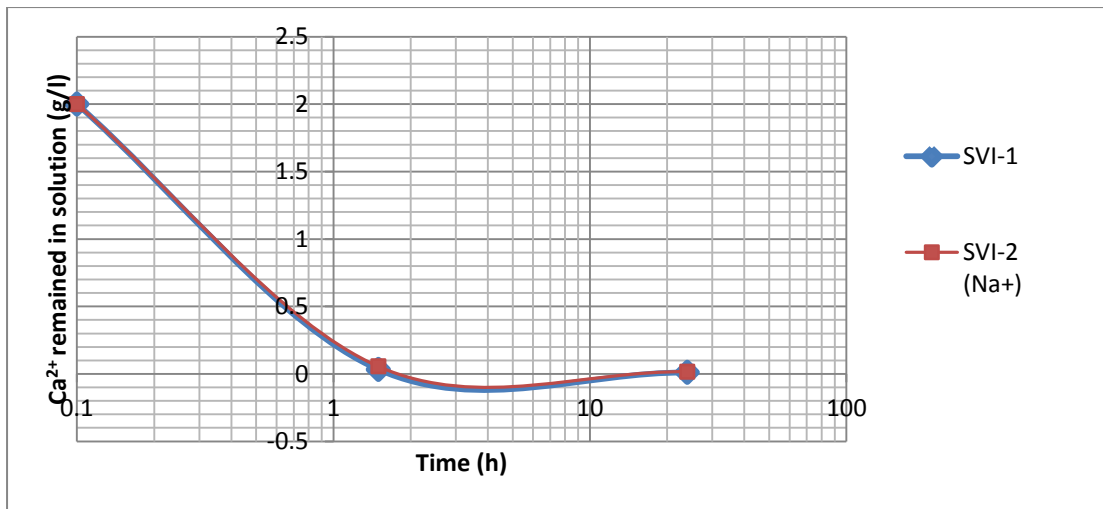
In this study, extra potassium is added on top of SV, thus testing metals including magnesium, calcium, sodium and potassium. The first two are for precipitates' formation and sequestration recording, while the latter two are for aqueous concentration and deposits' adsorption ability recording. The collection times of the samples were 1.5 hours and one day. All ions work independently except of the common-ion effect, which influences the dissociation and supersaturation degree. In order to provide reliable results, duplicated tests with errors were conducted and appear in Figure 6.16e.

It is noticeable that sodium has the tendency to increase the magnesium capture efficiency as SVI-2 illustrates (Figure 6. 16a-b), lessening calcium sequestration. Given that SVI-1 has a higher supersaturation degree by adding extra potassium, the outcome reveals a higher sequestration in calcium instead of magnesium (Figure 6. 16c-d), evaluated from a high concentrated solution. In terms of calcium alone, the result is acceptable within the errors, which are caused by uncontrollable factors. Moreover, Table 6.4 has proved adequate duration for the capture of metals after 1.5h.

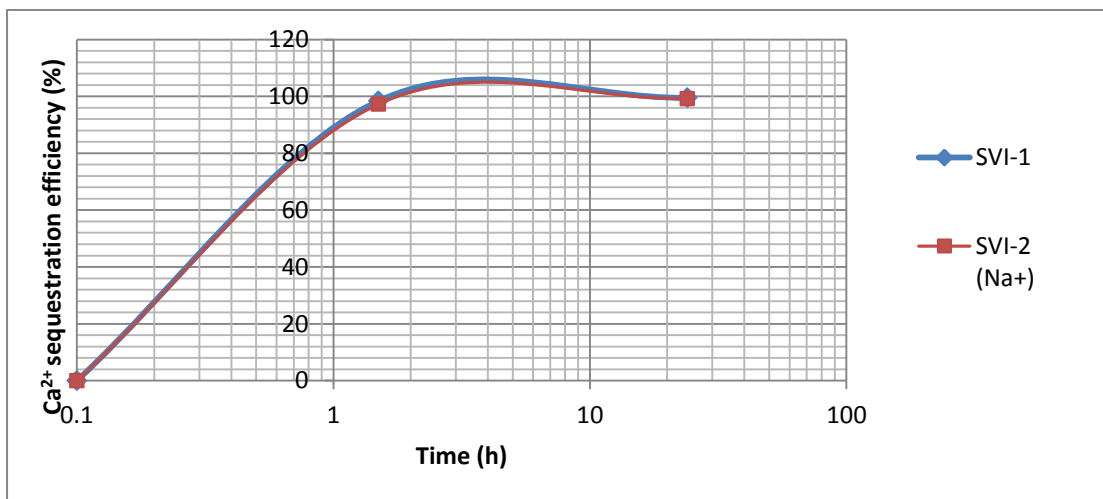
Table 6. 4: The kinetic studies of SVI-1/2 (Na^+)

Sample	Ca^{2+} (M)	Mg^{2+} (M)	Ca^{2+} (1.5h, g/l)	Sequest ration%	Mg^{2+} (1.5h, g/l)	Sequest ration %	$\text{Ca}^{2+}:\text{Mg}^{2+}$ (seques%:seques%)
SVI-1	0.05	0.25	0.032	98.38	0.326	94.57	1.04
SVI-2 (Na^+)	0.05	0.25	0.055	97.26	0.249	95.85	1.01

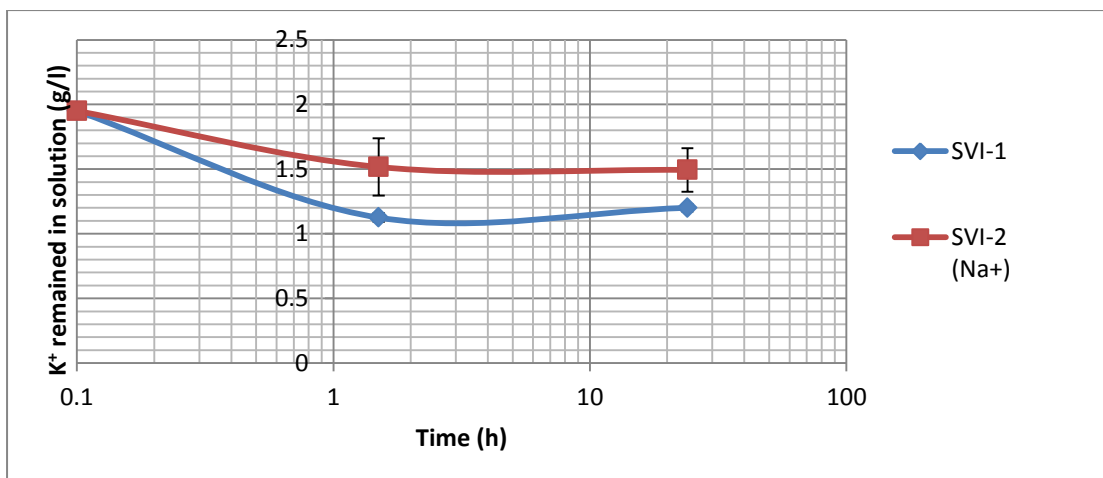
(a): SVI Mg^{2+} remained vs time(b): SVI Mg^{2+} sequestration efficiency vs time



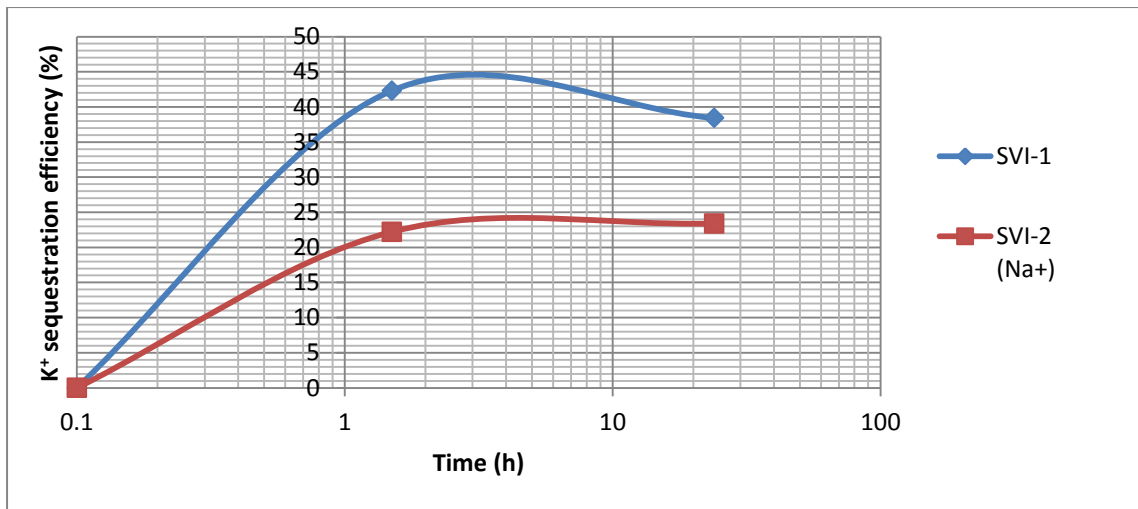
(c): SVI Ca²⁺ remained vs time



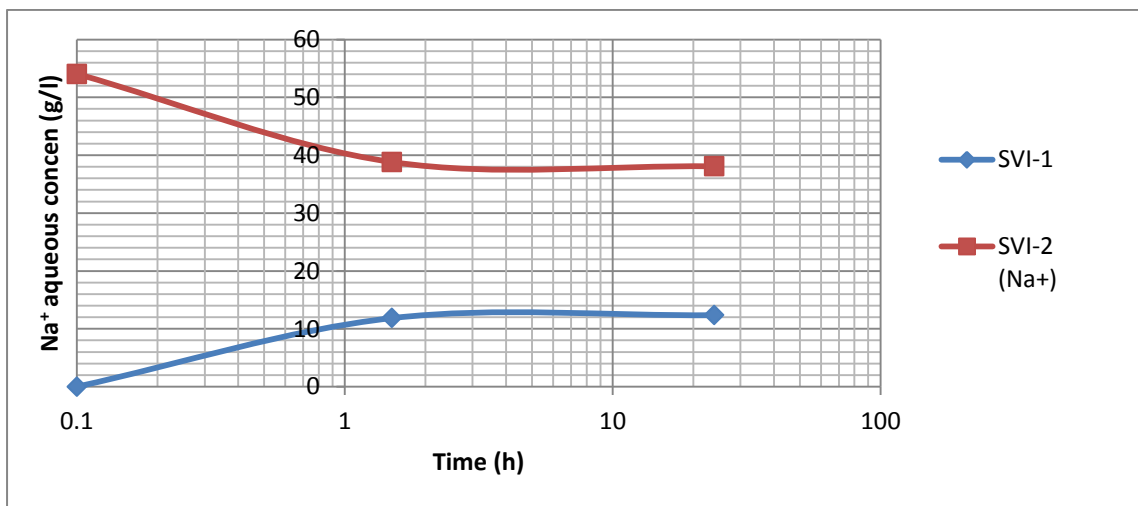
(d): SVI Ca²⁺ sequestration efficiency vs time



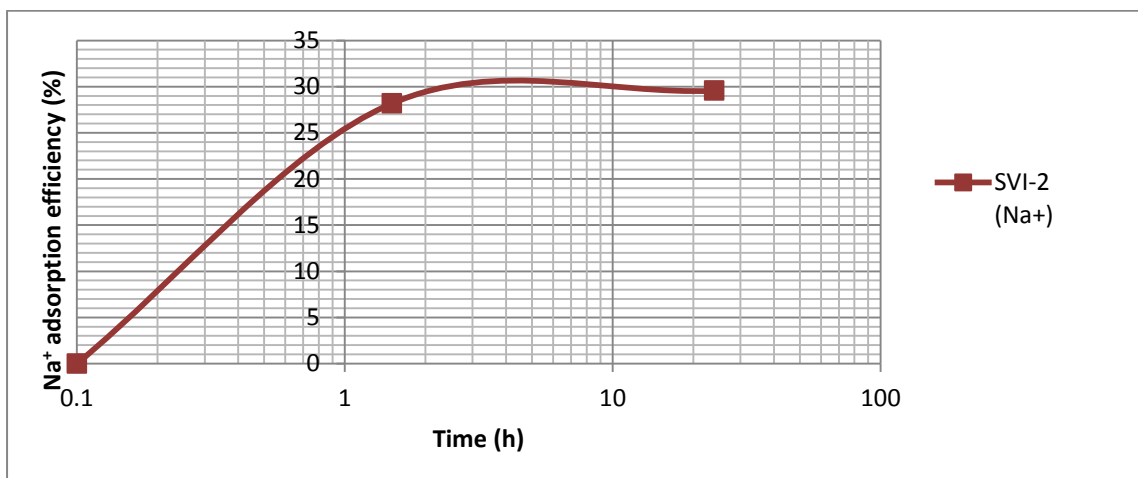
(e): SVI K⁺ remained vs time



(f): SVI K⁺ sequestration efficiency vs time



(g): SVI Na⁺ concentration vs time



(h): SVI Na⁺ adsorption efficiency vs time

Figure 6. 16: The kinetic studies of SVI-1/2 (Na⁺) over a day

Figure 6. 16 e-f demonstrate that added potassium is clearly adsorbed or incorporated within precipitates during the process because of its reduced level in the solutions after 1.5h and 1d. SVI-1 has higher sequestration value, reaching up to around 42% within 1.5h, while SVI-2 has only 22% after the same time. This is caused by extra sodium coprecipitation within the deposits of SVI-2. The sodium occupies the lattices, reducing the possibilities of potassium incorporation within the sample. It can also be estimated that, up to 40% of a specific soluble element can be physically absorbed by precipitates through incorporation within the lattice, after analysing this observation and Section 6.2.3.5. After one day, potassium sequestration efficiency declines in SVI-1 attributed to the dynamic movement of particle dissolution and reformation processes, causing embedded element potassium intake and release. Finally, separate sodium is investigated as the reaction of accompanied lattice adsorption in order to provide the information on the importance of efficient impurities' extraction.

Sample SVI-1 has no specific sodium addition. Therefore the amount of sodium found in the samples' testing is due to the process of pH adjustments as well as the precipitates' formation enhancement. 2.35M NaCl was added to sample SVI-2 at first as a reactant, based on the primary concentration of seawater. Sample SVI-1 has a starting sodium concentration of 0M, while sample SVI-2 (Na^+) is recorded based on the initial concentration of 2.35M. Finally SVI-1 sodium solution is raised to around 12g/l, enabling the alkaline input to reach the desired pH level of 10.5. This measurement can also vary in different conditions. Sodium adsorption after 1.5h in SVI-2 is around 28% (**Figure 6. 16g-h**), less than the usual 30-40% level recorded in SV, which is partially different from the potassium addition in the same aqueous phase.

6.3.4 Series VI-Thermal Property and Calcination

Detailed thermal investigations were conducted in this segment, as well as an 800°C calcination temperature. Although it is known that this temperature is not sufficient to fully calcine the carbonates, the moderate heat is easy to be operated, analysed and widely utilised, corresponding to one of the main themes of this study—to produce a light-burned reactive magnesia or dual-oxide (temperature range 700°C-1000°C).

6.3.4.1 The Analysis of Thermal Property

The thermal analysis of this test aims to provide a further illustration the effects of added salts. Irregular peak temperatures are presented by the increased salts' concentration and the interference of crystalline formation. No significant differences are noticed in SVI-1 and SVI-2 (**Figure 6.17**, DTG=Differential Thermogravimetry), and both samples are in the range of thermal loss percentages of magnesian calcite and HMCs. Especially in carbon weight loss, experiments display the almost theoretical magnesian calcite's carbonation degree, thus providing the validation of this test from temperature aspect.

6.3.4.2 The Analysis of Calcination at a Certain Temperature

800°C was used for decomposition, the most common investigated temperature. Likewise, this heat is not adequate to fully break down the carbonates, and the existence of portlandite is due to the rapid lime-hydration (**Figure 6.18 a-b**).

Morphology displays finer particles in SVI-2 than SVI-1 based on the sodium introduction, close to SV and SIV comparison's graph. Sodium distorts the natural carbonation, and embeds its metal within the intersection of particles, causing a more sodium-concentrated surface. In addition, sodium possesses a higher ability to increase the magnesium participation than potassium, after comparing the ratios of $\text{Ca}^{2+} : \text{Mg}^{2+}$ in SVI-1 and SVI-2 (**Figure 6.19**).

Sample	Step 1: Temp <200°C		Step 2: 200°C <Temp < 300°C		Water weight loss (%) (C3+C5)	Step 3: 300°C <Temp < 600°C		Step 4: 600°C<Temp <800°C		CO ₂ weight loss (%) (C8+C10)	Total weight loss (%) (C6+C11)
	Peak temp (°C)	Weight loss (%)	Peak temp (°C)	Weight loss (%)		Peak temp (°C)	Weight loss (%)	Peak temp (°C)	Weight loss (%)		
SVI-1	94.93	8.96	198.56	2.97	11.93	356.72; 410.63	30.00	680.22	14.40	44.4	56.38
SVI-2 (Na ⁺)	107.79	10.01	198.52	3.88	13.89	351.56; 402.37	29.18	712.68	15.40	44.58	58.47
SV-M5	84.15	11.83	193.64	4.07	15.9	339.42; 402.33	28.69	712.65	16.70	45.39	61.29
SIV-M5	94.89	12.27	201.65	2.71	14.98	376.91	21.04	728.26	8.14	29.18	44.16

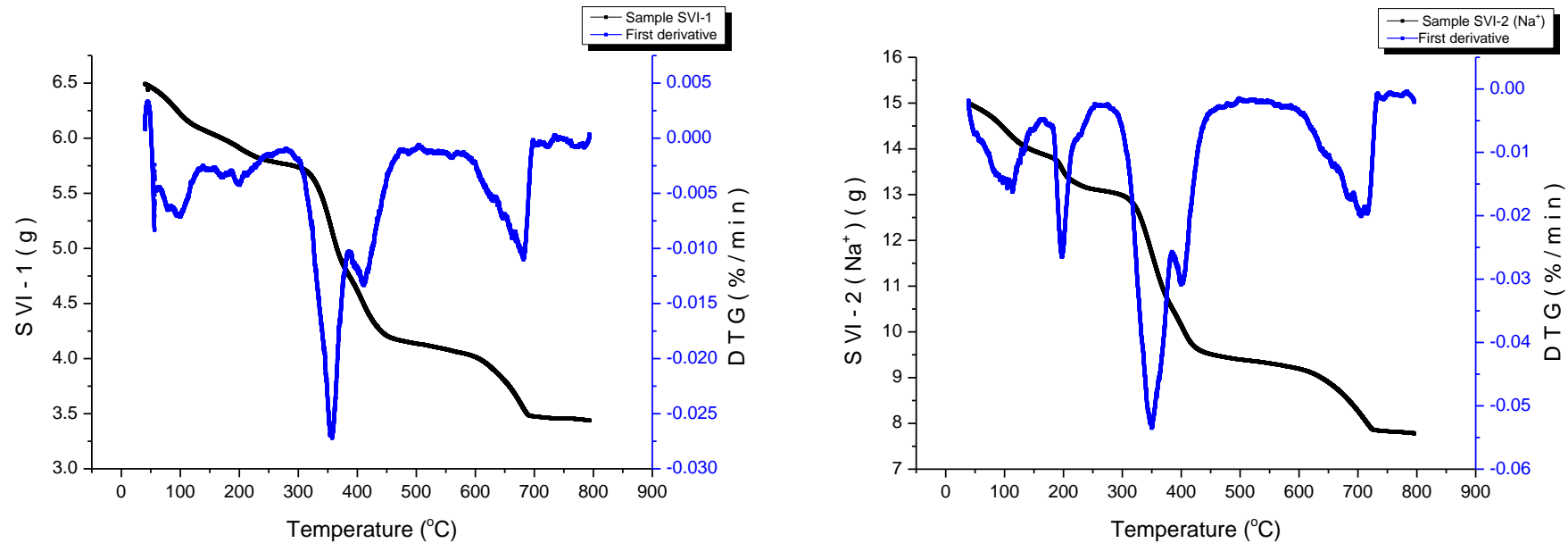
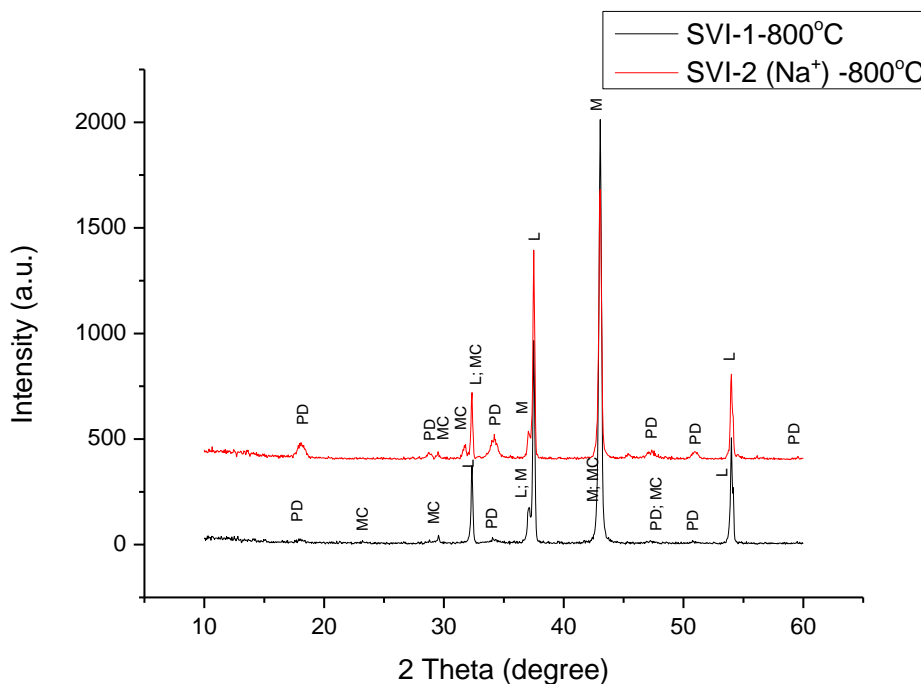


Figure 6. 17: The TGA thermal stages of SVI-1/2(Na⁺), SV-M5 & SIV-M5 (top), & TGA profiles of SVI-1 (bottom left) & SV-2 (Na⁺) (bottom right)

Sample			SVI-1-800°C		SVI-2 (Na ⁺)-800°C	
Ref. Code	Mineral Name	Chemical Formula	Score	SemiQuant (%)	Score	SemiQuant (%)
01-087-0673	Portlandite, syn	Ca(OH) ₂	23	--	65	--
01-077-2376	Lime	CaO	61	--	61	--
00-001-1235	Periclase	MgO	55	--	55	--
01-074-2220	Brucite	Mg(OH) ₂	Unmatched Strong	--	11	--
01-078-0751	Halite, syn	NaCl	Unmatched Strong	--	26	--
01-086-2335	Calcite, magnesian	(Mg _{0.064} Ca _{0.936})CO ₃	13	--	12	--
01-073-1403	Huntite	Mg ₃ Ca(CO ₃) ₄	3	--	9	--
Sample			SVI-1-800°C		SVI-2 (Na ⁺)-800°C	
Ref. Code	Mineral Name	Chemical Formula	Contained in precipitates? (Score)	SemiQuant (%)	Contained in precipitates? (Score)	SemiQuant (%)
01-087-0673	Portlandite, syn	Ca(OH) ₂	Yes (23)	--	Yes (65)	--
01-077-2376	Lime	CaO	Yes (61)	--	Yes (61)	--
00-001-1235	Periclase	MgO	Yes (55)	--	Yes (55)	--
01-074-2220	Brucite	Mg(OH) ₂	No	--	No	--
01-078-0751	Halite, syn	NaCl	No	--	No	--
01-086-2335	Calcite, magnesian	(Mg _{0.064} Ca _{0.936})CO ₃	Yes (13)	--	Yes (12)	--
01-073-1403	Huntite	Mg ₃ Ca(CO ₃) ₄	No	--	No	--

(a): The matching scores and semiquants of the SVI-1/2 (Na⁺) precipitates, calculated by software X'Per HighScore Plus



(b): The precipitates of SVI in XRD pattern

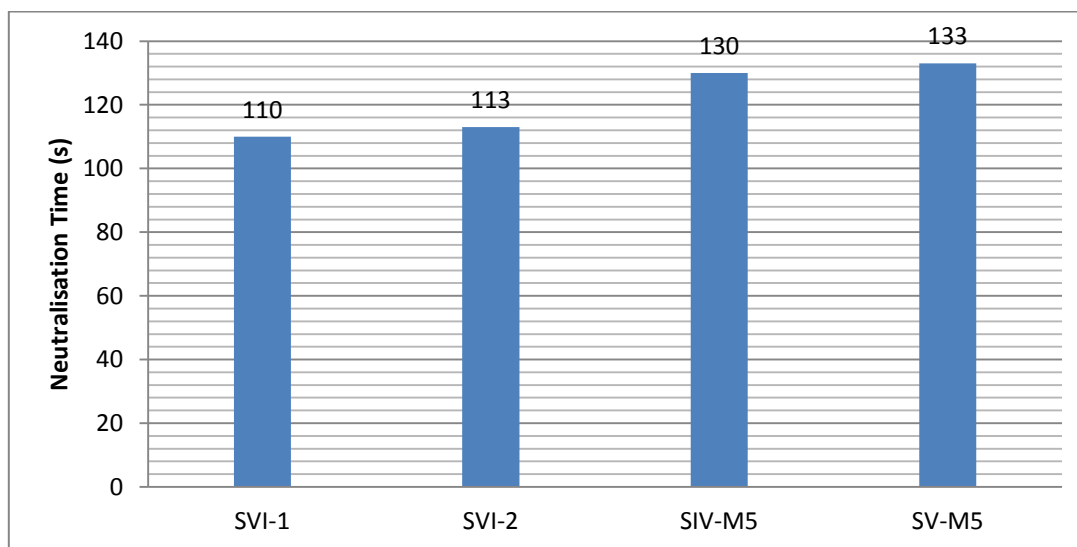
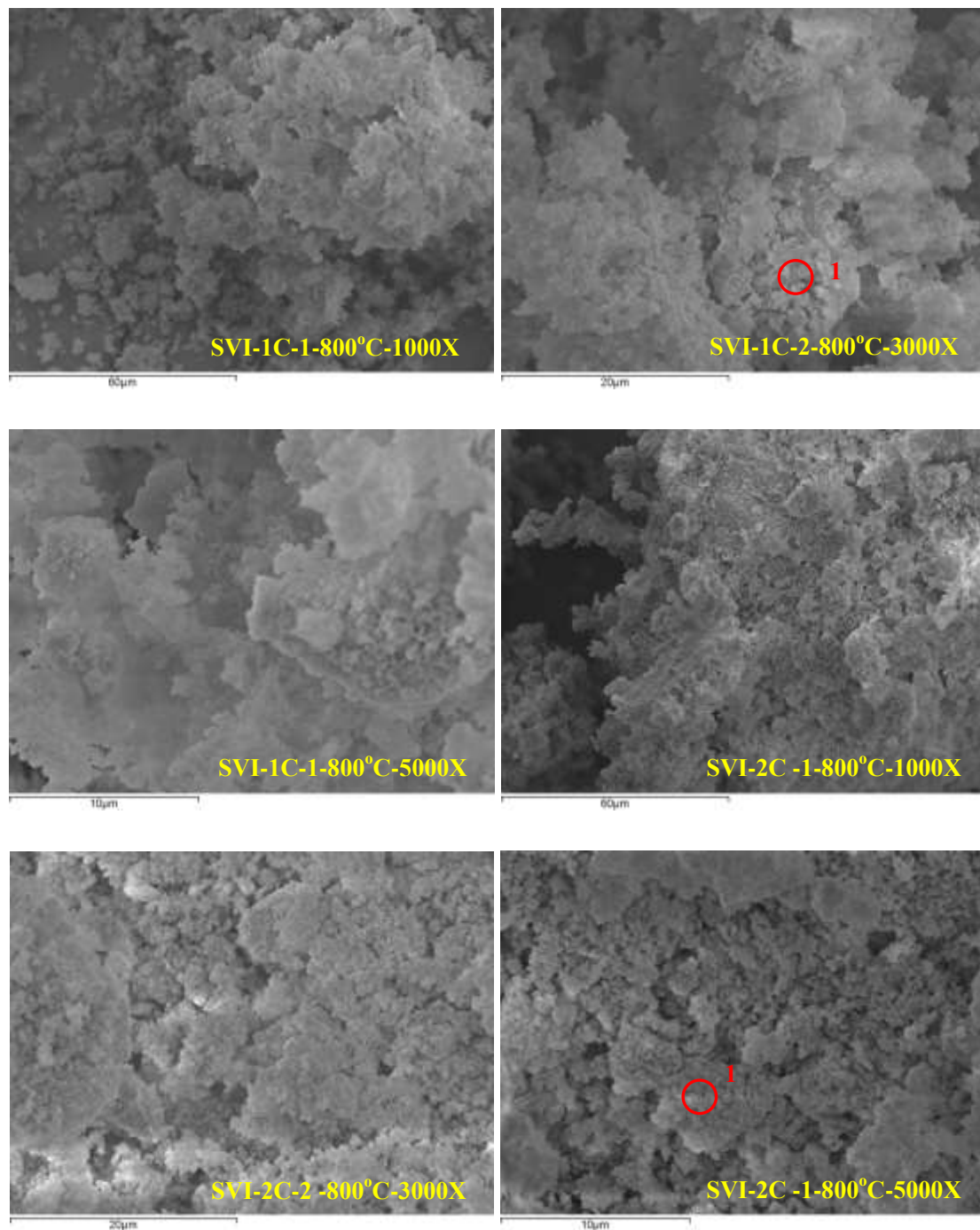
(c): The dolime reactivity results of SVI-1/2 (Na^+) & relevant comparisons

Figure 6. 18: The matching scores and semiquants of calcination SVI-1/2, calculated by software X'Per HighScore Plus (a), and their XRD patterns (b), and the relevant dolime reactivity tests (c). All samples are for SVI shown in Table 6.3.

The numbers in SVI reactivity test (**Figure 6.18c**) indicate that the higher impurity level, due to the sodium addition in SVI-2, resulted in a longer neutralisation time. This is also noticeable in SV-M5 and SIV-M5's evaluation. But as a whole, potassium has the property to reduce the overall reactivity, after analysing three series (SIV, SV, SVI) in total (**Figure 6.18c**).



Sample	Spectrum	C	O	Na	Mg	K	Ca	Ca ²⁺ :Mg ²⁺
SVI-1C-2-800oC-3000X	Spectrum 1	55.49	20.29	0.48	13.86	0.06	9.82	0.71
SVI-2C-1-800oC-5000X	Spectrum 1	69.48	11.46	0.81	16.34	0.35	1.56	0.10

Figure 6. 19: The SEM images of SVI-1/2 (Na⁺) dolime & corresponded EDX results (e.g. SVI-1C-2-800°C-3000X means that sample SVI-1, location 2, 800°C calcination temperature, 3000x magnification)

6.4 Conclusions

This chapter has described the sodium and potassium addition in the reactants. The model relied on PHREEQC because of high ionic strength in Visual Minteq. Selected samples M5 and M9 were tested in the segment. All physical and chemical types of studies were undertaken, including ICP, XRD, SEM, TGA and reactivity test. As the majority of these lack previous literature references, SIV's standards were mainly employed in this section.

The results of carbonation and pH stability studies were identical in SV and SVI because of the reactants' intrinsic properties. In SV, there were more magnesium based precipitates appearing than SIV, but this phenomenon was more obvious in SVI, assuming sodium induced higher magnesium incorporation. Potassium also enhanced this performance under the same condition. Aragonite was usually produced in a magnesium rich aqueous solution, and altered into monohydrocalcite when magnesium decreased. SEM strongly supported the idea with magnesium involvement in two series from both morphology and EDX $\text{Ca}^{2+}:\text{Mg}^{2+}$ ratios. However the addition of these impurities (sodium, potassium) increased the accumulation of finer particles into larger agglomerates. ICP was used to evaluate the metal's sequestration and it was found out that up to 40% of a specific soluble element was physically absorbed by precipitates through the mechanism of incorporation within the lattice. 1.5h was applicable for metals' sequestration and nucleation with both magnesium and calcium capture level over 90%, but might not be adequate for appropriate crystallisation. Five times washing procedures were required due to the large quantities of sodium interaction.

Analysis proved that 800°C was not sufficient to fully decompose the carbonates, and the increased salts led to higher abnormalities of the peak temperatures. Weight loss came well within the appropriate magnesian calcites' and HMCs' weight losses range, apart from the several incomplete drying or measuring errors. Finally the reactivity tests were conducted. In system SV, it was found that in a relatively simple system, lower pH led to magnesium carbonate formation resulting in the increased contamination due to its complicated aqueous system. While in a complex system, pH directly influenced on the reactivity outcome caused by the extra hydroxide ions. It can be concluded that a solution has the propensity to create a complex system, but when it reaches a certain level of concentration, each ion behaves more independently rather than interactively. Finally, sodium has the

ability to accelerate the neutralisation process; however, potassium reduces more in the neutralisation time of the calcined products.

Chapter 7: Conclusions & Recommendations for Future Research

7.1 Conclusions

This thesis focuses on the sustainable MgO production from waste magnesium resources, such as reject brines or seawater, through carbon sequestration, to provide a comparable low carbon manufacturing process. The produced minerals are further calcined to oxides used in the construction industry. The entire system is a closed loop to achieve both environmental optimisation and good productivity.

Six series of tests were conducted: (i) the individual magnesium ion (Mg^{2+}) with ammonia; (ii) the individual magnesium ion (Mg^{2+}) with sodium hydroxide; (iii) the individual calcium ion (Ca^{2+}) with sodium hydroxide; (iv) the dual ions (Mg^{2+} , Ca^{2+}) complex system; (v) the triple ions (Mg^{2+} , Ca^{2+} , Na^+) complex system; (vi) the quadruple ions (Mg^{2+} , Ca^{2+} , Na^+ , K^+) complex system integration. All studies were followed by a four-stage process: thermodynamic model estimation, experimental design, carbonation measurement, and calcination study. Sophisticated material analytical measurements were taken in all explorations, including XRD, SEM, TGA and ICP.

The simulation models are matched well with the tests, and experimentally the optimum carbonation parameters were found to be: $0.25MgCl_2 + 0.05CaCl_2 + 2.35NaCl + 0.05KCl$, 700rpm stirring speed, 25°C room temperature, pH=10.5, and 500cm³/min CO₂ infusion rate. The reaction time is within a day. These parameters were chosen based on the sequestration level, particle performance morphology and the operational convenience. The optimum calcination parameters were at 800°C heating temperature with a 4h retention time.

7.2 Literature Review

The literature review started from the climate change and carbon mitigation method. This research involves a CO₂ infusion, corresponding to carbon mineralisation process with advantages in permanent storage and potential construction materials utilisation.

Traditional Portland cement manufacture is one of the most polluting industries, arising from fossil fuel combustion and calcination phases. Alternative MgO cement possesses both

superior technical and sustainable advantages with a lower calcined temperature, and a good tendency of binding with waste, as well as higher recyclable properties and good durability taking into account its rehydration and recarbonation characteristics. Current industrialised MgO is mainly produced from magnesite (86%), while the rest is processed from seawaters by approximately 20 manufacturers. However, considering the geographic location and lack of natural magnesite deposit, for the UK and other European countries, waste water and seawater are more suitable resources. The constituents of seawater are mainly chloride, sodium and magnesium ions with pH level ranges from 7.8 to 8.3, buffered by the carbonates system. The increased solubility of CO₂ depends on the decreased temperature, the higher pressure at a constant temperature and salinity, as well as the reduced salts' concentration.

Various chemical reagents have been widely researched to sequester the magnesium element. The categories of magnesium carbonates are heavily dependent on the temperature, where a higher one will accelerate carbonation degree and a phase transformation from nesquehonite to dypingite and hydromagnesite. MgO grades are classified by calcined temperatures, with around 700-1000°C as light-burned and typically 1000-1400°C as hard-burned products. pH is the most important factor for magnesium carbonation, controlling the carbonates' formation at pH ≥9, while temperature is the second important parameter in the reaction, affecting sizes and the shapes of particles. Subsequently, concentration can influence the supersaturation degree and benefit the high quality crystals at more diluted solutions proposed by Hassan (2014). Stirring speed needs to be controlled at an appropriate level, and a longer reaction time produces more uniform crystals. Finally CO₂ pressure influences the precipitates phase transformation and growth rate.

Calcium is the second most abundant constituent in seawater among the tested elements. Within the calcium carbonate series, the most stable precipitate is calcite of rhombic/cubic morphology, while the metastable ones are vaterite and aragonite, greatly dependent on temperature. The most unstable forms are monohydrated calcite and hexahydrate calcite grouped as amorphous calcium carbonates with lower than a micrometer spherical shape. In a solution-mediated transformation process, amorphous precursor calcium carbonates (ACC) are formed at first. They are then aggregated and transformed into vaterite and

calcite at a low temperature (14 to 30°C), aragonite and calcite at a high temperature (60 to 80°C), and all three polymorphs at an intermediate temperature (40-50°C) within a few minutes. At even higher temperature, the solid-state changes from aragonite to calcite. Both calcium carbonates and calcined oxides are utilised in the construction industry or as materials additives. The particle size, distribution, morphologies and surface characteristics of calcium carbonates can be controlled through various parameters, including pH, temperature, reactant concentration, stirring speed, reaction time, CO₂ flux rate, and additives. Han et al. (2006) stated that primary calcium chloride concentration, CO₂ infusion rate and temperature play important roles on phase and morphology changes when compared to bubbling time and stirring rate, which are almost insignificant on particles' alterations.

In a complex dual-ion system, magnesium calcium carbonates can be broken down into a CaCO₃-MgCO₃-H₂O scheme. General magnesian calcites are separated into low-magnesian calcite and high-magnesian calcite at ≥4% MgCO₃ content. The latter is typically named as huntite and dolime. Magnesian calcium carbonates have several determining factors, for instance temperatures, CO₃²⁻ concentration (pH and CO₂ pressure), Mg²⁺:Ca²⁺ ratios, time and other additives (Meldrum & Hyde, 2001), on a broad range of morphologies and compositions. Temperature plays a positive correlation during magnesium participation, while the CO₂ partial pressure shows a negative one. Mg²⁺ incorporations within the crystallised solution have two effects: providing a much wider type of morphology, and a transition from a single crystal to crystallite aggregates.

Impurity salts have a significant impact on magnesium calcium carbonates' formation. Sodium coprecipitates at the interstitial sites of calcite lattice and enhances the magnesium proportion in the calcite precipitates until a certain level is reached. Increased pH value raises crystal abnormalities and the quantities of sodium intersection. Likewise, a higher initial reactants' concentration also leads to the defected morphologies. Potassium is another addition in experiment, as it has a similar effect to sodium's interference in carbonates. Magnesium can accelerate the alkali metals' engagement with calcite, but sodium-bearing aragonite decreases other alkali metals' quantities (e.g. Li⁺, K⁺ and Rb⁺) because of sodium's competitiveness in an ion-exchange mechanism as its ionic radius is similar to calcium.

Thermal decomposition occurs in a single step at a lower partial pressure of CO₂, and two steps in a higher temperature because of the immediate recombination of oxides into carbonates. The larger concentration of impurities in solids raises more abnormalities of peak temperatures in TGA.

Two widely recognised models PHREEQC and Visual Minteq were used in this study to simulate the thermodynamically favoured precipitates. PHREEQC is used in combination with Pitzer Sit.dat and Minteq is used in combination with an ion-association approach Thermo.dat. Calculated Saturation Index (SI) demonstrates the deposit formation. When Saturation Index > 0, precipitates are in a solid phase.

7.3 Materials and Experimental Methodology

Traditional chemical reactions have been widely explored and reviewed in Chapter 2, but the novel process of CO₂ diffusion under a controlled alkaline condition has not been discussed thus far. It is necessary to fully understand the reactions from the mechanism aspect of the components in seawater with CO₂ addition, together with their calcined products. Several physical and chemical properties were examined to achieve this target, from a simple system to multiple-ion composite systems. There were six systems in this research, where two of them were mixed with additional chemicals sodium chloride or potassium chloride. All produced carbonates were then calcined into oxides at 800°C or other temperatures -- 650°C & 1000°C. Commercial MgO N50 & 92-200 were recorded and tested as standards.

Apparatus' settings and experimental procedures were correspondingly documented, followed by filtration and purification of the produced carbonates. They were then ready for analytical measurements, consisting of pH and temperature recordings (pH thermometer), metals quantification (ICP-OES), precipitates identification (XRD), microstructure observation (SEM), and weight loss investigation (TGA). Five experimental studies were undertaken, including carbonation studies, pH stability studies, pH adjustment studies, reaction kinetic studies, and calcination studies, to ensure the success of carbonation and calcination stages. Finally, the reactivity was measured by using the citric acid to neutralise the calcined oxides. Tested calcined oxides were prepared at under 250µm particle sizes prior to reactivity examination.

7.4 Series I- Individual Magnesium Ion System with Ammonia

Preliminary and initial tests were carried out with ammonia involvement. Primary trials successfully proved the apparatus setting and the initialised process. Both PHREEQC and Visual Minteq were undertaken in SI, producing nesquehonite, artinite, magnesite, hydromagnesite and lansfordite formation thermodynamically. Among them, nesquehonite and hydromagnesite agree with the lab results, while the rest of modelled precipitates cannot be produced at this experimental condition.

The carbonation process was an exothermal reaction, particularly during the reactants' addition, where significant particles' interactions and collisions resulted in an obvious temperature increase. Precipitates started to form at pH=8.5 and reached the maximum at 9 and 9.25 in ammonia environment, with noticeable finer aggregated particles at a lower pH (e.g. pH=8.5) and larger independent particles' presence at a higher pH (e.g. pH=9.25). pH was monitored over three days, particularly when pH>9, ammonium displayed good buffering capacity to maintain a constant pH, while at pH≤9 the value gradually decreased about 0.2-0.5. All precipitates were formed as nesquehonite, irrespective of pH and time scale. Substantial magnesium removal efficiency was measured in the first 30min: 8.5<pH<10 (pH=8.75, 9, 9.25, 9.5) illustrated over 50% capture level, which was higher than pH≥10 (pH=10 & pH=10.3).

pH adjustment studies were then undertaken in Series I part II (SI.II). After a period of ¾ day or one day, the pH of all samples stabilised at a constant level, indicating the completion of the reaction. Magnesium had better sequestration quantities after pH adjustment compared to non-adjustment. Moreover, pH differences were found to have a direct relationship with the reaction degree, where the decreased pH revealed a more active progression than stable one.

7.5 Series II-Individual Magnesium Ion System with Sodium Hydroxide

The model performed in SII was indistinguishable from SI, considering both sodium and ammonium were contamination, and the mixed or the produced sodium chloride and ammonium salts were also largely soluble in an aqueous form. Carbonation studies showed an increase in temperature, while pH value kept constant over the experimental time. The deposits were then identified to have the mixtures of hydromagnesite (HM), dypingite (D),

nesquehonite (N), and the impurity halite. More reactants accelerated HM formation, but a higher pH induced more metastable phases or less uniform morphologies. Less CO₂ participation was due to no stirring, a high temperature and a smaller CO₂ infusion rate.

In terms of microstructure, a raised pH and temperature led to a more complex aggregation because of the enhanced nucleation rate and carbonates' activity. The complex particles are presented as sheet-like granules accumulated by needle-like nesquehonite and/or rosette-like HM. The degree of supersaturation was important on initial nucleation stage and the subsequent crystallisation. The lower concentrations of initial reactants triggered more regulated and smoother grains, while a less homogenous aqueous solution was caused by a lack of stirring speed. The decreased CO₂ flux rate was the main factor for the production of brucite, as well as combining nesquehonite into a tabular structure. Reaction kinetic studies illustrated that 1h was not adequate for proper crystallisation, and the captured metals were coprecipitated within hydromagnesite/dypingite porosities or accelerated as nuclei only, giving an illusion of high sequestration quantities after 1h. In the end, sample 3 with parameters 0.5M MgCl₂, 700rpm stirring speed, 25°C room temperature, pH=10.5 and 500 cm³/min CO₂ flux rate, was selected as the most appropriate specimen when taking into account the sequestration level, particle performance and morphology, as well as operational convenience. A better image and crystal formation were observed over one day. In short, during a limited period, pH=10 was beneficial to particles obtained with prominent peaks performance and regulated morphologies, but over time, pH=10.5 had better results as it supplied sufficient reactants and provided an adequate transformation process.

Thermal evaluation was operated by TGA heating from 40°C to 800°C with 10°C/min rate. Samples with brucite incorporated possessed a lower mass loss and a smaller carbonation degree compared to other HMCs. Moreover, a high temperature resulted in smaller H₂O and CO₂ weight losses, and one-day precipitates had no significant difference on thermal property in one hour. A few of the double peaks were presented within a range of 300-450°C, effected by a two-stage decomposition from immediate re-carbonation procedure, possibly caused by particle sizes, sample lid, atmosphere diffusion and ventilation conditions, etc. Generally, a higher supersaturation solution extends the MgO reaction time with non-uniform or sheet/plate-like particles' generation. Additionally, NaCl impurity also retarded the neutralisation process.

At other temperatures, 650°C had larger spherical grains, but the voids gradually reduced with the increasing temperatures. It was found that the temperature of 1000°C did not break down all carbonates because of the natural carbonation or long-time storage before test. A lower pH value introduced uniform particles with a longer growing time and larger spaces, while a higher one tended to have larger quantities of aggregations due to an elevated pH and supersaturation degree, leading to small particles' agglomeration. A higher hydration degree and lower carbonation extent up to 800°C were detected in the sample, illustrating that a lower pH trapped carbonates at higher temperatures.

In conclusion, the reactivity test corresponded to the initial predictions—an elevated temperature of the calcined product required a longer neutralisation time due to its decreased porosity and granular size. In the end, pure MgO was slower in reactivity than a dolime mixture, where CaO reduced the final reactivity.

In an ammonia and NaOH comparison study, NaOH's carbonation performance exhibited a lower temperature change per time compared to the ammonia reaction, due to fewer particles colliding, because the ammonia gas-liquid phase was more active than the NaOH solid-liquid phase. Its stability was also not as constant as ammonia because of ammonia's good buffering capacity. Nesquehonite was produced in an ammonia mediated solution because of the easy evaporation property, while NaOH was more likely to have HM and D within the same time by atom disturbance from sodium. Hence the alkalisated buffering solution can lubricate the phase transformation, while sodium hydroxide is a strong alkali causing the direct and tangible chemical reaction. It was also found that products produced at a higher pH of ammonia had better qualities for filtering and grinding, attributed to its good buffering ability. However, precipitates exhibited a more gelatinous property in NaOH system, generated by brucite at a higher pH value. Different from ammonia's long sequestration time, the increased level of NaOH had promising capture efficiency at the start, influenced by its immediate decomposition of strong alkaline. To conclude, sodium hydroxide has more advantages than ammonia because it theoretically needs shorter time to reach the balance and has a good economic approach as well as operational convenience.

7.6 Series III-Individual Calcium Ion System with Sodium Hydroxide

Preliminary thermodynamic modelling PHREEQC and Visual Minteq were operated to estimate the theoretical precipitates. Calculated potential deposits were aragonite, $\text{CaCO}_3 \cdot \text{H}_2\text{O}$, calcite and vaterite, based on the designed parameters. The practical results also show the same products experimentally.

Vaterite appeared under the condition of higher initial reactants, because the supplemented carbonates delayed the phase transformation into a more stable one; whereas the elevated temperature led to aragonite formation. Under 10000x magnification, calcite clearly presented as an assembled layered structure, vaterite was an integrated spherical shape, and aragonite appeared as arrows. A higher pH value and a CO_2 flux rate had more aggregated and denser particles, while a lower pH and a lower CO_2 flux rate displayed more uniform and individual granules. It is considered that an increased supersaturation degree resulted in more nuclei generation and less dissolution, thus preserving the crystal seeds and enhancing the growth. Kinetics illustrated a good capture value with over 90% sequestration; and the gap between the theoretical and practical weights was due to either procedural errors or insufficient time for crystallisation.

Overall sample 3 showed the best performance among all samples, considering both morphology presence and sequestration efficiency aspects. But one-day morphology of it was less uniform compared to 1h reaction, theorised from Ostwald's rule, that nuclei dissolve and reform into larger particles over time.

Thermal decomposition profiles illustrated the validity of this test, with the experimentally determined 44% weight loss, which was almost the same as theoretical mass reduction. Peak temperature was also located within a reasonable range according to the reference. It proved that the produced calcium carbonates possessed a high purity level, but one-day morphology changed slightly by more water molecular surface attachment. Calcined product CaO was highly reactive, and had fast neutralisation property with around 10 seconds only. The produced oxides were well matched with commercial CaO in the citric acid reactivity test and the XRD identification, proving the reliability of this practice.

7.7 Series IV-Dual Ions Complex System (Mg^{2+} , Ca^{2+})

PHREEQC predicted the potential sediments. The two represented magnesian calcites were dolomite and huntite recorded from Sit. database. In the pH range of interest, 10-10.5, and at the ratio of Mg: Ca=5:1, the potential outcomes were aragonite, artinite, brucite, monohydrocalcite, calcite, huntite, dolomite, magnesite, hydromagnesite and vaterite. This model is in a good agreement with the produced precipitates in SIV, except artinite, which cannot be produced at this experimental condition.

A carbonation study was conducted and revealed that a higher temperature was harder to maintain at a certain level over time, and the temperatures of other samples operated at room conditions increased naturally because of the exothermal reaction. pH stability was recorded at a constant value during the operation.

At a high calcium concentration (M1-4), magnesian calcite, calcite and brucite were found within the precipitates, whereas in high magnesium reactants (M5-10), samples had more varieties, by having magnesian calcite, dolomite and huntite. Brucite and halite were in the magnesium calcium carbonate series, while aragonite and monohydrocalcite were in the calcium carbonate series. The reason for the existence of halite only in high magnesium reactants (M5-10) was due to significant magnesium hydrophilic characteristics intersected by dissolved halite, which was different from calcium's high propensity in carbonation attachment (carbonphilic).

There were four stages during the carbonation studies: initial stage, intermediate stage, transitional stage and completed stage. Moreover, brucite was predicted to transfer into magnesian calcite after a long duration, while aragonite and monohydrocalcite were more stable compared to the transformed calcite, during magnesium participation. In short, calcite was formed at $Mg^{2+}: Ca^{2+} < 0.5$ when temperature was lower than 40°C; and aragonite and MHC appeared at $Mg^{2+}: Ca^{2+} > 1$ at room and elevated temperatures. The importance of parameters was ranked as:

pH > temperature > CO₂ flux rate > stirring speed,

from the most to least significance after analysis.

Smaller calcium reactant concentrations (M1 & 2) presented more rounded vaterite, with larger ratios of $\text{Ca}^{2+} : \text{Mg}^{2+}$, leading to different nucleation rate and mechanical incorporation. An increased temperature accelerated reaction and phase transformation, but also led to more irregular grains. Additionally, a reduced CO_2 flux rate shortened the required time to complete the nucleation, thus leaving a longer retention time for phase transformation. The formation of magnesian calcite was described as follows: (a) an elongated magnesian calcite appeared at first stage; (b) this was subsequently covered by rounded or cubic calcite particles; (c) it was then combined with tabular or rounded rosette-like grains as the exterior surface. This processing step was evaluated by means of growth kinetics: that is, the fastest growing nucleation may be expected to disappear at first and leave behind the slowest crystallisation as the outliers of granule. As a whole, the lower supersaturation accelerated the magnesium penetration within the same period of time, while the temperature developed the process positively by increasing the reaction rate. In contrast, stirring speed played a contrary influence on particles' crystallisation.

It is also concluded that a larger reaction degree was greatly affected by the increased temperature or longer duration, and products had the propensity to aggregate into a granule with more identical element accumulation as initial surplus metal.

Finally, additional miscellaneous studies were conducted with a high sodium impurity having obvious fish-scale-like particulates appearance.

TGA was utilised to show the thermal characteristics. Increased temperatures had a positive carbonation degree compared to others, and halite mixed as an impurity to reduce the entire weight loss. Lime was easily hydrated to portlandite over time after calcination, while magnesia tended to remain unchanged. In a reactivity test, hydrated portlandite from lime or dolime reduced the neutralisation time (M1-4), and typical magnesian calcite varied from 100s to 150s. An elevated temperature (samples 6 & 10) tended to induce a faster reactivity; similarly, a lower CO_2 flux rate (samples 7 & 8) as well as a higher pH, were also beneficial to decreasing this figure. In addition, a higher reaction level led to a poorer reactivity as magnesium participation created a more complex system by having the tendency to increase the impurity level.

Calcination at various temperatures was studied further. Obvious differences were noticed at 1000°C, no halite and carbon were present at 650°C and 800°C, explained by the high temperature beyond the melting point of NaCl and the completed decomposition stage. TGA analysis up to 1000°C clearly disclosed these calcination processes, results displayed that the final peak occurred at 800-1000°C referring to the incomplete decomposition at the initial designed 800°C calcination temperature. Reactivity tests, operating at three temperatures, found that higher endothermal calcined samples required a longer time to complete the neutralisation test.

7.8 Series V-Triple Ions Complex System (Mg^{2+} , Ca^{2+} , Na^+)

This work added extra sodium above the dual ions system, considering its large amounts of contamination within the natural seawater. A minimum five times of the washing procedure were conducted based on the investigation in Section 6.2.3.5. Model estimation showed no differences to Series IV, regarding the sodium as a type of impurity that was removed after the operation. More magnesium carbonates were present in the precipitates of Series V compared to Series IV, because of the sodium disturbance. When magnesium was less concentrated, monohydrocalcite was sensitive to form, but aragonite required larger magnesium proportion of $Mg^{2+}/Ca^{2+} \geq 4$. This result was in consistent with the microstructure of SEM. Both magnesium and calcium reached more than 90% capture level in kinetics, indicating that sodium did not have a significant effect on the capture of metals, but percentage was still less than the equivalent samples in SIV, which mainly attributed to the higher supersaturation degree of SV.

The peak of weight loss in the thermal phenomenon varied compared to literature, revealing that the increased salts' concentration caused more disordered peak temperatures. The results of TGA revealed more possibilities on magnesium carbonates production in SV. Three calcined temperatures (650°C, 800°C and 1000°C) were subsequently conducted. At all three temperatures, carbon remained, implying that the addition of sodium raised the completed calcination temperature for precipitates, through disordering the magnesium and calcium particles. The morphology presented smashed grains with less porosity compared to SIV because of sodium coprecipitation, although it was removed through cleaning procedure, the disruption to original structure occurred from the first carbonation stage.

The citric acid reactivity test was then measured to identify the neutralisation property of the products. Overall, a higher temperature led to a more difficult neutralisation process because of its reduced porosity by elevated temperatures. However, when making the comparisons of SIV and SV, it was found that in SIV's relative simple system, a lower pH accelerated the magnesium sequestration, and subsequently increased the impurity level through generating more complicated products.

This complexity influences the reactivity and the products during the test more than any other factors. While in an existing complex system, sodium achieved its maximum ability on magnesium sequestration. A more direct pH corresponding to hydroxide ion concentration dominated the reactive property. Therefore, the reactivity test relied on the complexity of the solution, and gave priority to generate a more supersaturated aqueous system. But when the solution reached a certain sequestration level, the compounds had a greater tendency to display their own intrinsic characteristics, for example, OH^- ion showed more alkali property rather than raising the supersaturation degree of the solution.

7.9 Series VI-Quadruple Ions Complex System (Mg^{2+} , Ca^{2+} , Na^+ , K^+)

This section described the addition of potassium. The model followed the previous two series of experiments without further precipitates extraction from the database. The estimated products, potassium carbonates and potassium hydroxide, were largely soluble in water, and existed as free ions within an aqueous phase. The concentration of the synthetic chemicals in this stage was applied to the 5 times concentrated solution compared to the original seawater components, excluding several minority elements, for instance strontium, boron and silicon because of their minute amounts as well as hazardous property when combining cation compounds during the lab operation. Chlorine was considered as an anion to balance the hydrous electric charge, and inorganic compounds generated from carbon series were replaced by CO_2 diffusion. Moreover, fluorine concentration is very low in seawater, so it was not considered in this investigation.

All four analytical measurements were identical to the previous measurements, and the TGA profile was disrupted due to the high volume of salts.

Carbonation studies and pH stabilities in Series VI were similar to the relevant studies in Series IV and Series V. The big difference occurred in XRD determination, as the potassium

had the equivalents effect or even better improvements in magnesium carbonates' formation, accompanied by more hydrated magnesium carbonates precipitates observation. Sodium was substituted by potassium to accelerate the reaction. SEM presented more flat crystals and conglomerated blocks with potassium participation. But SVI-2 (Na^+) had more independent particulates similar to rosette-like shapes, indicating the extra sodium had the ability to increase the magnesium penetration under the same conditions of others.

In kinetics study, it also proved that sodium accelerated the magnesium sequestration, which was lessened by calcium capture at the same time. Potassium incorporated within the sediments up to around 42% in 1.5 hours. Amalgamating these results and miscellaneous sodium study in SV, it was evaluated that up to 40% of a particular soluble product was physically absorbed by precipitates through the mechanism of incorporation within the deposits' porosities and lattices.

The thermal decomposition was operated at 800°C . This degree was selected for easy operation, convenient analysis, considerable decomposition and wide uses, although it was not sufficient to fully decompose the carbonates. Abnormal peak temperatures appeared with the increasing aqueous salts in TGA profiles. After calcination, fluffy particles emerged in samples illustrating that sodium disrupted the natural carbonates' formation and actively inserted its element within the voids of precipitates, leading to sodium-mediated pictures. Additionally, sodium had a larger capacity to capture magnesium than potassium. However, reactivity tests revealed that sodium's addition increased the impurity level and made it a longer time to complete the neutralisation. Conversely, potassium had a propensity to reduce the entire reactivity performance from the evaluations of all three series (SIV, SV, and SVI).

The final finding was that the optimum carbonation parameters were $0.25\text{MgCl}_2 + 0.05\text{CaCl}_2 + 2.35\text{NaCl} + 0.05\text{KCl}$ (5 times higher in concentration compared to seawater), 700rpm stirring speed, 25°C room temperature, $\text{pH}=10.5$ (using NaOH), and $500\text{cm}^3/\text{min}$ CO_2 infusion rate. The optimum calcination parameters were at 800°C heating temperature with a 4h retention time.

7.10 Recommendations for Future Research

This research consisted of 6 series of experiments in the study of the novel CO₂ infused system at a fixed pH, and producing a creative binary MgO-CaO reactivity test. The limitations of this work included procedural errors (e.g. sample transferring waste and a long-time duration) and the unavoidable limitations of machinery detection (e.g. TGA was limited to below 1000°C).

In the future, a broader range of complex systems needs further investigation. It is important to understand the extraction/isolation of magnesium compounds (mainly MgCl₂) from brine, the practical industrial process, and the further usage of the produced products. Therefore, three main aims in the next step are: (i) to explore seawater/brine pretreatment processes; (ii) to examine integrated natural brine or seawater pilot scale manufacturing; (iii) to investigate the commercial usage of the produced reactive MgO with traditional Portland cement mixture.

In the pretreatment of seawater, the methods of low temperature freezing and alkaline mixture can be considered to extract the magnesium. A low temperature will separate the components by different freezing points, in order to obtain the pure chemicals. The latter alkaline method will use lime and CO₂ to produce Mg(HCO₃)₂, which reacts with sodium chloride generating sodium bicarbonate precipitates and magnesium chloride solution. The bicarbonate can be then processed for soda ash manufacturing. Both of the methods have not been fully commercialised yet, a further research is necessary to form an integrated process from the raw material extraction (based on the future results) to the chemical formations (based on the current research).

Regarding the pilot scales of the entire process, a few conventional MgO production plants from seawater have been described in Chapter 2, but the novel process investigated in this thesis has not been widely used. This research has already provided the optimum conditions to synthetically produce the carbonates and oxides from the chemical engineering and mechanical manufacturing aspects. Therefore, the next step is important to test the reliability and validation of the data in practice, by using the natural seawater or industrialised reject brine. The scales of the operation should also be equivalent to the production capacity of Mg/Ca-carbonated precipitates from a small factory by using the

traditional production methods (e.g. calcination from the magnesite, or the reaction of strong alkalis with seawater without CO₂ involvement).

Finally, this thesis has not covered the application of produced oxides. The durability and the strength of these oxides need further investigations by mixing with other chemicals. This examination is essential for the usage of the experimental synthesised products, especially if we wish to approach its utilisation in cement industry. Current cement blending includes two novel reactive MgO-based binary cements, namely, reactive MgO-microsilica cement and reactive MgO-slag cement. Alongside, MgO is also promising in self-healing cement due to the good hydration and carbonation properties of MgO.

References:

- Aghakhani, a., Mousavi, S. F., Mostafazadeh-Fard, B., Rostamian, R., & Seraji, M. (2011). Application of some combined adsorbents to remove salinity parameters from drainage water. *Desalination*, 275(1-3), 217–223.
- Aizenberg, J., Lambert, G., Weiner, S., Addadi, L., Lucent, L., & Mountain, A. V. (2002). Factors Involved in the Formation of Amorphous and Crystalline Calcium Carbonate : A Study of an Ascidian Skeleton. *Journal of the American Chemical Society*, 124(10), 32-39.
- Al-Anezi, K., Somerfield, C., Mee, D., & Hilal, N. (2008). Parameters affecting the solubility of carbon dioxide in seawater at the conditions encountered in MSF desalination plants. *Desalination*, 222(1-3), 548–571.
- Al-handhaly, J. K., Mohamed, A. M. O., & Maraqa, M. (2003). Impact of chemical composition of reject brine from inland desalination plants on soil and groundwater, *Desalination*, 156, 89.
- Amiel, A. J., Friedman, G. M., & Miller, D. S. (1973). Distribution and nature of incorporation of trace elements in modern aragonitic corals. *Sedimentology*, 20(1), 47–64.
- Andreassen, J.-P., Beck, R., & Nergaard, M. (2012). Biomimetic type morphologies of calcium carbonate grown in absence of additives. *Faraday Discussions*, 159, 247.
- Aqueous Salt Solutions (2017). The CO₂-NH₃-H₂O system, [Online]. Available: <http://www.phasediagram.dk/ternary/CO2NH3H2O.htm> [13th Feb., 2017].
- Arita, Y., Mazilu, M., & Dholakia, K. (2013). Laser-induced rotation and cooling fo a trapped microgyroscope in vacuum. *Nature Communications*, 4, 2374.
- Bandi, W. R., & Krapf, G. (1976). The effect of CO₂ pressure and alkali salt on the mechanism of decomposition of dolomite. *Thermochimica Acta*, 14(1-2), 221–243.
- Baron, G. (1960) Sur la synthese de la dolomite, Application au phenomene de dolomitisation. *Rev. Inst. Franc. Petrole Ann. Combust. Liquides* 15, 3-68.
- BELL, P. M., and ENGLAND, J. L.(1964). High- pressure differential thermal analysis of a fast reaction with CaCO₃: *Carnegie Inst. Washington Year Book* 63, p. 176-178.
- Berner, R. A. (1975). The role of magnesium in the crystal growth of calcite and aragonite from sea water. *Geochimica et Cosmochimica Acta*, 39(4), 489–504.
- Berner, R. A., Westrich, J. T., Graber, R., Smith, J., & Martens, C. S. (1978). Inhibition of aragonite precipitation from supersaturated seawater; a laboratory and field study. *American Journal of Science*, 278, 816-837.
- Bert, M., Ogunlade, D., Heleen de, C., Manuela, L., & Leo, M. edt.(2005). *Carbon Dioxide Capture and Storage*. New York: Cambridge University Press. 5710-5716.

Bertram, M. A., Mackenzie, F. T., Bishop, F. C., & Bischoff, W. D. (1991). Influence of temperature on the stability of magnesian calcite. *American Mineralogist*, 76(11-12), 1889–1896.

Biedl, A. & Preisinger, A. (1962). Synthese von Huntit, $\text{CaMg}_3(\text{CO}_3)_4$. *Anzeiger Akad. Wiss. Wien*, 1962, No.10, pp.148-149.

Bischoff, W. D., Mackenzie, F. T., & Bishops, F. C. (1987). Stabilities of synthetic magnesian calcites in aqueous solution : Comparison with biogenic materials. *Geochimica et Cosmochimica Acta*, 51, 1413–1423.

Blanco-Gutierrez, V., Demourgues, A., Jubera, V., Gaudon, M. (2014). Eu(III)/Eu(II)-doped $(\text{Ca}_{0.7}\text{Sr}_{0.3})\text{CO}_3$ phosphors with vaterite/calcite/aragonite forms as shock/temperature detectors. *Royal Society of Chemistry*, 2, 9969-9977.

Blue, C. R., & Dove, P. M. (2015). Chemical controls on the magnesium content of amorphous calcium carbonate. *Geochimica et Cosmochimica Acta*, 148, 23–33.

Boeke, H. E. (1912). Die Schmelzerscheinungen und die umkehrbare Umwandlung des Calcium- carbonats: *Neues Jahrb. Mineralogie u., Geologie*, v. 1, p. 91-212.

Boettcher, A. L., & Wyllie, P. J. (1968). The Calcite-Aragonite Transition Measured in the System $\text{CaO-CO}_2\text{-H}_2\text{O}$. *The Journal of Geology*, 76(3), 314–330.

Bond, G. M., Stringer, J., Brandvold, D. K., Simsek, F. A., Medina, M., & Egeland, G. (2001). Development of Integrated System for Biomimetic CO_2 Sequestration Using the Enzyme Carbonic Anhydrase. *Energy Fuels*, 15(2), 309–316.

Botha, A., & Strydom, C. A. (2001). Preparation of a magnesium hydroxy carbonate from magnesium hydroxide. *Hydrometallurgy*, 62(3), 175–183.

Brian, J., & Peng, X. (2014). Signatures of biologically influenced CaCO_3 and Mg-Fe silicate precipitation in hot springs: Case study from the Ruidian geothermal area, western Yunnan Province, China. *Sedimentology*, 61 (1), 56-89.

Brečević, L., & Nielsen, A. E. (1993). Solubility of calcium carbonate hexahydrate. *Acta Chemica Scandinavica*, 47, 668-673.

Bridgman, P. W. (1939). The high pressure behavior of miscellaneous minerals. *American Journal of Science*, 237 (1), 7-18.

Brooks, R., Clark, L. M., & Thurston, E. F. (1950). Calcium Carbonate and Its Hydrates. *The Royal Society*, 243 (861), 145-168.

Brownlow, A.H. (1996). *Geochemistry*, 2nd Edition. U.S.A.: Prentice-Hall

Burton, E. A. (1993). Controls on marine carbonate cement mineralogy: review and reassessment. *Chemical Geology*, 105(1-3), 163–179.

Busenberg, E., & Niel Plummer, L. (1985). Kinetic and thermodynamic factors controlling the distribution of SO_4^{2-} and Na^+ in calcites and selected aragonites. *Geochimica et*

Cosmochimica Acta, 49(3), 713–725.

Busenberg, E., & Plummer, N. L. (1989). Thermodynamics of magnesian calcite solid-solutions at 25°C and 1 atm total pressure. *Geochimica et Cosmochimica Acta*, 53(6), 1189–1208.

Calcite crystals (2015). [Online] Available: <http://www.caveslime.org/fmd/calcite/#> [13th Feb., 2017]

Canterford, J. H., Tsambourakis, G., & Lambert, B. (1984). Some observations on the properties of dypingite, $Mg_5(CO_3)_4(OH)_2 \cdot 5H_2O$, and related minerals, *Mineralogical Magazine*, 48(September), 437-442.

Caponera, I., Fiori, S., and Pucci, R. (2013), Ritrovamento Di Artinite Nel Complesso Vulcanico Dei Colli Albani (RM), Gruppo Mineralogico Romano, [Online]. Available: <http://www.gminromano.it/Cercapietre/rivista04/testo/04A03.html> [13th Feb., 2017].

Chemias FT (2017). Inductively Coupled Plasma Optical Emission Spectrometry (ICP-OES), [Online]. Available: <http://www.chemiasoft.com/chemd/node/52> [13th Feb., 2017].

Chen, J., & Xiang, L. (2009). Controllable synthesis of calcium carbonate polymorphs at different temperatures. *Powder Technology*, 189(1), 64–69.

Cheng, W., & Li, Z. (2009). Precipitation of nesquehonite from homogeneous supersaturated solutions. *Crystal Research and Technology*, 44(9), 937–947.

Cheng, W., & Li, Z. (2010). Nucleation kinetics of nesquehonite ($MgCO_3 \cdot 3H_2O$) in the $MgCl_2$ – Na_2CO_3 system. *Journal of Crystal Growth*, 312(9), 1563–1571.

Cheng, W., Li, Z., & Demopoulos, G. P. (2009). Effects of Temperature on the Preparation of Magnesium Carbonate Hydrates by Reaction of $MgCl_2$ with Na_2CO_3 . *Chinese Journal of Chemical Engineering*, 17(4), 661–666.

Clarkson, J. R., Price, T. J., & Adams, C. J. (1992). Role of metastable phases in the spontaneous precipitation of calcium carbonate. *Journal of the Chemical Society, Faraday Transactions*, 88(2), 243.

Clark, S. P. (1957). A note on calcite-aragonite equilibrium. *Am. Mineralogist*, v. 42, p. 564-566.

Colfen, H. (2003). Precipitation of carbonates : recent progress in controlled production of complex shapes, 8, 23–31.

Company, T. water planet. (2013). Nitrification & Denitrification. The Water Planet Company, [Online]. Available: <https://www.yumpu.com/en/document/view/11509528/nitrification-amp-denitrification-the-water-planet-company> [13th, Feb., 2017].

Crawford, W. A., & Fyfe, W. S. (1964). Calcite-Aragonite Equilibrium at 100°C. *Science*, 144(3626), 1569-70.

- Culligan, S. A., Tinos, & NTUA. (2010). Report on the evaluation of existing methods on brine treatment and disposal practices. Sol-Brine team, [Online]. Available: http://solbrine.uest.gr/uploads/files/Deliverable_1.1.pdf [13th, Feb.,2017].
- Davey, R. J., Cardew, P. T., McEwan, D., & Sadler, D. E. (1986). Rate controlling processes in solvent-mediated phase transformation, 79, 648–653.
- Davies, P. J., & Bubela, B. (1973). The transformation of nesquehonite into hydromagnesite. *Chemical Geology*, 12(4), 289–300.
- Davies, P. J., Bubela, B., & Ferguson, J. (1977). Simulation of carbonate diagenetic processes: formation of dolomite, huntite and monohydrocalcite by the reactions between nesquehonite and brine. *Chemical Geology*, 19(1-4), 187-214.
- Davis, B. L. (1964). X-ray diffraction data on two high-pressure phases of calcium carbonate. *Science*, 145(3631), 489–491.
- Deelman, B. J. C. (1999). Low-temperature nucleation of magnesite and dolomite, *Neues Jahrbuch fuer Mineralogie, Monatshefte*, 1999(7), 289–302.
- Deelman, J. C. (1953). Low-temperature formation of dolomite and magnesite-Chapter 6: Magnesite & huntite. Version 2.3 (2011), 188–212.[Online]. Available: http://www.jcdeelman.demon.nl/dolomite/files/13_Chapter6.pdf [13th, Feb.,2017].
- DeGeer, B., Ford, J., Innes, S., Sargant, H. (2005). Demonstrations of sustainability. Rethinking Construction Ltd.[Online]. Available: http://constructingexcellence.org.uk/wp-content/uploads/2015/03/demonstrations_of_sustainability.pdf [13th, Feb.,2017]
- Dell, R. M., & Weller, S. W. (1959). The thermal decomposition of nesquehonite $MgCO_3 \cdot 3H_2O$ and magnesium ammonium carbonate $MgCO_3 \cdot (NH_4)_2CO_3 \cdot 4H_2O$. *Transactions of the Faraday Society*, 55, 2203-2220.
- DECC (2013). Annual report and accounts 2012-2013. Department of Energy and Climate Change, [Online]. Available: https://www.gov.uk/government/uploads/system/uploads/attachment_data/file/246692/0305.pdf [13th, Feb.,2017].
- Dowling, A., O'Dwyer, J., & Adley, C. C. (2015). Lime in the limelight. *Journal of Cleaner Production*, 92, 13–22.
- Dreybrodt, W., Eisenlohr, L., Madry, B., & Ringer, S. (1997). Precipitation kinetics of calcite in the system $CaCO_3-H_2O-CO_2$: The conversion to CO_2 by the slow process $H^+ + HCO_3^- \Rightarrow CO_2 + H_2O$ as a rate limiting step, *Geochimica et Cosmochimica Acta*, 61(18), 3897–3904.
- Druckenmiller, M. L., & Maroto-Valer, M. M. (2005). Carbon sequestration using brine of adjusted pH to form mineral carbonates. *Fuel Processing Technology*, 86(14-15), 1599–1614.
- Druckenmiller, M. L., Maroto-Valer, M. M., & Hill, M. (2006). Investigation of Carbon Sequestration via Induced Calcite Formation in Natural Gas Well Brine. *Energy & Fuels*, 20(1), 172–179.
- Duan, Z., & Sun, R. (2003). An improved model calculating CO_2 solubility in pure water and

- aqueous NaCl solutions from 273 to 533 K and from 0 to 2000 bar. *Chemical Geology*, 193(3-4), 257–271.
- Elfil, H., & Roquesb, H. (2001). Role of hydrate phases of calcium carbonate on the scaling phenomenon, *Desalination*, 137, 177–186.
- El-Naas, M. H. (2011). *Reject Brine Management*. United Arab Emirates University, UAE. [Online]. Available: http://cdn.intechopen.com/pdfs/13761/InTech-Reject_brine_management.pdf [13th, Feb., 2017].
- El-Naas, M. H., Al-Marzouqi, A. H., & Chaalal, O. (2010). A combined approach for the management of desalination reject brine and capture of CO₂. *Desalination*, 251(1-3), 70–74.
- Embassy of The Federal Democratic Republic of Ethiopia in London (2012). Profile on the production of calcium carbonate and lime. [Online]. Available: http://www.ethioembassy.org.uk/trade_and_investment/Investment_Profiles_EIA/Chemicals_and_Pharmaceuticals/Fertilizer.pdf [7th, Oct., 2016].
- Engler, P., Santana, M.W., Mittleman, M.A., & Balazs, D. (1988). Non-isothermal in situ XRD analysis of dolomite decomposition. *The Rigaku Journal*, 5(2), 3-8.
- Fakhru'l-Razi, A., Pendashteh, A., Abdullah, L. C., Biak, D. R. A., Madaeni, S. S., & Abidin, Z. Z. (2009). Review of technologies for oil and gas produced water treatment. *Journal of Hazardous Materials*, 170(2-3), 530–51.
- Falini, G., Gazzanob, M., & Ripamonti, A. (1996). Magnesium calcite crystallization from water-alcohol mixtures. *Chem. Commun.* 1996, 1037–1038. [Online]. Available: <http://pubs.rsc.org/en/Content/ArticlePDF/1996/CC/CC9960001037> [13th.Feb., 2017].
- Farm, H. E., Africa, S., & Berg, V. (1997). Chapter 5: Limestone. [Online]. Available: <https://ocw.mit.edu/courses/earth-atmospheric-and-planetary-sciences/12-110-sedimentary-geology-spring-2007/lecture-notes/ch5.pdf> [13th.Feb., 2017].
- Fernández Bertos, M., Simons, S. J. R., Hills, C. D., & Carey, P. J. (2004). A review of accelerated carbonation technology in the treatment of cement-based materials and sequestration of CO₂. *Journal of Hazardous Materials*, 112(3), 193–205.
- Fernandez-Diaz, L., Fernandez-Gonzalez, A., & Prieto, M. (2010). The role of sulfate groups in controlling CaCO₃ polymorphism. *Geochimica et Cosmochimica Acta*, 74(21), 6064–6076.
- Ferrini, V., De Vito, C., & Mignardi, S. (2009). Synthesis of nesquehonite by reaction of gaseous CO₂ with Mg chloride solution: its potential role in the sequestration of carbon dioxide. *Journal of Hazardous Materials*, 168(2-3), 832–7.
- Folk, R. L. (1974). The natural history of crystalline calcium carbonate: effect of manganese content and salinity. *Journal of Sedimentary Petrology*, 44(1), 40–53.
- Formia, A., Serra, C.L., Zerbinatti, M., Tulliani, J.M. (2014). The plasters of the Sacro Monte of Varallo Sesia. From the characterisation to the proposition of a restorative mix. *Case Studies in Construction Materials*, 1, 46-52.
- Gartner, E. (2004). Industrially interesting approaches to “low-CO₂” cements. *Cement and*

Concrete Research, 34(9), 1489–1498.

Georgiou, D., Petrolekas, P. D., Hatzixanthis, S., & Aivasidis, a. (2007). Absorption of carbon dioxide by raw and treated dye-bath effluents. *Journal of Hazardous Materials*, 144(1-2), 369–76.

Giammar, D. E., Bruant, R. G., & Peters, C. A. (2005). Forsterite dissolution and magnesite precipitation at conditions relevant for deep saline aquifer storage and sequestration of carbon dioxide. *Chemical Geology*, 217(3-4), 257–276.

Given, R. K., & Wilkinson, B. H. (1985). Kinetic control of morphology, composition, and mineralogy of abiotic sedimentary carbonates. *Journal of Sedimentary Research*, 55(6), 919–934.

Glasser, F.P., Jauffret, G., Morrison, J., Galvez-Martos, J.L., Patterson, N., & Imbabi, M.S. (2016). Sequestering CO₂ by mineralisation into useful nesquehonite-based products. *Frontiers in Energy Reserach*, 4, Article 3.

Glover, E. D., & Sippel, R. F. (1967). Synthesis of magnesium calcites. *Geochimica et Cosmochimica Acta*, 31(4), 603–613.

Goldsmith, J. R., Graf, D. L., & Joensuu, O. I. (1955). The occurrence of magnesian calcites in nature. *Geochimica et Cosmochimica Acta*, 7(5-6), 212–230.

Graf, D. L., & Goldsmith, J. R. (1955). Dolomite-magnesian calcite relations at elevated temperatures and CO₂ pressures. *Geochimica et Cosmochimica Acta*, 7, 109–128.

Gunning, P. J., Hills, C. D., & Carey, P. J. (2010). Accelerated carbonation treatment of industrial wastes. *Waste Management (New York, N.Y.)*, 30(6), 1081–90.

Guo, M., Li, Q., Ye, X., & Wu, Z. (2010). Magnesium carbonate precipitation under the influence of polyacrylamide. *Powder Technology*, 200(1-2), 46–51.

Han, Y. S., Hadiko, G., Fuji, M., & Takahashi, M. (2005). Effect of flow rate and CO₂ content on the phase and morphology of CaCO₃ prepared by bubbling method. *Journal of Crystal Growth*, 276(3-4), 541–548.

Han, Y. S., Hadiko, G., Fuji, M., & Takahashi, M. (2006). Factors affecting the phase and morphology of CaCO₃ prepared by a bubbling method. *Journal of the European Ceramic Society*, 26(4-5), 843–847.

Hänchen, M., Prigiobbe, V., Baciocchi, R., & Mazzotti, M. (2008). Precipitation in the Mg-carbonate system—effects of temperature and CO₂ pressure. *Chemical Engineering Science*, 63(4), 1012–1028.

Hangx, S. J.T. (2005). Behaviour of the CO₂-H₂O system and preliminary mineralisation model and experiments. CATO Workpackage WP 4.1 (December), 1–43. [Online]. Available: <https://www.co2-cato.org/publications/library1/behaviour-of-the-co2-h2o-system-and-preliminary-mineralisation-model-and-experiments-41-3-05-dec-2005> [13th.Feb.,2017].

Hardy, J.T. (2003). *Climate Change: Causes, Effects, and Solutions*. John Wiley & Sons, Ltd.

- Harned, S.H., & Davis, R. JR.(1942). The Ionization Constant of Carbonic Acid in Water and the Solubility of Carbon Dioxide in Water and Aqueous Salt Solutions from 0 to 50oC, New Haven, Connecticut, 65, 2030-2037.
- Harrison, A. J. W. (2004). Tececo Cements – Abatement , Sequestration and Waste, TecEco Pty. Ltd., [Online]. Available: <http://www.tececo.com/files/conference%20papers/CarbonationandWasteUtilisationWithTecandEcoCementsExtendedAbstractCementsCementConcreteScienceWarwickCoventryUK160904.pdf> [13th.Feb.,2017].
- Harrison, A. J. W., & Fcpa (2004a). Carbonating and Hydraulic Mortars - the difference is not only in the binder . Aggregates are also important. 10th Canadian Masonry Symposium, Banff, Alberta, June 8-12, 2005.[Online] Available: http://canadamasonrydesigncentre.com/download/10th_symposium/1a-3.pdf [13th.Feb.,2017].
- Harrison, A. J. W., & Fcpa (2004b). Emissions Reduction and other Advantages of TecEco Cements, TecEco Pty. Ltd., [Online]. Available: <https://www.tececo.com/files/political%20documents/EmissionsReductionandotherAdvantagesofTecEcoCements100803.pdf> [13th.Feb.,2017].
- Harrison, A. J. W., & Fcpa (2004c). The Properties of Reactive Magnesia--Portland Cement--Pozzolan Blends, TecEco Pty. Ltd., [Online]. Available: <http://www.tececo.com/files/conference%20papers/PropertiesofMagnesiaPortlandCementPozzolanBlends8thIntSemConcreteandBuildMatNewDelhi181103.pdf> [13th.Feb.,2017].
- Harrison, J. W. (2005). Reactive magnesium oxide cement. United States Patent Application Publication,[Online]. Available: <https://patentimages.storage.googleapis.com/pdfs/US20050103235.pdf> [13th.Feb.,2017].
- Hassan, D. (2014). Environmental Sustainability Assessment & Associated Experimental Investigations of Magnesia Production Routes, [Online]. Available: <http://www-geo.eng.cam.ac.uk/pdfs/abstract-2.pdf> [13th.Feb.,2017].
- Hollingbery, L.A., Hull, T.R. (2010). The fire retardant behaviour of huntite and hydromagnesite-a review. *Polymer Degradation and Stability*, 95, 2213-2225.
- House, W. A. (1987). Inhibition of Calcite Crystal-Growth By Inorganic-Phosphate. *Journal Of Colloid And Interface Science*, 119(2), 505–511.
- Hu, Z., & Deng, Y. (2003). Supersaturation control in aragonite synthesis using sparingly soluble calcium sulfate as reactants. *Journal of Colloid and Interface Science*, 266(2), 359–365.
- Hu, Z., & Deng, Y. (2004). Synthesis of needle-like aragonite from calcium chloride and sparingly soluble magnesium carbonate. *Powder Technology*, 140(1-2), 10–16.
- Huang, H. P., Shi, Y., Li, W., & Chang, S. G. (2001). Dual Alkali Approaches for the Capture and Separation of CO 2. *Energy & Fuels*, 15(2), 263–268.
- Huangjing Zhao, Nathan Dadap, Park, A. A. (2010). TAILORED SYNTHESIS OF PRECIPITATED

- MAGNESIUM CARBON-NEUTRAL FILLER MATERIALS DURING CARBON CARBONATES AS CARBON-NEUTRAL FILLER MATERIALS. The 13th International Conference on Fluidization - New Paradigm in Fluidization Engineering, RP6, Article 109.
- International Energy Agency. (2010). World Energy Outlook 2009. World Energy Outlook, 23(4), 326–328.
- Ishikawa, M., & Ichikuni, M. (1984). Uptake of sodium and potassium by calcite. *Chemical Geology*, 42(1-4), 137–146.
- Jager, A., Vins, V., Gernert, J., Span, R., & Hruby, J. (2013). Phase equilibria with hydrate formation in H₂O+CO₂ mixtures modeled with reference equations of state. *Fluid Phase Equilibria*, 338, 100–113.
- Jamieson, J. C. (1953). Phase Equilibrium in the System Calcite-Aragonite. *The Journal of Chemical Physics*, 21(8), 1385.
- Jarosinsk, A., & Madejska, L. (2010). MgCO₃ obtaining from wastewaters generated during the acidic leaching of zinc concentrates, 42, 317–320.
- Jeong, Y.-K., & Hwang, S.-J. (2005). Optimum doses of Mg and P salts for precipitating ammonia into struvite crystals in aerobic composting. *Bioresource Technology*, 96(1), 1–6.
- John A. Veil, Markus G. Puder, Deborah Elcock, Robert J. Redweik, J. (2004). A White Paper Describing Produced Water from Production of Crude Oil, Natural Gas, and Coal Bed Methane, Produce Water White Pape, [Online]. Available: <http://www.ipd.anl.gov/anlpubs/2004/02/49109.pdf> [13th.Feb.,2017].
- Kanagy, L. E., Johnson, B. M., Castle, J. W., & Rodgers, J. H. (2008). Design and performance of a pilot-scale constructed wetland treatment system for natural gas storage produced water. *Bioresource Technology*, 99(6), 1877–85.
- Kato, T., Sugawara, a., & Hosoda, N. (2002). Calcium Carbonate–Organic Hybrid Materials. *Advanced Materials*, 14(12), 869.
- Katz, A. (1973). The interaction of magnesium with calcite during crystal growth at 25-90oC and one atmosphere. *Geochimica et Cosmochimica Acta*, 37(6).
- Kinsman, D. J. J. (1967). Huntite from a carbonate-evaporite environment. *The American Minerologist*, 52 (9-10), 1332–1340.
- Kinsman, D. J. J., & Holland, H. D. (1969). The co-precipitation of cations with CaCO₃, -IV . The co-precipitation of Sr²⁺ with aragonite between 16°C and 96°C. *Geochimica et Cosmochimica Acta*, 33(October 1964), 1–17.
- Kisuma Chemicals (2017). Mangesium Hydroxide, Kisuma Chemicals, [Online]. Available: <https://www.kisuma.com/materials/magnesium-hydroxide> [13th.Feb.,2017].
- Kitamura, M. (2001). Crystallization and Transformation Mechanism of Calcium Carbonate Polymorphs and the Effect of Magnesium Ion. *Journal of Colloid and Interface Science*, 236(2), 318–327.

- Kitamura, M. (2002). Controlling factor of polymorphism in crystallization process. *Journal of Crystal Growth*, 237-239, 2205–2214.
- Kitamura, M., Konno, H., Yasui, A., & Masuoka, H. (2002). Controlling factors and mechanism of reactive crystallization of calcium carbonate polymorphs from calcium hydroxide suspensions. *Journal of Crystal Growth*, 236(1-3), 323–332.
- Kitano Okumura, M., Idogaki, M., Y. (1975). Incorporation of sodium, chloride and sulfate with calcium carbonate. *Geochemical Journal*, 9(2), 75–84.
- Klaus S. Lackner, Wendt, Christopher H, Darryl P. Butt, E. L. J. (1995). Carbon dioxide disposal in carbonate minerals. *Energy*, 20(1), 1153–1170.
- Kloprogge, J. T., Martens, W. N., Nothdurft, L., Duong, L. V., & Webb, G. E. (2003). Low temperature synthesis and characterization of nesquehonite. *Journal of Materials Science Letter*, 22(11), 825–829.
- Kodama, S., Nishimoto, T., Yamamoto, N., Yogo, K., & Yamada, K. (2008). Development of a new pH-swing CO₂ mineralization process with a recyclable reaction solution. *Energy*, 33(5), 776–784.
- Königsberger, E., Königsberger, L.-C., & Gamsjäger, H. (1999). Low-temperature thermodynamic model for the system Na₂CO₃-MgCO₃-CaCO₃-H₂O, 63(19), 3105–3119.
- Konno, H., Nanri, Y., & Kitamura, M. (2002). Crystallization of aragonite in the causticizing reaction. *Powder Technology*, 123(1), 33–39.
- Konno, H., Nanri, Y., & Kitamura, M. (2003). Effect of NaOH on aragonite precipitation in batch and continuous crystallization in causticizing reaction. *Powder Technology*, 129(1-3), 15–21.
- Kralj, D., & Brecevic, L. (1990). Vaterite growth and dissolution in aqueous solution I: Kinetics of crystal growth, 104, 793–800.
- Kralj, D., & Brečević, L. (1995). Dissolution kinetics and solubility of calcium carbonate monohydrate. *Colloids and Surfaces A: Physicochemical and Engineering Aspects*, 96(3), 287–293.
- Kralj, D., Breevi, L., & Kontrec, J. (1997). Vaterite growth and dissolution in aqueous solution III . Kinetics of transformation, 177, 248–257.
- Lackner, K. S. (2002). Carbonate Chemistry for Sequestering Fossil Carbon. *Annual Review of Energy and the Environment*, 27(1), 193–232.
- Lacson, J.G., Cometta, S. & Yoneyama, M. (2000) *Chemical Economics Handbook: Magnesium oxide and other magnesium chemicals*. [Online]. Available: <https://www.ihs.com/products/magnesium-oxide-chemical-economics-handbook.html> [13th Feb., 2017]
- Lafarge. (2013). Annual report registration document. Lafarge, 2014, [Online]. Available: http://www.lafarge.com/sites/default/files/atoms/files/03232015-press_publication-2014_annual_report-uk.pdf [13th.Feb.,2017].

- Lahann, R. W. (1978). A chemical model for calcite crystal growth and morphology control. *J.Sed.Petrol.*, 48(1), 337–344.
- Lanas, J., & Alvarez, J. I. (2004). Dolomitic lime: thermal decomposition of nesquehonite. *Thermochimica Acta*, 421(1-2), 123–132.
- Land, L. S., & Hoops, G. K. (1973). Sodium in carbonate sediments and rocks; a possible index to the salinity of diagenetic solutions. *Journal of Sedimentary Research*, 43(3), 614–617.
- Langmuir, D. (1965). Stability of carbonates in the system MgO-CO₂-H₂O, 73(5), 730–754.
- Lattemann, S., & Höpner, T. (2008). Environmental impact and impact assessment of seawater desalination. *Desalination*, 220(1-3), 1–15.
- Lee, I., Han, S. W., Choi, H. J., & Kim, K. (2001). Nanoparticle-Directed Crystallization of Calcium Carbonate. *Advanced Materials*, 13(21), 1617–1620.
- Li, Q., Ding, Y., Li, F., Xie, B., & Qian, Y. (2002). Solvothermal growth of vaterite in the presence of ethylene glycol, 1,2-propanediol and glycerin. *Journal of Crystal Growth*, 236(1-3), 357–362.
- Lide, D.R. (ed.), 2005, CRC Handbook of Chemistry and Physics, 86th edition
- Liebermann, O. (1967). Synthesis of Dolomite. *Nature*, 213, 241-245.
- Limin, Q., Li, J., & Ma, J. (2002). Biomimetic Morphogenesis of Calcium Carbonate in Mixed Solutions of Surfactants and Double-Hydrophilic Block Copolymers, *Advanced Materials*, 14(4), 300–303.
- Lioist (2016). What to know about...Lhoist Ltd., [Online]. Available: <http://www.lhoist.com/want-know-more-about%E2%80%A6> [13th Feb., 2017].
- Lippman, F. (1973). *Sedimentary Carbonate Minerals*. Berlin, Heidelberg: Springer-Verlag
- Liska, M., & Vandeperre, L. J. (2007). Influence of carbonation on the properties of reactive magnesia cement-based pressed masonry units. *Advances in Cement Research*, 20(2), 53-64.
- Liu, Q., & Maroto-Valer, M. M. (2010). Investigation of the pH effect of a typical host rock and buffer solution on CO₂ sequestration in synthetic brines. *Fuel Processing Technology*, 91(10), 1321–1329.
- Liu, Q., & Maroto-Valer, M. M. (2012). Studies of pH buffer systems to promote carbonate formation for CO₂ sequestration in brines. *Fuel Processing Technology*, 98, 6–13.
- Loste, E., Di, E., Zorbakhsh, A., & Meldrum, F. C. (2003). Study of Calcium Carbonate Precipitation under a Series of Fatty Acid Langmuir Monolayers Using Brewster Angle Microscopy. *Langmuir*, 19 (7), 2830–2837.
- Loste, E., Wilson, R. M., Seshadri, R., & Meldrum, F. C. (2003). The role of magnesium in stabilising amorphous calcium carbonate and controlling calcite morphologies. *Journal of*

Crystal Growth, 254(1-2), 206–218.

Lucas-Girot, A., Marie-Clemence, V., Tribut, O., & Oudadesse, H. (2005). Gentamicin-loaded calcium carbonate materials: Comparison of two drug-loading modes. *Journal of Biomedical Materials Research Part B Applied Biomaterials*, 73 (1), 164-70.

MacDonald, G. J. F. (1956). EXPERIMENTAL DETERMINATION OF CALCITE- ARAGONITE EQUILIBRIUM RELATIONS AT ELEVATED TEMPERATURES AND PRESSURES. *Institute of Geophysics, University of California, Los Angeles*, 24 (59), 744–756.

Malinin, S. D. (1959). The system water-carbon dioxide at high temperatures and pressures, *Geochem.*, 3, 292-306.

Markham, A. E., & Kobe, K. A. (1941). The Solubility of Carbon Dioxide and Nitrous Oxide in Aqueous Salt Solutions. *Journal of the American Chemical Society*, 63(2), 449-454.

Martin, Marietta (2013). Specialty Magnesium Oxide. Martin Marietta Magnesia Specialties, [Online]. Available: <http://magnesiaspecialties.com/category/specialty-magnesium-oxide/> [13th Feb., 2017].

Mathur, V. K., & Way, F. (2001). High speed manufacturing process for precipitated calcium carbonate employing sequential pressure carbonation. Patents, CA2416080 A1. [Online]. Available: <https://www.google.com/patents/CA2416080A1?cl=en> [13th.Feb.,2017].

McCauley, R. A., & Johnson, L. A. (1991). Decrepitation and thermal decomposition of dolomite. *Thermochimica Acta*, 185(2), 271–282.

McIntosh, R. M., Sharp, J. H., & Wilburn, F. W. (1990). The thermal decomposition of dolomite. *Thermochimica Acta*, 165(2), 281–296.

Medlin, W. L. (1956). The preparation of synthetic dolomite. *The American Mineralogist*, 44(9-10), 979-986.

Meldrum, F. C., & Hyde, S. T. (2001). Morphological influence of magnesium and organic additives on the precipitation of calcite. *Journal of Crystal Growth*, 231(4), 544–558.

Mignardi, S., De Vito, C., Ferrini, V., & Martin, R. F. (2011). The efficiency of CO₂ sequestration via carbonate mineralization with simulated wastewaters of high salinity. *Journal of Hazardous Materials*, 191(1-3), 49–55.

Ming, D. W., & Franklin, W. T. (1985). Synthesis and Characterization of Lansfordite and Nesquehonite, (1910), 1303–1308.

Mohamed, a. M. O., Maraqa, M., & Al Handhaly, J. (2005). Impact of land disposal of reject brine from desalination plants on soil and groundwater. *Desalination*, 182(1-3), 411–433.

Montes-Hernandez, G., Findling, N., Renard, F. (2016). Dissolution-precipitation reactions controlling fast formation of dolomite under hydrothermal conditions. *Applied Geochemistry*, 73, 169-177.

Morse, J. W., Arvidson, R. S., & Lüttge, A. (2007). Calcium carbonate formation and dissolution. *Chemical Reviews*, 107(2), 342–81.

- Morse, J. W., & Mackenzie, F. T. (1990). *Geochemistry of sedimentary carbonates*. Elsevier Science.
- Mucci, A. (1987). Influence of temperature on the composition of magnesian calcite overgrowths precipitated from seawater. *Geochimica et Cosmochimica Acta*, 76(11-12), 1889–1896.
- Mucci, A. (1988). Manganese uptake during calcite precipitation from seawater: Conditions leading to the formation of a pseudokutnahorite. *Geochimica et Cosmochimica Acta*, 52(7), 1859–1868.
- Mucci, A., & Morse, J. W. (1983). The incorporation of Mg²⁺ and Sr²⁺ into calcite overgrowths: influences of growth rate and solution composition. *Geochimica et Cosmochimica Acta*, 47, 217–233.
- Nan, Z., Shi, Z., Yan, B., Guo, R., & Hou, W. (2008). A novel morphology of aragonite and an abnormal polymorph transformation from calcite to aragonite with PAM and CTAB as additives. *Journal of Colloid and Interface Science*, 317(1), 77–82.
- Nielsen, A. E., & Sohnel, O. (1971). Interfacial tensions electrolyte crystal-aqueous solution, from nucleation data, *Journal of Crystal Growth*, 11(3), 233–242.
- Nishiyama, R., Munemoto, T., & Fukushi, K. (2013). Formation condition of monohydrocalcite from CaCl₂-MgCl₂-Na₂CO₃ solutions. *Geochimica et Cosmochimica Acta*, 100, 217–231.
- Nordbottne, J.M., & Celia, M.A. (2012). *Geological Storage of CO₂: Modeling Approaches for Large-Scale Simulation*. John Wiley & Sons, Inc.
- NRMCA (2012). Concrete CO₂ Fact Sheet. National Ready Mixed Concrete Association, [Online]. Available: <https://www.nrmca.org/sustainability/CONCRETE%20CO2%20FACT%20SHEET%20FEB%2012.pdf> [13th.Feb.,2017].
- Ogino, T., Suzuki, T., & Sawada, K. (1987). The formation and transformation mechanism of calcium carbonate in water. *Geochimica et Cosmochimica Acta*, 51(10), 2757–2767.
- Okumura, M., & Kitano, Y. (1986). Coprecipitation of alkali metal ions with calcium carbonate. *Geochimica et Cosmochimica Acta*, 50(1), 49–58.
- Oomori, T., Kaneshima, K., Taira, T., & Kitano, Y. (1983). Synthetic studies of protodolomite from brine waters. *Geochemical Journal*, 17(3), 147–152.
- Ota, Y., Inui, S., Tetsushi, I., Kasuga, T., & Abe, Y. (1995). Preparation of Aragonite Whiskers. *Journal of the American Ceramic Society*, 78(7), 1983-1984.
- Paquette, J., & Reeder, R. J. (1995). Relationship between surface structure, growth mechanism, and trace element incorporation in calcite. *Geochimica et Cosmochimica Acta*, 59(4), 735–749.
- Park, A.-H. A., & Fan, L.-S. (2004). mineral sequestration: physically activated dissolution of serpentine and pH swing process. *Chemical Engineering Science*, 59(22-23), 5241–5247.

- Park, W. K., Ko, S.-J., Lee, S. W., Cho, K.-H., Ahn, J.-W., & Han, C. (2008). Effects of magnesium chloride and organic additives on the synthesis of aragonite precipitated calcium carbonate. *Journal of Crystal Growth*, 310(10), 2593–2601.
- Parkhurst, D. L., & Appelo, C. A. J. (2013). Description of Input and Examples for PHREEQC Version 3 — A Computer Program for Speciation, Batch-Reaction, One-Dimensional Transport, and Inverse Geochemical Calculations. U.S. Geological Survey Techniques and Methods, Book 6, Chapter A43. [Online]. Available: <https://pubs.usgs.gov/tm/06/a43/pdf/tm6-A43.pdf> [13th.Feb.,2017].
- PCA (2009). Report on sustainable manufacturing. Portland Cement Association, [Online]. Available: http://cement.org/smreport09/images/shared_images/sustainreport08.pdf [13th.Feb.,2017].
- Peter Styring, D. J. (2011). Carbon Capture and Utilisation in the green economy. CO2Chem Carbon Dioxide Utilisation Network, [Online]. Available: <http://co2chem.co.uk/carbon-capture-and-utilisation-in-the-green-economy> [13th.Feb.,2017].
- Power, I. M., Wilson, S. a, Thom, J. M., Dipple, G. M., & Southam, G. (2007). Biologically induced mineralization of dypingite by cyanobacteria from an alkaline wetland near Atlin, British Columbia, Canada. *Geochemical Transactions*, 8, 13.
- Raz, S., Weiner, S., & Addadi, L. (2000). Formation of High-Magnesian Calcites via an Amorphous Precursor Phase: Possible Biological Implications. *Advanced Materials*, 12(1), 38–42.
- Read, A. J. (1975). The First Ionization Constant of Carbonic Acid from 25 to 250oC and to 2000bar. *Journal of Solution Chemistry*, 4(1), 53–70.
- Reddy, M. M. (1977). Crystallization of calcium carbonate in the presence of trace concentrations of phosphorus-containing anions. I. Inhibition by phosphate and glycerophosphate ions at pH 8.8 and 25°C. *Journal of Crystal Growth*, 41(2), 287–295.
- Reddy, M. M., & Gaillard, W. D. (1981). Kinetics of Calcium Carbonate (Calcite) -Seeded Crystallization : Influence of Solid / Solution Ratio on the Reaction Rate Constant, *Journal of Colloid and Interface Science*, 80(1), 171-178.
- Sánchez-Román, M., Romanek, C. S., Fernández-Remolar, D. C., Sánchez-Navas, A., McKenzie, J. A., Pibernat, R. A., & Vasconcelos, C. (2011). Aerobic biomineralization of Mg-rich carbonates: Implications for natural environments. *Chemical Geology*, 281(3-4), 143–150.
- Sanna, A., Dri, M., & Maroto-Valer, M. (2012). Carbon dioxide capture and storage by pH swing aqueous mineralisation using a mixture of ammonium salts and antigorite source. *Fuel*, 2–10.
- Sawada, K. (1997). The mechanisms of crystallization and transformation of calcium carbonates. *Pure and Applied Chemistry*, 69(5), 921–928.
- Sayles, F. L., & Fyfe, W. S. (1973). The crystallization of magnesite from aqueous solution. *Geochimica et Cosmochimica Acta.*, 37(1), 87-99.

- Schneider, M., Romer, M., Tschudin, M., & Bolio, H. (2011). Sustainable cement production—present and future. *Cement and Concrete Research*, 41(7), 642–650.
- SCLAR, C. B., CARRISON, L. C., and SCHWARTZ, C. M., 1962, The calcite-aragonite transition and the calibration of a belt-type apparatus between 15 and 35 kb, 700° to 1400° C. *Am. Soc. Mech. Engineers Paper 62-WA-248*, 7 p.
- Seitzinger, S., Harrison, J. a, Böhlke, J. K., Bouwman, a F., Lowrance, R., Peterson, B., Van Drecht, G. (2006). Denitrification across landscapes and waterscapes: a synthesis. *Ecological Applications : A Publication of the Ecological Society of America*, 16(6), 2064–90.
- Shakhashiri. (2006). Carbon dioxide. *Chemistry*, [Online]. Available: <http://www.scifun.org/GenChem/CHEMWEEK/CarbonDioxide.pdf> [13th.Feb.,2017].
- Shand, M. A. (2006). *THE CHEMISTRY AND TECHNOLOGY OF MAGNESIA*. New Jersey: John Wiley & Sons, Inc.
- Sheng Han, Y., Hadiko, G., Fuji, M., & Takahashi, M. (2006). Crystallization and transformation of vaterite at controlled pH. *Journal of Crystal Growth*, 289(1), 269–274.
- Siegel, F.R.(1961). Factors influencing the precipitation of dolomitic carbonates. *Geol. Surv. Kansas Bull.* 152, 129–158.
- Simmons, G., & Bell, P. (1963). Calcite-Aragonite Equilibrium. *Science*, 139(3560), 1197-1198.
- Soong, Y., Fauth, D. L., Howard, B. H., Jones, J. R., Harrison, D. K., Goodman, a. L., Frommell, E. A. (2006). CO₂ sequestration with brine solution and fly ashes. *Energy Conversion and Management*, 47(13-14), 1676–1685.
- Soong, Y., Goodman, a. ., McCarthy-Jones, J., & Baltrus, J. (2004). Experimental and simulation studies on mineral trapping of CO₂ with brine. *Energy Conversion and Management*, 45(11-12), 1845–1859.
- Span, R., Gernert, J., & Jäger, A. (2013). Accurate thermodynamic-property models for CO₂-rich mixtures. *Energy Procedia*, 37, 2914–2922.
- Span, R., & Wagner, W. (1996). A New Equation of State for Carbon Dioxide Covering the Fluid Region from the Triple-Point Temperature to 1100 K at Pressures up to 800 MPa. *Journal of Physical and Chemical Reference Data*, 25(6), 1509.
- Spanos, N., & Koutsoukos, P. G. (1998). The transformation of vaterite to calcite: effect of the conditions of the solutions in contact with the mineral phase. *Journal of Crystal Growth*, 191(4), 783–790.
- Steel, K. M., Alizadehhesari, K., Balucan, R. D., & Bašić, B. (2013). Conversion of CO₂ into mineral carbonates using a regenerable buffer to control solution pH. *Fuel*, 111, 40–47.
- Styring, P., Quadrelli, E.A., & Armstrong, K. edt.(2014). *Carbon Dioxide Utilization: Closing the Carbon Cycle*. Elsevier
- Styring, P., Jansen, D., de Coninck, H., Reith, H., & Armstrong, K. (2011). *Carbon Capture and*

- Utilisation in the green economy. Centre for Low Carbon Futures, [Online]. Available: <http://co2chem.co.uk/wp-content/uploads/2012/06/CCU%20in%20the%20green%20economy%20report.pdf> [13th.Feb.,2017].
- SURF (2017). Scanning Electron Microscopy & Energy Dispersive X-Ray Spectroscopy. Research Group Electrochemical and Surface Engineerin, [Online]. Available: <https://www.surfgroup.be/semedx> [13th Feb., 2017].
- Takenouchi, S., & Kennedy, G. C. (1964). The binary system H₂O-CO₂ at high temperatures and pressures. *American Journal of Science*, 262(9), 1055-1074.
- Taylor, H.F.W. (1997). *Cement chemistry*, 2nd Edition. Thomas Telford Ltd.
- Teir, S. (2008). Fixation of carbon dioxide by producing carbonates from minerals and steelmaking slags. Department of Energy Technology, Dissertations.
- Teir, S., Eloneva, S., Fogelholm, C. J., & Zevenhoven, R. (2007). Dissolution of steelmaking slags in acetic acid for precipitated calcium carbonate production. *Energy*, 32(4), 528–539.
- Teir, S., Eloneva, S., Fogelholm, C.-J., & Zevenhoven, R. (2009). Fixation of carbon dioxide by producing hydromagnesite from serpentinite. *Applied Energy*, 86(2), 214–218.
- Teir, S., Eloneva, S., & Zevenhoven, R. (2005). Production of precipitated calcium carbonate from calcium silicates and carbon dioxide. *Energy Conversion and Management*, 46(18-19), 2954–2979.
- Teir, S., Kuusik, R., Fogelholm, C.-J., & Zevenhoven, R. (2007). Production of magnesium carbonates from serpentinite for long-term storage of CO₂. *International Journal of Mineral Processing*, 85(1-3), 1–15.
- Teir, S., Revitzer, H., Eloneva, S., Fogelholm, C.-J., & Zevenhoven, R. (2007). Dissolution of natural serpentinite in mineral and organic acids. *International Journal of Mineral Processing*, 83(1-2), 36–46.
- The National (2014), Upending chemistry's atomic law. [Online], Available: <http://www.thenational.ae/uae/science/upending-chemistrys-atomic-law> [13th Feb., 2017].
- Tobler, D. J., Blanco, J. D. R., Dideriksen, K., Sand, K. K., Bovet, N., Benning, L. G., & Stipp, S. L. S. (2014). The Effect of Aspartic Acid and Glycine on Amorphous Calcium Carbonate (ACC) Structure, Stability and Crystallization. *Procedia Earth and Planetary Science*, 10, 143–148.
- Tödheide K. and Franck E. U. (1963) Das Zweiphasengebiet und die kritische Kurve im System Kohlendioxid–Wasser bis zu Drucken von 3500 bar. *Zeitschrift für Physikalische Chemie Neue Folge*, 37, 387-401.
- Unluer, C. (2012). ENHANCING THE CARBONATION OF REACTIVE MAGNESIA CEMENT - BASED POROUS BLOCKS. Department of Engineering University of Cambridge, Dissertations.
- U.S. Geological Survey. (2013). *Mineral Commodity Summaires 2013*. U.S. Geological Survey,

- 198p. [Online]. Available: <https://minerals.usgs.gov/minerals/pubs/mcs/2013/mcs2013.pdf> [13th Feb., 2017].
- USGS. (2001). Magnesium compounds. U.S. Geological Survey, 1(703), 98–99, 2000-2001. [Online]. Available: <https://minerals.usgs.gov/minerals/pubs/mcs/2001/mcs2001.pdf> [13th Feb., 2017].
- USGS. (2002). Mineral Commodity Summaries 2002. U.S. Geological Survey, [Online]. Available: <https://minerals.usgs.gov/minerals/pubs/mcs/2002/mcs2002.pdf> [13th Feb., 2017].
- USGS. (2003). 2003 Summaries 20 Mineral Commodity Summaries 2003. U.S. Geological Survey, [Online]. Available: <https://minerals.usgs.gov/minerals/pubs/mcs/2003/mcs2003.pdf> [13th Feb., 2017].
- USGS. (2016). Mineral Commodity Summaries 2016. U.S. Geological Survey, 198p. [Online]. Available: <https://minerals.usgs.gov/minerals/pubs/mcs/2016/mcs2016.pdf> [13th Feb., 2017].
- Wagner, W., Cooper, J. R., Dittmann, a., Kijima, J., Kretzschmar, H.-J., Kruse, A., Willkommen, T. (2000). The IAPWS Industrial Formulation 1997 for the Thermodynamic Properties of Water and Steam. *Journal of Engineering for Gas Turbines and Power*, 122(1), 150.
- Walsh, D., Lebeau, B., & Mann, S. (1999). Morphosynthesis of Calcium Carbonate (Vaterite) Microsponges. *Advanced Materials*, 11(4), 324–328.
- Wang, D., & Li, Z. (2011). Modeling Solid – Liquid Equilibrium of $\text{NH}_4\text{Cl} - \text{MgCl}_2 - \text{H}_2\text{O}$ System and Its Application to Recovery of NH_4Cl in MgO Production, 57(6), 1595–1606.
- Wang, H., Alfredsson, V., Tropsch, J., Ettl, R., & Nylander, T. (2013). Formation of CaCO_3 Deposits on Hard Surfaces Effect of Bulk Solution Conditions and Surface Properties. *Applied materials and Interfaces*, 5(10). 4035-4045.
- Wang, X., & Maroto-Valer, M. (2011a). Integration of CO_2 capture and storage based on pH-swing mineral carbonation using recyclable ammonium salts. *Energy Procedia*, 4, 4930–4936.
- Wang, X., & Maroto-Valer, M. M. (2011b). Dissolution of serpentine using recyclable ammonium salts for CO_2 mineral carbonation. *Fuel*, 90(3), 1229–1237.
- Wang, X., & Xue, D. (2006). Direct observation of the shape evolution of MgO whiskers in a solution system. *Materials Letters*, 60(25-26), 3160–3164.
- Wang, Y., Li, Z., & Demopoulos, G. P. (2008). Controlled precipitation of nesquehonite ($\text{MgCO}_3 \cdot 3\text{H}_2\text{O}$) by the reaction of MgCl_2 with $(\text{NH}_4)_2\text{CO}_3$. *Journal of Crystal Growth*, 310(6), 1220–1227.
- Wang, Z. (2012). Treatment of Reject Brine with Natural and Modified Zeolites. University of Cambridge, Dissertation.
- WBCSD. (2002). Toward a Sustainable Cement Industry. World Business Council for Sustainable Development, Geneva, Switzerland. [Online]. Available:

- <http://wbcscement.org/pdf/sdi.pdf> [13th Feb., 2017].
- WBCSD. (2007). Cement Sustainability Initiative. World Business Council for Sustainable Development, Geneva, Switzerland. [Online]. Available: <http://www.wbcscement.org/pdf/CSI%20Progress%20Report%202007.pdf> [13th Feb., 2017].
- WBCSD. (2012). The Cement Sustainability Initiative. World Business Council for Sustainable Development, Geneva, Switzerland. [Online]. Available: http://csiproggress2012.org/CSI_ProgressReport_Summary.pdf [13th Feb., 2017].
- Webmineral (2017), Mineralogy Database, [Online]. Available: <http://www.webmineral.com/> [13th Feb., 2017].
- Wei, H., Shen, Q., Zhao, Y., Wang, D.-J., & Xu, D.-F. (2003). Influence of polyvinylpyrrolidone on the precipitation of calcium carbonate and on the transformation of vaterite to calcite. *Journal of Crystal Growth*, 250(3-4), 516–524.
- White, A. F. (1977). Sodium and potassium coprecipitation in aragonite. *Geochimica et Cosmochimica Acta*, 41(5), 613–625.
- White, A. F. (1978). Sodium coprecipitation in calcite and dolomite. *Chemical Geology*, 23(1-4), 65–72.
- Wiebe, R., & Gaddy, V. L. (1939). The Solubility in Water of Carbon Dioxide at 50, 75 and 100°, at Pressures to 700 Atmospheres. *Journal of the American Chemical Society*, 61(2), 315–318.
- Wray, J. L., & Daniels, F. (1957). Precipitation of calcite and aragonite. *Journal of the American Chemical Society*, 79(9), 2031–2034.
- Xingqi, L., Dong, H., Rech, J. a., Matsumoto, R., Bo, Y., & Yongbo, W. (2008). Evolution of Chaka Salt Lake in NW China in response to climatic change during the Latest Pleistocene–Holocene. *Quaternary Science Reviews*, 27(7-8), 867–879.
- Xiong, Y., & Lord, A. S. (2008). Experimental investigations of the reaction path in the MgO–CO₂–H₂O system in solutions with various ionic strengths, and their applications to nuclear waste isolation. *Applied Geochemistry*, 23(6), 1634–1659.
- Yan, C., & Xue, D. (2005). Novel self-assembled MgO nanosheet and its precursors. *The Journal of Physical Chemistry. B*, 109(25), 12358–61.
- Yoshida, A. Y. & F. (1979). Carbon Dioxide in Aqueous Electrolyte Solutions, *American Chemical Society*, 24(7), 13–16.
- Zaitseva, L. V., Orleanskii, V. K., Gerasimenko, L. M., & Ushatinskaya, G. T. (2006). The role of cyanobacteria in crystallization of magnesium calcites. *Paleontological Journal*, 40(2), 125–133.
- Zawko, S.A., Schmidt, C.E. (2010). Assembly of sodium sope fibers and fibrillar particles triggered by dissolution of sodium chloride crystals. *Soft Matter*, 6, 3289–3297

- Zehr, J. P., & Kudela, R. M. (2011). Nitrogen Cycle of the Open Ocean: From Genes to Ecosystems. *Annual Review of Marine Science*, 3(1), 197–225.
- Zevenhoven, R., Wiklund, A., Fagerlund, J., Eloneva, S., In't Veen, B., Geerlings, H., Boerrigter, H. (2009). Carbonation of calcium-containing mineral and industrial by-products. *Frontiers of Chemical Engineering in China*, 4(2), 110–119.
- Zhan, G., & Guo, Z. (2015). Preparation of potassium salt with joint production of spherical calcium carbonate from sintering dust. *Transactions of Nonferrous Metals Society of China*, 25(2), 628–639.
- Zhang, J., Zhang, R., Geerlings, H., & Bi, J. (2012). Mg-Silicate Carbonation Based on an HCl- and NH₃-Recyclable Process: Effect of Carbonation Temperature. *Chemical Engineering & Technology*, 35(3), 525–531.
- Zhang, Z., Zheng, Y., Ni, Y., Liu, Z., Chen, J., & Liang, X. (2006). Temperature- and pH-dependent morphology and FT-IR analysis of magnesium carbonate hydrates. *The Journal of Physical Chemistry. B*, 110(26), 12969–73.